



FRIEDRICH-SCHILLER-
UNIVERSITÄT
JENA

DYNAMICS IN PRODUCTION AND EMISSION OF VOLATILE ORGANIC COMPOUNDS FROM SOIL, LEAVES, AND LITTER

Dissertation
(kumulativ)

zur Erlangung des Grades *Doctor rerum naturalium* (Dr. rer. nat.)

vorgelegt dem Rat der Chemisch-Geowissenschaftlichen Fakultät der
Friedrich-Schiller-Universität Jena

von M. Sc. (Chemie) Ann-Sophie Lehnert, geboren am 22.07.1993 in Mainz

Gutachter:

1. _____

2. _____

(3.) _____

Tag der Verteidigung: _____

Contents

List of Figures	v
List of Tables	vii
List of Abbreviations	ix
Summary	xiii
Zusammenfassung	xvii
1. Introduction	1
1.1. Role of VOCs in the Atmosphere	2
1.2. VOCs from Plants	3
1.2.1. Plant Stress Response	4
1.2.2. Plant–Microbe VOC Interactions	6
1.3. VOCs from Soils and Litter	7
1.3.1. VOCs from Litter Degradation	7
1.3.2. Soil VOCs	8
1.3.3. Microbial Soil VOCs	9
1.4. Terrestrial Sulfur Cycle, Formation and Degradation of Volatile Sulfur Compounds .	12
1.4.1. Sulfate Reduction and Oxidized Organic Sulfur Compounds	12
1.4.2. Amino Acid Formation	13
1.4.3. Cycling of Reduced VSCs	13
1.4.4. Formation and Cycling of Carbonyl Sulfide	19
1.4.5. Ecosystem Hotspots of Sulfur Cycling	21
1.4.6. The Marine Sulfur Cycle and the CLAW Hypothesis	27
1.5. Methods to Measure VOCs	29
1.5.1. PTR-MS and SIFT-MS	31
1.5.2. Sampling Methods	33
1.5.3. Field Setups	34
2. Scope of the Thesis	37

3. Publications	41
3.1. P1: SIFT-MS Optimization for Atmospheric Trace Gas Measurements at Varying Humidity	43
3.2. P2: Simultaneous Real-Time Measurement of Isoprene and 2-Methyl-3-Buten-2-ol Emissions From Trees Using SIFT-MS	57
3.3. P3: Dimethyl Sulfide Emissions from Peatlands Result more from Organic Matter Degradation than Sulfate Reduction	69
4. Unpublished Work - Volatile Organic Compound Emissions upon Leaf Litter Degradation	97
4.1. Introduction	97
4.2. Materials and Methods	99
4.2.1. Site Description	99
4.2.2. Incubations for VOC Emission Measurements	99
4.2.3. VOC Analysis	100
4.2.4. Terpene Analysis	101
4.2.5. CO ₂ , and N ₂ O Analysis	101
4.2.6. Microbial Community Analysis	102
4.2.7. Statistical Analysis	102
4.3. Results	103
4.3.1. VOC Emission Changes Upon Degradation	104
4.3.2. Tree Species Dependence of VOCs	105
4.3.3. Modelling VOC Emissions	107
4.3.4. Correlations with Litter Element Contents	108
4.3.5. Correlations with Microbial Community Abundance	109
4.3.6. Terpenes	110
4.4. Discussion	111
4.5. Conclusion	116
4.6. Author Contributions	117
4.7. Acknowledgements	117
5. Discussion	119
5.1. Instrument Advances for Accurate SIFT-MS Measurements	119
5.2. Dimethyl Sulfide, Methanethiol, and Hydrogen Sulfide from Soil	122
5.3. VOC Emissions from Litter	126
6. Conclusion	131
Bibliography	I
Acknowledgements	XLIII

Curriculum vitae	XLVII
Licenses	XLIX
Publikationsäquivalente	LI
Declarations	LIII
A. Supplement (Electronic)	LV
A.1. VSC Emissions in Different Regions of the World	LVI
A.2. Supplement of P1: SIFT-MS Optimization for Atmospheric Trace Gas Measurements at Varying Humidity	XCVIII
A.3. Supplement of P2: Simultaneous Real-Time Measurement of Isoprene and 2-Methyl- 3-Buten-2-ol Emissions From Trees Using SIFT-MS	CXXXI
A.4. Supplement of P3: Dimethyl Sulfide Emissions from Freshwater Wetlands Result more from Organic Matter Degradation than Sulfate Reduction	CXXXVII
A.5. Litter VOC Emissions over Time	CCXXX

List of Figures

1.1. Scheme of a typical VOC degradation and ozone formation process. R can be any organic residue	3
1.2. Scheme of common stress-induced plant VOC groups and their biosynthetic pathways	5
1.3. Main precursors and biosynthesis pathways of microbial VOCs	11
1.4. Scheme of the terrestrial sulfur cycle	14
1.5. Scheme of the marine sulfur cycle	28
1.6. General scheme of PTR-MS and SIFT-MS	31
4.1. Measured VOC headspace of the different tree species over time	104
4.2. Principal component analysis of VOC emissions of litter from different tree species over time	106
4.3. Correlations of the individual VOCs with each other	107
4.4. Correlations of the VOC emissions and litter elemental contents	108
4.5. Principal component analysis of the microbial community and VOC emissions from the litter at t = 0	109
5.1. Proposal for a VSC model	126
6.1. Thesis summary	132
A.1. Scheme of litter degradation field setup	CCXXX
A.2. Scheme of VOC sampling on litter degradation	CCXXXI
A.3. Methanol, acetaldehyde, acetic acid, acetonitrile, and hydrogen sulfide emission of the different tree litter types over time	CCXXXII
A.4. Sum sesquiterpene, geosmin, isoprene, dimethyl sulfide, and acetone emission of the different tree litter types over time	CCXXXIII
A.5. Sum monoterpene, β -pinene, camphene, and limonene emission of the different tree litter types over time	CCXXXIV
A.6. CO ₂ release rate, headspace and sample humidity, litter weight, and methanethiol emission of the different tree litter types over time	CCXXXV
A.7. PCAs of litter VOC emissions split by time	CCXXXVI
A.8. Carbon and nitrogen contents (mass percent relative to dry mass) as well as $\Delta^{13}\text{C}$ and $\Delta^{15}\text{N}$ signals of the different tree litter types over time	CCXXXIX

A.9. Ca, Fe, K, Mg, and P contents of the different tree litter types over time	CCXL
A.10. Relative abundance of the different bacterial/archaeal and fungal phyla at t = 0 for the different tree species	CCXLI
A.11. Correlation coefficients of the different VOCs correlating with the bacterial/archaeal and fungal phylum abundances at t = 0	CCXLII

List of Tables

1.1. Global sources and sinks of VSCs to the atmosphere (Watts, 2000)	22
1.2. Main global sources and sinks of VSCs to the atmosphere (Warneck and Williams, 2012)	22
4.1. Terpenes found in the litter samples via TD/SPME-GC-MS	112
4.2. Methanol and monoterpene emissions of different reference studies	115
A.1. Literature-documented VSC-emissions from plants	LVI
A.2. Literature-documented VSC-emissions from salt marshes	LIX
A.3. Literature-documented VSC-emissions from microbial mats	LXIV
A.4. Literature-documented VSC-emissions from mangrove forests	LXVII
A.5. Literature-documented VSC-emissions from freshwater wetlands and lakes	LXX
A.6. Literature-documented VSC-emissions from rice paddies	LXXXIII
A.7. Literature-documented VSC-emissions from temperate soils	LXXXV
A.8. Literature-documented VSC-emissions from subtropical soils	LXXXIX
A.9. Literature-documented VSC-emissions from tropical soils	LXXXIX
A.10. Literature-documented VSC-emissions from arctic soils	XCII
A.11. Literature-documented VSC-emissions from waste	XCV
A.12. Mixed-effect model for acetaldehyde emissions	CCXXXVII
A.13. Mixed-effect model for acetone emissions	CCXXXVII
A.14. Mixed-effect model for methanol emissions	CCXXXVIII
A.15. Mixed-effect model for monoterpene emissions	CCXXXVIII

List of Abbreviations

χ mixing ratio

φ release rate

ϕ gas flow

AdoHcy adenosylhomocysteine

AdoMet adenosylmethionine

AIC Akaike's information criterion

AMP adenosine monophosphate

ANOVA analysis of variance

AOM anaerobic oxidation of methane

APCI atmospheric pressure chemical ionization

APS adenosine-5'-phosphosulfate

ATP adenosine triphosphate

BIC Bayesian information criterion

BID barrier discharge ionization detector

br branching ratio

BTEX benzene, toluene, ethylbenzene, and xylene

BVOC biogenic volatile organic compound

CA carbonic anhydrase

CI confidence interval

CoA coenzyme A, [(2*R*,3*S*,4*R*,5*R*)-5-(6-amino-9*H*-purin-9-yl)-4-hydroxy-3-(phosphonoxy)tetrahydro-2-furanyl]methyl (3*R*)-3-hydroxy-2,2-dimethyl-4-oxo-4-(3-oxo-3-[(2-sulfanylethyl)amino]propyl-amino)butyl dihydrogen diphosphate

CoB coenzyme B, 2-[(7-mercapto-1-oxoheptyl)amino]-3-phosphonoxybutanoic acid

CoM coenzyme M, mercaptoethanesulfonate

cps counts per second, unit of signal intensity

CYP450 cytochrome P 450

DMAPP dimethylallyl pyrophosphate

DMDS dimethyl disulfide

DMS dimethyl sulfide

DMSHB 4-(dimethylsulfonio)-2-hydroxybutanoate

DMSO dimethyl sulfoxide

DMSOP 3-(dimethylsulfoxonio)-propionate

DMSP 3-(dimethylsulfonio)-propionate
DMTS dimethyl trisulfide
dw dry weight
E_H redox potential with reference to standard hydrogen electrode
ECD electron capture detector
EM electron multiplier
FAD flavine adenine dinucleotide
FEP fluorinated ethylene propylene
FID flame ionization detector
FKM fluorocarbon elastomer
GC gas chromatography
GCU gas calibration unit
HR high-resolution
I intensity
ICF instrument calibration factor
IG ion guide
IPr isoprene (2-methyl-1, 3-butadiene)
IPP isopentenyl pyrophosphate
k kinetic rate constant ($\frac{cm^3}{molec. s}$)
LOD limit of detection
logLik log likelihood ratio
LOV Leichtflüchtige organische Verbindungen, volatile organic compounds
LOX lipoxygenase
LSV Leichtflüchtige Schwefelverbindungen, volatile sulfur compounds
MBO 2-methyl-3-buten-2-ol
Me-CoM methylated coenzyme M, 2-(methylthio)-ethanesulfonate
MEP 2-C-methyl-D-erythritol-4-phosphate
MeSH methanethiol
MG methanogen
ML maximum likelihood approximation
MMPA 3-(methylthio)-propanoate
MPA 3-thiopropoanoate
MS mass spectrometry
MSA methanesulfonic acid
MTA-CoA methylthioacryloyl-CoA
MTHB 4-(methylthio)-2-hydroxybutanoate
MTOB 4-(methylthio)-2-oxobutanoate
MTPA 3-(methylthio)-propylamine
MVA mevalonic acid

nsim number of simulations
p pressure
PAPS 3'-phosphoadenosine-5'-phosphosulfate
PEEK polyether ether ketone
PEPCO phosphoenolpyruvate carboxylase
ppb parts per billion (mol/mol in air)
PPi pyrophosphate
ppt parts per trillion (mol/mol in air)
PTR-MS proton transfer reaction mass spectrometry
Q quadrupole (mass spectrometer)
REML restricted maximum likelihood approximation
ROS reactive oxygen species
RuBisCo ribulose-1,5-bisphosphate carboxylase/oxygenase
SD standard deviation
SIFT-MS selective ion flow tube mass spectrometry
SMM S-methyl-methionine
SNR signal-to-noise ratio
SPME solid-phase microextraction
SRB sulfate-reducing bacteria
SRI-MS switchable reagent ion mass spectrometry
T temperature
TD thermodesorption
TG Trockengewicht, dry weight
THF tetrahydrofolate
TMT thiol methyltransferase
ToF time of flight (mass spectrometer)
UHPLC ultra-high performance liquid chromatography
VOC volatile organic compound
VSC volatile sulfur compound

Summary

Volatile organic compounds (VOCs) are ubiquitous in our daily lives. As scents and infochemicals, they shape our perception of our environment and mediate numerous inter- and intraspecies interactions. Fish, birds, and other animals are known to orientate via their olfactory sense. Plants use many different volatiles, e.g. to attract pollinators, to defend against herbivores, and to combat abiotic stress. Also for microbes, VOCs are important for short- and long-range communication. They use them for biofilm assembly, mating, plant growth promotion, and defense against competitors and predators.

At the bigger picture, VOCs have a huge influence on our atmosphere and climate. Depending on their stability and properties, they can act as greenhouse gases on a regional to global scale. They can also contribute to ozone formation in summer smog and decrease air quality. Oxidation products of VOCs can aggregate to form secondary organic aerosols that influence global albedo. Sulfur and nitrogen-containing gases can even form sulfate and nitrate crystals in the atmosphere that can act as cloud condensation nuclei, changing cloud formation processes, the albedo and rain patterns.

Important substance classes for volatile organic compounds from soil, litter, and plants are small organic alcohols, aldehydes, and acids from primary metabolism as well as secondary metabolites like terpenes and terpenoids. Whereas the former are usually leaking from cells or emitted as waste products, the latter are often used on purpose as infochemicals. For example in trees, isoprene and 2-methyl-3-buten-2-ol are used to combat heat stress. Additionally, VOCs can be an important part of nutrient cycles: Volatile sulfur compounds emitted from soil, wetlands, and oceans link soil and water quality with microbial activity and the atmosphere. Hereby, sulfate reduction and methylation is the most important VSC source in wetlands, organic matter degradation in suboxic organic-rich soils and sediments, and DMSP degradation is the most important pathway in the oceans.

To understand these atmospheric and biotic processes, it is important to measure the concentration, net fluxes and composition of VOC mixtures. For this, a stable, sensitive instrument is needed. Gas Chromatography-Mass Spectrometry (GC-MS) is the method of choice for complex VOC mixtures of more unpolar volatiles with a higher boiling point, and Proton Transfer Reaction Mass Spectrometry (PTR-MS) and Selective Ion Flow Tube Mass Spectrometry (SIFT-MS) for time-resolved measurements of unpolar very volatile analytes. In this work I describe how I enhanced the sensitivity of our commercially-bought Voice 200 ultra SIFT-MS (Syft Technologies, Christchurch, New Zealand) to meet the requirements of our biogenic VOC research: By reducing the instrument background

and optimizing parameters like an increased sample gas flow, I could reduce the instrument's limits of detection (LOD) by a factor of 10 to low ppb values. I found that using FEP-coated FKM o-rings, a needle valve as an inlet, 100 ccm sample gas flow, 158 ccm helium carrier gas flow, 40 V flow tube voltage, and 140 °C flow tube temperature is optimal for our litter VOC and soil VSC emission research. This should be adjusted for each experimental setting though. The optimizations came at the cost of an enhanced humidity-dependence, so I developed and validated a calibration procedure for this setup. For us, it worked best to fit an equation derived from the theoretical calculation of concentration based on instrument parameters and the concentrations of water clusters of the products, but adding a linear humidity term also works fine. Upon comparison to a PTR-QMS 500 (Ionicon, Innsbruck, Austria), the PTR-MS still has lower LODs, but the SIFT-MS reached at least the same magnitude. Both instruments are equally sensitive to small concentration changes, and the SIFT-MS is still less humidity-dependent than the PTR-MS.

I then validated our SIFT-MS technique by investigating how to simultaneously measure isoprene and 2-methyl-3-buten-2-ol (MBO) emissions from trees in a time-resolved manner. Different tree species emit either isoprene or MBO upon heat stress, e.g. poplar and spruce emitting isoprene and ponderosa pine emitting MBO. Furthermore, spruce bark beetles emit MBO. To separate heat stress of different plant types at an ecosystem level or spruce heat stress from signals of bark beetle infestation, it can be important to measure both compounds in parallel, as can be done by SIFT-MS. I found that measuring isoprene on $m/z = 68$ u when ionizing with NO^+ and MBO on $m/z = 71$ u when ionizing with O_2^+ works best for a broad range of concentration ratios of the two compounds. There is some interference from one analyte on the signal of the other analyte, but with those two ions, it is below 2% and can be corrected for. With this method, I could capture the diurnal cycle of isoprene/MBO emissions of *Populus nigra*, *Pinus ponderosa*, *Picea abies*, and two *Picea glauca* accessions. The release rates were in the same magnitude as previously published release rates, and I even found that the *Picea abies* trees I investigated actually emitted both isoprene and MBO, which had not been reported before.

Having a sensitive and reliable technique to measure VOCs in hand, I went on to study the processes related to hydrogen sulfide (H_2S), methanethiol (MeSH), and dimethyl sulfide (DMS) cycling in an organic-rich fibric histosol fen known for its intense sulfur cycling. Volatile sulfur compounds (VSCs) are produced either by sulfate reduction or the degradation of amino acids and their derivatives, and can be converted to each other by methylation and demethylation. I found that DMS and MeSH are emitted over a much broader range of soil humidity and at higher redox potentials as H_2S , indicating that there might be different processes involved. By labelling with $^{34}\text{SO}_4^{2-}$, I found that only H_2S and MeSH are readily formed from sulfate. I then looked at organic compounds and identified organic sulfur compounds as potential VSC precursors from the peat's organic matter. When testing those compounds as well as literature-known VSC precursors, thiols were precursors for H_2S , methyl thio compounds were precursors for MeSH, and dimethyl sulfonio groups for DMS. I also found three sulfur cycling microbes (*Acidobacteria* SD1, *Desulfosporosinus*, *Pseudomonas*) cor-

relating with VSC emissions, which might be subject to further study on VSC emissions. When I incubated soil with static headspace, DMS mixing ratios were always a factor of 10 higher than MeSH and H₂S mixing ratios, regardless of the spiked precursor. These interconversion processes appear to be slower or less favorable than the immediate release of H₂S and MeSH from sulfate reduction and MeSH and DMS from organic matter degradation. By tracking VSC emissions, one could thus gain insights into the redox conditions in the soil and whether soil pore space is stable enough to equilibrate the VSCs to DMS, COS, and DMSO.

One main source of organic matter in soil is foliar litter. It contains labile organic carbon compounds that can be degraded quickly. Hence, I proceeded to investigate the VOC emissions from litter of 13 different temperate tree species over the course of 400 days. With up to 30 $\frac{\mu\text{g}}{\text{g}_{\text{dw}}}$ (microgram per gram litter dry weight), monoterpene emissions from conifer litter were the highest emissions that I found, and they persisted the longest. Methanol emissions could reach 1 $\frac{\mu\text{g}}{\text{g}_{\text{dw}}}$, but decayed quickly, and other emissions were much lower. I observed an exponential decay of the VOC emissions with time and litter quality such that most emissions from litter of deciduous tree species were negligible after the first burst of methanol emissions. An investigation of the identity of the terpenes showed similar monoterpenes and some sesquiterpenes like in other litter terpene studies, e.g. α - and β -pinene, 3-carene and β -caryophyllene, but especially terpenoid and sesquiterpene emissions were quite different. Correlating the emissions with microbial community composition showed no strong correlations, but *Firmicutes* correlated with acetonitrile, isoprene, mono- and sesquiterpenes, β -*proteobacteria* with methanol, acetonitrile, and hydrogen sulfide, and *basidiomycota* with dimethyl sulfide. When modelling acetaldehyde, acetone, methanol, and monoterpene emissions, the CO₂ respiration was not a significant factor, and the litter humidity only was important for acetaldehyde production. Thus, even for the small VOCs originating from primary metabolism, the litter quality and compound classes seem to matter more than the general microbial activity. These insights can now be used when including litter VOC emissions in atmospheric models.

My studies illustrate the different roles VOCs can have - sometimes being agents to fight stress, sometimes signalling molecules, sometimes just waste products of metabolism. In all these functions, their emissions can be quite high and with this, they can have a great impact on the atmosphere. However, the studies also illustrate that the formation mechanisms are complex and variable, and to understand the bulk signal takes considerable effort. Based on the three major topics of the thesis, there are three directions research could focus on: To advance measurement techniques, I propose merging the SIFT-MS ion source with the PTR-ToF-MS drift tube and mass spectrometer or even an ion trap, as this combines the enhanced structural identification possibilities of SIFT-MS with the sensitivity of the PTR-MS. To investigate the impact of soil volatile sulfur compounds further, I propose research on further organic precursors from soils as well as the enzymes related to them. Additionally, I proposed the framework for a soil VSC model. The most promising field for VOC research is currently litter, as even basic studies on the full VOC emission spectra from different litter types are still needed. This might be a long-overlooked source of VOCs, and we are

just beginning to understand its impact on soil and the atmosphere. With its studies on improving SIFT-MS instrument sensitivities and finding new analytical methods for measuring isoprene and 2-methyl-3-buten-2-ol simultaneously, on the origin and emission conditions of soil volatile sulfur compounds and on volatile organic compound during the degradation of 13 different litter species, this thesis contributed to our understanding of biogenic volatile organic compounds and how they shape the interactions between soil and the atmosphere.

Zusammenfassung

Leichtflüchtige organische Verbindungen (LOV) sind in unserem Leben allgegenwärtig. Gerüche als eine Form der chemischen Sprache bestimmen unsere Wahrnehmung der Umwelt und reguliert zahlreiche Interaktionen innerhalb und zwischen verschiedenen Spezies. Fische, Vögel und andere Tiere nutzen Gerüche zur Orientierung, während Pflanzen eine Vielzahl an LOV verwenden, bspw. um Bestäuber anzulocken oder Fraßfeinden und abiotischem Stress standzuhalten. Auch Mikroorganismen verwenden LOV zur Kommunikation über kurze oder längere Substanzen, etwa zur Bildung von Biofilmen, zur Fortpflanzung, zur Förderung des Pflanzenwachstums und als Verteidigung gegen Konkurrenten und Fraßfeinde.

All diese LOV haben einen großen Einfluss auf die Atmosphäre und das Klima. Je nach Stabilität und chemischen Eigenschaften können sie zum Treibhauseffekt auf lokaler oder globaler Ebene oder zur Bildung von Ozon im Sommer-Smog und zur Verringerung der Luftqualität beitragen. Ihre Oxidationsprodukte können zu sekundären organischen Aerosolen aggregieren, die die globale Albedo beeinflussen. Dies gilt insbesondere für schwefel- und stickstoffhaltige Gase, die Sulfat- und Nitratkristalle in der Atmosphäre bilden können und als Kondensationskeime die Wolkenbildung, globale Albedo und die Verteilung von Regen beeinflussen.

Wichtige Substanzklassen von LOV aus Boden, Laub und Pflanzen sind kleine organische Alkohole, Aldehyde und Säuren aus dem Primärmetabolismus sowie Sekundärmetaboliten wie Terpene und Terpenoide. Während erstere oft ungezielt aus Zellen herausdiffundieren oder als Metaboliten emittiert werden, werden letztere meist als Infochemikalien verwendet. Beispielsweise emittieren Bäume gezielt Isopren und 2-Methyl-3-buten-2-ol (MBO), um mit Hitzestress umzugehen. Zusätzlich können LOV ein wichtiger Bestandteil von Stoffkreisläufen sein: Leichtflüchtige Schwefelverbindungen (LSV), die aus Boden, Feuchtgebieten und Ozeanen emittiert werden, verbinden Boden- und Wasserqualität mit mikrobieller Aktivität und der Atmosphäre. Dabei ist Sulfatreduktion und Sulfidmethylierung die wichtigste LSV-Quelle in Feuchtgebieten, der Abbau organischer Materie am wichtigsten in suboxischen, organikreichen Böden und Sedimenten und Dimethylsulfoniopropionatabbau der wichtigste Biosyntheseweg in algenreichen Gewässern und den Ozeanen.

Um diese atmosphärischen und biotischen Prozesse zu verstehen, ist es wichtig, die Konzentration, Netto-Flüsse und Zusammensetzung von LOV zu messen. Dafür braucht es stabile und empfindliche Messgeräte. Gaschromatographie-Massenspektrometrie (GC-MS) ist die Methode der Wahl für komplexe LOV-Gemische, besonders wenn diese etwas unpolarer sind und einen höheren Siedepunkt

haben. Im Gegensatz dazu können SIFT-MS und PTR-MS zeitaufgelöst messen und erfassen besonders gut kleine, polare LOV mit hohem Dampfdruck. In einer ersten Studie habe ich die Empfindlichkeit des Voice 200 ultra SIFT-MS (Syft Technologies, Christchurch, Neuseeland) optimiert, damit es unsere Anforderungen für Forschung an biogenen LOV erfüllt: Indem ich den Hintergrund durch den Austausch VOC-emittierender Bauteile senkte, den Gasfluss erhöhte und einige Geräteparameter optimierte, konnte ich die Nachweisgrenzen des Geräts um Faktor 10 auf einstellige ppb-Werte reduzieren. Für unsere Forschung an Boden- und Laubemissionen sind FEP-ummantelte FKM-Dichtungsringe, ein Nadelventil als Probeneinlass, 100 ccm Probegasfluss, 158 ccm Helium Trägergasfluss, 40 V Flow Tube-Spannung und 140 °C Flow-Tube-Temperatur ideal, jedoch sollte dies für jedes experimentelle Design individuell optimiert werden. Die erhöhte Sensitivität wurde durch eine Zunahme der Feuchtigkeitsabhängigkeit erkauft, sodass ich zusätzlich eine feuchtigkeitsabhängige Kalibration implementierte und validierte. Die besten Ergebnisse erzielte ich mit einer von der theoretischen Berechnung der Konzentrationen abgeleiteten Kalibrierfunktion basierend auf den Wasserclustern aller Ionen, jedoch kann man auch einfach einen linearen Term für die Feuchtigkeit einführen. Im Vergleich mit einem PTR-QMS 500 (Ionicon, Innsbruck, Österreich) zeigt sich, dass das PTR-MS immer noch empfindlicher ist, allerdings das SIFT-MS Nachweisgrenzen in der gleichen Größenordnung wie das PTR-MS hat. Beide Geräte sind gleich empfindlich gegenüber kleinen Veränderungen der Konzentration, wobei die Messungen des SIFT-MS weniger feuchtigkeitsabhängig sind.

Die Anwendbarkeit des so optimierten SIFT-MS wurde in einer Fallstudie zu zeitaufgelösten Isopren- und MBO- Emissionen aus Bäumen getestet. Verschiedene Baumarten nutzen entweder Isopren oder MBO zur Bekämpfung von Hitzestress, bspw. nutzten Pappel und Fichte Isopren, aber Gelbkiefern MBO. Außerdem emittieren Borkenkäfer, die Fichten befallen, MBO. Um Hitzestress verschiedener Baumarten in Ökosystemen oder bei Fichten Hitzestress und Borkenkäferbefall zu unterscheiden, müssen beide Verbindungen simultan gemessen werden können, wie es mit SIFT-MS der Fall ist. Misst man Isopren auf $m/z(\text{NO}^+) = 68$ u und MBO auf $m/z(\text{O}_2^+) = 71$ u, ist dies für eine große Spanne von Konzentrationsverhältnissen der beiden Verbindungen möglich. Es gibt eine geringe Interferenz der Analyten mit dem Signal des jeweils anderen, aber mit den zwei genannten Ionen ist die Interferenz kleiner als 2% und kann herausgerechnet werden. Die Methode wurde von uns anhand von Standardmessungen untersucht und durch die Beobachtung des Tagesverlaufs der lichtabhängigen Emissionen beider Verbindungen in Pappel, Kiefer und verschiedenen Fichtenarten validiert. Die Freisetzungsraten beider Verbindungen waren in der gleichen Größenordnung wie publizierte Ergebnisse. Ich fand sogar Anzeichen darauf, dass *Picea abies* gleichzeitig Isopren und MBO emittiert - was bisher nicht beschrieben wurde.

Mit dieser empfindlichen und verlässlichen VOC-Messmethode untersuchte ich nun die Prozesse der Bildung von Schwefelwasserstoff (H_2S), Methanthiol (MeSH) und Dimethylsulfid (DMS) am Beispiel eines organikreichen Histosol-Flachmoors, dessen aktiver Schwefelkreislauf mit häufigen Redoxpotentialwechseln gut untersucht ist. Laut Literatur werden die drei leichtflüchtigen Schwe-

felverbindungen (LSV) entweder durch Sulfatreduktion oder den Abbau von schwefelhaltigen Aminosäuren und ihren Derivaten im Boden gebildet. Sie können durch Methylierung und Demethylierung ineinander umgewandelt werden. Unsere Untersuchungen ergaben, dass DMS und MeSH über eine wesentlich größere Spanne an Bodenfeuchtigkeit und bei höherem Redoxpotential als H₂S emittiert wurden, was darauf hindeutet, dass verschiedene Bildungsprozesse beteiligt sind. Durch Labelling mit ³⁴SO₄²⁻ und Zugabe verschiedener, literaturbekannter oder im Boden identifizierter organischer Schwefelsubstanzen konnte ich nachweisen, dass H₂S und MeSH durch Sulfatreduktion entsteht, und Moleküle mit Thio-, Methylthio- und Dimethylsulfonylgruppen zu H₂S, MeSH und DMS abgebaut werden können. Außerdem konnte ich drei für den Schwefelkreislauf relevante Bakterien identifizieren, die mit LSV-Emissionen korrelieren (*Acidobacteria* SD1, *Desulfosporosinus*, *Pseudomonas*) und somit Ausgangspunkt weiterer wissenschaftlicher Studien sein könnten. Wurde der mit Schwefelsubstanzen versetzte Boden in einer geschlossenen Kammer mit stabilem Gasraum inkubiert, bildete sich unabhängig vom Vorläufermolekül ein Gleichgewicht mit etwa 10x höherer DMS- als MeSH und H₂S-Konzentration aus. Diese Interkonversionen scheinen langsamer als die direkte Bildung von H₂S und MeSH aus der Sulfatreduktion und MeSH und DMS aus organischer Materie zu sein. Diese Erkenntnisse ermöglichen es nun, Rückschlüsse über die Redoxbedingungen im Boden und die Stabilität der Luft in den Bodenporen zu ziehen.

Eine große Quelle organischer Materie im Boden und damit von LOV-Emissionen aus dem Boden ist Laub. Es enthält labile organische Kohlenstoffverbindungen, die schnell abgebaut werden können. Deshalb habe ich in einer Studie die Emission von LOV während des Abbaus von Laub- und Nadelstreu 13 verschiedener Laub- und Nadelbäume der gemäßigten Klimazone über 400 Tage untersucht. Am größten waren die Terpenemissionen aus Nadelbaumstreu, die über mehr als 200 Tage bis zu $30 \frac{\mu\text{g}}{\text{g}_{TG}}$ (Mikrogramm pro Gramm Nadelrockengewicht) in den 24 h Inkubation produzierten. Die zweitwichtigste LOV-Emission war Methanol, von dem von frischem Laubbaumlaub (jünger als 100 Tage) bis zu $1 \frac{\mu\text{g}}{\text{g}_{TG}}$ in den 24 h Inkubation gemessen wurde. Andere LOV-Emissionen waren wesentlich geringer. Im Allgemeinen wurde ein exponentieller Abfall der Emissionen beobachtet, sodass die Emissionen von Laubbaumlaub lediglich kurz nach dem Fall der Blätter relevant sind. Eine Untersuchung der Struktur der Terpene ergab ähnliche Ergebnisse wie andere Terpen-Laub-Studien für Monoterpene und einige Sesquiterpene, z. B. α - und β -Pinen, 3-Caren oder β -Caryophyllen, allerdings waren vor allem Terpenoide und Sesquiterpenzusammensetzungen anders als in der Literatur. Eine Korrelation der LOV-Emissionen mit der Zusammensetzung der mikrobiellen Gemeinschaft ergab wenige starke Korrelationen: *Firmicutes* korrelieren mit Acetonitril, Isopren, Mono- und Sesquiterpenen, β -*Proteobacteria* mit Methanol, Acetonitril und Schwefelwasserstoff und *Basidiomycota* mit Dimethylsulfid. Eine Modellierung der Monoterpen-, Acetaldehyd-, Aceton- und Methanolemissionen zeigte, dass die CO₂-Emission als ein Maß für die mikrobielle Aktivität im Boden keinen signifikanten Faktor für die VOC-Emissionen darstellt und auch die Feuchtigkeit des Laubs nur für Acetaldehyd wichtig ist. Daraus lässt sich schließen, dass selbst für die kleinen LOV, die durch den Primärmetabolismus der Laubdestruenten entstehen, die Qualität und chemische Zusammensetzung der Streu wichtiger als die allgemeine mikrobielle Aktivität

zu sein scheint. Diese Ergebnisse können nun in die Modellierung von LOV in der Atmosphäre herangezogen werden.

Die Arbeit veranschaulicht die verschiedenen Rollen von biogenen LOV: Sie können zur Bekämpfung abiotischen Stresses oder zur Signalübertragung dienen und manchmal sind sie einfach Neben- und Endprodukte des Metabolismus. In allen diesen Funktionen können die Emissionen hoch sein und einen signifikanten Einfluss auf die Atmosphäre haben. Jedoch zeigt die Arbeit auch, dass die Bildungsprozesse kompliziert sind und die Interpretation schwierig sein kann. LOV-Messungen werden auf der makroskopischen Ebene gemacht, beinhalten aber Signale zum individuellen Metabolismus verschiedener Mikroben, Pflanzen etc. Manchmal überlagern sich die Prozesse, etwa wenn eine Verbindung direkt von der nächsten Mikrobe wieder aufgenommen und verändert wird, aber dennoch ermöglichen LOV es, nicht-destruktiv einen Einblick über den Status des Bodens, der Pflanze oder eines anderen Studienobjekts zu bekommen. Basierend auf den drei großen Themenblöcken der Arbeit können drei zukünftige Forschungsrichtungen abgeleitet werden: Um die Entwicklung von Messtechniken weiter voranzutreiben, schlage ich vor, die Ionenquelle von SIFT-MS mit dem Drift Tube und Massenspektrometer des PTR-MS oder sogar einer Ionenfallen zu vereinen, da dies die erweiterten Möglichkeiten der Substanzidentifikation mittels SIFT-MS mit der Sensitivität des PTR-MS verbindet. Im Bereich der LSV-Emissionen aus Boden wäre es interessant, weitere organische Vorläufermoleküle und die damit verbundenen Enzyme und Biosynthesewege zu untersuchen. Zusätzlich habe ich einen Rahmen für ein Boden-VSC-Modell vorgeschlagen. Das vielversprechendste Feld für LOV-Forschung ist gegenwärtig Laub, da selbst einfache Studien zu Gesamt-LOV-Emissionsspektren aus verschiedenen Laubsorten noch fehlen. Laub könnte eine lange übersehene Quelle von LOV sein und wir fangen erst an, seinen Einfluss auf den Boden und die Atmosphäre zu verstehen. Mit den Studien zur Verbesserung der Sensitivität von SIFT-MS, einer neuen analytischen Methode zur simultanen Messung von Isopren und MBO, einer Studie zu Vorläufern und Emissionsbedingungen leichtflüchtiger Schwefelverbindungen aus Boden und zu LOV-Emissionen während des Abbaus von 13 verschiedenen Laubsorten hat diese Arbeit zum Verständnis biogener LOV und ihrem Einfluss auf die Interaktionen von Boden und Atmosphäre beigetragen.

1. Introduction

Volatile Organic Compounds (VOCs) shape the medium we are living in: the air. As scents, infochemicals, leaking waste products, aerosol precursors, they are ubiquitous measures for the status of our surrounding environment. VOCs are generally considered compounds with a boiling point below 250 °C, so they comprise most chemical substance classes (Klose and Geldsetzer, 2013). Anthropogenic production is mostly linked to side products of oil, gas, coal, and wood combustion, by-products of manufacturing and landfills, solvent leakage, and their intended use as scents. Often, anthropogenic VOCs are rather unpolar, like benzene, toluene, ethylbenzene and xylene (BTEX). However, also the biota produces substantial amounts of VOCs, either involuntarily by general metabolism and cell leakage or on purpose as signalling compounds in intra- and inter-species communication or to combat abiotic stress. Biotic VOCs are often very polar, like methanol, formaldehyde or acetic acid (Lewis et al., 2020).

Understanding biotic VOCs helps understanding the state and wellbeing of its emitter: For example, if farmers or forest rangers can distinguish plant heat stress from stress caused by herbivores, they can adapt their management strategies accordingly. The same is true for understanding soil VOCs, as they might enable specific management strategies to improve soil quality. Additionally, we need to know under which circumstances which VOCs are emitted to assess their impact on the atmosphere and global climate.

In this thesis, a Selective Ion Flow Tube Mass Spectrometer was optimized for biogenic VOC emission measurements. Its ability to separate closely-related analytes like isoprene and 2-methyl-3-buten-2-ol (MBO) was shown for a number of isoprene and MBO-emitting tree species. With this instrument in hand, the precursors and emission conditions of volatile sulfur compound (VSC) emissions from peatlands were investigated. This contributes to our understanding of how the terrestrial sulfur cycle works and how biogenic VSC emissions contribute to the atmospheric sulfur burden. Additionally, VOC emissions from degrading leaf litter from 13 different species was investigated to deduce their formation and degradation processes in relation to the litter quality and microbial community. In the introduction, I will thus first shortly introduce the role of VOCs in the atmosphere, to highlight their impact. Then, I will give an overview over the main VOC classes and their roles in plants, litter, and soil. I will especially focus on the terrestrial sulfur cycle, the formation and degradation processes of VSCs and their emission rates in different ecosystems. Lastly, I explain the state of the art of different instruments and measurement techniques, explaining PTR-MS and SIFT-MS as well as dynamic chamber and static chamber systems in detail.

1.1. Role of VOCs in the Atmosphere

VOCs exhibit a broad gas phase chemistry in the atmosphere. Broadly speaking, they get oxidized until they are soluble enough to be washed out of the troposphere or aggregate to particles that precipitate *via* dry deposition. The atmospheric lifetime of VOCs depends on their water solubility and their susceptibility to reactions with atmospheric radicals like OH[•], NO₃, O₃, halogens and their oxides, as well as photolysis. These reactions are usually a sequence of hydrogen abstraction or radical additions to double bonds followed by an O₂ addition and then either O[•] abstractions by NO₂ or other radical recombinations, chain elongations etc. (Atkinson, 1997; Atkinson and Arey, 2003).

Their lifetime also determines the region they may reach. Lifetimes in the order of hours and days mean that the VOC is quickly deposited in the region of its emission, with lifetimes of weeks and months, countries and continents are affected, and with lifetimes of a year and above, VOCs can be transported into the stratosphere and distributed globally. Once in the stratosphere, deposition is more difficult, since the amount of air exchange between stratosphere and troposphere is limited. Additionally, the atmospheric chemistry changes - in the stratosphere, the ozone layer is formed by absorption of UV-B light (Baird and Cann, 2012).

VOCs can have different effects in the atmosphere. They can act as greenhouse gases, form aerosols and cloud condensation nuclei, reduce air quality, and contribute to the ozone formation.

Most volatile organic compounds can be excited by infrared radiation, as their total dipole moment can change and even be induced by vibrations. The wavelength of the excitation equals the resonance frequency of the transition between the vibrational ground state and the excited vibrational state, and its absorption intensity equals the transition dipole moment (Wedler and Freund, 2012). Since the excited molecules act as a Hertz dipole and emit light in every direction, parts of the IR radiation emitted by the earth's surface are scattered back into the atmosphere, and can be reabsorbed by other molecules. This way, the atmosphere is heated up - the greenhouse effect. Adding additional VOCs drastically changes the radiation balance and further heats up the atmosphere. This is especially important for VOCs with rare functional groups that absorb wavelengths that have rarely been absorbed before, e.g. fluorinated compounds (Baird and Cann, 2012). However, the lifetime of most VOCs is so short that their effect of greenhouse gases is negligible.

VOCs can form aerosols by condensation, freezing or resublimation. This usually happens to already partially degraded VOCs, forming secondary organic aerosols that mainly consist of aldehydes and acids (Mahilang et al., 2021). Aerosols enhance the albedo of the earth by increasing light scattering and are thus considered to have an overall cooling effect on the earth's climate. Atmospheric water tends to condense and freeze out on the surfaces of the aerosols, especially if they are hygroscopic. This way, aerosols can act as cloud condensation nuclei, impacting the type and location of the clouds that form. Heteroatom-containing VOCs are degraded to their corresponding oxides, which

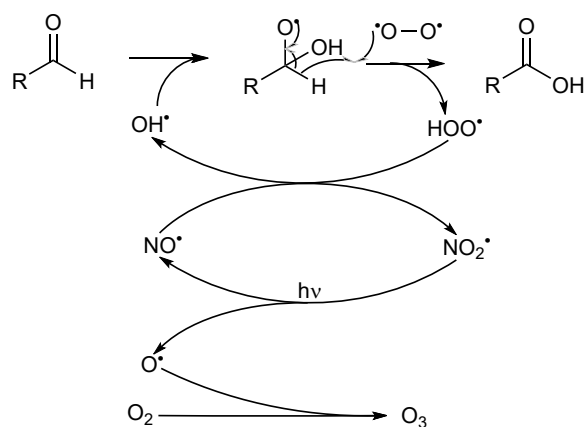


Figure 1.1.: Scheme of a typical VOC degradation and ozone formation process. R can be any organic residue.

are usually acidic. When these oxides aggregate and act as cloud condensation nuclei, they are usually dissolved to form the corresponding acids, significantly reducing the pH of the water droplet and causing acid rain (Baird and Cann, 2012).

VOCs can also play a role in smog and ozone formation. This has been mainly described for anthropogenic emissions of alkenes and aldehydes in cities, but also applies to biogenic alkene and aldehyde sources, e.g. terpenes. Put simply, OH^\bullet radicals add themselves to the double bond easily, forming an organic radical. This can also be induced by photochemical radical formation during hot summer days, which is why plant isoprene emissions also reduce air quality on long summer days (Ren et al., 2017). Oxygen in its normal triplet state can easily add to that, abstracting a hydrogen radical to form HOO^\bullet . The OH^\bullet can be regenerated from this by reaction with NO^\bullet , leading to NO_2^\bullet . This in turn can then be cleaved by UV-B light to form O^\bullet , which can react with molecular oxygen to form ozone (Figure 1.1, Baird and Cann (2012)).

VOCs in the atmosphere can be either caused by anthropogenic emissions, e.g. fuel or coal burning or solvent use, or they can be of biogenic origin. Biogenic VOCs can leak from the primary metabolism of organisms, like methanol or acetic acid, or they can be produced on purpose and serve specific aims, e.g. in stress response or communication. I will first focus on plant VOCs as plants are the main biogenic VOC source, and then continue with litter and soil VOCs.

1.2. VOCs from Plants

Plants exhibit complex VOC blends that vary between the different plant parts, their age and constitution, the environmental conditions the plant is facing, and other biotic factors like the composition of the microbial community that colonizes the plants surfaces or herbivory.

As indicator for general plant metabolism, methanol is an important factor. It is a side product of the pectin metabolism during cell wall synthesis. Methanol can leak to the atmosphere through the stomata. Thus, it is an indicator for plant growth, and shows stronger emissions from younger, developing leaves (Fall and Benson, 1996). Methanol emissions are so abundant that leaves are usually colonized in high densities by facultative methylotrophs like *Methylobacterium* (Junker and Tholl, 2013). Acetic, propanoic, and butyric acids and their respective aldehydes are also common plant VOCs (Hellén et al., 2017), which are side products of lipid degradation and the citrate cycle (Wongkittichote et al., 2017).

More importantly, VOCs from secondary metabolism might be used as signaling compounds and defense compounds in short and longer distances. Within one species, it might be quicker to use a volatile cue than to rely on the signaling pathways through the plant's ion canals, e.g. to warn neighboring leaves in case of a herbivore attack. Neighboring plants might also be warned this way, and predators of the herbivore could be called to help the plant fight the attack (Gols, 2014; Pierik et al., 2014). These indirect effects however are difficult to show and debated (Maag et al., 2015). Information about abiotic stress by drought or heat or light, the intention to bloom, or to prepare for winter can also be exchanged that way (Beck et al., 2014). It is important to note that usually, not a single VOC is specific for a specific situation, but that a blend of often more than 50, and up to 30.000 different VOCs is produced (Bitas et al., 2013). The exact composition and the relative concentrations of the VOCs in the blend represent the information on e.g. the type of stress, its severity, predator identity and number, sender age and position (Blande et al., 2014).

An overview over the most important compound classes and their biosynthetic pathways can be found in Figure 1.2. Terpenes and terpenoids are usually produced from dimethylallyl phosphate (DMAPP) and isopentenyl pyrophosphate (IPP) from methylerythritol phosphate (MEP) pathway, and often stored in glandular trichomes (deciduous trees) or resin ducts (conifers) (Niinemets and Reichstein, 2002). From there, they can be emitted whenever they are needed, but often, they are also synthesized on demand. Sesquiterpenes can additionally be produced from acetyl CoA via the mevalonate pathway (Hammerbacher et al., 2019). Indole, methyl salicylate, benzenoids, and phenylpropanoids originate from the shikimate pathway. Their emission is usually induced and occurs on longer time-scales (Hammerbacher et al., 2019). Green leaf volatiles are cleavage products of fatty acids, which are produced by lipoxygenase upon contact with O₂ (Hammerbacher et al., 2019). Methyl jasmonate is produced via the jasmonic acid pathway. Jasmonic acid and salicylic acid act highly antagonistically, suppressing the formation of each other for the different stress scenarios (Hammerbacher et al., 2019).

1.2.1. Plant Stress Response

The response to abiotic stress is similar for different types of stress (temperature, light, air pollution, heavy metals), since it mostly aims at reducing the amount of reactive oxygen species (ROS)

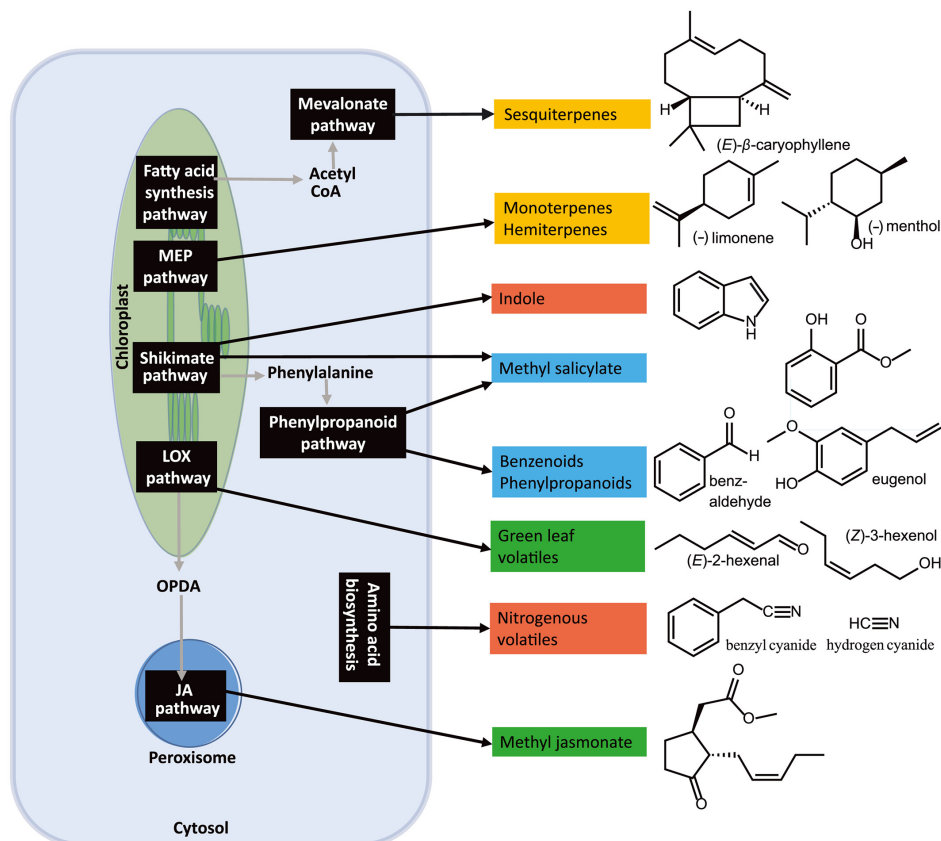


Figure 1.2.: Scheme of common stress-induced plant VOC groups and their biosynthetic pathways. CoA: coenzyme A, JA: jasmonic acid; LOX: lipoxygenase, MEP: methyletyrthitol phosphate. Reprinted with permission from Hammerbacher et al. (2019).

induced by the stress. This is achieved by emitting alkenes that can catch the ROS; most prominently isoprene, MBO, and sometimes terpenes. The VOC emission response is hormometric – only active at low to moderate stress – and usually ceases for very high stress levels (Agathokleous et al., 2018). Increases in the emission of simple VOCs like ethanol, methanol, and acetaldehyde have been observed when the plant suffers oxygen-deficiency, e.g. by flooding (Jansen et al., 2011), whereas green leaf volatiles, and methyl salicylate have been found to complement the terpenes upon exposure to ozone (Blande et al., 2014). Air pollution not only increases plant stress and thus plant VOC emissions, but also limits the distance plant signals are traceable significantly (Ghirardo et al., 2016; Manes et al., 2008), so it disrupts their communication channels as well.

Biotic stress can be induced by herbivore feeding on different plant parts, but also by infestation with microbial plant pathogens. In this case, the blend depends on the type of pathogen, and the affected plant part. VOC blends from roots are very different from VOC blends from leaves, shoots, or flowers (Junker and Tholl, 2013). After herbivore attack, green leaf volatiles are emitted immediately, followed by methyl salicylate, methyl jasmonate, ethylene and other inducible compounds minutes, hours or even days later. Terpene emissions can either be immediate, if storage reservoirs are damaged, or later, if they have to be synthesized (Dong et al., 2016). Predators of the herbivores can use these VOC blends to find their prey (Jansen et al., 2011).

To defend against microbial pathogens, different strategies are known: different terpenes and terpenoids, e.g. α/β -pinene, linalool, β -caryophyllene are used against bacteria and fungi, inhibiting their growth and sporulation, and damaging their cell walls. Aldehydes like acetaldehyde, benzaldehyde, and cinnamyl aldehyde inhibit the growth of epiphytic bacteria, and 2-hexenal, benzenoids, and phenylpropanoids are strong inhibitors against phytopathogens (Junker and Tholl, 2013). Salicylic acid is induced stronger by biotrophic pathogens, whereas jasmonic acid is induced stronger by necrotrophic pathogens and herbivores (Jansen et al., 2011). This is used by certain fungal pathogens, which increase the plant's jasmonic acid response by emitting 1-octen-3-ol, making it more vulnerable to the fungal attack (Bitas et al., 2013). Viruses are also known to alter the plant's VOC emission, thereby attracting potential vectors (Hammerbacher et al., 2019).

1.2.2. Plant–Microbe VOC Interactions

To combat plant's VOC defense, microbes have developed techniques to become resistant against them or even use them. Bacteria colonizing plant surfaces can use terpenes as a carbon source (Bitas et al., 2013), or convert HCN to formamide and use it as a nitrogen source (Hammerbacher et al., 2019).

They can in turn influence plant fitness and growth, e.g. 2,3-butanediol or a blend of different ketones and volatile sulfur compounds have been found to increase plant growth (Bitas et al., 2013; Cordovez

et al., 2018), but e.g. NH_3 , DMS, HCN, and 3-phenylpropionic acid from *Burkholderia*, *Chromobacterium*, *Pseudomonas*, *Serratia*, and *Stenotrophomonas* strains and 1-octen-3-ol and trans-2-octenal from truffles inhibited plant growth (Splivallo et al., 2007).

1.3. VOCs from Soils and Litter

Plant, litter and soil VOCs depend on each other: Since plant material is the input for litter, volatiles stored in the leaves as well as their degradation products can be released upon degradation. In turn, the input of fresh carbon sources as litter into the soil determines the microbial activity and thus the VOC emissions from soils. Soil microbes use VOCs to communicate with each other and with plants, such that they can alter the plant's emission profile as discussed in section 1.2.2.

1.3.1. VOCs from Litter Degradation

Litter can be a significant VOC source, especially in spring and fall, when the leaves are fresh and wet (Faiola et al., 2014). For boreal spruce and pine forests, mono- and sesquiterpene emissions in the same magnitude as the vegetation fluxes have been observed during these times (Aaltonen et al., 2011; Janson, 1993; Mäki et al., 2019b). Generally, litter VOCs are very diverse, reflecting the residual VOCs from the plant as well as products of microbial primary and secondary metabolism (Leff and Fierer, 2008). Emissions correlate with litter temperature and humidity (Faiola et al., 2014; Faubert et al., 2010), and the emissions are plant-specific (Gray et al., 2010).

Very important compounds for distinguishing between different plant species are terpenes: conifers and other aromatic plants like *Eucalyptus* or *Rosmarinus* show high emissions of their respective, very individual blend of terpenes (Isidorov et al., 2016; Viros et al., 2020). Additionally, fatty acid derivatives and other volatile compounds are important for distinguishing between broadleaf species, e.g. *Quercus* or *Populus*. Whatever is inside the leaf can be emitted upon degradation (Gray et al., 2010; Viros et al., 2020). Usually, these emissions decay exponentially with time (Gray et al., 2010), but a peak after 77-165 days has also been observed (Isidorov et al., 2010). Either microbes first had to degrade the surrounding plant tissue for the terpenes to escape, or the terpenes are produced by microbes feeding on the tissue.

Besides the compounds that were stored in the plant, there are compounds emerging from the microbial degradation process. The most ubiquitous and highest concentrated VOC is methanol, from the degradation of litter pectin and possibly lignin from woody parts (Asensio et al., 2012; Gray et al., 2010). Acetone, acetaldehyde, butanoic and propanoic acid from abiotic degradation and microbial primary metabolism are also reported (Bäck et al., 2010; Leff and Fierer, 2008).

Lastly, abiotic reactions can also contribute to litter VOC emissions. Acetone, acetaldehyde and other small VOCs can emerge from terpenes upon reaction with OH^\cdot , NO_3 or O_3 (Calogirou et al., 1999; Wisthaler et al., 2001).

1.3.2. Soil VOCs

Soil volatile emissions are usually one magnitude lower than litter emissions (Leff and Fierer, 2008), with the exception of the Amazon rainforest, where sesquiterpenes from soil are even as strong as emissions from the canopy (Bourtsoukidis et al., 2018). As litter is the primary input into soil organic carbon, the litter quality also strongly influences the microbial community in soils and soil VOC emissions (Asensio et al., 2012). Soils are even thought to take up up to 80% of the litter VOC emissions (Ramirez et al., 2010b; Rinnan and Albers, 2020). Especially arbuscular mycorrhizal or ectomycorrhizal fungi take up substantial amounts of VOCs - mainly from roots (Trowbridge et al., 2020). Source and sink strengths of soils depend on their temperature, moisture, pH, clay and humic acid content (Insam and Seewald, 2010; Stotzky et al., 1976; Wester-Larsen et al., 2020). An important source of VOCs from soil is when soil gets rewetted. Similar to the birch effect of peaking CO_2 emissions after rewetting, VOC emissions also peak after rewetting, but their dynamics are different from CO_2 . Besides the spike in microbial activity leading to increased VOC emissions, desorption reactions of the pore walls can contribute to these emission dynamics (Rossabi et al., 2018).

Roots can have mixed effects – an increase, a decrease and no effect on soil VOC emissions has been observed (Asensio et al., 2007a; Gray et al., 2014; Mäki et al., 2019a; Rinnan et al., 2013). They can themselves contribute VOCs and enhance microbial activity with their exudates, which facilitates VOC uptake and degradation (Tang et al., 2019). Root damaging, e.g. when setting up new soil chambers, leads to increased fatty-acid derived VOCs like 1,3-octadiene, 1-octen-3-ol, or hexanal, octanal and nonanal (Wester-Larsen et al., 2020).

Generally, VOC emissions increase with increased labile carbon sources. Besides litter, amending soils with sludge, manure and waste as well as alfalfa and straw increase VOCs emission rates. This usually leads to a variable bouquet of small VOCs like acetone, butanone, methanol, and acetaldehyde, terpenes, benzenoids, alkanes, alkenes, pyrazines, and in the presence of certain amino acids, volatile nitrogen and sulfur compounds (Abis et al., 2018; Stahl and Parkin, 1996; Zhao et al., 2016). Depending on the substrate, different bacteria and fungi are growing, which changes the VOC emissions (Stahl and Parkin, 1996).

Soils can act as sinks for VOCs not only by microbial VOC uptake and degradation, but also by adsorption to soil particles, dissolution in pore water (increasing bioavailability), and reactions with atmospheric radicals like NO_3^\cdot , OH^\cdot , O_3 or microbe-derived H_2O_2 (Stotzky et al., 1976; Tang et al., 2019).

An important concept for soil VOCs is the compensation concentration: As there are usually multiple different ways to form and degrade a volatile, it depends on the compound's mixing ratio in the headspace whether the compound is emitted or taken up. If the compound's mixing ratio is low, the emission processes are stronger than the uptake processes, and the resulting flux is an emission flux. If the headspace mixing ratio is high, uptake is more favorable and emission might even be suppressed, so that we only observe soil uptake. The compensation concentration is the headspace concentration at which soil emission equals soil uptake and we do not see a resulting flux (Conrad, 1994). Not all VOCs show a significant compensation concentration, but if they do, it is important to account for this in the experimental design. If the emission potential is the important factor, pure air should be used to flush dynamic chambers. If the actual net flux of an ecosystem is important, one has to use ambient air from this site and moment to get accurate results. In some cases, it might even make sense to determine the compensation concentration by measuring at different headspace concentrations of the compound (Conrad and Meuser, 2000; Lehmann and Conrad, 1996).

1.3.3. Microbial Soil VOCs

Microbial soil VOCs can be of very different compound classes, similar to plant VOCs. Microbial VOCs either originate from their primary metabolism or are used for chemical communication like in plants. The VOC emissions of different bacterial and fungal strains changes with the identity and number of microbes they are in contact with. The diversity of the microbial community has a direct impact on their VOC emission and their effects on plants: An intermediate community richness of 5 species leads to an emission of VOCs involved in plant pathogen suppression, and only with very few microbes, volatiles for plant growth promotion are emitted (Raza et al., 2020). Higher community richness was associated with lower VOC production (Raza et al., 2020), a trend that was also shown the other way round (Abis et al., 2020). Bacteria tend to produce more alkenes, ketones, pyrazines, and terpenes, whereas fungi produce more benzenoids, aldehydes, arsenics, chlorides, bromides, nitriles, thiofurans, and alkynes. This could be used to identify species in situ (Penuelas et al., 2014).

Again, a wide variety of compounds is known with a number of different functions: Ectomycorrhizal fungi use sesquiterpenes like thujopsene to induce lateral root formation and root hair growth (Ditengou et al., 2015), whereas arbuscular mycorrhizae use isobutyl alcohol, isopentyl alcohol, 3-methylbutanal, and 6-pentyl- α -pyrone for the same function (Sun et al., 2015b). Plant protection mechanisms are induced by different mycorrhizal fungi e.g. by *m*-cresol and methyl benzoate, and β -caryophyllene (Xin and He, 2013; Yamagiwa et al., 2011). Truffle fungi emit 1-octen-3-ol, 2-phenylethanol, 3-octanol, 1-hexanol, 3-methyl-1-butanol, 3-octanone, and *trans*-2-octenal that are mostly phytotoxic (Splivallo et al., 2007). These C8-compounds and other alcohols, ketones, and terpenes have antibiotic and antifungal activity (Stoppacher et al., 2010; Werner et al., 2016),

whereas the smaller alcohols like *iso*-propanol, ethanol, 2-/3-methyl-1-butanol and the terpene β -caryophyllene affect the motility and viability of nematodes (Fialho et al., 2012). Esters like ethyl acetate, ethyl pentanoate, and methyl cinnamate in turn are important olfactory cues used by spring-tails and earthworms to locate their fungal prey (Werner et al., 2016). Protist predators also use CO₂ gradients and olfactory cues to detect bacterial prey (Schulz-Bohm et al., 2017). Rhizosphere bacteria like *Pseudomonas donghuensis* inhibit fungal and oomycete pathogens with dimethyl sulfide, *S*-methyl thioacetate, methyl thioacetate, dimethyl trisulfide, 1-undecene, and HCN (Ossowicki et al., 2017). Trimethylamine, benzaldehyde, and *N,N*-dimethyloctylamine are other examples for bacterial fungistatic compounds (Chuankun et al., 2004).

The microbial pathways to many VOC classes are similar to plant production pathways. An overview can be found in Figure 1.3. The biggest group are primary metabolites, but secondary metabolites have been more the focus of research due to their role in microbial communication. The most important primary metabolites are short alcohols, aldehydes, and acids: The degradation of glucose and other sugars leads to lactate, acetate, pyruvate, and glyceraldehyde-3-phosphate, which can serve as precursors for C₂- and C₃-alcohols, aldehydes, and ketones (Effmert et al., 2012). *Saccharomyces*, *Lactobacillus*, *Enterobacteria*, and other organisms capable of homolactic and heterolactic fermentation produce ethanol under anaerobic conditions (Degelmann et al., 2009; Sniegowski et al., 2002; Yanagida et al., 2006). The oxidative deamination of aminoacids leads to ammonia, and subsequent decarboxylation of the acids and keto acids to short-chain aldehydes, ketones, and alcohols (Penuelas et al., 2014). As reported above, methanol and formaldehyde are commonly linked to pectin and lignin degradation (Fall and Benson, 1996), but can also be a methanotrophic degradation product of methane from methanogenesis, e.g. by methanotrophs in the classes of *Escherichia*, *Salmonella*, and *Vibrio* (Strong et al., 2015).

Like in plants, Terpenoids are synthesized from DMAPP and IPP via the mevalonate or deoxyxylulose phosphate pathway by a wide range of bacterial classes (Dickschat, 2011; Helfrich et al., 2019). Again, mostly mono- and sesquiterpenes are important in bacteria. Diterpenes have not been reported yet, but their volatility is also very low (Tyc et al., 2017).

Fatty acid derivatives like aldehydes, methyl ketones, alkenes, lactones, and esters can be formed from any intermediate of the fatty acid synthesis, starting from acetyl-CoA, adding malonyl-CoA units. Additional starters like propionyl-, isobutyryl-, isovaleryl-, and butyryl-CoA as well as the possible incorporation of methylmalonyl-CoA units further increase structural variability. Further transformation reactions include decarboxylation to form alkenes, or ketones from β -ketoacids, reductions of the carbonyl group to alcohols, and aldehydes, and α -oxidation to form aldehydes and alcohols with one carbon less than their precursor are possible. Esters, especially ethyl and butyl esters, and (γ)-lactones like γ -butyrolactone or γ -dodecalactone are also widespread (Penuelas et al., 2014; Schulz and Dickschat, 2007).

Like in plants, aromatic compounds are usually produced *via* the Shikimate pathway or by pheny-

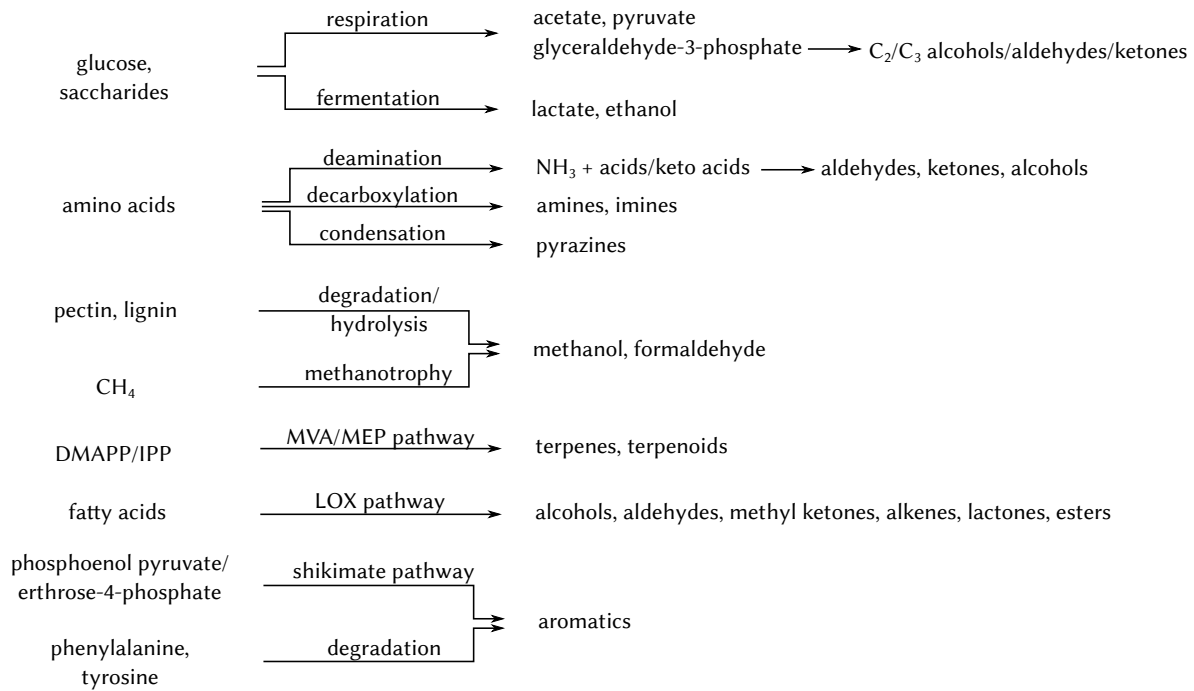


Figure 1.3.: Overview over main precursors and biosynthesis pathways of microbial VOCs. DMAPP: dimethylallyl pyrophosphate, IPP: isoprenyl pyrophosphate, MVA: mevalonate pathway, MEP: methyl erythritol phosphate pathway, LOX: lipoxygenase pathway.

alanine or tyrosine degradation. Cinnamic acid, phenylethanol and benzyl alcohol are widespread, especially in fungi (Penuelas et al., 2014; Schulz and Dickschat, 2007).

The degradation of amino acids leads to amines and imines, but also pyrazines are an important group of secondary metabolites with a high structural variability. They often have 1-4 methyl or ethyl groups that are most likely derived from alanine, valine, leucine, and isoleucine. The biosynthesis is not entirely elucidated, maybe acylloins are aminated, or pyrazines are produced by condensing two amino acids via a piperazine intermediate (Penuelas et al., 2014; Schulz and Dickschat, 2007). Indole formed from tryptophan by tryptophanase is also used as a bacteria pathogen and signaling molecule (Tyc et al., 2017).

Methylated halogens, phosphides, borides, selenides, tellurides, arsenides, antimonides, mercury and bismuth have been reported as well, usually resulting from detoxification procedures (Schulz and Dickschat, 2007). Another big group are methylated sulfides and other volatile sulfur compounds (VSCs), which will be described in detail in the following chapter.

1.4. Terrestrial Sulfur Cycle, Formation and Degradation of Volatile Sulfur Compounds

The terrestrial sulfur cycle comprises a complex system with many partners that influences climate and acid rain: Sulfur-containing gases are oxidized to SO_2/SO_3 , which form H_2SO_4 upon contact with water and oxygen. This way, sulfate crystals can form and serve as cloud condensation nuclei, contributing to cloud formation. Together with HNO_3 from NO_x , H_2SO_4 in the raindrops is the main cause for acid rain. On the other hand, the sulfur-containing amino acids methionine and cysteine are essential for life. In soil, the sulfur cycle is complex, because it comprises various different organic and inorganic compounds in all possible sulfur oxidation states. An overview over the discussed cycling processes can be found in Figure 1.4. The focus here will be on the most abundant VSCs dimethyl sulfide (DMS), methanethiol (MeSH), and hydrogen sulfide (H_2S) as they not only form a key part of the global sulfur cycle but also link to global climate and atmospheric chemistry. In the next chapters, I will briefly touch oxidized non-volatile sulfur compounds and the biosynthesis of amino acids before discussing the production and degradation pathways of VSCs in depth. Since the VSC production and degradation pathways vary between ecosystems and climate regimes, I will then highlight VSC emissions in the different systems.

1.4.1. Sulfate Reduction and Oxidized Organic Sulfur Compounds

Sulfate reduction is the most important process for sulfur assimilation - most microbes use it to satisfy their sulfur needs. Besides that, it is also a prominent electron acceptor for anaerobic respiration in nitrate-poor environments. Starting from sulfate in soil, adenosinetriphosphate (ATP) sulfurylase forms adenosine-5-phosphosulfonate (APS). APS is then phosphorylated to 3'-phosphoadenosine-5-phosphosulfate (PAPS) by APS kinase (Stefels, 2000). From PAPS, organic sulfates can be formed that comprise 30-40% of total sulfur contents in freshwater sediments (Losher and Kelts, 1989). Bacteria form a variety of different organic sulfate esters and sulfonates in this manner (Kertesz, 2000). Both bacteria and fungi cleave the esters by sulfatases to remobilize the sulfur (Gahan and Schmalenberger, 2014). Additionally, APS and PAPS can be reduced to sulfite (SO_3^{2-}) and thiosulfate ($\text{S}_2\text{O}_3^{2-}$) by APS reductase.

Both sulfite and thiosulfate are then further reduced to hydrogen sulfide by sulfite reductase (Höfgen et al., 2001; Oliveira et al., 2008). This process competes with denitrification and methanogenesis for electron donors like hydrogen, acetate, and propionate. It can be coupled to the anaerobic oxidation of methane (AOM), so CH_4 is oxidized to CO_2 while sulfate is reduced to H_2S (Meulepas et al., 2010; Le Mer and Roger, 2001). Both sulfate and sulfide can react abiotically with metal ions to form insoluble inorganic sulfur species (Rickard and Morse, 2005).

Besides the complete reduction of sulfite to H₂S, intermediate thiosulfate, thionates, and even elemental sulfur (Beard et al., 2011; Jones and Happold, 1961; Mangold et al., 2011) are formed under energy-limited conditions.

Hydrogen sulfide links sulfate reduction to amino acid formation and VSC formation. A fraction of it is oxidized back to sulfite, a process which is coupled to reduction of organic matter, e.g. quinones, as well as denitrification (Gu et al., 2012). Another fraction is emitted to the atmosphere where it is mainly oxidized by OH[•] to form SO₂. This reacts with water and dissolved oxygen to form sulfates. Ultimately, they are deposited to form terrestrial sulfate again (Castro and Dierberg, 1987).

1.4.2. Amino Acid Formation

H₂S is incorporated into amino acids - homocysteine and cysteine - by the reactions of *O*-succinyl-homoserine in bacteria and *O*-acetylserine in non-enteric bacteria, fungi and plants (Höfgen et al., 2001; Kertesz, 2000; Umbarger, 1987). Homocysteine is either derivatized to methionine or via cystathionine to cysteine (Kertesz, 2000). Methionine and cysteine are the building blocks from which many other organic sulfur compounds are derived, e.g. biotin (Streit and Entcheva, 2003). Under sulfur-limited conditions, direct scavenging of DMS and 2-(methylthio)-ethanol *via* nitrogenase-like enzymes for methionine formation has been observed (North et al., 2020).

These processes are reversed when amino acids are degraded. Both methionine and cysteine can also be methylated by thiol methyltransferases (Kadota and Ishida, 1972). *S*-methyl-methionine, *S*-methyl-cysteine, and cysteine can be cleaved by lyases to form dimethyl sulfide, methanethiol, and hydrogen sulfide, respectively (Lomans et al., 2002). As part of the regeneration of *S*-(methylthio)-adenosine, methanethiol can be generated from methylthioethanol or *S*-(methylthio)-glutathione (Miller et al., 2018).

1.4.3. Cycling of Reduced VSCs

There are several ways to form and degrade the reduced VSCs H₂S, MeSH, and DMS. Besides organic matter degradation, methylation and demethylation steps between the three compounds are important drivers of H₂S, MeSH, DMS, and CH₄ levels.

Formation of VSCs from Organic Matter

In terrestrial systems, microbial methionine from protein degradation is the most important organic VSC precursor. It is cleaved to α -ketobutyrate, ammonia, and MeSH by a PLP-dependent methionine- γ -lyase deaminase (Khan et al., 2013; Morcos et al., 2015; Tanaka et al., 1976). Additionally, DMS can be a product (Zinder et al., 1977). For the latter, probably the formed MeSH is

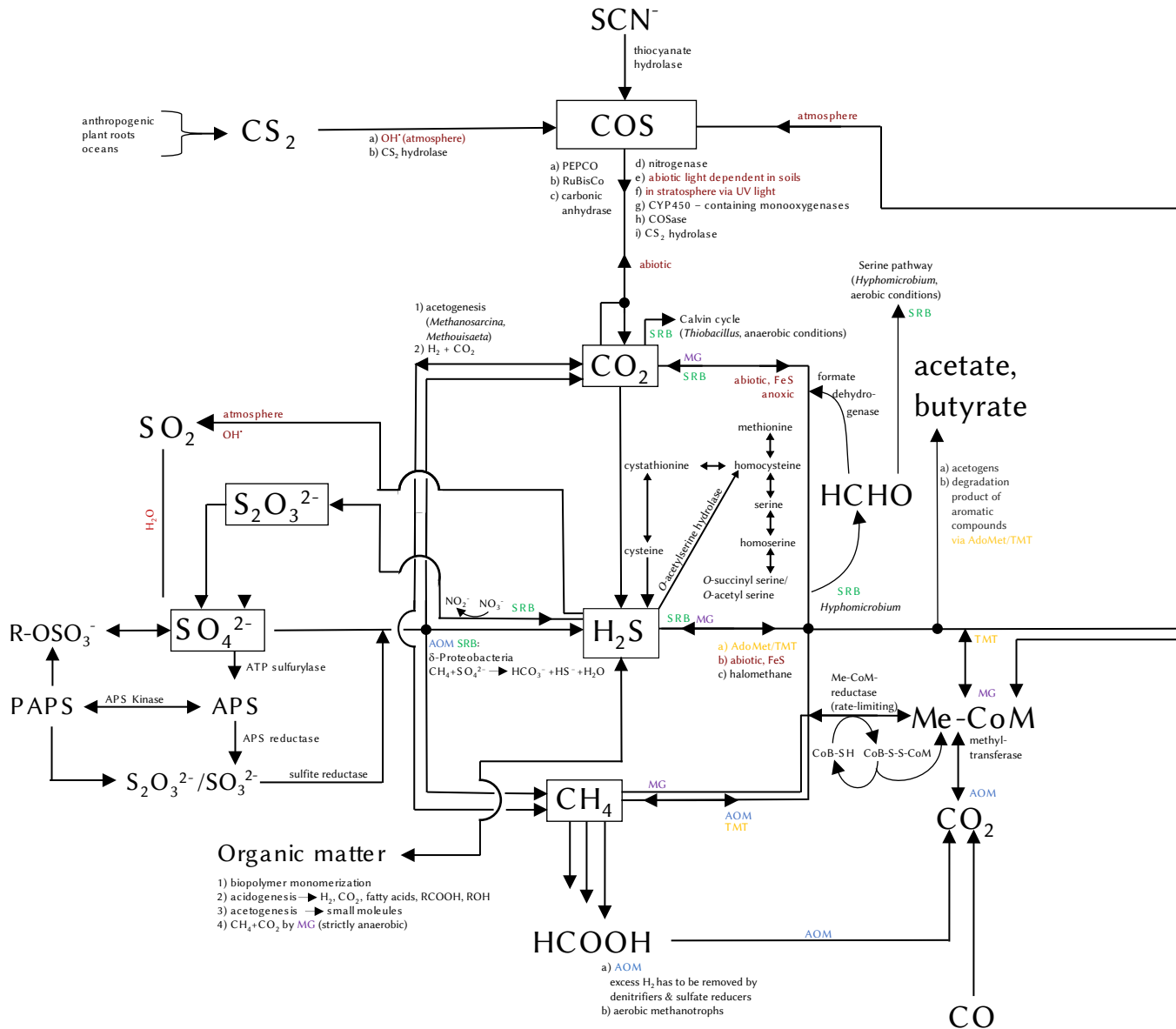
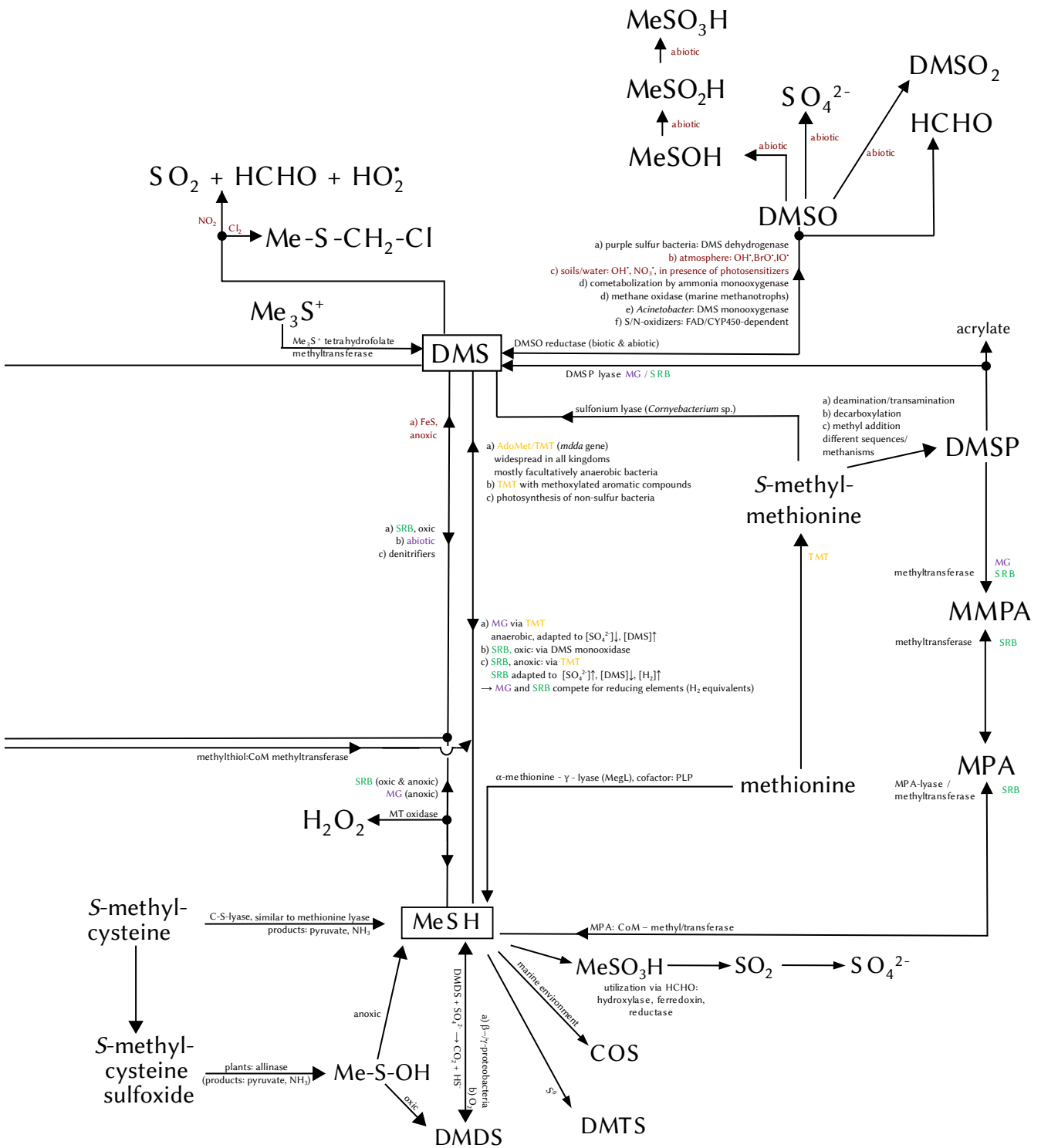


Figure 1.4.: Scheme of the terrestrial sulfur cycle. Microorganisms, enzymes, and/or abiotic reaction conditions are always noted close to the arrow head indicating the direction of the reaction. **Abiotic:** abiotic processes, **AOM:** anaerobic oxidation of methane, **MG:** methanogens, **SRB:** sulfate reducing bacteria, **thiol methyltransferase**, **PAPS:** 3'-phosphoadenosine-5'-phosphosulfate, **APS:** adenosine-5'-phosphosulfate, **AdoMet:** adenosyl methionine, **CYP450:** cytochrome P 450, **PEPCO:** phosphoenolpyruvate carboxylase, **RuBisCo:** ribulose-1,5-bisphosphate carboxylase/oxygenase, **CoM:** coenzyme M, **CoB:** coenzyme B, **MSA:** methylsulfonic acid, **FAD:** flavin adenine dinucleotide, **DMS:** dimethyl sulfide, **DMSP:** 3-(dimethylsulfonio)-propionate, **MMPA:** 3-(methylthio)-propionate, **MPA:** 3-mercapto-propionate, **DMDS:** dimethyl disulfide, **DMTS:** dimethyl trisulfide, **R:** any organic residue, $[X]_{\downarrow}$: important if concentration of X is low, $[X]_{\uparrow}$: important if concentration of X is high.

1.4. Terrestrial Sulfur Cycle, Formation and Degradation of Volatile Sulfur Compounds



methylated, e.g. by the adenosyl methionine-dependent membrane methyltransferase encoded in the *mddA* gene in *Pseudomonas deceptionensis* M1 (Carrion et al., 2015).

When H₂S and methionine are present at the same time, microbes use methionine and not H₂S to form MeSH (Dalby et al., 2018). Amongst others, different aerobic bacteria (*Bacillus* sp., *Arthrobacter* sp., *Delftia* sp.), *Pseudomonas fluorescens*, a strict anaerobe (*Clostridium* sp.), facultatively anaerobic bacteria (*Proteus vulgaris*, *Enterobacter aerogenes*, *Escherichia coli*), and fungi (*Penicillium* sp., *Candida* sp., *Aspergillus oryzae*, *Scopulariopsis* sp.) are able to cleave methionine to MeSH (Liu et al., 2017; Segal and Starkey, 1969; Taylor and Kiene, 1989). *Pseudomonas aeruginosa* even generates a suite of different VSCs (MeSH, DMS, DMDS, dithiapentane, 2-methylthiolan-3-one) from methionine, which promotes *Aspergillus fumigatus* growth and increases its pathogenicity (Scott et al., 2019). In contrast to that, *Geotrichum candidum* yeast growing on cheese does not cleave methionine directly, but uses 2-oxo-4-methylthiobutanoate as an intermediate to the production of MeSH, which then in turn could be converted to DMS, DMDS, DMTS, and 2,4-dithiapentane. Oxidative stress in the cells was found to increase casein hydrolysis to methionine, and thus VSC production (Pracharova et al., 2019).

In analogy to the cleavage of methionine, S-methyl-methionine can be cleaved to DMS and homoserine directly. It is present in a variety of different plants and algae (Bills and Keenan, 1963; Greene and Davis, 1960; Hattula and Granroth, 1974; White, 1981), and can be cleaved by soil bacteria like *Cornybacterium* sp. (Mazelis et al., 1965). Additionally, *Saccharomyces cerevisiae* yeast produces DMS from S-methyl-methionine in grape and melon juice (Deed et al., 2019; Pan et al., 2021).

Other organic precursors leading to VSC emissions were S-methyl-cysteine (to MeSH), 3-(methylthio)propionate (to DMS), 3-mercaptopyruvate (to DMS), 2-mercaptoacetate (to H₂S and MeSH), trimethyl sulfonium salts (to DMS), methionine sulfoxide and methionine sulfone (to MeSH, DMS, and DMDS), homocysteine (DMS and CS₂), cystine (CS₂), lanthionine (CS₂ and trace COS), and djenkolic acid (CS₂ and trace COS) (Kiene and Capone, 1988; Scholten et al., 2003; Challenger and Liu, 1950; Labarre and Bory, 1969; Wagner et al., 1967; Banwart and Bremner, 1975). Cysteic acid and taurine were found not to produce VSCs (Banwart and Bremner, 1975).

Dimethylsulfone (DMSO₂) and DMSO can also be reduced to DMS by DMSO reductase under anoxic conditions (Boden et al., 2011; Kiene and Capone, 1988; Taylor and Kiene, 1989).

Formation of MeSH and DMS from H₂S

Sulfate reduction not only leads to H₂S, but also to MeSH (Dalby et al., 2018; McCarthy et al., 1993). Kiene (1988) observed interconversions of MeSH to DMS and *vice versa*. From H₂S, subsequent methylations via thiomethyl transferase encoded in the *mddA* gene take place (Carrion et al., 2015). These are extremely widespread in all kingdoms, e.g. *Bradiorhizobium*, mycobacteria, cyanobacteria, *Pseudomonas deceptionensis*, *Parasporobacter paucivorans*, flavobacteria, *Rhizobium trifolii*, and

the phototrophs *Rhodocyclus tenuis* and *Rhodospirillum rubrum* S1 (Carrion et al., 2015, 2019; Lomans et al., 2001a; Drotar et al., 1987; McCarthy et al., 1993). The methylation cofactor is adenosylmethionine (Drotar et al., 1987).

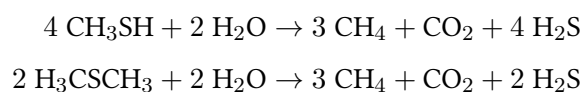
As for the carbon/methyl source, there are different theories. Besides a generic methyl group donor like methanol, aromatic methoxy compounds and even CO and CO₂ are discussed as the carbon precursor for VSCs (Visscher et al., 2003; van Leerdam et al., 2006; Moran et al., 2008; Lin et al., 2010). MeSH and DMS emissions can be stimulated by syringic acid and trimethoxybenzoic acid, but not by gallic acid, supporting the aromatic methoxy group theory (Lomans et al., 2001a,b; Finster et al., 1990; Stets et al., 2004). Two bacterial strains (likely homoacetogens) were isolated by enrichment on methoxylated aromatic compounds. They emit acetate, butyrate, DMS, and some MeSH (Bak et al., 1992), and cometabolism of methoxylated aromatic compounds by acetogenic bacteria and methylated thiols by methanogenic bacteria was proposed (Finster et al., 1990).

CO and CO₂ incorporation into VSCs were shown by the incorporation of the labelled compounds (Moran et al., 2008; Lin et al., 2010). They are hypothesized to occur via the pathway for the anaerobic oxidation of methane, but in reverse direction: They can bind to methanofurane, be reduced to a methyl group, transfer to coenzyme M, and from there transfer to H₂S or MeSH to form MeSH or DMS. This might be a mechanism to remove excess methylation of the coenzyme M inhibited by CO, and regenerate it again for further use (Moran et al., 2008; Lin et al., 2010). Besides these biotic methylation pathways, DMS can form abiotically when FeS, H₂S, and CO₂ interact at temperatures above 50 °C (Heinen and Lauwers, 1996).

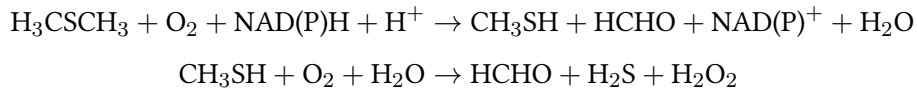
Demethylation of DMS and MeSH

DMS and methanethiol are degraded via three pathways. Most of it is oxidized to DMSO *via* DMS dehydrogenase in photoautotrophs in soil and by OH[•] and NO₃[•] radicals in the atmosphere. Further oxidation steps lead to dimethyl sulfone, MSA, formaldehyde, and ultimately to SO₂ (Chasteen and Bentley, 2004; Jensen et al., 1991). A smaller fraction is converted to COS in the atmosphere (Chasteen and Bentley, 2004), which itself is degraded by various processes, but much slower than DMS or MeSH. Besides these two oxidation pathways, DMS and MeSH can be demethylated to H₂S. Methanogens and sulfate-reducing bacteria compete for this oxidation. They use different processes for degrading the compounds in oxic and anoxic environments, which leads to different side products:

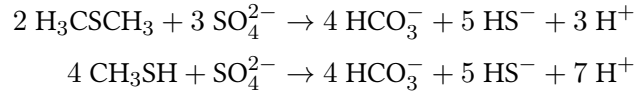
Methanogens (Finster et al., 1992; Lomans et al., 1999a):



Sulfate-reducing bacteria, aerobic conditions (Chasteen and Bentley, 2004):



Sulfate-reducing bacteria, anaerobic conditions (Scholten et al., 2003):



Methanogenic archaea and bacteria use their noncompetitive methyltransferases to metabolize DMS and MeSH (Lomans et al., 2001b; Moran et al., 2008). Often, cometabolism of methanol, trimethyl amine etc. can occur (Lee et al., 2012). Methanogens are active in anaerobic, sulfate-poor environments with relatively high dimethyl sulfide contents (Blodau et al., 2007). Oxygen, nitrate, free iron species, and magnesium hydroxide inhibit methanogenic activity (Sun et al., 2015a). Mechanistically, methanogens use methylated coenzyme M (Me-CoM) for methane formation, and Me-CoM reductase emitting CH₄ is the rate-limiting step (Tallant and Krzycki, 1997). Thus, when methanogens are active, intermediate accumulations of methanethiol are observed (Lomans et al., 1999a,b,c).

Sulfate-reducing bacteria use DMS monooxygenase and methanethiol oxidase to degrade DMS and MeSH (Taylor and Kiene, 1989). The key players investigated so far are the methylotroph hyphomicrobium and the photoautotroph thiobacillus (Kelly and Baker, 1990). Besides oxygen, they can also use nitrate and nitrite as electron acceptors (van Leerdam et al., 2006). Both bacteria further utilize the carbon from DMS, but hyphomicrobium incorporates it as formaldehyde *via* the serine pathway, and thiobacillus utilizes it as CO₂ and incorporates it into the Calvin cycle (Lomans et al., 2002). DMS monooxygenase has been purified from *Hyphomicrobium sulfonivorans* and *Arthrobacter globiformis*. It is a two-component flavin-dependent monooxygenase (Boden et al., 2011; Cao et al., 2018; Hammers et al., 2020). The methanethiol oxidase encoded in the *mtoX* gene in *Hyphomicrobium* sp. has recently been purified and is a Cu-dependent metalloenzyme (Eyice et al., 2018).

An in-depth study of DMS and MeSH degradation in *Hyphomicrobium denitrificans* X^T has shown that the DMS oxidation by DMS monooxygenase in the cytoplasm and MeSH oxidation to HS⁻ by methanethiol oxidase in the periplasm is coupled to a complex system of dissimilatory sulfide and sulfite oxidation via a membrane-bound heterodisulfide reductase-like system (Koch and Dahl, 2018). A similar system was found in *Methylophaga thiooxidans*: again, DMS is oxidized in the cytoplasm, then methanethiol is transported into the periplasm, where it is oxidized to sulfide. Both oxidation processes are coupled to membrane-bound and periplasmic sulfide and sulfite oxidases. In contrast to the first study, polythionates are not enzyme-bound and directly oxidized in the periplasm, but instead transported back into the cytoplasm for the oxidation to sulfite (Kröber and Schäfer, 2019).

In oxic environments, sulfate-reducing bacteria also utilize thiolmethyl transferases for DMS and MeSH metabolism (Visscher and Taylor, 1993). In general, sulfate-reducing bacteria operate in a high sulfate, low hydrogen environment. In hydrogen atmospheres, they accumulate methanethiol up to a toxic level (Lomans et al., 1999c). Sulfate-reducing bacteria do have a higher affinity for DMS than methanogens, enabling them to operate efficiently at low DMS levels (Kiene et al., 1986). Tungstate (Lomans et al., 1999b) and molybdate (Kiene and Capone, 1988) are inhibitors. During inhibition experiments, there were indications that methanogens degrade DMS to methanethiol which is then degraded by sulfate-reducing bacteria in sulfate-rich environments (Lomans et al., 1999b).

Abiotic Degradation of Reduced VSCs

There is some evidence for abiotic degradation of VSCs, mainly in the oceans. UV-B light degrades DMS in the presence of photosensitizers, which is more important in aqueous systems than in soils (Hatton, 2002; Ossola et al., 2019). In the oceans, this limits DMS emissions and leads to an increased sulfur recovery in the upper water columns.

Granular ferric hydroxide (Sun et al., 2014) and alkaline solutions (Smet and van Langenhove, 1998; van den Bosch et al., 2009) are used to reduce VSC emissions from anthropogenic sources to the environment. Both are of course extreme cases of what is happening in the soils as well: Iron and heavy metal ions form insoluble sulfides, and an increased pH leads to the formation of HS^- , which is not volatile as well. Therefore, emissions of H_2S are usually limited.

Atmospheric Fate of Reduced VSCs

H_2S , MeSH, and DMS are quickly degraded by OH^\cdot , NO_3^\cdot , and BrO^\cdot radicals (Breider et al., 2010; Jensen et al., 1991; Khan et al., 2016). The detailed reaction steps involve stepwise H^\cdot abstractions, O_2 and NO_2 additions, and oxidative divisions. Methanesulfonic acid and SO_2 are frequently observed intermediates until the wet and dry deposition of sulfates (Wallington et al., 1993). Global VSC models usually only focus on DMS, and try evaluating the CLAW hypothesis or general atmospheric behavior of DMS (Khan et al., 2016; Kloster et al., 2006; Lana et al., 2011). They have shown a short lifetime of < 1 d and the changing influence of the different radicals involved in degradation: OH^\cdot dominates daytime degradation, NO_3^\cdot nighttime degradation, and BrO^\cdot can be important over the southern ocean.

1.4.4. Formation and Cycling of Carbonyl Sulfide

Carbonyl sulfide (COS) cycling is controlled by very different processes than the reduced sulfur gases. Its mixing ratio in the atmosphere is about 500 ppt (Warneck and Williams, 2012). Most studies focus on COS net fluxes from soil into the atmosphere rather than separating it into production and

consumption. Hence, not much is known about possible precursors of COS production from soil. So far, only the formation of COS from thiocyanate via thiocyanate hydrolase is known, however, this only accounts for a small fraction of COS production (Banwart and Bremner, 1975; Conrad, 1996). Most of the thiocyanate is further degraded to ammonia and sulfate (Kwon et al., 2002). COS can also be generated upon decomposition of organic material (Turco et al., 1980). Stimulation of COS emissions occurs when adding a wide variety of sulfur compounds, so one theory is that mainly abiotic processes are involved (Conrad, 1995). However, COS emissions spike after rainfall events (Whelan and Rhew, 2016), which might either be due to physical desorption processes or microbial activity. For plants and for soils, compensation concentrations can be obtained where COS production equals COS uptake, but they vary strongly. Plants usually exhibit compensation mixing ratio smaller than 200 ppt (Kesselmeier et al., 1993), whereas soils mostly have compensation mixing ratios higher than the atmospheric mixing ratio, acting as a net source (Conrad and Meuser, 2000).

There are many processes involved in COS degradation in soil: (1) a steady COS production, (2) a linear, first-order kinetics COS uptake at low COS concentrations becoming saturated relatively quickly, and (3) a second first-order kinetics uptake when the mixing ratio of COS is rising over a certain threshold (Conrad, 1995; Conrad and Meuser, 2000). This suggests that two different microbial groups are involved in (2) and (3).

COS correlates with gross-primary production (Sandoval-Soto et al., 2005), but this is probably not a causal relationship since carbonic anhydrase (CA) is light-independent, and metabolization of COS was also observed during the night (Geng and Mu, 2004; Gimeno et al., 2017). It was then proposed to be an inverse tracer for biogenic VOC emissions since it seems to correlate with open stomata (de Gouw et al., 2009).

The most-studied pathway is the degradation by CA happening in plants as well as in soil. Normally, CA hydrolyzes CO₂ to hydrogen carbonate, but it can also cometabolize COS. Since there is a compensation mixing ratio, COS might be preferred at low CO₂ concentrations. β -CA does bind to COS more strongly than the other isoforms (Sauze et al., 2017). Since this form is more abundant in fungi than in bacteria, and fungi are most active in soil, it is concluded that fungi might be the main sink for COS in soil (Bunk et al., 2017; Sauze et al., 2017). However, *Mycobacterium sp.*, *Williamsia sp.*, and *Thiobacillus thioparus* also use β -CA for COS cleavage (Ogawa et al., 2017). In plants, the activity is dependent on the stomatal conductance (Goldan et al., 1988), but also in *T. thioparus*, transport hindrances are regulating COS consumption (Ogawa et al., 2017). In bryophytes which do not have stomata, there was also a compensation mixing ratio observed, and light appeared to act inhibitory on COS uptake (Gimeno et al., 2017).

Besides carbonic anhydrase, the other CO₂ fixing enzymes ribulose-1,5-biphosphate carboxylase oxygenase (RuBisCO, Whelan et al. (2018)) and phosphoenolpyruvate carboxylase (PEPCO) are also discussed as possible COS degraders. In plants, they do not seem to be involved (Protoschill-Krebs et al., 1996), but there are indications that those enzymes might be involved in COS degradation in

soil (Kesselmeier and Staudt, 1999). Other processes degrading COS are done by nitrogenases (Bunk et al., 2017), CYP-450 containing monooxygenases in mice (Chengelis and Neal, 1980), COSase, and CS₂ hydrolase (Kamezaki et al., 2016). Due to its lifetime of ca. 1 yr, COS is transported up into the stratosphere, where it gets degraded by UV light (Turco et al., 1980).

1.4.5. Ecosystem Hotspots of Sulfur Cycling

The most recent reduced sulfur gas budgets were estimated by Watts (2000) (Table 1.1). This study shows DMS to be the main contributor due to its marine emissions, followed by H₂S, COS, and CS₂. Main sources for H₂S are assumed to be by volcanic and geothermal origin as well as anthropogenic emissions, mostly from fuel burning. CS₂ is also considered to be mostly anthropogenic, and COS thus indirectly as well, as its main source is stated to be CS₂ oxidation. However, Watts mentioned that the budgets are fairly uncertain, as the number of studies on volatile sulfur gases is limited, especially since he excluded studies that used dynamic chambers with pure air. He argues that those are unreliable, because they tend to overestimate emission fluxes. This is of course important to consider, as compensation concentrations are known for many substances including COS (Conrad, 1994). Yet there is also a study showing that DMS emission fluxes are not overestimated when using DMS-free air (de Mello and Hines, 1994). It might have been reasonable to include studies using VOC-free air in Watts' budget, as this would have improved the data coverage substantially.

Conrad (1994) also budgeted atmospheric trace gas emissions from soils and estimates 0.58 Tg/a COS and <0.38 Tg/a DMS emissions from soils. Both values are higher than Watts' estimates. Warneck and Williams (2012), Table 1.2, did a much coarser global budgeting for the sulfur gases, and their estimates are also much higher than the ones by Watts.

Since even the latest budget is already eight years old, and there is considerable disagreement between the budgets, I will provide a summary of the available literature in the next subchapters. Tables with all VSC measurements known to the author can be found in the supplements, in section A.1.

Marine and Coastal Areas

Oceans are considered to be the by far major DMS emitter, due to cleavage of 3-(dimethylsulfonio)-propionate (DMSP) to DMS by microalgae and bacteria (Moran and Durham, 2019). Grazing by microzooplankton increases DMS emissions up to a factor of 20, which accounts to 32-96% of dark DMS production in the oceans (Simó et al., 2018). DMS emissions occur all over the oceans including the Arctic (Hines, 1992), but spike in coastal areas with high microalgae abundance. As DMS is mostly degraded by aerobic marine bacteria, low oxygen levels can increase DMS emissions. This can be further enhanced by the other bacterial VSC formation processes under anoxic conditions, sulfate reduction and organic sulfur compound degradation. For example, during South-West monsoon

Table 1.1.: Global sources and sinks of VSCs to the atmosphere in Tg/a as specified by Watts (2000). X: Since marine DMS emissions have been estimated using atmospheric lifetimes and boundary layer mixing ratios, it does not make sense to calculate the sinks the same way as the sources. Major removal processes include the reaction with OH[·] and NO₃ in the atmosphere. Reprinted with permission from Watts (2000).

Source /sink	H ₂ S	DMS	COS	CS ₂
Open ocean	1.50 ± 0.60	20.70 ± 5.20	0.10 ± 0.15	0.11 ± 0.04
Coastal ocean	0.30 ± 0.10		0.20 ± 0.10	0.07 ± 0.04
Salt marsh, estuary	0.50 ± 0.35	0.07 ± 0.06		
Vegetation	0.37 ± 0.07	1.58 ± 0.86		
Tropical forests	0.42 ± 0.12	1.60 ± 0.50		
Soils	0.002 ± 0.002	0.29 ± 0.17		
Anoxic soils			0.02 ± 0.01	0.07 ± 0.06
Wetlands	0.20 ± 0.21	0.12 ± 0.07	0.03 ± 0.03	0.02 ± 0.02
Volcanism (H ₂ S:+ Geothermal)	1.05 ± 0.94		0.05 ± 0.04	0.05 ± 0.04
Anthropogenic	3.30 ± 0.33	0.13 ± 0.04	0.12 ± 0.06	0.34 ± 0.17
Biomass burning			0.07 ± 0.05	
Precipitation			0.13 ± 0.08	
DMS oxidation			0.17 ± 0.04	
CS ₂ oxidation			0.42 ± 0.12	
COS + OH [·]	0.08 ± 0.07			
<i>Total source</i>	<i>7.72 ± 1.25</i>	<i>24.49 ± 5.30</i>	<i>1.31 ± 0.25</i>	<i>0.66 ± 0.19</i>
Reaction with OH [·]	-8.50 ± 2.80	X	-0.13 ± 0.10	-0.57 ± 0.25
Reaction with O [·]			-0.02 ± 0.01	
Reaction with NO ₃		X		
Photolysis			-0.03 ± 0.01	
Oxic soils			-0.92 ± 0.78	-0.44 ± 0.38
Vegetation			-0.56 ± 0.10	
<i>Total sink</i>	<i>-8.50 ± 2.80</i>		<i>-1.66 ± 0.79</i>	<i>-1.01 ± 0.45</i>
<i>Total imbalance</i>	<i>0.78 ± 3.1</i>		<i>0.35 ± 0.83</i>	<i>0.35 ± 0.49</i>

Table 1.2.: Main global sources and sinks of VSCs to the atmosphere in Tg/a as specified by Warneck and Williams (2012). X: sinks only mentioned, but strength not specified. Adapted from Warneck and Williams (2012), p. 71, with permission.

	H ₂ S	DMS	COS	CS ₂
Oceans		50	0.3	0.4
Soils (COS: + marshes)	0.5	1	0.3	
Vegetation	1.0			
Volcanic	1.0			
Anthropogenic	3.3			0.6
Oxidation of CS ₂ and DMS			0.6	
Uptake by vegetation			-0.5	
Reaction with OH [·]	X	X	-0.1	X
Reaction with NO ₃		X		
Loss to stratosphere			-0.1	

season at the west coast of India, oxygen levels quickly drop with depth, leading to spikes in DMS emissions (Naik et al., 2020).

Another marine environment with substantial DMS emissions are coral reefs, probably due to the endosymbiotic zooxanthellae in the corals (Broadbent and Jones, 2004; van Alstyne et al., 2008). Low tides with low wind speeds (Swan et al., 2017b,a) and low-level cloud cover (Jones et al., 2018) cause spikes in DMS emissions. This was found both when corals get exposed and when they get resubmerged, indicating this might be a stress response (Hopkins et al., 2016).

Microbial Mats

Microbial mats in both marine and freshwater environments also emit DMS. Estuarine cyanobacterial and diatom mats emit under both aerobic and anaerobic conditions. In this study, *Thiobacillus sp.*, *Thiocystis sp.*, and *Thiocapsa sp.* feed on the DMS emissions, and the authors discussed that microbial mats might actually serve as a DMS sink under anoxic conditions (Visscher et al., 1995).

Like in other environments, there seems to be a sharp separation of marine microbial mats mostly emitting DMS, and freshwater microbial mats, also emitting other VSCs. Microbial (mainly algal) mats from Yellowstone (USA) degrade by the formation of H₂S, some MeSH and very little DMS under anoxic conditions, which was attributed to algal protein constituents. One has to note that light decreased VSC production, which the authors attributed to O₂ production from the algae (Zinder et al., 1977).

This diurnal cycle was also shown by directly measuring O₂ and S²⁻ and VSC emissions in hypersaline mats in Mexico: DMS and MeSH emissions decreased with increasing oxygen abundance and salinity, and increased with temperature. The authors attributed this to an increased VSC consumption in the presence of oxygen (Visscher et al., 2003)

Vegetation

In general, plants emit H₂S and DMS, and are a sink for COS (Goldan et al., 1987). Root emissions of VSCs by brassica plants are discussed as chemical communication and warfare agents against fungal infestations (Eyice and Schäfer, 2016; Gamliel and Stapleton, 1993; Yang et al., 2006). Cabbage not only emits a broad blend of VSCs from roots, but also from the plant itself, though in lower release rates (Bailey et al., 1961). H₂S can be leaked involuntarily as an amino acid degradation product (Taylor and Kiene, 1989), but it is also a product of the cleavage of COS by carbonic anhydrase: $COS + H_2O \rightarrow H_2S + CO_2$ (Campbell et al., 2017). The main pathways to DMS are the cleavage of methionine to MeSH and then methylation by *S*-adenosyl-methionine-dependent thiolmethyl transferases (Drotar et al., 1987) or the other way round, first methylation to *S*-methylmethionine

involving *S*-adenosyl-methionine and then cleavage in a second step (Boden and Hutt, 2019; Taylor and Kiene, 1989).

For tropical plants, substantial DMS emissions with a diurnal cycle was shown (Jardine et al., 2015), and especially mahogany was highlighted as a DMS emitter (Vettikkat et al., 2020). In temperate plants, volatile sulfur emissions were reported for mainly for agricultural plants: Corn, carrot, celery, soybeans, onions, grass, and oats were found to emit VSCs, but the individual sulfur gases were not resolved (MacTaggart et al., 1987). More detailed work showed higher DMS and low H₂S emissions from corn and soybeans. Different deciduous and conifer trees emit H₂S, DMS, and COS, as well, although the authors note that they used VOC-free air and thus no sink activity could be tracked (Lamb et al., 1987). Soil covered with grass showed a diurnal pattern of VSC emissions, with DMS and H₂S being the dominant species. Soybeans and oats were moderate DMS and H₂S emitters, but corn emitted 10x as much. Grasses and clover only emitted DMS and H₂S at low rates. All of these plants took up COS (Goldan et al., 1987). Even seeds of Norway spruce can convert sulfate to hydrogen sulfide (Spálený, 1977), although the emissions also might originate from COS or amino acid cleavage, as they report a strong light-dependence and did not find an effect of sulfate-fertilization on the emissions.

Soil Emissions

Soil VSC fluxes reflect the net of all abiotic and biotic formation, degradation, dislocation processes. They integrate the net activity of roots and microbiota living in soil as well as abiotic processes. Even if the processes were the same in different ecosystems, their relative importance would change depending on the environmental conditions as well as the organisms living in the ecosystems, so for an overall estimate of global emission patterns, we need to know local emissions. Thus, in the next paragraphs I will discuss VSC quantification studies separately for different ecosystems and climate regions. The main microbial production pathways are either from sulfate reduction and subsequent methylation or organic matter degradation. The relative importance of those pathways depends on the soil properties and climate (Aneja and Cooper, 1989). In general, a correlation of VSC emissions with respiration rate (Kesselmeier and Hubert, 2002), an optimum of DMS emissions with soil moisture (Jardine et al., 2015), and decreasing DMS emissions with soil depth (Swan et al., 2019) suggest that VSC emissions from soil are mainly of biotic origin, and that abiotic processes only play a minor role.

Temperate Regions Temperate non-wetland soils have been shown to exhibit relatively low, but detectable VSC emissions, in the range of 0.1-20 mg S/(m² a) in Northern-American and German soils (Adams et al., 1979; Staubes et al., 1989). Maize fields have been reported to emit up to 100 mg S/(m² a) DMS, and wheat fields up to 50 mg S/(m² a) (Kanda et al., 1995). Leaf litter and the fermentation

layer are also sources of DMS, up to 14.5 pmol/(g_{dw} h) and 0.81 pmol/(g_{dw} h), comparable to fresh leaf emissions (Kesselmeier and Hubert, 2002).

Subtropical Forests Average DMS emissions from a subtropic Southern Chinese monsoon evergreen broadleaf forest, a pine and broad-leaf mixed forest and a pine forest appear to be slightly lower than emissions measured from temperate soils, with average emissions between 0.46 and 1.27 mg S/(m² a) (Yi et al., 2010).

Tropical Regions DMS emissions from the Amazon region have been studied on flights, tall towers, and at ground-level (Andreae and Andreae, 1988; Andreae, 1990; Jardine et al., 2015). A full model of the tropic sulfur budget was published by Delmas and Servant (1983), but they only included terrestrial H₂S from sulfate reduction, not other processes. Whereas DMS concentrations decrease with distance from the ocean and altitude, MeSH and H₂S show no such geographic trend (Simpson et al., 2001). DMS shows low diel variation, whereas MeSH drops by a factor of 10 between sunrise and noon. H₂S and DMS appear to be largely emitted by the canopy itself, even though those emissions are smaller than from crops. Soil emissions appear to be very low in general (Andreae, 1990), vegetated soils are even reported to be sinks for VSCs in unpolluted areas (Jaeschke et al., 1994). Wet season fluxes are generally up to 10-fold lower than dry-season fluxes (Andreae et al., 1990). These trends and similar emission magnitudes are also found in African rainforests (Bingemer et al., 1992; Kesselmeier et al., 1993).

Arctic Regions DMS emissions from the Arctic and Antarctic Oceans are similar to other ocean areas (Berresheim et al., 1989; Mungall et al., 2016). From Alaskan Tundra soils, DMS is the dominant sulfur gas in wet meadows, whereas COS is mainly emitted from upland lichens. The magnitude of the fluxes is similar to, but on the low end of temperate soil emissions (0.2-1.7 mg S/(m² a) DMS and 0.8-3.4 mg S/(m² a) COS) (Hines, 1992). This is much lower than oceanic emissions, but given the size of boreal and tundra areas might still be a relevant terrestrial source.

Wetlands

Salt marshes, mangrove forests, freshwater wetlands, lakes, and rice paddies show high VSC emissions originating from different pathways:

Salt Marshes Salt marshes, esp. when vegetated with *Spartina alterniflora*, are a big source of VSC emissions. The main DMS production comes from DMSP cleavage by *S. alterniflora* and to some extent microalgae (Dacey et al., 1987), whereas there are active communities of sulfate reducing bacteria and methanogens in the sediments that degrade DMS to H₂S (Kiene and Capone, 1988; Kiene, 1988).

The aerenchyma of *S. alterniflora* facilitate the transport of DMS from the water and soils to the atmosphere (Lamers et al., 2013). *S. alterniflora* emissions are so strong that they increase DMS and CH₄ emissions upon invasion into marshes (Tong et al., 2018; Wang and Wang, 2017). Marshes with *S. alterniflora* cover can reach emission rates of 328 µgS/(m² h) leading to an average of 5.8 g S/(m² a) (Stuedler and Peterson, 1985). DMS peaks at day, CS₂ at night, whereas for the others, no significant trend was observed (Stuedler and Peterson, 1985). The production of VSCs, mainly H₂S increases with decreasing redox potential, indicating a shift from DMSP degradation to sulfate reduction as the main VSC producing process (Devai and de Laune, 1995). Since the sulfate concentration in salt water is usually much higher than in freshwater (27 mmol/L vs. 0.005-20 mmol/L, Paul and Clark (1996); Rejmankova and Post (1996)), this again leads to much higher VSC emission potentials in marine and salt water ecosystems than in freshwater ecosystems.

Mangrove Forests Like in salt marshes, substantial H₂S and CH₄ emissions from DMS and MeSH degradation are found. Sulfate-reducing bacteria dominate the DMS degradation - apparently, methanogens are outcompeted by sulfate-reducing bacteria because of their higher substrate range (Lyimo et al., 2002a, 2009). Aerial roots correlate antiproportionally with H₂S and CH₄ (Lyimo et al., 2002b), maybe by increasing the redox potential in those areas.

Freshwater Wetlands and Lakes Wetland sediments are the perfect example of how the availability of energy-rich electron donors shapes microbial communities in soils: They tend to exhibit a strong layering of aerobic microorganisms, then nitrate reducers, iron reducers, sulfate reducers and finally methanogens (Conrad, 1996). VSC depth profiles show DMS and MeSH peaking in the redox transition zone between anoxic and oxic water layers in lakes (Fritz and Bachofen, 2000; Hu et al., 2007) or right above the sediment (Lomans et al., 1997), decreasing towards the water surface. MeSH and DMS are often completely degraded to H₂S, CH₄ and CO₂ before they reach the surface (Lomans et al., 2001b; Zinder and Brock, 1978), but not always (Cooper et al., 1987). Anoxic sphagnum peat and minerotrophic peatland sediments consume DMS, MeSH and COS (Lomans et al., 1999c; de Mello and Hines, 1994), indicating strong sulfur cycling under these conditions. The transient VSC concentrations in deeper, anoxic lake layers have been attributed to H₂S methylation in deep layers and then a demethylation under CH₄ and CO₂ formation in higher layers (Hu et al., 2007). In general, the more stratified, anoxic or eutrophic a lake gets, the more VSC emissions can be detected (Richards et al., 1991).

Besides these bacterial processes, algal DMS formation upon cleavage of DMSP (Ginzburg et al., 1998) and methionine (Caron and Kramer, 1994) can also be a significant contributor. DMS has been reported to spike around noon and to correlate with chlorophyll a contents in Canadian lakes (Steinke et al., 2018). The diurnal cycle was also observed in a different study on a freshwater lake (Leng et al., 2021), though no further investigation as to the cause was done there. Again, also DMS emissions from degrading algae have been found, and e.g. add up to ~230 t DMS/a from the Great

Lakes (Nriagu and Holdway, 1989), even though this volatilization is not a major pathway in sulfur cycling in those areas (Richards et al., 1991).

Rice Paddies VSC emissions from rice paddy fields reach 0.006-0.024 Tg S/a (Yang et al., 1998). The study on different Chinese rice paddies found mainly DMS, MeSH/DMDS and CS₂ emissions as well as very low COS and no H₂S emissions, diurnal cycles of VSC emissions as well as a spike shortly before harvest, in August (Yang et al., 1998). They also found a substantial increase of VSC emissions upon application of chemical fertilizer, yet did not state the composition of the fertilizer. Another study on COS and CS₂ only found the same diurnal cycle, but their results on nitrogen fertilizer application differed: Upon application of ammonium sulfate, CS₂ levels did not change, but the uptake of COS into the soil was increased by a factor of 2 (Jing et al., 2017).

Human and Animal Waste

Sulfur emissions from waste, landfills, wastewater treatment plants, sewers and manure are of concern due to odour complaints and health risks for the workers (He et al., 2018; Borrás et al., 2016; Cheng et al., 2005; Wang et al., 2015; Feilberg et al., 2010; Abis et al., 2018). Sewage influx into salt marshes also produces VSC emission hotspots (Adams et al., 1979), so environmental concerns are also present. Most of the emissions are due to organic sulfur compound degradation, probably mainly amino acids (He et al., 2018), but also letting the redox potential drop too low can lead to increased sulfate reduction and methylation (Smet and van Langenhove, 1998). Methanogens can also play a big role here (Sun et al., 2015a). A critical phase is when the activated sludge is aerated again; here, spikes of reduced sulfur species are observed (Kim et al., 2014). Handled well, activated sludge can also tremendously reduce VSC emissions and is thus a crucial step (van Leerdam et al., 2006).

1.4.6. The Marine Sulfur Cycle and the CLAW Hypothesis

Marine dimethyl sulfide emissions by microalgae are the main biogenic source of dimethyl sulfide. This is a major contributor to the atmospheric sulfur burden and cloud condensation nuclei over the ocean, as otherwise, the particle load over the oceans is low - one can even trace ship plumes days later (Capaldo et al., 1999). The important link of algal dimethyl sulfide emissions to cloud formation over the oceans led to the formation of the CLAW hypothesis. I will first discuss the DMS and MeSH formation pathways in the ocean, and then the CLAW hypothesis and its reception.

Marine micro- and macroalgae as well as some higher plants like *S. alterniflora* use 3-(dimethylsulfonio)-propionate (DMSP) as an osmolyte, chemoattractant and anti-freezing agent. Due to its wide abundance, predators of those species also use it as a chemical cue, and DMSP and DMS might play

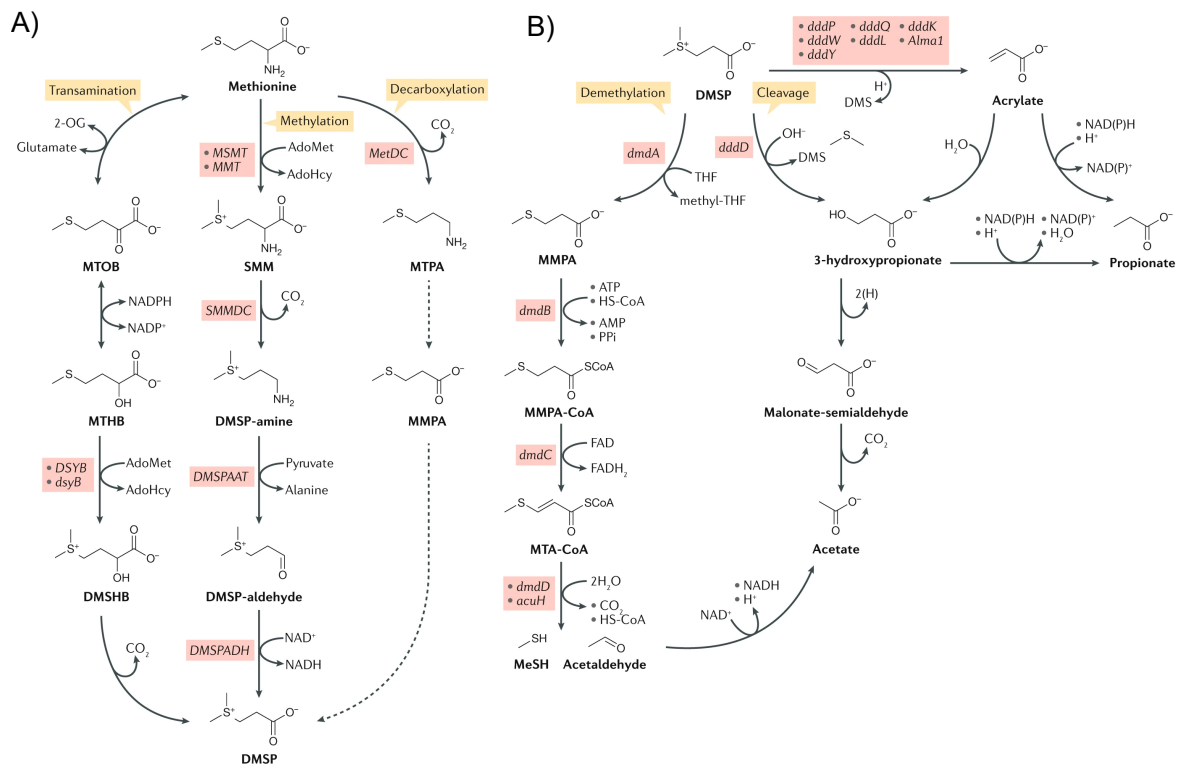


Figure 1.5.: Scheme of marine sulfur cycle. A) Formation of DMSP from methionine by algae (left), higher plants (middle), and dinoflagellates (right pathway). Red: genes involved in the pathways. MTOB: 4-(methylthio)-2-oxobutanoate, MTHB: 4-(methylthio)-2-hydroxybutanoate, DMSHB: 4-(dimethylsulfonio)-2-hydroxybutanoate, AdoHcy: adenosylhomocysteine, AdoMet: adenosylmethionine, SMM: S-methylmethionine, MTPA: 3-(methylthio)-propylamine, MMPA: 3-(methylthio)-propanoate. B) DMSP degradation pathways as done by bacteria (left) and algae (right). THF: tetrahydrofolate, ATP: adenosine triphosphate, AMP: adenosine monophosphate, PPi: pyrophosphate, CoA: coenzyme A, FAD: flavine adenine dinucleotide, MTA-CoA: methylthioacryloyl-CoA. Adapted from Moran and Durham (2019) with permission.

a crucial role in structuring the microbiota of algal reefs (Raina et al., 2010). It is formed from methionine by three different pathways (Figure 1.5A): In higher plants like *Spartina* and *Wollastonia*, methionine is first methylated to S-methylmethionine, then decarboxylated to 3-(dimethylsulfonio)-propionylamine, and then oxidized to 3-(dimethylsulfonio)-propionaldehyde and the DMSP. Macroalgae, diatoms, prymnesiophytes, and prasinophytes first oxidize methionine to 4-(methylthio)-2-oxobutanoate, which is reduced to 4-(methylthio)-2-hydroxybutanoate. This is methylated to 4-(dimethylsulfonio)-2-hydroxybutanoate and then decarboxylated to DMSP. In dinoflagellates, the biosynthesis is not entirely understood yet, but the first step is a decarboxylation to 3-(methylthio)-propylamine, which is the oxidized to 3-(methylthio)-propanoate and methylated to DMSP (Curson et al., 2017; Moran and Durham, 2019). Marine bacteria in sediments are also important DMSP producers, and their biosynthesis is likely the same as for *S. alterniflora*, as the methionine methyltransferase required for the first step was identified (Williams et al., 2019).

Algae can cleave DMSP to DMS and acrylate under certain conditions like temperature stress (Figure 1.5B). Depending on the DMSP lyase present, a substitution of the dimethylsulfonio group to form 3-hydroxypropanoate instead of the elimination to acrylate can also occur. Both compounds ultimately get degraded to acetyl CoA, whereas the DMS is released by the cells, e.g. as a temperature stress or wounding signal. Marine bacteria use a different way to catabolize DMSP (Figure 1.5B): They first demethylate it to 3-(methylthio)-propionic acid, which is then immediately coupled to coenzyme A and ultimately degraded to acetaldehyde, and methanethiol (Curson et al., 2011; Reisch et al., 2011). Some bacteria can use both pathways simultaneously (Sun et al., 2016). Often, the methanethiol is then further methylated to DMS as well (Kiene and Visscher, 1987; Kiene, 1996), or can be utilized for methanogenesis in intertidal sediments (van der Maarel and Hansen, 1997). A third degradation process of DMSP is the oxidation to 3-(dimethylsulfoxonio)-propionate (DMSOP), which can also be cleaved to dimethyl sulfoxide (DMSO) and acrylate in analogy to the DMSP-cleavage (Thume et al., 2018).

DMS abundance is strongly correlated with available irradiation (Vallina and Simo, 2007), temperature, salinity and nitrogen limitation (Stefels, 2000). In the water column, it can be degraded to sulfate, either *via* DMSO or *via* MeSH (González et al., 2010; Lidbury et al., 2016), but a significant fraction is leaked to the atmosphere, where it gets oxidized to DMSO, COS and methanesulfonic acid (MSA), and finally SO₂ within hours (Hatton, 2002). As SO₂ usually gets dissolved and oxidized to atmospheric sulfate and forms cloud condensation nuclei, Charlson, Lovelock, Andreae and Warren formulated the CLAW-hypothesis as a potential negative climate feedback loop (Charlson et al., 1987): Increased oceanic temperatures would lead to an increased algal growth and increased DMS emissions. These emissions would increase atmospheric sulfur compounds, enhancing cloud formation and increasing the albedo. This would lower the incoming radiation, which would cool the atmosphere and thus stabilize the current climate. Based on this hypothesis, many models were built trying to predict the magnitude of the atmospheric sulfur burden from oceanic DMS emissions, e.g. Fiddes et al. (2018); Kloster et al. (2006); Lana et al. (2011). However, the hypothesis has a few flaws, and the effect is likely much smaller than postulated. Firstly, oceanic aerosols are not only formed by DMS emissions, but also by sea salt and organic matter that are released from the ocean by turbulent mixing with winds. Those processes are not climate dependent, limiting the effect of DMS emissions (Quinn and Bates, 2011). Secondly, the increased temperature is due to increased CO₂ concentrations in the atmosphere, which also decrease the ocean's pH. This ocean acidification counteracts the productivity increase by warming, such that DMS emissions do not increase strongly with temperature (Six et al., 2013).

1.5. Methods to Measure VOCs

There are a number of different methods to measure VOCs. The most common way is the use of gas chromatography coupled to a range of different detectors like flame ionization detectors (FIDs)

for general organic compounds, electron capture detectors (ECDs) for halogenated analytes, barrier ionization detectors (BIDs) for non-helium compounds, or mass spectrometers (MS) (Hinshaw, 2018). Due to its additional structural information and low limits of detection, MS has been the detector of choice for years. GC-MS is an extremely selective and specific method, since the analytes can be first separated on the column based on their boiling point and polarity, and then identified by its fragments in the mass spectrometer. Using MS/MS-approaches in triple quadrupole-MS or using high-resolution mass spectrometers like time of flight- or ion trap-MS enhances the analyte specificity even further. Mass spectrometers are also very sensitive, so that low concentrations can be measured. However, GC-MS sensitivity is usually not high enough to allow for direct quantification of trace and ultratrace level compounds in headspace samples, due to the small sample size injected onto the column. Hence, GC-MS for trace level compound determination usually relies on preconcentration, e.g. on thermal desorption tubes, using SPME or liquid extraction techniques.

Besides GC-MS, there are direct ionization methods coupled to mass spectrometry, like atmospheric pressure chemical ionization (APCI-MS), proton transfer reaction (PTR-MS) or selective ion flow tube (SIFT-MS) mass spectrometry. In contrast to GC-MS, those techniques rely on a low fragmentation during the ionization, so that all analytes can be identified in a single mass spectrum and no chromatographic separation is needed. The missing column also allows for continuous, real-time measurements. An intermediate between the time-consuming separation on a chromatographic column and the full spectra obtained by non-separating methods is ion mobility-MS, which relies on a very short separation of the ionized analytes in a counter flow (McEwan, 2015).

Besides these destructive methods, spectroscopic methods like infrared (IR), ultraviolet and visible light (UV-Vis) and Raman-spectroscopy can be used. Since they are based on changes in molecular vibration states or electronic states, groups of molecules, e.g. aldehydes or thiols, can usually only be measured as a sum parameter rather than identifying individual compounds. Yet, since they are easy to use, reliable and cost-efficient instruments and analytes can be quantified reliably, they are the methods of choice for routine analyses in a situation with well-defined analytes and matrices (Otto, 2019).

Substance-class specific arrays of metal oxide sensors, surface or bulk acoustic wave sensors, metal oxide field effect transistor sensors or conducting polymer sensors are commonly used as e-noses and have been commercialized by different companies as well. It has been attempted to simplify them for untrained users, e.g. for drug or chemical weapon detection in airports, but their application remains constrained to very specific situations with well-known analytes and interferents, and often more on a presence-absence level than an actual quantification (Röck et al., 2008).

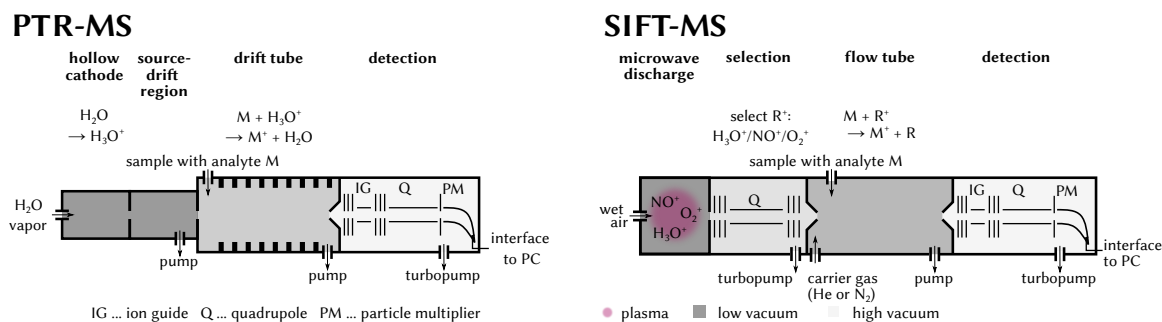


Figure 1.6.: General scheme of PTR-MS and SIFT-MS. Adapted from Lehnert et al. (2020a).

1.5.1. PTR-MS and SIFT-MS

SIFT-MS and PTR-MS were developed in the 1990s (Lagg et al., 1994; Smith and Spanel, 1996). Both are similar in their design: their working principle is based on a chemical ionization of gaseous analytes by reagent ions in a flow or a drift tube, and the detection of the analyte ions *via* mass spectrometry. The reaction time is important, as from knowing the kinetics of the ionization reaction, one can derive the original concentration (McEwan, 2015).

The three key differences in design become clear when looking more closely (Figure 1.6):

1. PTR-MS only uses H_3O^+ ions that are generated by a hollow cathode, whereas SIFT-MS uses a microwave plasma to ionize humid air. This generates many different ions and enables the use of the positive reagent ions H_3O^+ , NO^+ , O_2^+ , but also the negative reagent ions O^- , O_2^- , OH^- , NO_2^- , and NO_3^- in SIFT-MS (Hera et al., 2017). The desired reagent ion is then selected by a quadrupole. PTR-MS can also be expanded to Switchable Reagent Ion Mass Spectrometry (SRI-MS) by changing the source. This expands the number of possible reagent ions in PTR-MS/SRI-MS to H_3O^+ , NO^+ , O_2^+ , NH_4^+ , Kr^+ , and Xe^+ (Jordan et al., 2009a). In general, the hollow cathodes are able to produce higher numbers of ions, since they are optimized to just produce this one ion. Thus, the PTR-MS/SRI-MS tends to be more sensitive than the SIFT-MS. Hollow cathodes with electrostatic switching has been demonstrated for SIFT-MS as well (Španěl et al., 2019), but has not been commercialized yet. The range of reagent ions expands the field of possible analytes from proton acceptors (H_3O^+ , e.g. alcohols and aldehydes) to electron donors with an ionization potential up to 12 eV (NO^+ , O_2^+ , e.g. COS) and even higher (Kr^+ , Xe^+ , also inducing fragmentation), whereas the negative reagent ions in SIFT-MS also enable the ionization of proton donors and electron acceptors, e.g. HCN, CO_2 or SO_2 (Smith and Spanel, 2011b).
2. The reaction of the analyte with the reagent ion takes place in a drift tube in PTR-MS and a flow tube in SIFT-MS. The critical task in this region is to constrain the reaction time as good as possible, to obtain reliable results. In PTR-MS, this is solved by accelerating the ions in a high electric field with an accelerator voltage in the magnitude of kV (Hartungen et al., 2013).

In newer versions, the linear design was replaced by a field that facilitates a spiral path of the ions through the chamber, which increases the reaction time, thus the amount of ionized analyte and the instrument sensitivity substantially (Krechmer et al., 2018). SIFT-MS relies on a laminar flow of a carrier gas and only employs a small flow tube voltage for focusing the ions. This is a much milder technique, so less fragmentation of the analytes occurs, leading to cleaner spectra. The ions are also not excited strongly by the field, so the Maxwell-Boltzmann-distribution and gas phase chemistry kinetic constants are valid assumption and the direct mixing ratio calculations can be reliable (Španěl et al., 2006; Spesyvyi et al., 2015; Smith et al., 2014). PTR-MS usually cannot be used without calibration, while SIFT-MS is often used like this (Lourenço et al., 2017).

3. PTR-MS now uses only time of flight-mass spectrometers, whereas SIFT-MS still relies on quadrupole-mass spectrometers. Since SRI-MS is still rarely used, PTR-MS has overcome the issue of limited structural information by increasing mass accuracy. This enables the separation of isobaric compounds with different sum formulas and a much clearer identification of the analyte's sum formula. Additionally, full mass spectra can be obtained at a much higher frequency (200x higher if a mass range of $m/z = 15-250$ u is used). However, this comes at the cost of a more difficult handling, and the evaluation of the more complex dataset might be more challenging (Jordan et al., 2009b).
4. Newer developments in SIFT-MS include new sample introduction techniques. Besides the usual "nozzle" that draws in gas samples from a container or a flow, an autosampler with a needle for headspace samples from Tedlar bags, headspace incubation vials, and a TD tube sampler. This makes sampling more variable and extends the range of possible applications, as the instrument does not have to be placed directly at the point of the sample (Slingers et al., 2021).

Direct comparisons of the two instruments are rare. Reviews point out the higher sensitivity of PTR-MS at the cost of a higher humidity-sensitivity and less structural information (Biasioli et al., 2011; Shende et al., 2017; Smith and Spanel, 2011a). Measurement accuracies are reported to be higher for SIFT-MS (Lourenço et al., 2017). Smith et al. (2014) showed more hydrated product ions for SIFT-MS, and more fragment ions for PTR-MS. 10x higher sensitivity in cps/ppb due to the increased amount of reagent ions has been reported for PTR-MS (Smith et al., 2014), and is probably even higher for the newer instruments like PTR3 and Vocus.

In comparison to other atmospheric pressure ionization (APCI) techniques, PTR-MS has been proven to be more reliable in detecting smaller, more volatile compounds and primary VOCs, whereas other APCI techniques were better at detecting semivolatiles and atmospheric degradation products of VOCs (Riva et al., 2019). A comparison with TD-GC-MS also showed a much better performance for SIFT-MS and PTR-MS for small, very volatile, oxygenated compounds, and a worse performance

than TD-GC-MS for larger, semivolatile compounds. SIFT-MS and PTR-MS had a much bigger linear dynamic range than TD-GC-MS (Lourenço et al., 2017).

1.5.2. Sampling Methods

VOCs can be sampled very differently, depending on the analyte, analysis method, and experimental constraints.

For higher concentration analytes, direct analysis of gaseous samples is often used. Samples can be taken e.g. in metal cylinders, glass flasks, or Tedlar bags. Rigid containers are usually evacuated before the sampling and then just opened at the location, whereas the flexible Tedlar bags have to be filled using a pump. Caution has to be taken here, as all types of containers are contaminated easily, either if the vacuum is not good enough or by the pump utilized for the Tedlar bag filling (Marr et al., 1988). Additionally, one has to take care that the walls of the containers can adsorb compounds from the sample, desorb previously-adsorbed compounds, and in the case of Tedlar bags, can let gas exchange with the atmosphere happen. This can lead to reduced concentrations in the sample, and cross-contamination (Chandra et al., 2017).

Thus, direct gas analysis is usually only used when storage times are short. For example, one could measure directly in the field, incubate samples and measure the headspace after a certain time, or analyze breath samples directly.

When storage times are longer or a preconcentration of the analyte is required, adsorbents can be used. The most frequently used ones are polydimethylsiloxanes (PDMS) (Harshman et al., 2016), divinylbenzenes (Grossmannova et al., 2007), and activated carbon (Kaikiti et al., 2020), but also zeolites or silica (Li et al., 2019b), and even cotton pads (Prada et al., 2011). After exposure, the analytes can either be extracted with solvents (Ramirez et al., 2010b), or they can be thermally desorbed from thermal desorption tubes (TD tubes) or solid phase microextraction (SPME) fibres. TD tubes are commercially available, reliable sampling devices that can be used to sample in remote areas. The tubes can be placed upstream of a pump so that contamination by the pump is unlikely. Since their ends can be closed, long-time storage is possible, however, reactions can happen on the adsorbent material, altering the chemical composition of the sample (Merlen et al., 2017; Rosier et al., 2014). One drawback is that TD requires a special sample introduction systems for the GC-MS. SPME on the other hand can only be used for passive sampling, and storage should be kept as short as possible, as the fibres cannot be shielded well from the environment and are prone to contamination. But an SPME fibre can be injected into a normal GC injector, which makes handling easy and accessible (Bravo-Linares and Mudge, 2007; Kim and Park, 2008). Both techniques have in common that an accurate quantification can be difficult and is often imprecise, as one has to take into account the adsorption and desorption processes (Garcia-Alcega et al., 2017; Lourenço et al., 2020).

1.5.3. Field Setups

There are three main techniques for measuring VOC emission fluxes from soils or vegetation: static chambers, dynamic chambers, and eddy covariance measurements.

Chamber measurements are point measurements on a very small area: some air headspace is enclosed over some part of the soil or plant. This headspace can either be static, *i.e.* completely cut off the surrounding air, or dynamic, *i.e.* flushed continuously. Static chambers are very easy to use, as one just needs to close off the headspace and wait. Usually, after closing, the headspace is sampled at a number of pre-defined time points e.g. 5, 20, and 35 min, and from the increase in headspace concentration, the emission flux or release rate is calculated. The signal that is obtained is a combined signal of all release and uptake processes happening in the study object. This method is still widely used e.g. for soil respiration or soil methane emission measurements, and is very good to determine the general direction of a flow (Moore and Roulet, 1991). However, sometimes, the emission and uptake processes are concentration-dependent, and e.g. a higher headspace concentration reduces further production or desorption from the soil. This often leads to an underestimation of the source strengths (Rochette et al., 1992).

Dynamic chambers can help focusing on the emission potential of a soil. Since the air is constantly exchanged, accumulation of compounds is reduced greatly, and artefacts due to too high mixing ratios are removed. If one is interested only in emissions, one can use pure air to flush the chambers. With the concentration measured at the outlet of the chamber and the flow through the chamber, one can calculate the release rates of the soils directly. However, this can lead to artefacts if there are uptake processes of the compound in the soil or plant: These cannot be observed when no initial compound concentration is present (Castro and Galloway, 1991). Often, soils show distinct compensation concentrations, *i.e.* mixing ratios where the uptake rates are as big as the release rates. Below this concentration, the compound is emitted, above this concentration, it is taken up by the soil (Conrad, 1994). As an alternative, ambient air can be used for flushing the chambers. With this, one can measure the actual flux of a compound at its natural concentration into and from the study object. However, one has to measure the mixing ratio of the compound at the inlet and the outlet of the chamber, which doubles the measurement uncertainty of the flux result (Behrendt et al., 2014). Additionally, even when doing so, the concentrations of the compounds in the soils might be altered by flushing the system, so even this method might induce artefacts. For example for DMS, no compensation concentrations have been observed in previous studies (de Mello and Hines, 1994), so at least for this compound, pure air can be used without any problem.

Eddy covariance is a micrometeorological technique that does not rely on chamber enclosures, but makes use of the fact that wind is a turbulent flow. It extracts the covariance of atmospheric mixing ratio distributions and vertical wind components to estimate the overall ecosystem flux. Therefore, fast and accurate mixing ratio, wind speed and wind direction measurements have to be conducted (Baldocchi, 2003). One can extract accurate net ecosystem flux without the artefacts of enclosure

techniques, but cannot obtain contributions of individual components like individual plants or soil (Spirig et al., 2005). Compared to chamber systems, eddy covariance is a rather new technique. Whereas it has been used for greenhouse gas (CO_2 , CH_4 , N_2O , H_2O) measurements since the 1990s (e.g. Pederson et al. (1995)), studies with VOCs are more recent. Disjunct eddy covariance was already tried in 2014, but only with the new PTR-ToF-MS instruments, there is a tool to measure VOCs with eddy covariance, and the first studies have just been published within the last year (Acton et al., 2020; Peng and Sun, 2020; Seco et al., 2020; Loubet et al., 2021; Phillips et al., 2021). The ToF-MS was not only fast enough to be used for eddy covariance measurements, but also enabled untargeted VOC measurements, as the whole spectrum can be screened within milliseconds. Hence, there are not only targeted studies (Seco et al., 2020; Phillips et al., 2021), but also studies determining net fluxes of over 250 compounds simultaneously (Loubet et al., 2021). Thus, this technique will likely become more important in the future and enable a much clearer picture of VOC fluxes from a variety of different habitats.

2. Scope of the Thesis

Biogenic volatile organic compounds (VOCs) are important for three reasons:

1. They influence the atmosphere to the point where they can affect the global temperature both positively and negatively and substantially increase air pollution. It is important to understand under which environmental conditions they are emitted, to be able to predict the emissions under a changing climate.
2. As food sources and infochemicals, VOCs help shape microbial communities colonizing soil, leaves litter, and plant surfaces.
3. VOCs could help understand the activity of these microbes and plants and their individual status in the field undestructively *in vivo*.

In my study, I focused on understanding the environmental factors and formation mechanisms of microbial VOCs of soil and litter *in vitro*. This represents an intermediate step between the study of microbial isolates showing possible VOC emissions, but are conducted in a very unnatural, controlled environment, and field measurements, where the environment is natural, but uncontrolled and complex and thus interpretation can be challenging. Soil and litter incubations allowed me to control for some factors like temperature and humidity while still preserving the microbial community and natural growth surfaces, which makes data interpretation easier and more reliable.

SIFT-MS Optimization and Method Development To measure VOCs accurately, I needed a stable, time-resolved instrument with low limits of detection and the possibility to identify structures. GC-MS is excellent for structural identification, but takes a lot of time. Spectroscopic methods are usually not sensitive enough and mostly only yield information about structural motifs, but not individual analytes. PTR-MS has a low enough limit of detection (LOD) and a big linear dynamic range making quantification easy, but the structural information is very limited, as isomers cannot be separated. SIFT-MS provides more structural information than PTR-MS and can separate isomers due to the use of three different reagent ions, but our instrument, as purchased, lacked the sensitivity needed to conduct the desired measurements. I optimized instrument parameters to the point where I lowered the LOD by a factor of 10, and developed ways to quantify VOCs despite the introduced humidity-dependency (**Publication 1**). I then demonstrated its ability to separate isomers that would overlap in PTR-MS by developing a method to measure isoprene and 2-methyl-3-buten-2-ol in plants simultaneously (**Publication 2**).

VSC Emissions from Temperate Peatlands With this method in hand, I then focused on understanding volatile sulfur gas (VSC) emissions from temperate peat soils. Despite the importance of VSC emissions for global climate, freshwater wetlands and other terrestrial emissions are usually left out, as they are thought to be negligible besides anthropogenic and oceanic emissions. I investigated whether this assumption is valid, and which environmental parameters and which microbes are involved in the processes leading to the emission of VSCs. Our hypotheses were:

1. VSC emissions are mainly of microbial origin. Thus, the soil humidity and the redox potential are important drivers of VOC emissions.
2. There are two main processes for the emission of H₂S, MeSH, and DMS:
 - a) Sulfate reduction and subsequent methylation. This can only occur at low redox potentials, when sulfate reduction is active.
 - b) Degradation of organic matter. This is independent of the redox potential.

I thus expect sulfate reduction to be the dominating process under very anoxic conditions whereas organic matter degradation should be constant over the whole redox potential range.

3. Methylation and demethylation interconversions of H₂S, MeSH, and DMS can occur when their mixing ratios are high.
4. Sulfate reduction, organic matter degradation, VSC methylation and VSC demethylation are done by different microbial groups.

The soil humidity and redox potential were the drivers I focused on first, as they have been shown to govern VOC emissions in general and VSC emissions in particular. Since there are two main formation mechanisms involved – direct production of precursors during sulfate reduction followed by methylation, or by the degradation of organic matter –, the redox potential could help separate the two, as only the first one is redox-potential-dependent. I also fed different sulfur substances to the microbes, to see which pathways are indeed available and lead to VSC emissions. Lastly, I also investigated the change in microbial community and soil organic compounds correlating with soil VSC emissions, to get a clearer view on which microbes and metabolites are involved (**Publication 3**).

VOC Emissions during Litter Degradation Litter is the most important source of fresh, labile carbon into soils and its degradation could thus be a major VOC source. Numerous papers have worked on finding emission differences between plants, and have studied the temperature and humidity-dependence of litter VOC emissions, but it remains unclear to date how litter emissions change during degradation until the leaves are completely degraded. This I investigated by burying litterbags of 13 different temperate tree species below their original trees, and measuring VOC emissions from them. The microbial community and chemical litter analysis allows for the interpretation of different litter emissions. The hypotheses are:

1. Degrading litter is accompanied by a succession of different microbes growing on the litter,

depending on the compounds available. This is also reflected in changing VOC emission quantity and composition over time.

2. Indicators of microbial primary metabolism like ethanol or acetaldehyde correlate with CO₂ emissions from the sample.
3. Emissions of VOCs that were stored in the leaves decline exponentially with time.
4. The species of the original plant is reflected both in the VOC emissions of stored compounds and the microbial community colonizing the litter and their VOC emissions.

However, since the experiment is still ongoing and not all data has been collected yet, this is preliminary (**Chapter 4, Unpublished Work**).

3. Publications

- P1** Lehnert, A.-S., Behrendt, T., Ruecker, A., Pohnert, G., and Trumbore, S. E.: SIFT-MS optimization for atmospheric trace gas measurements at varying humidity, *Atmospheric Measurement Techniques*, 13, 3507-3520, 2020, reprinted under CC-BY 4.0 license.
- P2** Lehnert, A.-S., Perreca, E., Gershenzon, J., Pohnert, G., and Trumbore, S. E.: Simultaneous Real-Time Measurement of Isoprene and 2-Methyl-3-Buten-2-ol Emissions From Trees Using SIFT-MS. *Frontiers in Plant Science* 11, 578204, 2020, reprinted under CC-BY 4.0 license.
- P3** Lehnert, A.-S., Cooper, R., Ignatz, R., Ruecker, A., Gomes-Alves, E., Küsel, K., Pohnert, G., Trumbore, S. E.: Dimethyl sulfide originates from organic matter degradation in freshwater wetlands, and scarcely from sulfate reduction, submitted to *Environmental Science and Technology* on Feb 25, 2021.



SIFT-MS optimization for atmospheric trace gas measurements at varying humidity

Ann-Sophie Lehnert^{1,2}, Thomas Behrendt¹, Alexander Ruecker¹, Georg Pohnert², and Susan E. Trumbore¹

¹Department of Biogeochemical Processes, Max Planck Institute for Biogeochemistry, 07745 Jena, Germany

²Institute for Inorganic and Analytical Chemistry, Friedrich Schiller University, 07743 Jena, Germany

Correspondence: Ann-Sophie Lehnert (alehnert@bgc-jena.mpg.de)

Received: 18 September 2019 – Discussion started: 4 November 2019

Revised: 29 May 2020 – Accepted: 7 June 2020 – Published: 2 July 2020

Abstract. As direct real-time analysis techniques, selective ion flow tube mass spectrometry (SIFT-MS) and proton-transfer reaction mass spectrometry (PTR-MS) provide on-line measurement of volatile organic compounds (VOCs). Both techniques are widely used across several disciplines, e.g., atmospheric chemistry, food science, and medicine. However, the humidity of the sampled air greatly influences the quantified mixing ratio and must be accounted for. Here we present several improvements to a Voice200ultra SIFT-MS instrument to reduce background levels and enhance sensitivity. Increasing the sample gas flow to 125 sccm enables limits of detection (LODs) at the sub-parts-per-billion (subppb) level, and the resulting humidity dependence is overcome by calibrating for humidity as well. A comparison with a PTR-QMS 500 showed detection limits of the PTR-MS still being an order of magnitude lower, whereas sensitivity was higher for SIFT-MS, and its calibration was still more robust against humidity. Thus, SIFT-MS is a suitable, lower-cost, and easy-to-use alternative for atmospheric trace gas measurements of more complex mixtures, even with isomers, at a varying humidity range.

1 Introduction

Volatile organic compounds (VOCs) shape the medium in which we are living: the air. As odors, pheromones, reductants, greenhouse gases, and precursors for aerosols, they regulate key processes in the environment. Due to their reactivity, their atmospheric lifetimes are usually limited, and their mixing ratios are rather low and span several orders of magnitude, typically from tens of parts per trillion (ppt)

to low parts per million (ppm). Despite great improvements during the past years, methods of measuring VOC that rely on concentrating samples using adsorption tubes or trapping air in storage containers often have artifacts due to dissipation of the analytes to, or reactions with, the walls, sorptive materials, or tubing used in experimental setups (Herrington, 2015; Piennar et al., 2015; Deming et al., 2019).

Thus, an easy, fast, and direct analysis method is desirable. Proton-transfer reaction mass spectrometry (PTR-MS) and selective ion flow tube mass spectrometry (SIFT-MS) both provide these characteristics as they do not rely on time-consuming sample separation like gas chromatography/mass spectrometry. Both are used in a wide variety of fields comprising both natural and anthropogenic atmospheric chemistry (Milligan et al., 2002; Yuan et al., 2017), plant studies (Amelynck et al., 2013), food science (Davis et al., 2005), and medical applications like breath analysis (Schwarz et al., 2009; Shende et al., 2017; Smith et al., 2014).

The two techniques have been compared in various reviews, e.g., Bylinski et al. (2017), Casas-Ferreira et al. (2019), and Smith and Spanel (2011), and therefore, SIFT-MS and its main differences to PTR-MS are only discussed briefly here. The principle behind both instruments is the chemical ionization of the analyte during a defined reaction time. Thus, the amount of compound can be calculated from the number of detected product ions using the kinetic rate constants k of the ionization reaction of the analyte A with the reagent ion R^+ :



$$\frac{d[R]}{dt} = k \cdot [A] \cdot [R^+]. \quad (1)$$

Assuming a pseudo-first-order reaction with $[R^+] \ll [A]$, the differential equation can be solved by an exponential decay function (McEwan, 2015), and using theoretical knowledge of diffusion behavior and gas and ion velocities in an electric field as well as experimental factors correcting for mass discrimination, one can estimate the analyte concentrations (Smith and Spanel, 2005). Since SIFT-MS uses a flow tube that transports the ions through the gas flow and only uses a small voltage to minimize diffusion to the walls, near-thermal conditions apply unlike in PTR-MS, and mixing ratios can be determined with an accuracy of $\pm 35\%$ (Langford et al., 2014).

Both instruments are comprised of the same three components: an ion generation zone, a reaction zone, and a detection zone; see Fig. 1 for a scheme of SIFT-MS. Reagent ions H_3O^+ (both instruments), NO^+ , and O_2^+ (SIFT-MS only, with positive ion source) are generated and injected into the reaction zone, where they chemically ionize the analytes to form product ions, e.g., Reaction (R2) for methanol:



All ions are then analyzed by a mass spectrometer (MS), usually a quadrupole MS for SIFT-MS and a time of flight-MS for PTR-MS, separating the ions by their m/z ratio and then counting the number of ions hitting the multiplier.

There are two main differences between the two instruments. They differ first in the way the reagent ions are generated and second in whether the ions are reacting with the analyte in a drift tube vs. in a flow tube. Whereas PTR-MS uses hollow-cathode discharges to ionize water vapor generating H_3O^+ (Romano et al., 2015), SIFT-MS generates a wet air plasma via microwave discharge and then selects the reagent ions H_3O^+ , NO^+ , and O_2^+ with a quadrupole (Smith and Spanel, 2005). Since the three reagent ions react differently with the analyte and may form different association and fragmentation products, more structural information can be obtained. However, the efficiency of creating the reagent ions is lower than for PTR-MS, leading generally to higher limits of detection (LOD) for SIFT-MS.

The SIFT-MS uses a flow tube with an inert carrier gas (He or N_2) that is mixed with the sample gas containing the analyte and a low voltage to focus the ions, whereas PTR-MS uses a drift tube through which the ions are guided and accelerated by a much higher electric field. Due to collisions with the carrier gas, in SIFT-MS the analytes and reagent ions are approximately in thermal equilibrium. Because of their acceleration, the effective temperatures of the ions in the tube are much higher for PTR-MS than for SIFT-MS, and these differences in energy lead to different fragmentation patterns for the two methods (Biasioli et al., 2011). The carrier gas needed in SIFT-MS serves the additional role of reducing the amount of ion clustering, like water clustering (e.g., $\text{H}_3\text{O}^+ \cdot \text{H}_2\text{O}$ or $\text{CH}_3\text{OH}_2^+ \cdot \text{H}_2\text{O}$) that can occur at high humidity.

As mentioned above, the high LODs for SIFT-MS can be an issue when measuring atmospheric trace gases, so we op-

timized the Voice200ultra SIFT-MS (Syft Technologies, New Zealand) to reach sub-ppb LODs and systematically characterized the performance of the SIFT-MS under different humidity conditions. Lastly, the instrument's performance was compared to the performance of a PTR-QMS 500 (Ionicon, Austria).

2 Experimental section

2.1 Materials

VOC-free air was generated by a pure air generator (PAG 003, Ecophysics, Dürnten, Switzerland) and was further purified by a scrubber built into a gas calibration unit (GCU, Ionicon, Austria). Gas mixtures of known VOC mixing ratios were produced by diluting a VOC standard gas mixture (Ionicon, Austria) (1 ppm each of 2-butanone, acetaldehyde, acetonitrile, acrolein, benzene, chlorobenzene, crotonaldehyde, dichlorobenzene, ethanol, isoprene, methanol, α -pinene, toluene, and *o*-xylene in nitrogen). The GCU was used to dilute the standard to the mixing ratios used in the calibration. To minimize background, the tubing used was 1/8" black PFA tubing with 1/8" Swagelok stainless-steel connectors. Sample gas fluxes through the multiport-inlet system were measured via a Sensidyne Gilian Gilibrator-2 NIOSH primary standard air flow calibrator (Sensidyne, FL, USA).

2.2 SIFT-MS optimization

Hardware and parameters were changed to optimize the Syft Voice200ultra with a positive ion source and a multiport inlet. The shut-down valve in the carrier gas line was removed upon the advice of Marvin Shaw (University of York, GB). We also removed the vent valve for the backing pumps and just vent the system through the flow tube with purified air. All the Viton/FKM and nitrile O-rings delivered with the instrument were replaced by Hennlich FEP-coated FKM O-rings. Further, the VICI valve that was delivered with the multiport-inlet system was switched to a flow-through VICI valve (EUT-6CSF16MWE).

VICI silica-coated stainless-steel capillaries with capillary sizes of 0.007", 0.010", and 0.015" inner diameter (i.d.), PEEK capillaries (BOLA S1817-08, 0.25 mm i.d., Bohlander, Germany; ChromaTec, 0.3 mm i.d., Labomatic Instruments AG, Germany; PEEK Capillary Tubing 37010-20, 0.010" i.d., Thermo Scientific, USA; and Latek Blue PEEK capillaries 8560–6009, 0.25 mm i.d., Latek, Germany), and a Swagelok SS-SS2 needle valve were tested as inlet capillaries. For both dry and humid VOC-free air (90 % humidity at 25 °C), a background was measured between $m/z = 15$ and 250 u (100 ms count time per ion, 10 scans). The background was normalized to both 10^6 counts of the respective reagent ion and the flow rate through the inlet capillary; see Fig. S1 in the Supplement.

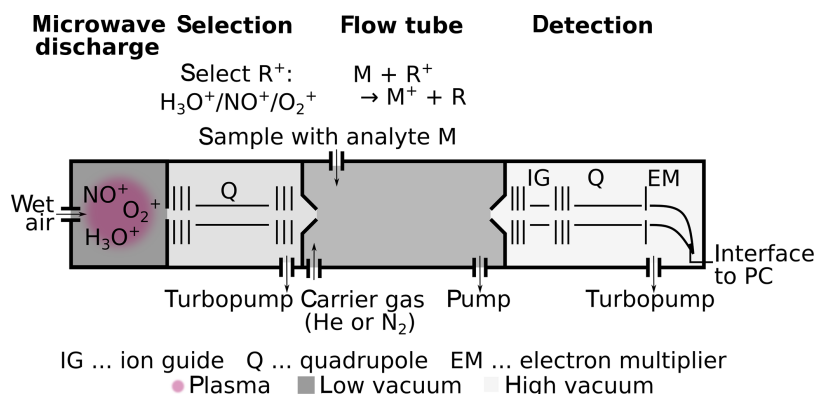


Figure 1. Scheme of SIFT-MS instrument components. SIFT-MS generates a plasma from wet air and then selects the reagent ion R (H_3O^+ , NO^+ or O_2^+) via a quadrupole (Q). In the flow tube, reagent ions R^+ and analytes M meet and react. Their reaction time is defined by the flow of the carrier gas through the tube and a small electric field to focus the ions. The ions are detected via a quadrupole MS.

Microwave cavity and power, the upstream and downstream lenses, the source pressure and the air stream into the source were tuned before the measurements. Flow tube voltage and temperature and carrier gas flow were optimized for VOCs with mixing ratios lower than 10 ppb. These experiments were performed using both helium and nitrogen as carrier gases; see Figs. S3–S14. Each time, 5 ppb of the VOC standard was mixed into dry and humid (90 % relative humidity at 25 °C) VOC-free air. The flow tube voltage was scanned in 5 V steps between 0 and 65 V; the flow tube temperature was stepwise increased in 5 °C intervals from 100 to 160 °C; and the carrier gas flow was scanned at 0, 7.89, 15.79, 31.57, 47.36, 63.14, 78.93, 118.39, 157.85, 236.78, 315.71, 394.63, and 473.56 ccm (0–6 TorrL s⁻¹). For the scan, 15 scans were conducted with 500 ms dwell time – the time the detector integrates the signal – per ion after 20 s settle time.

To select for nitrogen versus helium as a carrier gas, calibrations were done in the range from 0.1 to 10 ppb for the VOC standard in dry air as well as at 30 %, 60 %, and 90 % relative humidity (25 °C). For the measurement, after 20 s settle time, 15 scans were conducted with 500 ms dwell time per ion, except for α -pinene masses $m/z = 81$ and 137 u (H_3O^+ reagent ion), which were measured for 1 s, to account for its low mixing ratio due to its semivolatility in our soil samples.

2.3 Evaluation of different calibration procedures

The instrument calibration done with helium carrier gas (see Sect. 2.2) was used for evaluating different calibration procedures. Different regression equations and calibration procedures were tested. In the following equations, I_P is the product ion intensity; I_R is the reagent ion intensity; χ is the mixing ratio of the analyte; ϕ is the relative humidity; ICF is the experimentally determined instrument calibration factor

the SIFT-MS provides for correcting discrimination effects in flow tube and downstream quadrupole; k is the kinetic rate constant; $I_{\text{H}_3\text{O}^+}$ is the intensity of the H_3O^+ ion; $I_{\text{H}_3\text{O}^+\cdot\text{H}_2\text{O}}$ the intensity of the $\text{H}_3\text{O}^+\cdot\text{H}_2\text{O}$ ion; and m , a , b , c , and d are regression parameters that are fitted. In the equations where more than one reagent and product ion was included (e.g., water clusters of product ions), the different ions were indexed by i and j .

1. Calibration for each humidity:

a. Absolute product ion intensities:

$$I_P = m \cdot \chi_P + c. \quad (2)$$

b. Relative product ion intensities:

$$\frac{I_P}{I_R} = m \cdot \chi_P + c. \quad (3)$$

2. Calibration with linear humidity dependence:

a. Absolute product ion intensities:

$$\chi = m_1 \cdot I_P + m_2 \cdot \phi + c. \quad (4)$$

b. Relative product ion intensities:

$$\chi = m_1 \cdot \frac{I_P}{I_R} + m_2 \cdot \frac{I_{\text{H}_3\text{O}^+}}{I_{\text{H}_3\text{O}^+\cdot\text{H}_2\text{O}}} + c. \quad (5)$$

3. Based on the instrument's concentration result,

$$\chi_{\text{substance}} = \chi_{\text{measured}} \cdot \frac{k_1 \cdot I_{\text{H}_3\text{O}^+} + k_2 \cdot I_{\text{H}_3\text{O}^+\cdot\text{H}_2\text{O}}}{c_1 \cdot k_1 \cdot I_{\text{H}_3\text{O}^+} + c_2 \cdot k_2 \cdot I_{\text{H}_3\text{O}^+\cdot\text{H}_2\text{O}}}. \quad (6)$$

4. Calibration derived from physical parameters:

a. Completely de novo:

$$\chi_{\text{substance}} = a \cdot \frac{I_{\text{P}_1^+} + \sum_{i=2}^N (b_i \cdot I_{\text{P}_i^+})}{I_{\text{R}_1^+} + \sum_{j=2}^M (c_j \cdot I_{\text{R}_j^+})} + d. \quad (7)$$

b. Using the instrument calibration function:

$$\chi_{\text{substance}} = a \cdot \frac{\sum_i (I_{\text{P}_i^+} \cdot \text{ICF}_{\text{P}_i})}{I_{\text{R}_1^+} \cdot \text{ICF}_{\text{R}_1} + \sum_j (b_j \cdot I_{\text{R}_j^+} \cdot \text{ICF}_{\text{R}_j})} + c. \quad (8)$$

c. De novo with relative values derived from Eq. (7):

$$\chi_{\text{substance}} = a \cdot \frac{\frac{I_{\text{P}_1^+}}{I_{\text{R}_1^+}} + \sum_{i=2}^N \left(b_i \cdot \frac{I_{\text{P}_i^+}}{I_{\text{R}_1^+}} \right)}{1 + \sum_{j=2}^M \left(c_j \cdot \frac{I_{\text{R}_j^+}}{I_{\text{R}_1^+}} \right)} + d. \quad (9)$$

From the raw data taken at each calibration point, the five datapoints before the last datapoint were used for the regression to minimize the effect of instable flows. Based on the blank measurement, the critical intensity was calculated by Eq. (10).

$$I_{\text{crit}} = \bar{I}_{\text{Blank}} + 3 \cdot \text{SD}(I_{\text{Blank}}) \quad (10)$$

Only calibration points with means above the critical value were included in the regression. The evaluated ions are shown in Table S4. For the sake of simplicity, we will refer to the individual ions by m/z (reagent ion)/ m/z (product ion)/analyte, e.g., 19 u/33 u/methanol, throughout the paper.

To assess the quality of the regression models, the Bayesian information criterion (BIC) was calculated for each regression of the different compounds; see Eq. (11). Based on the variance in the residuals, it gives a measure of how well the model fits – a lower value shows a better fit of the model. In comparison to Akaike's information criterion, it more strongly punishes a higher number of parameters (Veres, 1990).

$$\text{BIC} = n \log(\hat{\sigma}_{\text{R}}^2) + k \log(n) \quad (11)$$

n is the number of samples; $\hat{\sigma}_{\text{R}}^2$ is the variance of the residuals; k is the number of model parameters.

The BICs were calculated individually for each compound, but to get an overall idea on how the regression functions perform, mean, median, maximum, and minimum of the BIC values of the compound obtained for each method were compared; see Table S5.

For the comparison of the SIFT-MS with the PTR-MS, each humidity was compared separately from the others following a basic calibration function; see Eq. (12).

$$\frac{I_{\text{product ion}}}{I_{\text{reagent ion}}} \cdot 10^6 = m \cdot \chi_{\text{substance}} + c \quad (12)$$

The limit of detection (LOD) was estimated to be 3 times the standard deviation of the blank. The sensitivity was defined as the change in signal response by mixing ratio change, i.e., the slope of the respective calibration function. The confidence interval (CI) of the sensitivity was calculated as Eq. (13).

$$\text{CI}_{m, 95\%} = t_{(p=95\%, df=26)} \cdot \frac{s_{y,x}}{\sqrt{\text{SS}_{xx}}} \quad (13)$$

$t_{(p=95\%, df=26)}$ is the 95 % value of Student's t distribution for 26 degrees of freedom; $s_{y,x}$ is the residual standard deviation, and $\text{SS}_{xx} = \sum_i (x_i - \bar{x})^2$ is the sum of squares of the mixing ratios.

The signal-to-noise ratio was calculated by dividing the normalized product ion intensity at 1 ppb standard gas by the normalized product ion intensity of the blank (no VOC standard), Eq. (14).

$$\text{SNR} = \frac{I_{1 \text{ ppb}}}{I_{\text{Blank}}} \quad (14)$$

For the signal-to-noise ratio, upper and lower CIs were calculated separately, the upper CI by Eq. (15), the lower CI as Eq. (16), where $\text{SD}()$ is the standard deviation of the respective intensity.

$$\text{CI}_{\text{SNR}, 95\%}^{\text{u}} = t_{p=95\%, df=7} \cdot \left(\frac{I_{1 \text{ ppb}} + \text{SD}(I_{1 \text{ ppb}})}{I_{\text{Blank}} - \text{SD}(I_{\text{Blank}})} - \text{SNR} \right) \quad (15)$$

$$\text{CI}_{\text{SNR}, 95\%}^{\text{l}} = t_{p=95\%, df=7} \cdot \left(\text{SNR} - \frac{I_{1 \text{ ppb}} - \text{SD}(I_{1 \text{ ppb}})}{I_{\text{Blank}} + \text{SD}(I_{\text{Blank}})} \right) \quad (16)$$

2.4 Comparison of SIFT-MS and PTR-MS

The SIFT-MS was compared to a PTR-QMS 500 (Ionicon, Austria) by calibrating both instruments in the same manner as Sect. 2.3. For the calibrations, 10 measurements were performed at each mixing ratio for each level of humidity. For both instruments, the ion dwell time was set to 500 ms to ensure comparability. The α -pinene masses $m/z = 81$ and 137 u (H_3O^+ reagent ion) were measured for 1 s. The masses measured for the different compounds can be found in Table S1. The counts were normalized to 10^6 counts of the reagent ion. The PTR-MS was operated at $E/N = 136 \text{ Td}$ (inlet temperature 85 °C; drift tube temperature 60 °C; drift tube voltage 600 V; drift tube pressure 2.25 mbar), and the counts of $m/z = 19 \text{ u}$ were inferred from its isotopic peak, $m/z = 21 \text{ u}$.

2.5 SIFT-MS robustness over time

To test the SIFT-MS robustness over time, we did three calibrations as described in Sect. 2.3 for 60 % humidity at 1 d (day 1) and repeated this 1 week later (day 8). All calibration curves were fitted with a linear regression. The significant difference of the slopes and intercepts of the 2 d was tested using an F test ($p = 95\%$, Bonferroni-corrected to

99.86 %, $n = 37$), and depending on the result of the F test, the homogeneous-variance or heterogeneous variance t test ($p = 95$ %, Bonferroni-corrected to 99.86 %, for the correction $n = 37$) was applied. In addition to that, the 2 ppb calibration points from day 1 and day 8 were compared using a Bartlett test and an ANOVA ($p = 95$ %, Bonferroni-corrected to 99.935 %, for the correction $n = 77$). Their relative standard deviation was calculated.

To evaluate a longer timescale, the measurement of a standard gas mixture of benzene, *o*-xylene, octafluorotoluene, hexafluorobenzene, ethylene, isobutane, tetrafluorobenzene, and toluene (2 ppm each in nitrogen; Syft, New Zealand) on each working day was evaluated. A Neumann trend test was used to test for trends ($p = 95$ %; $n = 10$).

To see the effect of venting the instrument on the calibrations, e.g., for maintenance or reparations, calibrations done in May 2018, December 2018, and January 2019, before and after the O-ring change and a detector shutdown, were conducted and compared as described above.

3 Results and discussion

Complete results of the different combinations of humidity conditions, carrier gas, flow tube temperature and voltage are given in the Supplement; here we show selected comparisons under a subset of experiments and conditions that best illustrate the performance of the SIFT-MS and how it compares to the PTR-MS.

3.1 SIFT-MS-optimization to improve sensitivity

Several changes were applied to the SIFT-MS to improve its limit of detection, inspired by the parameter optimizations done by Marvin Shaw (University of York, unpublished results) but considering different sample humidities. Amongst others, the inlet capillary was replaced by a needle valve (see Fig. S1), and all the O-rings in the instrument were replaced with FEP-coated FKM O-rings (see Fig. S2). All measures led to a significant reduction of the instrument background, by up to factor 5 for some masses (see Fig. S2).

Besides the hardware changes, we also optimized a number of running parameters, including the flow tube voltage, flow tube temperature, carrier gas flow, and sample gas flow. The observed effects of water clustering, adduct formation, fragmentation, and humidity sensitivity match the theoretical considerations of Smith and Spanel (2005):

As was expected, the product ions increase with increasing sample gas flow in most cases (see Fig. 2 or Figs. S3 and S4 for complete results), and also water clustering increases. However, we were surprised to see that the effect of water clustering was not critical for the chosen settings: the amount of unreactive $\text{H}_3\text{O}^+ \cdot 2\text{H}_2\text{O}$ ($m/z = 55$ u) was negligible, and no H_3O^+ signals were visible in the other two reagent ion channels. For methanol, one can already observe the effect of

an increased amount of $\text{H}_3\text{O}^+ \cdot 2\text{H}_2\text{O}$ with increasing sample gas flow, leading to less background on $m/z = 33$ u as also shown by de Guow and Warneke (2007). However, this experiment was performed at a medium humidity with a sample gas flow of 125 sccm. To further decrease the amount of $\text{H}_3\text{O}^+ \cdot \text{H}_2\text{O}$ formed, flow tube voltage and temperature as well as the carrier gas flow were also optimized.

With higher flow tube voltage, i.e., a higher kinetic energy of the ions, we expected (i) a higher reaction efficiency in general, leading to more ions; (ii) more secondary reagent ions, e.g., more H_3O^+ when O_2^+ was the reagent ion; (iii) less water clustering; (iv) less adduct formation; and (v) more fragmentation. In Fig. 2b (Fig. S6 for all ions), one can see that (iii) and (iv) are definitely true, (v) does occur a bit, but hardly at all, and (i) and (ii) did not occur the way we expected it. For (i), we assume that this is due to the fact that a third particle is needed in order to take up excess kinetic energy. If the kinetic energy is too high, the collisional cross section is too small, and the partner cannot take up the excess, and the reaction partners move away from each other again, as described by Smith and Spanel (2005). Interestingly, overall reagent ion counts of NO^+ and O_2^+ decrease at higher flow tube voltage, but the other ion counts do not increase at the same rate. We are unsure what causes this since we expected to see increased signals resulting from increased focusing of the ions. Perhaps they are hitting one of the accelerating electrodes instead of being focused by the lenses, or their increased kinetic energy leads to a stronger deviation from the ideal ion path. In newer PTR-MS instruments, for example the PTR3 (Breitenlechner et al., 2017) and the Vocus PTR-ToF (Krechmer et al., 2018), such effects have been overcome by applying an additional focusing field. A similar modification could also be considered to further improve SIFT-MS sensitivity. We chose to use a flow tube voltage of 40 V as a compromise between increased water clustering and losing NO^+ and O_2^+ reagent ions.

Increasing the flow tube temperature also increases the kinetic energy but randomly and for all molecules inside the flow tube, not just the ions. We expect effects of increased temperature to be similar to those for increased flow tube voltage but instead found that the effects are rather small. One can see a slight decrease in product ion counts – see Fig. 4 (Fig. S5 for all ions) – with increased flow tube temperature. However, reagent ion counts indicated a major shift due to decreases in interfering ions. Thus, a flow tube temperature as high as possible appears to be advantageous. However, we were concerned that for environmental samples, too high a temperature would reduce detection of more labile compounds with low thermal stability. Therefore, we decided on a flow tube temperature of 140 °C.

Increasing the carrier gas flow while keeping the sample gas flow stable meant increasing the pressure in the flow tube. This both decreases the main free path of the ions and provides more collision partners. While reactions are expected to be more efficient since surplus reaction can be dissipated

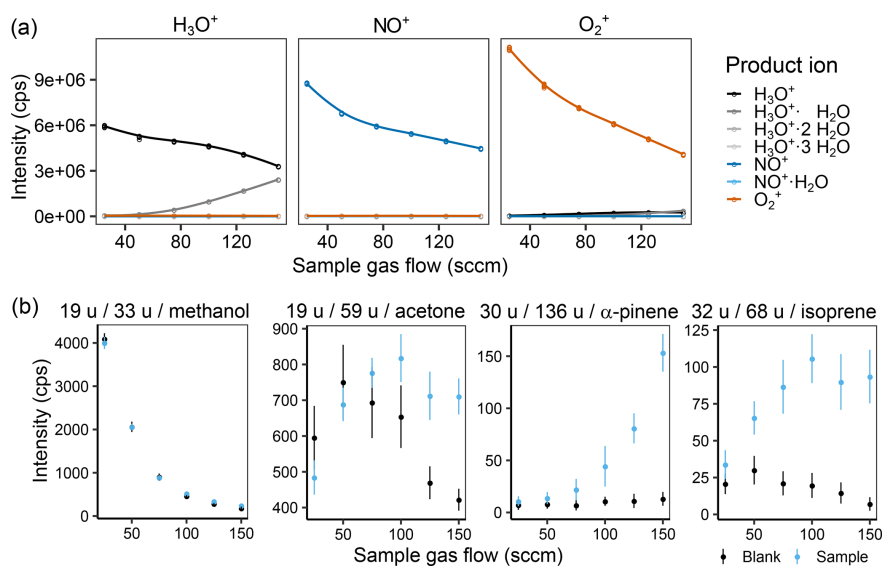


Figure 2. (a) Effect of the sample gas flow on the intensity of the different measured product ions when selecting for H_3O^+ (left), NO^+ (middle), and O_2^+ (right) in the first quadrupole and (b) the product ion intensity for a zero air blank and a 1 ppb VOC standard sample for methanol, acetone, α -pinene, and isoprene at 60% humidity (25 °C). In (b), the captions are labeled with m/z of the reagent ion, m/z of the product ion, and the corresponding substance. The helium carrier gas flow was kept at 158 sccm (2 TorrL s⁻¹).

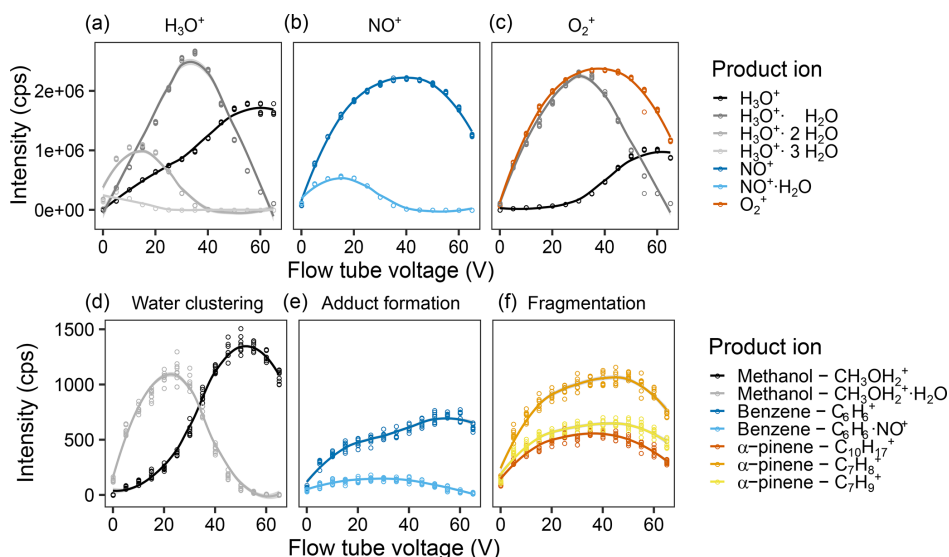


Figure 3. Effect of the flow tube voltage on reagent and product ion counts. Intensity of the different measured product ions when selecting for (a) H_3O^+ , (b) NO^+ , and (c) O_2^+ in the first quadrupole. Examples of the product ion behavior illustrating (d) the effect of water clustering on the methanol ions reacting with H_3O^+ , (e) adduct formation on the benzene ions upon reaction with NO^+ , and (f) fragmentation of the α -pinene ions upon reaction with O_2^+ . Measurements were done for a humid (90% at 25 °C) 5 ppb VOC standard air flow and were fit via LOESS. For the results of all ions, see Fig. S9.

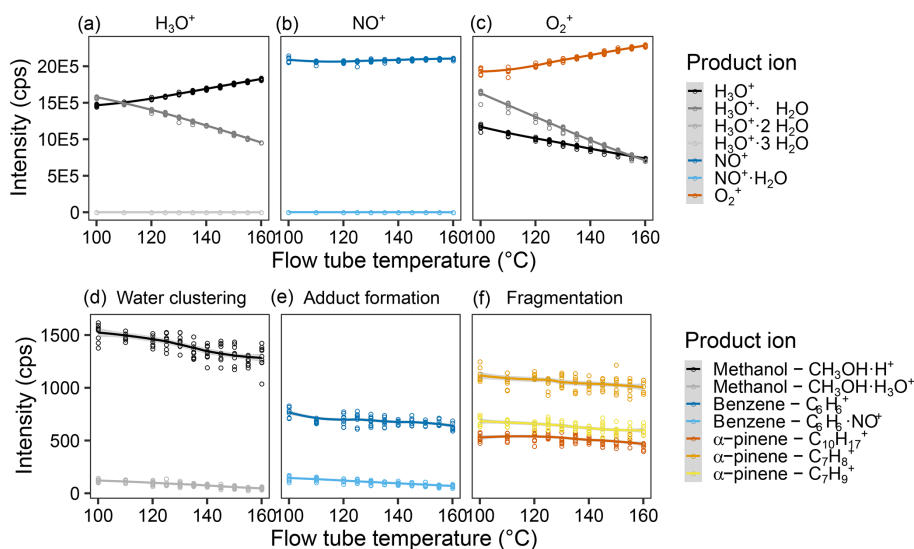


Figure 4. Effect of the flow tube temperature on reagent and product ion counts. Intensity of the different measured product ions when selecting for (a) H_3O^+ , (b) NO^+ , and (c) O_2^+ in the first quadrupole. Examples of the product ion behavior illustrating (d) the effect of water clustering on the methanol ions reacting with H_3O^+ , (e) adduct formation on the benzene ions upon reaction with NO^+ , and (f) fragmentation of the α -pinene ions upon reaction with O_2^+ . Measurements were done for a humid (90 % at 25 °C) 5 ppb VOC standard air flow and were fit via LOESS. For results of all measured ions, see Fig. S8.

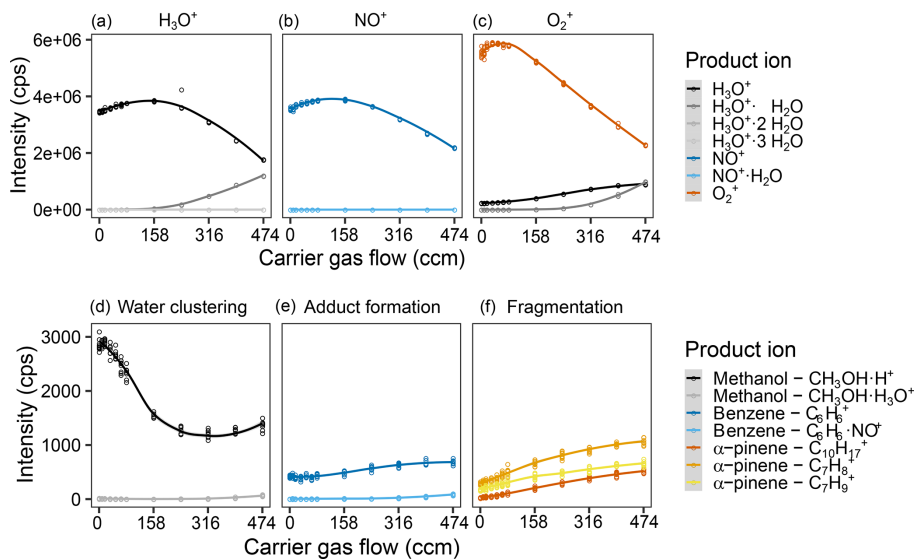


Figure 5. Effect of the helium carrier gas flow on reagent and product ion counts. Intensity of the different measured product ions when selecting for (a) H_3O^+ , (b) NO^+ , and (c) O_2^+ in the first quadrupole. Examples of the product ion behavior illustrating (d) the effect of water clustering on the methanol ions reacting with H_3O^+ , (e) adduct formation on the benzene ions upon reaction with NO^+ , and (f) fragmentation of the α -pinene ions upon reaction with O_2^+ . Measurements were done for a humid (90 % at 25 °C) 5 ppb VOC standard air flow and were fit via LOESS. The sample gas flow was 120 sccm (capillary with 0.010" inner diameter). For complete results of all measured ions, see Fig. S7.

more easily, the same dissipation will form ions with less average energy (closer to thermal equilibrium). The colder ions should be easier to focus leading to less diffusive loss to the flow tube walls, but the increased number of collisions should deflect ions more strongly. We observe an optimum for the reagent ion counts (approx. 200 ccm for H_3O^+ and NO^+ , 50 ccm for O_2^+) with strong intensity decreases afterwards. Product ion counts increase with higher carrier gas flows, but interestingly, the ratios do not seem to change strongly (cf. Figs. 5, S3 and S4). The decreasing reagent ion counts and increasing product ion counts are probably a result of the increased reaction efficiency. The increase in reagent ion counts is probably due to a minimized diffusive loss up to a certain point, before the increased reaction efficiency and increased ion deflection by collisions outweigh this effect. It is interesting that we do not see changes in adduct formation patterns and fragmentation patterns, as we expected adducts to be destabilized and fragmentations to be pushed towards the most stable ions by the increased number of collisions. The behavior of methanol was unexpected as well. Its counts are highest for low carrier gas flows, which counteracts the trends of the other product ions. What causes this is unclear but might be due to a contamination in the system, as a similar effect is observed for sample gas flows; cf. Fig. 2. For a carrier gas flow, 312 ccm (4 TorrL s^{-1}) were chosen to ensure high product ion counts while not losing too much reagent ion intensity.

We also tested helium and nitrogen as carrier gases, by optimizing the operating conditions with this carrier gas (Figs. S3–S10) and calibration (Tables S2–S4 in the Supplement) at the optimized values. We observed not only higher sensitivity using nitrogen carrier gas but also higher LODs and lower SNRs at 1 ppb. Further, humidity sensitivity of the reagent ions was also higher with nitrogen carrier gas, as was instrument background. In both cases 6.0-quality gases were used, and the nitrogen was even further purified with a filter, so that total amount of impurities should be similar for both gases. We thus attribute the higher background we observed with nitrogen to the higher collisional cross section of nitrogen molecules compared to helium atoms, which might have caused a higher ionization efficiency of the impurities in the nitrogen and the instrument itself, basically increasing the visibility of the impurities by increasing the amount of ionized background analytes. We also attribute the higher sensitivity we observed with nitrogen to the higher ionization efficiency. Final running conditions for the SIFT-MS were as follows: 40 V, 140 °C, 158 ccm (2 TorrL s^{-1}) helium, and 100 sccm sample.

3.2 SIFT-MS robustness over time

The company advertises that the SIFT-MS instrument is very stable in the long term, that you do not need to calibrate but can just use their daily validation routine for quality assurance (Syft Technologies Ltd., 2019). To test this, we per-

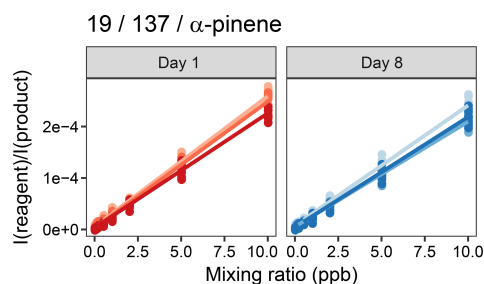


Figure 6. Robustness of the α -pinene calibration of the SIFT-MS. Three calibrations were conducted at 1 d and 1 week later, on day 8. Slopes and intercepts were not significantly different ($p = 0.9986$; $n = 3$) between the days.

formed three calibrations at 60 % humidity at 1 d (day 1) and repeated this 1 week later (day 8). Standard calibration curves for α -pinene are shown in Fig. 6. Results obtained on the 2 d were compared using F and t tests on the slopes and the intercepts of the calibration curves, performed separately for each reagent ion. The slopes were not heteroscedastic, and differences between the 2 d were not statistically significant ($p = 95\%$), whereas the F tests failed for the intercepts. The heterogeneous variance t tests on the intercepts again did not show statistically significant differences between the intercepts of day 1 and day 8 ($p = 95\%$). Thus, both calibrations were not significantly different between both days, so a calibration can be used for at least a week.

In addition, we tested the variance in signal intensity of the 2 ppb calibration point with time. Here, we included the two interacting factors, to which day and to which calibration of the raw data measurements belong. The Bartlett tests did not show heteroscedasticity, and the two-way ANOVA with the two interacting factors day and number of calibration only showed significant difference of the day for the ion 19 u/75 u/acrolein/ $\text{C}_3\text{H}_5\text{O}^+ \cdot \text{H}_2\text{O}$, i.e., the water cluster of acrolein. Perhaps the air humidity of the produced calibration standard varied enough to make it statistically significant. Thus, over the course of a week, the calibrations appear to be stable and can be used to calculate mixing ratios. We are not aware of a similar study published; however, Ammann et al. (2004) showed loss of detector signal intensity over a period of 2 months during their field experiment with PTR-MS. When comparing the signal intensity measured during weekly validation of the instrument, we observe the same trend (Fig. S12). A Neumann trend test was negative for the ions ($p = 95\%$; $n = 10$), but the signal appears to be dropping, and the trends might become significant over a longer time period. Combining the two experiments, we conclude that the calibration is stable over the course of days to weeks.

To test the robustness of calibrations over longer time periods, we compared the calibrations performed in May, December, and January. This time span included changes to the

instrument such as the O-ring change and a detector crash. We observed considerable variation in LOD and sensitivity (Fig. S13), indicating that calibrations need to be performed regularly, especially following repair or instrument maintenance. Syft tackles this problem by providing a daily automated validation procedure, but this only validates at 2 ppm of the standard substances in dry air. We adjusted the procedure to our low-mixing-ratio regime by diluting the standard to 20 ppb for validation. For routine measurements of a rather stable system with rather high mixing ratios (above ppb level), e.g., clean room air quality monitoring, the standard procedure using a multiple-gas standard and daily validation with the adapted Syft routine should be sufficient. However, for accurate quantification of dilute analytes in a varying system with different humidities, for example our soil VOC emission monitoring during dry-out-incubations from flooded to dry soil, we recommend calibrating the instrument before every experiment series.

3.3 Humidity dependence of product ion intensities of the SIFT-MS

Humidity can have a large influence on the product ion intensity when H_3O^+ reagent ions are used. For example, α -pinene at 10 ppb loses approximately one-fourth of the (H_3O^+) product ion intensity, whereas the product ion intensity upon reaction with NO^+ or O_2^+ remains stable; see Fig. 7. Even for H_3O^+ ions, influences are mixed – for lower-mass molecules like methanol (Fig. S13) and lower mixing ratios (α -pinene, Fig. 7), the effect appears to be less prominent.

For methanol, the intensity decrease of $m/z = 33$ u matches the intensity increase of $m/z = 51$ u, the water cluster (Fig. S13). Both are ca. 50 cps for the humidity increase from 30 % to 90 %. This could reflect either an increased association of water to protonated methanol in a three-body association involving a third collision partner M that takes up excess energy ($\text{CH}_3\text{OH} \cdot \text{H}^+ + \text{H}_2\text{O} + \text{M} \rightarrow \text{CH}_3\text{OH} \cdot \text{H}^+ \cdot \text{H}_2\text{O} + \text{M}^*$) or an increased ionization of methanol by $\text{H}_3\text{O}^+ \cdot \text{H}_2\text{O}$, where one water ligand is exchanged for methanol ($\text{CH}_3\text{OH} + \text{H}_3\text{O}^+ \cdot \text{H}_2\text{O} \rightarrow \text{CH}_3\text{OH} \cdot \text{H}_3\text{O}^+ + \text{H}_2\text{O}$) (Smith and Spanel, 2000). $\text{CH}_3\text{OH} \cdot \text{H}^+ \cdot 2\text{H}_2\text{O}$ (m/z (H_3O^+) = 69 u) could not be observed directly, as we used a mixed VOC standard, and at this m/z , isoprene is also detected. A quick calculation of the isoprene signal we should see based on the isoprene signal we see at m/z (NO^+) = 68 u showed us that most of the observed signal should be from isoprene, and if at all only a minor amount of the methanol dihydrate ion should be present. For the exact calculation, please refer to the Sect. S4.1 in the Supplement.

However, for acetaldehyde, we do not see the same effect – a decrease of ca. 250 cps from 30 % to 90 % humidity is accompanied by an increase of ca. 50 cps of the water cluster (Fig. S14). This difference can also not be explained if one assumes that the protonated product is the

product of the reaction with H_3O^+ and the water cluster is the product of the reaction with $\text{H}_3\text{O}^+ \cdot \text{H}_2\text{O}$ – the reaction rate difference is rather insignificant (3.7×10^{-9} vs. 3.1×10^{-9} $\text{cm}^3 \text{ molecule}^{-1} \text{ s}^{-1}$).

Overall, for acetaldehyde, acetonitrile, and ethanol, the water cluster intensity rise does not match the intensity of decline of the primary product ion, whereas for methanol and acrolein, it does. Thus, high moisture sensitivity of the compound appears to correspond to this mismatch, whereas a low moisture sensitivity avoids it. In accordance with Wilson et al. (2003), we conclude that a back-reaction of the product ion with water occurs via a ligand exchange of $\text{H}_3\text{O}^+ \cdot \text{M}$. The analyte M is exchanged by water again and thus not part of the ion anymore, leaving a thermally colder reagent ion behind: e.g., $\text{CH}_3\text{CHO} \cdot \text{H}_3\text{O}^+ + \text{H}_2\text{O} \rightarrow \text{H}_3\text{O}^+ \cdot \text{H}_2\text{O} + \text{CH}_3\text{CHO}$ (Spanel and Smith, 1998). This affinity to H_3O^+ should correspond to the proton affinity of the compound, as H_3O^+ is essentially a proton with one water ligand associated. Kebarle et al. (1976) published proton affinities of 187.3, 196.8, 185.4, and 182.3 kcal mol^{-1} for acetaldehyde, ethanol, acetonitrile, and methanol, respectively. The difference was greatest for ethanol, having the highest proton affinity, and smallest for methanol. Only acrolein does not fit in this picture as it has a proton affinity of 190.4 kcal mol^{-1} (Del Bene, 1978), but since this value is from a different source, it might have been calculated differently.

We further evaluated the effect of humidity when normalizing the product ion counts to the reagent ion counts. Figures 8 and S15 show that whether the absolute signal is humidity sensitive or not, both cases show a linear humidity dependence after being normalized. For all gases we tested, linear humidity dependence was observed for calibrations performed between 30 %–90 % relative humidity, when product ion counts were normalized to reagent counts. Usually, the dry samples were in line with the other results as well. This is not the case for toluene at lower mixing ratios: in dry air, the relative intensity is lower than for humid samples, but for the humidified samples, the trend is the same as for higher mixing ratios. This might be caused by problems with the bypass line of the humidifiers.

3.4 Evaluation of calibration procedures

To account for humidity effects on ion counts, several calibration procedures were tested. When using the chosen settings, the humidity has to be taken into account.

For the humidity-sensitive ions, we first investigated whether the humidity is better represented by the actual relative humidity or the ratio of the water cluster intensities, $\frac{I(\text{H}_3\text{O}^+ \cdot \text{H}_2\text{O})}{I(\text{H}_3\text{O}^+)}$. Since the ratio of the intensities correlates quite linearly with the relative humidity (Fig. S16) and is easy to measure in situ, the representation of the humidity as the intensity ratio appears to be more useful. Second, we tried normalizing to both $I(\text{H}_3\text{O}^+)$ and $I(\text{H}_3\text{O}^+) + I(\text{H}_3\text{O}^+ \cdot \text{H}_2\text{O})$.

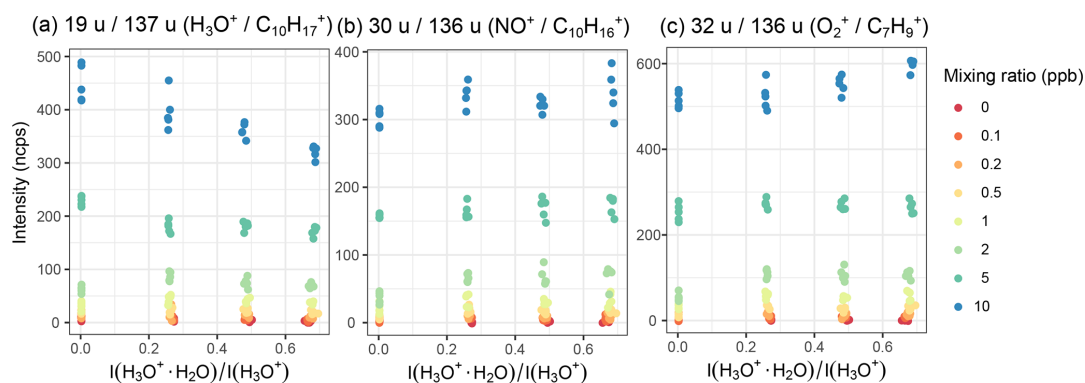


Figure 7. Humidity dependence of α -pinene signal at mixing ratios between 0.1 and 10 ppb upon reaction with the different reagent ions (a) H_3O^+ , (b) NO^+ , and (c) O_2^+ forming the product ions $\text{C}_{10}\text{H}_{17}^+$, $\text{C}_{10}\text{H}_{16}^+$, and C_7H_9^+ . Humidity is measured as the ratio of the $\text{H}_3\text{O}^+\cdot\text{H}_2\text{O}$ and the H_3O^+ intensity; cf. Fig. S20.

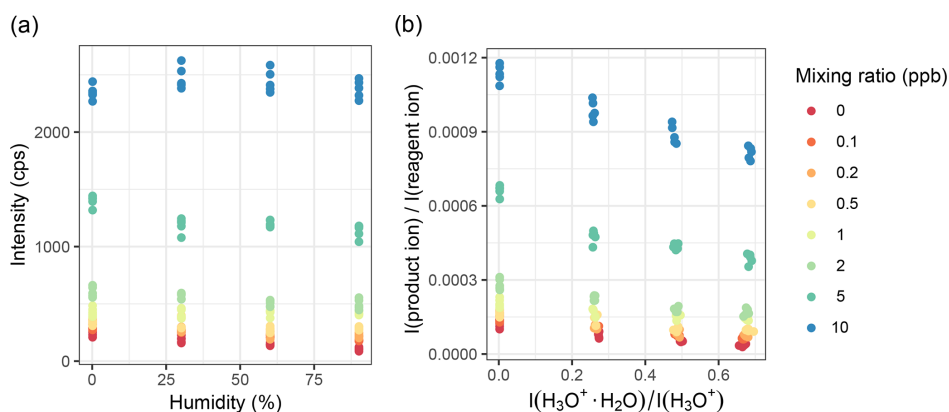


Figure 8. Humidity dependence of methanol $m/z = 33$ u intensity. (a) Absolute counts vs. relative humidity at 25 °C. (b) Relative intensity per reagent intensity vs. the ratio of H_3O^+ and its first water cluster as a measure of humidity.

Normalizing to both reagent ions makes the ion count more humidity dependent, but it also appears to make the humidity dependence more linear and decrease the variance in the data, (Fig. S17). Thus, we decided to normalize to both reagent ions. One has to keep in mind though that this is only valid if they react with the analyte on a similar rate. If the kinetic rate constants are too different, the influence of the two reacting ions is not equal, so they should be treated differently. This is also why higher water clusters were not considered – they generally react roughly 1000 times slower.

To account for air humidity in the calibration, we tested the different methods described in the Experimental section. Binning experimental results into humidity categories of 0 %, 30 %, 60 %, and 90 % as proposed in Eqs. (2) and (3) is very uncertain when applied to intermediate humidity (e.g., 45 %) where both calibration curves are not very close. Assuming a linear humidity dependence as in Eqs. (4) and (5) does not necessarily reflect the trends observed for lower mixing ra-

tios, e.g., Fig. S15 where responses are not as linear. In addition, a correction of the mixing ratio the instrument calculates was tested. This should be done carefully, as the results of all three reagent ions are averaged by the instrument if they do not differ too strongly, so one might actually induce error by correcting for humidity when the analyte is measured by multiple reagent ions. The most exact version is calibration function Eq. (7), which is derived from the function Syft uses to calculate mixing ratios based on the instrument parameters; Eq. (17):

$$\chi = k_B \cdot \frac{T_{\text{FT}}}{P_{\text{FT}}} \cdot \left(\frac{\varphi_{\text{carr}}}{\varphi_{\text{samp}}} + 1 \right) \cdot \frac{\sum_{i=1}^N (I_{P_i} \cdot \text{ICF}_{P_i})}{t_r \cdot b_{r_i} \cdot \sum_{j=1}^M (k_j \cdot I_{R_j} \cdot \text{ICF}_{R_j})}, \quad (17)$$

where k_B is the Boltzmann constant, T_{FT} is the flow tube temperature, P_{FT} is the flow tube pressure, φ_{carr} and φ_{samp} are the carrier gas and sample gas flows, I_{P_i} and I_{R_j} are product and reagent ion counts, ICF experimentally determined is the instrument calibration factor accounting for ion discrimination

of each ion, t_r is the reaction time, br_i is the branching ratio of the ion, and k_j is the rate constant of the reaction of the reagent ion with the analyte to form the product ion.

However, Eq. (8) quickly increases the number of parameters that need to be fitted. For example for methanol, the equation would be

$$\chi \text{ (ppbv)} = a \cdot \frac{I(\text{CH}_3\text{OH}_2^+) + b \cdot I(\text{CH}_3\text{OH}_2^+ \cdot \text{H}_2\text{O})}{I(\text{H}_3\text{O}^+) + c \cdot I(\text{H}_3\text{O}^+ \cdot \text{H}_2\text{O})} + d. \quad (18)$$

This is a 4D problem with four parameters. It cannot easily be plotted in two dimensions to see the quality of the fit, so one has to rely on the results of the fit without checking it visually. Using the ICFs determined during the validation reduces the number of fitted parameters, but still not the number of dimensions. The most versatile method we found is Eq. (9), derived from Eq. (7) by multiplying the fraction by $\frac{1}{I(\text{H}_3\text{O}^+) \cdot I(\text{H}_3\text{O}^+)}$. This way, the equation is reduced by one dimension, so that if there are no product ion water clusters, one can visualize the results in a 3D plot; see Fig. 9. As expected, the equation fits the data with a minimum of physical parameters without relying on experimentally determined parameters other than the ion intensities.

To compare the models, the Bayesian information criterion (BIC) was calculated for the calibration of each substance by each method; cf. Table S6. Although the BIC punishes for a larger number of parameters, still, Eqs. (7) and (9), the calibration functions based on actual theoretical considerations, consistently have the smallest BIC and thus fit the data best. This fits the considerations above. Thus, for humidity-dependent ions, this is the method of choice.

3.5 Comparison of SIFT-MS to PTR-MS

The optimized SIFT-MS was compared to our PTR-QMS 500 using the diluted Ionicon calibration standard (mixing ratios between 0.25 and 10 ppb) and for each mixing ratio at 10 %, 30 %, 60 %, and 90 % relative humidity (25 °C). Since to the knowledge of the authors parameters that access the quality of a calibration like LOD, sensitivity, SNR, precision, and robustness are only established for a 2D calibration curve, for the following comparison with the PTR-MS, we used the simple humidity-independent regression based on normalized ion counts, Eq. (3). This is the most accessible and the easiest to compare with the PTR-MS, especially because the humidity is known and does not need to be compared by $I(\text{H}_3\text{O}^+ \cdot \text{H}_2\text{O})/I(\text{H}_3\text{O}^+)$. In the graphs, the results for 30 % humidity are shown, and the results for all humidities are summarized in Tables S7–S12. The PTR-MS was operated at $E/N = 136 \text{ Td}$ with an inlet line temperature of 85 °C to reduce water clusters of the product ions and possible condensation of water droplets in the tube. The authors are aware that this increases fragmentation reactions; however, we found the settings to work well for humid samples: the formation of $m/z = 37 \text{ u}$ and water clusters of product ions is reduced substantially. Also, we reduced the risk of

water and VOCs condensing in the inlet tubes by using the stated high inlet temperature and drift tube temperature.

At all humidities, the limit of detection (LOD) was lower for our PTR-MS. While the LOD of the PTR-MS is between 10 and 100 ppt for most masses, the LODs of the SIFT-MS are generally 1 order of magnitude higher, between 100 ppt and 1 ppb; see Fig. 10 and Tables S7–S8. For PTR-QMS-systems, this matches the LODs reported for other instruments as well (Yuan et al., 2017). This is probably due to three factors. First, the flow into the PTR-MS is about 3 times as high, so that more analyte is ionized. Second, the reagent ion counts (e.g., H_3O^+) are twice as high for the PTR-MS, doubling the number of product ions, and thus more are detected. This was also discussed by Smith et al. (2014), who also report lower LODs for PTR-MS in their review. Third, the variation in the signal over time is much lower for PTR-MS, maybe due to more stable conditions and longer reaction times (approx. 5 ms in SIFT-MS vs. 0.2–1 s in PTR-MS; de Gouw and Warneke, 2007) in the flow tube. This can also be inferred from the calibration curves of Lourenço et al. (2017), as their R^2 value is lower for SIFT-MS than for PTR-MS. However, the difference in LOD between the instruments is smaller than was previously found. Blake et al. (2009), estimated a difference of 2 orders of magnitude, whereas we found only 1 order of magnitude. On the other hand, Milligan et al. (2007) presented a SIFT-MS with LODs in the mid-ppt range, so very low values are possible on custom-built instruments, and for PTR-MS, the PTR-Qi-TOF (Sulzer et al., 2014) and the Vocus PTR-TOF (Krechmer et al., 2018) even have LODs reported below ppt for 1 s scan time. Still, instrument improvements by Syft over the last 10 years as well as our improvements to the SIFT-MS instrument significantly improved LOD.

For the sensitivity analysis, the slopes of the calibration curve based on ion intensities normalized to 10^6 reagent ions were compared. In general, the SIFT-MS is more sensitive than the tested PTR-MS and appears to become even more sensitive the higher the m/z ratio becomes: for methanol, both instruments are comparable; for toluene, the sensitivity is at least twice as high; see Fig. S18 and Tables S9–S10. These results are different from the results of Lourenço et al. (2017), where PTR-MS shows a higher sensitivity by a factor of 10, and even higher sensitivities have been reported for the most recent PTR-MS developments (Sulzer et al., 2014; Breitenlechner et al., 2017; Krechmer et al., 2018), but match the reports of Prince et al. (2010) for SIFT-MS sensitivity. Still, due to a higher precision of the PTR-MS data that is also reflected in the much lower LOD, the signal-to-noise ratio at 1 ppb is still much higher for the PTR-MS than for the SIFT-MS.

This also influences the signal-to-noise ratios; see Fig. S19 and Tables S11–S12. For smaller masses, the tested PTR-MS has a much higher SNR, whereas for the higher masses of the aromatic molecules like dichlorobenzene, *o*-xylene, and toluene, the SIFT-MS has a higher SNR. With these

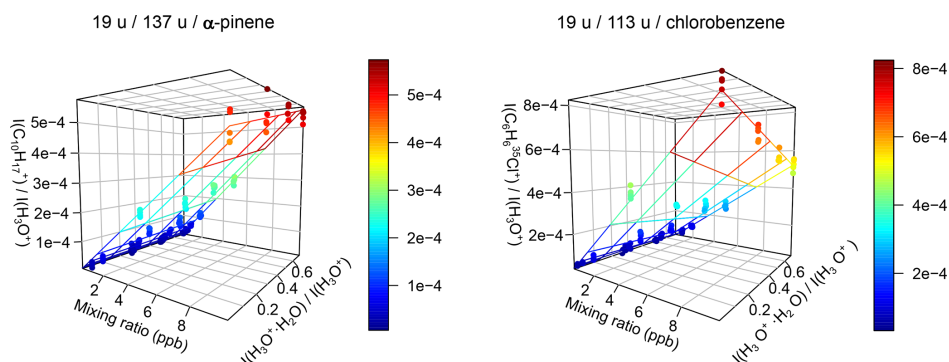


Figure 9. Relative product ion intensities and calibration plane for α -pinene and chlorobenzene using Eq. (9). Even strong humidity dependence like for chlorobenzene is accounted for using this method. $I(\text{C}_{10}\text{H}_{17}^+)/I(\text{H}_3\text{O}^+)$ and $I(\text{C}_6\text{H}_6^{35}\text{Cl}^+)/I(\text{H}_3\text{O}^+)$ are the relative product ion intensities of the two mentioned ions; $I(\text{H}_3\text{O}^+ \cdot \text{H}_2\text{O})/I(\text{H}_3\text{O}^+)$ serves as measure for the humidity.

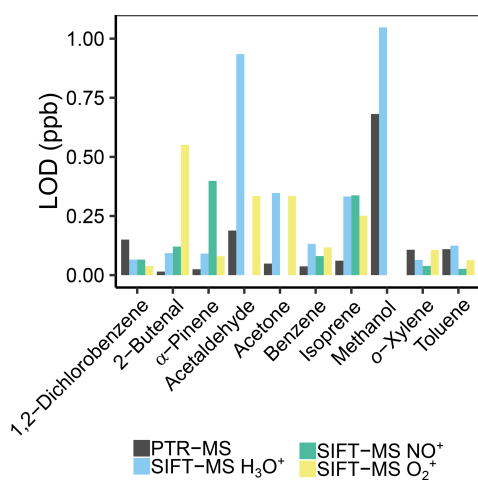


Figure 10. Comparison of the limit of detection (LOD) for PTR-MS and the different reagent ions of the SIFT-MS of the shown VOCs at 30 % humidity.

molecules, the tested PTR-MS has a comparable LOD and a lower sensitivity, so this adds up to a lower SNR. However again, with the higher sensitivity and lower LODs mentioned in the literature (Yuan et al., 2017), a higher signal-to-noise ratio should be found for state-of-the-art PTR-TOF-MS instruments. Still, the SIFT-MS has the advantage that isomeric compounds can be separated by the different reactions with different reagent ions, so for these analytical problems, it is better to use. Plus, the sensitivity is already low enough for regular atmospheric trace gas measurements, so it can be used as a robust lower-cost, easy-to-use alternative to the PTR-MS.

4 Conclusions

We successfully improved a purchased SIFT-MS to meet the requirements of sub-ppb atmospheric trace gas measurements. Hardware improvements like changing O-rings in the purchased instrument for materials with lower degassing and exchanging the capillary in the inlet system with a VICI valve helped reduce the SIFT-MS background. Increasing the sample gas flow by a factor of 5 also improved sensitivity greatly but made adjustments of the carrier gas flow, the flow tube voltage, and temperature necessary. In total, we achieved a decrease of the SIFT-MS LOD by a factor of 10. The humidity dependence resulting from the high sample gas flow could be corrected by a humidity-dependent calibration. The SIFT-MS is stable over shorter time periods, as we could demonstrate by comparing calibrations a week apart that are not significantly different. However, it shows considerable variations in signal intensity over longer periods, so that at least after each maintenance, the instrument should be calibrated. The LOD varied by up to a factor of 2, the sensitivity by up to a factor of 3. This drawback was addressed by Syft by implementing a workdaily validation routine that takes approx. 10 min that we adjusted to work for low mixing ratios, so the instrument calibration factor balancing out the mass discrimination should account for those instabilities. Still, we calibrate our instrument with humidity before every experiment series in addition to the one-point validation of the SIFT-MS procedure.

The comparison of SIFT-MS and PTR-MS confirmed that PTR-MS has a lower LOD than SIFT-MS, though modification of the SIFT-MS instrument improved its LOD to within an order of magnitude of the PTR-QMS. Both instruments are equally sensitive when responding to signal changes and have similar dynamic range. The calibration at multiple humidities demonstrated that PTR-QMS is more humidity dependent than SIFT-MS, indicating that it is important to cali-

brate for the humidity as well or take care that it remains constant during measurements. However, the Vocus PTR-TOF has overcome the humidity dependence by introducing high humidity in the drift tube (Krechmer et al., 2018). Still, the additional structural information that can be gained by SIFT-MS is especially helpful for mixtures of isomers like acetone and propanal. Overall, SIFT-MS is a good lower-cost alternative to PTR-MS for analyzing gases with a more complex mixtures of compounds including isomers at varying humidity.

Code and data availability. Code and data are published as <https://doi.org/10.17617/3.2u> (Lehnert et al., 2019).

Supplement. The supplement related to this article is available online at: <https://doi.org/10.5194/amt-13-3507-2020-supplement>.

Author contributions. The study was designed by A-SL, TB, and GP. Experiments were performed by A-SL with assistance from TB and AR. Data processing and analysis were done by A-SL with assistance from TB and AR. The paper was written by A-SL. All authors assisted with data interpretation and discussion of results and helped to improve the quality of the paper.

Competing interests. The authors declare that they have no conflict of interest.

Acknowledgements. Thanks to Paul Wilson, Vaughan Langford, Mar Viñallonga, and their colleagues at Syft Technologies Inc., New Zealand, for technical assistance during the instrument modifications as well as feedback to methodological considerations. We thank Marvin Shaw (University of York, GB) for input on how to decrease contamination by removing the carrier gas shut down valve. Alexander Ruecker and Ann-Sophie Lehnert received financial support from the Deutsche Forschungsgemeinschaft (DFG) in the frame of the collaborative research center CRC 1076 AquaDiva.

Financial support. The research was funded by the International Max Planck Research School for Global Biogeochemical Cycles and the Collaborative Research Centre AquaDiva (CRC 1076 AquaDiva, Project no 218627073) of the Friedrich Schiller University Jena, funded by the Deutsche Forschungsgemeinschaft.

The article processing charges for this open-access publication were covered by the Max Planck Society.

Review statement. This paper was edited by Joachim Curtius and reviewed by Patrik Spanel and two anonymous referees.

References

- Amelynck, C., Schoon, N., and Dhooghe, F.: SIFT Ion Chemistry Studies Underpinning the Measurement of Volatile Organic Compound Emissions by Vegetation, *Curr. Anal. Chem.*, 9, 540–549, <https://doi.org/10.2174/15734110113099990018>, 2013.
- Ammann, C., Spirig, C., Nefel, A., Steinbacher, M., Komenda, M., and Schaub, A.: Application of PTR-MS for measurements of biogenic VOC in a deciduous forest, *Int. J. Mass Spectrom.*, 239, 87–101, <https://doi.org/10.1016/j.ijms.2004.08.012>, 2004.
- Biasioli, F., Yeretzyan, C., Märk, T. D., Dewulf, J., and Van Langenhove, H.: Direct-injection mass spectrometry adds the time dimension to (B)VOC analysis, *TRAC-Trend. Anal. Chem.*, 30, 1003–1017, <https://doi.org/10.1016/j.trac.2011.04.005>, 2011.
- Blake, R. S., Monks, P. S., and Ellis, A. M.: Proton-Transfer Reaction Mass Spectrometry, *Chem. Rev.*, 109, 861–896, <https://doi.org/10.1021/cr800364q>, 2009.
- Breitenlechner, M., Fischer, L., Hainer, M., Heinritzi, M., Curtius, J., and Hansel, A.: PTR3: An Instrument for Studying the Lifecycle of Reactive Organic Carbon in the Atmosphere, *Anal. Chem.*, 89, 5824–5831, 2017.
- Bylinski, H., Gebicki, J., Dymerski, T., and Namiesnik, J.: Direct Analysis of Samples of Various Origin and Composition Using Specific Types of Mass Spectrometry, *Crit. Rev. Anal. Chem.*, 47, 340–358, <https://doi.org/10.1080/10408347.2017.1298986>, 2017.
- Casas-Ferreira, A. M., Nogal-Sanchez, M. D., Perez-Pavon, J. L., and Moreno-Cordero, B.: Non-separative mass spectrometry methods for non-invasive medical diagnostics based on volatile organic compounds: A review, *Anal. Chim. Acta*, 1045, 10–22, <https://doi.org/10.1016/j.aca.2018.07.005>, 2019.
- Davis, B. M. and McEwan, M. J.: Determination of Olive Oil Oxidative Status by Selected Ion Flow Tube Mass Spectrometry, *J. Agr. Food Chem.*, 55, 3334–3338, <https://doi.org/10.1021/cr800364q>, 2003.
- Davis, B. M., Senthilmohan, S. T., Wilson, P. F., and McEwan, M. J.: Major volatile compounds in head-space above olive oil analysed by selected ion flow tube mass spectrometry, *Rapid Commun. Mass Spectrom.*, 19, 2272–2278, <https://doi.org/10.1002/rcm.2056>, 2005.
- de Gouw, J. and Warneke, C.: Measurements of volatile organic compounds in the earth's atmosphere using proton-transfer-reaction mass spectrometry, *Mass Spectrom. Rev.*, 26, 223–257, <https://doi.org/10.1002/mas.20119>, 2007.
- Del Bene, J. E.: A molecular orbital study of protonation. 3. Equilibrium structures and energies of ions RCHOH, *J. Am. Chem. Soc.*, 100, 1673–1679, <https://doi.org/10.1021/ja00474a006>, 1978.
- Deming, B. L., Pagonis, D., Liu, X., Day, D. A., Talukdar, R., Krechmer, J. E., de Gouw, J. A., Jimenez, J. L., and Ziemann, P. J.: Measurements of delays of gas-phase compounds in a wide variety of tubing materials due to gas-wall interactions, *Atmos. Meas. Tech.*, 12, 3453–3461, <https://doi.org/10.5194/amt-12-3453-2019>, 2019.
- Herrington, J. S.: Ambient Air Sampling with Whole-Air, In-Field Concentration and Particulate Matter (PM) Methodologies, in: *Comprehensive Analytical Chemistry*, edited by: Forbes, P. B. C., Elsevier, 109–153, <https://doi.org/10.1016/bs.coac.2015.09.004>, 2015.
- Kebarle, P., Yamdagni, R., Hiraoka, K., and McMahon, T. B.: Ion molecule reactions at high pressure: recent proton affini-

- ties, gas phase acidities and hydrocarbon clustering results, *Int. J. Mass Spectrom.*, 19, 71–87, [https://doi.org/10.1016/0020-7381\(76\)83005-7](https://doi.org/10.1016/0020-7381(76)83005-7), 1976.
- Krechmer, J., Lopez-Hilfiker, F., Koss, A., Hutterli, M., Stoerner, C., Deming, B., Kimmel, J., Warneke, C., Holzinger, R., Jayne, J., Worsnop, D., Fuhrer, K., Gonin, M., and de Gouw, J.: Evaluation of a New Reagent-Ion Source and Focusing Ion-Molecule Reactor for Use in Proton-Transfer-Reaction Mass Spectrometry, *Anal. Chem.*, 90, 12011–12018, <https://doi.org/10.1021/acs.analchem.8b02641>, 2018.
- Langford, V. S., Graves, I., and McEwan, M. J.: Rapid monitoring of volatile organic compounds: a comparison between gas chromatography/mass spectrometry and selected ion flow tube mass spectrometry, *Rapid Commun. Mass Spectrom.*, 28, 10–18, <https://doi.org/10.1002/rcm.6747>, 2014.
- Lehnert, A.-S., Behrendt, T., Ruecker, A., Pohnert, G., Trumbore, S. E.: Raw data for “SIFT-MS optimization for atmospheric trace gas measurements at varying humidity”, Max Planck digital library, <https://doi.org/10.17617/3.2u>, 2019.
- Lourenço, C., González-Méndez, R., Reich, F., Mason, N., and Turner, C.: A potential method for comparing instrumental analysis of volatile organic compounds using standards calibrated for the gas phase, *Int. J. Mass Spectrom.*, 419, 1–10, <https://doi.org/10.1016/j.ijms.2017.05.011>, 2017.
- McEwan, M. J.: Direct Analysis Mass Spectrometry, in: *Ion/Molecule Attachment Reactions: Mass Spectrometry*, edited by: Fujii, T., Springer, Boston, USA, 263–317, https://dx.doi.org/10.1007/978-1-4899-7588-1_8, 2015.
- Milligan, D. P., Wilson, P. F., Mautner, M. N., Freeman, C. G., McEwan, M. J., Clough, T. J., and Sherlock, R. R.: Atmospheric Pollutants and Trace Gases, *J. Environ. Qual.*, 31, 515–524, <https://doi.org/10.2134/jeq2002.5150>, 2002.
- Milligan, D. P., Francis, G. J., Price, B. P., and McEwan, M. J.: Demonstration of Selected Ion Flow Tube MS Detection in the Parts per Trillion Range, *Anal. Chem.*, 79, 2537–2540, <https://doi.org/10.1021/ac0622678>, 2007.
- Pienaar, J. J., Beukes, J. P., Van Zyl, P. G., Lehmann, C. M. B., and Aherne, J.: Passive Diffusion Sampling Devices for Monitoring Ambient Air Concentrations, in: *Comprehensive Analytical Chemistry*, edited by: Forbes, P. B. C., Elsevier, 13–52, <https://doi.org/10.1016/bs.coac.2015.09.002>, 2015.
- Prince, B. J., Milligan, D. B., and McEwan, M. J.: Application of selected ion flow tube mass spectrometry to real-time atmospheric monitoring, *Rapid Commun. Mass Spectrom.*, 24, 1763–1769, <https://doi.org/10.1002/rcm.4574>, 2010.
- Romano, A., Capozzi, V., Spano, G., and Biasioli, F.: Proton transfer reaction-mass spectrometry: online and rapid determination of volatile organic compounds of microbial origin, *Appl. Microbiol. Biot.*, 99, 3787–3795, <https://doi.org/10.1007/s00253-015-6528-y>, 2015.
- Schwarz, K., Filipiak, W., and Amann, A.: Determining concentration patterns of volatile compounds in exhaled breath by PTR-MS, *J. Breath Res.*, 3, 027002, <https://doi.org/10.1088/1752-7155/3/2/027002>, 2009.
- Shende, P., Vaidya, J., Kulkarni, Y. A., and Gaud, R. S.: Systematic approaches for biodiagnostics using exhaled air, *J. Control. Release*, 268, 282–295, <https://doi.org/10.1016/j.jconrel.2017.10.035>, 2017.
- Smith, D. and Spanel, P.: Selected ion flow tube mass spectrometry (SIFT-MS) for on-line trace gas analysis, *Mass Spectrom. Rev.*, 24, 661–700, <https://doi.org/10.1002/mas.20033>, 2005.
- Smith, D. and Spanel, P.: Direct, rapid quantitative analyses of BVOCs using SIFT-MS and PTRMS obviating sample collection, *Trends Anal. Chem.*, 30, 945–959, <https://doi.org/10.1016/j.trac.2011.05.001>, 2011.
- Smith, D., Spanel, P., Herbig, J., and Beauchamp, J.: Mass spectrometry for real-time quantitative breath analysis, *J. Breath Res.*, 8, 027101, <https://doi.org/10.1088/1752-7155/8/2/027101>, 2014.
- Spanel, P. and Smith, D.: Selected ion flow tube studies of the reactions of H_3O^+ , NO^+ , and O_2^+ with several aromatic and aliphatic hydrocarbons, *Int. J. Mass Spectrom.*, 181, 1–10, [https://doi.org/10.1016/S1387-3806\(98\)14114-3](https://doi.org/10.1016/S1387-3806(98)14114-3), 1998.
- Spanel, P. and Smith, D.: Influence of water vapour on selected ion flow tube mass spectrometric analyses of trace gases in humid air and breath, *Rapid Commun. Mass Spectrom.*, 14, 1898–1906, [https://doi.org/10.1002/1097-0231\(20001030\)14:20<1898::AID-RCM110>3.0.CO;2-G](https://doi.org/10.1002/1097-0231(20001030)14:20<1898::AID-RCM110>3.0.CO;2-G), 2000.
- Sulzer, P., Hartungen, E., Hanel, G., Feil, S., Winkler, K., Mutschlechner, P., Haidacher, S., Schottkowsky, R., Gansch, D., Seehauser, H., Striednig, M., Jürschik, S., Breiev, K., Lanza, M., Herbig, J., Märk, L., Märk, T. D., and Jordan, A.: A Proton Transfer Reaction-Quadrupole interface Time-Of-Flight Mass Spectrometer (PTR-QiTOF): High speed due to extreme sensitivity, *Int. J. Mass Spectrom.*, 368, 1–5, <https://doi.org/10.1016/j.ijms.2014.05.004>, 2014.
- Syft Technologies Ltd.: SIFT-MS Technology Overview Brochure, available at: <https://www.syft.com/wp-content/uploads/2018/02/SIFT-MS-Technology-Overview.pdf> (last access: 27 January 2018), 2019.
- Veres, S. M.: Relations between information criteria for model-structure selection Part 1. The role of bayesian model order estimation, *Int. J. Control*, 52, 389–408, <https://doi.org/10.1080/00207179008953542>, 1990.
- Wilson, P. F., Freeman, C. G., and McEwan, M. J.: Reactions of small hydrocarbons with H_3O^+ , O_2^+ and NO^+ ions, *Int. J. Mass Spectrom.*, 229, 143–149, [https://doi.org/10.1016/s1387-3806\(03\)00290-2](https://doi.org/10.1016/s1387-3806(03)00290-2), 2003.
- Yuan, B., Koss, A. R., Warneke, C., Coggon, M., Sekimoto, K., and de Gouw, J. A.: Proton-Transfer-Reaction Mass Spectrometry: Applications in Atmospheric Sciences, *Chem. Rev.*, 117, 13187–13229, <https://doi.org/10.1021/acs.chemrev.7b00325>, 2017.



Simultaneous Real-Time Measurement of Isoprene and 2-Methyl-3-Buten-2-ol Emissions From Trees Using SIFT-MS

Ann-Sophie Lehnert^{1,2*†}, Erica Perreca^{3†}, Jonathan Gershenzon³, Georg Pohnert² and Susan E. Trumbore¹

¹ Department of Biogeochemical Processes, Max Planck Institute for Biogeochemistry, Jena, Germany, ² Institute for Inorganic and Analytical Chemistry, Biorganic Analytics, Friedrich Schiller University, Jena, Germany, ³ Department of Biochemistry, Max Planck Institute for Chemical Ecology, Jena, Germany

OPEN ACCESS

Edited by:

Roger Deal,
Emory University, United States

Reviewed by:

Phillippe Heynderickx,
Ghent University Global Campus,
South Korea
Murray McEwan,
University of Canterbury, New Zealand

*Correspondence:

Ann-Sophie Lehnert
alehnert@bgc-jena.mpg.de

[†]These authors have contributed
equally to this work

Specialty section:

This article was submitted to
Technical Advances in Plant Science,
a section of the journal
Frontiers in Plant Science

Received: 30 June 2020

Accepted: 04 November 2020

Published: 27 November 2020

Citation:

Lehnert A-S, Perreca E,
Gershenzon J, Pohnert G and
Trumbore SE (2020) Simultaneous
Real-Time Measurement of Isoprene
and 2-Methyl-3-Buten-2-ol Emissions
From Trees Using SIFT-MS.
Front. Plant Sci. 11:578204.
doi: 10.3389/fpls.2020.578204

The C5 hemiterpenes isoprene and 2-methyl-3-buten-2-ol (MBO) are important biogenic volatiles emitted from terrestrial vegetation. Isoprene is emitted from many plant groups, especially trees such as *Populus*, while emission of MBO is restricted to certain North American conifers, including species of *Pinus*. MBO is also a pheromone emitted by several conifer bark beetles. Both isoprene and MBO have typically been measured by proton-transfer reaction mass spectrometry (PTR-MS), but this method cannot accurately distinguish between them because of their signal overlap. Our study developed a method for using selective ion flow tube mass spectrometry (SIFT-MS) that allows simultaneous on-line measurement of isoprene and MBO by employing different reagent ions. The use of $m/z(\text{NO}^+) = 68$ u for isoprene and $m/z(\text{O}_2^+) = 71$ u for MBO gave minimal interference between the compounds. We tested the suitability of the method by measuring the emission of young trees of *Populus*, *Picea*, and *Pinus*. Our results largely confirm previous findings that *Populus nigra*, *Picea glauca*, and *Picea abies* emit isoprene and *Pinus ponderosa* emits MBO, but we also found MBO to be emitted by *Picea abies*. Thus SIFT-MS provides a reliable, easy to use, on-line measuring tool to distinguish between isoprene and MBO. The method should be of use to atmospheric chemists, tree physiologists and forest entomologists, among others.

Keywords: conifers, Picea, poplar, Pinus, VOC, isoprene, MBO, SIFT-MS

INTRODUCTION

The C5-hemiterpene isoprene, or 2-methyl-1,3-butadiene, is the most abundant biogenic volatile compound emitted from vegetation. Its annual global emission is estimated to be 350 to 769 Tg yr⁻¹, approximately half of the total estimated emissions of biogenic volatile organic compounds (BVOC) (Guenther et al., 2012). Isoprene is emitted from mosses, ferns and higher plants, especially trees (Tingey et al., 1987; Hanson et al., 1999; Loreto, 2015). Angiosperms including species of *Populus* emit large amounts of isoprene, while in gymnosperms this hemiterpene is known to be emitted from species belonging to the genus *Picea*, including *Picea abies* and *Picea glauca*,

but not from species belonging to the genus *Pinus*. Instead, the related hemiterpene 2-methyl-3-buten-2-ol (MBO), is emitted by *Pinus* species native to Northern America, e.g., *Pinus ponderosa*, *Pinus lodgepole*, and *Pinus jeffreyi* (Goldan et al., 1993; Harley et al., 1998). Globally, MBO contributions represent only a minor component of total BVOC emissions (Guenther et al., 2012), but in Northern American pine forests, their levels can reach 4–7 times the level of isoprene (Goldan et al., 1993; Harley et al., 1998; Schade and Goldstein, 2001).

2-Methyl-3-buten-2-ol and isoprene are often measured together as a sum parameter due to the experimental restrictions outlined below. However, it is important to distinguish between the two compounds during research in several different fields.

Atmospheric Sciences

The oxidation of BVOCs, such as isoprene and MBO, in the atmosphere can produce tropospheric ozone in sufficiently NO-rich environments (Steiner et al., 2007), influencing air quality and, as ozone is a greenhouse gas, radiative warming. These compounds can also form secondary organic aerosols (Carlton et al., 2009), with both direct and indirect (as cloud condensation nuclei) impacts on radiative balance. Oxidation of MBO by OH-radicals represents one of the most important sources of acetone in those areas where it is emitted (Ferronato et al., 1998). However, the very different lifetimes of isoprene (2.8 h) and MBO (7 h) lead to different spatial and temporal distributions around areas of high emissions (Fantechi et al., 1998; Atkinson and Arey, 2003). Thus, the ability to measure these gases individually with a high time resolution would provide important insights into their relative roles in atmospheric chemistry and climate.

Plant Sciences

Isoprene is thought to protect plants against abiotic stress by its antioxidant properties and stabilization of thylakoid membranes at high temperature (Perreca et al., 2020). Recently this molecule has also been proposed to activate gene networks involved in abiotic stress tolerance (Zuo et al., 2019). Although the role of MBO in plants has not been well studied, it is expected to be similar to that of isoprene based on a similar response of emission rates to light and temperature changes (Schade et al., 2000) and biosynthesis from the same substrate, dimethylallyl diphosphate (Gray et al., 2003). However, due to the differences in chemical properties, the way the two compounds serve in plant protection might differ. Especially the antioxidant properties of MBO might differ from those of isoprene. MBO was detected in the bark extracts of some angiosperms (Zhang et al., 2012) that are known to emit isoprene. Thus care should be taken to distinguish between the two compounds in simultaneous measurement in order to assess if their roles are different.

Entomology

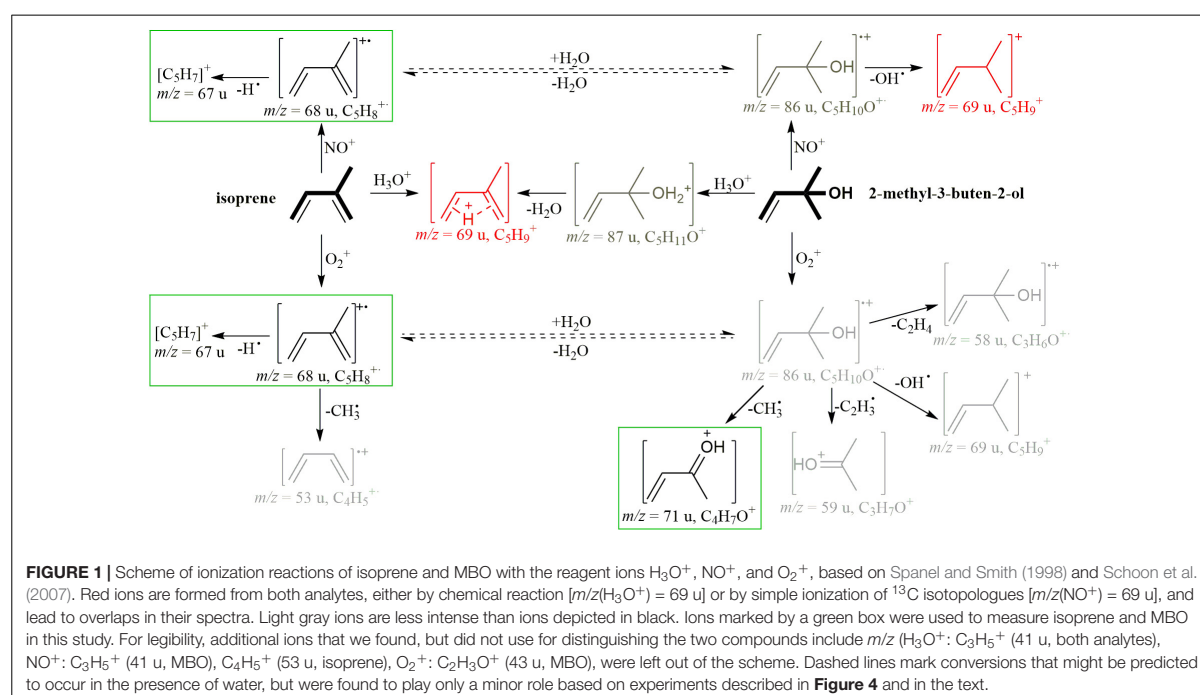
2-Methyl-3-buten-2-ol MBO is produced not only by trees, but also by tree pests. Several conifer bark beetles, e.g., the spruce bark beetle *Ips typographus*, produce MBO *de novo* as an aggregation pheromone (Bakke et al., 1977; Baader, 1989; Zhang et al., 2012). Thus simultaneous measurement of isoprene and MBO might

allow for distinguishing between abiotic stress and bark beetle infestation in field measurements.

Proton-transfer reaction mass spectrometry (PTR-MS) and gas chromatography-mass spectrometry (GC-MS) are the most widely used techniques for measuring BVOCs. PTR-MS ionizes gaseous analytes with H_3O^+ ions in a drift tube with a defined reaction time and detects them via mass spectrometry with a quadrupole or Time of Flight mass analyzer. This technique allows for online-measurements of gaseous analytes at low mixing ratios (Krechmer et al., 2018). However, with PTR-MS, the $[\text{M}+\text{H}-\text{H}_2\text{O}]^+$ fragment of MBO and the $[\text{M}+\text{H}]^+$ signal of isoprene have the same mass to charge ratio (cf. **Figure 1**, H_3O^+ pathway), so accurate distinction of the two compounds is difficult. GC-MS allows for a separation of the analytes based on differences in retention time and mass spectra, but is not suitable for online monitoring due to relatively long measurement times. In addition, GC-MS often requires pre-concentration on, e.g., cartridges before measurement. In practice, both techniques are usually employed side by side, using PTR-MS to acquire good time resolution and GC-MS for identification (Jardine et al., 2020). Another approach involves switchable reagent ion mass spectrometry (SRI-MS), a technique similar to PTR-MS, but including additional ion sources for NO^+ , O_2^+ , NH_4^+ , Kr^+ , and Xe^+ (Jordan et al., 2009). Using the NO^+ ion, isoprene can be detected at $m/z(\text{NO}^+) = 68$ u, and MBO at $m/z(\text{NO}^+) = 69$ u, as has been shown in a field study with SRI-MS (Karl et al., 2012), but these instruments are very costly and complex to operate. Because of the important role that isoprene and MBO play in different scientific fields, the possibility to distinguish between these compounds with accuracy using online measurements is desirable, but until now not realized technically with readily available instruments.

Selected ion flow tube mass spectrometry (SIFT-MS) is a cheaper (though still rather costly) and easy-to-use alternative to SRI-MS. Like PTR-MS and SRI-MS, SIFT-MS is a chemical ionization mass spectrometry technique for measuring gaseous analytes. Unlike PTR-MS, it utilizes multiple reagent ions that react differently with gaseous analytes, so one can obtain more structural information from the respective spectra. By measuring one analyte with more than one reagent ion, multiple spectra are generated. Comparison of these spectra allows identification of ions with the least interference from other VOCs and thus specific quantification of the target analyte.

In SIFT-MS, reagent ions are generated by a moist air plasma and then selected by a quadrupole. Reagent ions and gaseous analytes are mixed in a flow tube that is flushed continuously with a carrier gas. They travel together, and their reaction time is determined by the time they need to cross the flow tube (Smith and Spanel, 2011). During this time, the analytes are ionized during collision with the reagent ions. In our case, the reagent ions used were H_3O^+ , NO^+ , and O_2^+ , but it is also possible to use the negative ions OH^- , O^- , O_2^- , NO_2^- , and NO_3^- . With H_3O^+ , mostly proton transfer reactions occur, with NO^+ electrons are transferred or NO^+ adducts are formed and with O_2^+ , electrons are transferred and sometimes fragmentation reactions occur. The product ions and remaining reagent ions are detected via a quadrupole mass analyzer. A library is



implemented in the software of the manufacturer that can be used to calculate their mixing ratio directly from the measured counts.

When measuring isoprene and MBO with SIFT-MS, H_3O^+ generates $m/z(\text{H}_3\text{O}^+) = 69 \text{ u}$ for both analytes, like in PTR-MS (cf. **Figure 1** for a reaction scheme). However, with NO^+ , isoprene generates $m/z(\text{NO}^+) = 68 \text{ u}$, and MBO generates $m/z(\text{O}_2^+) = 69 \text{ u}$. With this difference, one can measure isoprene well, but the ^{13}C isotopologue of isoprene interferes with MBO measurement. With O_2^+ , isoprene forms two product ions, $m/z(\text{O}_2^+) = 67 \text{ u}$ and 68 u , at similar intensities, whereas MBO mostly forms $m/z(\text{O}_2^+) = 71 \text{ u}$ (Spanel and Smith, 1998; Schoon et al., 2007).

In this study, we demonstrate the use of SIFT-MS for simultaneous measurement of isoprene and MBO by monitoring isoprene with $m/z(\text{NO}^+) = 68 \text{ u}$ and MBO with $m/z(\text{O}_2^+) = 71 \text{ u}$. To validate our method, we performed measurements on three different isoprene-emitting tree species, *Populus nigra*, *Picea abies*, and *Picea glauca*, and on *Pinus ponderosa*, which is reported to emit MBO.

MATERIALS AND METHODS

Supplies and General Remarks

Isoprene, MBO, and dodecane were purchased from Sigma Aldrich (Darmstadt, Germany). Deuterated water was purchased from TCI (Eschborn, Germany). Distilled water was generated by a Enviro FALK GEO + EDI 200 electrode ionization cell (Enviro FALK, Westerbürg). The tubing used for the tree chamber experiment was opaque black 1/4" PFA-tubing, the tubing used

for the standard measurements was opaque black 1/8" PFA-tubing. Connectors for the tree experiment were Galtex PFA fittings (Entegris, United States), for the standard measurements and calibrations Swagelok stainless steel fittings (Swagelok, United States). All setups were built such that an overflow line to room air ensured ambient pressure in the chamber and at the SIFT-MS inlet.

SIFT-MS Settings

Measurements were conducted with a Voice 300 ultra SIFT-MS (Syft Technologies Ltd., Christchurch, New Zealand) with a positive ion source that was customized as described by Lehnert et al. (2019). 40 cm^3/min sample gas flow, 156 cm^3/min helium carrier gas flow, 50 V flow tube voltage, 120°C flow tube temperature, and 105°C sample plate and sampling line heater temperature were used. To suppress dimer formation at high mixing ratios, the larger trees (*P. nigra*, *P. abies*, and *P. glauca* #1) were measured at 390 cm^3/min carrier gas flow.

The ratio of the reagent ions NO^+ and O_2^+ varied between the different experiments. However, this did not affect our results significantly since for the interference calculation, measurements from the same ions were used, and for the calculation of mixing ratios and release rates, the ratios of product ion to reagent ion were used.

SIFT-MS Measurements of Isoprene and MBO Standards

Full mass spectra were measured for both standards using a diffusion cell flushed with VOC-free air from a pure air generator

(PAG 003, Ecophysics, Dürnten, Switzerland). An 1.5 mL vial with Teflon septum was filled with 50 μ L isoprene or MBO. A thin needle (23 G \times 1") was pierced through the septum, and then the vial was placed in a 40 mL headspace vial that was flushed with 0.5 L/min pure air humidified to 0, 25%, 50%, 75%, and 100% relative humidity at 25°C by a GCU gas calibration unit (IONICON Analytik GmbH, Innsbruck, Austria). The method captured ion counts between 10 and 250 u for all three reagent ions. The dwell time was 100 ms, and the count limit 10,000. 10 scans of each substance were measured and averaged.

For distinguishing the two standards, a selected ion monitoring (SIM) scan was set up for 10 min, with 500 ms dwell time/scan time and 100,000 cps count limit (36 scans, first and last omitted for averaging). The masses used are listed in **Supplementary Table S1**. The increased count limit and scan time compared to standard SIFT-MS settings was used to decrease variability in the measured reagent ion counts. The maximum ratio of product to reagent ions was 3%, so the assumption that the reagent ion counts remain unchanged in the flow tube is still valid.

Ionization of Isoprene and MBO in the Presence of Deuterated Water

We humidified pure air by bubbling it through deuterated water at room temperature. This moist air was mixed with pure air that was enriched in isoprene or MBO, respectively, by passing it over water with 1 μ L isoprene or MBO in the diffusion cell. Both flows were 400 mL/min. Mass spectra were recorded between $m/z = 15$ and 150 u, with a scan time limit 1 s, count limit 100,000 counts, and four repeats per measurement. As a control, the experiment was repeated with normal, non-deuterated water.

Tree Cultivation

Populus nigra trees were grown from stem cuttings obtained from trees grown in a common garden of *P. nigra* accessions in Isserstedt, Germany. The 1-year-old trees were grown in the greenhouse of the Max Planck Institute of Chemical Ecology (MPICÖ) Jena, Germany under the following conditions: 20/18°C (day/night), relative humidity 60%, natural light with 9–14 h photoperiod, and supplemental light for 12 h, with SON-T Agro lamps (Philips, Andover, MA, United States).

Three-year-old *Picea abies* trees were planted originally from seeds in 2016 and were grown outdoors in the garden of the MPICÖ, until the experiment was performed. Trees were irrigated every day. One-year-old *Pinus ponderosa* trees were obtained from a local nursery in Thuringia. Four-year-old *Picea glauca* trees (accession #1) were obtained from a local nursery in Thuringia in 2017 and grown prior to the experiment outdoors in the garden of the MPICÖ. Trees were irrigated every day. Three-year-old *Picea glauca* (accession #2) trees were obtained as seedlings from the Laurentian Forestry Centre, Quebec, Canada, in 2016, and grown under controlled environmental conditions in a growing chamber in the MPICÖ until the start of the experiment. Summer (16/8 h for day/night, 22°C and photosynthetically active radiation (PAR) 1000 μ mol/m²/s) and winter (8/12 h for day/night, 5°C and PAR 200 μ mol/m²/s)

conditions were alternated for 6 months (summer) and 3 months (winter) in the chamber.

Isoprene and MBO Emissions From Trees

Prior to the experiment, the trees were moved to the greenhouse of the Max Planck Institute of Biogeochemistry, Jena, Germany, and kept there for 4 weeks. The greenhouse was set up at 60% humidity and a 12 h day/night cycle (30°C/25°C). LED-lights (ultra violet, <400 nm, 1%; blue, 400–500 nm, 20%; green, 500–600 nm, 39%; red, 600–700 nm, 35%; far-red, 700–800 nm, 5%; Valoya, Finland) illuminated the trees with a PAR of 150 μ mol/m²/s and were supplemented by ambient light entering the greenhouse, reaching a PAR level of 300–400 μ mol/m²/s. Trees were watered daily. Before performing the measurement of isoprene and MBO with the SIFT-MS, trees were put into the chamber for 24 h [setup similar to Huang et al. (2018), scheme in **Supplementary Figure S1**].

The three tree-containing cylindrical chambers plus one reference chamber without a tree were made from FEP-foil. These chambers (height = 50 cm, diameter = 40 cm, volume = 60 L) were mounted in a polyacrylate scaffold. A Teflon tube ring with holes was placed at the bottom of the chambers and connected to an air inlet. Compressed air was dried and purified on adsorber columns, after which CO₂ was added back in to achieve levels of 400 ppm. Rotameters regulated the air flow through the chamber to 3 L/min. 1/4" black PFA tubing of 2 m length connected the chamber to the instrument. The outlets of the VICI-valve on the SIFT-MS were connected via T-pieces and 1 m tubing to a pump flushing the tubes from the chambers to the instrument at all times. Photosynthetically active radiation (PAR) and temperature were tracked in each chamber. Tree emissions were measured via the SIM scan described above for 24 h capturing a full diurnal cycle. After measuring each chamber with the SIM scan described above, additionally, one full mass spectrum was also measured for every chamber plus the instrument's internal background with the settings mentioned above with a single scan.

Mixing ratios were calculated as:

$$\chi_{\text{isoprene}} = 1.0035 \cdot 10^{-10} \cdot \frac{T_{FT}}{p_{FT}} \cdot \left(\frac{\varphi_{carr}}{\varphi_{samp}} + 1 \right) \cdot \frac{I(\text{NO}^+, 68 \text{ u}) \cdot \text{ICF}(\text{NO}^+, 68 \text{ u})}{k_{\text{isoprene, NO}^+} \cdot br_{\text{isoprene, NO}^+, 68 \text{ u}} \cdot I(\text{NO}^+, 30 \text{ u}) \cdot \text{ICF}(\text{NO}^+, 30 \text{ u})} \quad (1)$$

and

$$\chi_{\text{MBO}} = 1.0035 \cdot 10^{-10} \cdot \frac{T_{FT}}{p_{FT}} \cdot \left(\frac{\varphi_{carr}}{\varphi_{samp}} + 1 \right) \cdot \frac{I(\text{O}_2^+, 71 \text{ u}) \cdot \text{ICF}(\text{O}_2^+, 71 \text{ u})}{k_{\text{MBO, O}_2^+} \cdot br_{\text{MBO, O}_2^+, 71 \text{ u}} \cdot I(\text{O}_2^+, 32 \text{ u}) \cdot \text{ICF}(\text{O}_2^+, 32 \text{ u})} \quad (2)$$

χ is the mixing ratio in ppb, T_{FT} the flow tube temperature in K, p_{FT} the flow tube pressure in mTorr, φ_{carr} the carrier gas flow in Torr L/s, and φ_{samp} the sample gas flow in Torr L/s. $I()$ is the intensity of the ion ionized by the reagent ion and measured at

the mass stated, $ICF()$ the instrument calibration factor at the ion as specified, k the kinetic rate constant in $\text{cm}^3 \cdot \text{molecule/s}$ of the reaction with isoprene/MBO with the respective reagent ion, and br the branching ratio of the measured ion. The branching ratios were determined from the standard measurements at 100% humidity, which had the most similar 19/37 signal to the samples. The mixing ratios were calculated for each scan omitting the first and last scan of each measurement, and then the mean and standard deviation were calculated from this. The maximum observed ratio of product ion to reagent ion was 0.9% in the case of isoprene emissions from poplar, which is low enough to fulfill the assumption that the reagent ion counts did not change significantly. The maximum ion counts of $\text{NO}^+ \cdot \text{H}_2\text{O}$, an additional reagent ion water cluster, were always below 500 cps, which corresponded to less than 0.25% of the reagent ion counts and was thus not included in the calculation.

From there, the emission rate was calculated as

$$\phi = \frac{\chi \cdot M \cdot \varphi_{\text{air}}}{V_{\text{mol}} \cdot m_{\text{leaves/needles, dry}}} \quad (3)$$

ϕ is the release rate in $\mu\text{mol}/(\text{g h})$, M is the molar mass of the compound, φ_{air} is the air flow through the incubation chamber (cf. **Supplementary Table S3**), V_{mol} is the molar volume, used 24 L/mol as it was 25°C in the chamber, and $m_{\text{leaves/needles, dry}}$ is the leaf or needle dry mass (cf. **Supplementary Table S2**).

The error of the emission rate was calculated as

$$\Delta\phi = \frac{t(95\%, n_{\text{meas}} - 1)}{n_{\text{meas}} - 1} \cdot \sqrt{M \cdot \left(\left(\frac{\varphi_{\text{air}} \cdot \Delta\chi}{m_{\text{leaves/needles, dry}}} \right)^2 + \left(\frac{\chi \cdot \varphi_{\text{air}} \cdot \Delta V_{\text{mol}}}{V_{\text{mol}}^2 \cdot m_{\text{leaves/needles, dry}}} \right)^2 + \left(\frac{\chi \cdot \Delta\varphi_{\text{air}}}{V_{\text{mol}} \cdot m_{\text{leaves/needles, dry}}} \right)^2 + \left(\frac{\chi \cdot \varphi_{\text{air}} \cdot \Delta m_{\text{leaves/needles, dry}}}{V_{\text{mol}} \cdot m_{\text{leaves/needles, dry}}^2} \right)^2} \quad (4)$$

with $t(95\%, n_{\text{meas}} - 1)$ the result of the t-distribution at 95%. The degrees of freedom are the number of measurements per time point - 1 (21–22, depending on the measurement). $\Delta\chi$ is the standard deviation of the mixing ratios that was calculated based on the 21–22 individual measurements per time point. $\Delta V_{\text{mol}} = 0.72$ L/mol is the error of the molar volume for 5 K and 0.02 bar deviation of the temperature and pressure. $\Delta\varphi_{\text{air}}$ is the reading error of the gas flow measurements, and $\Delta m_{\text{leaves/needles, dry}}$ the reading error of the weight measurement.

RESULTS

Mass spectra of the standards (**Figure 2**) showed that isoprene and MBO react differently with NO^+ and O_2^+ than previously described (Spanel and Smith, 1998; Schoon et al., 2007). The biggest difference lies in the finding of a strong signal for isoprene at $m/z = 67$ u upon reaction with NO^+ . As the carrier gas flow used and moisture level were similar to those in our study (390 ccm at 100% humidity), we attribute the spectral changes to an increased ion energy leading to increased fragmentation

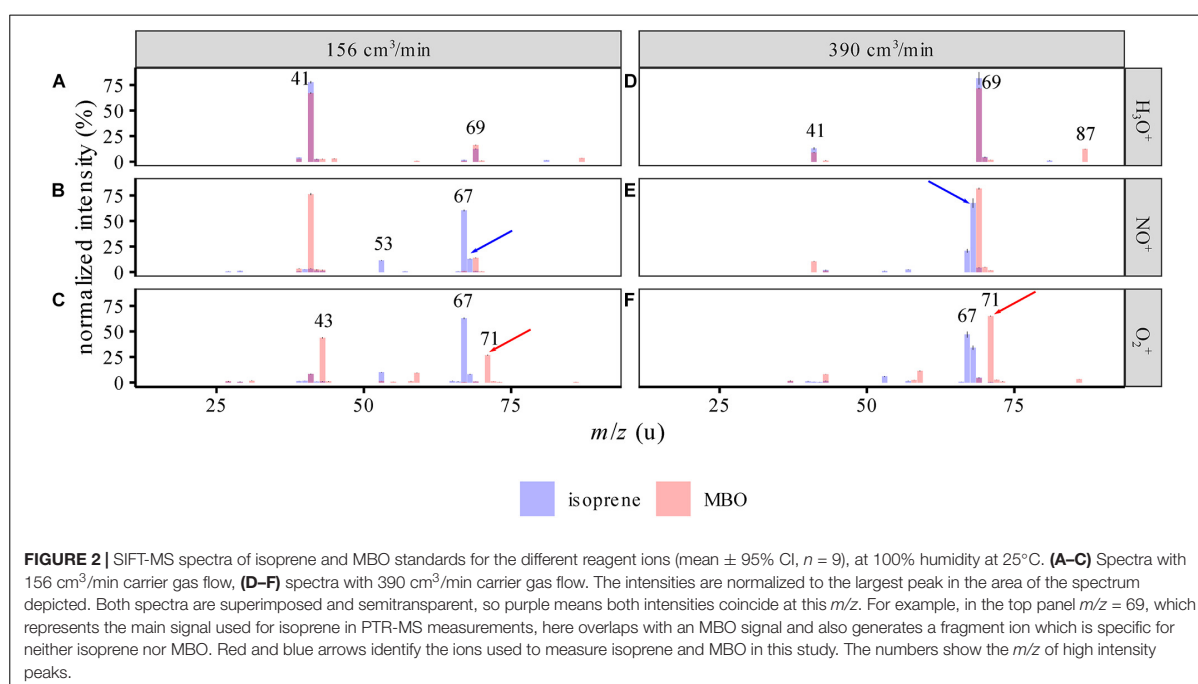
due to the higher flow tube voltage and temperature settings. We observed a decrease in fragmentation when increasing the carrier gas flow (**Figures 2A–C** vs. **D–F**), probably a result of product ions transferring excess energy more rapidly to the carrier gas due to an increased number of collisions.

Upon reaction with NO^+ , one could potentially use the $m/z = 67$ or 68 u signals for measuring isoprene and the $m/z = 69$ u for measuring MBO, as described by Karl et al. (2012). However, limitations in the mass resolution of the quadrupole used in the SIFT-MS resulted in a 5–6% interference [normalized to $m/z(\text{NO}^+) = 68$ u] due to the natural isotopologues of isoprene substituted with a single ^{13}C . When we measured the isoprene standard at different carrier gas flows and humidities, we determined 6% to 8% interference of isoprene with the MBO signal at $m/z(\text{NO}^+) = 69$ u (**Figure 3**). Corrected for the ^{13}C isotope peak, this calculates to a secondary reaction of isoprene to C_5H_9^+ ($m/z = 69$ u) with 1–2% abundance. An explanation for the formation of this ion could be H_2O addition and subsequent OH loss, cf. **Figure 1**. Using $m/z(\text{O}_2^+) = 71$ u for measuring MBO was more accurate than using $m/z(\text{NO}^+) = 69$ u, as the interference of isoprene at $m/z(\text{O}_2^+) = 71$ u was below 1% of that at $m/z(\text{O}_2^+) = 67$ u.

We also measured up to 0.7% interference of MBO on the isoprene signal at $m/z(\text{NO}^+) = 68$ u, normalized to $m/z(\text{NO}^+) = 69$ u. This interference was more prominent in dry samples since MBO ionized by NO^+ [$\text{C}_5\text{H}_{10}\text{O}^+$, $m/z(\text{NO}^+) = 86$ u] might not only eliminate OH radicals to form C_5H_9^+ [$m/z(\text{NO}^+) = 69$ u], but also eliminate water to form C_5H_8^+ [$m/z(\text{NO}^+) = 68$ u]. In this case, the presence of water would make this side reaction less favorable due to the principle of Le Chatelier. On the other hand, if we had used $m/z(\text{O}_2^+, 67$ u) to measure isoprene, the interference and thus the error would have been much higher, up to 1.9%.

To distinguish between isoprene and MBO, we sought signals of each compound that had the least interference from the other compound to minimize error, which scales with signal intensity. Thus, since the interference of isoprene on $m/z(\text{O}_2^+, 71$ u) is much smaller than on $m/z(\text{NO}^+) = 69$ u, we chose the former for measuring MBO. And, since the interference of MBO on $m/z(\text{NO}^+) = 68$ u is smaller than on $m/z(\text{O}_2^+, 67$ u), we chose the former for measuring isoprene. If the differences in mixing ratios between the two compounds are not anticipated to be large, and rapid measurements are needed with just a single reagent ion, it would be best to use both O_2^+ ions, $m/z(\text{O}_2^+, 67$ and 71 u), as the interference is lower than for the two NO^+ ions and one saves the time of measuring both reagent ions.

2-Methyl-3-buten-2-ol is formally an isoprene molecule with the addition of water to the substituted double bond. It could thus be possible that an ionized form of isoprene could react to form MBO in the presence of water. For example, isoprene ionized by NO^+ forms C_5H_8^+ , which could react with water to form $\text{C}_5\text{H}_{10}\text{O}^+$ with the same structure and m/z as ionized MBO. To evaluate the role of water in these proposed flow tube reactions, the standards were measured in air humidified by either H_2O or D_2O (**Figure 4**). If water is involved in the reaction, and a deuterium from water is added to or exchanged with the ion, the measured mass would be 1 u higher due to the higher



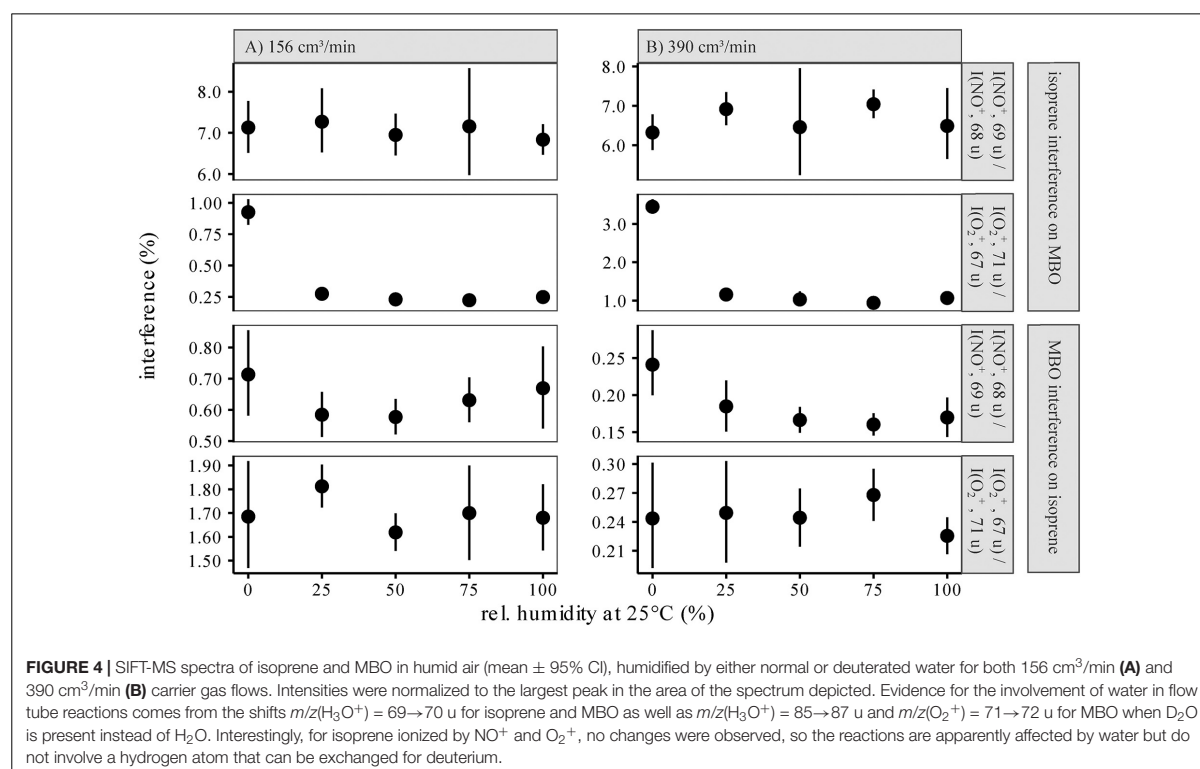
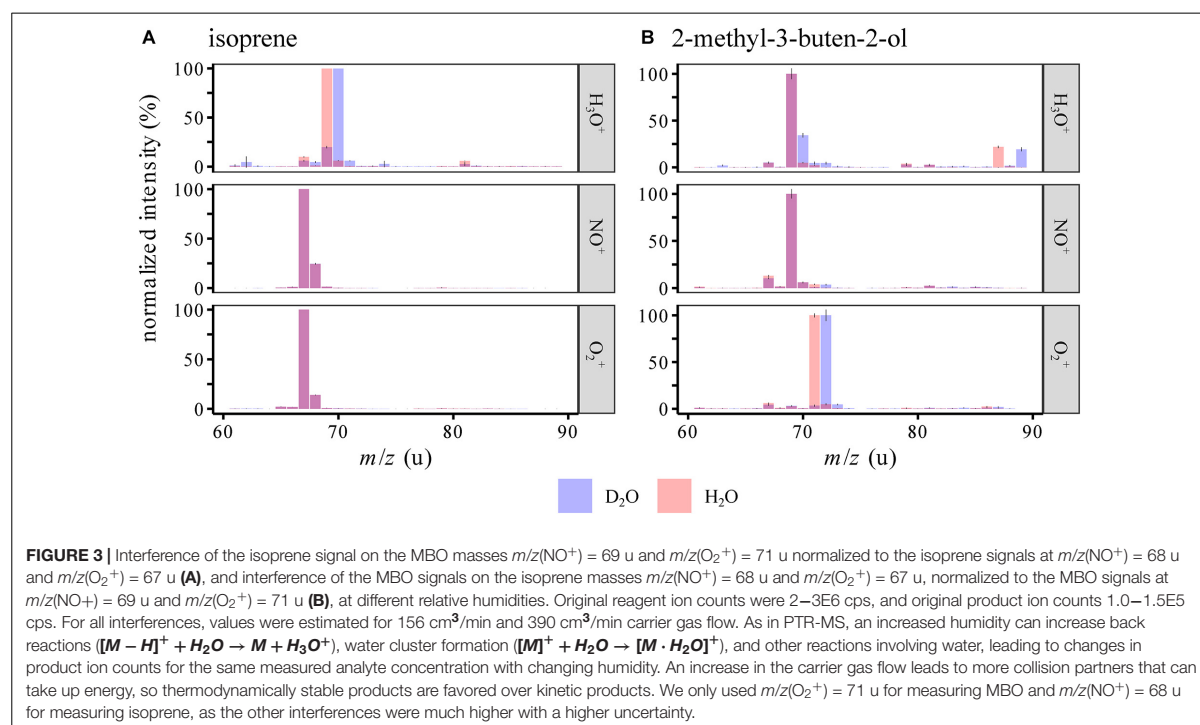
mass of deuterium compared to hydrogen. The reagent ions (see **Supplementary Figure S2**) showed an influence only in the H_3O^+ channel, where H_2DO^+ , HD_2O^+ , and D_3O^+ are detected. As expected, we saw a mass shift from $m/z(\text{H}_3\text{O}^+) = 69$ u to 70 u for both isoprene and MBO, as the reagent ions were both saturated and thus the protonation added a D to the analytes. $m/z(\text{O}_2^+) = 71$ u shifted to 72 u for MBO, so here, also water vapor was involved in forming this ion. Interestingly, for isoprene, the NO^+ and the O_2^+ signals did not change at all, so no proton exchange occurred in the formation of isoprene ions. This contradicts the hypothesis that water is involved in forming $m/z(\text{NO}^+) = 69$ u and $m/z(\text{O}_2^+) = 71$ u. However, we did observe an increase in the relative abundance of those two peaks when switching from dry to wet sample air. This could be due to suppression of the isoprene ions at $m/z(\text{NO}^+) = 68$ u and $m/z(\text{O}_2^+) = 67$ u by excess water.

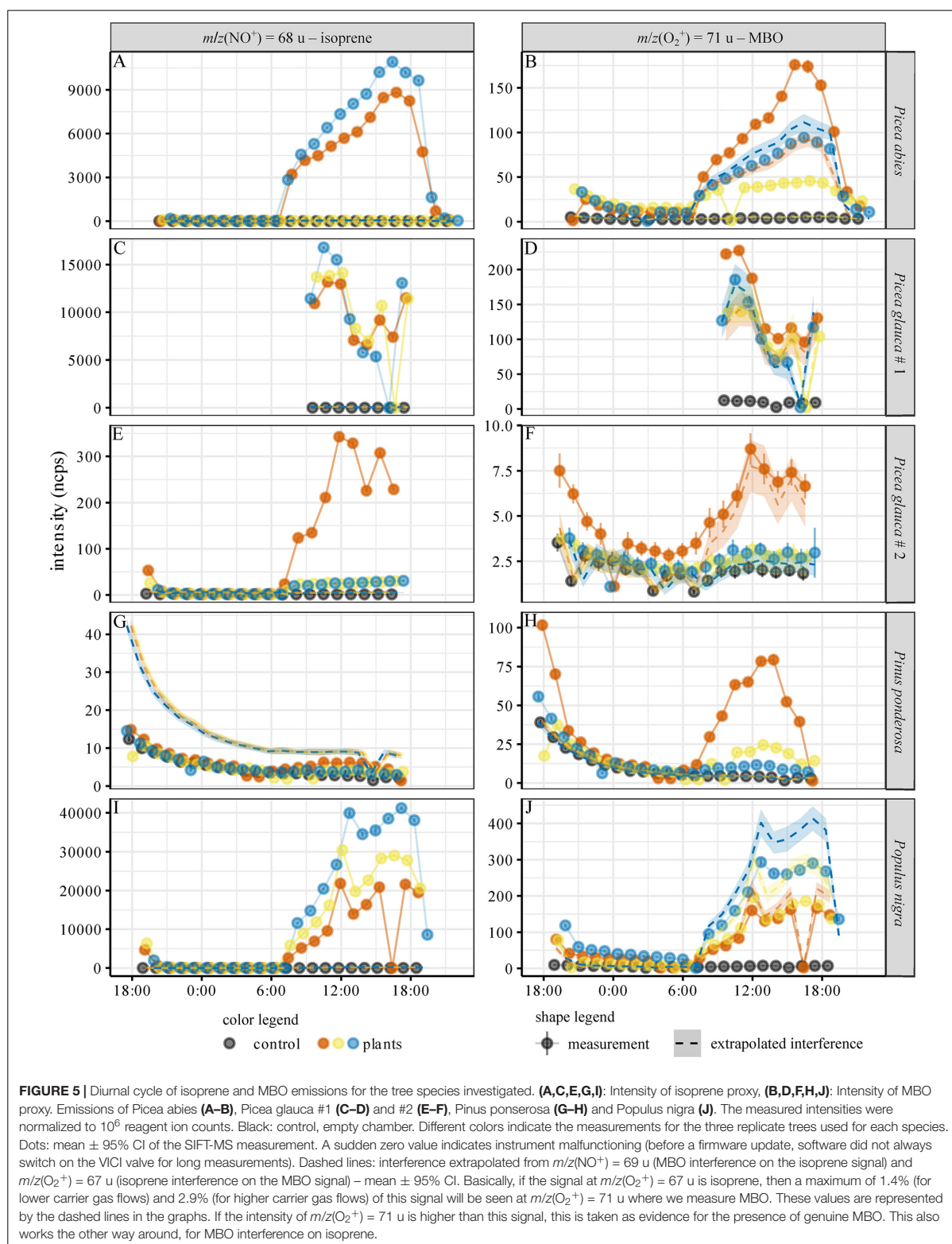
To test our ability to distinguish between isoprene and MBO in an experimental setup with natural sources of these gases, emissions from *Picea glauca*, *Picea abies*, *Populus nigra*, and *Pinus ponderosa* were measured over the course of a day. All trees exhibited a diurnal cycle of BVOC emissions related to the presence of light (**Figure 5**). Isoprene was measured from $m/z(\text{NO}^+) = 68$ u, and MBO was measured from $m/z(\text{O}_2^+) = 71$ u. We calculated the contribution of isoprene to the $m/z(\text{O}_2^+) = 71$ u signal with the equation $I(\text{O}_2^+, 71 \text{ u, isoprene interference}) = x \cdot I(\text{O}_2^+, 67 \text{ u, isoprene})$ (**Figure 3**). If the measured MBO signal is equal or below this value, the signal is not significantly different from the expected isoprene interference and no MBO is actually detected. If the signal is higher, it is measured as MBO. This of course

also applies also for the MBO interference on isoprene, with $I(\text{NO}^+, 68 \text{ u, MBO interference}) = x \cdot I(\text{NO}^+, 69 \text{ u, MBO})$. Again, we used the interference ratio that was determined measuring the standards at 100% humidity, as the trees transpired a substantial amount of water, leading to high air humidity in the chambers. A visualization of the potential isoprene interference with MBO for each species can be found in **Supplementary Figure S4**, where we plotted $I(\text{O}_2^+, 67 \text{ u})$ against $I(\text{O}_2^+, 71 \text{ u})$. Each species shows linear dependence of the two signals, but only *Picea abies* and *Pinus ponderosa* are found significantly above the black line, and so must emit MBO.

Relative humidity does not affect the ability to distinguish between isoprene and MBO except under very dry conditions (**Figure 3**). However, we suggest that interference rates should be determined with standards under conditions as close to the experiment as possible to rule out possible errors.

For each tree species, we analyzed the emission of isoprene and MBO from three individual trees, represented in **Figure 5** by different colors (blue, red, and yellow). The extrapolated interference signals are indicated with a dashed line in the color used for each individual tree. All species except *P. ponderosa* showed isoprene emissions (**Figure 5**), and within the tree species, the emission intensity mostly correlated with the needle or leaf dry mass, cf. **Supplementary Table S2**. For *P. abies*, the isoprene signal for one tree (shown in yellow) was a factor of 150 smaller than the other two (**Figure 5A** and **Supplementary Figure S3**), even though the biomass of this tree individual was the highest (**Supplementary Table S2**). For *P. glauca* (accession #2), one tree (red) had an isoprene signal 10 times higher than the other two, even though the biomass was comparable (**Figure 5E**





and **Supplementary Table S2**). Intraspecific variation was smaller among *P. glauca* (accession #1) and *P. nigra* (**Figures 5C,I**). As the isoprene signal of $m/z(\text{NO}^+) = 68$ u was much higher than the MBO signal of $m/z(\text{NO}^+) = 69$ u, and the calculated interference of MBO based on $m/z(\text{NO}^+) = 69$ u was close to the control in all cases, the isoprene signal did not result from interference of MBO. The isoprene signal for *P. ponderosa* trees was lower than the interference signal extrapolated from the MBO emissions on $m/z(\text{NO}^+) = 69$ u (**Figure 5G**), so we conclude that, as expected, these trees did not emit isoprene, and that the signal at $m/z(\text{NO}^+) = 68$ u in these cases arose from MBO.

A strong signal at $m/z(\text{O}_2^+) = 71$ u was observed from the emissions of *P. ponderosa*. It can be assigned to MBO since no isoprene emission was observed from this plant and thus no interference of this analyte has to be considered. The signals at $m/z(\text{O}_2^+) = 71$ u of both *P. glauca* accessions and *P. nigra* can be attributed to isoprene based on the isoprene signal [$m/z(\text{O}_2^+) = 67$ u]. These trees thus do not produce MBO. Interestingly, two of the *P. abies* individuals emitted MBO as well (**Figure 5B**). The ratio of isoprene and MBO signals differed substantially between the individual trees. Trees indicated with red and blue in **Figure 5** show much higher isoprene emissions at $m/z(\text{NO}^+) = 68$ u than the tree labeled with yellow. In contrast, the MBO emissions at $m/z(\text{O}_2^+) = 71$ u of the three trees are in the same intensity range. Possible interference by other terpenes was considered improbable since no other naturally occurring hemiterpenes are known, and monoterpene emissions measured at $m/z(\text{H}_3\text{O}^+) = 137$ u, $m/z(\text{NO}^+) = 136$ u, and $m/z(\text{O}_2^+) = 136$ u were a factor of 10–100 lower than the measured isoprene and MBO intensities. Only fragment ions from monoterpenes would overlap with isoprene and MBO, and their branching ratio should decrease the intensity even further.

Based on the measured intensities and eq. (1)–(4) above, we calculated the release rates of isoprene and MBO for mid-day (noon), cf. **Table 1** and **Supplementary Figure S4**. Given the low standard deviation, our results give a good idea of relative emission rates for the tree species and individuals involved. Since we could not calibrate the measured intensities as our VOC standard was not concentrated enough to capture the mixing ratio range of the plants, we had to rely on the internal instrument calibration described by Smith and Spanel (2005). As the uncertainty of measurements without external calibration is estimated to be at least $\pm 35\%$ (Langford et al., 2014) including systematic error, our results may not be very accurate. Calculating the isoprene emission rates based on $m/z(\text{O}_2^+) = 67$ u led to fluxes about 2/3 to 1/2 as high as the fluxes calculated from $m/z(\text{NO}^+) = 68$ u (**Supplementary Figure S6**). Thus when rigorous quantification is needed, we strongly recommend calibration.

DISCUSSION

Using SIFT-MS, we developed a method that allows distinguishing between isoprene and MBO in online measurements. For scientific questions where monitoring of both compounds is essential, e.g., for investigation of drought stress and bark beetle infestation or for monitoring BVOC

emissions at the ecosystem level, this is a reliable, easy method. Full scans of isoprene and MBO analytical standards allowed the selection of the ions $m/z(\text{NO}^+) = 68$ u for measuring isoprene and $m/z(\text{O}_2^+) = 71$ u for measuring MBO. These intense ions show the least interference with signals from the other compound and allow a stable and reliable online measurement of the analytes. As proof of concept we applied the method to the determination of isoprene and MBO emissions during the diurnal cycle in five tree species.

SIFT-MS is capable of measuring isoprene and MBO simultaneously under most conditions because of minimal interference between the two compounds for the diagnostic signals we have selected. However, the ratio of these signals depends on the operating conditions of the instrument, especially sample humidity. Thus, these ratios should be determined with standards under identical measurement conditions as used for the sample.

For more accurate quantification of small amounts of isoprene or MBO in the presence of large amounts of the other compound, one could include the humidity-dependence in the interference calculation. In $I(\text{O}_2^+, 71 \text{ u, isoprene interference}) = x \cdot I(\text{O}_2^+, 67 \text{ u, isoprene})$, x could be replaced by a term dependent on the sample humidity, e.g., $x = a \cdot I(\text{O}_2^+, 19 \text{ u}) + b$, which requires a humidity-dependent calibration of all ions. For simplicity, we decided to use the interference factors determined at very high humidity, as this was closest to the humidity in our experiment.

With SIFT-MS, isoprene and MBO can be determined in a single run. In previous approaches described for this analytical problem, a rather laborious measurement of the analytes with GC-MS for identification and PTR-MS for quantification was employed (Jardine et al., 2020). Using PTR-MS, complex calculations were required for a semiquantitative determination of the analytes. The SIFT-MS method introduced here represents a substantial simplification. With the Eqs (1) and (2), no tedious, humidity-dependent calibration is necessary as for PTR-MS. For increased accuracy, a calibration is advised for SIFT-MS as well (Langford et al., 2014; Lehnert et al., 2019).

Isoprene can even be determined in a 50-fold excess of MBO with SIFT-MS, as the MBO interference signal on the isoprene signal is only 0.5%. MBO determination can be accomplished in the presence of a 20-fold excess of isoprene. Limitations to the method are only to be expected if other analytes with the same mass to charge ratios as used for quantification of isoprene and MBO are present in the VOC mixture of the samples. Isoprene and MBO are abundant in natural BVOC samples (Penuelas and Staudt, 2010), thus this limitation should rarely be a major problem.

The ionization mechanism of the two structurally related analytes was investigated by using deuterated water for air humidification. If $m/z(\text{NO}^+) = 69$ u could form from isoprene by addition of water and than elimination of an OH-radical, in a D_2O atmosphere, we should see a mass shift to $\text{NO}^+/70$ u, and likewise for the O_2^+ ion. As we did not see any deuterated product ions forming when the analytes were ionized with NO^+ and O_2^+ in a deuterium-oxide saturated gas stream, the hydration-dehydration mechanism indicated by the dashed lines in **Figure 1** was not substantiated. Thus, the suppression of

TABLE 1 | Isoprene and MBO emission rates in $\mu\text{g}/(\text{g}_{\text{dryweight}} \times \text{h})$ at 12:00 noon.

	Isoprene			MBO		
	1	2	3	1	2	3
<i>P. abies</i>	8.8 ± 0.2	0.040 ± 0.002	19.5 ± 0.4	0.125 ± 0.006	0.029 ± 0.002	n.s.
<i>P. glauca</i> 1	41.7 ± 0.8	13.3 ± 0.2	64 ± 1	n.s.	n.s.	n.s.
<i>P. glauca</i> 2	25.2 ± 0.7	2.9 ± 0.2	3.3 ± 0.2	n.s.	n.s.	n.s.
<i>P. nigra</i>	175 ± 7	174 ± 4	126 ± 3	n.s.	n.s.	n.s.
<i>P. ponderosa</i>	n.s.	n.s.	n.s.	1.42 ± 0.05	0.79 ± 0.05	0.95 ± 0.05

Values listed represent the mean ± 95% CI. n.s.: After correcting for interference of the other analyte, the signal was not significantly different from 0 ($p = 95\%$). The confidence intervals are calculated based on the measured standard deviations of the intensities, however, these values can only be considered as estimates of the emissions, as the instrument is reported to have an actual error of ±34% (Langford et al., 2014) for the mixing ratio calculation employed.

the major ion under higher humidity-conditions is not caused by a formation of the detected side products, but possibly by suppressing the ionization reaction of the analyte itself.

The SIFT-MS measurement of volatiles from several tree species mostly confirmed previous literature reports of isoprene and MBO production (Kesselmeier and Staudt, 1999). *Picea glauca*, *Picea abies* and *Populus nigra* were found to emit isoprene but not MBO, and *Pinus ponderosa* to emit MBO but not isoprene (Figure 5). The relative release rates we measured allow qualitative comparisons among species and individuals over the entire diurnal cycle with a frequency of 15 min per measurement. If desired, this frequency can even be increased by reducing the number of scans per measurement.

In relation to previous measurements of isoprene, the emission rates determined with SIFT-MS were typically higher than those in the literature, though still of the same magnitude (Evans et al., 1982; Steinbrecher, 1989; Janson, 1993; Kempf et al., 1996; Staudt, 1997; Niinemets et al., 2011). Together they confirm previous observations that poplar trees are higher isoprene emitters than conifers (Sharkey et al., 2008; Laothawornkitkul et al., 2009). For MBO, our measurements of *Pinus ponderosa* were lower (Supplementary Figure S5H) than in the literature (Harley et al., 1998). Differences in isoprene and MBO emission between this study and others can be explained at least in part by natural genetic variation of the trees as well as the environmental conditions of measurement. The instrument was calibrated daily using a one-point calibration with a 2 ppm VOC standard as suggested by the manufacturer. This updated the reaction time and the instrument calibration function used in Eqs. (1) and (2) and ensured stable instrument performance. To avoid systematic errors, we recommend calibrating the SIFT-MS under conditions as close to those of the intended experiment as possible. In particular, matching relative humidity is necessary if precise, quantitative values are required.

Among the individuals of *P. glauca* accession #2, one tree emitted isoprene at much higher rates than the other two trees (Supplementary Figure S5E). Genetic variation in isoprenoid formation is very commonly observed within species of *Picea* and other conifers (Martin et al., 2003; Kännaste et al., 2012). Higher isoprene emission could also originate from exposure to slightly different environmental conditions. The high isoprene-emitting tree also had a greater number of flushing buds compared to the other two trees, which could also translate into a higher isoprene emission rate.

In *P. abies*, two of the three experimental trees (entries labeled red and yellow, Table 1) emitted MBO in addition to isoprene, confirming a previous report on simultaneous emission of both volatiles (Hakola et al., 2017) from a species usually considered to be an exclusive isoprene emitter. Since the young *P. abies* trees measured were reared under controlled conditions, MBO is unlikely to have arisen from bark beetle activity. MBO and isoprene are both biosynthesized from dimethylallyl diphosphate but by different terpene synthases (Gray et al., 2011). Neither enzyme has yet been identified in *P. abies*. Since the *P. ponderosa* MBO synthase also produces a trace amount of isoprene in *in vitro* assays (Zeidler and Lichtenthaler, 2001; Gray et al., 2011), one enzyme could in principle produce both isoprene and MBO. Further work is needed on the genetic and biochemical basis of hemiterpene formation in *P. abies*.

In conclusion, we demonstrated that SIFT-MS is suitable for the simultaneous quantification of isoprene and MBO. We introduced a robust easy-to-use online method that requires minimum data treatment. In a proof of principle study, we measured the diurnal cycle of volatile emission of five different tree species with high time resolution. Single 30 cm trees were sufficient to generate robust signals. This method should be useful in applications in plant sciences, entomology, chemical ecology, and atmospheric sciences.

DATA AVAILABILITY STATEMENT

The datasets presented in this study can be found in online repositories. The names of the repository/repositories and accession number(s) can be found in the article/Supplementary Material. Code and data are published as Lehnert, A., Perreca, E., Gershenson, J., Pohnert, G., Trumbore, S., doi: 10.17617/3.43,2020.

AUTHOR CONTRIBUTIONS

EP and A-SL planned and conducted the tree experiment together. EP organized the trees. A-SL conducted the standard measurements and evaluated all experimental data. EP and A-SL wrote the manuscript together. All authors assisted with data interpretation, discussion of results and helped to improve the quality of the manuscript.

FUNDING

A-SL was financially supported by the Deutsche Forschungsgemeinschaft (DFG) in the frame of the collaborative research center CRC 1076 AquaDiva Project no. 218627073. EP was financially supported by the Max Planck Society and a Max Planck Society-Fraunhofer Society cooperation grant.

ACKNOWLEDGMENTS

Thanks to Agnes Fastnacht and the gardeners of the MPI-CÖ for taking care of the trees in the greenhouse before the experiment, setting up the greenhouse for the experiment, and advice on

REFERENCES

- Atkinson, R., and Arey, J. (2003). Atmospheric degradation of volatile organic compounds. *Chem. Rev.* 103, 4605–4638. doi: 10.1021/cr0206420
- Baader, E. J. (1989). *Pityogenes* Spp.(Col., Scolytidae): investigations on semiochemicals and their application in forest protection. *J. Appl. Entomol.* 107, 1–31.
- Bakke, A., Froyen, P., and Skattebol, L. (1977). Field response to a new pheromonal compound isolated from *Ips typographus*. *Naturwissenschaften* 64, 98–99. doi: 10.1007/bf00437364
- Carlton, A. G., Wiedinmyer, C., and Kroll, J. H. (2009). A review of secondary organic aerosol (SOA) formation from isoprene. *Atmos. Chem. Phys.* 9, 4987–5005. doi: 10.5194/acp-9-4987-2009
- Evans, R. C., Tingey, D. T., Gumpertz, M. L., and Burns, W. F. (1982). Estimates of isoprene and monoterpene emission rates in plants. *Bot. Gaz.* 143, 304–310. doi: 10.1086/botanicalgazette.143.3.2474826
- Fantechi, G., Jensen, N. R., Hjorth, J., and Peeters, J. (1998). Determination of the rate constants for the gas phase reactions of methyl butenol with OH radicals, ozone, NO₃ radicals, and Cl atoms. *Int. J. Chem. Kinet.* 30, 589–594. doi: 10.1002/(sici)1097-4601(1998)30:8<589::aid-kin8>3.0.co;2-o
- Ferronato, C., Orlando, J. J., and Tyndall, G. S. (1998). Rate and mechanism of the reactions of OH and Cl with 2-methyl-3-buten-2-ol. *J. Geophys. Res. Atmos.* 103, 25579–25586. doi: 10.1029/98jd00528
- Goldan, P. D., Kuster, W. C., and Fehsenfeld, F. C. (1993). The observation of a C₅ alcohol emission in a North American pine forest. *Geophys. Res. Lett.* 20, 1039–1042. doi: 10.1029/93gl00247
- Gray, D. W., Breneman, S. R., Topper, L. A., and Sharkey, T. D. (2011). Biochemical characterization and homology modeling of methylbutenol synthase and implications for understanding hemiterpene synthase evolution in plants. *J. Biol. Chem.* 286, 20582–20590. doi: 10.1074/jbc.m111.237438
- Gray, D. W., Lerdau, M. T., and Goldstein, A. H. (2003). Influences of temperature history, water stress, and needle age on methylbutenol emissions. *Ecology* 84, 765–776. doi: 10.1890/0012-9658(2003)084[0765:iotwjs]2.0.co;2
- Guenther, A. B., Jiang, X., Heald, C. L., Sakulyanontvittaya, T., Duhl, T., Emmons, L. K., et al. (2012). The model of emissions of gases and aerosols from nature version 2.1 (MEGAN2.1): an extended and updated framework for modeling biogenic emissions. *Geosci. Model. Dev.* 5, 1471–1492. doi: 10.5194/gmd-5-1471-2012
- Hakola, H., Tarvainen, V., Praplan, A. P., Jaars, K., Hemmilä, M., Kulmala, M., et al. (2017). Terpenoid and carbonyl emissions from Norway Spruce in Finland during the growing season. *Atmos. Chem. Phys.* 17, 3357–3370. doi: 10.5194/acp-17-3357-2017
- Hanson, D. T., Swanson, S., Graham, L. E., and Sharkey, T. D. (1999). Evolutionary Significance of isoprene emission from mosses. *Am. J. Bot.* 86, 634–639. doi: 10.2307/2656571
- Harley, P., Fridd-Stroud, V., Greenberg, J., Guenther, A., and Vasconcellos, P. (1998). Emission of 2-methyl-3-buten-2-ol by pines: a potentially large natural source of reactive carbon to the atmosphere. *J. Geophys. Res. Atmos.* 103, 25479–25486. doi: 10.1029/98jd00820

how to treat the trees so that they are not stressed during the experiment. Thanks to Olaf Kolle for help with the PAR and temperature measurements and the whole tree measurement setup. Thanks to Hasan Mahmudul for helping to pick the trees. Thanks to Axel Schmidt, Thomas Fabisch, Danny Kessler, and Almuth Hammerbacher for providing the trees.

SUPPLEMENTARY MATERIAL

The Supplementary Material for this article can be found online at: <https://www.frontiersin.org/articles/10.3389/fpls.2020.578204/full#supplementary-material>

- Huang, J., Hartmann, H., Hellen, H., Wisthaler, A., Perreca, E., Weinhold, A., et al. (2018). New perspectives on CO₂, temperature and light effects on BVOC emissions using online measurements by PTR-MS and cavity ring-down spectroscopy. *Environ. Sci. Technol.* 52, 13811–13823. doi: 10.1021/acs.est.8b01435
- Janson, R. W. (1993). Monoterpene emissions from Scots pine and Norwegian spruce. *J. Geophys. Res.* 98, 2839–2850. doi: 10.1029/92jd02394
- Jardine, K. J., Zorzanelli, R. F., Gimenez, B. O., Oliveira Piva, L. R., Teixeira, A., Fontes, C. G., et al. (2020). Leaf isoprene and monoterpene emission distribution across hyperdominant tree genera in the Amazon basin. *Phytochemistry* 175:112366. doi: 10.1016/j.phytochem.2020.112366
- Jordan, A., Haidacher, S., Hanel, G., Hartungen, E., Herbig, J., Märk, L., et al. (2009). An online ultra-high sensitivity proton-transfer-reaction mass-spectrometer combined with switchable reagent ion capability (PTR+SRI-MS). *Int. J. Mass Spectrom.* 286, 32–38. doi: 10.1016/j.ijms.2009.06.006
- Kännaste, A., Zhao, T., Lindström, A., Stattin, E., Långström, B., and Borg-Karlson, A.-K. (2012). Odors of Norway spruce (*Picea abies* L.) seedlings: differences due to age and chemotype. *Trees* 27, 149–159. doi: 10.1007/s00468-012-0783-7
- Karl, T., Hansel, A., Cappellin, L., Kaser, L., Herdinger-Blatt, L., and Jud, W. (2012). Selective measurements of isoprene and 2-methyl-3-buten-2-ol based on NO⁺ ionization mass spectrometry. *Atmos. Chem. Phys.* 12, 11877–11884. doi: 10.5194/acp-12-11877-2012
- Kempf, K., Allwine, E. J., Westberg, H., Clariborn, C., and Lamb, B. K. (1996). Hydrocarbon emissions from spruce species using environmental chamber and branch enclosure methods. *Atmos. Environ.* 30, 1381–1389. doi: 10.1016/1352-2310(95)00462-9
- Kesselmeier, J., and Staudt, M. (1999). Biogenic volatile organic compounds (VOC): an overview on emission, physiology and ecology. *J. Atmos. Chem.* 22, 23–88.
- Krechmer, J., Lopez-Hilfiker, F., Koss, A., Hutterli, M., Stoermer, C., Deming, B., et al. (2018). Evaluation of a new reagent-ion source and focusing ion-molecule reactor for use in proton-transfer-reaction mass spectrometry. *Anal. Chem.* 90, 12011–12018. doi: 10.1021/acs.analchem.8b02641
- Langford, V. S., Graves, I., and Mcewan, M. J. (2014). Rapid monitoring of volatile organic compounds: a comparison between gas chromatography/mass spectrometry and selected ion flow tube mass spectrometry. *Rapid Commun. Mass Spectrom.* 28, 10–18. doi: 10.1002/rcm.6747
- Laothawornkitkul, J., Taylor, J. E., Paul, N. D., and Hewitt, C. N. (2009). Biogenic volatile organic compounds in the earth system. *New Phytol.* 183, 27–51. doi: 10.1111/j.1469-8137.2009.02859.x
- Lehnert, A.-S., Behrendt, T., Ruecker, A., Pohnert, G., and Trumbore, S. E. (2020). SIFT-MS optimization for atmospheric trace gas measurements at varying humidity. *Atmos. Meas. Tech.* 13, 3507–3520.
- Loreto, F. (2015). Reconciling functions and evolution of isoprene emission in higher plants. *New Phytol.* 206, 578–582. doi: 10.1111/nph.13242
- Martin, D. M., Gershenson, J., and Bohlmann, J. (2003). Induction of volatile terpene biosynthesis and diurnal emission by methyl Jasmonate in foliage of Norway spruce. *Plant Physiol.* 132, 1586–1599. doi: 10.1104/pp.103.021196
- Niinemetts, Ü, Kuhn, U., Harley, P. C., Staudt, M., Arneth, A., Cescaati, A., et al. (2011). Estimations of isoprenoid emission capacity from enclosure

- studies: measurements, data processing, quality and standardized measurement protocols. *Biogeosciences* 8, 2209–2246. doi: 10.5194/bg-8-2209-2011
- Penuelas, J., and Staudt, M. (2010). Bvocs and global change. *Trends Plant Sci.* 15, 133–144. doi: 10.1016/j.tplants.2009.12.005
- Perreca, E., Gershenzon, J., and Eberl, F. (2020). “Tree volatiles: effects of biotic and abiotic factors on emission and biological roles,” in *Biology of Plant Volatiles*, 2nd Edn, eds E. Pichersky and N. Dudareva (Boca Raton, FL: CRC Press), 361–375.
- Schade, G. W., and Goldstein, A. H. (2001). Fluxes of oxygenated volatile organic compounds from a ponderosa pine plantation. *J. Geophys. Res. Atmos.* 106, 3111–3123. doi: 10.1029/2000jd900592
- Schade, G. W., Goldstein, A. H., Gray, D. W., and Lerdau, M. T. (2000). Canopy and leaf level 2-methyl-3-buten-2-ol fluxes from a ponderosa pine plantation. *Atmos. Environ.* 34, 3535–3544. doi: 10.1016/s1352-2310(00)00120-5
- Schoon, N., Amelynck, C., Debie, E., Bultinck, P., and Arijs, E. (2007). A selected ion flow tube study of the reactions of H_3O^+ , NO^+ , and O_2^+ with a series of C5, C6 and C8 unsaturated biogenic alcohols. *Int. J. Mass Spectrom.* 263, 127–136. doi: 10.1016/j.ijms.2007.01.007
- Sharkey, T. D., Wiberley, A. E., and Donohue, A. R. (2008). Isoprene emission from plants: why and how. *Ann. Bot.* 101, 5–18. doi: 10.1093/aob/mcm240
- Smith, D., and Spanel, P. (2005). Selected ion flow tube mass spectrometry (SIFT-MS) for on-line trace gas analysis. *Mass Spectrom. Rev.* 24, 661–700. doi: 10.1002/mas.20033
- Smith, D., and Spanel, P. (2011). Direct, rapid quantitative analyses of BVOCs Using SIFT-MS and PTR-MS obviating sample collection. *TrAC Trends Analyt. Chem.* 30, 945–959. doi: 10.1016/j.trac.2011.05.001
- Spanel, P., and Smith, D. (1998). Selected ion flow tube studies of the reactions of H_3O^+ , NO^+ , and O_2^+ with several aromatic and aliphatic hydrocarbons. *Int. J. Mass Spectrom.* 181, 1–10. doi: 10.1016/s1387-3806(98)14114-3
- Staudt, M. (1997). *Untersuchungen Der Monoterpen-Abgabe an Europäischen Nadelbaumarten in Abhängigkeit Von Umweltfaktoren*. Ph.D. dissertation, Universität Hohenheim, Stuttgart.
- Steinbrecher, R. (1989). *Gehalt Und Emission Von Monoterpenen in Oberirdischen Organen Von Picea Abies*. Ph.D. dissertation, Technische Universität München, München.
- Steiner, A. L., Tonse, S., Cohen, R. C., Goldstein, A. H., and Harley, R. A. (2007). Biogenic 2-methyl-3-buten-2-ol increases regional ozone and HOx sources. *Geophys. Res. Lett.* 34, L15806–L15812.
- Tingey, D. T., Evans, R. C., Bates, E. H., and Gumpertz, M. L. (1987). Isoprene emissions and photosynthesis in three ferns – the influence of light and temperature. *Physiol. Plant* 69, 609–616. doi: 10.1111/j.1399-3054.1987.tb01974.x
- Zeidler, J., and Lichtenthaler, H. K. (2001). Biosynthesis of 2-methyl-3-buten-2-ol emitted from needles of *Pinus ponderosa* via the non-mevalonate DOXP/MEP pathway of isoprenoid formation. *Planta* 213, 323–326. doi: 10.1007/s004250100562
- Zhang, Q.-H., Schlyter, F., and Birgersson, G. (2012). 2-methyl-3-buten-2-ol: a pheromone component of conifer bark beetles found in the bark of nonhost deciduous trees. *Psyche* 2012:414508.
- Zuo, Z., Weraduwage, S. M., Lantz, A. T., Sanchez, L. M., Weise, S. E., Wang, J., et al. (2019). Isoprene acts as a signaling molecule in gene networks important for stress responses and plant growth. *Plant Physiol.* 180, 124–152. doi: 10.1104/pp.18.01391

Conflict of Interest: The authors declare that the research was conducted in the absence of any commercial or financial relationships that could be construed as a potential conflict of interest.

Copyright © 2020 Lehnert, Perreca, Gershenzon, Pohnert and Trumbore. This is an open-access article distributed under the terms of the Creative Commons Attribution License (CC BY). The use, distribution or reproduction in other forums is permitted, provided the original author(s) and the copyright owner(s) are credited and that the original publication in this journal is cited, in accordance with accepted academic practice. No use, distribution or reproduction is permitted which does not comply with these terms.

Dimethyl sulfide emissions from peatlands result more from organic matter degradation than sulfate reduction

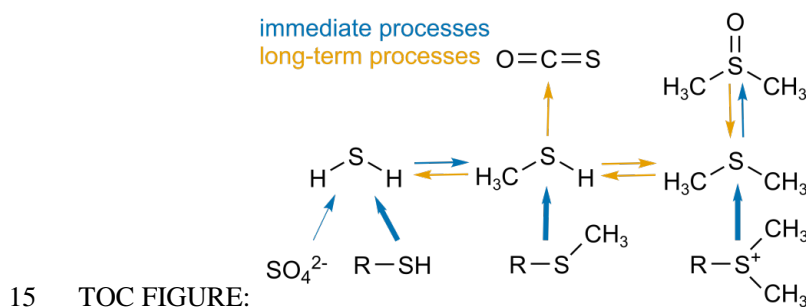
Ann-Sophie Lehnert^{1,2*}, Rebecca E. Cooper³, Rebecca Ignatz^{1,2}, Alexander Ruecker¹, Eliane
5 Gomes-Alves¹, Kirsten Kuesel^{3,4}, Georg Pohnert², Susan E. Trumbore¹

¹ Department of Biogeochemical Processes, Max Planck Institute for Biogeochemistry, Jena,
Germany

² Institute for Inorganic and Analytical Chemistry, Friedrich Schiller University, Jena, Germany

³ Institute for Biodiversity, Friedrich Schiller University, Jena, Germany

10 ⁴German Centre for Integrative Biodiversity Research (iDiv) Halle-Jena-Leipzig, Puschstraße 4,
04103 Leipzig, Germany



KEYWORDS: volatile sulfur compounds, methanethiol, DMS, hydrogen sulfide, sulfur cycle, fen, soil

ABSTRACT. Volatile sulfur compounds (VSCs) contribute to acid rain, cloud formation, and albedo, and thus influence the climate. Their global emissions are still quite uncertain, especially contributions from freshwater wetlands. We investigated the processes leading to hydrogen sulfide (H_2S), methanethiol (MeSH), and dimethyl sulfide (Me_2S) emissions in a slightly acidic peatland and found multiple indications that organic matter degradation rather than sulfate reduction is the main driver for MeSH and Me_2S emissions in this system. Evidence include a different humidity-dependence of emissions of H_2S and Me_2S , and increased emission rates when soils were amended with organic substrates containing thiol groups (H_2S emissions), methylthiols (MeSH), and dimethyl sulfonio groups (Me_2S). VSC precursors were identified from an *Untargeted Metabolomics* data set from the same soil. H_2S and MeSH but not Me_2S could be produced from sulfate reduction based on a ^{34}S -sulfate labelling experiment. Abundance of sulfur cycling microbes like *Acidobacteria* SD 1 and *Desulfosporosinus* correlated with VSC emissions. Our overall conclusion that organic matter degradation is more important than sulfate reduction as a peatlands source of VSC is generalizable to other organic-rich soils, as we found similar emission patterns at different locations around the world.

2

INTRODUCTION

Oceans and wetlands are major sources of reduced volatile sulfur compounds (VSCs), including hydrogen sulfide (H_2S), methanethiol (MeSH), and dimethyl sulfide (Me_2S).¹ These compounds are oxidized to SO_x in the atmosphere. In contact with water, SO_x forms acid rain, and cloud condensation nuclei. Thus, the distribution of VSCs influences local patterns of cloud formation, rainfall and sunlight reflection by the cloud albedo.² Enhanced VSC emissions have also been discussed as a negative climate feedback: As increased temperatures enhance biogenic activity and thus VSC emissions, the increased sulfur burden in the atmosphere will increase cloud formation and stabilizing the climate.³ Yet there are large uncertainties about the magnitude of and factors controlling VSC emissions, particularly on the contribution of freshwater wetlands and other terrestrial ecosystems.⁴

In the terrestrial and freshwater ecosystems, several mechanisms for release of volatile sulfur species exist: Firstly, MeSH and Me_2S emissions can be related to organic matter degradation, as amending soil with the amino acids cysteine, methionine, and S-methyl methionine has led to increased VSC emissions.^{5, 6} One of the identified involved enzymes is methionine- γ -lyase.^{7, 8} Generally, methylthio groups can be cleaved to MeSH and dimethyl sulfonio groups to Me_2S .^{9, 10} Secondly, H_2S can be generated by sulfate reduction.^{11, 12} This usually occurs at a pH-dependent redox potential between -100 mV and -200 mV.¹³ Acetogenic bacteria can methylate H_2S to MeSH and MeSH to Me_2S via methylthiol transferases.¹⁴ The methyl group can originate from methoxyaromatic compounds, e.g. lignin degradation products.^{15, 16} Thirdly, Me_2S formation from dimethylsulfoxide (DMSO) and MeSH formation from dimethyl disulfide (DMDS) are known.¹⁷ Together with methanogenesis, sulfate reduction is considered as a main pathway in anoxic lake sediments, with VSCs being degraded when going through the water column.

However, the relation to organic matter degradation was never explicitly investigated, so emissions could occur at a broader range of environmental conditions than previously thought.

In this study, we demonstrate that organic matter degradation is the more important and more widespread process leading to VSCs. Using soil from a peatland known for its active sulfur cycling and frequent fluctuations in redox potential,¹⁸⁻²¹ we investigated the link of VSC emissions to redox potential and water content of the peat soil. We combined dynamic and static chamber approaches that allowed us to separate VSC (de)-methylation reactions from the initial production of the VSCs in a variety of soils. Involvement of VSC precursors from soil organic matter and microbial community composition were also investigated. This way, we show that organic matter can be a significant source of VSCs, not only from wetlands, but also from forest soils.

MATERIALS AND METHODS

For details on the analysis methods, please refer to the supplementary information.

SITE DESCRIPTION AND SAMPLING PROCEDURES.

Peat soil was sampled from the well characterized Schläppnerbrunnen II fen, a mineratrophic peatland fed by mineral-rich surface water in the Lehstenbach catchment in the Fichtel Mountains in Germany (50°07'54.2"N, 11°52'51.4"E).¹⁸⁻²¹ The exact sampling locations were the same as in Kugler, et al.²² At the sampled site, a fibric histosol layer covers a Gleysol from granite bedrock at 70-90 cm depth.^{21, 23} It is mainly covered by the grass *Molinia caerulea*. The water table depths varies between 0.13-0.76 m.²¹ High concentrations of Fe(II) (mean(2001–2004) = 0.3 mmol L⁻¹), dissolved organic carbon (DOC, mean(2001–2004) = 5.1 mmol L⁻¹) and solid organic carbon (C_{org}; mean = 37%) have been reported previously.²³

The site was sampled in June 2019 and September 2019 for both the long-term incubation and the dry-out and rewetting experiments and again in July 2020 for the manipulation and labelling experiments. The water table depth was at approx. 50 cm for 06/2019 and 07/2020 and at 20 cm for 09/2020. Soil cores were taken with a Pürkheimer corer. After removal of plant debris, the cores were separated into depth intervals of 0-10 cm and 10-20 cm for the rewetting experiment, and pooled at 0-20 cm depth for the other experiments. Cores were stored at 4 °C in polyethylene ziplock bags from which the air was removed. Peat water was collected with a syringe and a ¼” silicone tube directly from the water table in the holes the Pürkheimer corer left and stored in completely filled 2 L Schott bottles at 4°C.

DRY-OUT INCUBATION.

3x 100 g field-moist peat soil pooled from 2019 campaigns were submerged in 150 mL distilled water. Two replicates were placed in chambers with redox probes in the bottom, and the third one was placed in a Teflon chamber on a balance (Figure S1-S2). Additionally, 2x 100 g acid-washed dry sand were submerged in 150 mL distilled water as controls, and one of them was placed in a redox chamber and the other one on the balance. All five chambers were flushed with 400±10 mL/min nitrogen for three weeks. Mass spectra of all chambers and a 1 ppb VSC standard were recorded every 1.5 h, the redox potential every second, the soil weights on the balance and the nitrogen gas flows were determined daily. After the dry-out, the soil’s residual water content, pH, sulfate and nitrate content were determined.

The experiment was then repeated with VOC-free air (20% O₂, 80% N₂) instead of pure nitrogen.

SAMPLE REWETTING.

100 Air-dried soil cores from the Schlöppnerbrunnen M and C site, from two different depths (1-10
cm and 10-20 cm) from 06/2019 were pooled and supplemented with distilled water until
reaching 30%, 60%, 100% and 150% of the soil's water holding capacity. They were incubated
in an open jar at room temperature for 24 h after which the water lost by evaporation was added
again. Then, they were put into the dynamic chamber system for 30 min (pure air flow =
105 400 mL/min), and the VSCs were measured with the SIFT-MS.

These experiments were also performed for soils from sites from other locations (Table S4).

PROLONGED INCUBATION IN STATIC CHAMBERS UNDER ARGON.

120 g of the pooled peat soil cores from 09/2020 were submerged in 100 mL peat water in 250
mL Schott bottles with 2 cm thick butyl rubber plugs and supplemented with 60 μ L solution of 1
110 M glucose, 1 M lactate, and 1 M acetate. The bottles were flushed with Argon for 1 h and then
incubated at 13°C in the dark for up to four weeks. Five bottles were autoclaved twice at 120°C
for 20 min before incubation. The next morning and then every week, five bottles plus one
autoclaved bottle were sampled. They were flushed with 400 mL/min nitrogen for 30 min
followed by a SIFT-MS measurement of the VOC emissions in the gas stream exiting the bottle.
115 Then, headspace samples for the greenhouse gas emission measurements were taken. Aliquots of
the soil were frozen to -80°C for subsequent soil metabolomics and 16S-RNA amplicon
sequencing. Nitrite content and pH were measured from the fresh soil. Another aliquot was dried
at 40°C and then used for the geochemical analyses (Figure S3).

SUBSTRATE MANIPULATION IN DYNAMIC CHAMBERS.

120 For each added substrate, 100 g field-moist pooled peat soil from 11/2019 was incubated under
200 mL/min nitrogen at room temperature. To achieve anoxic conditions, the soil was
preincubated for two days before the measurements started. After measuring the initial soil

6

emissions, 1.29 mmol of the substance (equal the total sulfur amount present based on the element analysis) dissolved in 10 mL distilled water was added through the outlet of the Teflon chamber using a syringe. For every six substances, one control with only distilled water was measured. The VSC emissions were tracked for four days immediately following addition. Every time each of the seven chambers incubated in parallel was measured, a one-point calibration at 1 ppb VSC-standard was made to account for changes in the instrument performance. Remaining soil moisture, sulfate and nitrite/nitrate content were measured after each incubation.

130 SULFUR SUBSTRATE ADDITION AND ANTIBIOTIC TREATMENT IN STATIC CHAMBERS.

Field-moist pooled peat soil from 07/2020 (8 g) was incubated under nitrogen in 120 mL glass bottles with a butyl rubber septum. The soil was flushed with nitrogen for 1 h. After 24 h, 103 μ mol of different sulfur substances dissolved in 3 mL distilled water were added to the bottles with a syringe. Glutaraldehyde, tungstate and bromoethanesulfonate were added to a final concentration of 2 mM, chloramphenicol to 25 mM, and chloroform to 1 mM.^{24, 25} Triplicates were analyzed for each treatment, as well as six control samples where only water was added. Immediately after the addition and then daily, VSC emissions were measured *via* a needle connected to the SIFT-MS via a short tube. The headspace air that was withdrawn for the measurement was replaced by N₂ via a second needle leading to a tube continuously flushed with N₂. This way, the headspace was not completely exchanged, but kept as stable as possible.

³⁴SO₄²⁻ LABELLING.

100 g field-moist pooled peat soil from 07/2020 were incubated under constant flushing with nitrogen (200 mL/min) for two days. Then, water was added through the gas outlet to meet the original water content. 4x 60 mg Na₂³⁴SO₄ dissolved in 10 mL freshly deionized water were added to four of the chambers. 60 mg unlabeled Na₂SO₄ in 10 mL deionized water were added to

a fifth chamber, and 10 mL deionized water without any sulfate salt was added to a sixth chamber. The gas emissions of the samples were measured continuously with SIFT-MS. After one week, the same amount (mol) of organic substances were dissolved in 10 mL fresh deionized water and added to chambers 1-3: (1) cysteine, (2) a 1:1 mixture of methionine and S-methyl methionine, and (3) a 1:1 mixture of syringic acid and 1-,3-,5-trimethoxybenzoate. The experiment was continued for another four days with continuous VSC-measurements.

RESULTS AND DISCUSSION

INFLUENCE OF REDOX POTENTIAL AND SOIL HUMIDITY ON VSC EMISSIONS

First, we investigated how changes in redox potential and soil humidity vary VSC emissions. When drying out soil under a constant stream of nitrogen over three weeks (Figure 2 and S4), the redox potential decreases from +400 mV at the initial 8 g H₂O/g_{dw} (g soil dry weight) to +220 mV at 3 g H₂O/g_{dw}; probes do not provide reliable results below 2 g H₂O/g_{dw}. The redox potential of ~200 mV matches the standard electrode potential of Fe(OH)₃/Fe²⁺ systems at the soil's pH (Table S6),²⁶ even with the slight decrease of the pH from pH = 4.5 to pH = 3.9 during the incubation (Table S5). H₂S emissions increase with decreasing redox potential and moisture content, but with an intermediate peak at 5–4 g H₂O/g_{dw} (Figure 2, S5). In contrast, Me₂S and MeSH emissions peak between 5–2 g H₂O/g_{dw}. A plot of the emissions against the redox potential shows a sharp increase of H₂S and MeSH emissions at 200-250 mV, and then a steady decline for MeSH and a constant value for H₂S (Figure S5). Me₂S steadily declines over the redox potential range, but shows a strong peak at 220 mV for one of the chambers. Under oxic conditions (the same experiment but purging the headspace with synthetic air at 20% O₂), we observe higher H₂S emissions at low moisture content, but strong reductions in other VSCs and volatile organic compounds (VOCs) (Figure S6, S7).

The increase of H₂S emissions at low soil moisture is not an artifact of the dryout: When
170 rewetting dry soil to different moisture contents, H₂S decreases with increasing soil moisture
(Figure S8). Me₂S and MeSH are less dependent on soil moisture, with maximum emissions at
~60% water holding capacity (~2 g H₂O/g_{dw}). This finding suggests Me₂S is likely not produced
from H₂S directly, and other processes might be involved.

A similar study that measured VSC emissions at different redox potentials in salt marsh
175 sediment slurries also found that H₂S was only emitted at E_H < -50 mV (pH = 6.3), whereas
MeSH, Me₂S, COS, and CS₂ were emitted regardless of the redox potential.²⁷ MeSH and Me₂S
are thus likely formed from organic matter in diverse environments. The pathways in salt marsh
sediments might however differ, since there Me₂S release is related to
dimethylsulfoniopropionate and not amino acids as precursors.

180 We repeatedly found a difference between H₂S and DMS emission patterns in soils sampled
from different locations around the world (Figure S9). The rainforest and temperate forest soils
show the same humidity-dependence as observed for the peat soils, whereas VSC emissions from
agricultural soils did not differ significantly from the control. The salt marsh soils from coastal
North Carolina, USA, emitted more DMS at low soil moisture, and had 10x higher MeSH
185 emissions than the soils we compared them to (Figure S9).

VSCS FROM SULFATE REDUCTION – LABELLING WITH Na₂³⁴SO₄ AND UNLABELED ORGANIC SUBSTANCES

Addition of ³⁴S labeled sulfate in amounts that doubled initial sulfate concentrations led to
build-up of labelled H₂³⁴S and Me³⁴SH emission rates, ending with the same emission rates as
190 non-labelled H₂³²S and Me³²SH in the same sample (Figure 3, S10-13, Table S7). However,
emissions of labelled Me₂³⁴S were close to the detection limit and not significantly different from

the control, whereas non-labelled Me_2^{32}S emissions remained constant at a relatively high level throughout the experiment.

We then tested whether organic compounds or sulfate are more important for the VSC
195 formation. We added cysteine with normal isotopic ratios as a sulfate reduction inhibitor and
potential H_2S precursor to the soils labelled with $\text{Na}_2^{34}\text{SO}_4$. This decreased H_2S formation (for
both labelled and unlabeled SO_4^{2-}) and decreased the amount of labelled MeSH by a factor of
three (Figure S14-16). As direct MeSH and Me_2S precursors, we added a mixture of methionine
and *S*-methyl methionine in the same manner as cysteine. This had no influence on H_2S
200 emissions, but non-labelled MeSH and Me_2S emissions increased by 2-3 orders of magnitude
(Figure S14-16).

To test whether we can enhance the conversion of H_2S to MeSH and MeSH to Me_2S by adding
methyl group donors, we added syringate and trimethoxybenzoic acid.^{28, 29} This increased the
emission of H_2^{32}S and Me^{32}SH by a factor of 10, but did not have an influence on H_2^{34}S ,
205 Me^{34}SH , Me_2^{32}S and Me_2^{34}S (Figure S14-16).

H_2^{34}S and Me^{34}SH emissions are in line with other labelling studies.^{30, 31} Since we could not
detect Me_2^{34}S , we conclude that the methylation of MeSH to Me_2S is less favorable or slower
than the methylation of H_2S to MeSH. We observed Me^{34}SH release rates in the same order of
magnitude as H_2^{34}S , whereas Me_2^{34}S was not detected (Figure 3). This is in contrast to the
210 studies claiming a high thiol methylation potential and thiol methyltransferase activity in soil,^{7, 8,}
¹⁴ with MeSH present only in trace concentrations.^{15, 16}

ORGANIC MATTER SULFUR COMPOUND PRECURSORS – IMMEDIATE RESPONSE OF VSC
EMISSION

215 Concluding that organic matter is likely a more important precursor for VSCs than sulfate, we
evaluated which organic compounds can be cleaved to VSCs. Based on an identification of
sulfur metabolites in the peat soil (Table S9, S10), we added different organic VSC precursors
known from the literature as well as structural analogues, and measured the immediate VSC
response in dynamic chamber incubations under N₂ (Figure 4A and S18-22, Table S8). Our
220 hypothesis was that dimethylsulfonio groups should be cleaved to Me₂S, methyl thiol groups to
MeSH, and thiol groups to H₂S by a substitution reaction with OH⁻³²⁻³⁴ or potentially also by an
elimination reaction analogous to the DMSP-lyase mediated cleavage.³⁵ Spiking substances with
oxidized or aromatic sulfur atoms like cysteic acid or thiophene carboxylate should not lead to
enhanced VSC emissions, as they cannot be converted to VSCs directly. Our results mostly
225 confirm our hypothesis – cystine, sodium sulfate, and coenzyme M lead to H₂S, methionine, S-
methyl cysteine, and N-formyl methionine lead to MeSH. S-methyl methionine and gonyol are
cleaved to form Me₂S, while cysteic acid and thiophene carboxylate do not increase Me₂S
emissions. Methionine S-oxide also enhances MeSH emissions, which might be due to a quick
reduction to methionine before it is cleaved. However, some compounds do not behave as
230 expected: dimethylsulfonio acetate is not utilized as Me₂S precursor. Cysteine leads to MeSH
emissions, N-acetyl methionine and 3-(methylthio)-propionic acid emit substantial amounts of
Me₂S, but hardly any MeSH. We conclude these compounds were methylated before cleavage,
as we did also not observe the methylation of MeSH.

CYCLING OF VSCs IN THE CHAMBER HEADSPACE

235 After analyzing the immediate VSC emission response to adding organic sulfur compounds to the soil, we tested if VSC mixing ratios reflect other reactions when allowed to build up in the chamber headspace, as they would in soil pores. Therefore, we incubated peat soil with the same added substrates in static chambers with a stable N₂ headspace, see Figure 4B, S26-29, and Table S8. In general, we observe stronger Me₂S formation during incubation in static chambers than in 240 dynamic chambers. Even for substances that mainly produce H₂S or MeSH in the dynamic chambers, Me₂S is the major component in the headspace when incubating in static chambers with an up to 10-fold excess of Me₂S over MeSH and H₂S (Figure 4B, S26-29, and Table S8). We thus conclude in accordance with literature^{36, 37} that cycling between the different VSCs determines VSC mixing ratios when their residence time in the pore space is high enough. To see 245 whether the ratio of Me₂S:MeSH reaches an equilibrium, we plotted all the measurements of the static chamber substance additions in one graph (Figure S26). We could still distinguish Me₂S precursor compounds from MeSH precursors, as the ratio of Me₂S to MeSH was much higher (100-1000:1 vs. 1-10:1) and had a higher slope than for all other samples. Since we can distinguish between situations where Me₂S was emitted initially and where H₂S or MeSH were 250 emitted initially, MeSH conversion to Me₂S is more eminent than Me₂S conversion to MeSH.

INVOLVED MICROBIAL PROCESSES

To assess which microbial process might be involved in VSC formation and cycling, we repeated the anoxic static chamber incubations with inhibitors for specific pathways. We used bromoethanesulfonate (BES) for inhibition of coenzyme M in methanogens, tungstate to inhibit 255 sulfate reducers, chloroform to inhibit methylotrophs, and glutaraldehyde and chloramphenicol for a general microbial inhibition (Figure S27-S29, 32).^{24, 25} Regardless of the inhibitor added, 12

Me₂S was increased compared to a control without inhibitors (Figure S29), which either means Me₂S is formed abiotically or that the activity of Me₂S degraders was inhibited more strongly than the activity of Me₂S producers. MeSH emission increased in treatments with
260 glutaraldehyde, chloramphenicol, and chloroform (Figure S28), which supports the hypothesis that VSC degraders were inhibited more strongly than VSC producers. Tungstate and BES showed no effect; suggesting that methanogens and sulfate reducers were not involved in MeSH formation. H₂S emissions decreased with all inhibitors except when adding BES (Figure S27). Maybe the inhibition of methanogens increased the amount of substrate available for sulfate
265 reducing bacteria, which in turn were more active in reducing sulfate to sulfide.

LONG-TERM ANOXIC INCUBATION, CORRELATION OF VSCS, ORGANIC MATTER, AND MICROBIAL COMMUNITY

To ensure we achieved active sulfate reduction, we submerged peat soil in pore water from the same location, and incubated it in a closed chamber under Argon for up to four weeks (Figure 5).
270 During this period, we measured volatile sulfur compounds, greenhouse gas emissions, and nutrient concentrations. The transition from nitrate reduction in the first two weeks to sulfate reduction and methanogenesis in the last 2 weeks of the incubation was observed in the changing makeup of pore waters and gas emissions (Figure 5B, S33-34). Parallel activities of sulfate reduction and methanogenesis in the Schlöppnerbrunnen fen was which is characterized as a
275 low-sulfate habitat was shown before.¹⁸ The decrease in sulfate correlated with an increase in H₂S and Me₂S levels, whereas MeSH first increased and then remained constant in the second half of the experiment (Figure 5A).

Non-volatile organic sulfur species were measured in water and acetonitrile extracts of organic matter using LC-MS and GC-MS. Principal Component Analyses (PCA) of the resulting

280 metabolome indicated alteration of the organic matter over time (Figure 5C and S35), with a
general decrease of H/C and O/C (Figure S36, S38), but not S/C ratios (Figure S37, S39). Our
hypotheses were: If a sulfur compound is degraded over time (i.e. its concentration correlates
negatively with time), it is consumed by microbes and thus could be a precursor for MeSH or
Me₂S. If a sulfur compound increases over time (positive correlation with time), it could be
285 produced from H₂S from sulfate reduction, and a fraction of its concentration could again be
degraded by other microbes to form MeSH and DMS. We could putatively identify 12 organic
sulfur compounds correlating positively with time and 34 organic compounds correlating
negatively with time, see Figure S40-41 and Table S9-S10. Of the 81 detected putative
compounds, 15 could be identified by MS²-experiments and five confirmed by co-injection of
290 standards. These five compounds were the ones we selected to add to peat soil in the experiments
above. Quantification of the compounds (Figure S42) showed that their concentrations were
between 0.004 and 0.1 nmol/g_{dw}. Relative to the soil's sulfur content, between 1 in 10⁶ to 10⁹ S
atoms were extracted as these organic sulfur compounds, and approx. 2% of all S atoms could be
extracted as sulfate – 98% of the sulfur could not be attributed to any compound class by these
295 extractions (Table S11).

LONG-TERM ANOXIC INCUBATION – CORRELATION WITH MICROBIAL COMMUNITIES

At all time points, microbial communities were dominated by Acidobacteria, Proteobacteria,
Firmicutes, Verrucomicrobia, and Actinobacteria accounting for up to 86.8% of the sequence
reads in the samples. All these genera have members associated with dissimilatory S cycling
300 processes (sulfate/sulfite reduction and sulfur oxidation). Overall, the microbial community
composition on the phylum level remained stable throughout the course of the incubation period,
with exception of Firmicutes, which increased from 0.13% (n=1) at T0 to 11.5% (n=4) after 3
14

weeks (Figure S43-44). A pronounced shift in the microbial community composition was not expected, as fen microbes should be adapted to water table fluctuations inducing redox
305 fluctuations.

On the Genus level, we found 33 genera linked to sulfur cycling (Figure 5D, S45). *Acidobacteria* SD 1 ($r = 0.71$), *Desulfosporosinus* ($r = 0.72$), and *Pseudomonas* ($r = 0.50$) correlated positively with time and VSC emissions, *Desulfobacca* ($r = -0.63$), uncultured *Desulfobulbaceae* ($r = -0.55$), *Synthrophobacter* ($r = -0.68$), and uncultured *Thermodesulfovibrio*
310 ($r = -0.57$) correlated negatively. Metatranscriptome analysis demonstrated expression of acidobacterial sulfur-metabolism genes and their upregulation in anoxic incubations of the Schlöppnerbrunnen fen.³⁸ Some of these *Acidobacteria* are also able to liberate sulfite from organosulfonates, which suggests organic sulfur compounds as complementary energy sources which would also affect VSC emissions. Despite its small population size in our incubations
315 *Desulfosporosinus* has been shown to be a keystone species in this fen, where it is responsible for a considerable part of sulfate reduction due to its high cell-specific sulfate reduction rates³⁹ showing the importance of rare species for ecosystem activities.⁴⁰ The other sulfur cycling species had correlation coefficients lower than 0.5. *Thiobacillus* and *Hyphomicrobium*, known for their VSC demethylation,⁴¹ only showed a low correlation with time/VSC emissions, $r = 0.19$
320 and 0.24. As outlined above, microbial abundance does not necessarily reflect microbial activity, so also other microbes might have contributed to VSCs cycling as well.

ALTERNATE MECHANISMS

MeSH and Me₂S emissions from H₂S involving methoxylated aromatic compounds, like in anoxic sphagnum peats,^{12, 15, 16, 24, 30} likely does not play a big role in other freshwater
325 environments.¹¹ MeSH formation from sulfate reduction without involvement of methoxylated
15

aromatic compounds might be a factor: either directly via thiol methyltransferases,^{14, 31} or with methane⁴², CO⁴³ or CO₂/bicarbonate^{11, 44} being involved. Me₂S emissions are most likely no by-products of inefficient methanogenesis, as methanogens were not involved (no inhibition by BES).^{11, 45} Alternatively, abiotic VSC formation with the help of FeS in the presence of CO₂,⁴⁶
330 would be supported by the fact that Me₂S emissions were always increased with inhibitors. However, temperatures above 50°C were needed to observe significant conversions,⁴⁶ supporting a biotic conversion.

When we allowed the headspace to build up to high VSC mixing ratios, we found that Me₂S emissions were always much higher than MeSH and H₂S emissions. However, this was not the
335 case for our long-term incubation. Me₂S might actually be formed to detoxify H₂S and MeSH,⁴⁷⁻⁴⁹ suggesting a threshold mixing ratio above which the conversion into the less toxic Me₂S occurs. Still, from our data, the most likely mechanism is organic matter degradation, as the mechanisms discussed in this paragraph rely on sulfate reduction to H₂S, and we found that Me₂S emissions were independent of sulfate reduction.

340 SIZE OF THE ORGANIC MATTER SULFUR POOL

The individual concentrations of the identified organic compounds are rather small; only 10⁻⁶-10⁻⁹ mol/mol S were found for the quantified organic compounds. Since both the organic sulfur compound and the sulfate analyses were only performed on extracts of the soils and this only accounts for ~2% of the total sulfur, the actual concentrations of the different sulfur compounds
345 in the soil remain unknown. In a survey of 30 different soils by Meredith, et al.⁵⁰ only 1-25% of the total sulfur was sulfate, but 20-55% were organic sulfur in the form of R-S-S-R, R-SH, or R-S-R, which could be potential VSC precursors. Since the carbon content of the soil was high, it is likely that much of the sulfur could be as reduced organic sulfur. Thus, it seems highly likely that
16

a high number of very different organic sulfur compounds are present, each individually at a low
350 concentration, but when adding them all up being the most abundant VSC precursor in the soil.

MAGNITUDE OF VSC EMISSIONS

The range of VSC emissions we observed from the peat soils under anoxic conditions was up
to 2 ng/(g_{dw} h) H₂S, 1 ng/(g_{dw} h) MeSH, and 1.5 ng/(g_{dw} h) Me₂S. These emissions correspond to
approx. 40 mg S/(m² a) H₂S, 15 mg S/(m² a) MeSH, and 20 mg S/(m² a) Me₂S. The H₂S
355 emissions are similar to the emissions from American histosol peats and bogs measured by
Adams,⁵¹ but the Me₂S emissions are a factor 2-5 higher than their reported values. In
comparison to different Florida wetlands, our H₂S and Me₂S release rates are well within the
reported range of release rates.⁵² Estimated Me₂S emissions were in a similar magnitude as the
maximum emissions observed from Canadian Shield lakes (1.5 μmol/(m² d) in our study vs. a
360 maximum of 1.2 μmol/(m² d) in ⁵³). Comparison to other lake studies is difficult, because
usually, only the concentration in the water column is reported.

IMPLICATIONS FOR GLOBAL VSC EMISSIONS

Organic matter as VSC precursor might be very widespread, since we not only observed VSC
emissions from wetlands, but also from forest soils. The emission rates observed for the
365 Würzbachgrund beech forest site were an order of magnitude lower than our wetland emissions.
However, considering that forests cover a global area five times larger than wetlands,⁴ forest soil
emissions globally could be as important as wetland emissions. This is accord with the
observation that methanethiol methyl transferases are widespread in soil environments, including
forests.⁷ In contrast to forests and wetlands, we did not observe significant VSC emissions from
370 agricultural sites. Land use change to generate more fields by drying out wetlands and
deforestation could thus decrease VSC emissions and alter the sulfur cycle in those areas.

We conclude that Me₂S emissions from organic matter as well as H₂S and MeSH emissions from sulfate reduction are immediate processes, whereas VSC interconversion is a slower, more long-term process generating energy and lowering VSC toxicity. This increases the number of
375 VSC-emitting soils greatly, since organic matter degradation not only occurs in wetlands, but also in more arid soils. Thus, future studies to measure VSC emissions from regions with high litter and soil organic matter contents are warranted, to better constrain their role in global sulfur budgeting.

ASSOCIATED CONTENT

380 Supporting Information: PDF-document with additional methods, results, and discussion including 45 figures and 11 tables

AUTHOR INFORMATION

Corresponding Author

*Ann-Sophie Lehnert, Max Planck Institute for Biogeochemistry, Department of
385 Biogeochemical Processes, Hans-Knöll-Str. 10, 07745 Jena, e-mail: alehnert@bgc-jena.mpg.de

Author Contributions

R.I. measured and analysed the VSC and greenhouse gas emissions as well as the geochemical soil parameters in the long-term incubation experiment. R.E.C. did the 16S rRNA amplicon sequencing and its analysis. A.S.L. designed the study, and conducted and evaluated the remaining experiments: the dryout and rewetting experiments, the labelling experiment, the substance
390 amendment experiments, the soil metabolomics for the long-term incubations, and the soil screening. She also mainly wrote the manuscript. All authors assisted with data interpretation, and discussion of results and helped to improve the quality of the manuscript.

Funding Sources

18

395 Funding was supplied by the Max-Planck Institute for Biogeochemistry, the Collaborative Research Centre AquaDiva (CRC 1076 AquaDiva, Project No. 218627073) and the Collaborative Research Centre ChemBioSys (CRC 1127 ChemBioSys, Project No. 239748522) of the Friedrich Schiller University Jena, funded by the Deutsche Forschungsgemeinschaft.

ACKNOWLEDGMENTS

We cordially thank Mariela Leidermann (Ben-Gurion University of the Negev, Israel), John Wang (University of North Carolina, USA), Magnus Kramshøj (University of Copenhagen, Denmark), Thomas Behrendt, and Elisa Catão (both formerly Max-Planck-Institute for Biogeochemistry, Jena), for providing the soil samples from international sites. Thanks to Cornelius Kappelhoff (Max Planck Institute for Biogeochemistry, Jena), who helped sampling at Schlöppnerbrunnen and the other German sites and assisted with conducting the static substance manipulation experiment. We also thank Jens D. Wurlitzer (Friedrich Schiller University, Jena) for assistance with sampling at the Schlöppnerbrunnen fen. Thanks to Xinyue Wang (Friedrich Schiller University, Jena) for assisting with the soil screening measurements, and to Erik Jäger (Friedrich Schiller University, Jena) for assisting with the dynamic chamber incubation with BES and chloramphenicol. We thank Joe von Fischer and Thomas Behrendt (both formerly Max-Planck-Institute for Biogeochemistry, Jena) for developing the redox chambers, and Karl Kübler (Max Planck Institute for Biogeochemistry, Jena) for building them.

CODE AND DATA AVAILABILITY

Code and data are available as a data publication Lehnert, A.-S. Cooper, R., Ignatz, R., Ruecker, A., Gomes-Alves, E., Küsel, K., Pohnert, G., Trumbore, S. E., Raw data for "Dimethyl sulfide emissions from freshwater wetlands result more from organic matter degradation than sulfate reduction". Max Planck Society, <https://dx.doi.org/10.17617/3.50>. Raw 16S rRNA amplicon sequencing reads were deposited at the ENA.

ABBREVIATIONS

BES: bromoethanesulfonate, COS: carbonyl sulfide, DMDS: dimethyl disulfide, DMSO: dimethyl sulfoxide, DMSP: 3-(dimethylsulfonio)-propionate, GC-MS: gas chromatography-mass spectrometry, LC-MS: liquid chromatography-mass spectrometry, MeSH: methanethiol, Me₂S: dimethyl sulfide, PCA: principle component analysis, SIFT-MS: selective ion flow tube mass spectrometry, VSC: volatile sulfur compound

REFERENCES

1. Aneja, V. P.; Cooper, W. J., Biogenic sulfur emissions. In *Biogenic Sulfur in the Environment*, American Chemical Society: 1989; Vol. 393, pp 2-13.
2. Berglen, T. F., A global model of the coupled sulfur/oxidant chemistry in the troposphere: The sulfur cycle. *J. Geophys. Res.* **2004**, *109*, (D19).
3. Charlson, R. J.; Lovelock, J. E.; Andreae, M. O.; Warren, S. G., Oceanic Phytoplankton, Atmospheric Sulfur, Cloud Albedo and Climate. *Nature* **1987**, *326*, (6114), 655-661.
4. Watts, S. F., The mass budgets of carbonyl sulfide, dimethyl sulfide, carbon disulfide and hydrogen sulfide. *Atmos. Environ.* **2000**, *34*, (5), 761-779.
5. Banwart, W. L.; Bremner, J. M., Formation of volatile sulfur compounds by microbial decomposition of sulfur-containing amino acids in soils. *Soil Biol. Biochem.* **1975**, *7*, (6), 359-364.
6. Segal, W.; Starkey, R. L., Microbial Decomposition of Methionine and Identity of the Resulting Sulfur Products. *J. Bacteriol.* **1969**, *98*, (3), 908-913.
7. Carrion, O.; Curson, A. R.; Kumaresan, D.; Fu, Y.; Lang, A. S.; Mercade, E.; Todd, J. D., A novel pathway producing dimethylsulphide in bacteria is widespread in soil environments. *Nat. Commun.* **2015**, *6*, 6579.
8. Carrion, O.; Pratscher, J.; Curson, A. R. J.; Williams, B. T.; Rostant, W. G.; Murrell, J. C.; Todd, J. D., Methanethiol-dependent dimethylsulfide production in soil environments. *ISME J.* **2017**, *11*, (10), 2379-2390.
9. Schäfer, H.; Eyice, Ö., Microbial cycling of methanethiol. *Curr. Issues Mol. Biol.* **2019**, *33*, 173-182.
10. Dahl, C., A biochemical view on the biological sulfur cycle. In *Environmental Technologies to Treat Sulphur Pollution: Principles and Engineering*, 2020; pp 55-96.
11. Lin, Y. S.; Heuer, V. B.; Ferdelman, T. G.; Hinrichs, K. U., Microbial conversion of inorganic carbon to dimethyl sulfide in anoxic lake sediment (Plußsee, Germany). *Biogeosciences* **2010**, *7*, (8), 2433-2444.
12. Stets, E. G.; Hines, M. E.; Kiene, R. P., Thiol methylation potential in anoxic, low-pH wetland sediments and its relationship with dimethylsulfide production and organic carbon cycling. *FEMS Microbiol. Ecol.* **2004**, *47*, (1), 1-11.

13. Kirchman, D. L., *Processes in Microbial Ecology*. Oxford University Press: Oxford, 2012.
- 455 14. Drotar, A.; Burton, G. A.; Tavernier, J. E.; Fall, R., Widespread Occurrence of Bacterial Thiol Methyltransferases and the Biogenic Emission of Methylated Sulfur Gases. *Appl. Env. Microbiol.* **1987**, *53*, (7), 1626-1631.
15. Finster, K.; Kling, G. M.; Bak, F., Formation of methylmercaptan and dimethylsulfide from methoxylated aromatic compounds in anoxic marine and fresh water sediments. *FEMS Microbiol. Lett.* **1990**, *74*, (4), 295.
- 460 16. Bak, F.; Finster, K.; Rochfuß, F., Formation of dimethylsulfide and methanethiol from methoxylated aromatic compounds and inorganic sulfide by newly isolated anaerobic bacteria. *Arch. Microbiol.* **1992**, *157*, (6), 529.
17. Kiene, R. P.; Capone, D. G., Microbial transformations of methylated sulfur compounds in anoxic salt marsh sediments. *Microb. Ecol.* **1988**, *15*, (3), 275-291.
- 465 18. Küsel, K.; Blöthe, M.; Schulz, D.; Reiche, M.; Drake, H. L., Microbial reduction of iron and porewater biogeochemistry in acidic peatlands. *Biogeosciences* **2008**, *5*, (6), 1537-1549.
19. Hausmann, B.; Knorr, K. H.; Schreck, K.; Tringe, S. G.; Glavina Del Rio, T.; Loy, A.; Pester, M., Consortia of low-abundance bacteria drive sulfate reduction-dependent degradation of fermentation products in peat soil microcosms. *ISME J.* **2016**, *10*, (10), 2365-75.
- 470 20. Loy, A.; Kusel, K.; Lehner, A.; Drake, H. L.; Wagner, M., Microarray and functional gene analyses of sulfate-reducing prokaryotes in low-sulfate, acidic fens reveal cooccurrence of recognized genera and novel lineages. *Appl. Environ. Microbiol.* **2004**, *70*, (12), 6998-7009.
21. Paul, S.; Kusel, K.; Alewell, C., Reduction processes in forest wetlands: Tracking down heterogeneity of source/sink functions with a combination of methods. *Soil Biol. Biochem.* **2006**, *38*, (5), 1028-1039.
- 475 22. Kugler, S.; Cooper, R. E.; Wegner, C. E.; Mohr, J. F.; Wichard, T.; Kusel, K., Iron-organic matter complexes accelerate microbial iron cycling in an iron-rich fen. *Sci. Total Environ.* **2019**, *646*, 972-988.
- 480 23. Reiche, M.; Torburg, G.; Küsel, K., Competition of Fe(III) reduction and methanogenesis in an acidic fen. *FEMS Microbiol. Ecol.* **2008**, *65*, (1), 88-101.
24. Kiene, R. P.; Hines, M. E., Microbial Formation of Dimethyl Sulfide in Anoxic Sphagnum Peat. *Appl. Env. Microbiol.* **1995**, *61*, (7), 2720-2726.
- 485 25. Visscher, P. T.; Taylor, B. F.; Kiene, R. P., Microbial consumption of dimethyl sulfide and methanethiol in coastal marine sediments. *FEMS Microbiol. Ecol.* **1995**, *18*, (2), 145-153.
26. Evangelou, V., *Environmental soil and water chemistry*. John Wiley: 1998.
27. Devai, I.; De Laune, R. D., Formation of volatile sulfur compounds in salt marsh sediment as influenced by soil redox condition. *Org. Geochem.* **1995**, *23*, (4), 283-287.
- 490 28. Lomans, B. P.; Pol, A.; Op den Camp, H. J., Microbial cycling of volatile organic sulfur compounds in anoxic environments. *Water Sci. Technol.* **2002**, *45*, (10), 55-60.
29. Lomans, B. P.; Luderer, R.; Steenbakkens, P.; Pol, A.; van Der Drift, C.; Vogels, G. D.; Op den Camp, H. J., Microbial populations involved in cycling of dimethyl sulfide and methanethiol in freshwater sediments. *Appl. Environ. Microbiol.* **2001**, *67*, (3), 1044-51.
- 495 30. Lomans, B. P.; Smolders, A.; Intven, L. M.; Pol, A.; Op, D.; Van Der Drift, C., Formation of dimethyl sulfide and methanethiol in anoxic freshwater sediments. *Appl. Environ. Microbiol.* **1997**, *63*, (12), 4741-7.

31. Dalby, F. R.; Hansen, M. J.; Feilberg, A., Application of Proton-Transfer-Reaction Mass Spectrometry (PTR-MS) and (33)S Isotope Labeling for Monitoring Sulfur Processes in Livestock Waste. *Environ. Sci. Technol.* **2018**.
- 500 32. Sawamura, M.; Shimoda, M.; Osajia, Y., Studies on Off-flavor Formed during Heating Process of Satsuma Mandarin Juice (III). *J. Agricult. Chem. Soc. Jpn.* **1978**, *52*, (7), 281-287.
33. Cooper, A. J. L., Chemical and Biochemical Properties of Sulfonium Compounds. In *Biological and Environmental Chemistry of DMSP and Related Sulfonium Compounds*, Kiene, R. P.; Visscher, P. T.; Keller, M. D.; Kirst, G. O., Eds. Plenum Press: New York, London, 1996; pp 13-28.
- 505 34. Bentley, R.; Chasteen, T. G., Environmental VOSCs—formation and degradation of dimethyl sulfide, methanethiol and related materials. *Chemosphere* **2004**, *55*, (3), 291-317.
35. Chasteen, T. G.; Bentley, R., Volatile Organic Sulfur Compounds of Environmental Interest: Dimethyl Sulfide and Methanethiol. An Introductory Overview. *J. Chem. Educ.* **2004**, *81*, (10), 1524.
- 510 36. Sun, Y.; Qiu, J.; Chen, D.; Ye, J.; Chen, J., Characterization of the novel dimethyl sulfide-degrading bacterium *Alcaligenes* sp. SY1 and its biochemical degradation pathway. *J. Hazard. Mater.* **2016**, *304*, 543-52.
37. Sun, J.; Hu, S.; Sharma, K. R.; Ni, B. J.; Yuan, Z., Degradation of methanethiol in anaerobic sewers and its correlation with methanogenic activities. *Water Res.* **2015**, *69*, 80-9.
- 515 38. Hausmann, B.; Pelikan, C.; Herbold, C. W.; Kostlbacher, S.; Albertsen, M.; Eichorst, S. A.; Glavina Del Rio, T.; Huemer, M.; Nielsen, P. H.; Rattei, T.; Stingl, U.; Tringe, S. G.; Trojan, D.; Wentrup, C.; Woebken, D.; Pester, M.; Loy, A., Peatland Acidobacteria with a dissimilatory sulfur metabolism. *ISME J.* **2018**, *12*, (7), 1729-1742.
- 520 39. Pester, M.; Bittner, N.; Deevong, P.; Wagner, M.; Loy, A., A 'rare biosphere' microorganism contributes to sulfate reduction in a peatland. *ISME J.* **2010**, *4*, (12), 1591-602.
40. Jousset, A.; Bienhold, C.; Chatzinotas, A.; Gallien, L.; Gobet, A.; Kurm, V.; Kusel, K.; Rillig, M. C.; Rivett, D. W.; Salles, J. F.; van der Heijden, M. G.; Youssef, N. H.; Zhang, X.; Wei, Z.; Hol, W. H., Where less may be more: how the rare biosphere pulls ecosystems strings. *ISME J.* **2017**, *11*, (4), 853-862.
- 525 41. Hayes, A. C.; Liss, S. N.; Allen, D. G., Growth kinetics of *Hyphomicrobium* and *Thiobacillus* spp. in mixed cultures degrading dimethyl sulfide and methanol. *Appl. Environ. Microbiol.* **2010**, *76*, (16), 5423-31.
42. Lee, J.-H.; Kim, T. G.; Cho, K.-S., Isolation and characterization of a facultative methanotroph degrading malodor-causing volatile sulfur compounds. *J. Hazard. Mater.* **2012**, *235-236*, (Supplement C), 224-229.
- 530 43. Moran, J. J.; House, C. H.; Vrentas, J. M.; Freeman, K. H., Methyl sulfide production by a novel carbon monoxide metabolism in *Methanosarcina acetivorans*. *Appl. Environ. Microbiol.* **2008**, *74*, (2), 540-2.
- 535 44. Moran, J. J.; Beal, E. J.; Vrentas, J. M.; Orphan, V. J.; Freeman, K. H.; House, C. H., Methyl sulfides as intermediates in the anaerobic oxidation of methane. *Environ. Microbiol.* **2008**, *10*, (1), 162-73.
45. Scholten, J. C.; Murrell, J. C.; Kelly, D. P., Growth of sulfate-reducing bacteria and methanogenic archaea with methylated sulfur compounds: a commentary on the thermodynamic aspects. *Arch. Microbiol.* **2003**, *179*, (2), 135-44.
- 540

46. Heinen, W.; Lauwers, A. M., Organic sulfur compounds resulting from the interaction of iron sulfide, hydrogen sulfide and carbon dioxide in an anaerobic aqueous environment. *Origins Life Evol. Biosphere* **1996**, *26*, (2), 131-150.
47. Lomans, B. P.; den Camp, H. J.; Pol, A.; Vogels, G. D., Anaerobic versus aerobic degradation of dimethyl sulfide and methanethiol in anoxic freshwater sediments. *Appl. Environ. Microbiol.* **1999**, *65*, (2), 438-43.
48. Lomans, B. P.; Op den Camp, H. J.; Pol, A.; van der Drift, C.; Vogels, G. D., Role of methanogens and other bacteria in degradation of dimethyl sulfide and methanethiol in anoxic freshwater sediments. *Appl. Environ. Microbiol.* **1999**, *65*, (5), 2116-21.
49. van Leerdam, R. C.; de Bok, F. A.; Lomans, B. P.; Stams, A. J.; Lens, P. N.; Janssen, A. J., Volatile organic sulfur compounds in anaerobic sludge and sediments: biodegradation and toxicity. *Environ. Toxicol. Chem.* **2006**, *25*, (12), 3101-9.
50. Meredith, L. K.; Boye, K.; Youngerman, C.; Whelan, M.; Ogée, J.; Sauze, J.; Wingate, L., Coupled Biological and Abiotic Mechanisms Driving Carbonyl Sulfide Production in Soils. *Soil Syst.* **2018**, *2*, (37), 1-27.
51. Adams, D. F.; Farwell, S. O.; Robinson, E.; Pack, M. R.; Bamesberger, W. L., Biogenic sulfur source strengths. *Environ. Sci. Technol.* **1981**, *15*, (12), 1493-1498.
52. Cooper, W. J.; Cooper, D. J.; Saltzman, E. S.; Demello, W. Z.; Savoie, D. L.; Zika, R. G.; Prospero, J. M., Emissions of Biogenic Sulfur-Compounds from Several Wetland Soils in Florida. *Atmos. Environ.* **1987**, *21*, (7), 1491-1495.
53. Richards, S. R.; Kelly, C. A.; John, W. M. R., Organic Volatile Sulfur in Lakes of the Canadian Shield and its Loss to the Atmosphere. *Limnol. Oceanogr.* **1991**, *36*, (3), 468-482.

SYNOPSIS. As suggested by Carrion *et al.*⁷ we found that organic matter degradation is the main process leading to volatile sulfur compounds from fen.

FIGURES AND TABLES

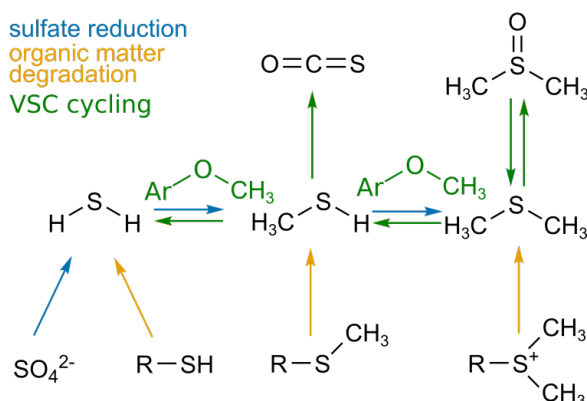


Figure 1. Scheme of known VSC production and cycling processes. The most important mechanisms involve sulfate reduction to H_2S and then methylation to MeSH and Me_2S and organic matter degradation. From amino acids, a degradation of the thiol in cysteine can be cleaved to H_2S , methyl thiols from methionine to MeSH , and dimethyl sulfonio groups from S-methyl methionine to Me_2S . This paper deals with the relative contribution of these processes to the sulfur flux to the atmosphere in freshwater wetlands.

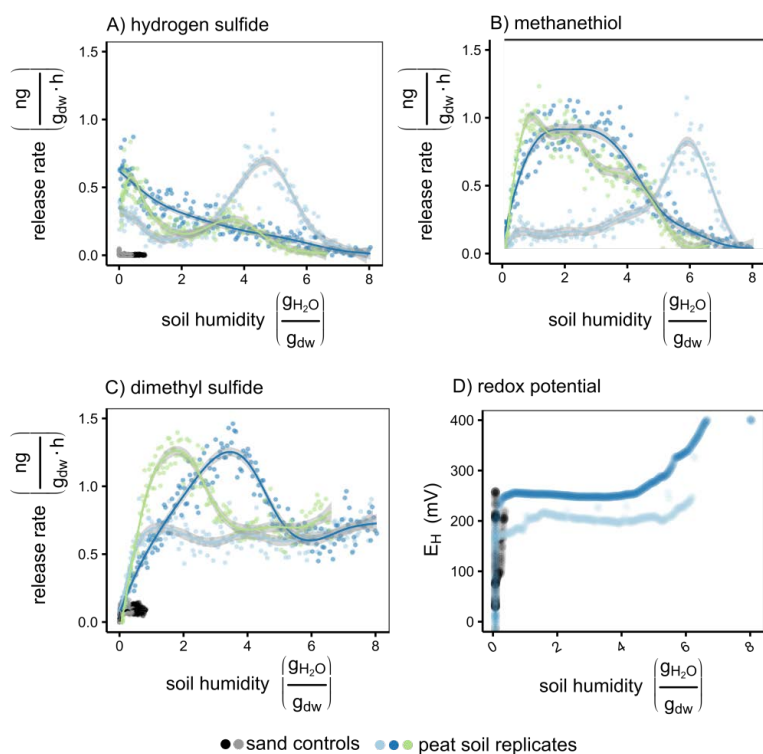
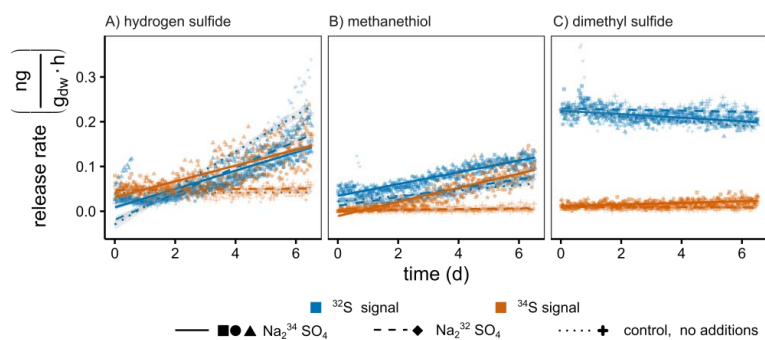
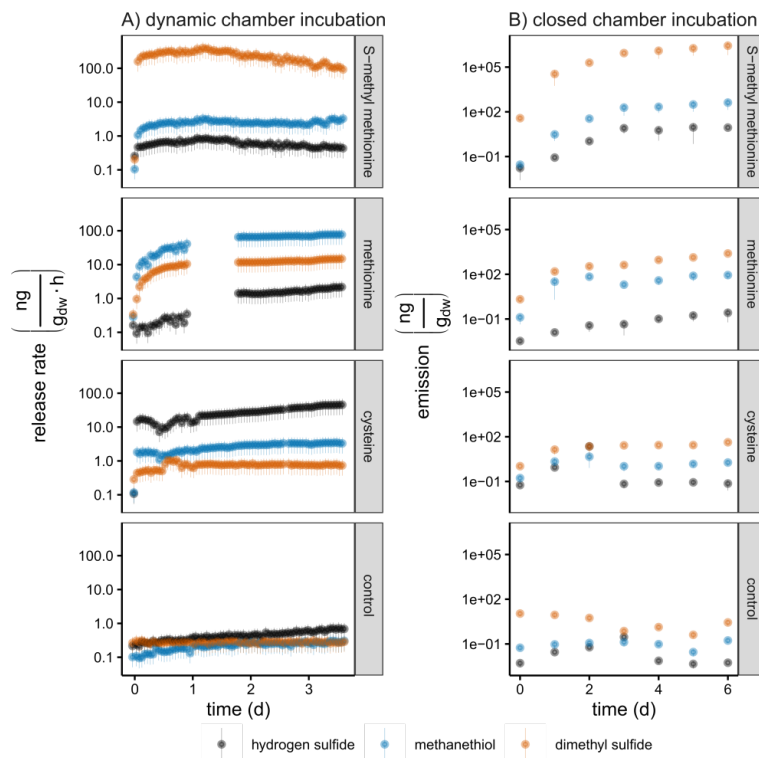


Figure 2. Volatile sulfur compound release rates and redox potential distribution during dry-out of soils (peat soil replicates $n=3$, acid-washed sand control $n=2$). A-C: Hydrogen sulfide, methanethiol, and dimethyl sulfide release rates per chamber with cubic spline GAM smoother ($\pm 95\%$ confidence interval (CI)). D: redox potential distribution in the first soil. Hourly averages of the measurements of the 30 electrodes in the soil $\pm 95\%$ CI. Below $2 \text{ g H}_2\text{O/g}_{\text{dw}}$, the redox

580 potential signal dropped drastically until the sensors failed, probably due to an interruption of the electric circuit when the soil's pore water is replaced by air. The redox potential distributions in the soil are displayed in Figure S4. We did not observe local "hotspots" of very low redox potentials that could explain the VSC emissions.



585 **Figure 3.** Release rates of unlabeled (blue) and labeled (red) hydrogen sulfide (A), methanethiol (B) and dimethyl sulfide (C) when spiking with Na₂³⁴SO₄ (n = 4, different point shapes represent the different chambers) with a Na₂³²SO₄ control and a control without any spiking. A linear fit was applied to the three groups (spiking with Na₂³⁴SO₄, spiking with Na₂³²SO₄, and control; solid, dashed, and dotted lines).



590

Figure 4. Effect of amending S-methyl methionine, methionine, and cysteine to peat soil. A) incubation in continuously N₂-flushed chambers. Release rates \pm 95% CI. $n_{\text{soil}} = 1$ per substance, $n_{\text{tech}} = 5$ per timepoint. Data of methionine are missing between day 1 and 2 due to an experimental failure. B) incubation in static, closed chambers with N₂ headspace. Headspace concentrations normalized to the soil dry weight \pm 95% CI, $n_{\text{soil}} = 3$ per substance, $n_{\text{tech}} = 3$ per timepoint.

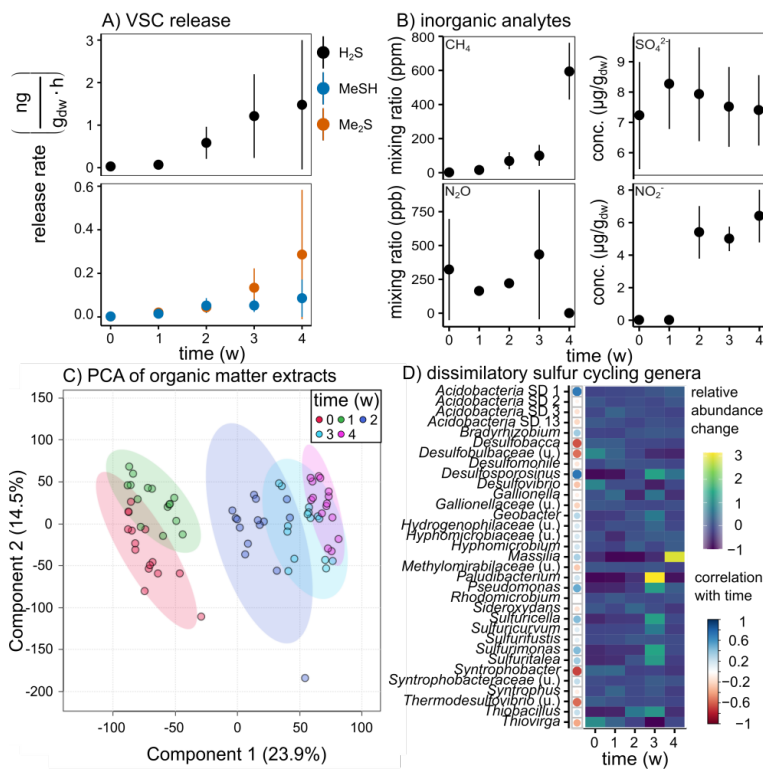


Figure 5. Long-term incubation over four weeks. A) Release rates (\pm 95% CI, $n_{\text{soil}} = 5$ at each time point) of the reduced sulfur compounds hydrogen sulfide, methanethiol, and dimethyl sulfide. B) Mixing ratios of methane, and nitrous oxide in the flasks (\pm 95% CI, $n_{\text{soil}} = 5$ at each time point) and nitrite concentration in the slurry (\pm 95% CI, $n_{\text{soil}} = 5$ at each time point). C) Principle component analysis scores plot of the organic matter extracts measured with UHPLC-Orbitrap-MS in positive polarity. Obtained from MetaboanalystR after log-transformation and Pareto-Scaling of the data. The five replicates analyzed each week were measured three times each ($n_{\text{total}} = 15$). The ellipses represent the 95% CI of each time point. D) 16S rRNA amplicon abundance of genera associated with dissimilatory S cycling (sulfate/sulfite reduction and S oxidation). Red and blue circles: Correlation of the relative 16S rRNA amplicon abundance with time. Purple/yellow heatmap: Change of the average relative abundance ($n = 5$) per time point,

centered and scaled by the average abundance of this species, *rel. A. change* (T_1) = $(A(T_1) - \bar{A})/\bar{A}$. Note, at t = 4 w, only 4 replicates are shown due to a failed library preparation for this sample prior to amplicon sequencing.

4. Unpublished Work - Volatile Organic Compound Emissions upon Leaf Litter Degradation

By: Ann-Sophie Lehnert^{1,2}, Eliane Gomes-Alves¹, Witoon Purahong³, Benjawan Tanunchai³, Nora Zannoni⁴, Simon Benk¹, Ernst-Detlev Schulze¹, Georg Pohnert², and Susan Trumbore¹

4.1. Introduction

Volatile Organic Compound (VOC) emissions from leaf litter can be significant contributors to the ecosystem's VOC emissions, especially in spring and autumn. During those times, litter emissions can reach the same magnitude as canopy emissions (Aaltonen et al., 2011; Janson, 1993).

Litter VOCs are more diverse and one order of magnitude higher than soil VOC emissions (Leff and Fierer, 2008) though net emissions depend the rates of uptake by underlying soils (Ramirez et al., 2010b). Specific VOCs emitted by litter can trigger microbial community shifts. For example, methanol and acetone can inhibit nitrification (McBride et al., 2019). They also form part of the 'mobile' and 'labile' carbon in soils, and when oxidized to CO₂ can contribute to soil respiration. (Asensio et al., 2012). Thus, VOCs not only serve as a food source, but also structure microbial communities by their inhibitory and allelopathic properties. Since VOCs can not only be dissolved the soil's aqueous phase, but also inhabit the soil's gas phase, they are very mobile and can diffuse easily throughout the entire soil pore space. ¹³C-labeled litter VOC carbon can be incorporated into all fractions of soil organic matter – dissolved organic matter, particulate organic matter, mineral-associated organic matter, and microbial biomass (McBride et al., 2020).

Generally, litter VOC emissions are diverse, spanning hydrocarbons, terpenes, terpenoids, carbonyl compounds, alcohols esters, and volatile sulfur compounds (VSCs) (Isidorov and Jdanova, 2002). The main classes of emitted VOCs are (i) small oxygenated volatiles (e. g. methanol or acetaldehyde) originating from microbial degradation of the labile carbon, (ii) compounds from the microbial secondary

¹Department of Biogeochemical Processes, Max Planck Institute for Biogeochemistry, Jena

²Institute for Inorganic and Analytical Chemistry, Friedrich Schiller University, Jena

³UFZ-Helmholtz Centre for Environmental Research, Department of Soil Ecology, Halle (Saale)

⁴Department of Atmospheric Chemistry, Max Planck Institute for Chemistry, Mainz

metabolism (terpenes, benzenoids, etc.) (Isidorov et al., 2016), or (ii) terpenes that were stored in the leaves themselves (Svendsen et al., 2016).

A number of environmental factors have been studied for their effect on litter VOC emissions. Litter/soil temperature has been identified as the main driver for VOC emissions (Faubert et al., 2010; Greenberg et al., 2012). Litter moisture only seems to have a minor effect on emissions in some studies (Greenberg et al., 2012), but can decrease emissions in others (Mäki et al., 2019b). Litter VOC emissions correlate with the percentage of labile carbon available for the decomposition process, so VOCs might actually be used as an indicator for litter quality (Leff and Fierer, 2008; Greenberg et al., 2012). UV light can increase abiotic VOC emissions, especially in humid air (Derendorp et al., 2011), but this seems to be insignificant on the global scale.

The VOC blend depends on the litter type. Most data comes from conifer litter, from pines, spruce, and larch. The main emitted compound class are terpenes from the resin ducts (Aaltonen et al., 2011; Asensio et al., 2008, 2012; Greenberg et al., 2012; Guénon et al., 2017; Isidorov et al., 2003, 2005; Janson, 1993; Mäki et al., 2019b; Ramirez et al., 2010b). Emissions from broadleaf species like oak, aspen, poplar, birch, willow, maple, eucalyptus, tulip, and holm oak are dominated by methanol (Isidorov and Jdanova, 2002; Ramirez et al., 2010b; McBride et al., 2020; Asensio et al., 2007b; Guénon et al., 2017).

How litter degradation affects its VOC emissions has been studied for litter and soil together via chamber measurements in the field (Faubert et al., 2010; Janson, 1993) or in the lab for up to 72 days (Ramirez et al., 2010b; Svendsen et al., 2018) on usually only 1-2 individual species, making it difficult to compare the results from different studies. On the other hand, surveys of litter emissions from different tree species and mixed sites have been conducted (Leff and Fierer, 2008), but these studies provide a single time point rather than comparing trajectories over time. Additionally, data on many temperate broadleaf species, e.g. beech, are missing. Thus, we designed a systematic survey measuring VOC emissions, dissolved organic carbon in leachate, and bacterial, fungal, and archaeal community shifts upon the degradation of litter from 13 different tree species dominating temperate forests over a year. The preliminary data presented here focus on the VOC emissions. Our hypotheses were: (1) Primary metabolite VOC emissions like methanol, formaldehyde, acetone, acetaldehyde, and acetic acid emissions depend on microbial activity and are thus correlated to the humidity and the CO₂ respiration. (2) Secondary metabolite VOC emissions vary among different plant types and correlate with the carbon content of the litter. (3) Over time, the impact of the litter type-related VOCs decrease and the microbial VOCs increases, so we see a convergence of VOC emissions from different litter types to similar VOCs over time. (4) VOC emissions decrease with time as the litter quality decreases.

4.2. Materials and Methods

Schemes of the general sampling setup and the VOC analyses can be found in Figures A.1 and A.2.

4.2.1. Site Description

In autumn 2019, conifer litter from *Pinus sylvestris* (Scots pine), *Picea abies* (Norway spruce), *Larix decidua* (European larch), and *Pseudotsuga menziesii* (Douglas fir) was retrieved from test plantations of the individual species in a forest near Keula (Thuringia, Germany, 51° 21'18.3"N, 10°32'10.6"E) by cropping branches and sampling the oldest needles (> 2 yr old). Broadleaf litter from *Acer pseudo-platanatus* (sycamore maple), *Carpinus betulus* (common hornbeam), *Fagus sylvatica* (common beech), *Fraxinus excelsior* (common ash), *Populus tremula* (common aspen), *Populus* hybrid (poplar), *Quercus* sp. (oak), and *Tilia* sp. (lime) was collected from a mixed-stand forest near Rehungen (Thuringia, Germany, 51°22'20.4"N 10°31'38.2"E). The senescent leaves of each species were collected directly from the trees themselves. Litter was dried in an oven at 25 °C for 72 h. 3 g air-dry litter of each individual tree was put into black nylon litter nets (mesh size 2 mm, with 6 holes (diameter = 5 mm) for access of meso-fauna and some macro-fauna) and buried below the litter layer right besides the respective tree on Nov. 20, 2019. To keep them in place and undisturbed by animals, a steel grate was put around the samples at each location. All five replicates per tree species were located with a minimum distance of 5 m to each other. At $t = 0$, 100 d, 200 d, and 383 d, two closely-located litter bags were sampled from each replicate grate, one for microbial community and DOC leachate analyses, and the other for VOC and chemical composition analyses. For simplicity, from now on, $t = 383$ d will be rounded to $t = 400$ d. Due to an error at $t = 0$, no VOC measurement could be done on those samples, so the sampling of newly collected leaf litter was repeated in November one year later. Here, the senescent leaves of the broadleaf trees were already fallen to the ground and sampled from there. Litter from coniferous trees were collected from the same trees with the same positions and methodology as one year before. The samples for VOC analysis were cooled to 4 °C directly after sampling, and processed within the next 72 h.

4.2.2. Incubations for VOC Emission Measurements

The litter from the litterbags was weighed and filled into a 250 mL Schott glass bottle, which was closed off with a butyl rubber stopper (4 of 5 samples), internally covered with PTFE foil. The fifth sample was put into a 280 mL Teflon chamber with two 1/8" Swagelok fittings, which were closed off for incubation. The bottles were incubated at 20 °C in the dark for 24 h. The samples in the Schott bottles were measured with the SIFT-MS, the VOCs of the one in the Teflon chamber were sucked onto a Tenax TA Carbograph 5TD thermal desorption tube (Markes International GmbH,

Offenbach a. M., Germany). On $t = 200$ d, SPME fibres (100 μm Polydimethylsiloxane, 24 Ga, Supelco, Darmstadt, Germany) were exposed to the fifth sample during the 24 h incubation. After the VOC measurement, the Schott bottle samples were opened for 5-10 min to equilibrate the headspace with the ambient air. Then, the bottles were closed again and after 5, 20, and 35 min, 20 mL of the headspace were filled into a 10 mL previously evacuated headspace vial for the greenhouse gas measurements. Afterwards, all samples were dried for 72 h at 60 °C in a ventilated drying oven (Heraeus Holding GmbH, Hanau, Germany), ground, and then used for chemical composition analysis.

4.2.3. VOC Analysis

Smaller VOCs were analyzed directly from the headspace via a Voice 200 ultra SIFT-MS with a positive ion source (Syft Technologies Ltd., Christchurch, New Zealand). It was customized acc. to Lehnert et al. (2020a) and operated at 40 mL/min sample gas flow, 156 mL/min helium carrier gas flow, 50 V flow tube voltage, and 120 °C flow tube temperature. The instrument was previously calibrated humidity-dependently acc. to Lehnert et al. (2020a). In 120 s scan time (4 scans), the following analytes (reagent ion / product ion m/z in brackets) were measured with a time limit of 500 ms and a count limit of 100.000 cps:

- acetaldehyde ($\text{H}_3\text{O}^+/45$, $\text{NO}^+/74$)
- acetic acid ($\text{H}_3\text{O}^+/61$, $\text{H}_3\text{O}^+/79$ (water cluster), $\text{NO}^+/90$)
- acetone ($\text{NO}^+/88$)
- acetonitrile ($\text{H}_3\text{O}^+/42$)
- dimethyl sulfide ($\text{H}_3\text{O}^+/63$)
- formic acid ($\text{H}_3\text{O}^+/47$, $\text{H}_3\text{O}^+/65$ (water cluster), $\text{O}_2^+/45$)
- furan ($\text{NO}^+/68$)
- geosmin ($\text{NO}^+/165$, $\text{O}_2^+/112$)
- hexanal ($\text{H}_3\text{O}^+/137$, $\text{NO}^+/99$)
- hydrogen sulfide ($\text{H}_3\text{O}^+/35$)
- isoprene ($\text{NO}^+/68$, $\text{O}_2^+/67$)
- methanol ($\text{H}_3\text{O}^+/33$, $\text{H}_3\text{O}^+/51$ (water cluster))
- methanethiol ($\text{H}_3\text{O}^+/49$)
- monoterpenes ($\text{H}_3\text{O}^+/81$ (fragment), $\text{H}_3\text{O}^+/137$, $\text{NO}^+/136$)
- β -pinene ($\text{O}_2^+/69$ (fragment))
- camphene ($\text{NO}^+/166$)
- limonene ($\text{NO}^+/135$ (fragment))
- sesquiterpenes ($\text{H}_3\text{O}^+/205$, $\text{NO}^+/204$, $\text{O}_2^+/204$)

The specific monoterpenes were measured on an additional mass that was individual to them (mostly with a low intensity); however, they were also included in the monoterpene signals. Acetaldehyde, Acetonitrile, furan, and hexanal not measured for $t = 100$ d.

4.2.4. Terpene Analysis

The SPME fibres were analyzed on an ISQ GC-MS (Thermo Scientific, Bremen, Germany) with a regenerated straight glass liner (5 mm inner diameter, CS-Chromatographie Service, Langerwehe, Germany), and a Zebron ZB-SemiVolatiles column (30 m x 0.25 mm x 0.25 μm , Phenomenex, Aschaffenburg, Germany). The oven was heated to 40 °C for 2 min, then heated to 200 °C at 15 °C/min, and then to 250 °C at a rate of 30 °C/min, where it was held for another minute. Splitless injection was done for 12 s, afterwards, the port was flushed with a split flow of 120 mL/min helium. Injector and transfer lines were kept at 250 °C. After manual peak detection and putative identification by comparison to the NIST spectral database, peaks were integrated using the built-in ICIS algorithm of Xcalibur. The retention time window was 10 s, the view width 0.3 min. A compound was considered detected in a sample if its area was larger than the mean area + CI ($n = 13, p = 95\%$) of all blank air samples.

The VOCs collected on sorbent tubes were analysed through thermodesorption gas chromatography time of flight mass spectrometry (TD-GC-TOF-MS, Bench ToF Tandem Ionisation from Markes International, UK). The analysis consists of three main steps: desorption of the analytes from the sorbent tubes (TD), separation of the analytes through gas chromatography (GC), and quantification and identification of the analytes through time of flight mass spectrometry (ToF-MS). Thermodesorption is carried out in two stages, both performed at 250 °C for 10 minutes through a TD 100xr (Markes International, UK). The desorbed components are carried in a flow of He into the GC column (dimethyl TBS β -cyclodextrin 0.15 μm , 0.15 mm ID, 25 mL, from MEGA, Italy). The method consists of an initial 5 min at 40 °C, after which the temperature was increased at a rate of 1.5 °C/min from 40 °C to 150 °C, and further increased at a rate of 30 °C/min from 150 °C to 200 °C. After the GC run, the analytes are fragmented through electron impact ionization at 70 eV in the ToF. Identification was obtained by comparing the MS spectra with the MS NIST library for the same ionization energy and by injection of gas mixtures (162 VOCs gas mixture, and 25 biogenic VOCs gas mixture, by Apel Riemer, USA) and liquid standards. The obtained chromatograms were integrated with TOF-DS (Markes International, UK). Gas standard cartridges were used to calibrate the instrument, determine the precision and LOD of the analysis, which is quantified as 23% and ≈ 1 pptv, respectively. More information on the material and method used can be found in Zannoni et al. (2020). Due to few blanks, a compound was only considered detected in a sample if its intensity was greater than 5 times the blank intensity, and the maximum intensity of the compound in all samples was at least 1E6.

4.2.5. CO₂, and N₂O Analysis

The headspace samples were analyzed with a Nexis GC-2030 with a BID discharge ionization detector, a HS-20 autosampler (Shimadzu, Jena, Germany), and a SH-Rt-QBond fused silica column (30 m

x 0.53 m x 20 μ m, Shimadzu, Jena, Germany). A split ratio of 1:9 and a purge flow of 2 mL/min was used upon injection. The temperature of the autosampler was 60 °C, the temperature of the sample and transfer lines 150 °C. The temperature gradient of the column was 40 °C for 2.5 min, then heat to 120 °C at 10 °C/min, then hold for 1.5 min, at 3.34 mL/min helium carrier gas flow. The retention times for CO₂ and N₂O were 2.9 and 3.1 min. For quantification, samples from four gas standards at different compound mixing ratios (ICOS Flask and Calibration Laboratory, Jena, Germany) were measured. Release rates were calculated as the slope of a linear regression of the headspace concentrations at the three time points.

4.2.6. Microbial Community Analysis

Microorganisms associated with leaf litter were characterised by 16S rRNA gene-and fungal internal transcribed spacer (ITS)-based amplicon sequencing on the Illumina MiSeq sequencing platform. Leaf litter samples were subjected to DNA extraction using DNeasy PowerSoil Kit (Qiagen, Hilden, Germany), according to the manufacturer's instructions. For construction of the bacterial and archaeal amplicon libraries, the 16S rRNA gene V4 region was amplified using the universal bacterial/archaeal primer pair 515F (5'-GTGCCAGCMGCCGCGGTAA-3') and 806R (5'-GGACTACHVGGTWTCTAAT-3') (Caporaso et al., 2011). For establishing fungal amplicon libraries, the fungal ITS2 gene was amplified using the fungal primer pair fITS7 [5GTGARTCATCGAATCTTTG-3] (Ihrmark et al., 2012) and ITS4 primer [5-TCCTCCGCTTATTGATATGC-3] (White et al., 1990). Amplifications were performed using 20 μ L reaction volumes with 5xHOT FIREPol Blend Master Mix (Solis BioDyne, Tartu, Estonia). The products from three technical replicates were pooled in equimolar concentrations. Paired-end sequencing (2 x 300 bp) was performed on the pooled PCR products using a MiSeq Reagent kit v3 on an Illumina MiSeq system (Illumina Inc., San Diego, CA, United States) at the Department of Soil Ecology, Helmholtz Centre of Environmental Research, Germany. The 16S and ITS rDNA sequences were quality-trimmed (for high quality sequences), filtered for chimeras, and merged using the DADA2 package (Callahan et al., 2016) through the pipeline dada-snake (Weißbecker et al., 2020). High-quality reads were clustered into different amplicon sequence variants (ASVs) for prokaryotes and fungi. Rare ASVs which potentially come from sequencing errors were removed. The SILVA SSU database v. 138 was used for taxonomic classification of the bacterial and archaeal ASVs. Fungal ASVs were classified against the UNITE v7.2database.

4.2.7. Statistical Analysis

The statistical analysis was done with R 4.0.2 (The R Foundation, USA) and RStudio 1.2.5033 (RStudio Inc., USA). The used packages were tidyverse 1.3.0 (Wickham et al., 2019), Hmisc 4.4-1 (Harrell Jr. Frank E. et al., 2020), corrplot 0.84 (Wei and Simko, 2017), factoextra 1.0.7 (Kassambara and

Mundt, 2020), and GGally 2.0.0 (Schloerke et al., 2021). Correlations and principle component analyses (PCAs) were calculated for all numeric variables of the whole dataset as well as different subsets: VOCs only, $t = 100$ and 200 d for VOCs and soil parameters, $t = 0$ for microbial community.

Linear Mixed Effect Modelling on the intensity data of acetaldehyde, acetone, methanol, and monoterpenes was done using nlme 3.1-149 (Pinheiro et al., 2020), lme4 1.1-26 (Bates et al., 2015), sjPlot 2.8.7 (Lüdtke, 2020), and boot 1.3-25 (Angelo and Ripley, 2020). We considered the following random and fixed factors for our model:

- ACETALDEHYDE/ACETONE/METHANOL/MONOTERPENES/ANALYTE: release rate of this specific compound, in ng/g_{dw}
- PLANT: the name of the tree (as a source for leaf litter) as a factor
- ISCONIFER: boolean variable, TRUE if the plant is a conifer
- TIME: sampling time, in d
- EXP TIME: negative exponential of sampling time in days, $\exp(-\text{time})$
- HUMIDITY: the litter humidity, in ng/g_{dw}
- CO₂: the CO₂ release rate, in $\text{ng}/(\text{g}_{\text{dw}} \text{ h})$

Following the procedure of Zuur et al. (2009), we first investigated the optimal error structure. For model selection procedure, we relied on ANalysis Of VAriance (ANOVA), the Akaike information criterion (AIC) and the log-likelihood function (logLik) to compare the model formation in a step-wise fashion. Using an overfit model containing all parameters and restricted maximum-likelihood (REML) approximation, the random effects were tested first. PLANT and PLANT:REPLICATE were considered as random intercept and random slope effects on TIME and ISCONIFER (RANDOM = (1|PLANT), (1|PLANT:REPLICATE), (TIME|PLANT), (ISCONIFER|PLANT)). Next, we tried overcoming variance heterogeneity by using the variance structures VARFIXED(\sim TIME), \sim I(1/ANALYTE), and VARIDENT(\sim PLANT). No model improvement was observed, so we left this out. Then, the fixed effects were determined in a forward selection approach, starting with TIME vs. EXP TIME, then including ISCONIFER and possible interactions, and lastly HUMIDITY and CO₂. Maximum likelihood (ML) approximation was used here. At every step, an ANOVA was done to compare the models with the simpler models based on the AIC, and logLik results. The final model was then refit with REML approximation, and reported with bootstrapped confidence intervals ($p = 95\%$, $\text{nsim} = 1000$).

4.3. Results

VOC emissions from litter from 13 different temperate tree species that degraded in the forest for 0, 100, 200, and 383 d were analyzed with static headspace incubation. For 100 and 200 d, we also analyzed C, N, P, Ca, Fe, K, Mg, organic C, ¹³C, and ¹⁵N contents and did an in-depth terpene analysis, and for $t = 0$, we also analyzed the microbial community. These data will be available for all time points including the yet-to-come 600 d for a final analysis, so these are preliminary results. From

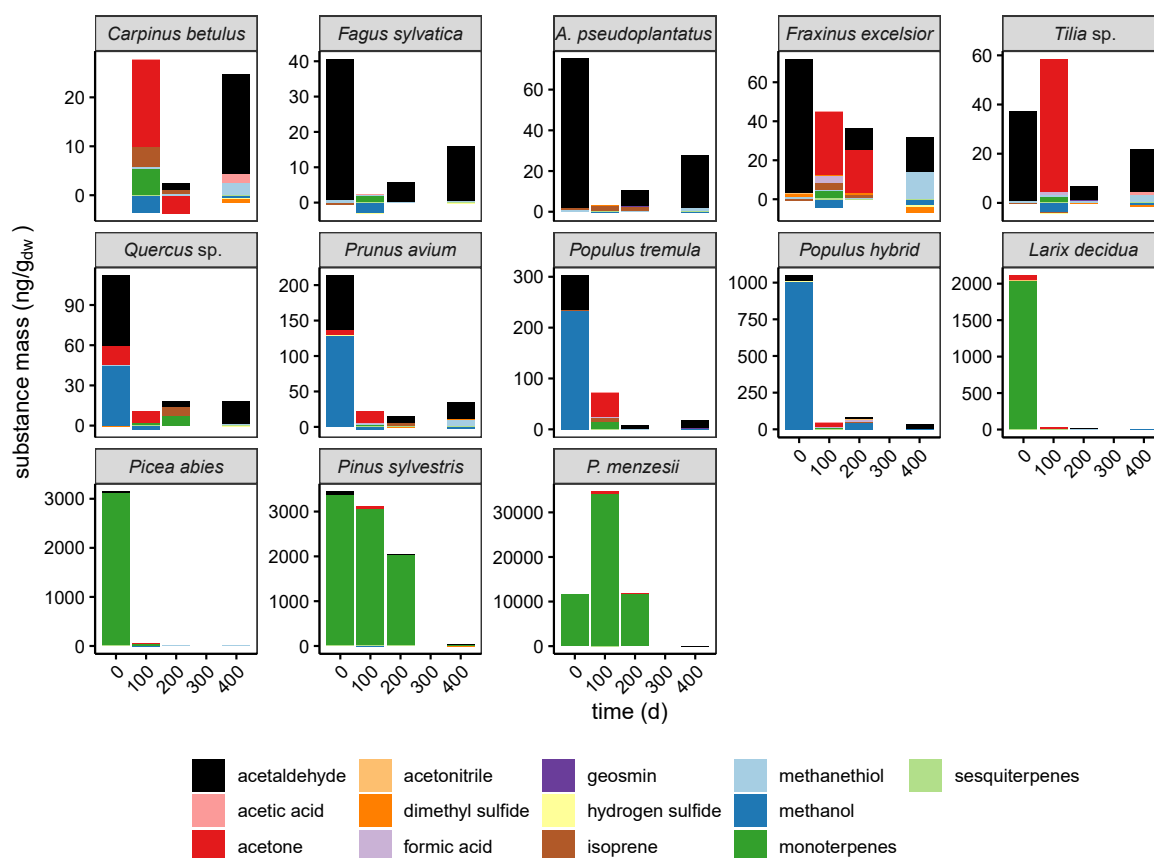


Figure 4.1.: Measured VOC headspace of the different tree species over time. The trees are sorted in ascending order of VOC emissions. Limonene, β -pinene, and camphene were left out since they are already included in the monoterpene measurements.

the behavior of the VOCs, we do not expect any change at 600 d though, since we observed a steady decay, and almost all VOC emissions were already diminished at 383 d.

4.3.1. VOC Emission Changes Upon Degradation

Keeping the difference in VOC emissions between deciduous and conifer trees in mind, the next important factor is the time as a measure of degradation status.

Figure 4.1 shows the VOC emissions of the different tree species, in ascending order of headspace concentrations. Despite the 1000-fold difference in headspace concentrations, a general trend is that emissions strongly decrease after the first measurement, and usually, emissions are dominated by one VOC. For the smaller emissions, this seems to be acetaldehyde and acetone. Methanol can be an important factor at the beginning of leaf degradation with an intermediate headspace mixing ratio. Monoterpene emissions of the conifers are the highest emissions observed, even over longer time frames.

For the low-molecular weight VOCs methanol, acetaldehyde, acetic acid, acetonitrile, hydrogen sulfide, and dimethyl sulfide, the strongest emissions are from fresh litter. The *Populus* hybrid has the highest emissions of these compounds and is the only species to emit acetic acid, acetonitrile, hydrogen sulfide and dimethyl sulfide. Acetaldehyde emissions seem to covariate with the litter humidity. Acetic acid emissions are a factor of 25 lower than acetaldehyde emissions, which is reasonable considering its lower volatility (15.8 hPa vs. 1006 hPa at 20 °C, GES (2021)). Acetonitrile is emitted not only by the *P. tremula* and *Populus* sp., but also by *P. menzesii* and *P. sylvestris*, and these emissions seem to persist for at least 200 days after emission.

Mono- and sesquiterpene emissions were tracked as sum parameters on their general $[M + H]^+$ ions, and we then looked for individual fragment ions that were specific of monoterpenes we might be interested in, namely β -pinene, camphene, and limonene. For α -pinene, there were no specific fragment ions listed in the SIFT-MS library. Given the large number of different terpenes, it is still very likely that even on the fragment m/z ratios, more than one terpene would be detected. This is the reason for the analysis of terpenes with GC-MS as discussed below. Generally, monoterpene emissions were up to four orders of magnitude higher in conifers than in broadleaf species, even though the measured sesquiterpene emissions were equally low for all litter types. *P. menzesii* emissions were increasing from $t = 0$ to 100 d. This does not seem to be the case for *L. decidua* and *P. abies*, where the emissions decrease very quickly. Small monoterpene emissions from broadleaf litter were observed after 100 d as well. Camphene, β -pinene, and limonene emissions mimic the general monoterpene emission patterns, though the relative intensity of conifer and deciduous tree emissions varies. Geosmin is an interesting exception - besides the general monoterpene trend observed for *P. menzesii*, it slowly, but steadily increases over time. This is probably due to its production by microorganisms. Isoprene emissions also correlate with monoterpene emissions, and acetone emissions in broadleaf species peak after 100 d as well, like deciduous tree monoterpene emissions.

4.3.2. Tree Species Dependence of VOCs

The most obvious difference when looking at VOC emissions is the distinction between deciduous and conifer litter. Besides the emissions of VOCs (ng/g_{dw}), we looked at the litter dry weight in the bag (litter weight), the litter water content (water), the air humidity in the chamber after incubation (humidity), and the time that passed after the litter was buried in the litterbags (time). We observed that conifer litter emitted up to 1000x more VOCs, mainly more terpenes. This is clearly visible when doing a principle component analysis (PCA) for all time points (Figure 4.2): The emissions of the conifers *L. decidua*, *P. sylvestris*, *P. abies*, and *P. menzesii* lie along the axes of the terpene emissions, whereas the deciduous trees spread out orthogonal to that. The two *Populus* species lie along the hydrogen sulfide, dimethyl sulfide, and methanol axes, whereas *P. avium* and *F. excelsior* correlate with the other direction, as specified by geosmin, methanethiol, water, humidity, and time. When looking at correlation plots for deciduous and conifer trees (Figure 4.3), this becomes even

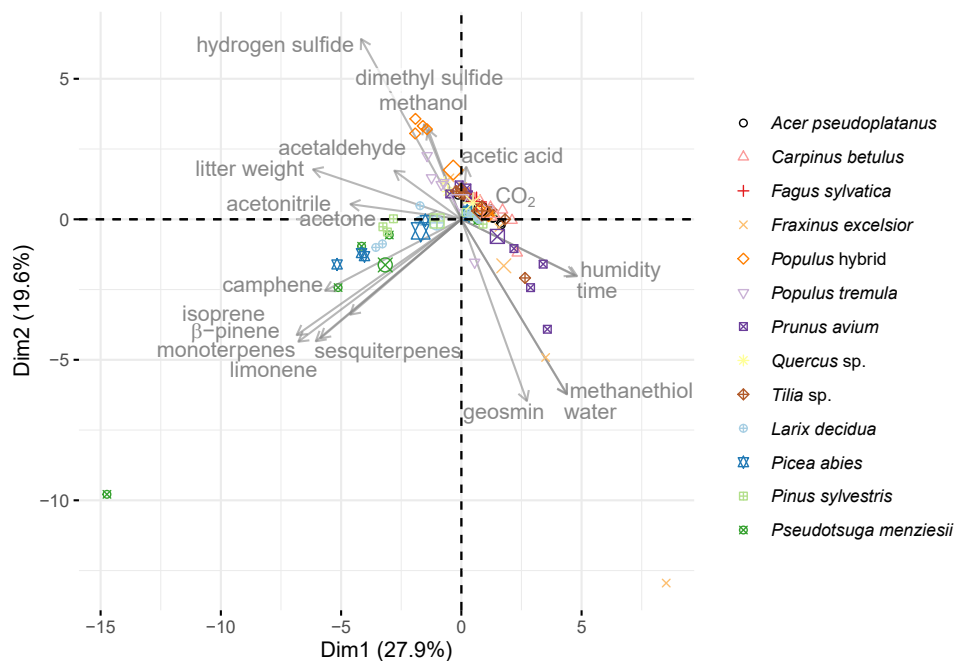


Figure 4.2.: Principal component analysis of VOC emissions of litter from different tree species over time. Bigger symbols represent the mean of each species. The data for the PCA was centered and scaled. The contributions of the third and higher axes are smaller than 10% and very similar to each other and thus considered negligible.

more visible: Whereas the conifers show strong correlations between the different measured mono-, and sesquiterpene measurements, the trends for deciduous trees are much weaker. However, it is important to note that conifer mono- and sesquiterpene emissions not only correlate with each other, but also with acetonitrile, acetone, and isoprene. All volatile sulfur compound emissions as well as geosmin show moderate to high correlations with the humidity measured by the SIFT-MS, so these emissions might be artefacts of the measurement. This also applies for methanol emissions in conifers. In conifers, CO_2 emissions are negatively correlated to acetaldehyde and acetic acid emissions, a trend which is not observed for deciduous trees. On the other hand, in deciduous trees, moderate correlations of the small VOCs methanol, acetaldehyde, acetic acid, and acetonitrile are observed that are not eminent for the conifers.

When doing a PCA for each time point (Figure A.7), one can see the shift of contributions. The first principal axis is dominated by terpene emissions and conifer litter for the first three timepoints and only becomes more mixed for the last time point. Its maximum contribution to the variance is 44% for $t = 100$ d, after which it decreases back to $\sim 30\%$. The second axis is determined by H_2S , DMS, methanol, acetonitrile, and acetic acid emissions on the first time point, which single out the *Populus hybrid* litter. On the second time point, *Populus hybrid* is joined by *F. excelsior* and *P. abies*, whereas the other broadleaf species and *L. decidua* are spread out on the opposite direction on the second axis. Over time, the contribution of the VOCs to the different axis becomes less straightforward until for $t = 400$ d, the PCA only separates a few extreme individual samples of each plant. This makes

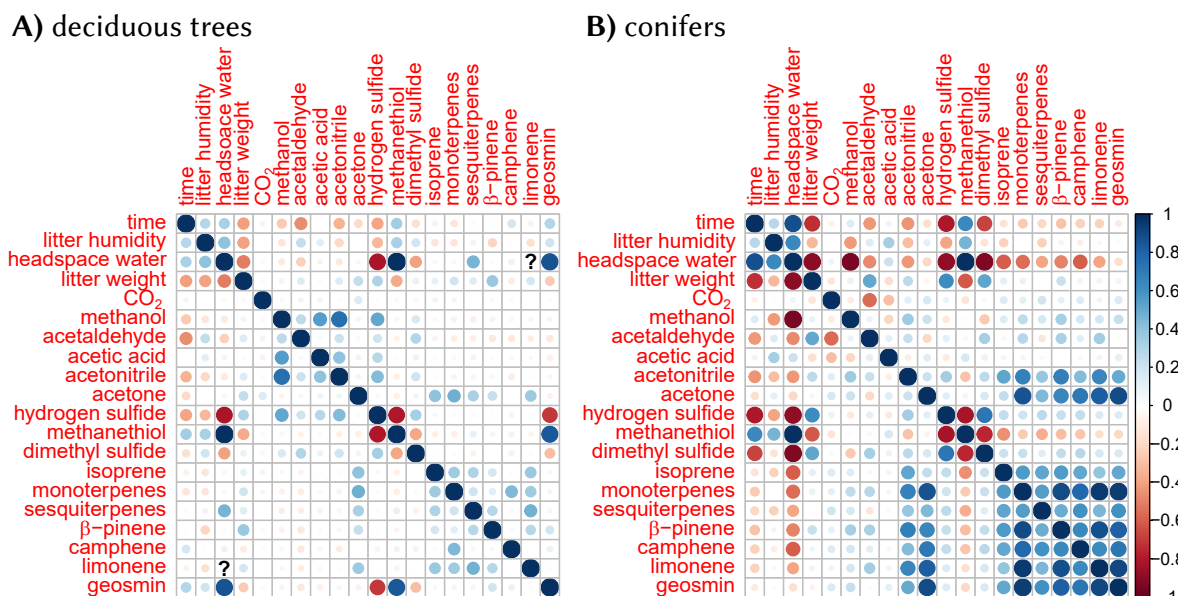


Figure 4.3.: Correlations of the individual VOCs with each other, for the deciduous trees (A) and the conifers (B).

sense since the overall VOC emissions decrease and with the lower value, the distinction between the different litter types becomes impossible.

4.3.3. Modelling VOC Emissions

Models of the four most outstanding emissions - acetaldehyde, acetone, methanol, and monoterpenes - as a function of the time, CO₂ respiration, litter humidity, and plant species were built, see Tables A.12–A.15. Since we were mostly interested in seeing the overall effect over all plant species, we usually modelled plant as a random effect and only included the boolean variable whether the plant is a conifer as a fixed effect. The four models were:

- ACETALDEHYDE \sim EXP TIME + HUMIDITY + (EXP TIME | PLANT)
- ACETONE \sim PLANT
- METHANOL \sim EXP TIME + (EXP TIME | PLANT)
- MONOTERPENE \sim TIME * ISCONIFER + (ISCONIFER | PLANT)

Terms in brackets signify the random effects, e.g. (EXP TIME|PLANT) is a random slope effect of EXP TIME for each plant species. Methanol and acetaldehyde emissions could be modelled better with an exponential time decay, whereas the monoterpene was better modelled with a linear time decay, and the acetone did not have a significant correlation with any of the two. We did not try other, more complex functions for modelling changes in VOC emissions with time, as there were only four time points. Monoterpenes are the only modelled analyte that needed the distinction between conifers and deciduous trees modelled as a fixed factor. We also needed to include the interaction between

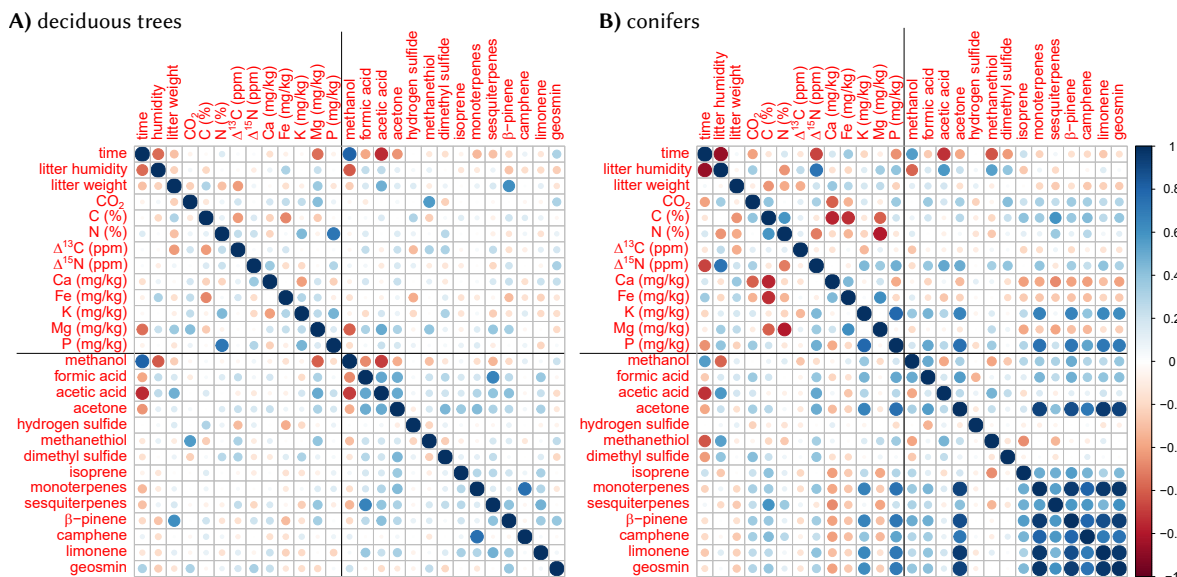


Figure 4.4.: Correlations of the VOC emissions and litter elemental contents for (A) deciduous and (B) coniferous trees after 100 and 200 d.

TIME and ISCONIFER into the model. For the three other models, this interaction was not significant. For acetone, PLANT was the only significant factor. For methanol, the exponential time decay was important and depended on the plant. Including CO₂ respiration rates decreased the MeOH model AIC and LogLik compared to the shown model, indicating this might be an even better model than the one shown above. Yet when investigating the contributions of the parameters to the model with an ANOVA, the CO₂ respiration was not significant, so we left it out.

4.3.4. Correlations with Litter Element Contents

The comparison with element compositions is only done on $t = 100$ and 200 d, since the rest of the data is still being acquired. In general, there are a few trends within the element data itself: The C, Ca, and Fe contents and the $\Delta^{13}\text{C}$ signal remain rather constant, whereas the other signals decrease at least for one of the two litter groups. Only the N and Fe contents appear to increase between the two data points for conifers. As all of these values are relative to the dry weight, this might just be the other elements leaching and degrading faster than those two. General observed correlations within the element composition are the correlation of P and K contents in all trees, accompanied by a correlation with the N content, a minor positive correlation with the Mg content and a minor negative correlation with the Ca content in deciduous trees (Figure 4.4). In deciduous trees, the carbon content is negatively correlated with the $\Delta^{13}\text{C}$ signal and the Fe content, whereas in conifers, it is negatively correlated with Ca, Fe, and Mg contents.

As before, correlations of broadleaf VOC emissions with other parameters are rather low ($|R| < 0.4$), whereas there are stronger correlations for the conifers ($0.4 \leq |R| \leq 0.7$), mainly due to the high

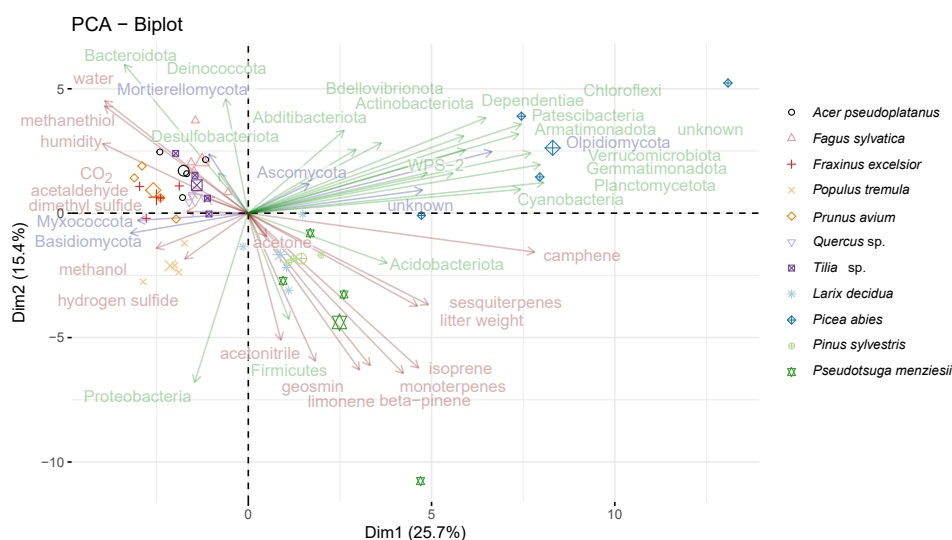


Figure 4.5.: Principal component analysis of the microbial community and VOC emissions from the litter at $t = 0$. VOC variables are colored red, bacterial/archaeal and fungal abundance variables green and blue. The other axes were considered negligible, since their contribution was $<10\%$ and the difference between the axes was rather small.

terpene emissions, see Figure 4.4. On this shorter time scale, they are actually positively correlated with the carbon content and the CO_2 respiration. The latter is not observed on the whole time scale, presumably due to the nonlinear behavior of the monoterpene emissions in *P. menziesii*. The terpene emissions also correlate positively with the $\Delta^{15}\text{N}$ signal, the K and P content, and negatively with the Ca, Fe, and Mg contents, but this probably is only an indirect relationship driven by the correlations with the C content.

4.3.5. Correlations with Microbial Community Abundance

The analysis on the microbial community structure with 16S-RNA sequencing was done on $t = 0$, and will be done for the other time points at the end of the experiments. Note that it was done for the original samples in 2019, whereas the VOC $t = 0$ was sampled a year later, so results have to be evaluated and discussed with caution. We only investigated the phylum level, as for the correlations with VOC emissions, there were not enough data points to do a strain-specific analysis. In general, the bacterial community is dominated by *Proteobacteria* and unknown clades, and the fungal community by *Ascomycota*. The differences between the species are rather small at this level. Only conifer litter tends to show a higher relative abundance of *Cyanobacteria* and *Acidobacteria* (Figure A.10).

In the PCA (Figure 4.5), the microbial phyla do not clearly correlate with VOCs. The microbial composition of *Picea abies* appears to be very different from the rest, hosting a big number of different phyla. Only *Firmicutes* and *Acidobacteria* seem to correspond to monoterpene-emissions, since both

separate the other conifers *L. decidua*, *P. sylvestris*, and *P. menzesii* from the deciduous tree litter, which in turn is more characterized by *Bacteriodota*, *Deinococcota*, and *Desulfobacteriota*.

Correlations of VOCs with microbes are similarly rare (Figure A.11). The microbial groups determining the first dimension, separating the *P. abies* from the other trees, also strongly correlate in the analysis. The camphene signal correlates with many microbial groups, but this might just be a coincidence due to its strongly negative correlation with the litter humidity, which is also reflected in the microbial data. *Firmicuites* correlate with acetonitrile and sesquiterpene and to some extent isoprene and monoterpene emissions again, whereas the *Acidobacteria* linked to the terpene emissions in the PCA do not show significant correlations here. *Proteobacteria* correlate with methanol, acetonitrile, and hydrogen sulfide emissions. For fungi, *Basidiomycota* correlate positively with dimethyl sulfide emissions, whereas *Ascomycota* correlate negatively with them.

4.3.6. Terpenes

The analysis of terpenes by GC-MS could only be done on a qualitative basis, as for most of the analytes, no standard was available for calibration. Structural identification was mainly done by comparison with the NIST spectral database, most of the assignments are putative. An overview over the found terpenes can be found in Table 4.1.

When comparing the TD-tube sampling with the SPME-sampling on $t = 200$ d (c.f. Figure A.2 for an overview over the sampling scheme), SPME shows a greater variety of compounds, and finds them in more samples. Some monoterpenes like α -pinene, 3-carene or *p*-cymene are even widespread over all samples, and the amount and variety of sesquiterpenes found is much higher than for the TD-tube sampling. This might have several reasons: Firstly, SPME fibres are much more sensitive to contamination, as they cannot be closed off. The fibres were stored in clean, previously heated-off glass tubes with taper joints between sampling and analysis, but still, the lab air might have caused contaminations. This is rather unlikely though, since our unexposed blank samples did not show those peaks. Secondly, the SPME fibre was inserted into the chamber before the TD tube sample was taken. Maybe, the adsorption capacity of the SPME fibre was high enough to extract the majority of terpenes in the vial, so that there was only very little left for the TD tube to sample. Thirdly, it is possible that the concentration on the TD tube was so low that the compounds did not readily desorb during the experiment. This might be the reason why only very few sesquiterpenes are found for the TD tubes in general compared to the SPME fibres.

Looking at the difference between $t = 100$ d and $t = 200$ d, one can see a sharp decrease in compound variability. Especially for the *Populus* hybrid and the conifers which were very strongly emitting monoterpenes and terpenoids before, the reduction in the number of terpene species is apparent. This is even more surprising as the cumulative monoterpene signal from SIFT-MS stays at the same

magnitude. Maybe, for the reasons stated above, the TD tube sampling of the second campaign was not very successful.

As a general trend, conifer species emit a higher number of monoterpenes and monoterpenoids, whereas for sesquiterpenes, the variety is equal for broadleaf and conifer species.

4.4. Discussion

In our investigation of VOC emissions during the degradation of litter from 13 different temperate tree species, we found that the most important emissions are monoterpene emissions from conifers, followed by methanol emissions from fresh leaves. Acetaldehyde, acetone, and some other small VOCs were detected only in small quantity.

The monoterpene emissions dominate the emissions from the conifer litter, contrary to the study by Gray et al. (2010) where methanol dominated, but in line with the studies by Isidorov et al. (2003, 2005, 2010, 2016) and the Finnish Meteorological Institute (Aaltonen et al., 2011; Mäki et al., 2019a,b; Hakola et al., 2012; Hellén et al., 2017) on boreal *P. abies* and *P. sylvestris* forests. The most common monoterpene emissions they reported are α - and β -pinene and 3-carene, and for sesquiterpenes β -caryophyllene, which are also emissions we found. Like in our results, Isidorov and Jdanova (2002) also found tricyclene, camphene, phellandrene, α -terpinene, limonene, and fenchone, Isidorov et al. (2010) sabinene, γ -terpinene, thujene, terpinolene, as well as the sesquiterpenes α -calacorene, α -copaene, and ylangene, Isidorov et al. (2003) additionally cymene, linalool, and 3-pinanone, and Mäki et al. (2019b) aromadendrene, bisabolene, and longifolene. A big difference between our study and the published literature is in the sesquiterpenes: most of the putatively identified compounds do not match the literature. However, since they are only putatively identified and the number of possible sesquiterpene isotopes with similar spectra is very high, they might not be correctly identified. Since those compounds are not very abundant, and our highest peaks (total ion count area) α - and β -pinene, 3-carene, and β -caryophyllene match the literature, we assume that most terpene emissions we observe with SIFT-MS are mainly those analytes. The planned additional analysis and identification of the terpenes that can be extracted from mature leaves and fresh litter will further help identify and correct the terpenes we found in the litter, and enable us to separate potential microbial terpenes from foliar litter terpenes.

For very fresh samples at $t = 0$, *Populus* hybrid litter is very different from the other litter. We observed strong methanol emissions in addition to smaller hydrogen sulfide, dimethyl sulfide, acetonitrile, and acetic acid emissions that were only significant at $t = 0$. Since the leaves of this *Populus* tree were still yellow upon sampling, whereas from the other trees, most of the leaves were already brown, these emissions might be due to a very rapid degradation of the most labile organic carbon in the leaves - the pectins, amino acids, sugars, and small molecules. A study similar to ours but

Table 4.1.: Terpenes found in the litter samples at t = 100 and 200 d, sampled with TD-sorbent tubes and SPME fibres. A dot indicates the presence of the analyte in the sample. Terpenes marked with a star are putative assignments. Blue: t = 100 d, TD-tube sampling. Gray: t = 200 d, TD-tube sampling. Red: t = 200 d, SPME-fibre sampling.

	<i>Acer pseudoplatanus</i>	<i>Carpinus betulus</i>	<i>Fagus sylvatica</i>	<i>Fraxinus excelsior</i>	<i>Populus hybrid</i>	<i>Populus tremula</i>	<i>Prunus avium</i>	<i>Quercus sp.</i>	<i>Tilia sp.</i>	<i>Larix decidua</i>	<i>Picea abies</i>	<i>Pinus sylvestris</i>	<i>Pseudotsuga menziesii</i>
monoterpenes													
alloocimene*						•							
2-bornene*						•						•	
camphene	•	•	•	•	•	•		•		•	•	•	•
3-carene		•	•	•	•	•	•	•	•	•	•	•	•
<i>m</i> -cymene		•											
<i>p</i> -cymene		•	•	•	•	•	•	•	•	•	•	•	•
limonene	•	•	•	•	•	•	•	•	•	•	•	•	•
β-phellandrene*	•	•	•	•	•	•	•	•	•	•	•	•	•
α-pinene		•	•	•	•	•	•	•	•	•	•	•	•
β-pinene			•		•	•				•	•	•	•
sabinene*			•			•						•	•
α-terpinene*						•						•	•
α-thujene*						•						•	•
γ-terpinene*						•				•	•	•	•
terpinolene*		•				•				•	•	•	•
tricyclene			•			•					•	•	•
monoterpene oxides													
carvone*													•
citronellal*			•					•	•			•	•
<i>p</i> -cymen-8-ol*												•	•
eucalyptol			•				•				•	•	•
fenchol*												•	•
fenchone*			•					•				•	•
geranylacetone*	•							•			•	•	•
isopulegol*		•	•					•	•			•	•
linalool			•					•				•	•
levoverbenone*					•							•	•
myrtenal*						•						•	•
myrtenol*												•	•
3-pinanone*												•	•
α-pinene epoxide*												•	•
pinene oxide*												•	•
pinocarvone*												•	•
thujenone*		•	•					•	•			•	•
thujol					•							•	•
thujone												•	•
sesquiterpenes													
alloaromadendrene*					•							•	•
aromadendrene oxide*				•								•	•
bisabolene			•									•	•
α-calacorene*			•	•				•				•	•
<i>trans</i> -calamene*		•	•	•	•			•		•		•	•
calarene*			•									•	•
β-caryophyllene			•									•	•
caryophyllene oxide*			•									•	•
chamigrene*	•											•	•
α-copaene		•	•	•	•	•	•	•				•	•
cubedol*		•	•	•	•	•	•	•				•	•
β-elemene*		•	•	•	•	•	•	•				•	•
α-/β-guaiene*	•											•	•
guia-1(10)-11-diene*												•	•
isoaromadendrene epoxide*			•					•				•	•
isocaryophyllene*		•	•					•				•	•
ledene oxide*		•	•	•				•				•	•
longifolene*		•	•	•	•			•		•	•	•	•
sativene*		•	•	•	•			•		•	•	•	•
sesquisabinene*			•							•		•	•
7-epi-silphiperfol-5-ene*				•	•	•			•		•	•	•
silphiperfol-5-ene*										•	•	•	•
α-ylangene*		•	•		•			•				•	•

targeting these first 3-4 weeks from the point where the leaves fall from the tree would be very interesting.

The observed acetone emissions are interesting, as their origin is not entirely clear. The correlation with monoterpene emissions from conifer litter and to some extent also deciduous tree litter indicates that the acetone might be formed by abiotic degradation of the terpenes and terpenoids by OH^\cdot and NO_3^\cdot . However, the acetone emission time dependence from *P. menziesii* and *P. sylvestris* do not match the time dependence of their monoterpene emissions. If it really were only a chemical process, we should see the highest acetone emissions in these two plants over a longer period of time than we do. So maybe, there are also microbial processes involved that are strongest for $t = 100$ d and that actually shapes the acetone emissions. There might also be microbes feeding on the abiotic acetone emissions on $t > 100$ d, which is a scenario we cannot distinguish from ceasing acetone production in our experiment.

It was surprising to see acetonitrile emissions in the dataset, as we originally planned to use this VOC as a negative control - we would not expect any acetonitrile emissions, as there are no biosyntheses known for it. Yet there are small but significant emissions of this compound that do not correlate strongly with the headspace water. A misassignment is unlikely, as the only other two compounds listed to form $m/z(\text{H}_3\text{O}^+) = 42$ u in the Syft library are butanone oxime and undecane. Also, acetonitrile was neither stored nor used in the lab and acetonitrile was also not seen in the control lab air samples, so a contamination from lab air is unlikely. There is no biosynthesis of acetonitrile listed in the KEGG and Metacyc databases, but its emission has been reported for some bacteria, fungi (Zhu et al., 2010; Wheatley et al., 1997), and soils (Li et al., 2019a; Veres et al., 2014). It is usually used as a tracer for biomass burning at ecosystem level though (Salisbury et al., 2003; Yáñez-Serrano et al., 2015). It might be interesting to look at other untargeted soil and plant VOC emission studies, to see whether biogenic acetonitrile emissions are really observed in nature. If the measured signal really is acetonitrile, it would be interesting to see whether the emissions are really by biosynthesis or just an abiotic degradation product, and to find its biosynthesis or formation mechanism. If these emissions are significant compared to biomass burning, this can influence the utility of acetonitrile as a biomass burning indicator at the ecosystem level and needs to be accounted for.

While we did not observe strong correlations of microbes with VOCs for most phyla, there was some correlation with *Firmicutes* with acetonitrile, isoprene, mono- and sesquiterpenes, of *Proteobacteria* with methanol, acetonitrile, and hydrogen sulfide, and of *Basidiomycota* with dimethyl sulfide. A similar study that added rice straw to soils and investigated food waste degradation found correlations of *Bacteroidetes*, *Firmicutes* and *Verrucomicrobia* with their 10 most important VOCs ethene, propene, ethanol, 2-propanol, 2-butanol, acetaldehyde, acetone, 2-butanone, 2-pentanone and acetophenone (Zhao et al., 2015), whereas another study that investigated food waste degradation found significant correlations of *Weissella*, *Leuconostoc*, *Enterobacteriaceae*, and *Lactotoccus* with carbonyl sulfide and dimethyl sulfide, *Bacteroides*, *Lactobacilliales*, *Peptoniphilus*, *Gallicola*, *Helcococcus*, and

Peptostreptococcus with dimethyl disulfide, methyl isobutyl ketone, acetone, and methyl methacrylate with *Eubacterium coprostanoligenes*, *Fusobacterium*, and *Sporanaerobacter*, and 2-butanone and vinyl acetate with *Cloacibacterium* and *Lactobacillus* (Zhang et al., 2020). In studies on fermented foods, *Lactobacillus*, *Weissella* and *Ascomycota* often correlate with flavor compounds and VOCs (Liang et al., 2020a; Liu et al., 2020; Lv et al., 2020). Generally, it looks like fast-growing bacteria respond almost immediately to fresh organic matter inputs and use the labile carbon as energy source, thereby releasing VOCs from primary metabolism and opening plant reservoirs of VOCs. The correlation of *Firmicutes* with terpenes might be caused by them producing the terpenes (Cane and Ikeda, 2012), but we rather think that this is due to them preferentially feeding on needle litter (Berger et al., 2021; Lladó and Baldrian, 2017; Zhou et al., 2020). The positive correlation of dimethyl sulfide with *Basidiomycota* and negative correlation of it with *Ascomycota* is interesting. *Basidiomycota* are usually discussed as being resistant to volatile sulfides and even feeding on them (Phae and Shoda, 1991; Yang et al.), marine clades of *Ascomycota* are known to be able to cleave DMSP and DMS (Kirkwood et al., 2010), and the truffle subclasses of *Ascomycotina* are well-known to produce various sulfides (Miranda et al., 1997). Yet, truffles inhibit their tyrosinase expression with the produced VSCs (Miranda et al., 1997). Possibly, the resistant *Basidiomycota* clades gained advantage over the DMS-susceptible *Ascomycota*. However, since we only have data on the first time point, this is all very speculative and might just be a coincidence.

Estimating net field emissions from laboratory incubation of litterbags is difficult, as factors like changing temperatures are not included. For example, winter emissions are usually low due to the exponential dependence of VOC-emissions on temperature (Greenberg et al., 2012), but we did not capture this effect, since we always incubated at 20 °C. However, this was also not purpose of our study, as we mainly wanted to investigate the trajectory of VOC emissions over litter degradation. There are only few studies to quantitatively compare the data to (Table 4.2), since often only GC-MS peak areas are reported for in-depth terpene analyses or the emission is normalized to the area that was sampled in field studies. The reported methanol emissions of Brown (2008) and Ramirez et al. (2010a) are up to a factor of 1000 higher than what we observe, whereas our monoterpene emissions in the same magnitude. On the other hand, the methanol emissions reported by Gray et al. (2010) and Svendsen et al. (2018) are as big as in our studies. The difference between the reported studies is difficult to find. All used dynamic chamber systems to measure the gas emissions, and all except for Svendsen et al. (2018) used static chamber incubations beforehand. All rewetted their samples, from 50% WHC (Ramirez et al., 2010b) to 100% WHC (Svendsen et al., 2018). Gray et al. (2010) and Svendsen et al. (2018) cut the litter before incubating, which might have increased their emissions. Yet their emissions are as low as ours and 1000x lower than the other reported emissions, so this is probably not the major criterium. For our study, there might be several reasons for the much lower methanol emissions. Firstly, we collected leaf litter that was already brown, approx. 2-3 weeks after the actual litterfall. During this time, the labile methanol precursor pectin might already have been consumed. Secondly, we incubated in static chambers. Potentially, the methanol reached its compensation concentration and a steady state early in the incubation. This is also the reason why

Table 4.2.: Methanol and monoterpene emissions of different reference studies.

Study	Investigated plant	emissions	
Gray et al. (2010)	<i>Pinus</i> , <i>Populus</i> , <i>Quercus</i> , <i>Thinopyrum</i> , <i>Rhododendron</i> , <i>Miscanthus</i> , <i>Eucalyptus</i> , <i>Fraxi-</i> <i>nus</i> , and <i>Centaurea</i>	methanol	13-380 ng/(g _{dw} h)
Brown (2008)	<i>Geum rossii</i> , <i>Deschampsia cespi-</i> <i>tosa</i> , <i>Rhododendron maximum</i>	methanol other VOCs	≤22000 μg/(g _{dw} h) ≤8 μg/(g _{dw} h)
Ramirez et al. (2010a)	fresh <i>Acer</i> litter fresh <i>Pinus</i> litter	methanol monoterpenes	≤1000 μg/(g _{dw} h) ≤180 μg/(g _{dw} h)
Svendsen et al. (2018)	Arctic shrub litter	methanol monoterpenes	≤40 ng/(g _{dw} h) ≤200 ng/(g _{dw} h)
Our study	<i>Populus</i> sp. <i>P. menzesii</i>	methanol monoterpenes	≤46 ng/(g _{dw} h) ≤1100 ng/(g _{dw} h)

we only reported the total emitted mass and did not normalize it to the time. Thirdly, the headspace concentrations of the analytes, especially of methanol, might be high enough to be toxic to microbes in the samples, and thus decrease their activity. Since the range of reported emissions is very high, tenths of nanograms to tenths of micrograms per gram dry weight per hour, our emissions are within the range, though rather low. But this reinforces the need for further studies, to constrain the emissions.

In general, we did not find the expected correlation of microbial VOCs with CO₂ respiration (Hypothesis 1), as CO₂ respiration only declined after 100 d, whereas VOCs related to microbial primary metabolism in literature declined much more rapidly. This was in spite of the fact that the litter humidity was a significant factor determining acetaldehyde emissions in the model. Potentially, litter quality decreased during the degradation and this masked the effect of microbial activity. Temperature and time of year should not have an impact, since the litter samples were incubated for 24 h before the measurement. Only the litter moisture might have an impact, but the correlations were rather low here as well. Future studies should not only include the analysis of general carbon and nitrogen contents, but also include an estimation of the remaining structural compound classes, e.g. pectins, amino acids/proteins, carbohydrates etc., to account for this. This might be something we can deduce once the litter wet-extractable organic matter data is evaluated, as from these, we might be able to see the increase and decrease of different compound classes in the leachate. Of course, this is only indirect, as it does not analyze the remaining contents, but only what can be leached from the foliage at this time point. Still, the amount of remaining labile and stable carbon compounds might be an important factor.

Our second hypothesis that secondary metabolite VOC emissions vary among different plant types and correlate with the litter carbon content was confirmed for monoterpenes. The main effect here was whether the plant is a conifer or not, but both from the quantity of monoterpene and sesquiterpene emissions and the nature of the different compounds, we could distinguish between the plants

easily. The suspected potential microbial monoterpene emissions are likely very small, such as the observed increase in geosmin emissions over time.

A convergence of litter VOC emissions (Hypothesis 3) to similar emissions from all species was not observed, as emissions dropped too quickly. The time-resolved PCA plots (Figure A.7) appear to show the convergence as in the end, only individual replicates are shown, but this is likely an effect of the centering and scaling. Most VOCs are very close to or below the limit of detection at this point. Hence, the results for organic leachate litter degradation (Benk et al.) was not found for VOCs.

Hypothesis 4, a decay of VOCs with time and litter quality, is also supported by the small VOC and monoterpene data as well as the models. We find an exponential decay for all VOC emissions except for monoterpene emissions from *P. menziesii* like Brown (2008). The exponential decay makes sense since the amount of readily degradable carbon and the litter quality decreases (Krishna and Mohan, 2017), which is probably the precursor for the litter.

4.5. Conclusion

The study investigated VOC emissions upon degradation of foliar litter from 13 different deciduous and conifer tree species. We found that the largest emissions originate from terpene emissions from conifers for up to 200 d after litterfall, followed by methanol emissions of fresh deciduous tree litter that degraded quickly. Emissions of other compounds, e.g. acetaldehyde, acetone, formic acid, and hydrogen sulfide were at least a factor of 10 lower than the methanol emissions, and up to a factor of 1000 lower than the terpenoid emissions. An analysis of the terpene composition with GC-MS showed mainly α - and β -pinene, 3-carene, and β -caryophyllene, and a few other, very low-concentration compounds. A preliminary analysis of correlations of the VOC emissions with litter elemental composition parameters as well as microbial phyla showed low correlations with VOCs, only a correlation of the terpenoids with the remaining carbon content of the litter, and distinctly different VOCs and microbial communities for broadleaf and conifer litter. Emissions of deciduous tree litter were rather low except for the methanol emissions right after litterfall. An exponential decay of the litter VOC emissions other than monoterpene emissions was found.

Thus, the study provides the link between previous studies looking at many litter species, but only at one time point (Gray et al., 2010), and studies looking at only a few species for systematic studies in the lab (Brown, 2008; Ramirez et al., 2010b) and in the field (Aaltonen et al., 2011; Mäki et al., 2019a,b; Räisänen et al., 2009). It highlights that VOC emissions are particularly high upon litterfall, and monoterpene emissions are still as high in the following spring, as also reported before (Isidorov et al., 2010). Future studies could focus more on the formation processes of VOCs, linking VOC emissions to their precursor compound classes in the leaves, like amino acids, pectins, and carbohydrates.

4.6. Author Contributions

EGA, WP, BT, SB, and EDS installed the litterbags. WP, BT, and EDS did the sampling with occasional help of ASL and EGA. ASL and EGA planned and conducted the litter incubations together. ASL evaluated the data and wrote the current version of the manuscript.

4.7. Acknowledgements

Funding was provided by the Deutsche Forschungsgemeinschaft through the CRC 1076 Aqua Diva. Thanks to Cornelius Kappelhoff for help during the sampling and the litter incubations. Thanks to Iris Kuhlmann, her student helpers, Ines Hilke, Dr. Michael Rässler, Heiko Moossen, and their teams at the central measurement facilities for processing and measuring the numerous different soil parameters.

5. Discussion

In the thesis, I investigated biogenic VOCs and VSCs from trees, litter, and soil. I first focused on SIFT-MS optimizations to enable the accurate measurements needed for environmental VOC research, validated its ability to separate structurally similar compounds on the example of isoprene and MBO emissions from trees, and then investigated the processes leading to VSC emissions from peatlands and VOC emissions from litter.

5.1. Instrument Advances for Accurate SIFT-MS Measurements

Real-time analysis of gaseous samples with a limited air volume and low mixing ratio VOCs is an important tool e.g. for eddy-covariance flux measurements of biogenic VOCs or the monitoring of breath samples. For these measurements, direct chemical ionization mass spectrometry like PTR-MS and SIFT-MS can be used. Those two systems are the two most-widely used in the field besides their offline pendant of GC-MS. Direct instrument comparisons are rare, but in general, PTR-MS is thought to have a higher sensitivity, a 1-3 magnitudes lower LOD, and a higher resolving power of isobars due to its time of flight mass spectrometer, whereas SIFT-MS is less humidity-sensitive, more reliable when using the internal calibration based on the instrument parameters, and offers more structural information for separating structural isomers (Bylinski et al., 2017; Casas-Ferreira et al., 2019).

To overcome the sensitivity limitations of SIFT-MS, we optimized the instrument parameters, by tuning the type and concentration of the carrier gas, and the flow tube voltage and temperature (Publication 1). Incidentally, the higher background we observed when using nitrogen as a carrier gas instead of helium was now explained by Španěl and Smith (2020), who found that the reagent ions react with nitrogen carrier gas to form impurity reagent ions, increasing the background. We could reduce the limit of detection by a factor of 10 at the cost of a higher humidity-dependence and the need for quantification via calibration (Publication 1), as the assumption of the energy distribution of the particles in the flow tube following Maxwell-Boltzmann statistics is no longer valid. This could be solved either by a closer look at the gas phase chemistry and modelling the reactions taking place (Lacko et al., 2020; Smith et al., 2020) or by the humidity-dependent calibration procedure we established (Publication 1). This way, our instrument is currently the most sensitive commercially

available instrument, and without changes of the ion source, the flow tube or ion guiding techniques, no more sensitivity improvement is to be expected.

Our subsequent comparison with PTR-MS (Publication 1) was one of the first direct comparisons of the instruments, together with Lourenço et al. (2017). While Schwarz et al. (2009) at least found a comparability of their PTR-MS measurements of breath acetone with earlier SIFT-MS measurements of breath acetone of a similar study group, it remains to be shown directly that the two methods are really comparable. Correlations of the two methods with GC-MS has been shown, but only to some extent: for PTR-MS, the measurement accuracy was only within $\pm 50\%$ of the GC-MS method (Dunne et al., 2018), and for the SIFT-MS/SPME-GC-MS comparison, the GC-MS data was not quantified due to the use of the SPME sampling (Olivares et al., 2011). It shows that SIFT-MS and PTR-MS measurements are precise, but not accurate. A protocol for comparing and validating breath volatile emission methods based on peppermint oil has recently been established (Gisler et al., 2020; Henderson et al., 2020) and used to compare PTR-MS, SIFT-MS, and TD-SIFT-MS (Lin et al., 2021). The study shows high correlations of measurement results and claims comparability of the methods, yet the systematic differences between PTR-MS and SIFT-MS results are up to a factor of 6.5 different for the two instruments. For me, this means that the two instruments do not really lead to the same results, but need a calibration to be comparable.

Other recent advances in SIFT-MS include the development of an autosampler system for head-space, Tedlar bag and even TD-tube samples (Slingers et al., 2021). This would enable separating sampling from analysis, and maybe also make mobile sampling easier than it is now. There have been attempts to put SIFT-MS and PTR-MS instruments on trucks (Liang et al., 2020b; Wojnarowska and Sawoszczuk, 2020) for mobile SIFT-MS measurements, but the desire to have portable instruments for fieldwork persists (La Nasa et al., 2020).

Combining the autosampler and ion source of SIFT-MS and the drift tube of PTR-MS might help to generate an instrument that has both the versatility and isomeric separation from SIFT-MS and the sensitivity of the PTR-MS. Attempts to increase the number of reagent ions for PTR-MS have been made with SRI-MS (Jordan et al., 2009a) and a new source that switched between NH_4^+ and H_3O^+ very quickly (Müller et al., 2020), but their functionality still lacks the ease of SIFT-MS for being able to switch between reagent ions and also use negative reagent ions in milliseconds. On the other hand, PTR-MS has observed magnificent improvements of the limits of detection by deflecting the ions on a spiral instead of a linear path through the flow tube, thus increasing reaction time greatly (Breitenlechner et al., 2017; Krechmer et al., 2018). Plus, by humidifying the air to 100% as done in the Vocus PTR-MS, humidity-dependence as the second major drawback of PTR-MS is overcome (Krechmer et al., 2020). Additionally, advances have been made recently to increase the measurement range to less volatile compounds (Piel et al., 2020), tackling the analyses for which secondary electrospray ionization MS and APCI-MS have been more successful than PTR-MS and SIFT-MS so far (Bruderer et al., 2020). Thus, it might be interesting to merge the more variable ion source of the SIFT-MS with the drift tube and detection system of the PTR-MS, combining the advantages of

both instruments. The first steps to merge the instruments to an selective ion-drift tube-time of flight-mass spectrometer have been done: a microwave plasma source has been incorporated into the PTR-MS (Zhao et al., 2020), though without the separating quadrupole yet, and the other way round, the flow tube of a SIFT-MS has been converged into a flow drift tube by enhancing the flow tube voltage and employing additional electronic lenses (Spesyvyi et al., 2015). However, it might be even more beneficial to rethink the design of the instrument: the selective ion technique is an extremely interesting CI-ion source, and could easily be combined not with a drift tube and ToF, but with an ion trap. One could use a collision cell as the place for doing the analyte ionization and then introduce the results into an ion trap. This way, we could achieve longer ionization times, which should further decrease limits of detection, and we could be able to do high-frequency measurements of high-mass-resolution spectra, enabling eddy covariance of the whole volatile metabolome at the same time. The first attempts in this direction have been done with PTR-ToF-MS (Acton et al., 2020; Peng and Sun, 2020; Seco et al., 2020; Loubet et al., 2021; Phillips et al., 2021), but given the size of a ToF-MS and the necessity to combine it with a drift tube, ion trap instruments might be smaller and more stable.

Since also the big trend of -omics techniques has arrived in VOC research, and chemometric analysis of the volatilome (entirety of all volatile organic compound) are increasingly employed for SIFT-MS data, e.g. in the examination of archaeological artifacts (La Nasa et al., 2020), paper quality (Langford et al., 2020), and the detection of human epileptic seizures (Catala et al., 2020), the sensitivity improvement we achieved (Publication 1) greatly helps identifying the whole spectrum of emitted compounds. Going further, the proposed selective ion drift tube mass spectrometer would be an extremely helpful complement to the existing GC-MS metabolomics analyses. There even have been attempts to couple a gas chromatograph to SIFT-MS and PTR-MS, which would then be similar to a conventional GC-CI-MS (Claflin et al., 2021; Španěl and Smith, 2011). This jack-of-all-trades might be interesting for volatilomics analysis when time-resolution is not so much of an issue and a reliable compound identification is required, but it introduces the drawbacks of GC-MS (lower time resolution and the need to preconcentrate on fibres or tubes) again.

As said before, the main advantage of SIFT-MS is its enhanced ability for structural identification and potential for separating structural isomers. To show the applicability of our improved SIFT-MS in a "real-world" analytical problem, I teamed up with Erica Perreca from the MPI for Chemical Ecology. In her research on isoprene emissions from *Picea* trees, she always had to prove that the ion she used as a proxy for isoprene in PTR-MS measurements is actually isoprene by additionally doing GC-MS measurements of air samples from the plant. 2-Methyl-3-buten-2-ol (MBO) was a common potential interferent, so we implemented a SIFT-MS method to separate the two. A similar attempt has been made with SRI-ToF-MS using $m/z = 68$ u for measuring isoprene and $m/z = 69$ u for measuring MBO (Karl et al., 2012). However, this seems not a very practical method since SRI-MS is not a very widely used technique: To date, there are only 25 papers using the 11-year-old SRI-MS technique on SciFinder, 15 of which are purely related to the instrument and the ionization reactions occurring

(<https://scifinder.cas.org>, search for SRI-MS, Jan 4, 2020). This is likely due to the high price and relatively difficult handling of the instrument compared to PTR-MS and SIFT-MS. Thus, the more widely-used, easier to handle, and more robust SIFT-MS would be a good alternative, which we successfully implemented and validated (Publication 2). We used standard measurements to identify the spectra of isoprene and MBO emissions and how they interfere with the measurement of one another under different conditions. We then validated our method by measuring the isoprene and MBO emissions from *Pinus*, *Picea*, and populus trees. We found indications that *Picea abies* might actually emit both analytes simultaneously during their diurnal cycle, which could not be done with time resolution before. Potential applications for this separation besides the mentioned examination of tree chemical ecology are the separation of MBO emissions from *Ips typographus* bark beetles from their *Picea* host plant's isoprene emissions in field studies of bark beetle attacks (Birgersson and Bergström, 1989; Zhang et al., 2009), or the simultaneous measurement of both analytes as stress markers for different trees in a mixed forest ecosystem via micrometeorological techniques (Schade et al., 2000; Sarkar et al., 2020; Rantala et al., 2014). Here, with PTR-MS so far scientists usually just measured both as a sum parameter (Rantala et al., 2014), and with our technique, this is not necessary anymore.

With these results, our study (Publication 2) could also be a template for separating other compounds that are difficult to separate with PTR-MS, e.g. acetone and propanal from soil VOC emissions (Mancuso et al., 2015) or breath (Lindinger et al., 1998; Rudnicka et al., 2011), or methacrolein and methyl vinyl ketone in atmospheric studies (Eerdeken et al., 2009; Ammann et al., 2004). The distinction between different xylenes and ethylbenzene in atmospheric BTEX concentrations has been a problem with PTR-MS (de Gouw et al., 2003), but was recently realized with SIFT-MS (Allpress et al., 2019). With this, SIFT-MS has a great potential to be increasingly used in atmospheric research in the next years.

5.2. Dimethyl Sulfide, Methanethiol, and Hydrogen Sulfide from Soil

Traditionally, terrestrial VSC emissions were thought to be negligible since studies of temperate soils were found to only emit MeSH and DMS only at low rates (Adams et al., 1981). The only significant sources of DMS and MeSH in terrestrial systems were thought to be anaerobic sediments of stratified lakes and wetlands, and even there, most MeSH and DMS was found to be consumed in the well-mixed water columns above the sediments (Hu et al., 2007). The main production pathways were considered to be sulfate reduction and subsequent methylation in those anaerobic sediments (Lomans et al., 2001a), or MeSH production from methionine and DMS production from methylated methionine (Drotar et al., 1987). Since only low methanethiol emission rates were found and the pool for methylated methionine is small, this was considered a negligible source (Aneja and Cooper,

1989), and only oceanic DMS emissions were further considered in models (Kloster et al., 2006; Fiddes et al., 2018).

The finding of a widespread methanethiol methyltransferase (Carrion et al., 2015) and high MeSH methylation activities of microbes in agricultural, grassland, and forest soils as well as in lake, river, and marine sediments (Carrion et al., 2017) opened the possibility that terrestrial VSC emissions actually contribute significantly to the global sulfur budget. This is further supported by a study of Wilkening et al. (2019), who reported VSC emission rates 10x higher than previous studies and showed that this might be due to the rapid degradation of VSCs during sample storage. We observed significant H₂S, MeSH, and DMS emissions at redox potentials too high for sulfate reduction in an organic-rich peat sample, so we conclude that in this case, organic matter is the VSC precursor (Publication 3). Assuming that the emission behavior of our soil incubations is similar to natural peatland emissions and we can use the surface area in our chamber as a proxy for the natural area, we get an emission of approx. 20 μg/(m² a) DMS, which is well in the range of emissions reported from Florida wetlands (Cooper et al., 1987), but a factor of 2-20 higher than the emissions reported from other US-American histosols (Adams et al., 1981). This is similar for the other VSCs. Thus, revisiting terrestrial soils and wetlands to measure their emissions might be useful.

When taking into account our results of the litter degradation under oxic conditions in Chapter 4, it becomes clear that litter itself under oxic conditions is not a big source of VSCs, even though it contains fresh amino acids and proteins. Assuming a linear increase of VSC emissions over time in the static chambers, the VSC emissions from fresh litter are 20-fold lower than from soil. It seems like some oxygen restriction is necessary to enhance VSC emissions, but from our results of the Hainich and Würzbadgrund forest sites, this can easily be accomplished in mineral topsoil layers below the litter layer. So the VSC emissions in mineral topsoil might be a secondary effect of litter input. Leaching litter with water would transport methionine, cysteine, and other sulfur-containing organic compounds into the mineral soil layers, where it is then degraded under the formation of VSCs. Of course, if litter is submerged, e.g. by falling into a lake, this could also directly lead to VSC emissions from the litter itself. Still, litter likely matters as organic matter input for VSC emissions, but is not a big direct contributor to the emissions.

Besides the atmospheric implications, VSCs have repeatedly been observed to mediate interspecies interactions in soils, e.g. brassica plants exude them from their roots and *Pseudomonas aeruginosa* bacteria emit them to promote *Aspergillus fumigatus* growth (Scott et al., 2019). So even if emissions of VSCs are not high, they might give us insights into which organisms are present and active in the soil, and how they interact with each other. With the recent enzyme purifications and elucidations of biosynthetic pathways, closer investigations on their genetic regulation and potential biotic and abiotic stress factors triggering the VSC emission and degradation are possible. Examples for these newer developments are the methylation and demethylation by methanethiol methyltransferase (Carrion et al., 2015) and MeSH and DMS monooxygenases (Boden et al., 2011; Cao et al., 2018; Eyice et al., 2018; Hammers et al., 2020) and their coupling to dissimilatory sulfide and sulfite

reductase (Koch and Dahl, 2018; Kröber and Schäfer, 2019). Potentially, abiotic and biotic processes could be intertwined or coupled to each other, like in the genesis of COS (Meredith et al., 2018). We found that sulfate reduction and subsequent methylation to methanethiol as well as the formation of MeSH and DMS from methylthio and dimethyl sulfonio groups is faster than the interconversion of MeSH to DMS and *vice versa*, the demethylation of MeSH to H₂S, and the oxidation of MeSH to COS and DMS to DMSO (Publication 3). This indicates that these steps are governed by different biotic and abiotic processes and provides further motivation to investigate their regulating factors.

Still, precursors for VSCs are mostly discussed as sulfate and methionine (Liu et al., 2017). With the vast variety of compounds in soil organic matter, a restriction to sulfate and methionine as sole precursors of VSCs seems unlikely. Thus, we expanded the search for potential precursors of VSCs to methylthio-group- and dimethylsulfonio-group-containing substances. We used a metabolomics approach to search for other potential precursors, and then spiked them and other literature-known methylthio-group-containing compounds like gonyol to soil. We found proof for our hypothesis, as all compounds with these functionalities that we examined led to an increase in VSC emissions (Publication 3). This scavenging of methylthio and dimethyl sulfonio groups might not only occur when detoxifying VSC-precursors or using them for growth, but also when scavenging sulfur from organic material in sulfur-starvation conditions analogous to the use of DMS and 2-(methylthio)-ethanol by a nitrogenase-like methylthio-alkane reductase for methionin formation (North et al., 2020).

The last comprehensive study on soil VSC emissions is 40 years old, and only comprised US-American soils (Adams et al., 1981). As pointed out above, the detected emissions are considerably lower than what we measured ourselves (Publication 3). Of course, our high emissions might be an artifact since we did not measure in the field, but considering the results of Wilkening et al. (2019), maybe the emissions of Adams et al. (1981) are too low. Hence, systematic emission measurements for both freshwater wetlands and more arid soils would be beneficial. Besides wetlands, agricultural soils should be in the focus, as they are frequently fertilized with sulfate and organic matter like manure or organic waste. Since these products are known to be substantial VSC emitters (Feilberg et al., 2010; He et al., 2018), it is very likely that these emissions also persist in soil.

As pointed out in the introduction, the number of plants that were investigated for VSC emissions is very small, a few crops, and some trees and shrubs temperate, mediterranean, and tropical. Even though VSC emissions are usually only of minor importance when studying vegetation VOC emissions, they are still sometimes reported, e.g. Tang et al. (2018). As already pointed out by Watts (2000), a focused study on VSC emissions from plants that enables an accurate determination of the contribution of vegetation to the global sulfur budget would thus be very helpful.

As discussed above, it is very unlikely that only amino acids are precursors for VSC emissions. One step to identify other precursors was done by us (Publication 3), and this could be continued. For example, one should also include glucosinolates from root extracts of e.g. horseradish, as they can

be degraded to VSCs by fungi (Plaszkó et al., 2020). However, one should not only identify the precursors, but also the biosynthetic pathways involved. There is currently more work done on enzymes and microbes involved in VSC degradation than on their formation pathways, presumably because it is easier to identify microbes and enzymes differentially expressed when growing on VSCs. To my knowledge (and as described in the Metacyc database (Caspi et al., 2020)), neither a H₂S methylation enzyme to form MeSH nor an enzyme cleaving *S*-methyl methionine to DMS was completely characterized yet. The latter was purified and investigated for its kinetic properties, substrate specificity and inhibitor studies were done (Mazelis et al., 1965), but neither the crystal structure nor the encoding gene has been identified. Also, the putative link between MeSH and COS that we found in our study (Publication 3) should be investigated further – the exact biochemical pathway and its involved microorganisms and enzymes are interesting. Of course, there is always the possibility to find new pathways to VSCs, either from previously unknown VSC precursors or just by different ways from existing precursors, like the pathway to DMS from methionine via *S*-methyl methionine, DMSP, and gonyol in *Burkholderia pseudomallei* (Trottmann et al. (2020) and personal communication by him).

Besides the obvious triggers like a low redox potential, a medium soil humidity, a warm temperature, and high sulfate and methionine contents, there is little information on what governs VSC emissions. This is especially of interest in the context of VSCs as infochemicals. As they are used for both pathogen growth promotion (Scott et al., 2019) and defense compounds against flies (Crespo et al., 2012) and nematodes (Sikder and Vestergård, 2019), it is very likely that some of these VSCs also escape to the atmosphere and contribute to the global sulfur budget. Understanding why which plants and microbes use VSCs for which purpose under which circumstances would not only help understanding how soil communities form, but would also help assessing their impact on the global sulfur cycle.

To my knowledge, terrestrial VSC emissions have not been modelled yet. A conceptual model of the cycling processes will show us which processes we already understand well and where we do not understand the system well enough to represent it in a model. In analogy to the recent VOC model proposal by Tang et al. (2019) and the COS model by Ogée et al. (2016), one could model soil VSCs like depicted in Figure 5.1: Generally, the model is determined by the soil properties, like its texture and porosity. The main sulfur sources are litter and minerals. They feed into the soil organic matter and soil sulfate pools. Both processes can be abiotic or biotic, through microbes. From soil organic matter and soil sulfate, VSCs can be formed. Potentially, one could also include litter degradation as an input for VSC emissions, but as discussed above, I believe the indirect influence of litter *via* SOM is more important and the direct link is negligible. VSCs can be adsorbed on particles, dissolved in soil water, or part of the pore gases in soil. H₂S, MeSH, and DMS can be converted into each other. These processes are all biotic and could be modelled by Michaelis-Menten kinetics. H₂S can also be caught by metal ions to form minerals again, and the other way round – an abiotic process that can be modelled as a second-order kinetic reaction, or just an equilibrium. Release of VSCs to the

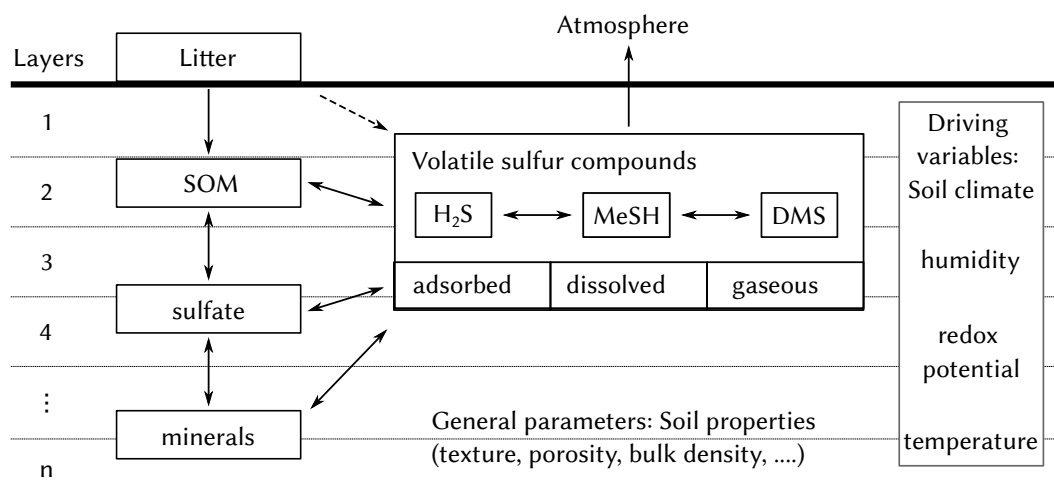


Figure 5.1.: Proposal for a VSC model. The litter sulfur pool feeds into soil organic matter (SOM). SOM and sulfate feed volatile sulfur compounds (H₂S, MeSH, DMS) in soil. The magnitude of the feed is driven by soil humidity, redox potential, and temperature. As these are microbial processes, they could be modelled as Michaelis Menthen kinetics. VSCs absorbed on particles, dissolved in soil water and gaseous in the soil air are in equilibrium to each other, again depending on the driving parameters. VSCs can be emitted to the atmosphere; here, diffusion laws govern the process. One can model different soil layers to account for the variation of conditions with depth.

atmosphere depends on diffusion, desorption and dissolution, so Fick's and Henry's laws have to be taken into account here. To capture the effect of soil depth, one can model different soil layers. With such a model, the processes we found could complement what is known in literature, and a deeper understanding of the soil's sulfur cycle would be achieved.

5.3. VOC Emissions from Litter

Leaf litter VOC emissions are often considered to be the main biogenic VOC source besides vegetation (Asensio et al., 2008; Tang et al., 2019), but on an ecosystem level, litter VOCs are usually only determined together with soil emissions as ground VOC emissions (Aaltonen et al., 2011; Barreira et al., 2017; Gray et al., 2014). However, leaf litter emissions can reach the same magnitude as vegetation emissions in spring and fall (Viros et al., 2020), so an understanding of these emissions is necessary for accurate VOC emission inventories. Since litter is an important source of organic carbon for soils and contains a lot of labile carbon as well, its VOC emissions are usually resembled by the soil below, but on a lower magnitude and with less variability (Leff and Fierer, 2008). So by understanding litter VOC emissions, we can infer knowledge to soil VOC emissions as well. There are a few studies investigating species specificity of VOC emissions on a broad range of different plants (Gray et al., 2010; Isidorov and Jdanova, 2002; Leff and Fierer, 2008; Viros et al., 2020), but

when it comes to long-term studies, only different pine and spruce species are well-covered (Barreira et al., 2017; Gray et al., 2014; Greenberg et al., 2012; Haapanala et al., 2012; Hayward et al., 2001; Isidorov et al., 2003; Mäki et al., 2019a,b; Räisänen et al., 2009). One in-depth time dependence study has been done on *Geum rossii*, *Deschampsia cespitosa*, and *Rhododendron maximum* (Brown, 2008), and the change of VOC emissions from green leaves to fresh litter has been studied on birch (Batish et al., 2006).

We performed a systematic study on how litter of different temperate broadleaf and conifer litter is degrading in its natural environment (Chapter 4, unpublished manuscript). To our knowledge, this is the first litter VOC emission data for a few of the plants, e.g. *C. betulus*, *Tilia* sp., and *F. sylvatica*. We observed strong monoterpene emissions for conifers that decreased slowly over time, and a spike in small polar VOC emissions (methanol, acetaldehyde, acetic acid, H₂S) for fresh broadleaf species. The exponential decay of VOC emissions that Brown (2008) reported matches our findings. Gray et al. (2010) report an increase in biotic emission over a period of 20 days for some of their litter species. We also observed an increase of monoterpene emissions for *P. menziesii* from t = 0 to t = 100 d, so this might be an effect. Summarizing our study as well as other published studies, it seems litter VOC emissions quickly rise to a peak and then decay exponentially. However, our data are rather coarse, measuring only at 0, 100, 200, and 400 d, and most emissions cease after 200 d the latest. We could show that the VOC emissions depend on the labile carbon in the leaves and the emission rates are very low when only the leaf skeleton is left. However, for a more accurate description, it might be interesting to do a more short-term study again and sample the litter e.g. once a week from November till March or do a long-term soil & litter VOC emission experiment in single-species and mixed-species forests.

In terms of the driving factors for VOC emissions, Tang et al. (2019) proposed using a plant-storage derived litter VOC pool and a microbial-derived litter pool. The former would be governed by its averaged residence time in the pool and the litter temperature, and the latter governed by the litter moisture and temperature and other biochemical characteristics. The temperature-dependence was shown by Greenberg et al. (2012), Gray et al. (2014), and Svendsen et al. (2018). The humidity influence was shown by Asensio et al. (2012), and Faiola et al. (2014), even showing a burst of VOC emissions after rewetting similar to the Birch-Effect for CO₂ respiration. We only observed the humidity-effect for acetaldehyde, and we did not find a correlation with the CO₂ respiration rate. But we could confirm the pool size as an important factor governing monoterpene emissions in conifers, and even the simple carbon content could be used as a proxy for this (Chapter 4, Unpublished Work). In general, it seems like modelling broadleaf litter methanol and conifer litter monoterpene emissions is sufficient for larger scale VOC emission and atmospheric models.

For future research, it would be interesting to relate structural compound classes to VOC emissions, to see which precursors are used to produce which VOC. Some steps in this direction have been made, e.g. by showing that nitrogen limitation in conifer litter degradation can be overcome by either nitrogen fertilization or the addition of broadleaf (maple) litter and that this decreases VOC

emissions (Guénon et al., 2017; Huang et al., 2020). This is in line with the observation that the bulk C:N:P stoichiometry is not kept by the microbes, but rather the C:N:P stoichiometry of the labile carbon fraction (Fanin et al., 2013). Isidorov et al. (2005) have started relating structural carbon classes to monoterpene emissions in larch needle litter, but this is probably even more important for broadleaf species. It remains to be shown in litter itself that the pectins degrade to methanol and that acetate originates from sugar metabolism. As far as I know, this is only inferred from our knowledge of biosynthesis and metabolism pathways in isolated microbial strains, but it has never been shown that the amount of those compounds and the activity of the microbes degrading these compound classes influences the VOC emissions. Yet this would improve our understanding of litter VOC emissions and enable us to model them more accurately.

With regards to the tree species, especially litter from pine and spruce both in boreal forests and mediterranean forests plus oak from mediterranean forests have been studied extensively (Aaltonen et al., 2011; Asensio et al., 2007a; Gray et al., 2010; Hakola et al., 2012; Hellén et al., 2017; Isidorov et al., 2003, 2005, 2010, 2016; Mäki et al., 2019a,b; Viros et al., 2020), and there is at least some data on understorey and shrub litter in those regions as well (Asensio et al., 2012; Batish et al., 2006; Brown, 2008; Svendsen et al., 2018; Viros et al., 2020). Our study adds knowledge on temperate tree litter (Chaper 4, Unpublished Work) and there is one study on a tropical forest (Huang et al., 2020). So regional study areas would thus be temperate, subtropical and tropical forest litters, and the extension of litter research from tree litter to litter of understorey vegetation, shrubs, herbs, and grasses. Experiments on VOC emissions from rotting wood and tree stumps as other degrading organic material as demonstrated by Haapanala et al. (2012) and Kulmala et al. (2014) are also needed to complete the picture of biogenic degradation-based VOC emissions.

Another research direction might be a systematic inventory of all the different VOCs that are emitted from tree species. Isidorov and Jdanova (2002), Isidorov et al. (2003), Leff and Fierer (2008), Svendsen et al. (2018), and Viros et al. (2020) have found numerous non-terpenoid aldehydes, ketones, aromatics, and even halogen, nitrogen, and sulfur compounds for their boreal pine and spruce and mediterranean broadleaf, conifer and shrub litter respectively, and this could and should be continued for the missing tree litter sources. Especially the emission of methyl chloride and other chlorinated compounds from litter (Derendorp et al., 2011, 2012) is interesting, as these emissions influence the ozone depletion in the stratosphere and absorb light in wavelength areas not usually covered by other greenhouse gases. Yet the overall emissions of halogenated compounds from litter is likely rather small. Distinguishing the different terpenes of course also still remains an interesting field of study for conifers, especially since it seems that the chirality of the compounds might enable a separation of vegetation and ground/litter terpene emissions (Staudt et al., 2019).

In addition to that, the influence of litter VOCs on soil and generally the interactions of litter and soil in VOC production, degradation, emission, and uptake dynamics still needs further investigation. Litter VOCs can directly be used as a carbon source by soil microbes (Ramirez et al., 2010b) and contribute to the soil's carbon content (Asensio et al., 2012). Labelled litter VOC emissions were

found in all SOC fractions including dissolved organic matter, particulate organic matter, mineral-bound organic matter, and microbial matter (McBride et al., 2019, 2020), and litter VOCs were found to change the activity of microbes by inhibiting nitrification processes (McBride et al., 2019). So far, litter VOCs were only treated as potential carbon sources though. There might also be compounds used as signals and triggers of microbial activity, as shown for nitrification (McBride et al., 2019). Plus, this might not only be litter VOCs influencing soil microbial activity, but also the other way round. In contrast to nonvolatile leachate organic compounds, VOCs can actually travel from the soil to the litter, and even if the amounts are smaller than the other way round, the mixture of the blend or specific compounds can probably work as allelopathic compounds to influence microbial activity in the litter.

Taking this into account, analyzing the soil's volatilome offers a unique opportunity to investigate the underlying soil and litter biogeochemistry nondestructively and in situ. Of course, we can only observe the net effect and not all VOCs will be informative, but if we can identify specific VOCs as biomarkers for specific processes, we can track those processes in situ. Thus, by measuring multiple VOCs in parallel like with an untargeted metabolomics approach, we might be able to observe the soil's response to environmental conditions while it is evolving.

Not only the flora, but also the fauna contributes to the soil's organic matter pool upon degradation. To my knowledge, there are no studies on VOC emissions from decaying soil fauna. There are studies of VOC emissions from forensic investigation of human and other mammal cadavers showing high emissions of hydrocarbons and carbonyl compounds (Dekeirsschieter et al., 2009; Martin et al., 2021; Stefanuto et al., 2015) as well as insects living on them (Blonar and Prada-Tiedemann, 2020; Dubie et al., 2017), but not from other animals. Whereas the VOC emissions of decaying bacteria and fungi will be captured by the investigation of soil organic matter and soil VOCs, annelides, nematodes and other soil macrofauna are usually sorted out when doing incubations. Given the fact that annelides can make up 5% of the soil's weight (Gisi, 1997), this might be a huge missing VOC source we have not investigated yet.

Lastly, not only bulk soil, the rhizosphere, and leaves litter should be considered for VOC emissions, but also earthworm burrows. As organic carbon and microbial activity is enhanced in the drilosphere due to the excretion of mucus by the earthworms (Guhra et al., 2020), it is very probable that also VOC emissions are enhanced here. Since the pores of *Lumbricus terrestris* are vertical (van Schaik et al., 2014), air should be exchanged with the atmosphere easily, so these earthworm pores could contribute to VOC emissions from deeper layers of the soils as well.

The common theme of Publication 3 and Chapter 4 is thus the investigation of volatile compounds from degrading organic matter. The investigated histosol in Publication 3 is essentially also decaying plant parts and litter. What always dominates the VOC and VSC emissions is the availability of organic precursors that usually originally stem from vegetation. The amino acid degradation for

MeSH and DMS emissions is tied to relatively fresh, labile organic carbon, either from litter or microbial origin. We also found small H₂S, MeSH, and DMS emissions from fresh litter in Chapter 4 (a factor of 20 lower than soil VSC emissions), probably produced by the organic matter degradation pathways described in Publication 3. Probably, the variety and release rate of litter VOCs is to increase once oxygen gets limiting. This would explain the close relation to litter humidity mentioned above. Submerging litter would then even start fermentation processes. This is more likely to happen to the organic carbon leached from the litter into the deeper soil layers, where the air exchange is more limited than in the litter layer with its big pore spaces. Thus, soil and litter VOC emissions should not only be treated separately, but their interactions are important as well.

6. Conclusion

Volatilomics has the potential to give deeper insights into biochemical and biogeochemical processes as we can monitor a multitude of volatile analytes nondestructively in situ. With the rise of new, selective and sensitive real-time analysis techniques like PTR-ToF-MS and SIFT-MS, we are now reaching a level where it actually becomes possible to closely monitor environmental processes in situ and capture both small and large VOC concentrations. This will enable us to understand the chemical language of plants, microbes, and animals better and better, until we eventually might be able to enter into some sort of communication.

Thereby, the four major contributions of this work are firstly, that we can now use SIFT-MS for soil and litter VOC emission analysis reliably (Publication 1). Secondly, our validated method to distinguish isoprene from 2-methyl-3-buten-2-ol in real time enables phytologists and ecologists to distinguish heat stress signals from different tree species, like we demonstrated for *Populus nigra*, *Picea glauca*, *Picea abies*, and *Pinus ponderosa* (Publication 2). Thirdly, our detailed study of the soil's sulfur cycle and processes leading to the reduced volatile sulfur compounds hydrogen sulfide, methanethiol, and dimethyl sulfide showed that dimethyl sulfide mainly originates from organic matter degradation in peatlands and other at least partially oxygen-restricted soils and thus dimethyl sulfide fluxes from terrestrial ecosystems might be underestimated. We could also show that higher VSC levels in the headspace lead to a convergence of the headspace to mainly dimethyl sulfide, 3x less methanethiol, and 10x less hydrogen sulfide as well as some carbonyl sulfide and dimethyl sulfoxide. Lastly, we could show that litter VOC emissions are mainly caused by oxygenated low-molecular weight VOCs like methanol or acetaldehyde for fresh broadleaf litter, and terpene and terpenoid emissions from conifer litter over longer timeframes (Chapter 4).

Each chapter of this thesis opens up the possibility for further research: Based upon my first publication, researchers can now adjust their SIFT-MS to their needs: whether they want to measure small headspace concentrations of specific compounds in a rather dry environment like in soil VOC research or bigger concentrations in a humid atmosphere as in plant VOC research, the publication shows how to optimize the parameters to suit their needs best.

Based upon the second publication, phytologists and ecologists can now do field studies on isoprene and 2-methyl-3-buten-2-ol in parallel, and gain insights into the heat stress of different plants in an ecosystem or into bark beetle infestations. Furthermore, this study can serve as a template for similar method developments to separate different analytes.

With the deeper understanding of the sulfur cycle that was provided in Publication 3, we opened an ensemble of new research questions: How important are VSC emissions from other terrestrial ecosystems like organic-rich forest soils? Which other organic VSC precursors exist? How are the enzymatic mechanisms involved in these precursor degradations? And how are the contributions of litter, soil organic matter, sulfate, and minerals to volatile sulfur compounds?

Lastly, the work in Chapter 4 shows that we should focus our litter degradation studies on the small period directly after litterfall for broadleaf litter, but for conifer litter, much longer time frames are necessary. We also see a big suite of different compounds, so for field studies investigating litter, it might be useful to try measuring the whole volatilome to get an idea of the magnitude and diversity of VOC emissions.

As a whole, the thesis links microbial, biosynthetic, metabolic, and abiotic pathways leading to VOC emissions with environmental emission observations. Studies like this one narrow the gap between the simple two- or three-way interaction systems of the chemical ecology world and the large-scale cycle-focused biogeochemistry world. It helps explaining the results we see on the bulk soil and ecosystem emissions by the numerous processes we know from chemical ecology. By tying organic precursor compounds and compound classes with VOC emissions and investigating the microbial community composition and activity, we will be able to gain full understanding of the soil system, which will then allow us to select the necessary parameters for a model of the system.

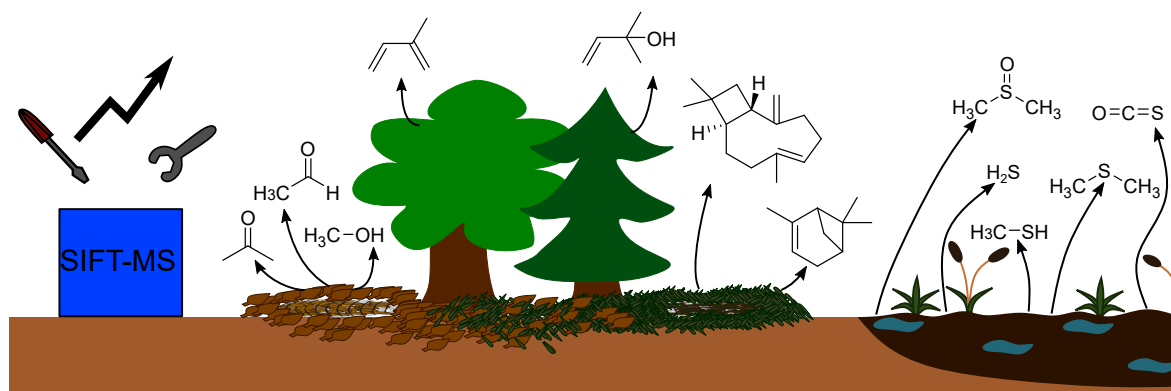


Figure 6.1.: Thesis summary: SIFT-MS was optimized for ambient VOC measurements. Isoprene and MBO are emitted from trees and can now be simultaneously measured. Upon degradation, broadleaf litter mainly emits small VOCs when it is fresh and emissions decrease quickly, whereas needle litter emits terpenoids as stored in the leaves over longer periods of time. DMS from peatlands is mainly caused by organic matter degradation, whereas H_2S and methanethiol also originate from sulfate reduction and can be converted to DMS easily.

Bibliography

GESTIS Substance Database, URL www.dguv.de/ifa/gestis-database, 2021.

Aaltonen, H., Pumpanen, J., Pihlatie, M., Hakola, H., Hellén, H., Kulmala, L., Vesala, T., and Bäck, J.: Boreal pine forest floor biogenic volatile organic compound emissions peak in early summer and autumn, *Agricult. For. Meteorol.*, 151, 682–691, <https://doi.org/10.1016/j.agrformet.2010.12.010>, 2011.

Abis, L., Loubet, B., Ciuraru, R., Lafouge, F., Dequiedt, S., Houot, S., Maron, P. A., and Bourgeteau-Sadet, S.: Profiles of volatile organic compound emissions from soils amended with organic waste products, *Sci. Tot. Environ.*, 636, 1333–1343, <https://doi.org/10.1016/j.scitotenv.2018.04.232>, 2018.

Abis, L., Loubet, B., Ciuraru, R., Lafouge, F., Houot, S., Nowak, V., Tripied, J., Dequiedt, S., Maron, P. A., and Sadet-Bourgeteau, S.: Reduced microbial diversity induces larger volatile organic compound emissions from soils, *Sci. Rep.*, 10, 6104, <https://doi.org/10.1038/s41598-020-63091-8>, 2020.

Acton, W. J. F., Huang, Z., Davison, B., Drysdale, W. S., Fu, P., Hollaway, M., Langford, B., Lee, J., Liu, Y., Metzger, S., Mullinger, N., Nemitz, E., Reeves, C. E., Squires, F. A., Vaughan, A. R., Wang, X., Wang, Z., Wild, O., Zhang, Q., Zhang, Y., and Hewitt, C. N.: Surface–atmosphere fluxes of volatile organic compounds in Beijing, *Atmos. Chem. Phys.*, 20, 15 101–15 125, <https://doi.org/10.5194/acp-20-15101-2020>, 2020.

Adams, D. F., Farwell, S. O., Pack, M. R., and Bamesberger, W. L.: Preliminary measurements of biogenic sulfur-containing gas emissions from soils, *J. Air Poll. Control Assoc.*, 29, 380–383, <https://doi.org/10.1080/00022470.1979.10470805>, 1979.

Adams, D. F., Farwell, S. O., Robinson, E., Pack, M. R., and Bamesberger, W. L.: Biogenic sulfur source strengths, *Env. Sci. Technol.*, 15, 1493–1498, <https://doi.org/10.1021/es00094a012>, 1981.

Agathokleous, E., Kitao, M., and Calabrese, E. J.: Emission of volatile organic compounds from plants shows a biphasic pattern within an hormetic context, *Environ. Pollut.*, 239, 318–321, <https://doi.org/10.1016/j.envpol.2018.04.031>, 2018.

Allpress, C., Crittenden, D., Ma, J., McEwan, M., Robinson, S., Wilson, P., and Wu, M.: Real-time differentiation of ethylbenzene and the xylenes using selected ion flow tube mass spectrometry, *Rapid Commun. Mass Spectrom.*, 33, 1844–1849, <https://doi.org/10.1002/rcm.8550>, 2019.

- Ammann, C., Spirig, C., Neftel, A., Steinbacher, M., Komenda, M., and Schaub, A.: Application of PTR-MS for measurements of biogenic VOC in a deciduous forest, *Int. J. Mass Spectrom.*, 239, 87–101, <https://doi.org/10.1016/j.ijms.2004.08.012>, 2004.
- Andreae, M. O.: Ocean-atmosphere interactions in the global biogeochemical sulfur cycle, *Marine Chem.*, 30, 1–29, [https://doi.org/10.1016/0304-4203\(90\)90059-L](https://doi.org/10.1016/0304-4203(90)90059-L), 1990.
- Andreae, M. O. and Andreae, T. W.: The cycle of biogenic sulfur compounds over the Amazon Basin: 1. Dry season, *J. Geophys. Res.*, 93, 1487–1497, <https://doi.org/10.1029/JD093iD02p01487>, 1988.
- Andreae, M. O., Berresheim, H., Bingemer, H., Jacob, D. J., Lewis, B. L., Li, S. M., and Talbot, R. W.: The atmospheric sulfur cycle over the Amazon basin 2. wet season, *J. Geophys. Res.: Atmos.*, 95, 16 813–16 824, <https://doi.org/10.1029/JD095iD10p16813>, 1990.
- Aneja, V. P. and Cooper, W. J.: Biogenic sulfur emissions, in: Biogenic sulfur in the environment, vol. 393 of *ACS Symposium Series*, pp. 2–13, American Chemical Society, <https://doi.org/10.1021/bk-1989-0393.ch001>, 1989.
- Aneja, V. P., Overton, J. H., Cupitt, L. T., Durham, J. L., and Wilson, W. E.: Carbon disulphide and carbonyl sulphide from biogenic sources and their contributions to the global sulphur cycle, *Nature*, 282, 493–496, 1979.
- Angelo and Ripley, B. D.: boot: Bootstrap R (S-Plus) Functions, URL <https://cran.r-project.org/web/packages/boot/index.html>, 2020.
- Asensio, D., Peñuelas, J., Filella, I., and Llusà, J.: On-line screening of soil VOCs exchange responses to moisture, temperature and root presence, *Plant Soil*, 291, 249–261, <https://doi.org/10.1007/s11104-006-9190-4>, 2007a.
- Asensio, D., Peñuelas, J., Llusà, J., Ogaya, R., and Filella, I.: Interannual and interseasonal soil CO₂ efflux and VOC exchange rates in a Mediterranean holm oak forest in response to experimental drought, *Soil Biol. Biochem.*, 39, 2471–2484, <https://doi.org/10.1016/j.soilbio.2007.04.019>, 2007b.
- Asensio, D., Owen, S., Llusia, J., and Penuelas, J.: The distribution of volatile isoprenoids in the soil horizons around *Pinus halepensis* trees, *Soil Biol. Biochem.*, 40, 2937–2947, <https://doi.org/10.1016/j.soilbio.2008.08.008>, 2008.
- Asensio, D., Yuste, J. C., Mattana, S., Ribas, À., Llusà, J., and Peñuelas, J.: Litter VOCs induce changes in soil microbial biomass C and N and largely increase soil CO₂ efflux, *Plant Soil*, 360, 163–174, <https://doi.org/10.1007/s11104-012-1220-9>, 2012.
- Atkinson, R.: Gas-phase tropospheric chemistry of volatile organic compounds: 1. Alkanes and Alkenes, *J. Phys. Chem. Ref. Data*, 26, 215–290, <https://doi.org/10.1063/1.556012>, 1997.
- Atkinson, R. and Arey, J.: Atmospheric degradation of volatile organic compounds, *Chem. Rev.*, 103, 4605–4638, 2003.

- Bäck, J., Aaltonen, H., Hellén, H., Kajos, M. K., Patokoski, J., Taipale, R., Pumpanen, J., and Heinonsalo, J.: Variable emissions of microbial volatile organic compounds (MVOCs) from root-associated fungi isolated from Scots pine, *Atmos. Environ.*, 44, 3651–3659, <https://doi.org/10.1016/j.atmosenv.2010.06.042>, 2010.
- Bailey, S. D., Bazinet, M. L., Driscoll, J. L., and McCarthy, A. I.: The volatile sulfur components of cabbage, *J. Food Sci.*, 26, 163–170, <https://doi.org/10.1111/j.1365-2621.1961.tb00787.x>, 1961.
- Baird, C. and Cann, M.: *Environmental Chemistry*, W. H. Freeman and Company, New York, 2012.
- Bak, F., Finster, K., and Rochfuß, F.: Formation of dimethylsulfide and methanethiol from methoxylated aromatic compounds and inorganic sulfide by newly isolated anaerobic bacteria, *Arch. Microbiol.*, 157, 529, <https://doi.org/10.1007/BF00276773>, 1992.
- Baldocchi, D. D.: Assessing the eddy covariance technique for evaluating carbon dioxide exchange rates of ecosystems: past, present and future, *Glob. Chang. Biol.*, 9, 479–492, <https://doi.org/10.1046/j.1365-2486.2003.00629.x>, 2003.
- Banwart, W. L. and Bremner, J. M.: Formation of volatile sulfur compounds by microbial decomposition of sulfur-containing amino acids in soils, *Soil Biol. Biochem.*, 7, 359–364, [https://doi.org/10.1016/0038-0717\(75\)90050-4](https://doi.org/10.1016/0038-0717(75)90050-4), 1975.
- Barreira, L. M. F., Duporte, G., Parshintsev, J., Hartonen, K., Jussila, M., Aalto, J., Bäck, J., Kumala, M., and Riekkola, M. L.: Emissions of biogenic volatile organic compounds from the boreal forest floor and understory: a study by solid-phase microextraction and portable gas chromatography-mass spectrometry, *Boreal Environ. Res.*, 22, 393–413, 2017.
- Bates, D., Mächler, M., Bolker, B., and Walker, S.: Fitting linear mixed-effects models using lme4, *J. Stat. Soft.*, 67, 1–48, <https://doi.org/10.18637/jss.v067.i01>, 2015.
- Batish, D. R., Singh, H. P., Setia, N., Kaur, S., and Kohli, R. K.: Chemical composition and phytotoxicity of volatile essential oil from intact and fallen leaves of *Eucalyptus citriodora*, *Z. Naturforsch. C: J. Biosci.*, 61, 465–471, <https://doi.org/10.1515/znc-2006-7-801>, 2006.
- Beard, S., Paradela, A., Albar, J. P., and Jerez, C. A.: Growth of *Acidithiobacillus ferrooxidans* ATCC 23270 in thiosulfate under oxygen-limiting conditions generates extracellular sulfur globules by means of a secreted tetrathionate hydrolase, *Front. Microbiol.*, 2, 79, <https://doi.org/10.3389/fmicb.2011.00079>, 2011.
- Beck, J. J., Smith, L., and Baig, N.: An overview of plant volatile metabolomics, sample treatment and reporting considerations with emphasis on mechanical damage and biological control of weeds, *Phytochem. Anal.*, 25, 331–341, <https://doi.org/10.1002/pca.2486>, 2014.
- Behrendt, T., Veres, P. R., Ashuri, F., Song, G., Flanz, M., Mamtimin, B., Bruse, M., Williams, J., and Meixner, F. X.: Characterisation of NO production and consumption: new insights by an

- improved laboratory dynamic chamber technique, *Biogeosciences*, 11, 5463–5492, <https://doi.org/10.5194/bg-11-5463-2014>, 2014.
- Bending, G. D. and Lincoln, S. D.: Characterisation of volatile sulphur-containing compounds produced during decomposition of *Brassica juncea* tissues in soil, *Soil Biol. Biochem.*, 31, 695–703, 1999.
- Benk, S., Eveillard, D., Taubert, M., Küsel, K., and Gleixner, G.: The Coupled Nature of DOM: Combining Microbial and Molecular Perspectives on Plant Litter Decomposition, in: *AGU Fall Meeting Abstracts 2019*, vol. B13G, p. 2585.
- Berger, T., Poyntner, C., and Margesin, R.: Culturable bacteria from an Alpine coniferous forest site: biodegradation potential of organic polymers and pollutants, *Folia Microbiol.*, 66, 87–98, <https://doi.org/10.1007/s12223-020-00825-1>, 2021.
- Berresheim, H., Andreae, M. O., Ayers, G. P., and Gillett, R. W.: Distribution of biogenic sulfur compounds in the remote southern hemisphere, in: *Biogenic sulfur in the environment*, vol. 393 of *ACS Symposium Series*, pp. 352–366, American Chemical Society, <https://doi.org/10.1021/bk-1989-0393.ch021>, 1989.
- Biasioli, F., Yeretzyan, C., Märk, T. D., Dewulf, J., and van Langenhove, H.: Direct-injection mass spectrometry adds the time dimension to (B)VOC analysis, *Trends Anal. Chem.*, 30, 1003–1017, <https://doi.org/10.1016/j.trac.2011.04.005>, 2011.
- Bills, D. D. and Keenan, T. W.: Dimethyl sulfide and its precursor in sweet corn, *J. Agricult. Food Chem.*, 16, 643–645, <https://doi.org/10.1021/jf60158a029>, 1963.
- Bingemer, H. G., Andreae, M. O., Andreae, T. W., Artaxo, P., Helas, G., Jacob, D. J., Mihalopoulos, N., and Nguyen, B. C.: Sulfur gases and aerosols in and above the equatorial African rain forest, *J. Geophys. Res.*, 97, 6207–6217, <https://doi.org/10.1029/91JD01112>, 1992.
- Birgersson, G. and Bergström, G.: Volatiles released from individual spruce bark beetle entrance holes: quantitative variations during the first week of attack, *J. Chem. Ecol.*, 15, 2465–2483, <https://doi.org/10.1007/bf01020377>, 1989.
- Bitas, V., Kim, H. S., Bennett, J. W., and Kang, S.: Sniffing on microbes: diverse roles of microbial volatile organic compounds in plant health, *Mol. Plant Microbe Interact.*, 26, 835–843, <https://doi.org/10.1094/MPMI-10-12-0249-CR>, 2013.
- Blanar, K. and Prada-Tiedemann, P. A.: Characterization of the volatile odor profile from larval masses in a field decomposition setting, *Forensic Chem.*, 21, 100 288, <https://doi.org/10.1016/j.forc.2020.100288>, 2020.
- Blande, J. D., Holopainen, J. K., and Niinemets, U.: Plant volatiles in polluted atmospheres: stress responses and signal degradation, *Plant Cell Environ.*, 37, 1892–1904, <https://doi.org/10.1111/pce.12352>, 2014.

- Blodau, C., Mayer, B., Peiffer, S., and Moore, T. R.: Support for an anaerobic sulfur cycle in two Canadian peatland soils, *J. Geophys. Res.: Biogeosci.*, 112, G2, 1–10, <https://doi.org/10.1029/2006jg000364>, 2007.
- Boden, R. and Hutt, L. P.: Bacterial metabolism of C1 sulfur compounds, in: *Aerobic Utilization of Hydrocarbons, Oils and Lipids*, pp. 1–43, https://doi.org/10.1007/978-3-319-39782-5_9-1, 2019.
- Boden, R., Borodina, E., Wood, A. P., Kelly, D. P., Murrell, J. C., and Schafer, H.: Purification and characterization of dimethylsulfide monooxygenase from *Hyphomicrobium sulfonivorans*, *J. Bacteriol.*, 193, 1250–1258, <https://doi.org/10.1128/JB.00977-10>, 2011.
- Borras, E., Tortajada-Genaro, L. A., and Munoz, A.: Determination of reduced sulfur compounds in air samples for the monitoring of malodor caused by landfills, *Talanta*, 148, 472–477, <https://doi.org/10.1016/j.talanta.2015.11.021>, 2016.
- Bourtsoukidis, E., Behrendt, T., Yanez-Serrano, A. M., Hellen, H., Diamantopoulos, E., Catao, E., Ashworth, K., Pozzer, A., Quesada, C. A., Martins, D. L., Sa, M., Araujo, A., Brito, J., Artaxo, P., Kesselmeier, J., Lelieveld, J., and Williams, J.: Strong sesquiterpene emissions from Amazonian soils, *Nat. Commun.*, 9, 2226–2237, <https://doi.org/10.1038/s41467-018-04658-y>, 2018.
- Bravo-Linares, C. M. and Mudge, S. M.: Analysis of volatile organic compounds (VOCs) in sediments using in situ SPME sampling, *J. Environ. Monit.*, 9, 411–418, <https://doi.org/10.1039/b617215f>, 2007.
- Breider, T. J., Chipperfield, M. P., Richards, N. A. D., Carslaw, K. S., Mann, G. W., and Spracklen, D. V.: Impact of BrO on dimethylsulfide in the remote marine boundary layer, *Geophys. Res. Lett.*, 37, L02 807, 1–10, <https://doi.org/10.1029/2009gl040868>, 2010.
- Breitenlechner, M., Fischer, L., Hainer, M., Heinritzi, M., Curtius, J., and Hansel, A.: PTR3: an instrument for studying the lifecycle of reactive organic carbon in the atmosphere, *Anal. Chem.*, 89, 5824–5831, <https://doi.org/10.1021/acs.analchem.6b05110>, 2017.
- Broadbent, A. D. and Jones, G. B.: DMS and DMSP in mucus ropes, coral mucus, surface films and sediment pore waters from coral reefs in the Great Barrier Reef, *Marine Freshw. Res.*, 55, 849–855, <https://doi.org/10.1071/MF04114>, 2004.
- Brown, E. M.: VOC emissions from decomposing leaf litter: Revising the conceptual framework for decay-related emissions, M. Sc., University of Colorado at Boulder, Ann Arbor, 2008.
- Bruderer, T., Gaugg, M. T., Cappellin, L., Lopez-Hilfiker, F., Hutterli, M., Perkins, N., Zenobi, R., and Moeller, A.: Detection of volatile organic compounds with secondary electrospray ionization and proton transfer reaction high-resolution mass spectrometry: a feature comparison, *J. Am. Soc. Mass Spec.*, 31, 1632–1640, <https://doi.org/10.1021/jasms.0c00059>, 2020.

- Bunk, R., Behrendt, T., Yi, Z. G., Andreae, M. O., and Kesselmeier, J.: Exchange of carbonyl sulfide (OCS) between soils and atmosphere under various CO₂ concentrations, *J. Geophys. Res.: Biogeosci.*, 122, 1343–1358, <https://doi.org/10.1002/2016jg003678>, 2017.
- Bylinski, H., Gebicki, J., Dymerski, T., and Namiesnik, J.: Direct analysis of samples of various origin and composition using specific types of mass spectrometry, *Crit. Rev. Anal. Chem.*, 47, 340–358, <https://doi.org/10.1080/10408347.2017.1298986>, 2017.
- Callahan, B. J., McMurdie, P. J., Rosen, M. J., Han, A. W., Johnson, A. J. A., and Holmes, S. P.: DADA2: High-resolution sample inference from Illumina amplicon data, *Nat. Methods*, 13, 581–583, <https://doi.org/10.1038/nmeth.3869>, 2016.
- Calogirou, A., Larsen, B. R., and Kotzias, D.: Gas-phase terpene oxidation products: a review, *Atmos. Environ.*, 33, 1423–1439, [https://doi.org/10.1016/S1352-2310\(98\)00277-5](https://doi.org/10.1016/S1352-2310(98)00277-5), 1999.
- Campbell, J. E., Whelan, M. E., Berry, J. A., Hilton, T. W., Zumkehr, A., Stinecipher, J., Lu, Y., Kornfeld, A., Seibt, U., Dawson, T. E., Montzka, S. A., Baker, I. T., Kulkarni, S., Wang, Y., Hernon, S. C., Zahniser, M. S., Commane, R., and Loik, M. E.: Plant uptake of atmospheric carbonyl sulfide in coast redwood forests, *J. Geophys. Res.: Biogeosci.*, 122, 3391–3404, <https://doi.org/10.1002/2016jg003703>, 2017.
- Cane, D. E. and Ikeda, H.: Exploration and mining of the bacterial terpenome, *Acc. Chem. Res.*, 45, 463–472, <https://doi.org/10.1021/ar200198d>, 2012.
- Cao, H. Y., Wang, P., Peng, M., Shao, X., Chen, X. L., and Li, C. Y.: Crystal structure of the dimethylsulfide monooxygenase DmoA from *Hyphomicrobium sulfonivorans*, *Acta Crystallogr., Sect. F: Struct. Biol. Commun.*, F74, 781–786, <https://doi.org/10.1107/S2053230X18015844>, 2018.
- Capaldo, K., Corbett, J. J., Kasibhatla, P., Fischbeck, P., and Pandis, S. N.: Effects of ship emissions on sulphur cycling and radiative climate forcing over the ocean, *Nature*, 400, 743–746, <https://doi.org/10.1038/23438>, 1999.
- Caporaso, J. G., Lauber, C. L., Walters, W. A., Berg-Lyons, D., Lozupone, C. A., Turnbaugh, P. J., Fierer, N., and Knight, R.: Global patterns of 16S rRNA diversity at a depth of millions of sequences per sample, *Proc. Natl. Acad. Sci. U. S. A.*, 108 Suppl 1, 4516–4522, <https://doi.org/10.1073/pnas.1000080107>, 2011.
- Caron, F. and Kramer, J. R.: Formation of volatile sulfides in freshwater environments, *Sci. Tot. Environ.*, 153, 177–194, [https://doi.org/10.1016/0048-9697\(94\)90197-X](https://doi.org/10.1016/0048-9697(94)90197-X), 1994.
- Carrion, O., Curson, A. R., Kumaresan, D., Fu, Y., Lang, A. S., Mercade, E., and Todd, J. D.: A novel pathway producing dimethylsulphide in bacteria is widespread in soil environments, *Nat. Commun.*, 6, 6579–6587, <https://doi.org/10.1038/ncomms7579>, 2015.

- Carrion, O., Pratscher, J., Curson, A. R. J., Williams, B. T., Rostant, W. G., Murrell, J. C., and Todd, J. D.: Methanethiol-dependent dimethylsulfide production in soil environments, *ISME J.*, 11, 2379–2390, <https://doi.org/10.1038/ismej.2017.105>, 2017.
- Carrion, O., Pratscher, J., Richa, K., Rostant, W. G., Farhan Ul Haque, M., Murrell, J. C., and Todd, J. D.: Methanethiol and dimethylsulfide cycling in stiffkey saltmarsh, *Front. Microbiol.*, 10, 1040–1055, <https://doi.org/10.3389/fmicb.2019.01040>, 2019.
- Casas-Ferreira, A. M., Nogal-Sanchez, M. D., Perez-Pavon, J. L., and Moreno-Cordero, B.: Non-separative mass spectrometry methods for non-invasive medical diagnostics based on volatile organic compounds: A review, *Anal. Chim. Acta*, 1045, 10–22, <https://doi.org/10.1016/j.aca.2018.07.005>, 2019.
- Caspi, R., Billington, R., Keseler, I. M., Kothari, A., Krummenacker, M., Midford, P. E., Ong, W. K., Paley, S., Subhraveti, P., and Karp, P. D.: The MetaCyc database of metabolic pathways and enzymes - a 2019 update, *Nucleic Acids Res.*, 48, D445–D453, <https://doi.org/10.1093/nar/gkz862>, 2020.
- Castro, M. S. and Dierberg, F. E.: Biogenic hydrogen sulfide emissions from selected Florida wetlands, *Water Air Soil Poll.*, 33, 1–13, <https://doi.org/10.1007/Bf00191372>, 1987.
- Castro, M. S. and Galloway, J. N.: A comparison of sulfur-free and ambient air enclosure techniques for measuring the exchange of reduced sulfur gases between soils and the atmosphere, *J. Geophys. Res.: Atmos.*, 96, 15 427–15 437, <https://doi.org/10.1029/91jd01399>, 1991.
- Catala, A., Levasseur-Garcia, C., Pagès Marielle, Schaff Jean-Luc, Till Ugo, Vitola Pasetto Leticia, Hausberger Martine, Cousillas Hugo, Violleau Frederic, and Grandgeorge Marine: Prediction and detection of human epileptic seizures based on SIFT-MS chemometric data, *Sci. Rep.*, 10, 18 365–18 371, <https://doi.org/10.1038/s41598-020-75478-8>, 2020.
- Challenger, F. and Liu, Y. C.: The elimination of methylthiol and dimethyl sulphide from methylthiol- and dimethyl-sulphonium compounds by moulds, *Recl. Trav. Chim. Pays-Bas*, 69, 334–342, <https://doi.org/10.1002/recl.19500690313>, 1950.
- Chandra, B. P., Sinha, V., Hakkim, H., and Sinha, B.: Storage stability studies and field application of low cost glass flasks for analyses of thirteen ambient VOCs using proton transfer reaction mass spectrometry, *Int. J. Mass Spectrom.*, 419, 11–19, <https://doi.org/10.1016/j.ijms.2017.05.008>, 2017.
- Charlson, R. J., Lovelock, J. E., Andreae, M. O., and Warren, S. G.: Oceanic phytoplankton, atmospheric sulfur, cloud albedo and climate, *Nature*, 326, 655–661, <https://doi.org/10.1038/326655a0>, 1987.
- Chasteen, T. G. and Bentley, R.: Volatile organic sulfur compounds of environmental interest: dimethyl sulfide and methanethiol. An introductory overview, *J. Chem. Ed.*, 81, 1524, <https://doi.org/10.1021/ed081p1524>, 2004.

- Cheng, X., Peterkin, E., and Burlingame, G. A.: A study on volatile organic sulfide causes of odors at Philadelphia's Northeast Water Pollution Control Plant, *Water Res.*, 39, 3781–3790, <https://doi.org/10.1016/j.watres.2005.07.009>, 2005.
- Chengelis, C. P. and Neal, R. A.: Studies of carbonyl sulfide toxicity: Metabolism by carbonic anhydrase, *Toxicol. Appl. Pharmacol.*, 55, 198–202, [https://doi.org/10.1016/0041-008X\(80\)90236-7](https://doi.org/10.1016/0041-008X(80)90236-7), 1980.
- Chuankun, X., Minghe, M., Leming, Z., and Keqin, Z.: Soil volatile fungistasis and volatile fungistatic compounds, *Soil Biol. Biochem.*, 36, 1997–2004, 2004.
- Clafin, M. S., Pagonis, D., Finewax, Z., Handschy, A. V., Day, D. A., Brown, W. L., Jayne, J. T., Worsnop, D. R., Jimenez, J. L., Ziemann, P. J., de Gouw, J., and Lerner, B. M.: An in situ gas chromatograph with automatic detector switching between PTR- and EI-TOF-MS: isomer-resolved measurements of indoor air, *Atmos. Meas. Tech.*, 14, 133–152, <https://doi.org/10.5194/amt-14-133-2021>, 2021.
- Conrad, R.: Compensation concentration as critical variable for regulating the flux of trace gases between soil and atmosphere, *Biogeochemistry*, 27, 155, <https://doi.org/10.1007/BF00000582>, 1994.
- Conrad, R.: Soil microbial processes involved in production and consumption of atmospheric trace gases, in: *Advances in microbial ecology*, edited by Jones, J. G., vol. 14, Plenum Press, New York London, 1995.
- Conrad, R.: Soil microorganisms as controllers of atmospheric trace gases (H₂, CO, CH₄, OCS, N₂O, and NO), *Microbiol. Rev.*, 60, 609–640, 1996.
- Conrad, R. and Meuser, K.: Soils contain more than one activity consuming carbonyl sulfide, *Atmos. Environ.*, 34, 3635–3639, [https://doi.org/10.1016/S1352-2310\(00\)00136-9](https://doi.org/10.1016/S1352-2310(00)00136-9), 2000.
- Cooper, W. J., Cooper, D. J., Saltzman, E. S., Demello, W. Z., Savoie, D. L., Zika, R. G., and Prospero, J. M.: Emissions of biogenic sulfur compounds from several wetland soils in Florida, *Atmos. Environ.*, 21, 1491–1495, [https://doi.org/10.1016/0004-6981\(87\)90311-8](https://doi.org/10.1016/0004-6981(87)90311-8), 1987.
- Cordovez, V., Schop, S., Hordijk, K., de Boulois, H. D., Raaijmakers, J. M., and Carriona, V. J.: Priming of plant growth promotion by volatiles of root-associated *Microbacterium* spp., *App. Environ. Microbiol.*, 84, 1–16, <https://doi.org/10.1128/AEM.01865-18>, 2018.
- Crespo, E., Hordijk, C. A., de Graaf, R. M., Samudrala, D., Cristescu, S. M., Harren, F. J. M., and van Dam, N. M.: On-line detection of root-induced volatiles in *Brassica nigra* plants infested with *Delia radicum* L. root fly larvae, *Phytochemistry*, pp. 68–77, <https://doi.org/10.1016/j.phytochem.2012.08.013>, 2012.
- Curson, A. R., Todd, J. D., Sullivan, M. J., and Johnston, A. W.: Catabolism of dimethylsulphonio-propionate: microorganisms, enzymes and genes, *Nat. Rev. Microbiol.*, 9, 849–859, <https://doi.org/10.1038/nrmicro2653>, 2011.

- Curson, A. R., Liu, J., Bermejo Martinez, A., Green, R. T., Chan, Y., Carrion, O., Williams, B. T., Zhang, S. H., Yang, G. P., Bulman Page, P. C., Zhang, X. H., and Todd, J. D.: Dimethylsulfoniopropionate biosynthesis in marine bacteria and identification of the key gene in this process, *Nat. Microbiol.*, 2, 17 009, <https://doi.org/10.1038/nmicrobiol.2017.9>, 2017.
- Dacey, J. W. H., King, G. M., and Wakeham, S. G.: Factors controlling emission of dimethylsulphide from salt marshes, *Nature*, 330, 643–645, <https://doi.org/10.1038/330643a0>, 1987.
- Dalby, F. R., Hansen, M. J., and Feilberg, A.: Application of proton-transfer-reaction mass spectrometry (PTR-MS) and ^{33}S isotope labeling for monitoring sulfur processes in livestock waste, *Environ. Sci. Technol.*, <https://doi.org/10.1021/acs.est.7b04570>, 2018.
- de Gouw, J. A., Goldan, P. D., Warneke, C., Kuster, W. C., Roberts, J. M., Marchewka, M., Bertman, S. B., Pszenny, A. A. P., and Keene, W. C.: Validation of proton transfer reaction-mass spectrometry (PTR-MS) measurements of gas-phase organic compounds in the atmosphere during the New England Air Quality Study (NEAQS) in 2002, *J. Geophys. Res.: Atmos.*, 108, <https://doi.org/10.1029/2003jd003863>, 2003.
- de Gouw, J. A., Warneke, C., Montzka, S. A., Holloway, J. S., Parrish, D. D., Fehsenfeld, F. C., Atlas, E. L., Weber, R. J., and Flocke, F. M.: Carbonyl sulfide as an inverse tracer for biogenic organic carbon in gas and aerosol phases, *Geophys. Res. Lett.*, 36, L05 804, 1–5, <https://doi.org/10.1029/2008GL036910>, 2009.
- de Mello, W. Z. and Hines, M. E.: Application of static and dynamic enclosures for determining dimethyl sulfide and carbonyl sulfide exchange in *Sphagnum* peatlands: Implications for the magnitude and direction of flux, *J. Geophys. Res.: Atmos.*, 99, 14 601–14 607, <https://doi.org/10.1029/94jd01025>, 1994.
- Deed, R. C., Pilkington, L. I., Herbst-Johnstone, M., Miskelly, G. M., Barker, D., and Fedrizzi, B.: A new analytical method to measure *S*-methyl-L-methionine in grape juice reveals the influence of yeast on dimethyl sulfide production during fermentation, *J. Sci. Food Agric.*, 99, 6944–6953, <https://doi.org/10.1002/jsfa.9983>, 2019.
- Degelmann, D. M., Kolb, S., Dumont, M., Murrell, J. C., and Drake, H. L.: *Enterobacteriaceae* facilitate the anaerobic degradation of glucose by a forest soil, *FEMS Microbiol. Ecol.*, 68, 312–319, <https://doi.org/10.1111/j.1574-6941.2009.00681.x>, 2009.
- Dekeirsschieter, J., Verheggen, F. J., Gohy, M., Hubrecht, F., Bourguignon, L., Lognay, G., and Haubruge, E.: Cadaveric volatile organic compounds released by decaying pig carcasses (*Sus domesticus* L.) in different biotopes, *Forensic Sci. Int.*, 189, 46–53, <https://doi.org/10.1016/j.forsciint.2009.03.034>, 2009.
- Delmas, R. and Servant, J.: Atmospheric balance of sulphur above an equatorial forest, *Tellus B: Chem. Phys. Meteorol.*, 35, 110–120, <https://doi.org/10.3402/tellusb.v35i2.14791>, 1983.

- Derendorp, L., Holzinger, R., Wishkerman, A., Keppler, F., and Röckmann, T.: Methyl chloride and C₂–C₅ hydrocarbon emissions from dry leaf litter and their dependence on temperature, *Atmos. Environ.*, 45, 3112–3119, <https://doi.org/10.1016/j.atmosenv.2011.03.016>, 2011.
- Derendorp, L., Wishkerman, A., Keppler, F., McRoberts, C., Holzinger, R., and Röckmann, T.: Methyl chloride emissions from halophyte leaf litter: Dependence on temperature and chloride content, *Chemosphere*, 87, 483–489, <https://doi.org/10.1016/j.chemosphere.2011.12.035>, 2012.
- Devai, I. and de Laune, R. D.: Formation of volatile sulfur compounds in salt marsh sediment as influenced by soil redox condition, *Org. Geochem.*, 23, 283–287, 1995.
- Dickschat, J. S.: Isoprenoids in three-dimensional space: the stereochemistry of terpene biosynthesis, *Nat. Prod. Rep.*, 28, 1917–1936, <https://doi.org/10.1039/C1NP00063B>, 2011.
- Ditengou, F. A., Müller, A., Rosenkranz, M., Felten, J., Lasok, H., van Doorn, M. M., Legué, V., Palme, K., Schnitzler, J.-P., and Polle, A.: Volatile signalling by sesquiterpenes from ectomycorrhizal fungi reprogrammes root architecture, *Nat. Commun.*, 6, 6279, <https://doi.org/10.1038/ncomms7279>, 2015.
- Dong, F., Fu, X., Watanabe, N., Su, X., and Yang, Z.: Recent advances in the emission and functions of plant vegetative volatiles, *Molecules*, 21, 124, 1–10, <https://doi.org/10.3390/molecules21020124>, 2016.
- Drotar, A., Burton, G. A., Tavernier, J. E., and Fall, R.: Widespread occurrence of bacterial thiol methyltransferases and the biogenic emission of methylated sulfur gases, *Appl. Env. Microbiol.*, 53, 1626–1631, 1987.
- Dubie, T. R., Talley, J. L., Payne, J. B., Wayadande, A. W., Dillwith, J., and Richards, C.: Filth fly activity associated with composted and noncomposted beef cadavers and laboratory studies on volatile organic compounds, *J. Med. Entomol.*, 54, 1299–1304, <https://doi.org/10.1093/jme/tjx073>, 2017.
- Dunne, E., Galbally, I. E., Cheng, M., Selleck, P., Molloy, S. B., and Lawson, S. J.: Comparison of VOC measurements made by PTR-MS, adsorbent tubes–GC-FID-MS and DNPH derivatization–HPLC during the Sydney Particle Study, 2012: a contribution to the assessment of uncertainty in routine atmospheric VOC measurements, *Atmos. Meas. Tech.*, 11, 141–159, <https://doi.org/10.5194/amt-11-141-2018>, 2018.
- Eerdeken, G., Ganzeveld, L., Vilà-Guerau de Arellano, J., Klüpfel, T., Sinha, V., Yassaa, N., Williams, J., Harder, H., Kubistin, D., Martinez, M., and Lelieveld, J.: Flux estimates of isoprene, methanol and acetone from airborne PTR-MS measurements over the tropical rainforest during the GABRIEL 2005 campaign, *Atmos. Chem. Phys.*, 9, 4207–4227, <https://doi.org/10.5194/acp-9-4207-2009>, 2009.

- Effmert, U., Kalderás, J., Warnke, R., and Piechulla, B.: Volatile mediated interactions between bacteria and fungi in the soil, *J. Chem. Ecol.*, 38, 665–703, <https://doi.org/10.1007/s10886-012-0135-5>, 2012.
- Eyice, O. and Schäfer, H.: Culture-dependent and culture-independent methods reveal diverse methylophilic communities in terrestrial environments, *Arch. Microbiol.*, 198, 17–26, <https://doi.org/10.1007/s00203-015-1160-x>, 2016.
- Eyice, O., Myronova, N., Pol, A., Carrion, O., Todd, J. D., Smith, T. J., Gurman, S. J., Cuthbertson, A., Mazard, S., Mennink-Kersten, M. A., Bugg, T. D., Andersson, K. K., Johnston, A. W., Op den Camp, H. J., and Schäfer, H.: Bacterial SBP56 identified as a Cu-dependent methanethiol oxidase widely distributed in the biosphere, *ISME J.*, 12, 145–160, <https://doi.org/10.1038/ismej.2017.148>, 2018.
- Faiola, C. L., Vanderschelden, G. S., Wen, M., Elloy, F. C., Cobos, D. R., Watts, R. J., Jobson, B. T., and Vanreken, T. M.: SOA formation potential of emissions from soil and leaf litter, *Environ. Sci. Technol.*, 48, 938–946, <https://doi.org/10.1021/es4040045>, 2014.
- Fall, R. and Benson, A. A.: Leaf methanol – the simplest natural product from plants, *Trends Plant Sci.*, 1, 296–301, [https://doi.org/10.1016/S1360-1385\(96\)88175-0](https://doi.org/10.1016/S1360-1385(96)88175-0), 1996.
- Fanin, N., Fromin, N., Buatois, B., and Hättenschwiler, S.: An experimental test of the hypothesis of non-homeostatic consumer stoichiometry in a plant litter-microbe system, *Ecol. Lett.*, 16, 764–772, <https://doi.org/10.1111/ele.12108>, 2013.
- Faubert, P., Tiiva, P., Rinnan, A., Michelsen, A., Holopainen, J. K., and Rinnan, R.: Doubled volatile organic compound emissions from subarctic tundra under simulated climate warming, *New phytol.*, 187, 199–208, <https://doi.org/10.1111/j.1469-8137.2010.03270.x>, 2010.
- Feilberg, A., Liu, D., Adamsen, A. P. S., Hansen, M. J., and Jonassen, K. E. N.: Odorant emissions from intensive pig production measured by online proton-transfer-reaction mass spectrometry, *Environ. Sci. Technol.*, 44, 5894–5900, <https://doi.org/10.1021/es100483s>, 2010.
- Fialho, M. B., Bessi, R., Inomoto, M. M., and Pascholati, S. F.: Nematicidal effect of volatile organic compounds (VOCs) on the plant-parasitic nematode *Meloidogyne javanica*, *Summa phytopathol.*, 38, 152–154, <https://doi.org/10.1590/S0100-54052012000200008>, 2012.
- Fiddes, S. L., Woodhouse, M. T., Nicholls, Z., Lane, T. P., and Schofield, R.: Cloud, precipitation and radiation responses to large perturbations in global dimethyl sulfide, *Atmos. Chem. Phys.*, 18, 10 177–10 198, <https://doi.org/10.5194/acp-18-10177-2018>, 2018.
- Finster, K., Kling, G. M., and Bak, F.: Formation of methylmercaptan and dimethylsulfide from methoxylated aromatic compounds in anoxic marine and fresh water sediments, *FEMS Microbiol. Lett.*, 74, 295–301, [https://doi.org/10.1016/0378-1097\(90\)90682-G](https://doi.org/10.1016/0378-1097(90)90682-G), 1990.

- Finster, K., Tanimoto, Y., and Bak, F.: Fermentation of methanethiol and dimethylsulfide by a newly isolated methanogenic bacterium, *Arch. Microbiol.*, 157, 425–430, <https://doi.org/10.1007/BF00249099>, 1992.
- Fritz, M. and Bachofen, R.: Volatile organic sulfur compounds in a meromictic alpine lake, *Acta Hydrochim. Hydrobiol.*, 28, 185–192, [https://doi.org/10.1002/1521-401X\(20004\)28:4<185::AID-AHEH185>3.0.CO;2-V](https://doi.org/10.1002/1521-401X(20004)28:4<185::AID-AHEH185>3.0.CO;2-V), 2000.
- Gahan, J. and Schmalenberger, A.: The role of bacteria and mycorrhiza in plant sulfur supply, *Front. Plant Sci.*, 5, 723, <https://doi.org/10.3389/fpls.2014.00723>, 2014.
- Gamliel, A. and Stapleton, J. J.: Characterization of antifungal volatile compounds evolved from solarized soil amended with cabbage residues, *Phytopathology*, 83, 899–905, 1993.
- Garcia-Alcega, S., Nasir, Z. A., Ferguson, R., Whitby, C., Dumbrell, A. J., Colbeck, I., Gomes, D., Tyrrel, S., and Coulon, F.: Fingerprinting outdoor air environment using microbial volatile organic compounds (MVOCs) – A review, *Trends Anal. Chem.*, 86, 75–83, <https://doi.org/10.1016/j.trac.2016.10.010>, 2017.
- Geng, C. and Mu, Y. J.: Carbonyl sulfide and dimethyl sulfide exchange between lawn and the atmosphere, *J. Geophys. Res.: Atmos.*, 109, D12 302, <https://doi.org/10.1029/2003JD004492>, 2004.
- Ghirardo, A., Xie, J., Zheng, X., Wang, Y., Grote, R., Block, K., Wildt, J., Mentel, T., Kiendler-Scharr, A., Hallquist, M., Butterbach-Bahl, K., and Schnitzler, J.-P.: Urban stress-induced biogenic VOC emissions and SOA-forming potentials in Beijing, *Atmos. Chem. Phys.*, 16, 2901–2920, <https://doi.org/10.5194/acp-16-2901-2016>, 2016.
- Gimeno, T. E., Ogee, J., Royles, J., Gibon, Y., West, J. B., Burlett, R., Jones, S. P., Sauze, J., Wohl, S., Bernard, C., Genty, B., and Wingate, L.: Bryophyte gas-exchange dynamics along varying hydration status reveal a significant carbonyl sulphide (COS) sink in the dark and COS source in the light, *New phytol.*, 215, 965–976, <https://doi.org/10.1111/nph.14584>, 2017.
- Ginzburg, B., Chalifa, I., Gun, J., Dor, I., Hadas, O., and Lev, O.: DMS formation by dimethylsulfoniopropionate route in freshwater, *Environ. Sci. Technol.*, 32, 2130–2136, 1998.
- Gisi, U.: *Bodenökologie: 51 Tabellen*, Bücher Biowissenschaften, Thieme, Stuttgart, 2nd edn., 1997.
- Gisler, A., Lan, J., Singh, K. D., Usemann, J., Frey, U., Zenobi, R., and Sinues, P.: Real-time breath analysis of exhaled compounds upon peppermint oil ingestion by secondary electrospray ionization-high resolution mass spectrometry: technical aspects, *J. Breath Res.*, 14, 046 001, <https://doi.org/10.1088/1752-7163/ab9f8b>, 2020.
- Goldan, P. D., Kuster, W. C., Albritton, D. L., and Fehsenfeld, F. C.: The measurement of natural sulfur emissions from soils and vegetation: three sites in the Eastern United States revisited, *J. Atmos. Chem.*, 5, 439–467, 1987.

- Goldan, P. D., Fall, R., Kuster, W. C., and Fehsenfeld, F. C.: Uptake of COS by growing vegetation: A major tropospheric sink, *J. Geophys. Res.: Atmos.*, 93, 14 186, <https://doi.org/10.1029/JD093iD11p14186>, 1988.
- Goldberg, AB, Maroulis, P. J., La Wilner, and Bandy, A. R.: Study of H₂S emissions from a salt water marsh, *Atmos. Environ.*, 15, 11–18, 1981.
- Gols, R.: Direct and indirect chemical defences against insects in a multitrophic framework, *Plant Cell Environ.*, 37, 1741–1752, <https://doi.org/10.1111/pce.12318>, 2014.
- González, J. M., Johnston, A. W. B., Vila-Costa, M., and Buchan, A.: Genetics and molecular features of bacterial dimethylsulfoniopropionate (DMSP) and dimethylsulfide (DMS) transformations, in: *Handbook of Hydrocarbon and Lipid Microbiology*, edited by Timmis, K. N., pp. 1201–1211, Springer Berlin Heidelberg, Berlin, Heidelberg, https://doi.org/10.1007/978-3-540-77587-4_83, 2010.
- Gray, C. M., Monson, R. K., and Fierer, N.: Emissions of volatile organic compounds during the decomposition of plant litter, *J. Geophys. Res.: Atmos.*, 115, <https://doi.org/10.1029/2010jg001291>, 2010.
- Gray, C. M., Monson, R. K., and Fierer, N.: Biotic and abiotic controls on biogenic volatile organic compound fluxes from a subalpine forest floor, *J. Geophys. Res.: Biogeosci.*, 119, 547–556, <https://doi.org/10.1002/2013JG002575>, 2014.
- Greenberg, J. P., Asensio, D., Turnipseed, A., Guenther, A. B., Karl, T., and Gochis, D.: Contribution of leaf and needle litter to whole ecosystem BVOC fluxes, *Atmos. Environ.*, 59, 302–311, <https://doi.org/10.1016/j.atmosenv.2012.04.038>, 2012.
- Greene, R. C. and Davis, N. B.: Biosynthesis of S-methylmethionine in the jack bean, *Biochim. Biophys. Act.*, 43, 360–362, [https://doi.org/10.1016/0006-3002\(60\)90457-1](https://doi.org/10.1016/0006-3002(60)90457-1), 1960.
- Grossmannova, H., Ciganek, M., and Krma, F.: High-molecular products analysis of VOC destruction in atmospheric pressure discharge, *J. Phys. Conf. Ser.*, 63, <https://doi.org/10.1088/1742-6596/63/1/012011>, 2007.
- Gu, C. H., Laverman, A. M., and Pallud, C. E.: Environmental controls on nitrogen and sulfur cycles in surficial aquatic sediments, *Front. Microbiol.*, 3, 11, <https://doi.org/10.3389/fmicb.2012.00045>, 2012.
- Guénon, R., Day, T. A., Velazco-Ayuso, S., and Gros, R.: Mixing of Aleppo pine and Holm oak litter increases biochemical diversity and alleviates N limitations of microbial activity, *Soil Biol. Biochem.*, 105, 216–226, <https://doi.org/10.1016/j.soilbio.2016.11.023>, 2017.
- Guhra, T., Stolze, K., Schweizer, S., and Totsche, K. U.: Earthworm mucus contributes to the formation of organo-mineral associations in soil, *Soil Biol. Biochem.*, 145, 107 785, <https://doi.org/10.1016/j.soilbio.2020.107785>, 2020.

- Haapanala, S., Hakola, H., Hellén, H., Vestenius, M., Levula, J., and Rinne, J.: Is forest management a significant source of monoterpenes into the boreal atmosphere?, *Biogeosciences*, 9, 1291–1300, <https://doi.org/10.5194/bg-9-1291-2012>, 2012.
- Hakola, H., Hellén, H., Hemmilä, M., Rinne, J., and Kulmala, M.: In situ measurements of volatile organic compounds in a boreal forest, *Atmos. Chem. Phys.*, 12, 11 665–11 678, <https://doi.org/10.5194/acp-12-11665-2012>, 2012.
- Hammerbacher, A., Coutinho, T. A., and Gershenzon, J.: Roles of plant volatiles in defence against microbial pathogens and microbial exploitation of volatiles, *Plant Cell Environ.*, 42, 2827–2843, <https://doi.org/10.1111/pce.13602>, 2019.
- Hammers, D. S., Donaghy, C. M., Heiss, S. L., Harris, L. M., Gordon, J. M., Stevens, J. W., Murray, L. P., Schwab, A. D., Hester, B. C., and Culpepper, M. A.: Identification and characterization of a DmoB flavin oxidoreductase from a putative two-component DMS C-monooxygenase, *ACS omega*, 5, 9830–9838, <https://doi.org/10.1021/acsomega.9b04489>, 2020.
- Harrell Jr. Frank E., Dupont, C., and many others: Hmisc: Harrell Miscellaneous, URL <https://CRAN.R-project.org/package=Hmisc>, 2020.
- Harshman, S. W., Mani, N., Geier, B. A., Kwak, J., Shepard, P., Fan, M., Sudberry, G. L., Mayes, R. S., Ott, D. K., Martin, J. A., and Grigsby, C. C.: Storage stability of exhaled breath on Tenax TA, *J. Breath Res.*, 10, 046 008, <https://doi.org/10.1088/1752-7155/10/4/046008>, 2016.
- Hartungen, E., Jürschik, S., Jordan, A., Edtbauer, A., Feil, S., Hanel, G., Seehauser, H., Haidacher, S., Schottkowsky, R., Märk, L., Jaksch, S., Agarwal, B., Becker, K., Mayhew, C. A., Sulzer, P., and Märk, T. D.: Proton transfer reaction-mass spectrometry: fundamentals, recent advances and applications, *Eur. Phys. J. Appl. Phys.*, 61, 24 303, <https://doi.org/10.1051/epjap/2012120401>, 2013.
- Hatton, A. D.: Influence of photochemistry on the marine biogeochemical cycle of dimethylsulphide in the northern North Sea, *Deep-Sea Res. II*, 49, 3039–3052, 2002.
- Hattula, T. and Granroth, B.: Formation of dimethyl sulphide from S-methylmethionine in onion seedlings (*Allium cepa*), *J. Sci. Food Agric.*, 25, 1517–1521, 1974.
- Hayward, S., Muncey, R., James, A., Halsall, C., and Hewitt, C.: Monoterpene emissions from soil in a Sitka spruce forest, *Atmos. Environ.*, 35, 4081–4087, [https://doi.org/10.1016/S1352-2310\(01\)00213-8](https://doi.org/10.1016/S1352-2310(01)00213-8), 2001.
- He, R., Yao, X. Z., Chen, M., Ma, R. C., Li, H. J., Wang, C., and Ding, S. H.: Conversion of sulfur compounds and microbial community in anaerobic treatment of fish and pork waste, *Waste Manage.*, 76, 383–393, <https://doi.org/10.1016/j.wasman.2018.04.006>, 2018.
- Heinen, W. and Lauwers, A. M.: Organic sulfur compounds resulting from the interaction of iron sulfide, hydrogen sulfide and carbon dioxide in an anaerobic aqueous environment, *Origins Life Evol. Biospheres*, 26, 131–150, <https://doi.org/10.1007/bf01809852>, 1996.

- Helfrich, E. J. N., Lin, G.-M., Voigt, C. A., and Clardy, J.: Bacterial terpene biosynthesis: challenges and opportunities for pathway engineering, *Beilstein J. Org. Chem.*, 15, 2889–2906, <https://doi.org/10.3762/bjoc.15.283>, 2019.
- Hellén, H., Schallhart, S., Praplan, A. P., Petäjä, T., and Hakola, H.: Using in situ GC-MS for analysis of C2-C7 volatile organic acids in ambient air of a boreal forest site, *Atmos. Meas. Tech.*, 10, 281–289, <https://doi.org/10.5194/amt-10-281-2017>, 2017.
- Henatsch, J. and Jüttner, F.: Capillary gas chromatographic analysis of low-boiling organic sulphur compounds in anoxic lake-water by cryoadsorption, *J. Chromatogr.*, 445, 97–105, 1988.
- Henderson, B., Ruszkiewicz, D. M., Wilkinson, M., Beauchamp, J. D., Cristescu, S. M., Fowler, S. J., Salman, D., Di Francesco, F., Koppen, G., Langejürgen, J., Holz, O., Hadjithekli, A., Moreno, S., Pedrotti, M., Sinues, P., Slingers, G., Wilde, M., Lomonaco, T., Zanella, D., Zenobi, R., Focant, J.-F., Grassin-Delyle, S., Franchina, F. A., Malásková, M., Stefanuto, P.-H., Pugliese, G., Mayhew, C., and Thomas, C. L. P.: A benchmarking protocol for breath analysis: the peppermint experiment, *J. Breath Res.*, 14, 046 008, <https://doi.org/10.1088/1752-7163/aba130>, 2020.
- Hera, D., Langford, V., McEwan, M., McKellar, T., and Milligan, D.: Negative reagent ions for real time detection using SIFT-MS, *Environments*, 4, 16, <https://doi.org/10.3390/environments4010016>, 2017.
- Hines, M. E.: Emissions of biogenic sulfur gases from Alaskan tundra, *J. Geophys. Res.: Atmos.*, 97, 16 703–16 707, 1992.
- Hinshaw, J. V.: A compendium of GC detection, past and present, *LCGC North Am.*, 36, 178–182, URL <https://www.chromatographyonline.com/view/compendium-gc-detection-past-and-present-0>, 2018.
- Höfgen, R., Kreft, O., Willmitzer, L., and Hesse, H.: Manipulation of thiol contents in plants, *Amino Acids*, 20, 291–299, <https://doi.org/10.1007/s007260170045>, 2001.
- Hopkins, F. E., Bell, T. G., Yang, M., Suggett, D. J., and Steinke, M.: Air exposure of coral is a significant source of dimethylsulfide (DMS) to the atmosphere, *Sci. Rep.*, 6, 36 031, 2016.
- Hu, H., Mylon, S. E., and Benoit, G.: Volatile organic sulfur compounds in a stratified lake, *Chemosphere*, 67, 911–919, <https://doi.org/10.1016/j.chemosphere.2006.11.012>, 2007.
- Huang, X., Lai, J., Liu, Y., Zheng, L., Fang, X., Song, W., and Yi, Z.: Biogenic volatile organic compound emissions from *Pinus massoniana* and *Schima superba* seedlings: Their responses to foliar and soil application of nitrogen, *Sci. Total Environ.*, 705, 135 761, <https://doi.org/10.1016/j.scitotenv.2019.135761>, 2020.
- Ihrmark, K., Bödeker, I. T. M., Cruz-Martinez, K., Friberg, H., Kubartova, A., Schenck, J., Strid, Y., Stenlid, J., Brandström-Durling, M., Clemmensen, K. E., and Lindahl, B. D.: New primers to amplify

- the fungal ITS2 region—evaluation by 454-sequencing of artificial and natural communities, *FEMS Microbiol Ecol*, 82, 666–677, <https://doi.org/10.1111/j.1574-6941.2012.01437.x>, 2012.
- Insam, H. and Seewald, M. S. A.: Volatile organic compounds (VOCs) in soils, *Biol. Fertil. Soils*, 46, 199–213, <https://doi.org/10.1007/s00374-010-0442-3>, 2010.
- Isidorov, V. and Jdanova, M.: Volatile organic compounds from leaves litter, *Chemosphere*, 48, 975–979, 2002.
- Isidorov, V., Vinogorova, V., and Rafałowski, K.: Gas chromatographic determination of extractable compounds composition and emission rate of volatile terpenes from larch needle litter, *J. Atmos. Chem.*, 50, 263–278, <https://doi.org/10.1007/s10874-005-5078-6>, 2005.
- Isidorov, V., Tyszkiewicz, Z., and Pirożnikow, E.: Fungal succession in relation to volatile organic compounds emissions from Scots pine and Norway spruce leaf litter-decomposing fungi, *Atmos. Environ.*, 131, 301–306, <https://doi.org/10.1016/j.atmosenv.2016.02.015>, 2016.
- Isidorov, V. A., Vinogorova, V. T., and Rafałowski, K.: HS-SPME analysis of volatile organic compounds of coniferous needle litter, *Atmos. Environ.*, 37, 4645–4650, <https://doi.org/10.1016/j.atmosenv.2003.07.005>, 2003.
- Isidorov, V. A., Smolewska, M., Purzyńska-Pugacewicz, A., and Tyszkiewicz, Z.: Chemical composition of volatile and extractive compounds of pine and spruce leaf litter in the initial stages of decomposition, *Biogeosciences*, 7, 2785–2794, <https://doi.org/10.5194/bg-7-2785-2010>, 2010.
- Jaeschke, W., Dippell, J., Sitals, R., and Haunold, W.: Measurements of reduced sulphur compounds in an industrialized tropical region – Cubatão (Brazil), *Int. J. Environ. Anal. Chem.*, 54, 315–337, <https://doi.org/10.1080/03067319408034097>, 1994.
- Jansen, R. M., Wildt, J., Kappers, I. F., Bouwmeester, H. J., Hofstee, J. W., and van Henten, E. J.: Detection of diseased plants by analysis of volatile organic compound emission, *Annu. Rev. Phytopathol.*, 49, 157–174, <https://doi.org/10.1146/annurev-phyto-072910-095227>, 2011.
- Janson, R. W.: Monoterpene emissions from Scots Pine and Norwegian Spruce, *J. Geophys. Res.*, 98, 2839–2850, <https://doi.org/10.1029/92JD02394>, 1993.
- Jardine, K., Yanez-Serrano, A. M., Williams, J., Kunert, N., Jardine, A., Taylor, T., Abrell, L., Artaxo, P., Guenther, A., Hewitt, C. N., House, E., Florentino, A. P., Manzi, A., Higuchi, N., Kesselmeier, J., Behrendt, T., Veres, P. R., Derstroff, B., Fuentes, J. D., Martin, S. T., and Andreae, M. O.: Dimethyl sulfide in the Amazon rain forest, *Global Biogeochem. Cycles*, 29, 19–32, <https://doi.org/10.1002/2014gb004969>, 2015.
- Jensen, N. R., Hjorth, J., Lohse, C., Skov, H., and Restelli, G.: Products and mechanism of the reaction between NO₃ and dimethylsulphide in air, *Atmos. Environ.*, 25A, 1897–1904, [https://doi.org/10.1016/0960-1686\(91\)90272-9](https://doi.org/10.1016/0960-1686(91)90272-9), 1991.

- Jing, W. W., Li, N., Li, X. F., Li, D. Q., and Wang, L. L.: Exchange fluxes of VOSCs between rice paddy fields and the atmosphere in the oasis of arid area in Xinjiang, China, *J. Atmos. Chem.*, 75, 17–32, <https://doi.org/10.1007/s10874-017-9360-1>, 2017.
- Jones, G. L. and Happold, F. C.: The occurrence of polythionates as intermediates in the metabolism of thiosulphate by the *Thiobacilli*, *J. Gen. Microbiol.*, 26, 361–366, 1961.
- Jones, R. M., Goordial, J. M., and Orcutt, B. N.: Low energy subsurface environments as extraterrestrial analogs, *Front. Microbiol.*, 9, 1605, <https://doi.org/10.3389/fmicb.2018.01605>, 2018.
- Jordan, A., Haidacher, S., Hanel, G., Hartungen, E., Herbig, J., Märk, L., Schotchkowsky, R., Seehauser, H., Sulzer, P., and Märk, T. D.: An online ultra-high sensitivity proton-transfer-reaction mass spectrometer combined with switchable reagent ion capability (PTR+SRI–MS), *Int. J. Mass Spectrom.*, 286, 32–38, <https://doi.org/10.1016/j.ijms.2009.06.006>, 2009a.
- Jordan, A., Haidacher, S., Hanel, G., Hartungen, E., Märk, L., Seehauser, H., Schotchkowsky, R., Sulzer, P., and Märk, T. D.: A high resolution and high sensitivity proton-transfer-reaction time-of-flight mass spectrometer (PTR-TOF-MS), *Int. J. Mass Spectrom.*, 286, 122–128, <https://doi.org/10.1016/j.ijms.2009.07.005>, 2009b.
- Junker, R. R. and Tholl, D.: Volatile organic compound mediated interactions at the plant–microbe interface, *J. Chem. Ecol.*, 39, 810–825, <https://doi.org/10.1007/s10886-013-0325-9>, 2013.
- Kadota, H. and Ishida, Y.: Production of volatile sulfur compounds by microorganisms, *Annu. Rev. Microbiol.*, 26, 127–138, <https://doi.org/10.1146/annurev.mi.26.100172.001015>, 1972.
- Kaikiti, K., Stylianou, M., and Agapiou, A.: Use of biochar for the sorption of volatile organic compounds (VOCs) emitted from cattle manure, *Environ. Sci. Pollut. Res.*, <https://doi.org/10.1007/s11356-020-09545-y>, 2020.
- Kamezaki, K., Hattori, S., Ogawa, T., Toyoda, S., Kato, H., Katayama, Y., and Yoshida, N.: Sulfur isotopic fractionation of carbonyl sulfide during degradation by soil bacteria, *Environ. Sci. Technol.*, 50, 3537–3544, <https://doi.org/10.1021/acs.est.5b05325>, 2016.
- Kanda, K.-i., Tsuruta, H., and Minami, K.: Emissions of biogenic sulfur gases from maize and wheat fields, *Soil Sci. Plant Nutr.*, 41, 1–8, <https://doi.org/10.1080/00380768.1995.10419553>, 1995.
- Karl, T., Hansel, A., Cappellin, L., Kaser, L., Herdinger-Blatt, I., and Jud, W.: Selective measurements of isoprene and 2-methyl-3-buten-2-ol based on NO⁺ ionization mass spectrometry, *Atmos. Chem. Phys.*, 12, 11 877–11 884, <https://doi.org/10.5194/acp-12-11877-2012>, 2012.
- Kassambara, A. and Mundt, F.: factoextra: extract and visualize the results of multivariate data analyses, URL <https://CRAN.R-project.org/package=factoextra>, 2020.

- Kelly, D. P. and Baker, S. C.: The organosulphur cycle: aerobic and anaerobic processes leading to turnover of C1-sulphur compounds, *FEMS Microbiol. Rev.*, 7, 241–246, <https://doi.org/10.1111/j.1574-6968.1990.tb04919.x>, 1990.
- Kertesz, M. A.: Riding the sulfur cycle - metabolism of sulfonates and sulfate esters in Gram-negative bacteria, *FEMS Microbiol. Rev.*, 24, 135–175, [https://doi.org/10.1016/S0168-6445\(99\)00033-9](https://doi.org/10.1016/S0168-6445(99)00033-9), 2000.
- Kesselmeier, J. and Hubert, A.: Exchange of reduced volatile sulfur compounds between leaf litter and the atmosphere, *Atmos. Environ.*, 36, 4679–4686, [https://doi.org/10.1016/S1352-2310\(02\)00413-2](https://doi.org/10.1016/S1352-2310(02)00413-2), 2002.
- Kesselmeier, J. and Staudt, M.: Biogenic volatile organic compounds (VOC): An overview on emission, physiology and ecology, *J. Atmos. Chem.*, 22, 23–88, <https://doi.org/10.1023/A:1006127516791>, 1999.
- Kesselmeier, J., Meixner, F. X., Hofmann, U., Ajavon, A. L., and Leimbach, S.: Reduced sulfur compound exchange between the atmosphere and tropical tree species in Southern Cameroon, *Biogeochemistry*, 23, 23–45, <https://doi.org/10.1007/BF00002921>, 1993.
- Khan, M. A., López-Muñoz, M. M., Kaspar, C. W., and Hung, K. F.: Activities of methionine-gamma-lyase in the acidophilic archaeon *Ferroplasma acidarmanus* strain fer1, *Res. Rep. Biol.*, <https://doi.org/10.2147/rrb.S41345>, 2013.
- Khan, M. A. H., Gillespie, S. M. P., Razis, B., Xiao, P., Davies-Coleman, M. T., Percival, C. J., Derwent, R. G., Dyke, J. M., Ghosh, M. V., Lee, E. P. F., and Shallcross, D. E.: A modelling study of the atmospheric chemistry of DMS using the global model, STOCHEM-CRI, *Atmos. Environ.*, 127, 69–79, <https://doi.org/10.1016/j.atmosenv.2015.12.028>, 2016.
- Kiene, R. P.: Dimethyl sulfide metabolism in salt marsh sediments, *FEMS Microbiol. Ecol.*, 4, 71–78, <https://doi.org/10.1111/j.1574-6968.1988.tb02649.x>, 1988.
- Kiene, R. P.: Production of methanethiol from dimethylsulfoniopropionate in marine surface waters, *Marine Chem.*, 54, 69–83, [https://doi.org/10.1016/0304-4203\(96\)00006-0](https://doi.org/10.1016/0304-4203(96)00006-0), 1996.
- Kiene, R. P. and Capone, D. G.: Microbial transformations of methylated sulfur compounds in anoxic salt marsh sediments, *Microb. Ecol.*, 15, 275–291, <https://doi.org/10.1007/bf02012642>, 1988.
- Kiene, R. P. and Visscher, P. T.: Production and fate of methylated sulfur compounds from methionine and dimethylsulfoniopropionate in anoxic salt marsh sediments, *Appl. Environ. Microbiol.*, 53, 2426–2434, 1987.
- Kiene, R. P., Oremland, R. S., Catena, A., Miller, L. G., and Capone, D. G.: Metabolism of reduced methylated sulfur compounds in anaerobic sediments and by a pure culture of an estuarine methanogen, *Appl. Environ. Microbiol.*, 52, 1037–1045, 1986.

- Kim, H., Lee, H., Choi, E., Choi, I., Shin, T., Im, H., and Ahn, S.: Characterization of odor emission from alternating aerobic and anoxic activated sludge systems using real-time total reduced sulfur analyzer, *Chemosphere*, 117, 394–401, <https://doi.org/10.1016/j.chemosphere.2014.08.008>, 2014.
- Kim, K.-H. and Park, S.-Y.: A comparative analysis of malodor samples between direct (olfactometry) and indirect (instrumental) methods, *Atmos. Environ.*, 42, 5061–5070, <https://doi.org/10.1016/j.atmosenv.2008.02.017>, 2008.
- Kirkwood, M., Todd, J. D., Rypien, K. L., and Johnston, A. W. B.: The opportunistic coral pathogen *Aspergillus sydowii* contains dddP and makes dimethyl sulfide from dimethylsulfoniopropionate, *ISME J*, 4, 147–150, <https://doi.org/10.1038/ismej.2009.102>, 2010.
- Klose, F. and Geldsetzer, F.: Roempp Online: VOC, Thieme Gruppe, URL <https://roempp.thieme.de/lexicon/RD-22-01040>, 2013.
- Kloster, S., Feichter, J., Maier-Reimer, E., Six, K. D., Stier, P., and Wetzal, P.: DMS cycle in the marine ocean-atmosphere system – a global model study, *Biogeosciences*, 3, 29–51, <https://doi.org/10.5194/bg-3-29-2006>, 2006.
- Koch, T. and Dahl, C.: A novel bacterial sulfur oxidation pathway provides a new link between the cycles of organic and inorganic sulfur compounds, *ISME J.*, 12, 2479–2491, <https://doi.org/10.1038/s41396-018-0209-7>, 2018.
- Krechmer, J., Lopez-Hilfiker, F., Koss, A., Hutterli, M., Stoermer, C., Deming, B., Kimmel, J., Warneke, C., Holzinger, R., Jayne, J., Worsnop, D., Fuhrer, K., Gonin, M., and de Gouw, J.: Evaluation of a new reagent-ion source and focusing ion-molecule reactor for use in proton-transfer-reaction mass spectrometry, *Anal. Chem.*, 90, 12 011–12 018, <https://doi.org/10.1021/acs.analchem.8b02641>, 2018.
- Krechmer, J., Canagaratna, M. R., Onasch, T., Shilling, J. E., Thornton, J. A., and Worsnop, D.: Vocus proton transfer reaction time-of-flight mass spectrometer (Vocus PTR-MS), ARM Aerial Instrumentation Workshop White Paper Call, URL https://www.arm.gov/capabilities/observatories/aaf/workshop-march2020/Krechmer_Vocus_PTR-MS.pdf, 2020.
- Krishna, M. P. and Mohan, M.: Litter decomposition in forest ecosystems: a review, *Energ. Ecol. Environ.*, 2, 236–249, <https://doi.org/10.1007/s40974-017-0064-9>, 2017.
- Kröber, E. and Schäfer, H.: Identification of proteins and genes expressed by *Methylophaga thiooxydans* during growth on dimethylsulfide and their presence in other members of the genus, *Front. Microbiol.*, 10, 1132, <https://doi.org/10.3389/fmicb.2019.01132>, 2019.
- Kulmala, L., Aaltonen, H., Berninger, F., Kieloaho, A.-J., Levula, J., Bäck, J., Hari, P., Kolari, P., Korhonen, J. F. J., Kulmala, M., Nikinmaa, E., Pihlatie, M., Vesala, T., and Pumpanen, J.: Changes in

- biogeochemistry and carbon fluxes in a boreal forest after the clear-cutting and partial burning of slash, *Agric. For. Meteorol.*, 188, 33–44, <https://doi.org/10.1016/j.agrformet.2013.12.003>, 2014.
- Kwon, H. K., Woo, S. H., and Park, J. M.: Thiocyanate degradation by *Acremonium strictum* and inhibition by secondary toxicants, *Biotechnol. Lett.*, 24, 1347–1351, <https://doi.org/10.1023/a:1019825404825>, 2002.
- La Nasa, J., Nardella, F., Modugno, F., Colombini, M. P., Ribechini, E., and Degano, I.: SIFT-ing archaeological artifacts: Selected ion flow tube-mass spectrometry as a new tool in archaeometry, *Talanta*, 207, 120–123, <https://doi.org/10.1016/j.talanta.2019.120323>, 2020.
- Labarre, C. and Bory, J.: Gas liberated by *Clostridium oedematiens* cultivated on sodium thioglycolate medium in a vacuum, *Ann. Inst. Pasteur*, 117, 222–225, 1969.
- Lacko, M., Piel, F., Mauracher, A., and Španěl, P.: Chemical ionization of glyoxal and formaldehyde with H_3O^+ ions using SIFT-MS under variable system humidity, *Phys. Chem. Chem. Phys.*, 22, 10 170–10 178, <https://doi.org/10.1039/D0CP00297F>, 2020.
- Lagg, A., Taucher, J., Hansel, A., and Lindinger, W.: Applications of proton transfer reactions to gas analysis, *Int. J. Mass Spectrom. Ion Proc.*, 134, 55–66, 1994.
- Lamb, B., Westberg, H., Allwine, G., Bamesberger, L., and Guenther, A.: Measurement of biogenic sulfur emissions from soils and vegetation: Application of dynamic enclosure methods with Natusch filter and GC/FPD analysis, *J. Atmos. Chem.*, 5, 469–491, 1987.
- Lamers, L. P. M., Govers, L. L., Janssen, I. C. J. M., Geurts, J. J. M., van der Welle, M. E. W., van Katwijk, M. M., van der Heide, T., Roelofs, J. G. M., and Smolders, A. J. P.: Sulfide as a soil phytotoxin – a review, *Front. Plant Sci.*, 4, 268, <https://doi.org/10.3389/fpls.2013.00268>, 2013.
- Lana, A., Bell, T. G., Simó, R., Vallina, S. M., Ballabrera-Poy, J., Kettle, A. J., Dachs, J., Bopp, L., Saltzman, E. S., Stefels, J., Johnson, J. E., and Liss, P. S.: An updated climatology of surface dimethylsulfide concentrations and emission fluxes in the global ocean, *Global Biogeochem. Cycles*, 25, GB1004, 1–17, <https://doi.org/10.1029/2010gb003850>, 2011.
- Langford, V. S., Du Bruyn, C., and Padayachee, D.: An evaluation of selected ion flow tube mass spectrometry for rapid instrumental determination of paper type, origin and sensory attributes, *Packag. Technol. Sci.*, 2555, 1–16, <https://doi.org/10.1002/pts.2555>, 2020.
- Le Mer, J. and Roger, P.: Production, oxidation, emission and consumption of methane by soils: a review, *Eur. J. Soil Biol.*, 37, 25–50, [https://doi.org/10.1016/S1164-5563\(01\)01067-6](https://doi.org/10.1016/S1164-5563(01)01067-6), 2001.
- Lee, J.-H., Kim, T. G., and Cho, K.-S.: Isolation and characterization of a facultative methanotroph degrading malodor-causing volatile sulfur compounds, *J. Haz. Mat.*, 235–236, 224–229, <https://doi.org/10.1016/j.jhazmat.2012.07.047>, 2012.

- Leff, J. W. and Fierer, N.: Volatile organic compound (VOC) emissions from soil and litter samples, *Soil Biol. Biochem.*, 40, 1629–1636, <https://doi.org/10.1016/j.soilbio.2008.01.018>, 2008.
- Lehmann, S. and Conrad, R.: Characteristics of turnover of carbonyl sulfide in four different soils, *Journal of Atmospheric Chemistry*, 23, 193–207, <https://doi.org/10.1007/BF00048260>, 1996.
- Lehnert, A.-S., Behrendt, T., Ruecker, A., Pohnert, G., and Trumbore, S. E.: SIFT-MS optimization for atmospheric trace gas measurements at varying humidity, *Atmos. Meas. Tech.*, 13, 3507–3520, <https://doi.org/10.5194/amt-13-3507-2020>, 2020a.
- Lehnert, A.-S., Perreca, E., Gershenzon, J., Pohnert, G., and Trumbore, S. E.: Simultaneous real-time measurement of isoprene and 2-methyl-3-buten-2-ol emissions from trees using SIFT-MS, *Front. Plant Sci.*, 11, 1867, <https://doi.org/10.3389/fpls.2020.578204>, 2020b.
- Leng, G., Jin, C.-F., Bell, T. G., Ussher, S. J., Worsfold, P. J., and Li, W.-Y.: Automated, high frequency, on-line dimethyl sulfide measurements in natural waters using a novel "microslug" gas-liquid segmented flow method with chemiluminescence detection, *Talanta*, pp. 121 595, 1–8, <https://doi.org/10.1016/j.talanta.2020.121595>, 2021.
- Lewis, A. C., Hopkins, J. R., Carslaw, D. C., Hamilton, J. F., Nelson, B. S., Stewart, G., Dernie, J., Passant, N., and Murrells, T.: An increasing role for solvent emissions and implications for future measurements of volatile organic compounds, *Philos. Trans. A: Math. Phys. Eng. Sci.*, 378, 20190 328, <https://doi.org/10.1098/rsta.2019.0328>, 2020.
- Li, G., Cheng, Y., Kuhn, U., Xu, R., Yang, Y., Meusel, H., Wang, Z., Ma, N., Wu, Y., Li, M., Williams, J., Hoffmann, T., Ammann, M., Pöschl, U., Shao, M., and Su, H.: Physicochemical uptake and release of volatile organic compounds by soil in coated-wall flow tube experiments with ambient air, *Atmos. Chem. Phys.*, 19, 2209–2232, <https://doi.org/10.5194/acp-19-2209-2019>, 2019a.
- Li, L., Guenther, A. B., Xie, S., Gu, D., Seco, R., Nagalingam, S., and Yan, D.: Evaluation of semi-static enclosure technique for rapid surveys of biogenic volatile organic compounds (BVOCs) emission measurements, *Atmos. Environ.*, 212, 1–5, <https://doi.org/10.1016/j.atmosenv.2019.05.029>, 2019b.
- Liang, H., He, Z., Wang, X., Song, G., Chen, H., Lin, X., Ji, C., and Li, S.: Effects of salt concentration on microbial diversity and volatile compounds during suancai fermentation, *Food microbiology*, 91, 103 537, <https://doi.org/10.1016/j.fm.2020.103537>, 2020a.
- Liang, Q., Bao, X., Sun, Q., Zhang, Q., Zou, X., Huang, C., Shen, C., and Chu, Y.: Imaging VOC distribution in cities and tracing VOC emission sources with a novel mobile proton transfer reaction mass spectrometer, *Environ. Pollut.*, 265, 114 628, <https://doi.org/10.1016/j.envpol.2020.114628>, 2020b.
- Lidbury, I., Krober, E., Zhang, Z., Zhu, Y., Murrell, J. C., Chen, Y., and Schafer, H.: A mechanism for bacterial transformation of dimethylsulfide to dimethylsulfoxide: a missing link in the marine

- organic sulfur cycle, *Environ. Microbiol.*, 18, 2754–2766, <https://doi.org/10.1111/1462-2920.13354>, 2016.
- Lin, G.-P., Vadhwana, B., Belluomo, I., Boshier, P. R., Španěl, P., and Hanna, G. B.: Cross Platform Analysis of Volatile Organic Compounds Using Selected Ion Flow Tube and Proton-Transfer-Reaction Mass Spectrometry, *Journal of the American Society for Mass Spectrometry*, <https://doi.org/10.1021/jasms.1c00027>, 2021.
- Lin, Y. S., Heuer, V. B., Ferdelman, T. G., and Hinrichs, K. U.: Microbial conversion of inorganic carbon to dimethyl sulfide in anoxic lake sediment (Plußsee, Germany), *Biogeosciences*, 7, 2433–2444, <https://doi.org/10.5194/bg-7-2433-2010>, 2010.
- Lindinger, W., Hansel, A., and Jordan, A.: On-line monitoring of volatile organic compounds at pptv levels by means of Proton-Transfer-Reaction Mass Spectrometry (PTR-MS) Medical applications, food control and environmental research, *Int. J. Mass Spectrom. Ion Proc.*, 173, 191–241, 1998.
- Liu, H., Shi, C., Wu, T., Jia, Q., Zhao, J., and Wang, X.: Isolation and characterization of methanethiol-producing bacteria from agricultural soils, *Pedosphere*, 27, 1083–1091, [https://doi.org/10.1016/s1002-0160\(17\)60411-9](https://doi.org/10.1016/s1002-0160(17)60411-9), 2017.
- Liu, N., Pan, J., Miao, S., and Qin, L.: Microbial community in Chinese traditional fermented acid rice soup (rice-acid) and its correlations with key organic acids and volatile compounds, *Food research international (Ottawa, Ont.)*, 137, 109 672, <https://doi.org/10.1016/j.foodres.2020.109672>, 2020.
- Lladó, S. and Baldrian, P.: Community-level physiological profiling analyses show potential to identify the copiotrophic bacteria present in soil environments, *PLoS ONE*, 12, e0171 638, <https://doi.org/10.1371/journal.pone.0171638>, 2017.
- Lomans, B. P., Smolders, A., Intven, L. M., Pol, A., Op den Camp, H. J. M., and van der Drift, C.: Formation of dimethyl sulfide and methanethiol in anoxic freshwater sediments, *Appl. Environ. Microbiol.*, 63, 4741–4747, 1997.
- Lomans, B. P., Maas, R., Luderer, R., Op den Camp, H. J., Pol, A., van der Drift, C., and Vogels, G. D.: Isolation and characterization of *Methanomethylovorans hollandica* gen. nov., sp. nov., isolated from freshwater sediment, a methylotrophic methanogen able to grow on dimethyl sulfide and methanethiol, *Appl. Environ. Microbiol.*, 65, 3641–3650, 1999a.
- Lomans, B. P., Op den Camp, H. J., Pol, A., van der Drift, C., and Vogels, G. D.: Role of methanogens and other bacteria in degradation of dimethyl sulfide and methanethiol in anoxic freshwater sediments, *Appl. Environ. Microbiol.*, 65, 2116–2121, 1999b.
- Lomans, B. P., Op den Camp, H. J. M., Pol, A., and Vogels, G. D.: Anaerobic versus aerobic degradation of dimethyl sulfide and methanethiol in anoxic freshwater sediments, *Appl. Environ. Microbiol.*, 65, 438–443, 1999c.

- Lomans, B. P., Leijdekkers, P., and Wesselink, J.-J.: Obligat sulfide-dependent degradation of methoxylated aromatic compounds and formation of methanethiol and dimethyl sulfide by a freshwater sediment isolate, *Parasporobacterium paucivorans* gen. nov., sp. nov, Appl. Env. Microbiol., 67, 4017, 2001a.
- Lomans, B. P., Luderer, R., Steenbakkers, P., Pol, A., van der Drift, C., Vogels, G. D., and Op den Camp, H. J.: Microbial populations involved in cycling of dimethyl sulfide and methanethiol in freshwater sediments, Appl. Environ. Microbiol., 67, 1044–1051, <https://doi.org/10.1128/AEM.67.3.1044-1051.2001>, 2001b.
- Lomans, B. P., van der Drift, C., Pol, A., and Op den Camp, H. J. M.: Microbial cycling of volatile organic sulfur compounds, Cell. Mol. Life Sci., 59, 575–588, <https://doi.org/10.1007/s00018-002-8450-6>, 2002.
- Losher, A. J. and Kelts, K. R.: Organic sulphur fixation in freshwater lake sediments and the implication for US ratios, Terra Nova, 1, 253–261, <https://doi.org/10.1111/j.1365-3121.1989.tb00366.x>, 1989.
- Loubet, B., Buysse, P., Gonzaga-Gomez, L., Lafouge, F., Ciuraru, R., Decuq, C., Kammer, J., Bsaiibes, S., Boissard, C., Durand, B., Gueudet, J.-C., Fanucci, O., Zurfluh, O., Abis, L., Zannoni, N., Truong, F., Baisnée, D., Sarda-Estève, R., Staudt, M., and Gros, V.: Volatile organic compound fluxes over a winter wheat field by PTR-Qi-TOF-MS and eddy covariance, <https://doi.org/10.5194/acp-2020-1328>, 2021.
- Lourenço, C., González-Méndez, R., Reich, F., Mason, N., and Turner, C.: A potential method for comparing instrumental analysis of volatile organic compounds using standards calibrated for the gas phase, Int. J. Mass Spectrom., 419, 1–10, <https://doi.org/10.1016/j.ijms.2017.05.011>, 2017.
- Lourenço, C., Bergin, S., Hodgkinson, J., Francis, D., Staines, S. E., Saffell, J. R., Walton, C., and Tatam, R. P.: Instrumentation for quantitative analysis of volatile compounds emission at elevated temperatures. Part 1: Design and implementation, Sci. Rep., 10, 8700, <https://doi.org/10.1038/s41598-020-65472-5>, 2020.
- Lüdecke, D.: sjPlot: Data visualization for statistics in social science, URL <https://CRAN.R-project.org/package=sjPlot>, 2020.
- Lv, J., Xu, W., Ji, C., Liang, H., Li, S., Yang, Z., Zhang, S., and Lin, X.: Relationships between the bacterial diversity and metabolites of a Chinese fermented pork product, sour meat, International Journal of Food Science & Technology, <https://doi.org/10.1111/ijfs.14905>, 2020.
- Lyimo, T. J., Pol, A., and Op den Camp, H. J.: Methane emission, sulphide concentration and redox potential profiles in Mtoni mangrove sediment, Tanzania, Western Indian Ocean J. Mar. Sci., 1, 71–80, 2002a.

- Lyimo, T. J., Pol, A., and Op den Camp, Huub J. M.: Sulfate reduction and methanogenesis in sediments of Mtoni mangrove forest, Tanzania, *AMBIO: J. Human Environ.*, 31, 614–616, <https://doi.org/10.1579/0044-7447-31.7.614>, 2002b.
- Lyimo, T. J., Pol, A., Harhangi, H. R., Jetten, M. S. M., and Op den Camp, Huub J. M.: Anaerobic oxidation of dimethylsulfide and methanethiol in mangrove sediments is dominated by sulfate-reducing bacteria, *FEMS Microbiol. Ecol.*, 70, 483–492, <https://doi.org/10.1111/j.1574-6941.2009.00765.x>, 2009.
- Maag, D., Erb, M., Köllner, T. G., and Gershenson, J.: Defensive weapons and defense signals in plants: some metabolites serve both roles, *BioEssays*, 37, 167–174, <https://doi.org/10.1002/bies.201400124>, 2015.
- MacTaggart, D. L., Adams, D. F., and Farewell, S. O.: Measurement of biogenic sulfur emissions from soils and vegetation using dynamic enclosure methods: total sulfur gas emissions via MFC/FD/FPD Determinations, *J. Atmos. Chem.*, 5, 417–437, <https://doi.org/10.1007/BF00113904>, 1987.
- Mahilang, M., Deb, M. K., and Pervez, S.: Biogenic secondary organic aerosols: A review on formation mechanism, analytical challenges and environmental impacts, *Chemosphere*, 262, 127 771, <https://doi.org/10.1016/j.chemosphere.2020.127771>, 2021.
- Mäki, M., Aalto, J., Hellén, H., Pihlatie, M., and Bäck, J.: Interannual and seasonal dynamics of volatile organic compound fluxes from the boreal forest floor, *Front. Plant Sci.*, 10, 191, <https://doi.org/10.3389/fpls.2019.00191>, 2019a.
- Mäki, M., Krasnov, D., Hellén, H., Noe, S. M., and Bäck, J.: Stand type affects fluxes of volatile organic compounds from the forest floor in hemiboreal and boreal climates, *Plant Soil*, 441, 363–381, <https://doi.org/10.1007/s11104-019-04129-3>, 2019b.
- Mancuso, S., Taiti, C., Bazihizina, N., Costa, C., Menesatti, P., Giagnoni, L., Arenella, M., Nannipieri, P., and Renella, G.: Soil volatile analysis by proton transfer reaction-time of flight mass spectrometry (PTR-TOF-MS), *Appl. Soil Ecol.*, 86, 182–191, <https://doi.org/10.1016/j.apsoil.2014.10.018>, 2015.
- Manes, F., Salvatori, E., La Torre, G., Villari, P., Vitale, M., Biscontini, D., and Incerti, G.: Urban green and its relation with air pollution: ecological studies in the Metropolitan area of Rome, *It. J. Publ. Health*, 5, 278–283, 2008.
- Mangold, S., Valdes, J., Holmes, D. S., and Dopson, M.: Sulfur metabolism in the extreme acidophile *Acidithiobacillus caldus*, *Front. Microbiol.*, 2, 17, <https://doi.org/10.3389/fmicb.2011.00017>, 2011.
- Marr, I. L., Cressner, M. S., and Ottendorfer, L. J.: Probenahme von Gasen und der Atmosphäre, in: *Umweltanalytik: eine allgemeine Einführung*, pp. 105–135, Georg Thieme Verlag, Stuttgart, 1988.

- Martin, C., Maesen, P., Minchilli, D., Francis, F., and Verheggen, F.: Forensic taphonomy: Characterization of the gravesoil chemistry using a multivariate approach combining chemical and volatile analyses, *Forensic Sci. Int.*, 318, 110–114, <https://doi.org/10.1016/j.forsciint.2020.110569>, 2021.
- Mazelis, M., Levin, B., and Mallinson, N.: Decomposition of methyl methionine sulfonium salts by a bacterial enzyme, *Biochim. Biophys. Act.*, 105, 106–114, 1965.
- McBride, S. G., Osburn, E. D., Barrett, J. E., and Strickland, M. S.: Volatile methanol and acetone additions increase labile soil carbon and inhibit nitrification, *Biogeochemistry*, 145, 127–140, <https://doi.org/10.1007/s10533-019-00595-0>, 2019.
- McBride, S. G., Choudoir, M., Fierer, N., and Strickland, M. S.: Volatile organic compounds from leaf litter decomposition alter soil microbial communities and carbon dynamics, *Ecology*, 101, e03130, <https://doi.org/10.1002/ecy.3130>, 2020.
- McCarthy, S., Chasteen, T., Marshall, M., Fall, R., and Bachofen, R.: Phototrophic bacteria produce volatile, methylated sulfur and selenium compounds, *FEMS Microbiol. Lett.*, 112, 93–97, <https://doi.org/10.1111/j.1574-6968.1993.tb06429.x>, 1993.
- McEwan, M. J.: Direct analysis mass spectrometry, in: *Ion/molecule attachment reactions: mass spectrometry*, edited by Fujii, T., pp. 263–317, Springer US, Boston, MA, https://doi.org/10.1007/978-1-4899-7588-1_8, 2015.
- Meredith, L. K., Boye, K., Youngerman, C., Whelan, M., Ogée, J., Sauze, J., and Wingate, L.: Coupled biological and abiotic mechanisms driving carbonyl sulfide production in soils, *Soil Syst.*, 2, 1–27, <https://doi.org/10.3390/soilsystems2030037>, 2018.
- Merlen, C., Verrièle, M., Crunaire, S., Ricard, V., Kaluzny, P., and Locoge, N.: Quantitative or only qualitative measurements of sulfur compounds in ambient air at ppb level? Uncertainties assessment for active sampling with Tenax TA, *Microchem. J.*, 132, 143–153, <https://doi.org/10.1016/j.microc.2017.01.014>, 2017.
- Meulepas, R. J., Jagersma, C. G., Khadem, A. F., Stams, A. J., and Lens, P. N.: Effect of methanogenic substrates on anaerobic oxidation of methane and sulfate reduction by an anaerobic methanotrophic enrichment, *Appl. Microbiol. Biotechnol.*, 87, 1499–1506, <https://doi.org/10.1007/s00253-010-2597-0>, 2010.
- Miller, A. R., North, J. A., Wildenthal, J. A., and Tabita, F. R.: Two distinct aerobic methionine salvage pathways generate volatile methanethiol in *Rhodospseudomonas palustris*, *mBio*, <https://doi.org/10.1128/mBio.00407-18>, 2018.
- Miranda, M., Zarivi, O., Bonfigli, A., Amicarelli, F., Aimola, P., Ragnelli, A. M., and Pacioni, G.: Melanogenesis, tyrosinase expression, and reproductive differentiation in black and white truffles (Ascomycotina), *Pigment cell research*, 10, 46–53, <https://doi.org/10.1111/j.1600-0749.1997.tb00465.x>, 1997.

- Moore, T. R. and Roulet, N. T.: A comparison of dynamic and static chambers for methane emission measurements from subarctic fens, *Atmosph. Ocean*, 29, 102–109, <https://doi.org/10.1080/07055900.1991.9649395>, 1991.
- Moran, J. J., Beal, E. J., Vrentas, J. M., Orphan, V. J., Freeman, K. H., and House, C. H.: Methyl sulfides as intermediates in the anaerobic oxidation of methane, *Environ. Microbiol.*, 10, 162–173, <https://doi.org/10.1111/j.1462-2920.2007.01441.x>, 2008.
- Moran, M. A. and Durham, B. P.: Sulfur metabolites in the pelagic ocean, *Nat. Rev. Microbiol.*, <https://doi.org/10.1038/s41579-019-0250-1>, 2019.
- Morcos, D., Schmier, B. J., Malhotra, A., and Venkatachalam, K. V.: Purification and characterization of methionine gamma lyase-deaminase (Mgld) from the oral pathogenic organism *Porphyromonas gingivalis*, *Biochemistry and Analytical Biochemistry*, 4, 2015.
- Müller, M., Piel, F., Gutmann, R., Sulzer, P., Hartungen, E., and Wisthaler, A.: A novel method for producing NH_4^+ reagent ions in the hollow cathode glow discharge ion source of PTR-MS instruments, *Int. J. Mass Spectrom.*, 447, 116–254, <https://doi.org/10.1016/j.ijms.2019.116254>, 2020.
- Mungall, E. L., Croft, B., Lizotte, M., Thomas, J. L., Murphy, J. G., Levasseur, M., Martin, R. V., Wentzell, J. J. B., Liggio, J., and Abbatt, J. P. D.: Dimethyl sulfide in the summertime Arctic atmosphere: measurements and source sensitivity simulations, *Atmos. Chem. Phys.*, 16, 6665–6680, <https://doi.org/10.5194/acp-16-6665-2016>, 2016.
- Naik, B. R., Gauns, M., Bepari, K., Uskaikar, H., and Shenoy, D. M.: Variation in phytoplankton community and its implication to dimethylsulphide production at a coastal station off Goa, India, *Mar. Environ. Res.*, 157, <https://doi.org/10.1016/j.marenvres.2020.104926>, 2020.
- Niinemets, Ü. and Reichstein, M.: A model analysis of the effects of nonspecific monoterpenoid storage in leaf tissues on emission kinetics and composition in Mediterranean sclerophyllous *Quercus* species, *Global Biogeochem. Cycles*, 16, 57, 1–26, <https://doi.org/10.1029/2002GB001927>, 2002.
- North, J. A., Narrowe, A. B., Xiong, W., Byerly, K. M., Zhao, G., Young, S. J., Murali, S., Wildenthal, J. A., Cannon, W. R., Wrighton, K. C., Hettich, R. L., and Tabita, F. R.: A nitrogenase-like enzyme system catalyzes methionine, ethylene, and methane biogenesis, *Science*, 369, 1094–1098, <https://doi.org/10.1126/science.abb6310>, 2020.
- Nriagu, J. O. and Holdway, D. A.: Production and release of dimethyl sulfide from the Great Lakes, *Tellus B: Chem. Phys. Meteorol.*, 41, 161–169, <https://doi.org/10.3402/tellusb.v41i2.15065>, 1989.
- Ogawa, T., Hattori, S., Kamezaki, K., Kato, H., Yoshida, N., and Katayama, Y.: Isotopic fractionation of sulfur in carbonyl sulfide by carbonyl sulfide hydrolase of *Thiobacillus thioparus* THI115, *Microbes Environ.*, 32, 367–375, <https://doi.org/10.1264/jsme2.ME17130>, 2017.

- Ogée, J., Sauze, J., Kesselmeier, J., Genty, B., van Diest, H., Launois, T., and Wingate, L.: A new mechanistic framework to predict OCS fluxes from soils, *Biogeosciences*, 13, 2221–2240, <https://doi.org/10.5194/bg-13-2221-2016>, 2016.
- Olivares, A., Dryahina, K., Navarro, J. L., Smith, D., Španěl, P., and Flores, M.: SPME-GC-MS versus selected ion flow tube mass spectrometry (SIFT-MS) analyses for the study of volatile compound generation and oxidation status during dry fermented sausage processing, *J. Agricult. Food Chem.*, 59, 1931–1938, <https://doi.org/10.1021/jf104281a>, 2011.
- Oliveira, T. F., Vonnrhein, C., Matias, P. M., Venceslau, S. S., Pereira, I. A., and Archer, M.: The crystal structure of *Desulfovibrio vulgaris* dissimilatory sulfite reductase bound to DsrC provides novel insights into the mechanism of sulfate respiration, *J. Biol. Chem.*, 283, 34 141–34 149, <https://doi.org/10.1074/jbc.M805643200>, 2008.
- Ossola, R., Tolu, J., Clerc, B., Erickson, P. R., Winkel, L. H. E., and McNeill, K.: Photochemical production of sulfate and methanesulfonic acid from dissolved organic sulfur, *Environ. Sci. Technol.*, 53, 13 191–13 200, <https://doi.org/10.1021/acs.est.9b04721>, 2019.
- Ossowicki, A., Jafra, S., and Garbeva, P.: The antimicrobial volatile power of the rhizospheric isolate *Pseudomonas donghuensis* P482, *PLoS ONE*, 12, e0174 362, <https://doi.org/10.1371/journal.pone.0174362>, 2017.
- Otto, M.: *Analytische Chemie*, John Wiley and Sons, Weinheim, fünfte auflage edn., 2019.
- Pan, X., Zhang, W., Lao, F., Mi, R., Liao, X., Luo, D., and Wu, J.: Isolation and identification of putative precursors of the volatile sulfur compounds and their inhibition methods in heat-sterilized melon juices, *Food Chem.*, 343, 128 459, <https://doi.org/10.1016/j.foodchem.2020.128459>, 2021.
- Paul, A. and Clark, F. E.: *Soil Microbiology and Biochemistry*, Academic Press, San Diego, 2 edn., 1996.
- Pederson, J. R., Massman, W. J., Mahrt, L., Delany, A., Oncley, S., Hartog, G., Neumann, H. H., Mickle, R. E., Shaw, R. H., Paw U, K. T., Grantz, D. A., MacPherson, J. I., Desjardins, R., Schuepp, P. H., Pearson, R., and Arcadio, T. E.: California ozone deposition experiment: Methods, results, and opportunities, *Atmospheric Environment*, 29, 3115–3132, [https://doi.org/10.1016/1352-2310\(95\)00136-M](https://doi.org/10.1016/1352-2310(95)00136-M), 1995.
- Peng, L. and Sun, J.: Advances in marine dimethyl sulfide observation and its air-sea flux estimation, *Acta Ecologica Sinica*, 40, <https://doi.org/10.5846/stxb201807131524>, 2020.
- Penuelas, J., Asensio, D., Tholl, D., Wenke, K., Rosenkranz, M., Piechulla, B., and Schnitzler, J. P.: Biogenic volatile emissions from the soil, *Plant Cell Environ.*, 37, 1866–1891, <https://doi.org/10.1111/pce.12340>, 2014.

- Phae, C.-G. and Shoda, M.: A new fungus which degrades hydrogen sulfide, methanethiol, dimethyl sulfide and dimethyl disulfide, *Biotechnology Letters*, 13, 375–380, <https://doi.org/10.1007/BF01027686>, 1991.
- Phillips, D. P., Hopkins, F. E., Bell, T. G., Liss, P. S., Nightingale, P. D., Reeves, C. E., Wohl, C., and Yang, M.: Air-sea exchange of acetone, acetaldehyde, DMS and isoprene at a UK coastal site, <https://doi.org/10.5194/acp-2021-108>, 2021.
- Piel, F., Müller, M., Winkler, K., Skytte af Sättra, J., and Wisthaler, A.: Introducing the extended volatility range proton-transfer-reaction mass spectrometer (EVR PTR-MS), *Atmos. Meas. Tech. Discuss.* [preprint], 2020, 1–12, <https://doi.org/10.5194/amt-2020-241>, URL <https://amt.copernicus.org/preprints/amt-2020-241/>, 2020.
- Pierik, R., Ballaré, C. L., and Dicke, M.: Ecology of plant volatiles: taking a plant community perspective, *Plant Cell and Environment*, 37, 1845–1853, <https://doi.org/10.1111/pce.12330>, 2014.
- Pinheiro, J., Bates, D., DebRoy, S., Sarkar, D., and R Core Team: nlme: Linear and nonlinear mixed effects models, URL <https://CRAN.R-project.org/package=nlme>, 2020.
- Plaszko, T., Szűcs, Z., Kállai, Z., Csoma, H., Vasas, G., and Gonda, S.: Volatile organic compounds (VOCs) of endophytic fungi growing on extracts of the host, horseradish (*Armoracia rusticana*), *Metabolites*, 10, 451, <https://doi.org/10.3390/metabo10110451>, 2020.
- Pracharova, P., Lieben, P., Pollet, B., Beckerich, J. M., Bonnarme, P., Landaud, S., and Swennen, D.: *Geotrichum candidum* gene expression and metabolite accumulation inside the cells reflect the strain oxidative stress sensitivity and ability to produce flavour compounds, *FEMS Yeast Res.*, 19, foy111, <https://doi.org/10.1093/femsyr/foy111>, 2019.
- Prada, P. A., Curran, A. M., and Furton, K. G.: The evaluation of human hand odor volatiles on various textiles: a comparison between contact and noncontact sampling methods, *J. Forensic Sci.*, 56, 866–881, <https://doi.org/10.1111/j.1556-4029.2011.01762.x>, 2011.
- Protoschill-Krebs, G., Wilhelm, C., and Kesselmeier, J.: Consumption of carbonyl sulphide (COS) by higher plant carbonic anhydrase (CA), *Atmos. Environ.*, 30, 3151–3156, [https://doi.org/10.1016/1352-2310\(96\)00026-x](https://doi.org/10.1016/1352-2310(96)00026-x), 1996.
- Quinn, P. K. and Bates, T. S.: The case against climate regulation via oceanic phytoplankton sulphur emissions, *Nature*, 480, 51–56, <https://doi.org/10.1038/nature10580>, 2011.
- Raina, J.-B., Dinsdale, E. A., Willis, B. L., and Bourne, D. G.: Do the organic sulfur compounds DMSP and DMS drive coral microbial associations?, *Trends Microbiol.*, 18, 101–108, <https://doi.org/10.1016/j.tim.2009.12.002>, 2010.
- Räisänen, T., Ryyppö, A., and Kellomäki, S.: Monoterpene emission of a boreal Scots pine (*Pinus sylvestris* L.) forest, *Agric. For. Meteorol.*, 149, 808–819, <https://doi.org/10.1016/j.agrformet.2008.11.001>, 2009.

- Ramirez, K. S., Lauber, C. L., and Fierer, N.: Microbial consumption and production of volatile organic compounds at the soil-litter interface, *Biogeochemistry*, 99, 97–107, <https://doi.org/10.1007/s10533-009-9393-x>, 2010a.
- Ramirez, N., Cuadras, A., Rovira, E., Borrull, F., and Marce, R. M.: Comparative study of solvent extraction and thermal desorption methods for determining a wide range of volatile organic compounds in ambient air, *Talanta*, 82, 719–727, <https://doi.org/10.1016/j.talanta.2010.05.038>, 2010b.
- Rantala, P., Taipale, R., Aalto, J., Patokoski, J., Ruuskanen, T. M., Kajos, M. K., and Rinne, J.: Continuous flux measurements of VOCs using PTR-MS – reliability and feasibility of disjunct-eddy-covariance, surface-layer-gradient, and surface-layer-profile methods, *Boreal Environ. Res.*, 19, 87–107, 2014.
- Raza, W., Wang, J., Jousset, A., Friman, V. P., Mei, X., Wang, S., Wei, Z., and Shen, Q.: Bacterial community richness shifts the balance between volatile organic compound-mediated microbe-pathogen and microbe-plant interactions, *Proc. Biol. Sci.*, 287, 20200403, <https://doi.org/10.1098/rspb.2020.0403>, 2020.
- Reisch, C. R., Moran, M. A., and Whitman, W. B.: Bacterial catabolism of dimethylsulfoniopropionate (DMSP), *Front. Microbiol.*, 2, 172, <https://doi.org/10.3389/fmicb.2011.00172>, 2011.
- Rejmankova, E. and Post, R. A.: Methane in sulfate-rich and sulfate-poor wetland sediments, *Biogeochemistry*, 34, 57–70, <https://doi.org/10.1007/BF02180973>, 1996.
- Ren, Y., Qu, Z., Du, Y., Xu, R., Ma, D., Yang, G., Shi, Y., Fan, X., Tani, A., Guo, P., Ge, Y., and Chang, J.: Air quality and health effects of biogenic volatile organic compounds emissions from urban green spaces and the mitigation strategies, *Environ. Pollut.*, 230, 849–861, <https://doi.org/10.1016/j.envpol.2017.06.049>, 2017.
- Richards, S. R., Kelly, C. A., and John, W. M. R.: Organic volatile sulfur in lakes of the Canadian shield and its loss to the atmosphere, *Limnol. Oceanogr.*, 36, 468–482, <https://doi.org/10.4319/lo.1991.36.3.0468>, 1991.
- Richards, S. R., Rudd, J. W. M., and Kelly, C. A.: Organic volatile sulfur in lakes ranging in sulfate and dissolved salt concentration over five orders of magnitude, *Limnol. Oceanogr.*, 39, 562–572, <https://doi.org/10.4319/lo.1994.39.3.0562>, 1994.
- Rickard, D. and Morse, J. W.: Acid volatile sulfide (AVS), *Mar. Chem.*, 97, 141–197, <https://doi.org/10.1016/j.marchem.2005.08.004>, 2005.
- Rinnan, R. and Albers, C. N.: Soil Uptake of Volatile Organic Compounds: Ubiquitous and Underestimated?, *Journal of Geophysical Research: Biogeosciences*, 125, <https://doi.org/10.1029/2020JG005773>, 2020.

- Rinnan, R., Gierth, D., Bilde, M., Rosenørn, T., and Michelsen, A.: Off-season biogenic volatile organic compound emissions from heath mesocosms: responses to vegetation cutting, *Front. Microbiol.*, 4, 1–10, <https://doi.org/10.3389/fmicb.2013.00224>, 2013.
- Riva, M., Rantala, P., Krechmer, J. E., Peräkylä, O., Zhang, Y., Heikkinen, L., Garmash, O., Yan, C., Kulmala, M., Worsnop, D., and Ehn, M.: Evaluating the performance of five different chemical ionization techniques for detecting gaseous oxygenated organic species, *Atmos. Meas. Tech.*, 12, 2403–2421, <https://doi.org/10.5194/amt-12-2403-2019>, 2019.
- Rochette, P., Gregorich, E. G., and Desjardins, R. L.: Comparison of static and dynamic closed chambers for measurement of soil respiration under field conditions, *Can. J. Soil. Sci.*, 72, 605–609, <https://doi.org/10.4141/cjss92-050>, 1992.
- Röck, F., Barsan, N., and Weimar, U.: Electronic nose: current status and future trends, *Chem. Rev.*, 106, 705–725, <https://doi.org/10.1021/cr068121q>, 2008.
- Rosier, E., Cuypers, E., Dekens, M., Verplaetse, R., Develter, W., van de Voorde, W., Maes, D., and Tytgat, J.: Development and validation of a new TD-GC/MS method and its applicability in the search for human and animal decomposition products, *Anal. Bioanal. Chem.*, 406, 3611–3619, <https://doi.org/10.1007/s00216-014-7741-8>, 2014.
- Rossabi, S., Choudoir, M., Helmig, D., Hueber, J., and Fierer, N.: Volatile organic compound emissions from soil following wetting events, *J. Geophys. Res.: Biogeosci.*, 123, 1988–2001, <https://doi.org/10.1029/2018jg004514>, 2018.
- Rudnicka, J., Kowalkowski, T., Ligor, T., and Buszewski, B.: Determination of volatile organic compounds as biomarkers of lung cancer by SPME-GC-TOF/MS and chemometrics, *J. Chromatogr. B*, 879, 3360–3366, <https://doi.org/10.1016/j.jchromb.2011.09.001>, 2011.
- Salisbury, G., Williams, J., Holzinger, R., Gros, V., Mihalopoulos, N., Vrekoussis, M., Sarda-Estève, R., Berresheim, H., von Kuhlmann, R., Lawrence, M., and Lelieveld, J.: Ground-based PTR-MS measurements of reactive organic compounds during the MINOS campaign in Crete, July–August 2001, *Atmos. Chem. Phys.*, 3, 925–940, <https://doi.org/10.5194/acp-3-925-2003>, 2003.
- Sandoval-Soto, L., Stanimirov, M., von Hobe, M., Schmitt, V., Valdes, J., Wild, A., and Kesselmeier, J.: Global uptake of carbonyl sulfide (COS) by terrestrial vegetation: Estimates corrected by deposition velocities normalized to the uptake of carbon dioxide (CO₂), *Biogeosciences*, 2, 125–132, <https://doi.org/10.5194/bg-2-125-2005>, 2005.
- Sarkar, C., Guenther, A. B., Park, J.-H., Seco, R., Alves, E., Batalha, S., Santana, R., Kim, S., Smith, J., Tóta, J., and Vega, O.: PTR-TOF-MS eddy covariance measurements of isoprene and monoterpene fluxes from an eastern Amazonian rainforest, *Atmos. Chem. Phys.*, 20, 7179–7191, <https://doi.org/10.5194/acp-20-7179-2020>, 2020.

- Sauze, J., Ogee, J., Maron, P. A., Crouzet, O., Nowak, V., Wohl, S., Kaisermann, A., Jones, S. P., and Wingate, L.: The interaction of soil phototrophs and fungi with pH and their impact on soil CO₂, CO¹⁸O and OCS exchange, *Soil Biol. Biochem.*, 115, 371–382, <https://doi.org/10.1016/j.soilbio.2017.09.009>, 2017.
- Schade, G. W., Goldstein, A. H., Gray, D. W., and Lerdau, M. T.: Canopy and leaf level 2-methyl-3-buten-2-ol fluxes from a ponderosa pine plantation, *Atmos. Environ.*, 34, 3535–3544, [https://doi.org/10.1016/S1352-2310\(00\)00120-5](https://doi.org/10.1016/S1352-2310(00)00120-5), 2000.
- Schloerke, B., Di Cook, Larmarange, J., Briatte, F., Marbach, M., Thoen, E., Elberg, A., and Crowley, J.: GGally: Extension to 'ggplot2', URL <https://CRAN.R-project.org/package=GGally>, 2021.
- Scholten, J. C., Murrell, J. C., and Kelly, D. P.: Growth of sulfate-reducing bacteria and methanogenic archaea with methylated sulfur compounds: a commentary on the thermodynamic aspects, *Arch. Microbiol.*, 179, 135–144, <https://doi.org/10.1007/s00203-002-0509-0>, 2003.
- Schulz, S. and Dickschat, J. S.: Bacterial volatiles: the smell of small organisms, *Nat. Prod. Rep.*, 24, 814–842, <https://doi.org/10.1039/B507392H>, 2007.
- Schulz-Bohm, K., Geisen, S., Wubs, E. R., Song, C., de Boer, W., and Garbeva, P.: The prey's scent - Volatile organic compound mediated interactions between soil bacteria and their protist predators, *ISME J.*, 11, 817–820, <https://doi.org/10.1038/ismej.2016.144>, 2017.
- Schwarz, K., Filipiak, W., and Amann, A.: Determining concentration patterns of volatile compounds in exhaled breath by PTR-MS, *J. Breath Res.*, 3, 027 002, <https://doi.org/10.1088/1752-7155/3/2/027002>, 2009.
- Scott, J., Sueiro-Olivares, M., Ahmed, W., Heddergott, C., Zhao, C., Thomas, R., Bromley, M., Latge, J. P., Krappmann, S., Fowler, S., Bignell, E., and Amich, J.: *Pseudomonas aeruginosa*-derived volatile sulfur compounds promote distal *Aspergillus fumigatus* growth and a synergistic pathogen-pathogen interaction that increases pathogenicity in co-infection, *Front. Microbiol.*, 10, 2311, <https://doi.org/10.3389/fmicb.2019.02311>, 2019.
- Seco, R., Holst, T., Matzen, M. S., Westergaard-Nielsen, A., Li, T., Simin, T., Jansen, J., Crill, P., Friborg, T., Rinne, J., and Rinnan, R.: Volatile organic compound fluxes in a subarctic peatland and lake, *Atmospheric Chemistry and Physics*, 20, 13 399–13 416, <https://doi.org/10.5194/acp-20-13399-2020>, 2020.
- Segal, W. and Starkey, R. L.: Microbial decomposition of methionine and identity of the resulting sulfur products, *J. Bacteriol.*, 98, 908–913, 1969.
- Shende, P., Vaidya, J., Kulkarni, Y. A., and Gaud, R. S.: Systematic approaches for biodiagnostics using exhaled air, *J. Control. Release*, 268, 282–295, <https://doi.org/10.1016/j.jconrel.2017.10.035>, 2017.

- Sikder, M. M. and Vestergård, M.: Impacts of root metabolites on soil nematodes, *Front. Plant Sci.*, 10, 1792, <https://doi.org/10.3389/fpls.2019.01792>, 2019.
- Simó, R., Saló, V., Almeda, R., Movilla, J., Trepal, I., Saiz, E., and Calbet, A.: The quantitative role of microzooplankton grazing in dimethylsulfide (DMS) production in the NW Mediterranean, *Biogeochemistry*, 141, 125–142, <https://doi.org/10.1007/s10533-018-0506-2>, 2018.
- Simpson, I. J., Colman, J. J., Swanson, A. L., Bandy, A. R., Thornton, D. C., Blake, D. R., and Rowland, F. S.: Aircraft measurements of dimethyl sulfide (DMS) using a whole air sampling technique, *J. Atmos. Chem.*, 39, 191–213, <https://doi.org/10.1023/a:1010608529779>, 2001.
- Six, K. D., Kloster, S., Ilyina, T., Archer, S. D., Zhang, K., and Maier-Reimer, E.: Global warming amplified by reduced sulphur fluxes as a result of ocean acidification, *Nat. Clim. Change*, 3, 975–978, <https://doi.org/10.1038/nclimate1981>, 2013.
- Slingers, G., Vanden Eede, M., Lindekens, J., Spruyt, M., Goelen, E., Raes, M., and Koppen, G.: Real-time versus thermal desorption selected ion flow tube mass spectrometry for quantification of breath volatiles, *Rapid Commun. Mass Spectrom.*, 35, e8994, <https://doi.org/10.1002/rcm.8994>, 2021.
- Smet, E. and van Langenhove, H.: Abatement of volatile organic sulfur compounds in odorous emissions from the bio-industry, *Biodegradation*, 9, 273–284, <https://doi.org/10.1023/A:1008281609966>, 1998.
- Smith, D. and Spanel, P.: The novel selected-ion flow tube approach to trace gas analysis of air and breath, *Rapid Commun. Mass Spectrom.*, 10, 1183–1196, [https://doi.org/10.1002/\(SICI\)1097-0231\(19960731\)10:10<1183::AID-RCM641>3.0.CO;2-3](https://doi.org/10.1002/(SICI)1097-0231(19960731)10:10<1183::AID-RCM641>3.0.CO;2-3), 1996.
- Smith, D. and Spanel, P.: Direct, rapid quantitative analyses of BVOCs using SIFT-MS and PTRMS obviating sample collection, *Trends Anal. Chem.*, 30, 945–959, <https://doi.org/10.1016/j.trac.2011.05.001>, 2011a.
- Smith, D. and Spanel, P.: Ambient analysis of trace compounds in gaseous media by SIFT-MS, *Analyst*, 136, 2009–2032, <https://doi.org/10.1039/c1an15082k>, 2011b.
- Smith, D., Spanel, P., Herbig, J., and Beauchamp, J.: Mass spectrometry for real-time quantitative breath analysis, *J. Breath Res.*, 8, 027 101, <https://doi.org/10.1088/1752-7155/8/2/027101>, 2014.
- Smith, D., McEwan, M. J., and Španěl, P.: Understanding gas phase ion chemistry is the key to reliable selected ion flow tube-mass spectrometry analyses, *Analyt. Chem.*, 92, 12 750–12 762, <https://doi.org/10.1021/acs.analchem.0c03050>, 2020.
- Sniegowski, P. D., Dombrowski, P. G., and Fingerman, E.: *Saccharomyces cerevisiae* and *Saccharomyces paradoxus* coexist in a natural woodland site in North America and display different levels of reproductive isolation from European conspecifics, *FEMS Yeast Res.*, 1, 299–306, <https://doi.org/10.1111/j.1567-1364.2002.tb00048.x>, 2002.

- Spálený, J.: Sulphate transformation to hydrogen sulphide in spruce seedlings, *Plant Soil*, 48, 557–563, <https://doi.org/10.1007/BF00145767>, 1977.
- Španěl, P. and Smith, D.: Progress in SIFT-MS: Breath analysis and other applications, *Mass Spectrom. Rev.*, 30, 236–267, <https://doi.org/10.1002/mas.20303>, 2011.
- Španěl, P. and Smith, D.: Dissociation of H_3O^+ , NO^+ and O_2^+ reagent ions injected into nitrogen carrier gas in SIFT-MS and reactivity of the ion fragments, *Int. J. Mass Spectrom.*, 458, 116–1438, <https://doi.org/10.1016/j.ijms.2020.116438>, 2020.
- Španěl, P., Dryahina, K., and Smith, D.: A general method for the calculation of absolute trace gas concentrations in air and breath from selected ion flow tube mass spectrometry data, *Int. J. Mass Spectrom.*, 249–250, 230–239, <https://doi.org/10.1016/j.ijms.2005.12.024>, 2006.
- Španěl, P., Spesyvyi, A., and Smith, D.: Electrostatic Switching and Selection of H_3O^+ , NO^+ , and O_2^+ reagent ions for selected ion flow-drift tube mass spectrometric analyses of air and breath, *Anal. Chem.*, 91, 5380–5388, <https://doi.org/10.1021/acs.analchem.9b00530>, 2019.
- Spesyvyi, A., Smith, D., and Španěl, P.: Selected ion flow-drift tube mass spectrometry: Quantification of volatile compounds in air and breath, *Anal. Chem.*, 87, 12 151–12 160, <https://doi.org/10.1021/acs.analchem.5b02994>, 2015.
- Spirig, C., Neftel, A., Ammann, C., Dommen, J., Grabmer, W., Thielmann, A., Schaub, A., Beauchamp, J., Wisthaler, A., and Hanse, A.: Eddy covariance flux measurements of biogenic VOCs during ECHO 2003 using proton transfer reaction mass spectrometry, *Atmos. Chem. Phys.*, 5, 465–481, 2005.
- Splivallo, R., Novero, M., Berteà, C. M., Bossi, S., and Bonfante, P.: Truffle volatiles inhibit growth and induce an oxidative burst in *Arabidopsis thaliana*, *New phytol.*, 175, 417–424, <https://doi.org/10.1111/j.1469-8137.2007.02141.x>, 2007.
- Stahl, P. D. and Parkin, T. B.: Microbial production of volatile organic compounds in soil microcosms, *Soil Sci. Soc. Am. J.*, 60, 821–828, <https://doi.org/10.2136/sssaj1996.03615995006000030020x>, 1996.
- Staubes, R., Georgii, H. W., and Ockelmann, G.: Flux of COS, DMS and CS₂ from various soils in Germany, *Tellus B: Chem. Phys. Meteorol.*, 41, 305–313, <https://doi.org/10.3402/tellusb.v41i3.15084>, 1989.
- Staudt, M., Byron, J., Piquemal, K., and Williams, J.: Compartment specific chiral pinene emissions identified in a Maritime pine forest, *Sci. Total Environ.*, 654, 1158–1166, <https://doi.org/10.1016/j.scitotenv.2018.11.146>, 2019.
- Stefanuto, P.-H., Perrault, K. A., Stadler, S., Pesesse, R., LeBlanc, H. N., Forbes, S. L., and Focant, J.-F.: GC × GC-TOFMS and supervised multivariate approaches to study human cadaveric decomposition olfactive signatures, *Anal. Bioanal. Chem.*, 407, 4767–4778, <https://doi.org/10.1007/s00216-015-8683-5>, 2015.

- Stefels, J.: Physiological aspects of the production and conversion of DMSP in marine algae and higher plants, *J. Sea Res.*, 43, 183–197, [https://doi.org/10.1016/S1385-1101\(00\)00030-7](https://doi.org/10.1016/S1385-1101(00)00030-7), 2000.
- Steinke, M., Hodapp, B., Subhan, R., Bell, T. G., and Martin-Creuzburg, D.: Flux of the biogenic volatiles isoprene and dimethyl sulfide from an oligotrophic lake, *Sci. Rep.*, 8, 630, <https://doi.org/10.1038/s41598-017-18923-5>, 2018.
- Stets, E. G., Hines, M. E., and Kiene, R. P.: Thiol methylation potential in anoxic, low-pH wetland sediments and its relationship with dimethylsulfide production and organic carbon cycling, *FEMS Microbiol. Ecol.*, 47, 1–11, [https://doi.org/10.1016/S0168-6496\(03\)00219-8](https://doi.org/10.1016/S0168-6496(03)00219-8), 2004.
- Stuedler, P. A. and Peterson, B. J.: Annual cycle of gaseous sulfur emissions from a New England *Spartina alterniflora* marsh, *Atmos. Env.*, 19, 1411–1416, [https://doi.org/10.1016/0004-6981\(85\)90278-1](https://doi.org/10.1016/0004-6981(85)90278-1), 1985.
- Stoppacher, N., Kluger, B., Zeilinger, S., Krska, R., and Schuhmacher, R.: Identification and profiling of volatile metabolites of the biocontrol fungus *Trichoderma atroviride* by HS-SPME-GC-MS, *J Microbiol Methods*, 81, 187–193, <https://doi.org/10.1016/j.mimet.2010.03.011>, 2010.
- Stotzky, G., Schenck, S., and Papavizas, G. C.: Volatile organic compounds and microorganisms, *Crit. Rev. Microbiol.*, 4, 333–382, <https://doi.org/10.3109/10408417609102303>, 1976.
- Streit, W. R. and Entcheva, P.: Biotin in microbes, the genes involved in its biosynthesis, its biochemical role and perspectives for biotechnological production, *Appl. Microbiol. Biotechnol.*, 61, 21–31, <https://doi.org/10.1007/s00253-002-1186-2>, 2003.
- Strong, P. J., Xie, S., and Clarke, W. P.: Methane as a resource: can the methanotrophs add value?, *Environ Sci Technol*, 49, 4001–4018, <https://doi.org/10.1021/es504242n>, 2015.
- Sun, J., Hu, S., Sharma, K. R., Ni, B. J., and Yuan, Z.: Stratified microbial structure and activity in sulfide- and methane-producing anaerobic sewer biofilms, *Appl. Environ. Microbiol.*, 80, 7042–7052, <https://doi.org/10.1128/AEM.02146-14>, 2014.
- Sun, J., Hu, S., Sharma, K. R., Ni, B. J., and Yuan, Z.: Degradation of methanethiol in anaerobic sewers and its correlation with methanogenic activities, *Water Res.*, 69, 80–89, <https://doi.org/10.1016/j.watres.2014.11.004>, 2015a.
- Sun, J., Todd, J. D., Thrash, J. C., Qian, Y., Qian, M. C., Temperton, B., Guo, J., Fowler, E. K., Aldrich, J. T., Nicora, C. D., Lipton, M. S., Smith, R. D., de Leenheer, P., Payne, S. H., Johnston, A. W., Davie-Martin, C. L., Halsey, K. H., and Giovannoni, S. J.: The abundant marine bacterium *Pelagibacter* simultaneously catabolizes dimethylsulfoniopropionate to the gases dimethyl sulfide and methanethiol, *Nat. Microbiol.*, 1, 16 065, <https://doi.org/10.1038/nmicrobiol.2016.65>, 2016.
- Sun, X.-G., Bonfante, P., and Tang, M.: Effect of volatiles versus exudates released by germinating spores of *Gigaspora margarita* on lateral root formation, *Plant Physiol. Biochem.*, 97, 1–10, <https://doi.org/10.1016/j.plaphy.2015.09.010>, 2015b.

- Svendsen, S. H., Lindwall, F., Michelsen, A., and Rinnan, R.: Biogenic volatile organic compound emissions along a high arctic soil moisture gradient, *Sci. Tot. Environ.*, 573, 131–138, <https://doi.org/10.1016/j.scitotenv.2016.08.100>, 2016.
- Svendsen, S. H., Priemé, A., Voriskova, J., Kramshøj, M., Schostag, M., Jacobsen, C. S., and Rinnan, R.: Emissions of biogenic volatile organic compounds from arctic shrub litter are coupled with changes in the bacterial community composition, *Soil Biol. Biochem.*, 120, 80–90, <https://doi.org/10.1016/j.soilbio.2018.02.001>, 2018.
- Swan, H. B., Deschaseaux, E. S. M., Jones, G. B., and Eyre, B. D.: Quantification of dimethylsulfoniopropionate (DMSP) in *Acropora* spp. of reef-building coral using mass spectrometry with deuterated internal standard, *Anal. Bioanal. Chem.*, 409, 1929–1942, 2017a.
- Swan, H. B., Jones, G. B., Deschaseaux, E. S. M., and Eyre, B. D.: Coral reef origins of atmospheric dimethylsulfide at Heron Island, southern Great Barrier Reef, Australia, *Biogeosciences*, 14, 229, <https://doi.org/10.5194/bg-14-229-2017>, 2017b.
- Swan, H. B., Deschaseaux, E. S. M., Eyre, B. D., and Jones, G. B.: Surface flux and vertical profile of dimethyl sulfide in acid sulfate soils at Cudgen Lake, northern New South Wales, Australia, *Chemosphere*, 228, 309–317, <https://doi.org/10.1016/j.chemosphere.2019.04.129>, 2019.
- Tallant, T. C. and Krzycki, J. A.: Methylthiol:coenzyme M methyltransferase from *Methanosarcina barkeri*, an enzyme of methanogenesis from dimethylsulfide and methylmercaptopropionate, *J. Bacteriol.*, 179, 6902–6911, 1997.
- Tanaka, H., Esaki, N., Yamamoto, T., and Soda, K.: Purification and properties of methioninase from *Pseudomonas ovalis*, *FEBS Lett.*, 66, 307–311, 1976.
- Tang, J., Valolahti, H., Kivimäenpää, M., Michelsen, A., and Rinnan, R.: Acclimation of biogenic volatile organic compound emission from subarctic heath under long-term moderate warming, *J. Geophys. Res. Biogeosci.*, 123, 95–105, <https://doi.org/10.1002/2017jg004139>, 2018.
- Tang, J., Schurgers, G., and Rinnan, R.: Process understanding of soil BVOC fluxes in natural ecosystems: A review, *Rev. Geophys.*, <https://doi.org/10.1029/2018rg000634>, 2019.
- Taylor, B. F. and Kiene, R. P.: Microbial metabolism of dimethyl sulfide, in: Biogenic sulfur in the environment, vol. 393 of *ACS Symposium Series*, pp. 202–221, American Chemical Society, <https://doi.org/10.1021/bk-1989-0393.ch013>, 1989.
- Thume, K., Gebser, B., Chen, L., Meyer, N., Kieber, D. J., and Pohnert, G.: The metabolite dimethylsulfonium propionate extends the marine organosulfur cycle, *Nature*, 563, 412–415, <https://doi.org/10.1038/s41586-018-0675-0>, 2018.
- Tong, C., Morris, J. T., Huang, J., Xu, H., and Wan, S.: Changes in pore-water chemistry and methane emission following the invasion of *Spartina alterniflora* into an oligohaline marsh, *Limnol. Oceanogr.*, 63, 384–396, <https://doi.org/10.1002/lno.10637>, 2018.

- Trottmann, F., Ishida, K., Franke, J., Stanisic, A., Ishida-Ito, M., Kries, H., Pohnert, G., and Hertweck, C.: Sulfonium acids loaded onto an unusual thiotemplate assembly line construct the cyclopropanol warhead of a *Burkholderia* virulence factor, *Angew. Chem. Int. Ed.*, 59, 13 511–13 515, <https://doi.org/10.1002/anie.202003958>, 2020.
- Trowbridge, A. M., Stoy, P. C., and Phillips, R. P.: Soil Biogenic Volatile Organic Compound Flux in a Mixed Hardwood Forest: Net Uptake at Warmer Temperatures and the Importance of Mycorrhizal Associations, *Journal of Geophysical Research: Biogeosciences*, 125, <https://doi.org/10.1029/2019JG005479>, 2020.
- Turco, R. P., Whitten, R. C., Toon, O. B., Pollack, J. B., and Hamill, P.: OCS, stratospheric aerosols and climate, *Nature*, 283, 283, <https://doi.org/10.1038/283283a0>, 1980.
- Tyc, O., Song, C., Dickschat, J. S., Vos, M., and Garbeva, P.: The ecological role of volatile and soluble secondary metabolites produced by soil bacteria, *Trends Microbiol.*, 25, 280–292, <https://doi.org/10.1016/j.tim.2016.12.002>, 2017.
- Umbarger, H. E.: Amino acid biosynthesis and its regulation, *Annu. Rev. Biochem.*, 47, 533–606, 1987.
- Vallina, S. M. and Simo, R.: Strong relationship between DMS and the solar radiation dose over the global surface ocean, *Science*, 315, 506–508, <https://doi.org/10.1126/science.1133680>, 2007.
- van Alstyne, K. L., Dominique, V. J., and Müller-Parker, G.: Is dimethylsulfoniopropionate (DMSP) produced by the symbionts or the host in an anemone–zooxanthella symbiosis?, *Coral Reefs*, 28, 167–176, <https://doi.org/10.1007/s00338-008-0443-y>, 2008.
- van den Bosch, P. L., de Graaff, M., Fortuny-Picornell, M., van Leerdam, R. C., and Janssen, A. J.: Inhibition of microbiological sulfide oxidation by methanethiol and dimethyl polysulfides at natron-alkaline conditions, *Appl. Microbiol. Biotechnol.*, 83, 579–587, <https://doi.org/10.1007/s00253-009-1951-6>, 2009.
- van der Maarel, M. J. E. C. and Hansen, T. A.: Dimethylsulfoniopropionate in anoxic intertidal sediments: a precursor of methanogenesis via dimethyl sulfide, methanethiol, and methiolpropionate, *Marine Geol.*, 137, 5–12, [https://doi.org/10.1016/S0025-3227\(96\)00074-6](https://doi.org/10.1016/S0025-3227(96)00074-6), 1997.
- van Leerdam, R. C., de Bok, F. A., Lomans, B. P., Stams, A. J., Lens, P. N., and Janssen, A. J.: Volatile organic sulfur compounds in anaerobic sludge and sediments: biodegradation and toxicity, *Environ. Toxicol. Chem.*, 25, 3101–3109, <https://doi.org/10.1897/06-106R.1>, 2006.
- van Schaik, L., Palm, J., Klaus, J., Zehe, E., and Schröder, B.: Linking spatial earthworm distribution to macropore numbers and hydrological effectiveness, *Ecohydrology*, 7, 401–408, <https://doi.org/10.1002/eco.1358>, 2014.

- Veres, P. R., Behrendt, T., Klapthor, A., Meixner, F. X., and Williams, J.: Volatile Organic Compound emissions from soil: using Proton-Transfer-Reaction Time-of-Flight Mass Spectrometry (PTR-TOF-MS) for the real time observation of microbial processes, *Biogeosci. Discuss.*, 11, 12 009–12 038, <https://doi.org/10.5194/bgd-11-12009-2014>, 2014.
- Vettikkat, L., Sinha, V., Datta, S., Kumar, A., Hakkim, H., Yadav, P., and Sinha, B.: Significant emissions of dimethyl sulfide and monoterpenes by big-leaf mahogany trees: discovery of a missing dimethyl sulfide source to the atmospheric environment, *Atmos. Chem. Phys.*, 20, 375–389, <https://doi.org/10.5194/acp-20-375-2020>, 2020.
- Viros, J., Fernandez, C., Wortham, H., Gavinet, J., Lecareux, C., Ormeño, E., J, V., C, F., H, W., J, G., C, L., and E, O.: Litter of mediterranean species as a source of volatile organic compounds, *Atmos. Environ.*, 242, 117 815, <https://doi.org/10.1016/j.atmosenv.2020.117815>, 2020.
- Visscher, P. T. and Taylor, B. F.: A new mechanism for the aerobic catabolism of dimethyl sulfide, *Appl. Environ. Microbiol.*, 59, 3784–3789, 1993.
- Visscher, P. T., Taylor, B. F., and Kiene, R. P.: Microbial consumption of dimethyl sulfide and methanethiol in coastal marine sediments, *FEMS Microbiol. Ecol.*, 18, 145–153, <https://doi.org/10.1111/j.1574-6941.1995.tb00172.x>, 1995.
- Visscher, P. T., Baumgartner, L. K., Buckley, D. H., Rogers, D. R., Hogan, M. E., Raleigh, C. D., Turk, K. A., and Des Marais, D. J.: Dimethyl sulphide and methanethiol formation in microbial mats: potential pathways for biogenic signatures, *Environ. Microbiol.*, 5, 296–308, <https://doi.org/10.1046/j.1462-2920.2003.00418.x>, 2003.
- Wagner, C., Lusty, S. M., Kung, H.-F., and Rogers, N. L.: Preparations and properties of trimethylsulfonium tetrahydrofolate methyltransferase, *J. Biol. Chem.*, 242, 1287–1293, 1967.
- Wallington, T. J., Ellermann, T., and Nielsen, O. J.: Atmospheric chemistry of dimethyl sulfide: UV spectra and self-reaction kinetics of CH_3SCH_2 and $\text{CH}_3\text{SCH}_2\text{O}_2$ radicals and kinetics of the reactions $\text{CH}_3\text{SCH}_2 + \text{O}_2 \rightarrow \text{CH}_3\text{SCH}_2\text{O}_2$ and $\text{CH}_3\text{SCH}_2\text{O}_2 + \text{NO} \rightarrow \text{CH}_3\text{SCH}_2\text{O} + \text{NO}_2$, *J. Phys. Chem.*, 97, 8442–8449, <https://doi.org/10.1021/j100134a013>, 1993.
- Wang, B., Sivret, E. C., Parsci, G., and Stuetz, R. M.: Determination of VOSCs in sewer headspace air using TD-GC-SCD, *Talanta*, 137, 71–79, <https://doi.org/10.1016/j.talanta.2014.11.072>, 2015.
- Wang, J. and Wang, J.: *Spartina alterniflora* alters ecosystem DMS and CH_4 emissions and their relationship along interacting tidal and vegetation gradients within a coastal salt marsh in Eastern China, *Atmos. Environ.*, 167, 346–359, <https://doi.org/10.1016/j.atmosenv.2017.08.041>, 2017.
- Warneck, P. and Williams, J.: *The Atmospheric Chemist's Companion*, Springer, Dordrecht, 2012.
- Watts, S. F.: The mass budgets of carbonyl sulfide, dimethyl sulfide, carbon disulfide and hydrogen sulfide, *Atmos. Environ.*, 34, 761–779, [https://doi.org/10.1016/S1352-2310\(99\)00342-8](https://doi.org/10.1016/S1352-2310(99)00342-8), 2000.

- Wedler, G. and Freund, H.-J.: Lehrbuch der physikalischen Chemie, John Wiley & Sons, 2012.
- Wei, T. and Simko, V.: R package "corrplot": Visualization of a Correlation Matrix, URL <https://github.com/taiyun/corrplot>, 2017.
- Weißbecker, C., Schnabel, B., and Heintz-Buschart, A.: Dadasnake, a Snakemake implementation of DADA2 to process amplicon sequencing data for microbial ecology, *GigaScience*, 9, <https://doi.org/10.1093/gigascience/giaa135>, 2020.
- Werner, S., Polle, A., and Brinkmann, N.: Belowground communication: impacts of volatile organic compounds (VOCs) from soil fungi on other soil-inhabiting organisms, *Appl. Microbiol. Biotech.*, 100, 8651–8665, <https://doi.org/10.1007/s00253-016-7792-1>, 2016.
- Wester-Larsen, L., Kramshøj, M., Albers, C. N., and Rinnan, R.: Biogenic volatile organic compounds in arctic soil: A field study of concentrations and variability with vegetation cover, *J. Geophys. Res. Biogeosci.*, 125, <https://doi.org/10.1029/2019jg005551>, 2020.
- Wheatley, R., Hackett, C., Bruce, A., and Kundzewicz, A.: Effect of substrate composition on production of volatile organic compounds from *Trichoderma* spp. Inhibitory to wood decay fungi, *Int. Biodeterior. Biodegrad.*, 39, 199–205, [https://doi.org/10.1016/S0964-8305\(97\)00015-2](https://doi.org/10.1016/S0964-8305(97)00015-2), 1997.
- Whelan, M. E. and Rhew, R. C.: Reduced sulfur trace gas exchange between a seasonally dry grassland and the atmosphere, *Biogeochemistry*, 128, 267–280, <https://doi.org/10.1007/s10533-016-0207-7>, 2016.
- Whelan, M. E., Lennartz, S. T., Gimeno, T. E., Wehr, R., Wohlfahrt, G., Wang, Y., Kooijmans, L. M. J., Hilton, T. W., Belviso, S., Peylin, P., Commane, R., Sun, W., Chen, H., Le Kuai, Mammarella, I., Maseyk, K., Berkelhammer, M., Li, K.-F., Yakir, D., Zumkehr, A., Katayama, Y., Ogée, J., Spielmann, F. M., Kitz, F., Rastogi, B., Kesselmeier, J., Marshall, J., Erkkilä, K.-M., Wingate, L., Meredith, L. K., He, W., Bunk, R., Launois, T., Vesala, T., Schmidt, J. A., Fichot, C. G., Seibt, U., Saleska, S., Saltzman, E. S., Montzka, S. A., Berry, J. A., and Campbell, J. E.: Reviews and syntheses: Carbonyl sulfide as a multi-scale tracer for carbon and water cycles, *Biogeosciences*, 15, 3625–3657, <https://doi.org/10.5194/bg-15-3625-2018>, 2018.
- White, R. H.: Analysis of dimethyl sulfonium compounds in marine algae, *J. Marine Res.*, 40, 529–536, 1981.
- White, T. J., Bruns, T., Lee, S., and Taylor, J.: Amplification and direct sequencing of fungal ribosomal RNA genes for phylogenetics, in: *PCR Protocols: A Guide to Methods and Applications*, edited by Innis, M. A., Gelfand, D. H., Sninsky, J. J., and White, T. J., pp. 315–322, Elsevier, New York, <https://doi.org/10.1016/B978-0-12-372180-8.50042-1>, 1990.
- Wickham, H., Averick, M., Bryan, J., Chang, W., McGowan, L., François, R., Grolemond, G., Hayes, A., Henry, L., Hester, J., Kuhn, M., Pedersen, T., Miller, E., Bache, S., Müller, K., Ooms, J., Robinson,

- D., Seidel, D., Spinu, V., Takahashi, K., Vaughan, D., Wilke, C., Woo, K., and Yutani, H.: Welcome to the Tidyverse, *J. Open Source Softw.*, 4, 1686, <https://doi.org/10.21105/joss.01686>, 2019.
- Wilkening, J. V., Turchyn, A. V., Redeker, K. R., Mills, J. V., Antler, G., Carrión, O., and Todd, J. D.: The production and fate of volatile organosulfur compounds in sulfidic and ferruginous sediment, *J. Geophys. Res. Biogeosci.*, 124, 3390–3402, <https://doi.org/10.1029/2019JG005248>, 2019.
- Williams, B. T., Cowles, K., Bermejo Martinez, A., Curson, A. R. J., Zheng, Y., Liu, J., Newton-Payne, S., Hind, A. J., Li, C. Y., Rivera, P. P. L., Carrion, O., Spurgin, L. G., Brearley, C. A., Mackenzie, B. W., Pinchbeck, B. J., Peng, M., Pratscher, J., Zhang, X. H., Zhang, Y. Z., Murrell, J. C., and Todd, J. D.: Bacteria are important dimethylsulfoniopropionate producers in coastal sediments, *Nat. Microbiol.*, <https://doi.org/10.1038/s41564-019-0527-1>, 2019.
- Wisthaler, A., Jensen, N. R., Winterhalter, R., Lindinger, W., and Hjorth, J.: Measurements of acetone and other gas phase product yields from the OH-initiated oxidation of terpenes by proton-transfer-reaction mass spectrometry (PTR-MS), *Atmos. Environ.*, 35, 6181–6191, [https://doi.org/10.1016/S1352-2310\(01\)00385-5](https://doi.org/10.1016/S1352-2310(01)00385-5), 2001.
- Wojnarowska, M. and Sawoszczuk, T.: The assessment of the Voice 200Ultra apparatus applicability to field investigations of air quality and odours, *Environ. Impact Assess. Rev.*, 85, 106–160, <https://doi.org/10.1016/j.eiar.2020.106460>, URL <http://www.sciencedirect.com/science/article/pii/S0195925520303851>, 2020.
- Wongkittichote, P., Ah Mew, N., and Chapman, K. A.: Propionyl-CoA carboxylase - A review, *Mol. Genet. Metab.*, 122, 145–152, <https://doi.org/10.1016/j.ymgme.2017.10.002>, 2017.
- Xin, X.-F. and He, S. Y.: *Pseudomonas syringae* pv. *tomato* DC3000: a model pathogen for probing disease susceptibility and hormone signaling in plants, *Annu. Rev. Phytopathol.*, 51, 473–498, <https://doi.org/10.1146/annurev-phyto-082712-102321>, 2013.
- Yamagiwa, Y., Inagaki, Y., Ichinose, Y., Toyoda, K., Hyakumachi, M., and Shiraishi, T.: *Talaromyces wortmannii* FS2 emits beta-caryophyllene, which promotes plant growth and induces resistance, *J. Gen. Plant Pathol.*, 77, 336–341, <https://doi.org/10.1007/s10327-011-0340-z>, 2011.
- Yanagida, F., Chen, Y.-s., and Shinohara, T.: Searching for bacteriocin-producing lactic acid bacteria in soil, *J. Gen. Microbiol.*, 52, 21–28, <https://doi.org/10.2323/jgam.52.21>, 2006.
- Yáñez-Serrano, A. M., Nölscher, A. C., Williams, J., Wolff, S., Alves, E., Martins, G. A., Bourtsoukidis, E., Brito, J., Jardine, K., Artaxo, P., and Kesselmeier, J.: Diel and seasonal changes of biogenic volatile organic compounds within and above an Amazonian rainforest, *Atmos. Chem. Phys.*, 15, 3359–3378, <https://doi.org/10.5194/acp-15-3359-2015>, 2015.
- Yang, L., Stulen, I., and de Kok, L. J.: Impact of sulfate nutrition on the utilization of atmospheric SO₂ as sulfur source for Chinese cabbage, *J. Plant Nutr. Soil Sci.*, 169, 529–534, <https://doi.org/10.1002/jpln.200520574>, 2006.

- Yang, Z., Haneklaus, S., de Kok, L. J., Schnug, E., and Singh, B. R.: Effect of H₂S and dimethyl sulfide (DMS) on growth and enzymatic activities of *Rhizoctonia solani* and its implications for sulfur-induced resistance (SIR) of agricultural crops, in: *Phyton-Annales rei botanicae*, pp. 55–70.
- Yang, Z., Kong, L., Zhang, J., Wang, L., and Xi, S.: Emission of biogenic sulfur gases from Chinese rice paddies, *Sci. Tot. Environ.*, 224, 1–8, [https://doi.org/10.1016/S0048-9697\(98\)00207-1](https://doi.org/10.1016/S0048-9697(98)00207-1), 1998.
- Yi, Z., Wang, X., Ouyang, M., Zhang, D., and Zhou, G.: Air-soil exchange of dimethyl sulfide, carbon disulfide, and dimethyl disulfide in three subtropical forests in south China, *J. Geophys. Res.: Atmos.*, 115, <https://doi.org/10.1029/2010JD014130>, 2010.
- Zannoni, N., Leppla, D., Lembo Silveira de Assis, P. I., Hoffmann, T., Sá, M., Araújo, A., and Williams, J.: Surprising chiral composition changes over the Amazon rainforest with height, time and season, *Commun. Earth Environ.*, 1, <https://doi.org/10.1038/s43247-020-0007-9>, 2020.
- Zhang, Q.-H., Song, L.-W., Ma, J.-H., Han, F.-Z., and Sun, J.-H.: Aggregation pheromone of a newly described spruce bark beetle, *Ips shangrila* Cognato and Sun, from China, *Chemoecology*, 19, 203–210, <https://doi.org/10.1007/s00049-009-0026-6>, 2009.
- Zhang, Y., Liang, Z., Tang, C., Liao, W., Yu, Y., Li, G., Yang, Y., and An, T.: Malodorous gases production from food wastes decomposition by indigenous microorganisms, *Sci Total Environ*, 717, 137 175, <https://doi.org/10.1016/j.scitotenv.2020.137175>, 2020.
- Zhao, J., Wang, Z., Wu, T., Wang, X., and Dai, W.: Volatile organic compound emissions from straw-amended agricultural soils and their relations to bacterial communities: A laboratory study, *J. Environ. Sci.*, 45, 257–269, <https://doi.org/10.1016/j.jes.2015.12.036>, 2016.
- Zhao, T., Axelsson, K., Krokene, P., and Borg-Karlson, A. K.: Fungal Symbionts of the Spruce Bark Beetle Synthesize the Beetle Aggregation Pheromone 2-Methyl-3-buten-2-ol, *J. Chem. Ecol.*, 41, 848–852, <https://doi.org/10.1007/s10886-015-0617-3>, 2015.
- Zhao, Z., Dai, J., Wang, T., Niu, G., He, F., and Duan, Y.: Development of microwave plasma proton transfer reaction mass spectrometry (MWP-PTR-MS) for on-line monitoring of volatile organic compounds: Design, characterization and performance evaluation, *Talanta*, 208, 120 468, <https://doi.org/10.1016/j.talanta.2019.120468>, 2020.
- Zhou, T., Wang, C., and Zhou, Z.: Impacts of forest thinning on soil microbial community structure and extracellular enzyme activities: A global meta-analysis, *Soil Biol. Biochem.*, 149, 107 915, <https://doi.org/10.1016/j.soilbio.2020.107915>, 2020.
- Zhu, J., Bean, H. D., Kuo, Y.-M., and Hill, J. E.: Fast detection of volatile organic compounds from bacterial cultures by secondary electrospray ionization-mass spectrometry, *J. Clin. Microbiol.*, 48, 4426–4431, <https://doi.org/10.1128/JCM.00392-10>, 2010.

Zinder, S. H. and Brock, T. D.: Production of methane and carbon dioxide from methane thiol and dimethyl sulphide by anaerobic lake sediments, *Nature*, 273, 226–228, <https://doi.org/10.1038/273226a0>, 1978.

Zinder, S. H., Doemel, W. N., and Brock, T. D.: Production of volatile sulfur compounds during the decomposition of algal mats, *Appl. Env. Microbiol.*, 34, 859–860, 1977.

Zuur, A. F., Ieno, E., Walker, N. J., Saveliev, A. A., and Smith, G. M.: Mixed effects models and extensions in ecology with R, *Statistics for Biology and Health*, Springer, New York, 2009.

Acknowledgements

My biggest *Thank You* goes to both of you, Susan and Georg. Not only for trusting me and giving me my PhD position, but for your constant support during the last three years. You gave me the freedom to take my own decisions - to develop my own research question, do my own experiments, and write my own papers. Yet you were always there when I needed you, both emotionally and with your amazing insights into science. You helped me focus and cut my research plans to a realistic level, but also to trust my own results and their implications, and to communicate them well. When I came to you to talk about what I need in supervision, you were understanding and adjusted to my needs. Without your amazing supervision, I would not have been able to grow as much as I did during my thesis.

The same is true for my daily supervisors, Thomas, Alex, and Eliane. Thomas, thank you for helping me to start off. You taught me how to handle gases, measure soil emissions, and develop my setup. You helped me broaden my views on VOC science and possible experiments, and guided me towards my first results. Alex, thank you so much for your support when Thomas decided to leave and I had to reconsider my PhD project. You taught me how to do meaningful soil experiments. Your pragmatic way of thinking together with your experience in VOCs from soils enabled me to skip a lot of detours I might otherwise have taken. And Eliane, thank you so much for our creative discussions during the paper club meetings and our experiments together. You helped me out and gave your feedback whenever I needed it, but trusted me and my work. By involving me in the paper discussion with Deborah and you and the litter degradation experiment with you, Witoon and the others, you gave me a sense of community and actually working together. Plus, you organized what would have been the most amazing research stay without Corona.

Thank you, Erica, for collaborating with me on the isoprene/MBO separation project, and you, Becca, for collaborating on the VSC project. I really enjoyed working and doing field trips with you and learning about your different perspectives on our joint research. Thank you Witoon, Benjawan, and Dr. Schulze for inviting me to join the litter degradation project and the plastic degradation projects. Without your planning, this huge study would not have been possible. Field trips with you all were always fun.

Thank you Rebecca for being my master student. I really enjoyed working with you - it was super-nice to have someone as well-spirited, motivated and hardworking as you to work on my project. The same is true for you, Júlia, Xinyue, and Eric, thank you! Thank you Cornelius, for your long-term and outstanding work as a Hiwi. Not only did you get a lot of things done that sped up my progress by a lot, but going on field trips with you was supereasy and I really enjoyed your company. Thanks to Hasan and Lara for your occasional help as Hiwis as well.

Thank you Martin, Karl, Agnes, Hannes, and Iris for helping me out in the lab. Martin, Karl, you built a lot of my equipment and taught me how to use it. Agnes, you taught me how to do meaningful plant experiments. Hannes and Iris, without you as my premier source of where I can find this and that and how I can do this and that extraction, I would have had a much harder time around the MPI and the uni. Thanks to you, and your Hiwis, Iris, for doing the plant sample preparation for me. Thanks to the central facility labs, RoMA, the SpecLab, the IsoLab, and the Field Experiments and Instrumentation group for measuring samples with element contents, inorganic ions, and isotope signals. Without all of you, my experiments would not have been as successful as they were. Thanks to the CRC 1076 AquaDiva and the Max Planck Society for providing the funding of the thesis. I also really want to thank the Max Planck Society for their Open Access Initiative. I could publish all my papers Open Access without any problem. Accessibility of scientific research is so important for diminishing equality and enabling everyone to get the information they seek, so I really appreciate this initiative.

Thank you Sabrina, Uta, Annett, Carsten, Simon, Alice, and Akanksha for sharing lunch breaks and offices with me, helping me out in soil science and DOM Metabolomics as well as general PhD-related questions, the Corona Christmas Party online games, and just chatting about all sorts of non-Science-related stuff. Thanks to all fellow PhDs, postdocs and technicians I had the pleasure to work with at the institute. You really made me feel welcome by your genuine interest in me as a person and helped me out tons of times with my questions.

Thank you Arite, Marcel, Marine, Nils, Franzi, Kathleen, Carlos, Simona, Emilio, Remington, Daniel, Lydia, Stefan, Michiel, Gianmaria, Mona, Kristy, Yun, Christian, Justus, Cristina, Nico, David, Hans, Marine, Chuner, Lu, Tim, Johanna, Ioannis, Marino, Thomas, Sarah for a great time at the Pohnert Lab. Even though I was only there every once in a while, it always felt like I was part of the group. Thank you for the most amazing lunch and coffee breaks, office and lab discussions, hat-crafting sessions, pen and paper evenings, waffle breakfasts, cake afternoons, group seminars, group outings, and retreats, and your genuine interest and help for my research problems and daily life.

Thanks to Steffi, Stefanie and John for being the life and soul of the IMPRS. Whenever I had a question or a problem, I could come to you and talk about it. Thanks to my fellow PhD reps, Gan, Martijn, Tina, Jasper, Santiago, Nora, Sophie, Shane, Ingrid, Katharina and Eldho. You organized so much for us PhDs and working with you was really nice. We got more more vacation and a pay raise, more relaxed rules for the research stay during the pandemic, the expectation alignment sheet, a high turnout at the N3 questionnaire, successful summer parties, retreats, bar evenings and hikes.

Veit, I don't even know where to start. Being able to share my life with you is such a wonderful experience. Your calm, happy, down-to-earth, one-step-at-a-time attitude helped me so much during the smaller and bigger crises in my PhD. You laugh with me when I need a laugh, and hold me tight when I need to cry. You show me the wonder of the simple things, the garden, self-grown food and mushrooms, hiking, cycling, and canoeing tours, an icecream on a warm summer night. You are always in for adventures, be it sleeping in the garden, paragliding or diving. Even now that we are both stuck in home office together, there is harmony and good spirit, and good food and making

ourselves a good time. Living with you is so easy, lightweight, relaxed. Thank you for being in my life. I love you.

One last big thank you goes to my friends and family, for your being there for me and supporting me always. Stefan, Gabi, Justus, Charlotte, Else, Gertrud, you know myself best. Not only did you support me financially during my studies, you also lived through the good and the bad times with me, and were always there for me when I needed you. You trust in me and made me have faith in myself, showing me my potential and watching me grow. I owe a lot to you, thank you so much for everything you have done! Milena, Chiara, Johannes, whenever I need to talk, you are just one phone call away. You really understand my feelings, so we can share deep conversations about life, the universe, and everything. Thank you! Thank you Mona, Lars, Erik, Maria, Marlene, Max, Verena, Timo, Annika, and Paul for making my life here in Jena so enjoyable. The busy evenings at Steinheid and in Paradise park with a lot of fun and laughter and sometimes lighter and sometimes deeper conversations, the hikes, the frisbee and boardgame evenings, the barbecues, and the singing. Thank you Anne, for listening to me and enabling me to learn so much about myself.

SDG.

Curriculum vitae

Education and Professional Experience

- Since 2017 **PhD researcher**
Prof. Dr. Susan E. Trumbore, Max Planck Institute for Biogeochemistry
Prof. Dr. Georg Pohnert, Friedrich Schiller University, Jena
International Max Planck Research School for Global Biogeochemical Cycles
- 2015-2017 **Chemistry M. Sc.**, Friedrich Schiller University, Jena
Thesis: Study on the transformation of organic matter in leachate by microbes *via* Metabolomics methods, Prof. Dr. Georg Pohnert
- 2015-2016 **Study Exchange**, Queen's University, Kingston ON, Canada
- 2012-2015 **Chemistry B. Sc.**, Friedrich Schiller University, Jena
Thesis: Photoinduced ligand dissociation of ruthenium-polypyridine complexes and their interaction with DNA, Prof. Dr. Benjamin Dietzek
- 2012 **Civil service** (Bundesfreiwilligendienst) as a lab assistant at the Landesanstalt für Umwelt, Messungen und Naturschutz Baden Württemberg
- 2011 **Au Pair** in Valencia, Spain
- 2011 **Abitur**, St. Dominikus-Gymnasium Karlsruhe

Awards and Scholarships

- 2017 exams price in chemistry at Friedrich Schiller University, Jena
- 2015-2016 Scholarship of the Transatlantic Science Student Exchange Program
- 2014-2017 Scholarship of the German Academic Scholarship Foundation
- 2012-2017 Scholarship of the Cusanuswerk e.V.

Teaching

- 2017-2020 Supervision of 1 master thesis, 5 research projects (F-Praktikum) and (co-) supervision of 3 student helpers (HiWi)
- 2018-2020 Teaching of seminar on IR spectroscopy in BC 3.4 Analytical Chemistry I at Friedrich Schiller University, Jena
- 2017-2020 Teaching of Ballett Revolution and Classical Ballett sports courses at the university sports of the Friedrich Schiller University, Jena
- 2017 Teaching of Metabolomics Data Evaluation Session in Phycomorph COST-Action Workshop Crossing the kingdoms: Macroalgae-Bacteria Interactions

Scientific Publications and Presentations

- **Lehnert, A.-S.**, Behrendt, T., Ruecker, A., Pohnert, G., Trumbore, S. E.: SIFT-MS optimization for atmospheric trace gas measurements at varying humidity, *Atmospheric Measurement Techniques*, 13, 3507-3520, <https://doi.org/10.5194/amt-13-3507-2020>, 2020.
- **Lehnert, A.-S.**, Perreca, E., Gershenson, J., Pohnert, G., Trumbore, S. E.: Simultaneous Real-Time Measurement of Isoprene and 2-Methyl-3-Buten-2-ol Emissions from Trees Using SIFT-MS, *Frontiers in Plant Science*, 11, 1867, <https://doi.org/10.3389/fpls.2020.578204>, 2020.
- **Lehnert, A.-S.**, Cooper, R., Ignatz, R., Ruecker, A., Gomes-Alves, E., Küsel, K., Pohnert, G., Trumbore, S. E.: Dimethyl sulfide originates from organic matter degradation in freshwater wetlands, and scarcely from sulfate reduction, *submitted*, 2021.
- Tanunchai, B., Juncheed, K., Wahdan, S. F. M., Guliyev, V., **Lehnert, A.-S.**, Gomes-Alves, E., Schädler, M., Glaser, B., Heintz-Buschart, A., Buscot, F., Noll, M., Blagodatskaya, E., Purahong, W.: The light and dark sides of bio-based and biodegradable plastics in soil systems, *submitted*, 2021.
- **Lehnert, A.-S.**, Cooper, R., Ignatz, R., Ruecker, A., Gomes-Alves, E., Küsel, K., Pohnert, G., Trumbore, S. E.: Biogeochemical pathways to reduced volatile sulfur compounds, Oral Presentation, European SIFT-MS User Meeting, 2020.
- **Lehnert, A.-S.**, Behrendt, T., Ruecker, A., Pohnert, G., Trumbore, S. E.: Sensitivity improvement of SIFT-MS for soil VOSC emission studies, Oral Presentation, Advances in applications of SIFT-MS, 2019.
- **Lehnert, A.-S.**, Ruecker, A., Trumbore, S. E., Pohnert, G., Behrendt, T.: Improved monitoring of Volatile Organic Compounds using SIFT-MS, Poster Presentation, 21st Spring Meeting of the German Young Chemist's Association, 2019.
- **Lehnert, A.-S.**, Ruecker, A., Trumbore, S. E., Pohnert, G., Behrendt, T.: Improved monitoring of Volatile Organic Compounds using SIFT-MS, Poster Presentation, Earth System PhD Conference, 2019.
- **Lehnert, A.-S.**, Ueberschaar, N., Baumeister, T., Pohnert, G.: Microbial Transformation of Organic Components in Seepage Water, Poster Presentation, EMBL Summer School Microbial Geobiology, 2018.

Licenses

Figure 1.2 Reprinted from Hammerbacher et al. (2019) with permission of John Wiley and Sons, by Copyright Clearance Center (Licence # 4971911463816).

Figure 1.5 Adapted from Moran and Durham (2019) with permission of Springer Nature, by Copyright Clearance Center (License # 5037210541589)

Figure 1.6 Reprinted from Lehnert et al. (2020a) under the rights of the CC-BY 4.0 license.

Table 1.1 Adapted from Watts (2000) with permission of Elsevier, by Copyright Clearance Center (License # 4979291109555).

Table 1.2 Adapted from Warneck and Williams (2012) with permission of Springer, by Copyright Clearance Center (License # 1087537-1).

Publication 1 Reprinted from (Lehnert et al., 2020a) in Atmospheric Measurement Techniques under the rights of the CC-BY 4.0 license (https://www.atmospheric-measurement-techniques.net/policies/licence_and_copyright.html, last access 02.01.2021)

Publication 2 Reprinted from (Lehnert et al., 2020b) in Frontiers in Plant Sciences under the rights of the CC-BY 4.0 license (<https://www.frontiersin.org/journals/plant-science/sections/technical-advances-in-plant-science#about>, last access 02.01.2021)

Publikationsäquivalente

Publikation 1: Lehnert, A.-S., Behrendt, T., Ruecker, A., Pohnert, G., and Trumbore, S. E.: SIFT-MS optimization for atmospheric trace gas measurements at varying humidity, Atmospheric Measurement Techniques 13, 3507-3520, 2020.

	ASL	TB	AR	GP	SET
Konzeption des Forschungsansatzes	X	X		X	
Planung der Untersuchungen	X				
Datenerhebung	X				
Datenanalyse und -interpretation	X				
Schreiben des Manuskripts	X	X	X	X	X
Vorschlag Anrechnung Publikationsäquivalente	1.0				

Publikation 2: Lehnert, A.-S.*, Perreca, E.*, Gershenzon, J., Pohnert, G., Trumbore, S. E.: Simultaneous real-time measurement of isoprene and 2-methyl-3-buten-2-ol emissions from trees using SIFT-MS, Frontiers in Plant Science, 11, 1867, 2020.

	ASL	EP	JG	GP	SET
Konzeption des Forschungsansatzes	X	X			
Planung der Untersuchungen ⁺	X	X			
Datenerhebung ⁺	X	X			
Datenanalyse und -interpretation ⁺	X	X			
Schreiben des Manuskripts ⁺	X	X	X	X	X
Vorschlag Anrechnung Publikationsäquivalente	1.0	1.0			

* Diese Autorinnen haben in gleichen Anteilen zur Publikation beigetragen.

⁺ ASL hat die Planung, Datenerhebung und -analyse für die Messung der analytischen Standards die Methodvalidierung durchgeführt, für die Experimente an Pflanzen haben ASL und EP sich diese Aufgaben geteilt.

Publikation 3: Lehnert, A.-S., Cooper, R., Ignatz, R., Ruecker, A., Gomes-Alves, E., Küsel, K., Pohnert, G., Trumbore, S. E.: Dimethyl sulfide originates from organic matter degradation in freshwater wetlands, and scarcely from sulfate reduction, submitted to Environmental Science and Technology, 2021.

	ASL	RC	RI	AR	EGA	KK	GP	SET
Konzeption des Forschungsansatzes	X							
Planung der Untersuchungen*	X	X	X					
Datenerhebung*	X	X	X					
Datenanalyse und -interpretation*	X	X	X					
Schreiben des Manuskripts*	X	X	X	X	X	X	X	X
Vorschlag Anrechnung Publikationsäquivalente	1.0							

* RC hat die Analyse des Mikrobioms geplant, durchgeführt, teilweise analysiert, und im Manuskript beschrieben, RI die VOC-Emissionen in der Langzeitinkubation. ASL hat die restlichen Experimente (Austrocknungen, Manipulationen mit Schwefelsubstanzen, Labelling, Metabolomics der Schwefelverbindungen im Boden) sowie das Gesamtkonzept geplant, durchgeführt, analysiert und im Manuskript beschrieben.

Declarations

Selbstständigkeitserklärung

Ich erkläre, dass ich die vorliegende Arbeit selbständig und unter Verwendung der angegebenen Hilfsmittel, persönlichen Mitteilungen und Quellen angefertigt habe.

Ann-Sophie Lehnert		Jena	
Name der Promovendin	Datum	Ort	Unterschrift

Erklärung zu den Eigenanteilen der Promovendin sowie der weiteren Doktorand*innen als Co-Autor*innen an den Publikationen und Zweitpublikationsrechten bei einer kumulativen Dissertation

Für alle in dieser kumulativen Dissertation verwendeten Manuskripte liegen die notwendigen Genehmigungen der Verlage („Reprint permissions“) für die Zweitpublikation vor.

Die Co-Autor*innen der in dieser kumulativen Dissertation verwendeten Manuskripte sind sowohl über die Nutzung, als auch über die oben angegebenen Eigenanteile der weiteren Doktorand*innen als Co-Autor*innen an den Publikationen und Zweitpublikationsrechten bei einer kumulativen Dissertation informiert und stimmen dem zu.

Die Anteile der Promovendin sowie der weiteren Doktorand*innen als Co-Autor*innen an den Publikationen und Zweitpublikationsrechten bei einer kumulativen Dissertation sind in der Anlage aufgeführt.

Ann-Sophie Lehnert		Jena	
Name der Promovendin	Datum	Ort	Unterschrift

Ich bin mit der Abfassung der Dissertation als publikationsbasierte Dissertation, d.h. kumulativ, einverstanden und bestätige die vorstehenden Angaben.

Georg Pohnert

Name des Betreuers	Datum	Ort	Unterschrift
--------------------	-------	-----	--------------

Susan Trumbore

Name der Betreuerin	Datum	Ort	Unterschrift
---------------------	-------	-----	--------------

A. Supplement (Electronic)

Please find the supplemental data on the attached CD.

Supplement Table of Contents

A.1. VSC Emissions in Different Regions of the World	LVI
A.2. Supplement of P1: SIFT-MS Optimization for Atmospheric Trace Gas Measurements at Varying Humidity	XCVIII
A.3. Supplement of P2: Simultaneous Real-Time Measurement of Isoprene and 2-Methyl- 3-Buten-2-ol Emissions From Trees Using SIFT-MS	CXXXI
A.4. Supplement of P3: Dimethyl Sulfide Emissions from Freshwater Wetlands Result more from Organic Matter Degradation than Sulfate Reduction	CXXXVII
A.5. Litter VOC Emissions over Time	CCXXX

A.1. VSC Emissions in Different Regions of the World

Table A.1.: VSC emissions from plants according to literature.

species	part	location	T(°C)	measurement method	instrument	H ₂ S	MeSH	DMS	COS	CS ₂	DMDS	unit	source
<i>Brassica juncea</i>	leaf-amended sandy loam	Wellesbourne, UK	20	static chamber	SPME-GC-FID		200-1000	0-400		0-50	0-10	μmol/kg	(Bending and Lincoln, 1999)
<i>Brassica juncea</i>	leaf-amended clay loam	Wellesbourne, UK	20	static chamber	SPME-GC-FID		50-500	0-150		0-150	0-10	μmol/kg	(Bending and Lincoln, 1999)
Soybeans	whole	USA	27-53	dynamic chamber, VOC-free	mobile GC-FPD	690		1150	-575			μmol/kg/a	(Goldan et al., 1987)
Oats	whole	USA	30-40	dynamic chamber, VOC-free	mobile GC-FPD	164		707	-82.2			μmol/kg/a	(Goldan et al., 1987)
Orchard grass	whole soil	+ USA	27-31	dynamic chamber, VOC-free	mobile GC-FPD	164		247	-493			μmol/kg/a	(Goldan et al., 1987)
Purple clover	whole soil	+ USA	32-36	dynamic chamber, VOC-free	mobile GC-FPD	822		214	-214			μmol/kg/a	(Goldan et al., 1987)
Corn	whole	USA	44377	dynamic chamber, VOC-free	mobile GC-FPD	526		8550	0			μmol/kg/a	(Goldan et al., 1987)
Mahogany (<i>Swietenia macrophylla</i> King)- summer	branch	Northwestern Indo-Gangetic Plain	30-40	branch enclosure chamber, VOC-free	PTR-MS			2.7±2.7				μmol/kg/a	(Vettikkat et al., 2020)
Mahogany (<i>Swietenia macrophylla</i> King) - Monsoon	branch	Northwestern Indo-Gangetic Plain	22-38	branch enclosure chamber, VOC-free	PTR-MS			2.4±2.4				μmol/kg/a	(Vettikkat et al., 2020)

species	part	location	T(°C)	measurement method	instrument	H ₂ S	MeSH	DMS	COS	CS ₂	DMDS	unit	source
Mahogany (<i>Swietenia macrophylla</i> King) - Post-Monsoon	branch	Northwestern Indo-Gangetic Plain	14-28	branch enclosure chamber, VOC-free	PTR-MS			2.7±3.1				μmol/kg/a	(Vettikkat et al., 2020)
Mahogany (<i>Swietenia macrophylla</i> King) - Winter	branch	Northwestern Indo-Gangetic Plain	5-30	branch enclosure chamber, VOC-free	PTR-MS			0.41±0.60				μmol/kg/a	(Vettikkat et al., 2020)
Norway spruce	seedling	lab	20	dynamic chamber, VOC-free	photometric	0.571						μmol/kg/a	(Spálený, 1977)
oat grass	whole (over soil)	Ames, Iowa, USA	25.5	dynamic chamber, VOC-free	mobile GC-FPD	49 ± 16		102 ± 56	32 ± 13	9.9 ± 3.3		μmol/m ² /a	(Goldan et al., 1987)
gramma gras	whole (over soil)	Ames, Iowa, USA	25.5	dynamic chamber, VOC-free	mobile GC-FPD	38 ± 13		58 ± 16	29 ± 10	6.6 ± 3.3		μmol/m ² /a	(Goldan et al., 1987)
soy plants	whole (over soil)	Ames, Iowa, USA	25.5	dynamic chamber, VOC-free	mobile GC-FPD	16 ± 7		87 ± 48	12 ± 5	8.2 ± 3.3		μmol/m ² /a	(Goldan et al., 1987)
Purple clover	whole (over soil)	Celeryville, Ohio, USA	22	dynamic chamber, VOC-free	mobile GC-FPD	110 ± 25		123 ± 25	20 ± 5	20 ± 2		μmol/m ² /a	(Goldan et al., 1987)
Orchard grass	whole (over soil)	Celeryville, Ohio, USA	22	dynamic chamber, VOC-free	mobile GC-FPD	112 ± 13		44 ± 6	36 ± 7	23 ± 7		μmol/m ² /a	(Goldan et al., 1987)
"Quack" grass	whole (over soil)	Celeryville, Ohio, USA	22	dynamic chamber, VOC-free	mobile GC-FPD	16 ± 7		87 ± 48	12 ± 5	8.2 ± 3.3		μmol/m ² /a	(Goldan et al., 1987)
<i>Alpinia zerumbet</i>	branch	Biosphere2 Mesocosm, Oracle, Arizona, USA	20-27	branch enclosure chamber, VOC-free?	PTR-MS			3.2				μmol/m ² /a	(Jardine et al., 2015)

species	part	location	T(°C)	measurement method	instrument	H ₂ S	MeSH	DMS	COS	CS ₂	DMDS	unit	source
<i>Canna indica</i> L.	branch	Biosphere2 Mesocosm, Oracle, Arizona, USA	20-27	branch enclosure chamber, VOC-free?	PTR-MS			5.3				μmol/ m ² /a	(Jardine et al., 2015)
<i>Cissus sicyodes</i>	branch	Biosphere2 Mesocosm, Oracle, Arizona, USA	20-27	branch enclosure chamber, VOC-free?	PTR-MS			5.3				μmol/ m ² /a	(Jardine et al., 2015)
<i>Hibiscus rosa-sinensis</i> L.	branch	Biosphere2 Mesocosm, Oracle, Arizona, USA	20-27	branch enclosure chamber, VOC-free?	PTR-MS			3.2				μmol/ m ² /a	(Jardine et al., 2015)
<i>Inga vera</i> W.	branch	Biosphere2 Mesocosm, Oracle, Arizona, USA	20-27	branch enclosure chamber, VOC-free?	PTR-MS			2.6				μmol/ m ² /a	(Jardine et al., 2015)
<i>Mangifera indica</i>	branch	Biosphere2 Mesocosm, Oracle, Arizona, USA	20-27	branch enclosure chamber, VOC-free?	PTR-MS			3.2				μmol/ m ² /a	(Jardine et al., 2015)
<i>Pterocarpus Indicus</i> Wild.	branch	Biosphere2 Mesocosm, Oracle, Arizona, USA	20-27	branch enclosure chamber, VOC-free?	PTR-MS			2.6				μmol/ m ² /a	(Jardine et al., 2015)

Table A.2.: VSC emissions from salt marshes according to literature.

site specifics		location	T (°C)	measurement method	instrument	H ₂ S	MeSH	DMS	COS	CS ₂	DMDS	other	other	unit	source	
<i>Juncus romerianus</i>		tidally flooded marsh	Cedar land, North Carolina, USA	dynamic chamber, VOC-free	mobile GC-FPD								net avg flux	7070	μmol/m ² /a	(Goldan et al., 1987)
		marsh above high tide	Cedar land, North Carolina, USA	dynamic chamber, VOC-free	mobile GC-FPD								net avg flux	1970	μmol/m ² /a	(Goldan et al., 1987)
<i>Spartina terniflora</i>	<i>al-</i>	tidally flooded, low tide	Cedar land, North Carolina, USA	dynamic chamber, VOC-free	mobile GC-FPD	99-130	130-180	8200-16400							μmol/m ² /a	(Goldan et al., 1987)
		tidally flooded, high tide	Cedar land, North Carolina, USA	dynamic chamber, VOC-free	mobile GC-FPD	330-3300	66-99	8200							μmol/m ² /a	(Goldan et al., 1987)
salt sandy pool	water tidal	both tides	Cedar land, North Carolina, USA	dynamic chamber, VOC-free	mobile GC-FPD	49000-120000	660-1300	4900-5700							μmol/m ² /a	(Goldan et al., 1987)
<i>Spartina terniflora</i>	<i>al-</i>	flooded marsh	East USA?	static chamber							5300±900				μmol/m ² /a	(Dacey et al., 1987)
<i>Spartina terniflora</i>	<i>al-</i>	open surface marsh	East USA?	static chamber							2600±900				μmol/m ² /a	(Dacey et al., 1987)

site specifics	location	T (°C)	measurement method	instrument	H ₂ S	MeSH	DMS	COS	CS ₂	DMDS	other	other	unit	source
<i>Spartina alterniflora</i> salt marsh sediment	Flax Pond, New York, USA	22	static soil core incubation	headspace-GC-FID			260						μmol/m ² /a	(Kiene, 1988)
glutaraldehyde-killed <i>Spartina alterniflora</i> salt marsh sediment	Flax Pond, New York, USA	22	static soil core incubation	headspace-GC-FID			2500						μmol/m ² /a	(Kiene, 1988)
<i>Spartina alterniflora</i> salt marsh sediment	Flax Pond, New York, USA	22	static slurry incubation	headspace-GC-FID		0.36E6	-						μmol/m ³ /a	(Kiene, 1988)
<i>Spartina alterniflora</i> -invaded salt marsh	Min River Estuary, China	20	pore water	GC-FPD				20-120					μmol/m ³	(Tong et al., 2018)
native <i>Cyperus malaccensis</i> salt marsh	Min River Estuary, China	20	pore water	GC-FPD				20-80					μmol/m ³	(Tong et al., 2018)
<i>Spartina alterniflora</i> invaded coastal salt marsh	Yancheng Natural Reserve, Jiangsu, China		static chambers	GC-MS (cryofocusing)				(1.8±0.9)E6					μmol/m ³ /a	(Wang and Wang, 2017)
<i>Suaeda salsa</i> coastal salt marsh	Yancheng Natural Reserve, Jiangsu, China		static chambers	GC-MS (cryofocusing)				(0.3±0.1)E6					μmol/m ³ /a	(Wang and Wang, 2017)

site specifics		location	T (°C)	measurement method	instrument	H ₂ S	MeSH	DMS	COS	CS ₂	DMDS	other	other	unit	source
<i>Aeluropus lit-</i> <i>toralis</i> coastal salt marsh	August	Yancheng Natural Reserve, Jiangsu, China		static chambers	GC-MS (cryofo- cusing)				(0.4±0.3)E6					μmol/ m ³ /a	(Wang and Wang, 2017)
coastal salt marsh mudflat	August	Yancheng Natural Reserve, Jiangsu, China		static chambers	GC-MS (cryofo- cusing)				(0.6±0.4)E6					μmol/ m ³ /a	(Wang and Wang, 2017)
<i>Spartina al-</i> <i>terniflora</i> invaded coastal salt marsh	December	Yancheng Natural Reserve, Jiangsu, China		static chambers	GC-MS (cryofo- cusing)				(83±7)E6					μmol/ m ³ /a	(Wang and Wang, 2017)
<i>Suaeda salsa</i> coastal salt marsh	December	Yancheng Natural Reserve, Jiangsu, China		static chambers	GC-MS (cryofo- cusing)				(3.5±0.2)E6					μmol/ m ³ /a	(Wang and Wang, 2017)
<i>Aeluropus lit-</i> <i>toralis</i> coastal salt marsh	December	Yancheng Natural Reserve, Jiangsu, China		static chambers	GC-MS (cryofo- cusing)				(1.7±1.7)E6					μmol/ m ³ /a	(Wang and Wang, 2017)
coastal salt marsh mudflat	December	Yancheng Natural Reserve, Jiangsu, China		static chambers	GC-MS (cryofo- cusing)				0					μmol/ m ³ /a	(Wang and Wang, 2017)

site specifics			location	T (°C)	measurement method	instrument	H ₂ S	MeSH	DMS	COS	CS ₂	DMDS	other	other	unit	source
<i>Spartina terniflora</i>	al-	year-round	Great Sippewissett Marsh, Falmouth, Massachusetts, USA		dynamic chamber, ambient air	TD-GC-FPD	(-56-220)E6		(0-700)E6	(0-22)E6	(0-11)E6	(0-420)E6			μmol/m ³ /a	(Steudler and Peterson, 1985)
<i>Spartina terniflora</i>	al-	July	Cedar Island, North Carolina, USA		dynamic chamber, VOC-free	GC-FPD			0.42E6				H ₂ S+COS	6.1E6	μmol/m ³ /a	(Aneja et al., 1979)
<i>Spartina terniflora</i>	al-	September	Cox's Landing, North Carolina, USA		dynamic chamber, VOC-free	GC-FPD			5.8E6				H ₂ S+COS	1.3E6	μmol/m ³ /a	(Aneja et al., 1979)
<i>Spartina terniflora</i>	al-	July/August	North Carolina		dynamic chamber, VOC-free	GC-FPD	0.3E6	1.6E6	1.3E6	1.0E6	4.8E6	1.6E6			μmol/m ³ /a	(?)
<i>Spartina terniflora</i>	al-	July	Wallops Island, Virginia		ambient air directly	GC-FPD	(34-180)E6								μmol/m ³ /a	(Goldberg, AB et al., 1981)
saline marsh			Aransas W. R., TX, USA		dynamic chamber, VOC-free	GC-FPD	1880	63	2200	0	11900	160			μmol/m ² /a	(Adams et al., 1981)
saline marsh			Cedar Island, North Carolina, USA		dynamic chamber, VOC-free	GC-FPD	630-5000	0-9	220-49100	63-630	0-1900	0-16			μmol/m ² /a	(Adams et al., 1981)

site specifics	location	T (°C)	measurement method	instrument	H ₂ S	MeSH	DMS	COS	CS ₂	DMSD	other	other	unit	source
saline marsh	Cox's Landing, North Carolina, USA		dynamic chamber, VOC-free	GC-FPD	(4.4- 16)E6	(0.21- 0.36)E6	0- 55000	28000- 200000	0- 30000	0- 2300			μmol/ m ² /a	(Adams et al., 1981)
saline marsh	E. Ware- ham, Mas- sachusetts. USA		dynamic chamber, VOC-free	GC-FPD	0	0	19000	120	880	190			μmol/ m ² /a	(Adams et al., 1981)
saline marsh	Everglades National Park, Florida, USA		dynamic chamber, VOC-free	GC-FPD	2.3E6	6900	8100	1300	12000	1600			μmol/ m ² /a	(Adams et al., 1981)
saline marsh	Georgetown, South Car- olina, USA		dynamic chamber, VOC-free	GC-FPD	29000	190	15000	1600	6900	160			μmol/ m ² /a	(Adams et al., 1981)
saline marsh	Jeanerette, LA, USA		dynamic chamber, VOC-free	GC-FPD	0	0	900	6	31	0			μmol/ m ² /a	(Adams et al., 1981)
saline marsh	Lewes, Delaware, USA		dynamic chamber, VOC-free	GC-FPD	3000	0	15000	41000	2200	16			μmol/ m ² /a	(Adams et al., 1981)
saline marsh	Rockefeller W. R., LA, USA		dynamic chamber, VOC-free	GC-FPD	2800	31	250	31	630	94			μmol/ m ² /a	(Adams et al., 1981)
saline marsh	St. Marks W. R., Florida, USA		dynamic chamber, VOC-free	GC-FPD	41000	2500	38000	1900	33000	2200			μmol/ m ² /a	(Adams et al., 1981)

site specifics			location	T (°C)	measurement method	instrument	H ₂ S	MeSH	DMS	COS	CS ₂	DMDS	other	other	unit	source
saline marsh			Sanibel Island, W. R., Florida, USA		dynamic cham- ber, VOC-free	GC-FPD	19E6	730000	25000	63	34000	51000			μmol/ m ² /a	(Adams et al., 1981)
saline marsh			Wallops Island, Virginia, USA		dynamic cham- ber, VOC-free	GC-FPD	0	6900	58000	940	43000	1300			μmol/ m ² /a	(Adams et al., 1981)

Table A.3.: VSC emissions from microbial mats according to literature.

site specifics			location	T (°C)	measurement method	instrument	H ₂ S	MeSH	DMS	COS	CS ₂	DMDS	other	other	unit	source
cyanobacterial mat	0-5 oxic	mm,	Sapelo Island, Georgia, USA	20	1/1 diluted slurry, headspace	headspace- GC-FID						- 130E6			μmol/ m ³ /a	(Visscher et al., 1995)
cyanobacterial mat	0-5 anoxic	mm,	Sapelo Island, Georgia, USA	20	1/1 diluted slurry, headspace	headspace- GC-FID						- 96E6			μmol/ m ³ /a	(Visscher et al., 1995)
cyanobacterial mat	5-10 oxic	mm,	Sapelo Island, Georgia, USA	20	1/1 diluted slurry, headspace	headspace- GC-FID						- 11E6			μmol/ m ³ /a	(Visscher et al., 1995)
cyanobacterial mat	5-10 anoxic	mm,	Sapelo Island, Georgia, USA	20	1/1 diluted slurry, headspace	headspace- GC-FID						-6E6			μmol/ m ³ /a	(Visscher et al., 1995)

site specifics		location	T (°C)	measurement method	instrument	H ₂ S	MeSH	DMS	COS	CS ₂	DMDS	other	other	unit	source
diatom mat	0-10 oxic	mm, Biscaye Bay, Florida, USA	20	1/1 diluted slurry, headspace	headspace-GC-FID		70E6	32E6						μmol/ m ³ /a	(Visscher et al., 1995)
diatom mat	0-10 anoxic	mm, Biscaye Bay, Florida, USA	20	1/1 diluted slurry, headspace	headspace-GC-FID		79E6	39E6						μmol/ m ³ /a	(Visscher et al., 1995)
diatom mat	10-20 oxic	mm, Biscaye Bay, Florida, USA	20	1/1 diluted slurry, headspace	headspace-GC-FID									μmol/ m ³ /a	(Visscher et al., 1995)
carbonate sediment	0-10 oxic	mm, Biscaye Bay, Florida, USA	20	1/1 diluted slurry, headspace	headspace-GC-FID						2.6E6			μmol/ m ³ /a	(Visscher et al., 1995)
carbonate sediment	0-10 anoxic	mm, Biscaye Bay, Florida, USA	20	1/1 diluted slurry, headspace	headspace-GC-FID						1.8E6			μmol/ m ³ /a	(Visscher et al., 1995)
algal mat in hotspring effluent	0-3 mm	Octopus Spring, Yellowstone National Park, USA		core	headspace GC-FPD		(0.6± 0.2)E6	33000						μmol/ m ³	(Zinder et al., 1977)
algal mat in hotspring effluent	3-18 mm	Octopus Spring, Yellowstone National Park, USA		core	headspace GC-FPD		6000							μmol/ m ³	(Zinder et al., 1977)

site specifics		location	T (°C)	measurement method	instrument	H ₂ S	MeSH	DMS	COS	CS ₂	DMDS	other	other	unit	source
phototrophic bacteria	July- Octo- ber	Lake Cardagno					0-15	25- 230		20- 150	0-6			μmol/ m ³	(Fritz and Bachofen, 2000)
hypersaline cyanobacterial mat	0-5 mm	seawater evapora- tion pond, Guerrero Negro, Mexico	20	mat in aquar- ium	GC-FPD	0- 1E5		20- 200						μmol/ m ³	(Visscher et al., 2003)
hypersaline cyanobacterial mat	0-5 mm	seawater evapora- tion pond, Guerrero Negro, Mexico	20	pond oxic	water, GC-FPD				(12±10)E3					μmol/ m ² /a	(Visscher et al., 2003)
hypersaline cyanobacterial mat	0-5 mm	seawater evapora- tion pond, Guerrero Negro, Mexico	20	pond anoxic	water, GC-FPD					4800±1700				μmol/ m ² /a	(Visscher et al., 2003)

Table A.4.: VSC emissions from mangrove forests according to literature.

site specifics	location	T (°C)	measurement method	instrument	H ₂ S	MeSH	DMS	COS	CS ₂	DMDS	other	other	unit	source
more inland, 1-60 cm open spaces, abundant man- grove litter, non-rooted	Mzinga creek, Mtoni mangrove forest, Dar es Salam, Tanzania	25-32	dissolved, situ	in electrodes	(2- 25)E6								μmol/ m ³	(Lyimo et al., 2002a)
more inland, 1-60 cm open spaces, abundant man- grove litter, rooted	Mzinga creek, Mtoni mangrove forest, Dar es Salam, Tanzania	25-32	dissolved, situ	in electrodes	(15)E6								μmol/ m ³	(Lyimo et al., 2002a)
landside, close to land, less deep mud, lit- ter, non-rooted	Mzinga creek, Mtoni mangrove forest, Dar es Salam, Tanzania	25-32	dissolved, situ	in electrodes	(2- 6)E6								μmol/ m ³	(Lyimo et al., 2002a)
intermediate between other stations, non- rooted	Mzinga creek, Mtoni mangrove forest, Dar es Salam, Tanzania	25-32	dissolved, situ	in electrodes	(1- 5)E5								μmol/ m ³	(Lyimo et al., 2002a)

site specifics		location	T (°C)	measurement method	instrument	H ₂ S	MeSH	DMS	COS	CS ₂	DMDS	other	other	unit	source
intermediate between other stations, rooted	1-60 cm	Mzinga creek, Mtoni mangrove forest, Dar es Salam, Tanzania	25-32	dissolved, situ	in electrodes	(0.5- 2)E6								μmol/ m ³	(Lyimo et al., 2002a)
seaside, no lit- ter, Sonneratia alba-rich, crab- holes, rooted	1-60 cm	Mzinga creek, Mtoni mangrove forest, Dar es Salam, Tanzania	25-32	dissolved, situ	in electrodes	(0.02- 2)E6								μmol/ m ³	(Lyimo et al., 2002a)
Mangrove sediment with open areas (inland site from above?)	0-5 cm	Mzinga creek, Mtoni mangrove forest, Dar es Salam, Tanzania	30	static cham- ber, CO ₂ /N ₂ headspace	GC-FPD	(0.7±0.3)E6								μmol/ kg/a	(Lyimo et al., 2002b)
Mangrove sediment with open areas (inland site from above?)	5-10 cm	Mzinga creek, Mtoni mangrove forest, Dar es Salam, Tanzania	30	static cham- ber, CO ₂ /N ₂ headspace	GC-FPD	(0.3±0.1)E6								μmol /kg/a	(Lyimo et al., 2002b)

site specifics		location	T (°C)	measurement method	instrument	H ₂ S	MeSH	DMS	COS	CS ₂	DMS	other	other	unit	source
Mangrove sediment with open areas	10-15 cm	Mzinga creek, Mtoni mangrove forest, Dar es Salam, Tanzania	30	static chamber, CO ₂ /N ₂ headspace	GC-FPD	(0.3±0.2)E6								μmol/kg/a	(Lyimo et al., 2002b)
Mangrove sediment with open areas	15-20 cm	Mzinga creek, Mtoni mangrove forest, Dar es Salam, Tanzania	30	static chamber, CO ₂ /N ₂ headspace	GC-FPD	(0.3±0.2)E6								μmol/kg/a	(Lyimo et al., 2002b)
Mangrove sediment with open areas	20-25 cm	Mzinga creek, Mtoni mangrove forest, Dar es Salam, Tanzania	30	static chamber, CO ₂ /N ₂ headspace	GC-FPD	0.2E6								μmol/kg/a	(Lyimo et al., 2002b)
Mangrove sediment with open areas	25-30 cm	Mzinga creek, Mtoni mangrove forest, Dar es Salam, Tanzania	30	static chamber, CO ₂ /N ₂ headspace	GC-FPD	0.1E6								μmol/kg/a	(Lyimo et al., 2002b)

site specifics	location	T (°C)	measurement method	instrument	H ₂ S	MeSH	DMS	COS	CS ₂	DMDS	other	other	unit	source
Mangrove sediment with open areas (inland site from above?)	Mzinga creek, Mtoni mangrove forest, Dar es Salam, Tanzania	30	static chamber, CO ₂ /N ₂ headspace	GC-FPD		33000	14000±900						μmol/kg/a	(Lyimo et al., 2009)

Table A.5.: VSC emissions from freshwater wetlands and lakes according to literature.

site specifics	location	T (°C)	measurement method	instrument	H ₂ S	MeSH	DMS	COS	CS ₂	DMDS	other	other	unit	source
Stratified alpine lake (summer)	mixolimnium Lake Cadagno, Piora valley, Switzerland	7.17	direct water/sediment samples	photometric, GC-FPD	2E6	0	0		(0-10)E6	0			μmol/m ³	(Fritz and Bachofen, 2000)
Stratified alpine lake (summer)	transition zone Lake Cadagno, Piora valley, Switzerland	5-7	direct water/sediment samples	photometric, GC-FPD	(1-4)E6	(0-15)E6	(0-40)E6		(0-20)E6	0-30000			μmol/m ³	(Fritz and Bachofen, 2000)
Stratified alpine lake (summer)	mimolimnium Lake Cadagno, Piora valley, Switzerland	4-5	direct water/sediment samples	photometric, GC-FPD	(0.25-0.3)E6	0	(0-10)E6		(80-100)E6	0			μmol/m ³	(Fritz and Bachofen, 2000)

site specifics		location	T (°C)	measurement method		instrument	H ₂ S	MeSH	DMS	COS	CS ₂	DMDS	other	other	unit	source
Stratified alpine lake (summer)	water column	Lake Cadagno, Piora valley, Switzerland	4-17	direct	water/sediment samples	photometric, GC-FPD	0	0			80E6				μmol/m ³	(Fritz and Bachofen, 2000)
Stratified alpine lake (summer)	sediment	Lake Cadagno, Piora valley, Switzerland	4-5	direct	water/sediment samples	photometric, GC-FPD	(10-40)E6	(40-70)E6			(250-400)E6				μmol/m ³	(Fritz and Bachofen, 2000)
Stratified lake	epilimnion/metalimnion	Linsley Pond, North Branford, Connecticut, USA	10-24	direct	water samples	GC-PFPD			(0-5)E6		(0-2)E6	(0-4)E6			μmol/m ³	(Hu et al., 2007)
Stratified lake	anoxic hypolimnium	Linsley Pond, North Branford, Connecticut, USA	5-10	direct	water samples	GC-PFPD			(0-90)E6		(0-10)E6	(1-18)E6			μmol/m ³	(Hu et al., 2007)
Canal	water	Desjardins Canal, Ontario, Canada		direct	water samples	GC-ELCD (purge and trap)		430-5400	120-350				H ₂ S + COS		μmol/m ³	(Caron and Kramer, 1994)

site specifics		location	T (°C)	measurement method	instrument	H ₂ S	MeSH	DMS	COS	CS ₂	DMDS	other	other	unit	source
Great Lakes	water	Lake Ontario, Ontario, Canada		direct water samples	GC-ELCD (purge and trap)		450-4000	640-2000				H ₂ S COS	+	μmol/ m ³	(Caron and Kramer, 1994)
Great Lakes	sediment	Lake Ontario, Ontario, Canada		direct water samples	GC-ELCD (purge and trap)		270	320				H ₂ S COS	+	μmol/ m ³	(Caron and Kramer, 1994)
Lake	sediment	Harp Lake, Huntsville, Ontario, Canada		direct water samples	GC-ELCD (purge and trap)		400	520				H ₂ S COS	+	μmol/ m ³	(Caron and Kramer, 1994)
Bog lake	soil water	Luther Lake, Ontario, Canada		direct water samples	GC-ELCD (purge and trap)		6100	170				H ₂ S COS	+	μmol/ m ³	(Caron and Kramer, 1994)
Bog lake	lake water	Luther Lake, Ontario, Canada		direct water samples	GC-ELCD (purge and trap)		1200	820				H ₂ S COS	+	μmol/ m ³	(Caron and Kramer, 1994)
Bog lake	bog water (shade)	Luther Lake, Ontario, Canada		direct water samples	GC-ELCD (purge and trap)		7100	2200				H ₂ S COS	+	μmol/ m ³	(Caron and Kramer, 1994)
Bog lake	bog water (sunlight)	Luther Lake, Ontario, Canada		direct water samples	GC-ELCD (purge and trap)		11000	760				H ₂ S COS	+	μmol/ m ³	(Caron and Kramer, 1994)

site specifics			location	T (°C)	measurement method	instrument	H ₂ S	MeSH	DMS	COS	CS ₂	DMDS	other	other	unit	source
Prairie salt lake	May	-	Humboldt		water sample at	GC-FPD	0-8	0.9-	0.4-	0-3	0.7-				μmol/ m ³	(Richards et al., 1994)
	September		Lake, Saskatchewan, Canada		50 cm depth	(purge and trap)		3.9	0.6		4.5					
Prairie salt lake	May	-	Patience		water sample	GC-FPD	0-	1.7-	0.5-	0.8-	0-				μmol/ m ³	(Richards et al., 1994)
	September		Lake, Saskatchewan, Canada		at50 cm depth	(purge and trap)	2.5	8.3	1.4	3.6	3.6					
Prairie salt lake	May	-	Waldsea		water sample at	GC-FPD	0-	6.3-	0-	0-	0-				μmol/ m ³	(Richards et al., 1994)
	September		Lake, Saskatchewan, Canada		50 cm depth	(purge and trap)	4.7	130	0.9	1.8	3.0					
Prairie salt lake	May	-	Bid Quill		water sample at	GC-FPD	1.4-	60-	0.6-	0-6	0-				μmol/ m ³	(Richards et al., 1994)
	September		Lake, Saskatchewan, Canada		50 cm depth	(purge and trap)	18	230	1.2		3.2					
Prairie salt lake	May	-	Little Man-		water sample at	GC-FPD	0-22	3.2-	0.4-	0-	0-13				μmol/ m ³	(Richards et al., 1994)
	September		itou Lake, Saskatchewan, Canada		50 cm depth	(purge and trap)		170	1	3.6						
Prairie salt lake	May	-	Chaplin		water sample at	GC-FPD	23-	52-	1.5-	0-	5.0-				μmol/ m ³	(Richards et al., 1994)
	September		Lake East, Saskatchewan, Canada		50 cm depth	(purge and trap)	600	1400	1.9	480	2100					
Prairie salt lake	May	-	Chaplin		water sample at	GC-FPD	0-	110-	1.7-	0-	18-				μmol/ m ³	(Richards et al., 1994)
	September		Lake west, Saskatchewan, Canada		50 cm depth	(purge and trap)	650	3100	27	130	200					

site specifics		location	T (°C)	measurement method	instrument	H ₂ S	MeSH	DMS	COS	CS ₂	DMDS	other	other	unit	source
Kinosheo	May	- Hudson		water sample at	GC-FPD	0-	0.4-	0.4-	0-	0-				μmol/ m ³	(Richards et al., 1994)
	September	Bay Low-lands, Ontario, Canada		50 cm depth	(purge and trap)	2.4	7.8	2.4	2.7	1.8					
Coastal fen	May	- Hudson		water sample at	GC-FPD	0	0-	0-	0	0				μmol/ m ³	(Richards et al., 1994)
	September	Bay Low-lands, Ontario, Canada		50 cm depth	(purge and trap)		2.8	1.6							
Interior fen	May	- Hudson		water sample at	GC-FPD	0	0-1	0.3-	0-	0				μmol/ m ³	(Richards et al., 1994)
	September	Bay Low-lands, Ontario, Canada		50 cm depth	(purge and trap)			0.7	1.4						
Prairie salt lake	May September	- Humboldt Lake, Ontario, Canada		stagnant film gas exchange model		0-91	4.5- 34	2.3- 8.0	0-18	2.3- 57				μmol/ m ² /a	(Richards et al., 1994)
Prairie salt lake	May September	- Patience Lake, Ontario, Canada		stagnant film gas exchange model		0- 4.5	3.4- 18	1.1- 4.6	2.3- 11	0- 8.0				μmol/ m ² /a	(Richards et al., 1994)
Prairie salt lake	May September	- Waldsea Lake, Ontario, Canada		stagnant film gas exchange model		0-50	24- 1800	0- 8.0	0- 8.0	0-25				μmol/ m ² /a	(Richards et al., 1994)

site specifics			location	T (°C)	measurement method	instrument	H ₂ S	MeSH	DMS	COS	CS ₂	DMSD	other	other	unit	source
Prairie salt lake	May	-	Bid Quill Lake,		stagnant film		0-	410-	2.3-	0-46	0-23				μmol/ m ² /a	(Richards et al., 1994)
	September		Ontario, Canada		gas exchange model		100	820	10							
Prairie salt lake	May	-	Little Manitou Lake,		stagnant film		0-	14-	2.3-	0-14	0-91				μmol/ m ² /a	(Richards et al., 1994)
	September		Ontario, Canada		gas exchange model		180	1100	6.9							
Prairie salt lake	May	-	Chaplin Lake East,		stagnant film		130-	300-	8.0-	0-70	30-				μmol/ m ² /a	(Richards et al., 1994)
	September		Ontario, Canada		gas exchange model		4500	8700	140		1200					
Prairie salt lake	May	-	Chaplin Lake west,		stagnant film		0-	910-	11-	0-	100-				μmol/ m ² /a	(Richards et al., 1994)
	September		Ontario, Canada		gas exchange model		3500	12000	210	910	1200					
Open bog with acidic ponds	May	-	Kinosheo, Hudson Bay Low-		stagnant film		0-25	0-82	1.1-	0-25	0-				μmol/ m ² /a	(Richards et al., 1994)
	September		lands, Ontario, Canada		gas exchange model				22		8.0					
Coastal fen	May	-	Hudson Bay Low-		stagnant film		0	0-39	4.6-	0	0				μmol/ m ² /a	(Richards et al., 1994)
	September		lands, Ontario, Canada		gas exchange model				17							

site specifics		location	T (°C)	measurement method	instrument	H ₂ S	MeSH	DMS	COS	CS ₂	DMDS	other	other	unit	source
Interior fen	May - September	Hudson Bay Low-lands, Ontario, Canada		stagnant film gas exchange model		0	0-17		2.3-9.1	0-17	0			μmol/ m ² /a	(Richards et al., 1994)
Hypolimnetic zone	Small experimental lakes	Experimental Lakes Area, North-western Ontario, Canada		sediment pore water	GC-FPD (cryofocused)	(0.30-0.36)E6	24000-210000	84000-400000			0-70000			μmol/ m ² /a	(Richards et al., 1991)
Small experimental lakes		Experimental Lakes Area, North-western Ontario, Canada		direct water samples	GC-FPD (cryofocused)	0-2.8	0.3-2.7	0-0.9			0-3.0			μmol/ m ³	(Richards et al., 1991)
Small experimental lakes fed with sulfuric acid		Experimental Lakes Area, North-western Ontario, Canada		direct water samples	GC-FPD (cryofocused)	0-32	0.3-110	0.2-1.1			0-0.3			μmol/ m ³	(Richards et al., 1991)
NE bog		Experimental Lakes Area, North-western Ontario, Canada		direct water samples	GC-FPD (cryofocused)	0.38	0.7-110	0			0-0.3			μmol/ m ³	(Richards et al., 1991)

site specifics	location	T (°C)	measurement method	instrument	H ₂ S	MeSH	DMS	COS	CS ₂	DMDS	other	other	unit	source
Lakes in Red Lake Area	Canadian Shield near Red Lake, Ontario, Canada		direct water samples	GC-FPD (cryofo- cused)	0	0-	0-	0-	0				μmol/ m ³	(Richards et al., 1991)
Anoxic Hy- polimnion Stratified Lake	Schleinsee, Germany		direct water samples	GC-SSD (cryofo- cused)		62	11	traces	0.7				μmol/ m ³	(Henatsch and Jüttner, 1988)
Minerotrophic Peatland	surface De Bruck, Nether- lands				590- 19000	0.06- 1.6	0.02- 0.71		0.03- 0.40	0.02- 0.03			μmol/ m ³	(Lomans et al., 1997)
Minerotrophic Peatland	sediment De Bruck, Nether- lands				0.3- 0.9	0.02- 0.16	0.01- 0.32		0.13- 0.30	(1- 6)E- 3			μmol/ m ³	(Lomans et al., 1997)
organic/sulfate rich sediment	Zegveld I, Nether- lands				(0.16- 0.18)E6								μmol/ m ³	(Lomans et al., 2001b)
organic/sulfate rich sediment	Zegveld II, Nether- lands				(0.14- 0.19)E6								μmol/ m ³	(Lomans et al., 2001b)
organic/iron rich sediment	Hatertse Vennen, Nether- lands				6000- 26000								μmol/ m ³	(Lomans et al., 2001b)
organic/iron rich sediment	Bruuk I, Nether- lands				0- 1300								μmol/ m ³	(Lomans et al., 2001b)
organic/sulfate rich sediment	Bruuk II, Nether- lands				(0.13- 0.30)E6								μmol/ m ³	(Lomans et al., 2001b)

site specifics	location	T (°C)	measurement method	instrument	H ₂ S	MeSH	DMS	COS	CS ₂	DMDS	other	other	unit	source
organic/sulfate rich sediment	Dekkerswald, Nether- lands				(0.14- 0.24)E6								μmol/ m ³	(Lomans et al., 2001b)
organic/sulfate rich sediment	Breukelen, Nether- lands				15000- 110000								μmol/ m ³	(Lomans et al., 2001b)
organic/sulfate/iron rich sediment	Tienhoven I, Nether- lands				2000- 3000								μmol/ m ³	(Lomans et al., 2001b)
organic-rich sediment	Tienhoven II, Nether- lands				3000- 8000								μmol/ m ³	(Lomans et al., 2001b)
organic-rich sediment	Maarssen, Nether- lands				(0.10- 0.25)E6								μmol/ m ³	(Lomans et al., 2001b)
moist, cal- careous C. <i>jamaicense</i> freshwater wetland	Everglades National Park, Florida, USA	12-37	dynamic cham- ber, VOC-free		27- 1300		0- 1900		0- 140	0- 190			μmol /m ² /a	(Cooper et al., 1987)
moist, sandy wetland with <i>J.</i> <i>roemerianus</i>	St. Marks National Wildlife Refuge, Florida, USA	19-38	dynamic cham- ber, VOC-free		160- 770		27- 1800		0	0			μmol/ m ² /a	(Cooper et al., 1987)

site specifics	location	T (°C)	measurement method	instrument	H ₂ S	MeSH	DMS	COS	CS ₂	DMDS	other	other	unit	source
moist, peaty wetland with <i>D. spicata</i>	Merritt Island National Wildlife Refuge, Florida, USA	15- 32.5	dynamic cham- ber, VOC-free		0- 42000		0- 6300		0- 470	0- 410			μmol/ m ² /a	(Cooper et al., 1987)
moist, peaty wetland with <i>A. germians</i>	Rookery Bay Na- tional Estuarine Sanctuary, Florida, USA	13-34	dynamic cham- ber, VOC-free		82- 220		0- 2700		0- 160	0- 160			μmol/ m ² /a	(Cooper et al., 1987)
dry, calcareous wetland with <i>B.</i> <i>maritima</i>	Everglades National Park, Florida, USA	19-23	dynamic cham- ber, VOC-free		160- 270		270- 1900		27- 82	27- 140			μmol/ m ² /a	(Cooper et al., 1987)
Sphagnum peat	Sallie's Fen, Barring- ton, New Hampshire, USA	3-29.3	static and dy- namic chamber incubations (S- free air)	GC-FPD			35- 3800	32- 480					μmol/ m ² /a	(de Mello and Hines, 1994)
Lake of Galilee	Israel		water samples (0, 5, 20 m depth)	GC-MS	0		0-25						μmol/ m ³	(Ginzburg et al., 1998)

site specifics				location	T (°C)	measurement method	instrument	H ₂ S	MeSH	DMS	COS	CS ₂	DMDS	other	other	unit	source
Lake stance	Con- stance	depth file	pro-	Germany/ Switzer- land/ Austria		water samples	GC-FID (cryo- genic purge and trap)			0.2- 0.4						μmol/ m ³	(Steinke et al., 2018)
Lake stance	Con- stance	surface emissions		Germany/ Switzer- land/ Austria		water samples	GC-FID (cryo- genic purge and trap)			7.0- 110						μmol/ m ² /a	(Steinke et al., 2018)
East University of Electronic Science and Technology of China)	Lake, Electronic and Technology of China)			Chengu, China		water samples	MSSF- CL			5.0- 60						μmol/ m ³	(Leng et al., 2021)
		Qingsgui river		Chengdu, China		water samples	MSSF- CL			0-10						μmol/ m ³	(Leng et al., 2021)
		Zipingpu and Tuanjie Reservoir		Chengu, China		water samples	MSSF- CL			20- 40						μmol/ m ³	(Leng et al., 2021)
		Lake Superior off-shore		Canada		water samples	GC-FPD (cryo- genic purge and trap)			(5- 44)E6						μmol/ m ² /a	(Nriagu and Hold- way, 1989)

site specifics	location	T (°C)	measurement method	instrument	H ₂ S	MeSH	DMS	COS	CS ₂	DMDS	other	other	unit	source
Lake Erie	Canada		water samples	GC-FPD (cryo- genic purge and trap)			0.02- 0.05						μmol/ m ² /a	(Nriagu and Hold- way, 1989)
Lake Ontario	Canada		water samples	GC-FPD (cryo- genic purge and trap)			0.04- 1.5						μmol/ m ² /a	(Nriagu and Hold- way, 1989)
nonsaline swamp	Brunswick Co., NC, USA		dynamic cham- ber, VOC-free	GC-FPD	2800		160	750	690				μmol/ m ² /a	(Adams et al., 1981)
nonsaline swamp	Elba, NY, USA		dynamic cham- ber, VOC-free	GC-FPD	5000		130	190	190				μmol/ m ² /a	(Adams et al., 1981)
nonsaline swamp	Okefenokee W. R., GA, USA		dynamic cham- ber, VOC-free	GC-FPD	31		660	160	690	31			μmol/ m ² /a	(Adams et al., 1981)
wet suborder	Ames, IA, USA		dynamic cham- ber, VOC-free	GC-FPD	4500		94	530	500				μmol/ m ² /a	(Adams et al., 1981)
wet suborder	Clarkedale, AR, USA		dynamic cham- ber, VOC-free	GC-FPD	9.3		3.1	31	94				μmol/ m ² /a	(Adams et al., 1981)
wet suborder	Georgetown, SC, USA		dynamic cham- ber, VOC-free	GC-FPD	250		63	250	160				μmol/ m ² /a	(Adams et al., 1981)
wet suborder	Hastings, FL, USA		dynamic cham- ber, VOC-free	GC-FPD	31		94	31	63	22			μmol/ m ² /a	(Adams et al., 1981)
wet suborder	Jeanerette, LA, USA		dynamic cham- ber, VOC-free	GC-FPD	310		31	31	94				μmol/ m ² /a	(Adams et al., 1981)

site specifics	location	T (°C)	measurement method	instrument	H ₂ S	MeSH	DMS	COS	CS ₂	DMDS	other	other	unit	source
freshwater pond	Belle Valley, OH, USA		dynamic chamber, VOC-free	GC-FPD	2200		160	630	880	63			μmol/ m ² /a	(Adams et al., 1981)
histosol	Belle Glade, FL, USA		dynamic chamber, VOC-free	GC-FPD	160		31	63	130	6.3			μmol/ m ² /a	(Adams et al., 1981)
histosol	Brunswick Co., NC, USA		dynamic chamber, VOC-free	GC-FPD	2800		190	220	530				μmol/ m ² /a	(Adams et al., 1981)
histosol	Celeryville, OH, USA		dynamic chamber, VOC-free	GC-FPD	1500		94	380	190				μmol/ m ² /a	(Adams et al., 1981)
histosol	Dismal Swamp, NC, USA		dynamic chamber, VOC-free	GC-FPD	560- 1400		22- 63	0- 250	3.1- 63	6.3- 9.4			μmol/ m ² /a	(Adams et al., 1981)
histosol	E. Ware- ham, MA, USA		dynamic chamber, VOC-free	GC-FPD	0		410	0	13	94			μmol/ m ² /a	(Adams et al., 1981)
histosol	Elba, NY, USA		dynamic chamber, VOC-free	GC-FPD	4900		190	720	4300				μmol/ m ² /a	(Adams et al., 1981)
histosol	Fairhope, AL, USA		dynamic chamber, VOC-free	GC-FPD	0		31	31	440				μmol/ m ² /a	(Adams et al., 1981)
histosol	Fens, MN, USA		dynamic chamber, VOC-free	GC-FPD	1300		94	310	94				μmol/ m ² /a	(Adams et al., 1981)
histosol	Lakeland, FL, USA		dynamic chamber, VOC-free	GC-FPD	2200		340	0	250				μmol/ m ² /a	(Adams et al., 1981)
histosol	Laingsburg, MI, USA		dynamic chamber, VOC-free	GC-FPD	1400		340	340	130				μmol/ m ² /a	(Adams et al., 1981)
histosol	One Stone Lake, WI, USA		dynamic chamber, VOC-free	GC-FPD	2600		31	750	380				μmol/ m ² /a	(Adams et al., 1981)

Table A.6.: VSC emissions from rice paddies according to literature.

site specifics	location	T (°C)	measurement method	instrument	H ₂ S	MeSH	DMS	COS	CS ₂	DMDS	other	other	unit	source
Zhanjiang rice paddy field	chemically fertilized	Guangdong Province, China	closed chamber	GC-FPD (sorbent traps)	0	0	980	160	0	0			μmol/kg/a	(Yang et al., 1998)
Zhanjiang rice paddy field	organic and chemically fertilized	Guangdong Province, China	closed chamber	GC-FPD (sorbent traps)	0	0	1300	330	160	0			μmol/kg/a	(Yang et al., 1998)
Changsha rice paddy field	chemically fertilized	Hunan Province, China	closed chamber	GC-FPD (sorbent traps)	0	0	1100	160	660	8200			μmol/kg/a	(Yang et al., 1998)
Changsha rice paddy field	organic and chemically fertilized	Hunan Province, China	closed chamber	GC-FPD (sorbent traps)	0	0	1800	330	490	1100			μmol/kg/a	(Yang et al., 1998)
Yingtian rice paddy field	chemically fertilized	Jianxi Province, China	closed chamber	GC-FPD (sorbent traps)	0	160	330	160	0	0			μmol/kg/a	(Yang et al., 1998)
Yingtian rice paddy field	organic and chemically fertilized	Jianxi Province, China	closed chamber	GC-FPD (sorbent traps)	0	330	490	0	0	0			μmol/kg/a	(Yang et al., 1998)
Wuxian rice paddy field	chemically fertilized	Jiangsu Province, China	closed chamber	GC-FPD (sorbent traps)	160	490	8800	330	2000	2900			μmol/kg/a	(Yang et al., 1998)
Wuxian rice paddy field	organic and chemically fertilized	Jiangsu Province, China	closed chamber	GC-FPD (sorbent traps)	0	650	11000	330	3300	3400			μmol/kg/a	(Yang et al., 1998)

site specifics			location	T (°C)	measurement method	instrument	H ₂ S	MeSH	DMS	COS	CS ₂	DMDS	other	other	unit	source
Nanjing paddy field	rice chemically fertilized		Jiangsu Province, China		closed chamber	GC-FPD (sorbent traps)	160	490	6200	160	1800	2600			μmol/ kg/a	(Yang et al., 1998)
Nanjing paddy field	rice organic and chem- ically fertilized		Jiangsu Province, China		closed chamber	GC-FPD (sorbent traps)	0	490	9100	330	2600	3100			μmol/ kg/a	(Yang et al., 1998)
Rice Paddy	annual cy- cle		Xiaolingwei, Nanjing, China		closed chamber	GC-FPD (sorbent traps)			0- 2300				other	0- 1300	μmol/ m ² /a	(Yang et al., 1998)
Arid Oase Paddy field	no rice		Sandaoba, Urumqi, Xinjiang Uygur Au- tonomous Region, China		static chambers	GC-FPD (cryofo- cusing)				-53- 220	0- 110				μmol/ m ² /a	(Jing et al., 2017)
Arid Oase Paddy field	rice planted		Sandaoba, Urumqi, Xinjiang Uygur Au- tonomous Region, China		static chambers	GC-FPD (cryofo- cusing)				- 310- 0	16- 200				μmol/ m ² /a	(Jing et al., 2017)

site specifics	location	T (°C)	measurement method	instrument	H ₂ S	MeSH	DMS	COS	CS ₂	DMDS	other	other	unit	source
Arid Oase Rice Paddy field	rice planted, urea at 10 g N/m ²	Sandaoba, Urumqi, Xinjiang Uygur Au- tonomous Region, China	static chambers	GC-FPD (cryofo- cusing)				- 480- 16	0- 250				μmol/ m ² /a	(Jing et al., 2017)
Arid Oase Rice Paddy field	rice planted, urea and (NH ₄) ₂ SO ₄ at 10 g N/m ² and 2.5 g S/m ²	Sandaoba, Urumqi, Xinjiang Uygur Au- tonomous Region, China	static chambers	GC-FPD (cryofo- cusing)				- 430- 47	0- 160				μmol/ m ² /a	(Jing et al., 2017)

Table A.7.: VSC emissions from temperate soils according to literature.

site specifics	location	T (°C)	measurement method	instrument	H ₂ S	MeSH	DMS	COS	CS ₂	DMDS	other	other	unit	source
agricultural soil	Ames, Iowa	25.5	dynamic cham- ber, VOC-free	mobile GC-FPD	9.9		15	46	9.9				μmol/ m ² /a	(Goldan et al., 1987)
agricultural soil	Celeryville, Ohio, USA	22	dynamic cham- ber, VOC-free	mobile GC-FPD	76		9.9	110	23				μmol/ m ² /a	(Goldan et al., 1987)
Alfisol	Wadesville, IN, USA		dynamic cham- ber, VOC-free	GC-FPD	31	0	31	63	63	63			μmol/ m ² /a	(Adams et al., 1979)
Inceptisol	Philo, OH, USA		dynamic cham- ber, VOC-free	GC-FPD	88	0	6.3	69	38	44			μmol/ m ² /a	(Adams et al., 1979)
Histosol	Dismal Swamp, NC, USA		dynamic cham- ber, VOC-free	GC-FPD	560	0	22	0	3.1	3.1			μmol/ m ² /a	(Adams et al., 1979)

site specifics	location	T (°C)	measurement method	instrument	H ₂ S	MeSH	DMS	COS	CS ₂	DMDS	other	other	unit	source
Saline Swamp	Cedar Island, NC, USA		dynamic chamber, VOC-free	GC-FPD	610	0	220	50	0	0			μmol/m ² /a	(Adams et al., 1979)
Saline Marsh	Cox's Landing, NC, USA		dynamic chamber, VOC-free	GC-FPD	4.4E6	0.2E6	0	0.2E6	0	0			μmol/m ² /a	(Adams et al., 1979)
Alluvial Clay	Clarkedale, AR, USA		dynamic chamber, VOC-free	GC-FPD	13	0	3.1	44	0	0			μmol/m ² /a	(Adams et al., 1979)
mollisol	Linneus, MO, USA		dynamic chamber, VOC-free	GC-FPD	3300	0	94	280	160	0			μmol/m ² /a	(Adams et al., 1981)
mollisol	Shreveport, LA, USA		dynamic chamber, VOC-free	GC-FPD	0	0	31	63	120	0			μmol/m ² /a	(Adams et al., 1981)
mollisol	Yankeetown, IN, USA		dynamic chamber, VOC-free	GC-FPD	2300	0	63	720	660	0			μmol/m ² /a	(Adams et al., 1981)
alfisol	Kearnsyville, WV, USA		dynamic chamber, VOC-free	GC-FPD	2600	0	63	910	690	3.1			μmol/m ² /a	(Adams et al., 1981)
alfisol (wooded)	R.T.P., NC, USA		dynamic chamber, VOC-free	GC-FPD	0	0	0	130	31	0			μmol/m ² /a	(Adams et al., 1981)
alfisol (cultivated)	R.T.P., NC, USA		dynamic chamber, VOC-free	GC-FPD	250	0	160	94	31	0			μmol/m ² /a	(Adams et al., 1981)
alfisol	Shreveport, LA, USA		dynamic chamber, VOC-free	GC-FPD	0	0	190	63	160	0			μmol/m ² /a	(Adams et al., 1981)
alfisol	Stephenville, TX, USA		dynamic chamber, VOC-free	GC-FPD	0	0	9.4	6.3	94	0			μmol/m ² /a	(Adams et al., 1981)
alfisol	Wadesville, IN, USA		dynamic chamber, VOC-free	GC-FPD	310	0	31	63	63	63			μmol/m ² /a	(Adams et al., 1981)
inceptisol	Belle Vally, OH, USA		dynamic chamber, VOC-free	GC-FPD	2300	0.6E6	130	130	310	0			μmol/m ² /a	(Adams et al., 1981)
inceptisol	Philo, OH, USA		dynamic chamber, VOC-free	GC-FPD	94	0	6.2	63	31	44			μmol/m ² /a	(Adams et al., 1981)

site specifics	location	T (°C)	measurement method	instrument	H ₂ S	MeSH	DMS	COS	CS ₂	DMDS	other	other	unit	source
Spodosols	E. Wareham, MA, USA		dynamic chamber, VOC-free	GC-FPD	0	0	410	0	0	6.3			μmol/m ² /a	(Adams et al., 1981)
ultisol	Calhoun, GA, USA		dynamic chamber, VOC-free	GC-FPD	280	0	63	94	340	3.1			μmol/m ² /a	(Adams et al., 1981)
ultisol	Fairhope, AL, USA		dynamic chamber, VOC-free	GC-FPD	16	0	63	31	160	9.4			μmol/m ² /a	(Adams et al., 1981)
Rendzina	Germany	9-13	dynamic chamber, VOC-free	GC-FPD (cryofocusing)			2200	1700	890				μmol/m ² /a	(Staubes et al., 1989)
Gleysol	Germany		dynamic chamber, VOC-free	GC-FPD (cryofocusing)			630	1600	1400				μmol/m ² /a	(Staubes et al., 1989)
Acrisol	Germany	9.8-22.5	dynamic chamber, VOC-free	GC-FPD (cryofocusing)			2200	1700	1300				μmol/m ² /a	(Staubes et al., 1989)
Acrisol	Germany	9.7-22.0	dynamic chamber, VOC-free	GC-FPD (cryofocusing)			2500	2400	1500				μmol/m ² /a	(Staubes et al., 1989)
Acrisol	Germany	9.0-20.2	dynamic chamber, VOC-free	GC-FPD (cryofocusing)			970	3100	5000				μmol/m ² /a	(Staubes et al., 1989)
Hortisol	Germany	0.1-24.6	dynamic chamber, VOC-free	GC-FPD (cryofocusing)			1300	2600	2000				μmol/m ² /a	(Staubes et al., 1989)
Fluvisol	Germany	9.0-20.8	dynamic chamber, VOC-free	GC-FPD (cryofocusing)			4100	3000	3100				μmol/m ² /a	(Staubes et al., 1989)

site specifics		location	T (°C)	measurement method	instrument	H ₂ S	MeSH	DMS	COS	CS ₂	DMDS	other	other	unit	source
Histosol	May-Oct	Germany	10.0- 22.3	dynamic chamber, VOC-free	GC-FPD (cryofocusing)			3000	3900	2500				μmol/ m ² /a	(Staubes et al., 1989)
Histosol	May	Germany	7.3- 22.8	dynamic chamber, VOC-free	GC-FPD (cryofocusing)			13000	10000	1000				μmol/ m ² /a	(Staubes et al., 1989)
Histosol	May	Germany	6.5- 26.0	dynamic chamber, VOC-free	GC-FPD (cryofocusing)			2700	10000	950				μmol/ m ² /a	(Staubes et al., 1989)
Histosol	May	Germany	13.2	dynamic chamber, VOC-free	GC-FPD (cryofocusing)			48000	30000	620				μmol/ m ² /a	(Staubes et al., 1989)
Histosol	May	Germany	16.0	dynamic chamber, VOC-free	GC-FPD (cryofocusing)			18000	8000	520				μmol/ m ² /a	(Staubes et al., 1989)
Maize field	year-round	Tsukuba, Japan	0-30	closed chamber	GC-FPD (cryofocusing)			0- 110000	0- 16000	0- 26000				μmol/ m ² /a	(Kanda et al., 1995)
wheat field	year-round	Tsukuba, Japan	0-30	closed chamber	GC-FPD (cryofocusing)			0- 53000	0- 26000	0- 26000				μmol/ m ² /a	(Kanda et al., 1995)
beech forest - fermentation layer		Darmstadt, Germany	20	dynamic chamber, ambient air	GC-FPD (cryofocusing)	0		0- 7.1	-22- 7.0	-5.8- 0				μmol/ kg/a	(Kesselmeier and Hubert, 2002)
beech forest - leaf litter layer		Darmstadt, Germany	20	dynamic chamber, ambient air	GC-FPD (cryofocusing)	0-33		0- 130	-85- 50	-4.6- 7.5				μmol/ kg/a	(Kesselmeier and Hubert, 2002)

Table A.8.: VSC emissions from subtropical soils according to literature.

site	location	T (°C)	measurement method	instrument	H ₂ S	MeSH	DMS	COS	CS ₂	DMDS	other	other	unit	source
monsoon broadleaf forest litter	evergreen soil with litter						6.0- 32		-33- 4.1	-3.5- 6.0			μmol/ m ² /a	(Yi et al., 2010)
monsoon broadleaf forest out litter	evergreen soil with- out litter						13- 66		-32 - -11	-3.8- 1.6			μmol/ m ² /a	(Yi et al., 2010)
broadleaf mixed forest soil with litter							5.4- 21		-19- 24	0- 5.0			μmol/ m ² /a	(Yi et al., 2010)
broadleaf mixed forest soil without litter							9.8- 25		-68- 11	0.9- 5.0			μmol/ m ² /a	(Yi et al., 2010)
pine forest with litter							3.5- 12		-15- 140	1.6- 2.8			μmol/ m ² /a	(Yi et al., 2010)
pine forest without litter							9.2- 33		-81- 92	2.2- 14			μmol/ m ² /a	(Yi et al., 2010)

Table A.9.: VSC emissions from tropical soils according to literature.

site specifics	location	T (°C)	measurement method	instrument	H ₂ S	MeSH	DMS	COS	CS ₂	DMDS	other	other	unit	source
rainforest veg- etation + soil	Wet season Brazil		aircraft mea- surement	GC-FPD (gold wool trapping, cryofo- cusin)	840	210	420		53				μmol/ m ² /a	(Andreae and An- dreae, 1988)

site specifics		location	T (°C)	measurement method	instrument	H ₂ S	MeSH	DMS	COS	CS ₂	DMDS	other	other	unit	source
rainforest soil	wet season	Ducke Reserve, Brazil		dynamic chamber (VOC-free)	GC-FPD (gold wool trapping, cryofocusin)	37±16	21±5.3	210±21						μmol/m ² /a	(Andreae and Andreae, 1988)
rainforest vegetation + soil	dry season	Brazil		aircraft measurement	GC-FPD (gold wool trapping, cryofocusin)	580	53	240±100						μmol/m ² /a	(Andreae et al., 1990)
rainforest soil		Suriname	25 °C	dynamic chamber (VOC-free)	PTR-MS						200±800			μmol/m ² /a	(Jardine et al., 2015)
well-drained rainforest soil		Ivory coast			fluorescence	3200								μmol/m ² /a	(Delmas and Servant, 1983)
flooded rainforest soil		Ivory coast			fluorescence	77000								μmol/m ² /a	(Delmas and Servant, 1983)
Abidjan soil	dry season	Ivory coast			fluorescence	10000								μmol/m ² /a	(Delmas and Servant, 1983)
rainforest		La Selva, Costa Rica			GC-FPD (gold wool trapping, cryofocusin)				5.3-	210				μmol/m ² /a	(Andreae and Andreae, 1988)

site specifics	location	T (°C)	measurement method	instrument	H ₂ S	MeSH	DMS	COS	CS ₂	DMDS	other	other	unit	source	
rainforest soil	Billings Reservoir, Brazil		dynamic chamber (ambient air)	GC-FPD (cryofocusing)	- 9500- 92000	0- 140000	0	22000- 170000	3200- 22000				μmol/ m ² /a	(Jaeschke et al., 1994)	
vegetated rain- forest soil	Serra do Mar, Brazil		dynamic chamber (ambient air)	GC-FPD (cryofocusing)	- 320- 100	0-53	0- 320	- 210- 0	-26- 26				μmol/ m ² /a	(Jaeschke et al., 1994)	
estuary	Radio Universal, Brazil		dynamic chamber (ambient air)	GC-FPD (cryofocusing)	32- 410	0	0- 520	530- 12000	74- 1400				μmol/ m ² /a	(Jaeschke et al., 1994)	
Sacoglottis gab. Forest edge ground level	Reserve de Campo, Cameroon		plant cuvette	GC-FPD (cryofocusing)								total S	850- 2400	μmol/ m ² /a	(Kesselmeier et al., 1993)
Sacoglottis gab. In the forest canopy top (45 m)	Reserve de Campo, Cameroon		plant cuvette	GC-FPD (cryofocusing)								total S	19000	μmol/ m ² /a	(Kesselmeier et al., 1993)
Porterandia clad. Forest edge near ground	Reserve de Campo, Cameroon		plant cuvette	GC-FPD (cryofocusing)								total S	1000	μmol/ m ² /a	(Kesselmeier et al., 1993)
Amazon rain- forest	ATTO, Brasil		eddy covariane	PTR-MS			0.8- 6.0						μmol/ m ³	(Jardine et al., 2015)	
rainforest veg- etation + soil at 35 m height	Reserve de Campo, Cameroon		tower measure- ment	GC-FPD (cryofocusing)			n.d.	18	4.4				μmol/ m ³	(Kesselmeier et al., 1993)	

site specifics	location	T (°C)	measurement method	instrument	H ₂ S	MeSH	DMS	COS	CS ₂	DMDS	other	other	unit	source
rainforest vegetation + soil	Impfondo, Congo		direct air sampling ground	GC-FPD (gold wool trapping, cryofocusin)	1.7±0.7		1.2±0.6	24					μmol/m ³	(Bingemer et al., 1992)
rainforest vegetation + soil	Impfondo, Congo		simulation	GC-FPD (gold wool trapping, cryofocusin)	330±170								μmol/m ² /a	(Bingemer et al., 1992)

Table A.10.: VSC emissions from arctic soils according to literature.

site specifics	location	T (°C)	measurement method	instrument	H ₂ S	MeSH	DMS	COS	CS ₂	DMDS	other	other	unit	source
Antarctic Ocean Atmosphere	Drake Passage, Antarctica		direct air sampling	GC-FPD (gold wool trapping, cryofocusin)	0-3	(1.7-0.15E-3)	(8.3E-3)						μmol/m ³	(Berresheim et al., 1989)
Antarctic Ocean Atmosphere	Gerlache Strait, Antarctica		direct air sampling	GC-FPD (gold wool trapping, cryofocusin)	0-3	(0.7-0.09E-3)	(9.8E-3)						μmol/m ³	(Berresheim et al., 1989)

site specifics	location	T (°C)	measurement method	instrument	H ₂ S	MeSH	DMS	COS	CS ₂	DMDS	other	other	unit	source
Antarctic Ocean Atmo- sphere	Bransfield Strait, Antarctica		direct air sam- pling	GC-FPD (gold wool trapping, cryofo- cusin)	0		(4.6- 5.7)E- 3						μmol/ m ³	(Berresheim et al., 1989)
Antarctic Ocean Atmo- sphere	Coastal Shelf / Gerlache Strait, Antarctica		direct air sam- pling	GC-FPD (gold wool trapping, cryofo- cusin)	0		(1.5- 2.8)E- 3						μmol/ m ³	(Berresheim et al., 1989)
Arctic Ocean Atmosphere	Baffin Bay, Lancaster Sound, Nares Strait, Canada/Greenland		direct air sam- pling	HR-ToF- CIMS			7.3- 4400						μmol/ m ² /a	(Mungall et al., 2016)
wet meadow grass and sedge	Yukon- Kuskokwim delta, Bethel, Alaska, USA		dynamic cham- ber (VOC-free air)	GC-FPD (cryofo- cusing)			24- 89	11- 46	0- 9.6				μmol/ m ² /a	(Hines, 1992)
wet meadow moss	Yukon- Kuskokwim delta, Bethel, Alaska, USA		dynamic cham- ber (VOC-free air)	GC-FPD (cryofo- cusing)			13- 83	2.0- 78	0-29				μmol/ m ² /a	(Hines, 1992)

site specifics	location	T (°C)	measurement method	instrument	H ₂ S	MeSH	DMS	COS	CS ₂	DMDS	other	other	unit	source
upland mixed	Yukon-Kuskokwim delta, Bethel, Alaska, USA		dynamic chamber (VOC-free air)	GC-FPD (cryofocusing)			0-44	20-110	0-11				μmol/m ² /a	(Hines, 1992)
upland Labrador Tea	Yukon-Kuskokwim delta, Bethel, Alaska, USA		dynamic chamber (VOC-free air)	GC-FPD (cryofocusing)			4.4-73	25-88	0				μmol/m ² /a	(Hines, 1992)
upland moss	Yukon-Kuskokwim delta, Bethel, Alaska, USA		dynamic chamber (VOC-free air)	GC-FPD (cryofocusing)			0-67	29-74	0				μmol/m ² /a	(Hines, 1992)
upland lichen	Yukon-Kuskokwim delta, Bethel, Alaska, USA		dynamic chamber (VOC-free air)	GC-FPD (cryofocusing)			7.0-9.6	96-110	0				μmol/m ² /a	(Hines, 1992)
lake	Yukon-Kuskokwim delta, Bethel, Alaska, USA		dynamic chamber (VOC-free air)	GC-FPD (cryofocusing)			6.1-7.0	25	0-9.6				μmol/m ² /a	(Hines, 1992)

Table A.11.: VSC emissions from human and animal waste according to literature.

site specifics	location	T (°C)	measurement method	instrument	H ₂ S	MeSH	DMS	COS	CS ₂	DMS	other	other	unit	source
fish waste			static chamber	GC-MS	64000	230000	1.8		4.8	190	DMTS	2300	μmol/ kg/a	(He et al., 2018)
fish waste			static chamber	GC-MS							EtSH	2900	μmol/ kg/a	(He et al., 2018)
pork waste			static chamber	GC-MS	97	190000				390	DMTS	290	μmol/ kg/a	(He et al., 2018)
pork waste			static chamber	GC-MS							EtSH	59	μmol/ kg/a	(He et al., 2018)
suburban and rural landfills	Southeast Spain		cartridge sampling	GC-MS	0-59		0-		0.6-	0-	EtSH	0-26	μmol/ m ³	(Borras et al., 2016)
Reactive Activated sludge	Philadelphia's Northeast Water Pollution Control Plant, USA		water samples	GC-MS (purge and trap)	32	62	0		0	0-74			μmol/ m ³	(Cheng et al., 2005)
Primary tank	Philadelphia's Northeast Water Pollution Control Plant, USA		water samples	GC-MS (purge and trap)	0-44	0-810	80-12000		0	0-64			μmol/ m ³	(Cheng et al., 2005)
Aeration tank	Philadelphia's Northeast Water Pollution Control Plant, USA		water samples	GC-MS (purge and trap)	0-97	0-5300	0-20000		0	0-440			μmol/ m ³	(Cheng et al., 2005)

site specifics		location	T (°C)	measurement method	instrument	H ₂ S	MeSH	DMS	COS	CS ₂	DMDS	other	other	unit	source
Upstream of a siphon	winter	Sydney, Australia		direct air	GC-SCD (cryofocusing)	110	18	1.8		0.18	0.21	EtSH	0	μmol/m ³	(Wang et al., 2015)
Upstream of a siphon	summer	Sydney, Australia		direct air	GC-SCD (cryofocusing)	330	27	3.3		0.36	0.47	EtSH	0	μmol/m ³	(Wang et al., 2015)
pump stations wet well	winter	Sydney, Australia		direct air	GC-SCD (cryofocusing)	11	1.5	0.8		0.08	0.16	EtSH	0	μmol/m ³	(Wang et al., 2015)
pump stations wet well	summer	Sydney, Australia		direct air	GC-SCD (cryofocusing)	34	7.5	1.4		0.12	0.21	EtSH	0	μmol/m ³	(Wang et al., 2015)
inlet (downstream of siphon)	winter	Sydney, Australia		direct air	GC-SCD (cryofocusing)	32	86	1.0		0.05	0.08	EtSH	0	μmol/m ³	(Wang et al., 2015)
inlet (downstream of siphon)	summer	Sydney, Australia		direct air	GC-SCD (cryofocusing)	140	15	1.0		0.13	0.17	EtSH	0	μmol/m ³	(Wang et al., 2015)
outlet (after ac unit)	winter	Sydney, Australia		direct air	GC-SCD (cryofocusing)	0.8	0.4	1.1		0.14	0.44	EtSH	0	μmol/m ³	(Wang et al., 2015)
outlet (after ac unit)	summer	Sydney, Australia		direct air	GC-SCD (cryofocusing)	3.2	0.1	1.0		0.23	0.76	EtSH	0	μmol/m ³	(Wang et al., 2015)
intensive pig production facility		Groenhoej, Jutland, Denmark		direct air	PTR-MS		2000-3600	2000-3500						μmol/a	(Feilberga et al., 2010)

site specifics	location	T (°C)	measurement method	instrument	H ₂ S	MeSH	DMS	COS	CS ₂	DMSD	other	other	unit	source
agricultural soil	QualiAgro site, Feucherolles, France		dynamic cham- ber (VOC-free air)	PTR-MS			(1.6± 0.6)E6			(0.82± 0.16)E6	diethyl sulfide	(3.2± 0.7)E6	μmol/ kg/a	(Abis et al., 2018)
soil amended with bio-waste compost	QualiAgro site, Feucherolles, France		dynamic cham- ber (VOC-free air)	PTR-MS			(0.76± 0.44)E6			(1.1± 0.25)E6	diethyl sulfide	(3.2± 1.8)E6	μmol/ kg/a	(Abis et al., 2018)
soil with farm- yard manure	QualiAgro site, Feucherolles, France		dynamic cham- ber (VOC-free air)	PTR-MS			(1.35± 0.03)E6			(0.95± 0.22)E6	diethyl sulfide	(3.8± 0.5)E6	μmol/ kg/a	(Abis et al., 2018)
soil amended with co- composting green wastes with sewage sludge	QualiAgro site, Feucherolles, France		dynamic cham- ber (VOC-free air)	PTR-MS			(1.2± 0.3)E6			(1.45± 0.25)E6	diethyl sulfide	(12± 2)E6	μmol/ kg/a	(Abis et al., 2018)
soil with mu- nicipal solid waste compost	QualiAgro site, Feucherolles, France		dynamic cham- ber (VOC-free air)	PTR-MS			(1.3± 0.4)E6			(0.95± 0.32)E6	diethyl sulfide	(5.1± 0.6)E6	μmol/ kg/a	(Abis et al., 2018)

Supplement of Atmos. Meas. Tech., 13, 3507–3520, 2020
<https://doi.org/10.5194/amt-13-3507-2020-supplement>
© Author(s) 2020. This work is distributed under
the Creative Commons Attribution 4.0 License.



Atmospheric
Measurement
Techniques



Supplement of

SIFT-MS optimization for atmospheric trace gas measurements at varying humidity

Ann-Sophie Lehnert et al.

Correspondence to: Ann-Sophie Lehnert (alehnert@bgc-jena.mpg.de)

The copyright of individual parts of the supplement might differ from the CC BY 4.0 License.

S1 Experimental

Table S1: Measured ions (m/z in u) for SIFT-MS and PTR-MS to compare the compounds of the VOC standard.

substance	m/z (SIFT-MS) in u			m/z (PTR-MS) in u
	H_3O^+	NO^+	O_2^+	
α -pinene	81, 137, 155	136	93	81, 137
1,4-dichlorobenzene	147	146	146	148
2-butenal	71, 89	69	69, 70	71
acetaldehyde	45, 63	43	43	45
acetone	59, 77	88	43, 58	59
acetonitrile	42, 60	71	-	42
acrolein	57, 75	55, 86	28, 55	75
benzene	79	78, 108	78	79

S2 SIFT-MS optimization to reduce background

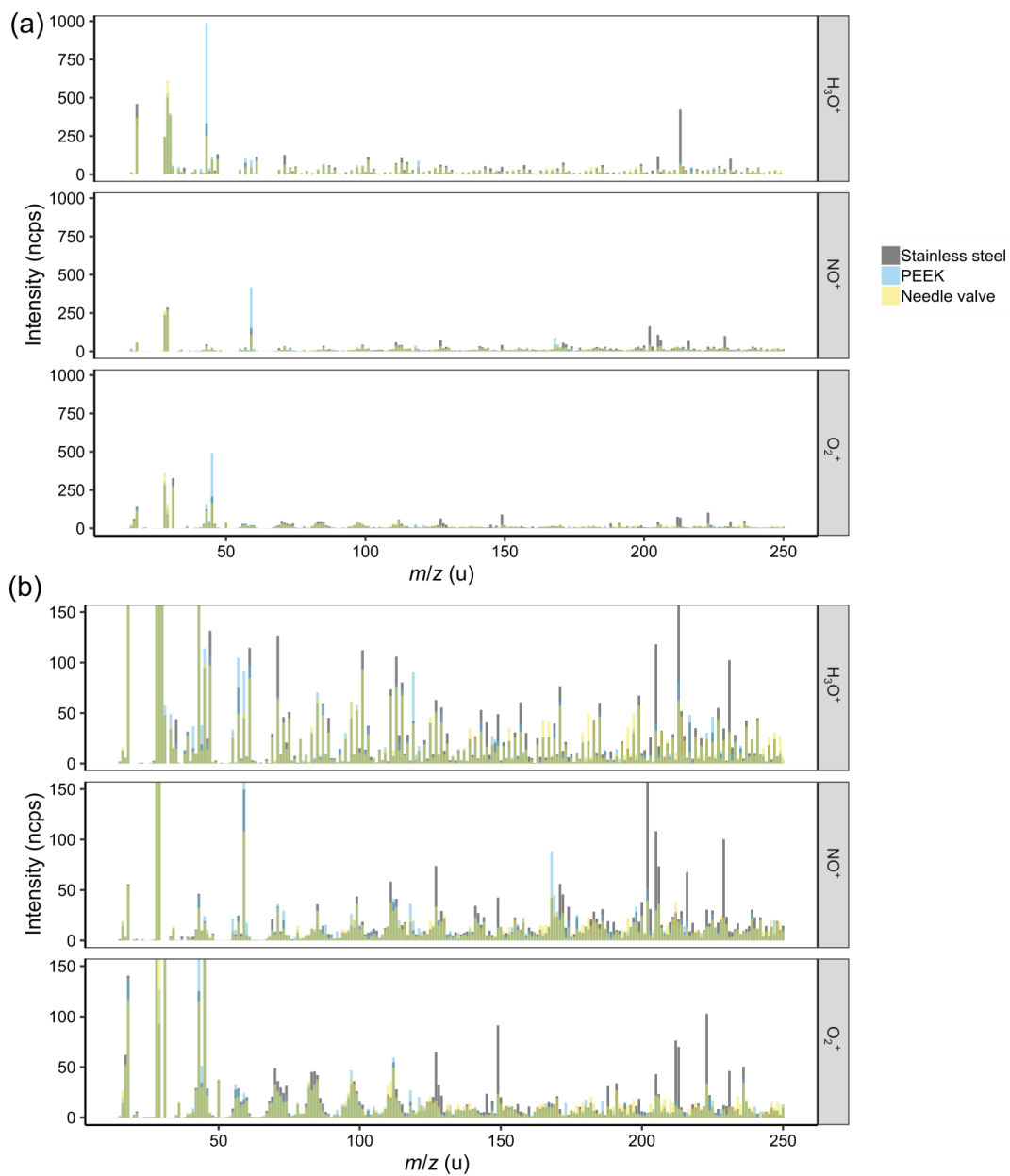


Figure S1: Background as recorded for different flow restrictors in the multi-port inlet: capillaries from silica coated stainless steel (as provided by Syft Technologies, grey bars), from PEEK (blue bars), and a Swagelok needle valve (yellow bars). The ion intensity is normalized to 10^6 counts of the reagent ion and the air flow entering the system in sccm. (b) is a zoomed-in version of (a), to visualize differences better. The reagent ions as well as their water clusters and isotopic peaks are not shown to improve clarity.

We chose to use the needle valve since it consistently shows lowest contamination in the range <150 u.

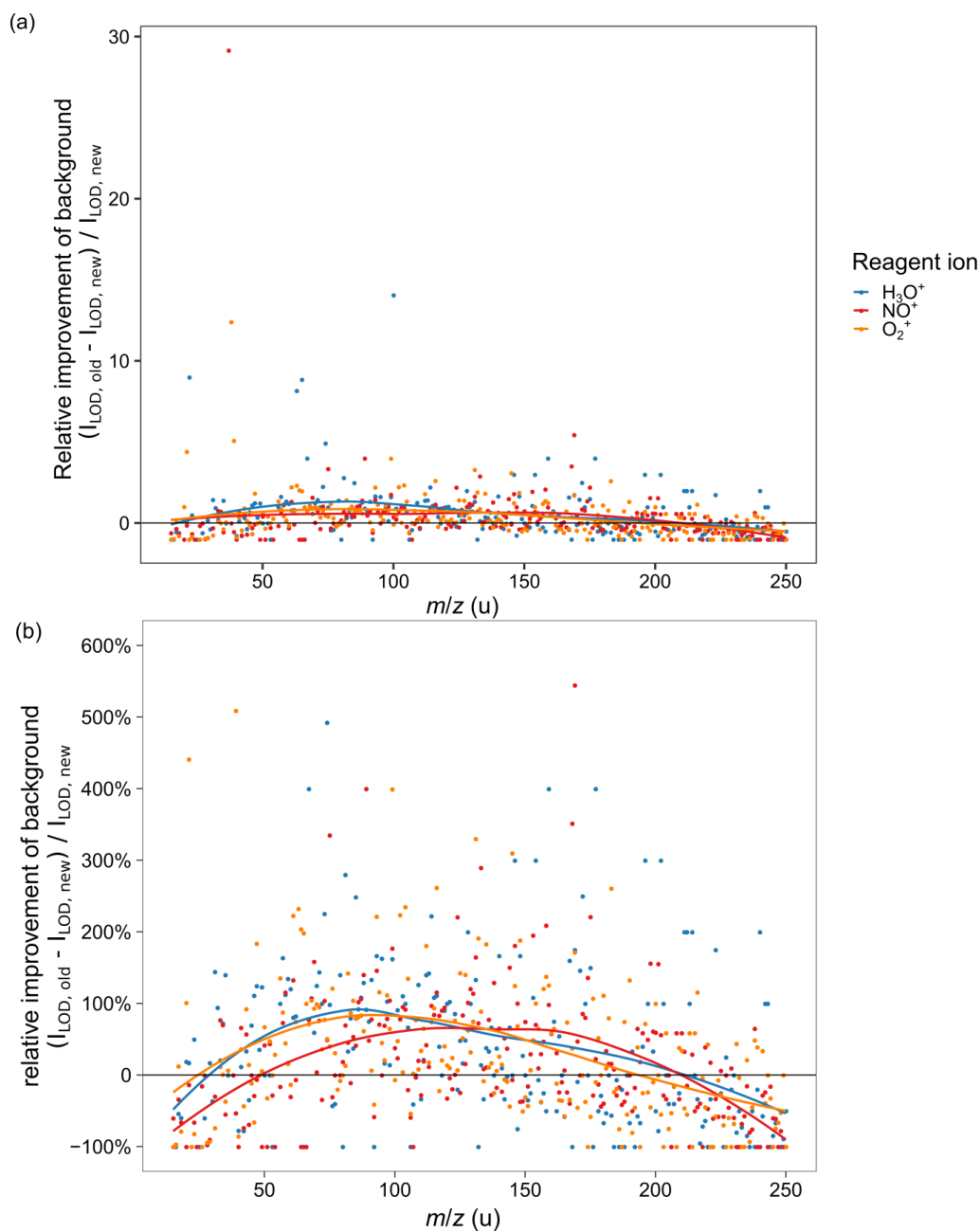


Figure S2: Relative improvement of the instrument background (instrument being flushed with VOC free air) after changing the o-rings in the system to FEP coated FKM o-rings. Comparing the critical intensity $I_{LOD} = \overline{I_{background}} + 3 \cdot sd(I_{background})$ before (old) and after (new) the change, normalized to the critical intensity after the o-ring change. (a) complete display of all improvement factors, (b) zoomed plot for lower relative improvements. The data was normalized to 10^6 reagent ion counts before comparing it. Changes in secondary reagent ions, i.e. H₃O⁺/ 30, 32, 37, 55, 73, NO⁺/ 19, 32, 37, 48, O₂⁺/ 19, 30, 37 as well as reagent ion isotopic peaks were removed from the data before plotting. The curves are LOESS fits of the critical intensities with regard to the three reagent ions.

We found H₃O⁺ 63, 65, 67, and 114 u and O₂⁺ 63, and 64, which might all be different ions of difluorovinylidene quenching products and residual monomers, [CF₂CH]⁺, [CF₂CH₃]⁺, [CF₂CH₃]⁺, [C₂F₄CH₂]⁺, and [CF₂CH₂]⁺. H₃O⁺ 100 u might be [C₂F₄]⁺, 202 u might be [C₄F₈H₂]⁺, 196 and 146 u could be [HC₂F₄CO₂H]⁺ and [HCF₂CO₂H]⁺, NO⁺ 169 could be [C₃F₇]⁺, and O₂⁺ 102 amu could be [C₂F₄H₂]⁺ which might be

byproducts in the PTFE production or degradation. This all hints to the fact that the previous o-rings in the system degassed small contaminants that could come from their production process.

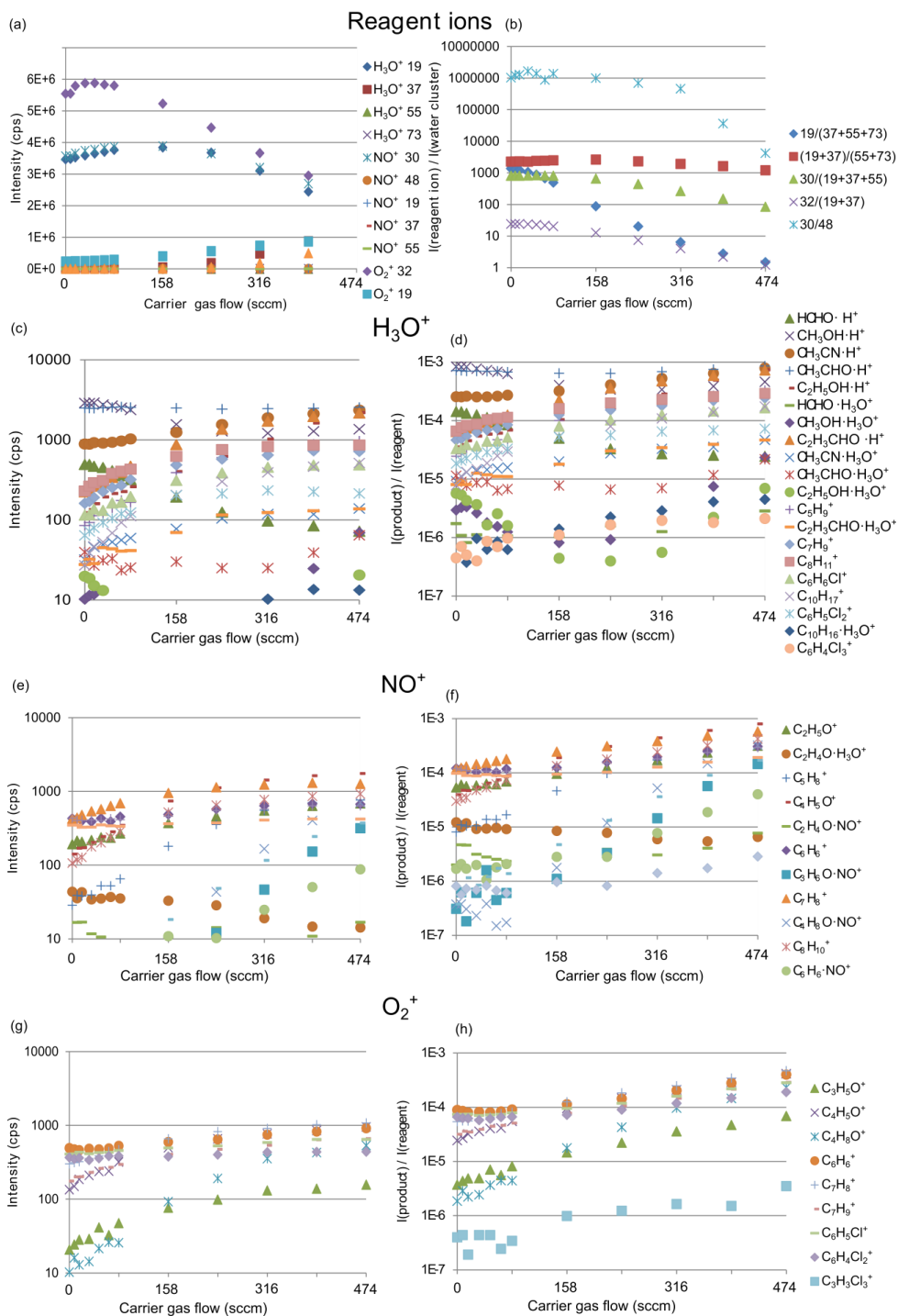


Figure S3: Complete results of the carrier gas flow optimization for helium carrier gas and zero air dilution gas, $U_{\text{FT}} = 50$ V, $T_{\text{FT}} = 140^\circ\text{C}$, 90% humidity at 25°C . (a), (b): for the different reagent ions H_3O^+ , NO^+ , and O_2^+ , the detected primary and secondary reagent ions symbolized by their mass are shown 19 = H_2O^+ , 37 = $\text{H}_3\text{O}^+ \cdot \text{H}_2\text{O}$, 55 = $\text{H}_3\text{O}^+ \cdot 2 \text{H}_2\text{O}$, 73 = $\text{H}_3\text{O}^+ \cdot 3 \text{H}_2\text{O}$, 30 = NO^+ , 48 = $\text{NO}^+ \cdot \text{H}_2\text{O}$, 32 = O_2^+ . (a): absolute

ion counts, (b): proportion of reagent ions relative to the water clusters. (c–h): behaviour of the product ions upon reaction with H_3O^+ (19 + 37 + 55, (c, d)), NO^+ (e, f), and O_2^+ (g, h) as reagent ions. (c, e, g): absolute ion counts, (d, f, h): counts normalized to reagent ion counts.

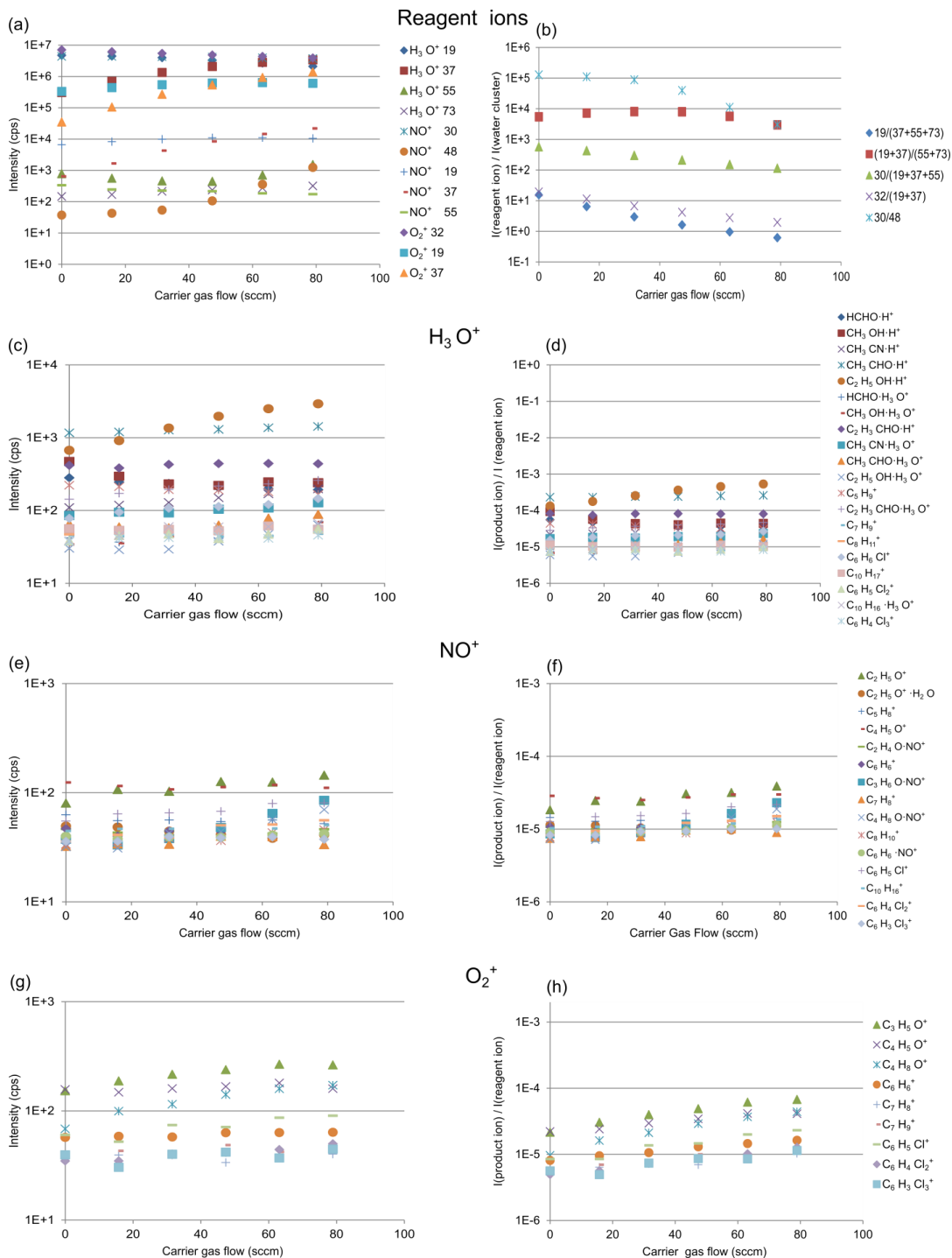


Figure S4: Complete results of the carrier gas flow optimization for helium carrier gas and zero air dilution gas, $U_{FT} = 50$ V, $T_{FT} = 140^\circ\text{C}$, 90% humidity at 25°C , picture section of Fig. S3 for low carrier gas flows <100 sccm. (a), (b): for the different reagent ions H_3O^+ , NO^+ , and O_2^+ , the detected primary and secondary reagent ions symbolized by their mass are shown $19 = \text{H}_2\text{O}^+$, $37 = \text{H}_3\text{O}^+$, $55 = \text{H}_3\text{O}^+ \cdot \text{H}_2\text{O}$, $73 = \text{H}_3\text{O}^+ \cdot 2 \text{H}_2\text{O}$, $30 = \text{NO}^+$, $48 = \text{NO}^+ \cdot \text{H}_2\text{O}$, $32 = \text{O}_2^+$. (a): absolute ion counts, (b): proportion of reagent ions relative to the water clusters. (c–h): behaviour of the product ions upon reaction with H_3O^+ (19 + 37 + 55, (c, d)), NO^+ (e, f), and O_2^+ (g, h) as reagent ions. (c, e, g): absolute ion counts, (d, f, h): counts normalized to reagent ion counts.

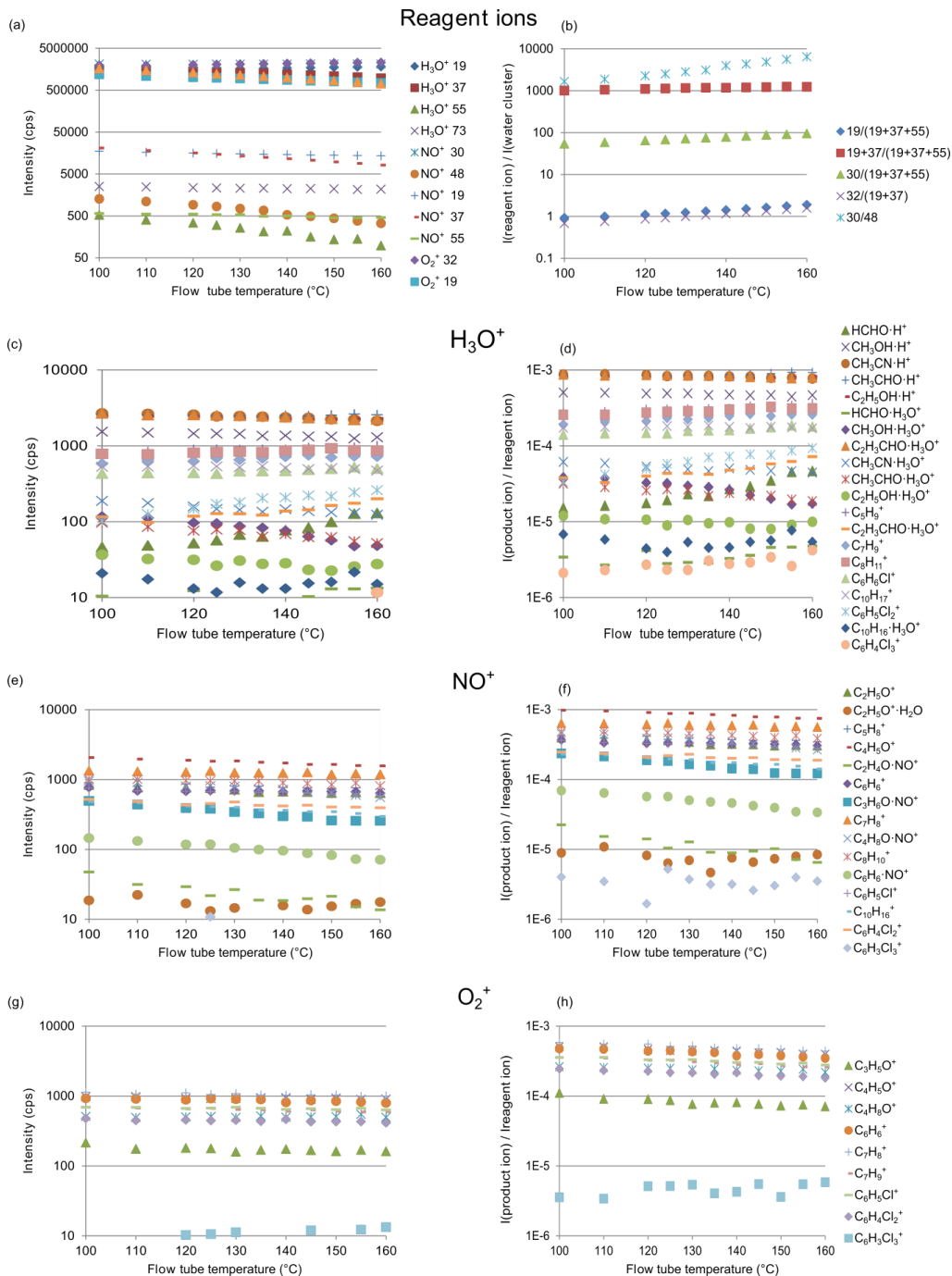


Figure S5: Complete results of the flow tube temperature for helium carrier gas and zero air dilution gas, $U_{FT} = 50$ V, $\phi_{FT} = 395$ sccm, 90% humidity at 25°C. (a–b) for the different reagent ions H_3O^+ , NO^+ , and O_2^+ , the detected primary and secondary reagent ions symbolized by their mass are shown 19 = H_2O^+ , 37 = $H_3O^+ \cdot H_2O$, 55 = $H_3O^+ \cdot 2 H_2O$, 73 = $H_3O^+ \cdot 3 H_2O$, 30 = NO^+ , 48 = $NO^+ \cdot H_2O$, 32 = O_2^+ . (a) absolute ion counts, (b) proportion of reagent ions relative to the water clusters. (c–h) behaviour of the product ions upon reaction with H_3O^+ (19 + 37 + 55, c, d), NO^+ (e, f), and O_2^+ (g, h) as reagent ions. (c, e, g) absolute ion counts, (d, f, h) counts normalized to reagent ion counts.

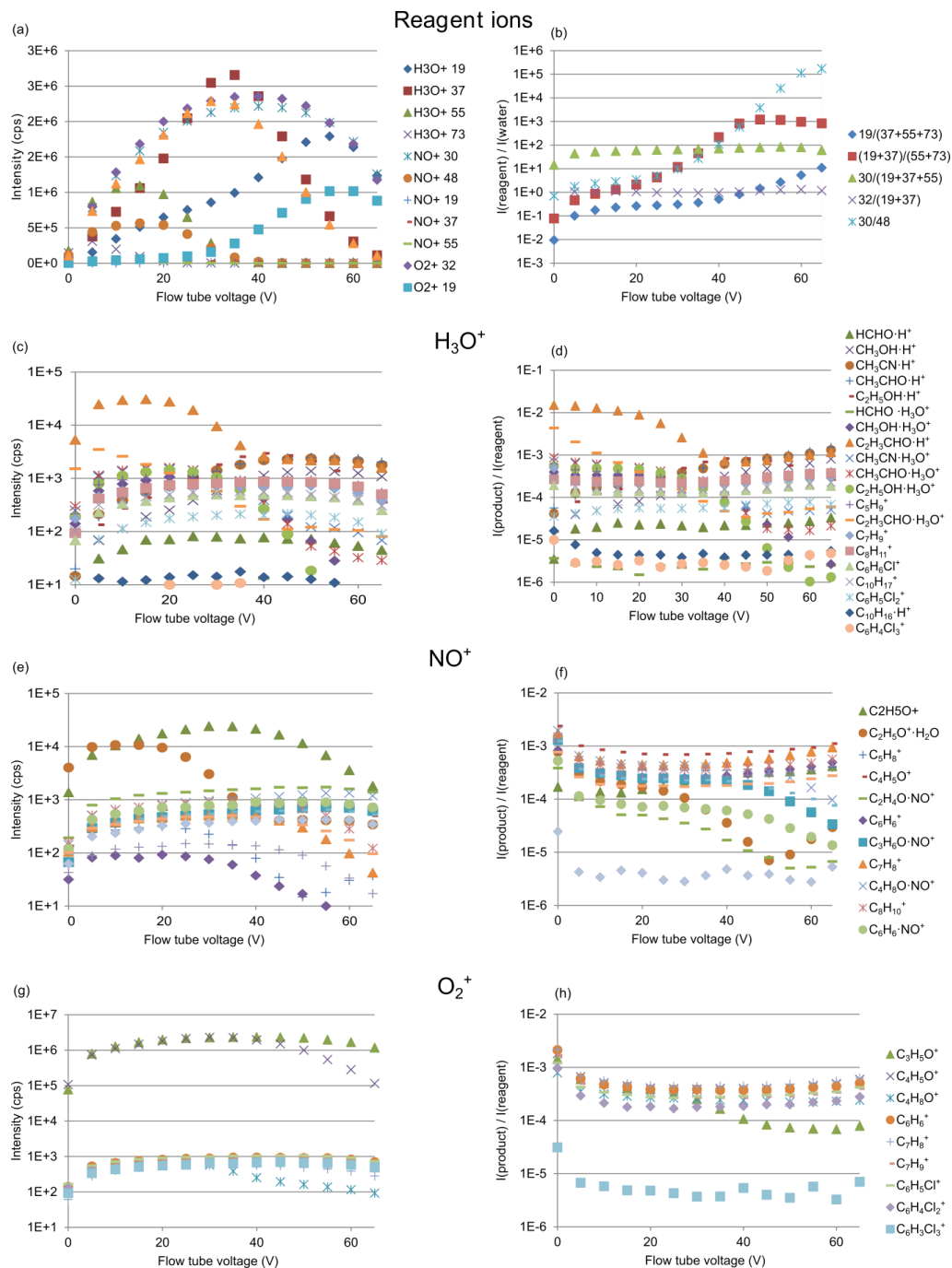


Figure S6: Flow tube voltage optimization for helium carrier gas and zero air dilution gas, $\phi_{FT} = 395$ sccm, $T_{FT} = 140^\circ\text{C}$, 90% humidity at 25°C . (a–b) for the different reagent ions H_3O^+ , NO^+ , and O_2^+ , the detected primary and secondary reagent ions symbolized by their massare shown 19 = H_2O^+ , 37 = $\text{H}_3\text{O}^+ \cdot \text{H}_2\text{O}$, 55 = $\text{H}_3\text{O}^+ \cdot 2 \text{H}_2\text{O}$, 73 = $\text{H}_3\text{O}^+ \cdot 3 \text{H}_2\text{O}$, 30 = NO^+ , 48 = $\text{NO}^+ \cdot \text{H}_2\text{O}$, 32 = O_2^+ . (a) absolute ion counts, (b) proportion of reagent ions relative to the water clusters. (c–h) behaviour of the product ions upon reaction with H_3O^+ (19 + 37 + 55, c, d), NO^+ (e, f), and O_2^+ (g, h) as reagent ions. (c, e, g) absolute ion counts, (d, f, h) counts normalized to reagent ion counts.

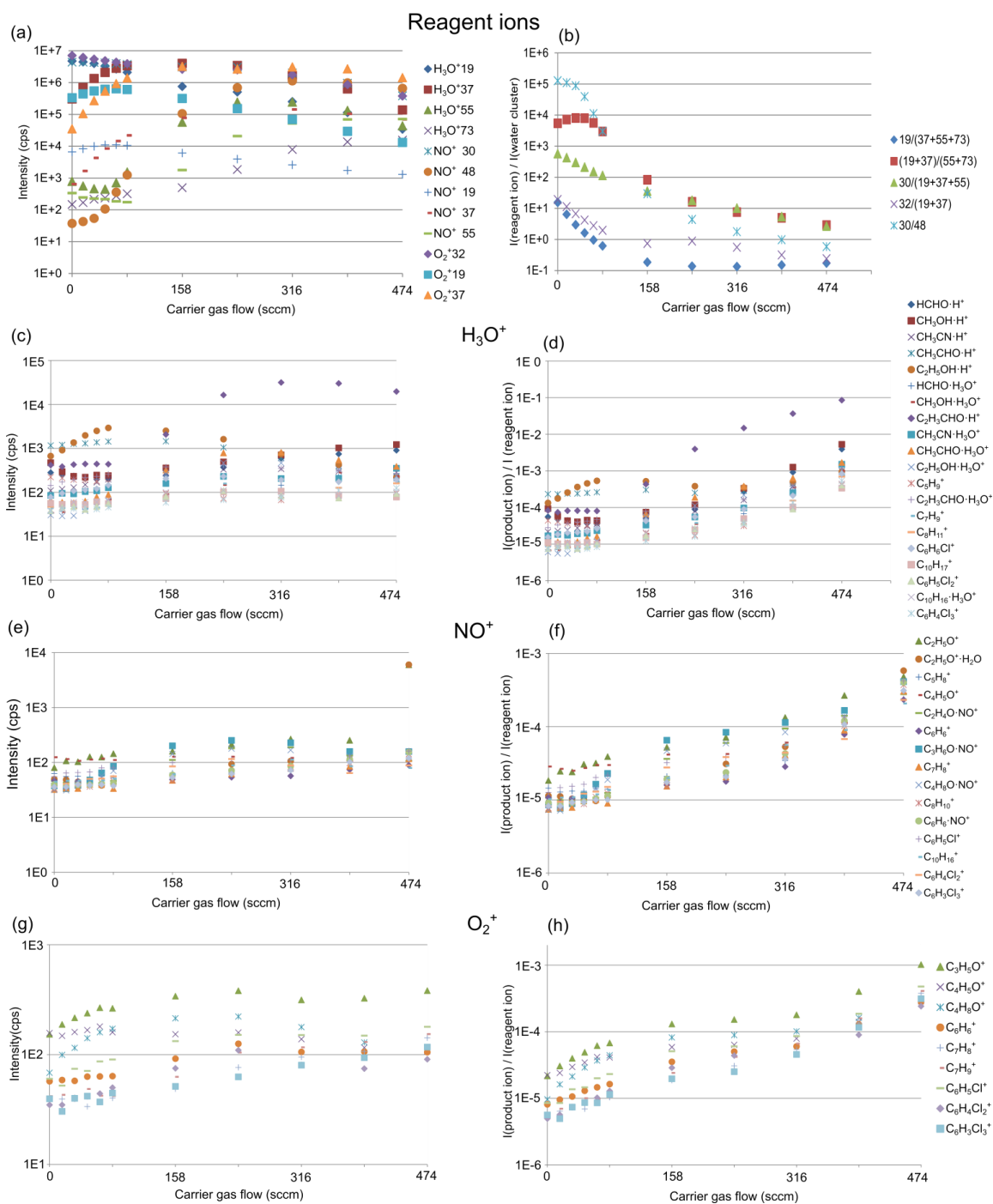


Figure S7: Carrier gas flow optimization for nitrogen carrier gas and zero air dilution gas, $U_{\text{FT}} = 50$ V, $T_{\text{FT}} = 140^\circ\text{C}$, 90% humidity at 25°C . (a–b) for the different reagent ions H_3O^+ , NO^+ , and O_2^+ , the detected primary and secondary reagent ions symbolized by their mass are shown 19 = H_2O^+ , 37 = $\text{H}_3\text{O}^+ \cdot \text{H}_2\text{O}$, 55 = $\text{H}_3\text{O}^+ \cdot 2 \text{H}_2\text{O}$, 73 = $\text{H}_3\text{O}^+ \cdot 3 \text{H}_2\text{O}$, 30 = NO^+ , 48 = $\text{NO}^+ \cdot \text{H}_2\text{O}$, 32 = O_2^+ . (a) absolute ion counts, (b) proportion of reagent ions relative to the water clusters. (c–h) behaviour of the product ions upon reaction with H_3O^+ (19 + 37 + 55, c, d), NO^+ (e, f), and O_2^+ (g, h) as reagent ions. (c, e, g) absolute ion counts, (d, f, h) counts normalized to reagent ion counts.

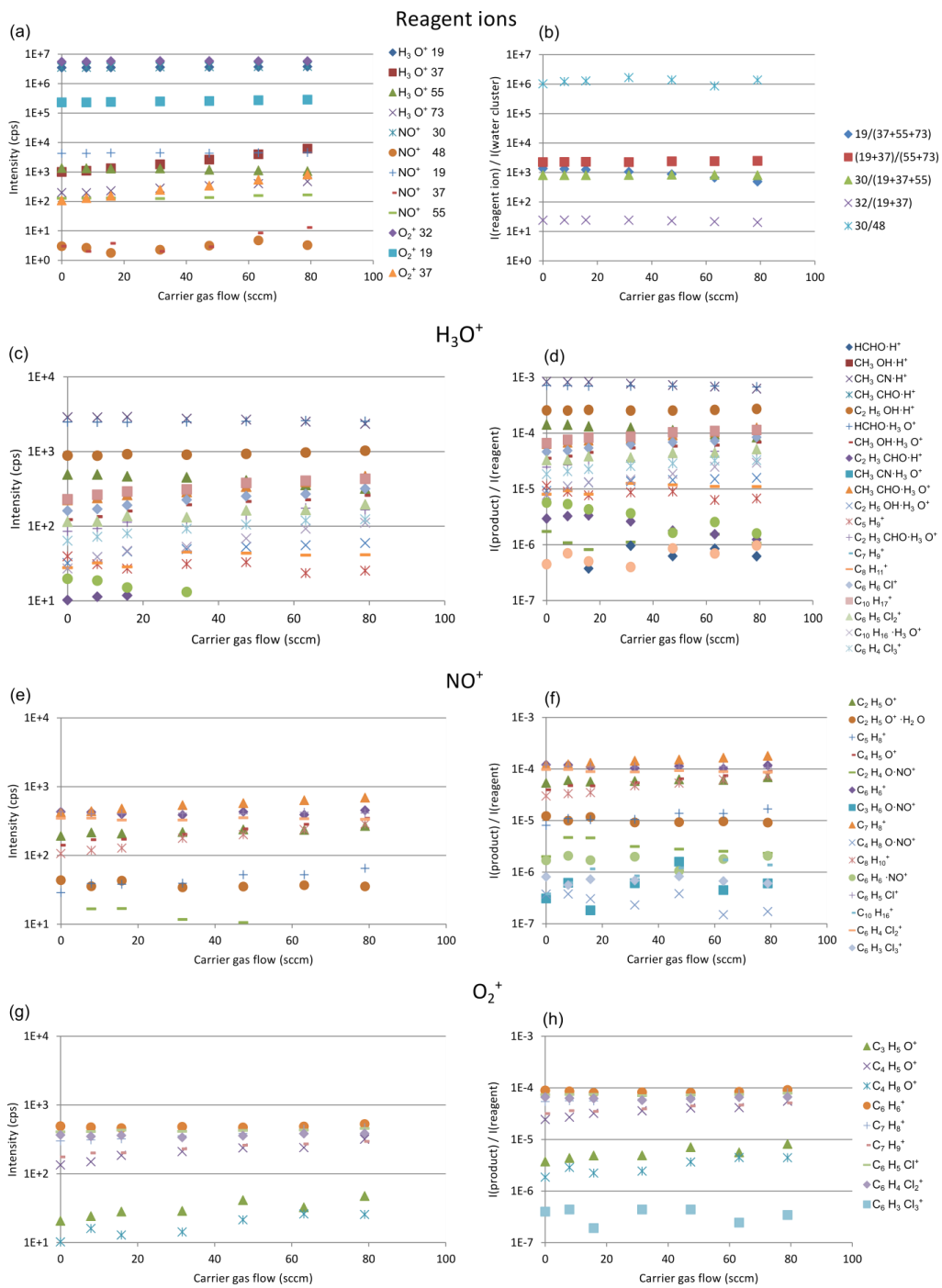


Figure S8: Carrier gas flow optimization for nitrogen carrier gas and zero air dilution gas, $U_{FT} = 50$ V, $T_{FT} = 140^\circ\text{C}$, 90% humidity at 25°C , picture section of Fig. S7 for low carrier gas flows. (a–b) for the different reagent ions H_3O^+ , NO^+ , and O_2^+ , the detected primary and secondary reagent ions symbolized by their mass are shown $19 = H_2O^+$, $37 = H_3O^+ \cdot H_2O$, $55 = H_3O^+ \cdot 2 H_2O$, $73 = H_3O^+ \cdot 3 H_2O$, $30 = NO^+$, $48 = NO^+ \cdot H_2O$, $32 = O_2^+$. (a) absolute ion counts, (b) proportion of reagent ions relative to the water clusters. (c–h) behaviour of the product ions upon

reaction with H_3O^+ (19 + 37 + 55, c, d), NO^+ (e, f), and O_2^+ (g, h) as reagent ions. (c, e, g) absolute ion counts, (d, f, h) counts normalized to reagent ion counts.

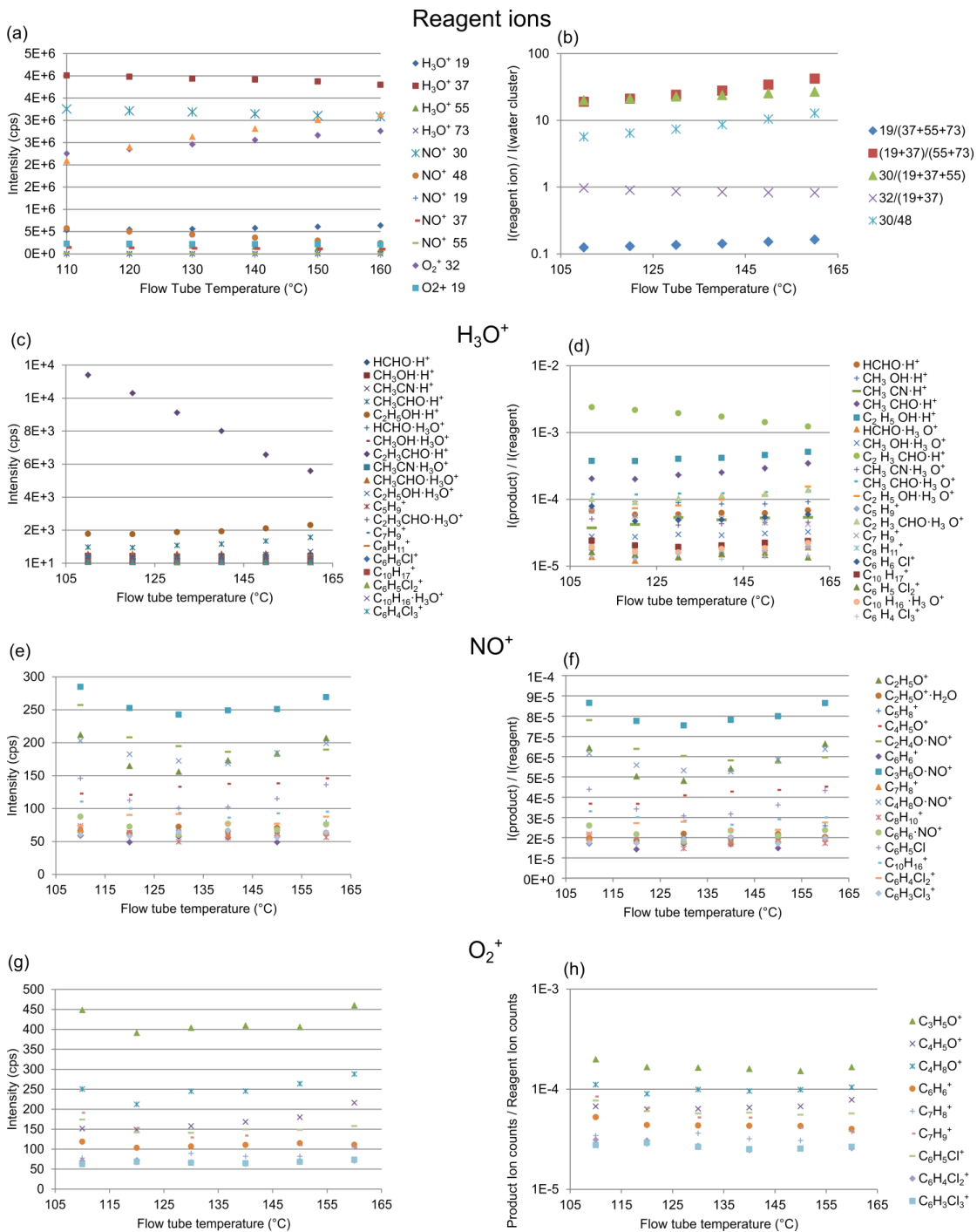


Figure S9: Flow tube temperature optimization for nitrogen carrier gas and zero air dilution gas, $U_{FT} = 50$ V, $\phi_{FT} = 5$ TorrL s^{-1} , 90% humidity at 25°C. (a–b) for the different reagent ions H_3O^+ , NO^+ , and O_2^+ , the detected primary and secondary reagent ions symbolized by their mass are shown $19 = H_2O^+$, $37 = H_3O^+ \cdot H_2O$, $55 = H_3O^+ \cdot 2 H_2O$, $73 = H_3O^+ \cdot 3 H_2O$, $30 = NO^+$, $48 = NO^+ \cdot H_2O$, $32 = O_2^+$. (a) absolute ion counts, (b) proportion of reagent ions relative to the water clusters. (c–h) behaviour of the product ions upon reaction with H_3O^+ ($19 + 37 + 55$, c, d), NO^+ (e, f), and O_2^+ (g, h) as reagent ions. (c, e, g) absolute ion counts, (d, f, h) counts normalized to reagent ion counts.

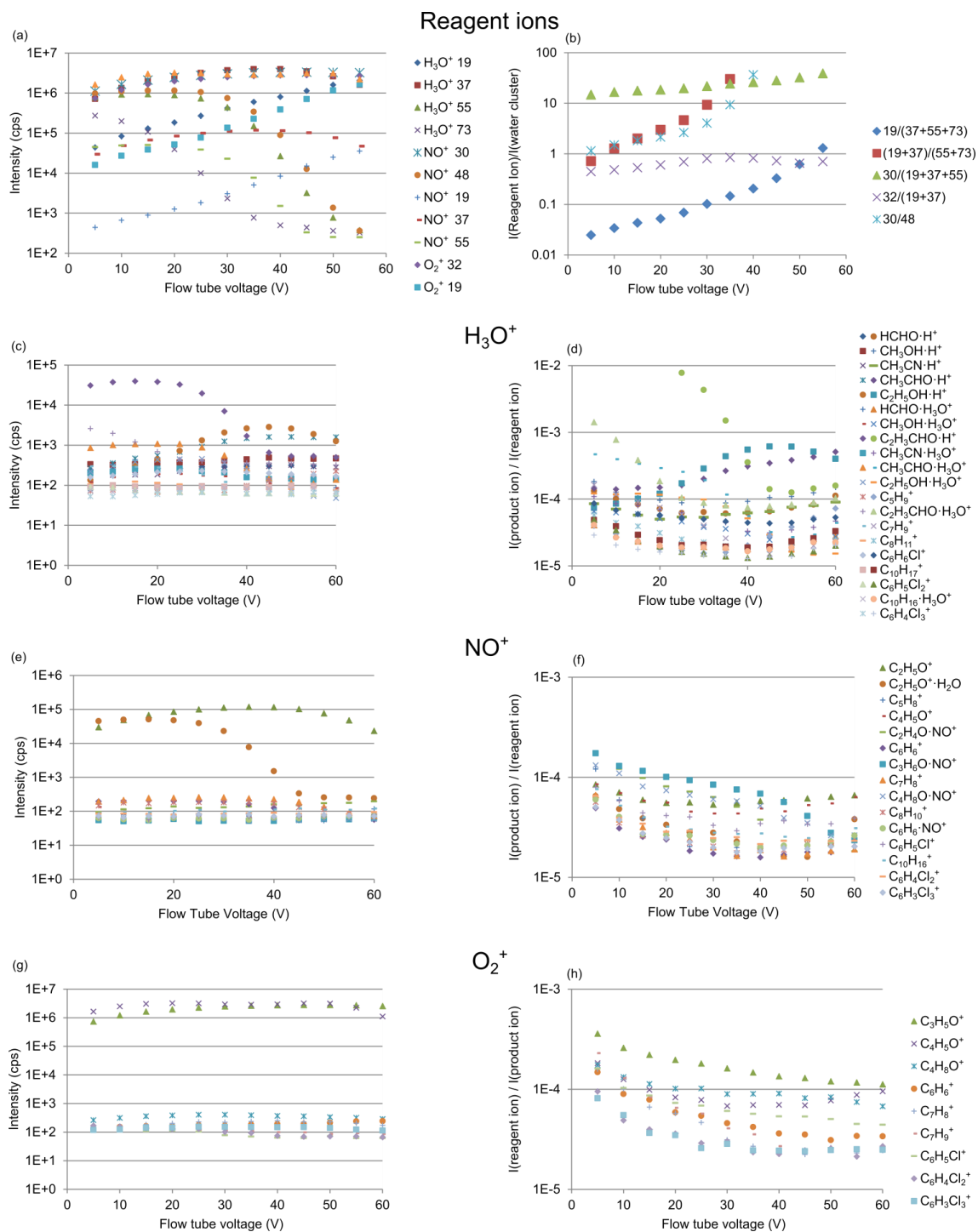


Figure S10: Flow tube voltage optimization for nitrogen carrier gas and zero air dilution gas, $\phi_{\text{FT}} = 5 \text{ TorrL s}^{-1}$, $T_{\text{FT}} = 140^\circ\text{C}$, 90% humidity at 25°C . (a–b) for the different reagent ions H_3O^+ , NO^+ , and O_2^+ , the detected primary and secondary reagent ions symbolized by their mass are shown 19 = H_2O^+ , 37 = $\text{H}_3\text{O}^+ \cdot \text{H}_2\text{O}$, 55 = $\text{H}_3\text{O}^+ \cdot 2 \text{H}_2\text{O}$, 73 = $\text{H}_3\text{O}^+ \cdot 3 \text{H}_2\text{O}$, 30 = NO^+ , 48 = $\text{NO}^+ \cdot \text{H}_2\text{O}$, 32 = O_2^+ . (a) absolute ion counts, (b)

proportion of reagent ions relative to the water clusters. (c–h) behaviour of the product ions upon reaction with H_3O^+ (19 + 37 + 55, c, d), NO^+ (e, f), and O_2^+ (g, h) as reagent ions. (c, e, g) absolute ion counts, (d, f, h) counts normalized to reagent ion counts.

Table S2: LODs (in ppb, derived from Blank, $3 \cdot \text{sd}$), of the SIFT-MS with nitrogen carrier gas of the different compounds and relative humidities at 25°C.

compound	$m/z_{\text{reag}} / m/z_{\text{prod}}$	Dry	30% humidity	60% humidity	90% humidity
methanol	19 / 33	0.720	0.342	0.385	0.803
acetonitrile	19 / 42	0.075	0.053	0.063	0.251
acetaldehyde	19 / 45	0.429	0.288	0.240	0.281
acrolein	19 / 57	0.112	0.219	0.348	1.077
isoprene	19 / 69	0.120	0.142	0.167	0.264
butanone	19 / 73	0.112	0.191	0.152	0.229
toluene	19 / 93	0.048	0.164	0.100	0.222
<i>o</i>-xylene	19 / 107	0.074	0.126	0.193	0.272
α-pinene	19 / 137	0.317	0.064	0.319	0.168
dichlorobenzene	19 / 147	0.131	0.120	0.196	2.609
isoprene	30 / 68	0.094	0.110	0.141	0.182
2-butenal	30 / 69	0.084	0.077	0.033	0.060
benzene	30 / 78	0.063	0.181	0.098	0.215
toluene	30 / 92	0.127	0.058	0.094	0.098
butanone	30 / 102	0.116	0.093	0.116	0.114
<i>o</i>-xylene	30 / 106	0.073	0.212	0.106	0.090
chlorobenzene	30 / 112	0.145	0.193	0.238	0.219
α-pinene	30 / 136	0.125	0.240	0.292	0.359
dichlorobenzene	30 / 146	0.175	0.144	0.155	0.239
2-butenal	32 / 69	0.026	0.177	0.166	0.181
butanone	32 / 72	0.113	0.140	0.192	0.460
benzene	32 / 78	0.080	0.109	0.064	0.136
toluene	32 / 92	0.066	0.050	0.081	0.087
α-pinene	32 / 93	0.049	0.088	0.130	0.214
chlorobenzene	32 / 112	0.132	0.219	0.079	0.192
dichlorobenzene	32 / 146	0.194	0.093	0.117	0.171

Table S3: Sensitivities \pm 95% confidence interval (in cps/ppb, based on product ion counts normalized to 10^6 reagent ion counts, $df = 26$), of the SIFT-MS with nitrogen carrier gas of the different compounds and relative humidities at 25°C. NA: LOD was over 2 ppb so that not enough calibration points remained for a calibration.

compound	$m/z_{\text{reag}} / m/z_{\text{prod}}$	Dry	30% humidity	60% humidity	90% humidity
methanol	19 / 33	111 \pm 2	104 \pm 2	110 \pm 2	36.2 \pm 0.8
acetonitrile	19 / 42	235 \pm 2	236 \pm 1	232 \pm 2	109.0 \pm 0.8
acetaldehyde	19 / 45	200 \pm 2	195 \pm 2	194 \pm 2	85 \pm 1
acrolein	19 / 57	220 \pm 4	223 \pm 3	219 \pm 3	118 \pm 3
isoprene	19 / 69	135 \pm 1	129 \pm 1	124 \pm 2	29.8 \pm 0.4
butanone	19 / 73	264 \pm 1	252 \pm 2	250 \pm 2	148 \pm 2
toluene	19 / 93	137 \pm 1	130.2 \pm 0.9	127 \pm 1	21.5 \pm 0.7
<i>o</i>-xylene	19 / 107	144.4 \pm 0.8	137.2 \pm 0.9	135 \pm 1	28.4 \pm 0.3
α-pinene	19 / 137	63.1 \pm 0.6	63.4 \pm 0.9	59.0 \pm 0.6	36.1 \pm 0.5
dichlorobenzene	19 / 147	71.0 \pm 0.9	64.1 \pm 0.6	62.8 \pm 0.8	3.4 \pm 0.3
isoprene	30 / 68	82.9 \pm 0.9	83.2 \pm 0.8	79.6 \pm 0.8	71.1 \pm 0.6
2-butenal	30 / 69	204 \pm 2	201 \pm 2	194 \pm 1	186 \pm 3
benzene	30 / 78	71.6 \pm 0.6	72.3 \pm 0.7	67.3 \pm 0.9	60.3 \pm 0.6
toluene	30 / 92	131.7 \pm 0.8	134 \pm 1	125 \pm 1	115.9 \pm 0.5
butanone	30 / 102	130 \pm 1	127.0 \pm 0.9	121.0 \pm 0.8	130 \pm 2
<i>o</i>-xylene	30 / 106	114 \pm 0.8	111 \pm 1	106 \pm 1	103.5 \pm 0.9
chlorobenzene	30 / 112	87.8 \pm 0.9	86 \pm 1	80.1 \pm 0.7	75 \pm 1
α-pinene	30 / 136	61.4 \pm 0.5	60.4 \pm 0.9	56.1 \pm 0.7	62.1 \pm 0.9
dichlorobenzene	30 / 146	60.0 \pm 0.7	59.2 \pm 0.7	56.2 \pm 0.6	48.6 \pm 0.9
2-butenal	32 / 69	136 \pm 1	132.2 \pm 0.9	128 \pm 1	109 \pm 2
butanone	32 / 72	51.5 \pm 0.5	50.9 \pm 0.7	48.6 \pm 0.7	60.1 \pm 0.9
benzene	32 / 78	88.8 \pm 0.6	86.4 \pm 0.5	85.3 \pm 0.7	108.8 \pm 0.7
toluene	32 / 92	113.6 \pm 0.7	112.1 \pm 0.8	104.9 \pm 0.7	133.9 \pm 0.7
α-pinene	32 / 93	64.6 \pm 0.6	66.2 \pm 0.5	62.1 \pm 0.4	80 \pm 1
chlorobenzene	32 / 112	75.0 \pm 0.8	74 \pm 1	72.6 \pm 0.7	89 \pm 1
dichlorobenzene	32 / 146	54.2 \pm 0.5	53.2 \pm 0.7	48.3 \pm 0.5	62.0 \pm 0.7

Table S4: SNR at 1 ppb \pm 95% upper and lower confidence interval (CI^u and CI^l), based on product ion counts normalized to 10⁶ reagent ion counts, df = 7) of the SIFT-MS with nitrogen carrier gas of the different compounds and relative humidities at 25°C. NA: LOD was over 2 ppb so that not enough calibration points remained for a calibration.

compound	$m/z_{\text{reag}} / m/z_{\text{prod}}$	dry			30% humidity			60% humidity			90% humidity		
		SNR	CI ^u	CI ^l	SNR	CI ^u	CI ^l	SNR	CI ^u	CI ^l	SNR	CI ^u	CI ^l
methanol	19 / 33	1.6	0.7	0.5	1.9	0.4	0.4	1.7	0.5	0.4	1.8	0.6	0.4
acetonitrile	19 / 42	6.6	3.0	2.2	8.6	3.8	2.9	5.4	1.5	1.2	3.6	2.6	1.5
acetaldehyde	19 / 45	1.6	0.4	0.3	1.3	0.2	0.2	1.4	0.2	0.2	1.4	0.2	0.2
acrolein	19 / 57	5.4	1.2	1.1	2.6	0.5	0.4	2.0	0.5	0.5	1.1	0.1	0.1
isoprene	19 / 69	6.7	5.1	3.1	5.3	2.9	2.0	5.1	3.5	2.2	2.6	1.7	1.2
butanone	19 / 73	3.6	1.0	0.9	2.3	0.7	0.6	2.6	0.5	0.4	1.5	0.3	0.3
toluene	19 / 93	8.3	2.1	1.7	6.6	6.0	3.4	6.4	2.8	2.0	3.4	1.3	1.1
<i>o</i> -xylene	19 / 107	7.4	3.3	2.5	5.8	2.7	1.9	5.3	4.7	2.7	2.1	0.9	0.7
α -pinene	19 / 137	5.4	6.4	3.2	5.1	0.9	0.8	3.5	3.2	2.0	2.5	0.8	0.6
dichlorobenzene	19 / 147	5.5	4.1	2.7	5.2	2.7	2.0	4.8	4.7	3.0	1.5	1.3	0.9
isoprene	30 / 68	6.4	3.6	2.7	5.1	2.7	2.0	6.2	4.6	3.0	4.6	2.7	1.7
2-butenal	30 / 69	6.6	5.0	3.0	5.7	1.9	1.5	5.8	1.0	0.9	1.8	1.0	0.8
benzene	30 / 78	3.9	1.1	1.0	4.4	3.0	2.0	4.4	1.7	1.4	4.8	4.5	2.5
toluene	30 / 92	8.2	8.7	4.7	9.4	4.5	3.3	7.3	4.3	2.9	6.4	3.9	2.7
butanone	30 / 102	4.3	2.1	1.5	4.1	1.2	1.0	3.6	1.0	0.8	2.3	1.1	0.9
<i>o</i> -xylene	30 / 106	5.4	1.7	1.4	5.1	5.2	2.9	5.3	3.2	2.3	6.0	3.6	2.5
chlorobenzene	30 / 112	4.5	1.5	1.1	3.8	2.0	1.5	3.9	2.3	1.6	3.6	2.6	1.7
α -pinene	30 / 136	4.6	1.5	1.2	5.4	4.2	2.6	3.5	2.9	1.9	3.5	2.9	1.6
dichlorobenzene	30 / 146	5.9	4.3	2.6	5.4	3.5	2.5	4.6	2.7	2.0	3.0	1.5	1.1
2-butenal	32 / 69	4.2	1.0	0.9	3.7	1.9	1.4	3.9	1.9	1.3	1.7	1.0	0.8
butanone	32 / 72	3.4	0.7	0.7	1.9	0.3	0.3	2.2	0.5	0.4	1.6	0.7	0.5
benzene	32 / 78	5.5	3.2	2.4	6.9	4.1	2.8	5.0	1.2	1.0	3.4	1.2	0.9
toluene	32 / 92	9.1	3.8	2.7	7.5	2.4	1.9	7.3	4.8	3.5	6.4	3.8	2.7
α -pinene	32 / 93	5.8	1.6	1.4	4.9	1.7	1.4	4.4	2.3	1.7	3.7	1.7	1.2
chloro-benzene	32 / 112	5.0	2.6	2.0	3.7	2.3	1.6	3.3	0.8	0.7	2.7	1.0	0.8
dichloro-benzene	32 / 146	5.5	5.1	2.8	7.3	4.2	3.1	5.1	2.6	1.9	3.4	2.1	1.6

S3 robustness of SIFT-MS over time

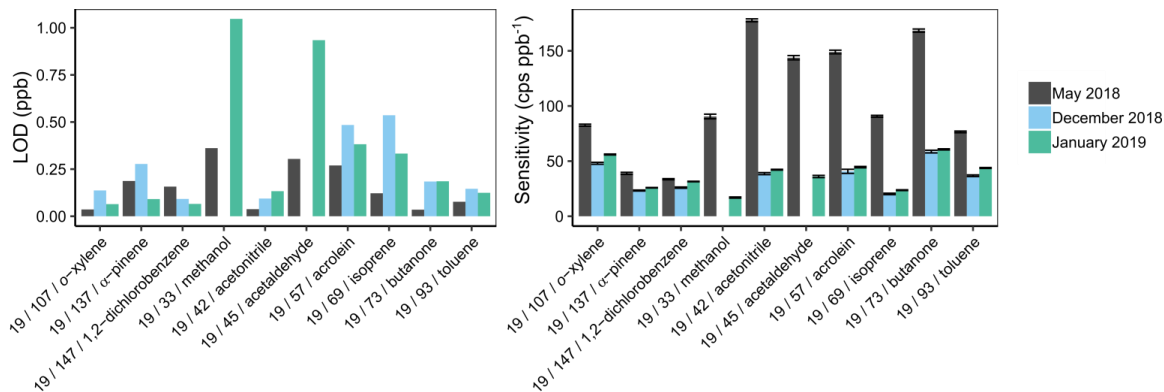


Figure S11: Robustness of calibrations of the SIFT-MS. The calibrations in May, December and January show considerable differences as one can see from the LOD changes (left panel) and sensitivity changes (right panel). This might be due to the o-ring change in September and a detector breakdown end-December. Both times, repairs were necessary. Still, a regular calibration should be done at least after each maintenance and if possible before every important experiment.

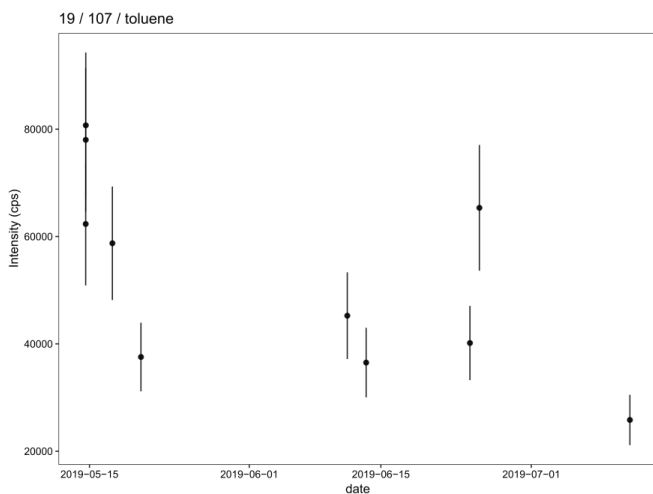


Figure S12: Long-term signal stability of the SIFT-MS tested with a standard of 2 ppm toluene. The Neumann trend test does not indicate a trend ($p = 95\%$, $n = 10$).

S4 Humidity dependence of product ion intensities of the SIFT-MS

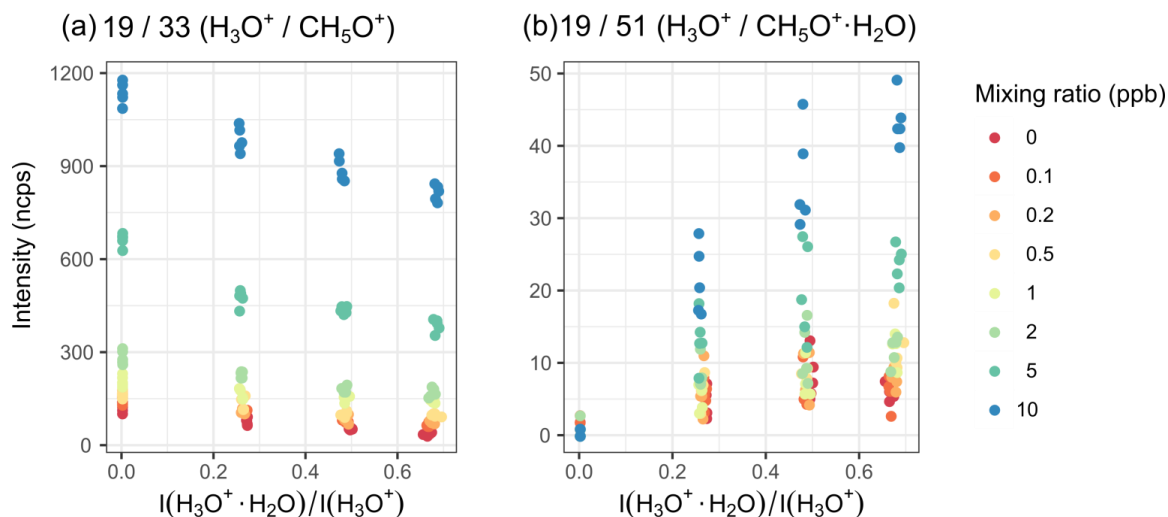


Figure S13: Humidity dependence of methanol signal, CH_3OH_2^+ (19 / 33) (a) and its first water cluster, $\text{CH}_3\text{OH}\cdot\text{H}_3\text{O}^+$ (19 / 51) (b). Humidity is measured as the ratio of the $\text{H}_3\text{O}^+\cdot\text{H}_2\text{O}$ and the H_3O^+ intensity, cf. Fig. 8.

S4.1 Calculation of the expected isoprene count on $m/z(\text{H}_3\text{O}^+) = 69 \text{ u}$

The intensity of $\text{H}_3\text{O}^+/69 \text{ u}$ is ca. 1800 cps for 10 ppb VOC standard. However, the standard contains isoprene, so we think what we see here is more isoprene emissions than methanol. We quickly checked that by calculating how much isoprene signal should be there from $\text{NO}^+/68 \text{ u}$, at the highest calibration standard of 10 ppb and 90% humidity:

$$\begin{aligned}
 I_{\text{H}_3\text{O}^+/69\text{u}} &= I_{\text{NO}^+/68\text{u}} \cdot \frac{k_{\text{H}_3\text{O}^+} \cdot I_{\text{H}_3\text{O}^+} + k_{\text{H}_3\text{O}^+} \cdot I_{\text{H}_3\text{O}^+/37\text{u}}}{k_{\text{NO}^+} \cdot I_{\text{NO}^+/30\text{u}}} \\
 &= 1800 \text{ cps} \cdot \frac{2.0 \cdot 10^{-9} \frac{\text{cm}^3}{\text{molec} \cdot \text{s}} \cdot 1.75 \cdot 10^6 \text{ cps} + 1.5 \cdot 10^{-9} \frac{\text{cm}^3}{\text{molec} \cdot \text{s}} \cdot 1.2 \cdot 10^{-9} \text{ cps}}{1.7 \cdot 10^{-9} \frac{\text{cm}^3}{\text{molec} \cdot \text{s}} \cdot 2.15 \cdot 10^6 \text{ cps}} = 2320 \text{ cps}
 \end{aligned}$$

The higher count rate than observed probably shows that the system is not in thermal equilibrium anymore and the kinetic constants do not fit perfectly. However, it still implies that the $\text{H}_3\text{O}^+/68 \text{ u}$ signal is mostly from isoprene and not from methanol.

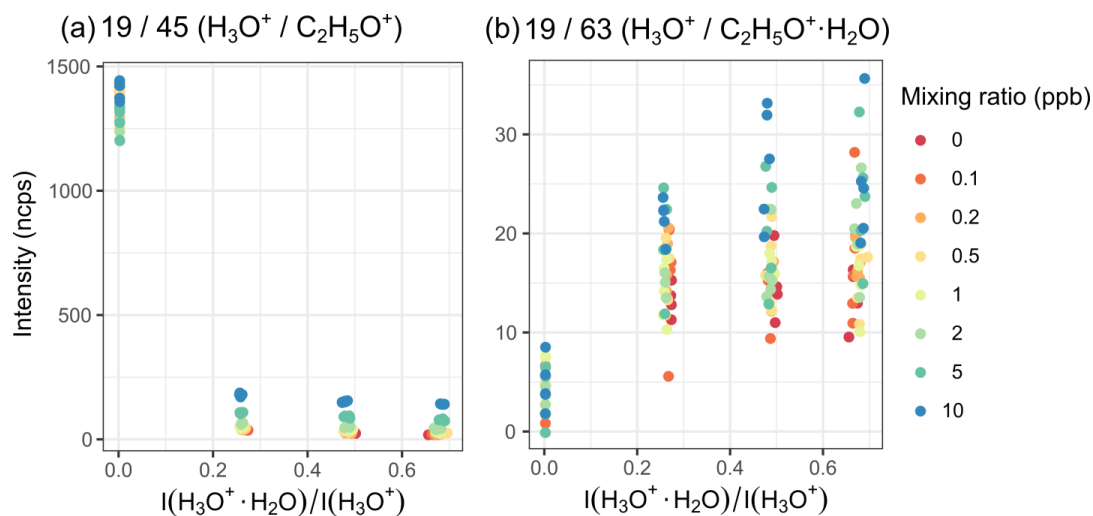


Figure S14: Humidity dependence of acetaldehyde (19/45) (a) and its water cluster (19/63) (b). Humidity is measured as the ratio of the $\text{H}_3\text{O}^+ \cdot \text{H}_2\text{O}$ and the H_3O^+ intensity, cf. Fig. S20.

In dry air, $m/z = 45$ amu shows a very high background. In dry state there is a very high background that does not occur when the system is wet. It cannot be found when reacting with NO^+ , but the reaction is roughly five times slower, so that the intensity is not high enough to detect acetaldehyde via this reaction. The background might either be due to the transfer line bypassing the water bubbler in dry state or desorption of a compound forming $m/z = 45$ when all the surfaces are dry.

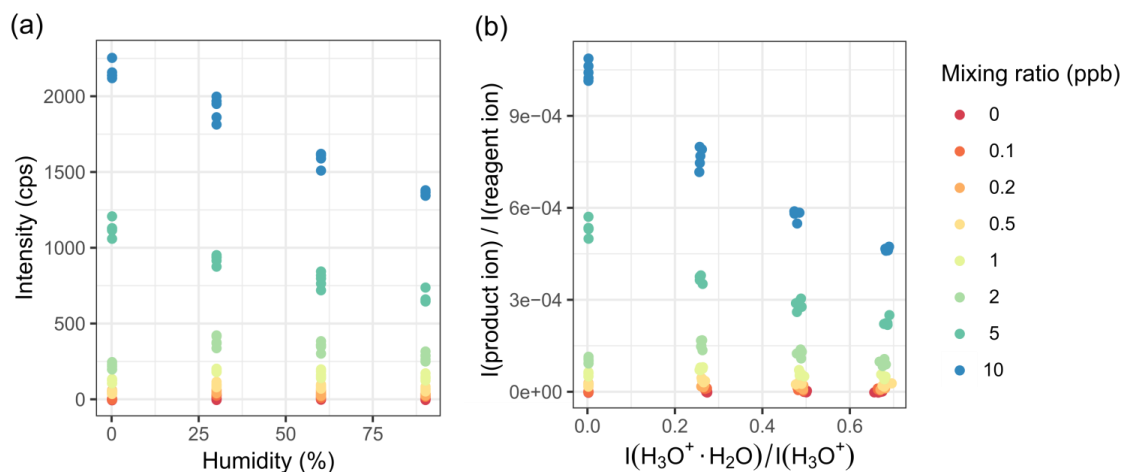


Figure S15: Humidity dependence of toluene ($m/z = 93$ u) intensity. (a) Absolute counts vs. relative humidity at 25°C. (b) Relative intensity per reagent intensity vs. the ratio of H_3O^+ and its first water cluster as a measure of humidity.

At mixing ratios smaller than 2 ppb, none of the plots is linear for the dry state.

S5 Evaluation of calibration procedures

Table S5: Compounds and their ions evaluated for the calibration.

reagent ion	m/z (u)	compound	product ion
H ₃ O ⁺	33	methanol	CH ₅ O ⁺
H ₃ O ⁺	42	acetonitrile	CH ₄ CN ⁺
H ₃ O ⁺	45	acetaldehyde	C ₂ H ₅ O ⁺
H ₃ O ⁺	47	ethanol	C ₂ H ₇ O ⁺
H ₃ O ⁺	51	methanol	CH ₃ OH ₂ ⁺ · H ₂ O
H ₃ O ⁺	57	acrolein	C ₃ H ₅ O ⁺
H ₃ O ⁺	60	acetonitrile	CH ₄ CN ⁺ · H ₂ O
H ₃ O ⁺	63	acetaldehyde	C ₂ H ₅ O ⁺ · H ₂ O
H ₃ O ⁺	65	ethanol	C ₂ H ₇ O ⁺ · H ₂ O
H ₃ O ⁺	69	isoprene	C ₅ H ₉ ⁺
H ₃ O ⁺	75	acrolein	C ₃ H ₅ O ⁺ · H ₂ O
H ₃ O ⁺	93	toluene	C ₇ H ₉ ⁺
H ₃ O ⁺	107	<i>o</i> -xylene	C ₈ H ₁₁ ⁺
H ₃ O ⁺	113	chlorobenzene	C ₆ H ₅ ³⁵ Cl ⁺
H ₃ O ⁺	137	α -pinene	C ₁₀ H ₁₇ ⁺
H ₃ O ⁺	147	1, 4-dichlorobenzene	C ₆ H ₄ ³⁵ Cl ₂ ⁺
NO ⁺	45	ethanol	C ₂ H ₅ O ⁺
NO ⁺	55	acrolein	C ₃ H ₃ O ⁺
NO ⁺	63	ethanol	C ₂ H ₅ O ⁺ · H ₂ O
NO ⁺	68	isoprene	C ₅ H ₈ ⁺
NO ⁺	69	2-butenal	C ₄ H ₅ O ⁺
NO ⁺	74	acetaldehyde	C ₂ H ₄ O · NO ⁺
NO ⁺	78	benzene	C ₆ H ₆ ⁺
NO ⁺	88	acetone	C ₃ H ₆ O · NO ⁺
NO ⁺	92	toluene	C ₇ H ₈ ⁺
NO ⁺	102	butanone	C ₄ H ₈ O · NO ⁺
NO ⁺	106	<i>o</i> -xylene	C ₈ H ₁₀ ⁺
NO ⁺	108	benzene	C ₆ H ₆ · NO ⁺
NO ⁺	112	chlorobenzene	C ₆ H ₅ ³⁵ Cl ⁺
NO ⁺	136	α -pinene	C ₁₀ H ₁₆ ⁺
NO ⁺	146	1, 4-dichlorobenzene	C ₆ H ₄ ³⁵ Cl ₂ ⁺
O ₂ ⁺	39	benzene	CH ₃ O ⁺ · H ₂ O
O ₂ ⁺	58	acetone	C ₃ H ₅ O ⁺
O ₂ ⁺	69	2-butenal	C ₄ H ₅ O ⁺
O ₂ ⁺	72	butanone	C ₄ H ₈ O ⁺
O ₂ ⁺	78	benzene	C ₆ H ₆ ⁺
O ₂ ⁺	92	toluene	C ₇ H ₈ ⁺
O ₂ ⁺	93	α -pinene	C ₇ H ₉ ⁺
O ₂ ⁺	112	chlorobenzene	C ₆ H ₅ ³⁵ Cl ⁺
O ₂ ⁺	146	1, 4-dichlorobenzene	C ₆ H ₄ ³⁵ Cl ₂ ⁺

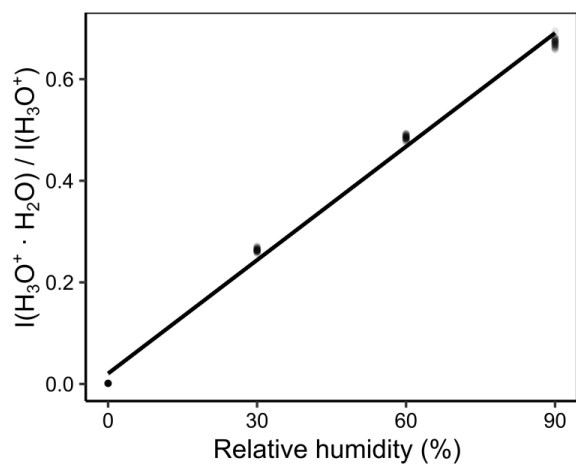


Figure S16: Correlation of the intensity ratio of the reagent ion water clusters with the relative humidity. The results are not entirely linear, but the deviance is so small that they were approximated linearly.

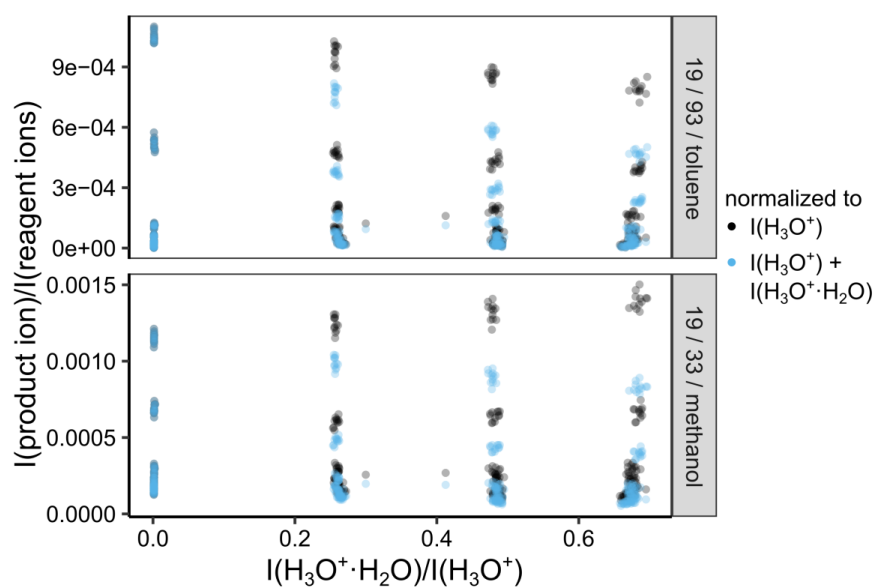


Figure S17: Effect of normalization to H_3O^+ vs. to both H_3O^+ and $\text{H}_3\text{O}^+ \cdot \text{H}_2\text{O}$. The latter makes the data more humidity dependent, but it accounts for effects seen for methanol, where a drop in H_3O^+ leads to a pseudo signal increase if not corrected for the first water cluster.

Table S6: Bayesian Information Criteria (BIC) of the different substances and their mean, median, minimum and maximum value for the different regression methods, named by the equations numbers they were calculated on. Equation (6) was not calculated for the reagent ions separately, but for the total mixing ratio result of the substance.

substance	ion	Eq. (2) dry	Eq. (2) 30%	Eq. (2) 60%	Eq. (2) 90%	Eq. (3) dry	Eq. (3) 30%	Eq. (3) 60%	Eq. (3) 90%	Eq. (4)	Eq. (5)	Eq. (6)	Eq. (7)	Eq. (8)	Eq. (9)
methanol	19/33	236	361	408	302	348	433	627	442	101	192	921	103	101	103
	19/42	462	402	407	416	557	632	628	625	4	231	33	18	0	18
acetonitrile	19/45		298	298	290		437	447	455	3	64	2045	40	0	40
	19/47	475	387	403	175	387	499	634	273	349	298	1664		395	
acrolein	19/57	400	418	397	290	473	615	641	453	59	260	1071	23	57	23
	19/69	369	376	320	351	507	663	571	689	208	348	235	65	68	65
isoprene	19/73	394	411	399	277	478	626	641	467	15	220	128	33	62	33
	19/93	362	358	346	317	511	671	694	724	301	423	267	57	73	57
toluene	19/107	243	373	308	263	340	655	478	480	190	297	467	69	101	69
	19/113	288	301	250	197	441	583	493	397	267	344	336	98	102	98
chlorobenzene	19/137	216	323	319	275	369	563	721	620	115	218	2218	106	128	106
	19/147	274	283	295	308	453	601	744	734	418	483	132	253	132	132
ethanol	30/45		224	211	262		362	370	464	213	220		266		266
	30/55	230	356	336	195	353	660	681	391	220	229	266	73	266	266
isoprene	30/68	346	330	340	355	524	695	680	671	65	71	73	112	73	73
	30/69	383	405	337	241	486	621	529	338	64	57	62	343	62	62
2-butenal	30/78	336	345	307	320	537	675	559	557	101	94	92	198	92	92
	30/88	146	242	218	191	291	488	511	395	181	164	198	38	198	198
acetone	30/92	369	349	361	363	502	669	659	656	27	32	38	62	38	38
	30/102	222	287	252	303	355	585	479	566	96	93	112	35	112	112
butanone	30/106	393	338	330	371	621	675	691	659	42	25	35	35	35	35
	30/108	170	135	176	162	410	302	405	420	234	234	124		124	

chlorobenzene	30/ 112	331	261	258	368	541	468	465	654	119	126	124	147	124
α-pinene	30/ 136	282	316	271	253	590	705	602	470	148	127	23	136	23
dichlorobenzene	30/ 146	313	289	333	307	555	585	686	562	141	136	136	163	136
acetone	32/58	155				288				152	151	163	245	163
2-butenal	32/69	246	284	277	266	349	459	455	462	250	200	246		246
butanone	32/72	170	203	258	206	277	388	474	374	118	103		112	
benzene	32/78	353	350	355	292	530	686	682	583	78	44	112	68	112
toluene	32/92	357	353	368	380	527	672	659	639	107	46	67	68	67
α-pinene	32/93	330	364	331	352	554	679	694	667	94	91	48	73	48
chlorobenzene	32/ 112	271	282	250	304	469	610	482	563	91	48	73	142	73
dichlorobenzene	32/ 146	318	343	324	289	567	697	692	584	122	124	142	134	142
mean		305	323	314	289	458	583	587	532	142	175	853	125	95
median		318	341	322	291	478	618	628	560	118	151	467	102	73
min		146	135	176	162	277	302	370	273	3	25	33	18	18
max		475	418	408	416	621	705	744	734	418	483	2218	395	266

S6 Comparison of SIFT-MS to PTR-MS

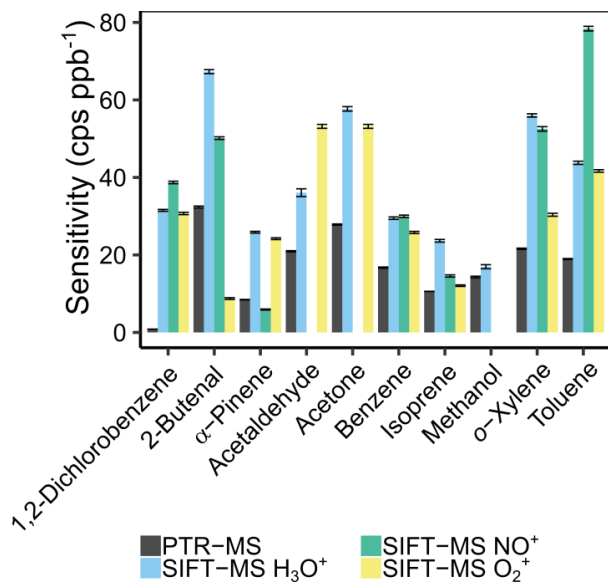


Figure S18: Instrument sensitivity \pm 95 % confidence interval ($df = 26$) of PTR-MS and the different SIFT-MS reagent ions for different VOCs at 30 % humidity. Sensitivity is defined here as the slope of the calibration curve.

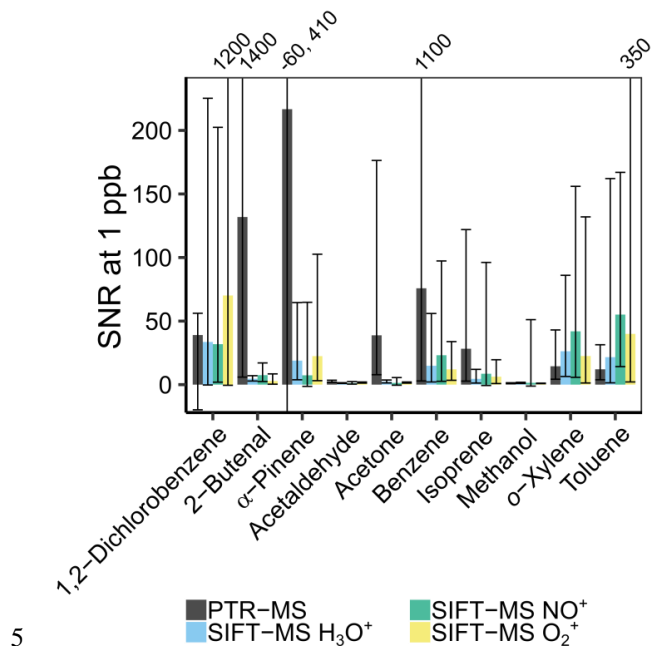


Figure S19: Signal to noise ratio (SNR) at 1 ppb (\pm 95 % CI, $df = 7$) of PTR-MS and the different SIFT-MS reagent ions for different VOCs at 30 % humidity. The values above the biggest error bars resemble the values of the confidence intervals out of the depicted range. The high positive confidence interval is due to the high relative error of the blank.

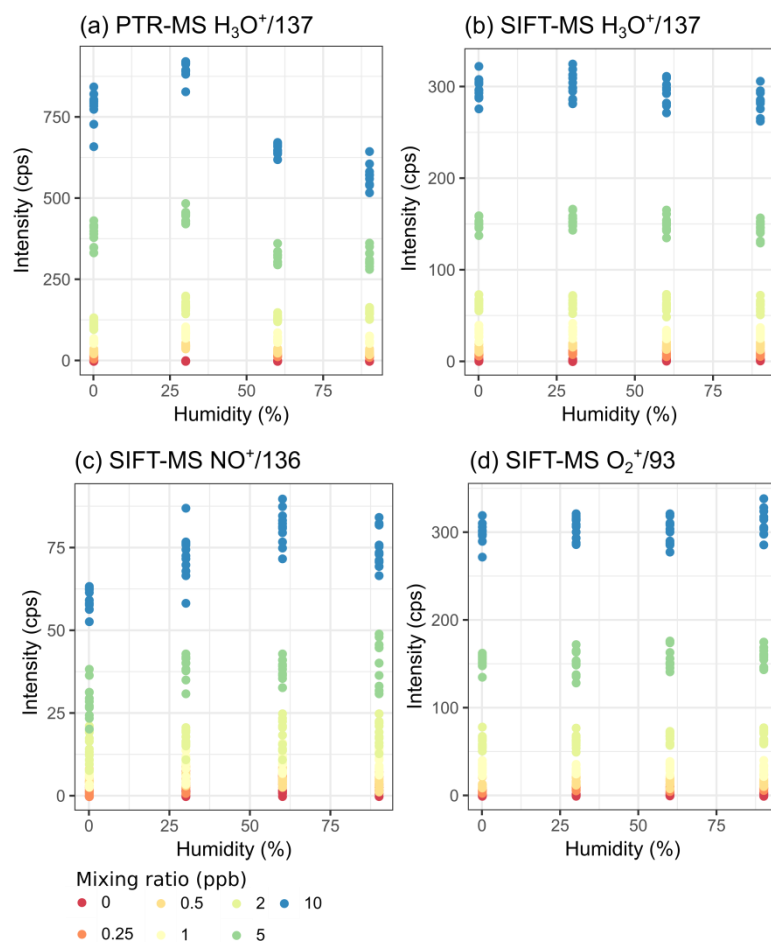


Figure S20: Humidity-dependence as a change in signal intensity with humidity for mixing ratios between 0.25 and 10 ppb of the α -pinene signal for PTR-MS (a) and the different SIFT-MS reagent ions (b–d) with their most abundant product ion.

5 We observed that PTR-MS tends to be less robust against humidity. As the example for α -pinene in Fig. 4 shows, PTR-MS has an optimum at low humidity whereas the SIFT-MS with H_3O^+ and O_2^+ shows a rather stable signal. However, one has to note that this has to be tested for each compound product ion separately, as the humidity dependence of α -pinene upon reaction with NO^+ illustrates. Humidity affects the sensitivity to a greater extent than the LOD, so especially for PTR-MS, a calibration in the targeted humidity-range or calibrating also for humidity using Eq. (9) is advisable.

Table S7: LODs (in ppb, derived from Blank, 3*sd) of the PTR-MS of the different compounds for the different humidities at 25°C. n.d.: intensities were not measured at this *m/z* and humidity.

Compound	m/z	dry	30% humidity	60% humidity	90% humidity
methanol	33	0.618	0.681	0.685	0.835
acetonitrile	42	0.026	0.020	n.d.	n.d.
acetaldehyde	45	0.266	0.188	n.d.	n.d.
acrolein	57	0.055	0.051	n.d.	n.d.
acetone	59	0.043	0.049	0.029	0.028
isoprene	69	0.070	0.061	0.065	0.159
2-butenal	71	0.024	0.015	0.024	0.034
butanone	73	0.095	0.033	0.072	0.072
benzene	79	0.066	0.060	0.019	0.026
toluene	93	0.137	0.110	0.077	0.071
<i>o</i>-xylene	107	0.061	0.107	n.d.	n.d.
α-pinene	137	0.049	0.025	0.050	0.037
dichlorobenzene	148	0.000	0.150	n.d.	n.d.

Table S8: LODs (in ppb, derived from Blank, 3*sd), of the SIFT-MS with Helium carrier gas of the different compounds and relative humidities at 25°C.

compound	$m/z_{\text{reag}} / m/z_{\text{prod}}$	LOD (ppb)			
		dry	30% humidity	60% humidity	90% humidity
methanol	19 / 33	>2	1.047	>2	1.367
acetonitrile	19 / 42	0.111	0.133	0.081	0.139
acetaldehyde	19 / 45	1.315	0.934	0.999	0.852
acrolein	19 / 57	0.332	0.382	0.341	0.281
acetone	19 / 59	0.378	0.347	0.501	0.416
isoprene	19 / 69	0.460	0.333	0.318	0.434
2-butenal	19 / 71	0.176	0.093	0.159	0.109
butanone	19 / 73	0.142	0.186	0.126	0.164
benzene	19 / 79	0.107	0.132	0.195	0.171
toluene	19 / 93	0.072	0.124	0.120	0.154
<i>o</i>-xylene	19 / 107	0.093	0.064	0.106	0.100
α-pinene	19 / 137	0.088	0.091	0.147	0.078
dichlorobenzene	19 / 147	0.047	0.066	0.138	0.195
isoprene	30 / 68	0.189	0.337	0.242	0.175
2-butenal	30 / 69	0.171	0.121	0.117	0.136
benzene	30 / 78	0.082	0.081	0.080	0.070
toluene	30 / 92	0.031	0.026	0.025	0.027
butanone	30 / 102	0.452	0.497	0.390	0.393
<i>o</i>-xylene	30 / 106	0.098	0.039	0.074	0.074
chlorobenzene	30 / 112	0.091	0.157	0.137	0.124
α-pinene	30 / 136	0.489	0.398	0.498	0.457
dichlorobenzene	30 / 146	0.057	0.066	0.065	0.051
2-butenal	32 / 69	0.217	0.239	0.250	0.249
butanone	32 / 72	0.652	0.455	0.866	0.528
benzene	32 / 78	0.151	0.117	0.151	0.118
toluene	32 / 92	0.084	0.063	0.091	0.063
α-pinene	32 / 93	0.098	0.080	0.121	0.144
chlorobenzene	32 / 112	0.122	0.097	0.087	0.128
dichlorobenzene	32 / 146	0.079	0.038	0.087	0.078

Table S9: Sensitivities \pm 95% confidence interval (in cps/ppb, based on product ion counts normalized to 10^6 reagent ion counts, $df = 26$) of the PTR-MS of the different compounds for the different humidities at 25°C. n.d.: intensities were not measured at this m/z and humidity.

compound	m/z	sensitivity \pm 95% CI (cps/ppb)			
		dry	30% humidity	60% humidity	90% humidity
methanol	33	14.3 \pm 0.6	14.3 \pm 0.4	12.2 \pm 0.2	9.2 \pm 0.4
acetonitrile	42	25.5 \pm 0.4	25.1 \pm 0.3	n.d.	n.d.
acetaldehyde	45	21.4 \pm 0.3	20.9 \pm 0.3	n.d.	n.d.
acrolein	57	19 \pm 1	21.4 \pm 0.3	n.d.	n.d.
acetone	59	28.8 \pm 0.4	27.8 \pm 0.3	26.2 \pm 0.2	24.7 \pm 0.4
isoprene	69	9.39 \pm 0.05	10.60 \pm 0.03	4.22 \pm 0.04	4.17 \pm 0.02
2-butenal	71	31 \pm 1	32.4 \pm 0.4	14.9 \pm 0.2	12.8 \pm 0.3
butanone	73	28 \pm 1	28.4 \pm 0.3	16.2 \pm 0.2	14.1 \pm 0.3
benzene	79	17.0 \pm 0.3	16.7 \pm 0.3	n.d.	n.d.
toluene	93	20.1 \pm 0.3	19.0 \pm 0.2	15.8 \pm 0.1	16.7 \pm 0.3
o-xylene	107	22.6 \pm 0.2	21.6 \pm 0.3	n.d.	n.d.
a-pinene	137	8.2 \pm 0.2	8.5 \pm 0.1	6.08 \pm 0.07	6.1 \pm 0.2
dichlorobenzene	148	0.90 \pm 0.04	0.84 \pm 0.04	n.d.	n.d.

5

Table S10: Sensitivities \pm 95% confidence interval (in cps/ppb, based on product ion counts normalized to 10^6 reagent ion counts, $df = 26$), of the SIFT-MS of the different compounds and relative humidities at 25°C. NA: LOD was over 2 ppb so that not enough calibration points remained for a calibration.

compound	$m/z_{\text{reag}} / m/z_{\text{prod}}$	sensitivity \pm 95% CI (cps/ppb)			
		dry	30% humidity	60% humidity	90% humidity
methanol	19 / 33	NA	17 ± 0.5	NA	14.7 ± 0.4
acetonitrile	19 / 42	48.2 ± 0.3	42.2 ± 0.3	38.6 ± 0.4	34.8 ± 0.3
acetaldehyde	19 / 45	42 ± 1	36 ± 1	32.7 ± 0.7	29.5 ± 0.5
acrolein	19 / 57	51.2 ± 0.8	44.6 ± 0.6	40.5 ± 0.5	38.8 ± 0.5
acetone	19 / 59	68.7 ± 0.8	57.7 ± 0.6	52.2 ± 0.6	47.0 ± 0.5
isoprene	19 / 69	27.2 ± 0.4	23.7 ± 0.3	18.7 ± 0.3	15.6 ± 0.2
2-butenal	19 / 71	76.3 ± 0.8	67.3 ± 0.5	61.6 ± 0.8	56.6 ± 0.4
butanone	19 / 73	71.7 ± 0.8	60.6 ± 0.5	56.1 ± 0.5	51.4 ± 0.3
benzene	19 / 79	43.3 ± 0.4	29.5 ± 0.3	20.9 ± 0.3	16.2 ± 0.2
toluene	19 / 93	29.6 ± 0.2	26.0 ± 0.2	23.0 ± 0.2	20.4 ± 0.2
o-xylene	19 / 107	56.6 ± 0.6	43.8 ± 0.4	33.1 ± 0.4	25.0 ± 0.3
α -pinene	19 / 137	30.3 ± 0.2	25.9 ± 0.2	22.3 ± 0.2	19.5 ± 0.2
dichlorobenzene	19 / 147	50.6 ± 0.3	31.5 ± 0.2	19.8 ± 0.2	12.2 ± 0.2
isoprene	30 / 68	13.5 ± 0.2	14.6 ± 0.3	15.6 ± 0.2	15.6 ± 0.2
2-butenal	30 / 69	46.2 ± 0.5	50.2 ± 0.3	53.5 ± 0.5	52.9 ± 0.4
benzene	30 / 78	27.8 ± 0.3	30.0 ± 0.3	30.0 ± 0.3	29.6 ± 0.3
toluene	30 / 92	73.6 ± 0.5	78.4 ± 0.6	78.4 ± 0.5	77.9 ± 0.4
butanone	30 / 102	4.7 ± 0.2	6.3 ± 0.2	7.6 ± 0.2	7.7 ± 0.1
o-xylene	30 / 106	48.8 ± 0.4	52.5 ± 0.6	53.2 ± 0.4	52.4 ± 0.4
chlorobenzene	30 / 112	42.6 ± 0.4	46.4 ± 0.3	47.5 ± 0.4	47.0 ± 0.4
α -pinene	30 / 136	4.7 ± 0.1	5.9 ± 0.1	6.5 ± 0.2	5.7 ± 0.2
dichlorobenzene	30 / 146	27 ± 0.4	25.2 ± 0.3	24.1 ± 0.4	23.2 ± 0.3
2-butenal	32 / 69	5.3 ± 0.2	6.8 ± 0.2	6.9 ± 0.3	7.1 ± 0.2
butanone	32 / 72	23.4 ± 0.3	25.8 ± 0.3	26.4 ± 0.3	26.9 ± 0.2
benzene	32 / 78	37.1 ± 0.3	41.7 ± 0.3	43.2 ± 0.3	44.2 ± 0.3
toluene	32 / 92	21.9 ± 0.2	24.2 ± 0.2	25.1 ± 0.3	26.3 ± 0.2
α -pinene	32 / 93	32.7 ± 0.3	35.6 ± 0.2	38.3 ± 0.3	38.4 ± 0.3
chlorobenzene	32 / 112	28.2 ± 0.3	30.7 ± 0.3	33.0 ± 0.3	32.6 ± 0.4
dichlorobenzene	32 / 146	NA	17.0 ± 0.5	NA	14.7 ± 0.4

Table S11: SNR at 1 ppb, upper and lower confidence interval (based on product ion counts normalized to 10^6 reagent ion counts, $p = 95\%$, $df = 7$) of the PTR-MS of the different compounds for the different humidities at 25°C. n.d.: intensities were not measured at this m/z and humidity. Inf: infinite value, I(Blank) = 0.

compound	m/z	dry			30% humidity			60% humidity			90% humidity		
		SNR	CI ^u	CI ^l	SNR	CI ^u	CI ^l	SNR	CI ^u	CI ^l	SNR	CI ^u	CI ^l
methanol	33	1.2	1.5	0.9	1.2	1.5	0.9	1	1.8	0.4	1.2	1.4	1
acetonitrile	42	130	2330	-10	190	830	-40	n. d.	n. d.	n. d.	n. d.	n. d.	n. d.
acetaldehyde	45	2.4	3.3	1.6	2.5	3.5	1.7	n. d.	n. d.	n. d.	n. d.	n. d.	n. d.
acrolein	57	16	81	2	33	138	6	n. d.	n. d.	n. d.	n. d.	n. d.	n. d.
acetone	59	49	526	2	39	176	8	31	60	15	67	265	16
isoprene	69	25	527	-6	28	122	3	54	1125	-6	22	918	-1
2-butenal	71	23	109	3	132	1377	6	165	647	-32	70	465	7
butanone	73	6.7	15.3	2.5	42	125	12	21	70	5	1	179	-1
benzene	79	34	156	6	76	1067	3	n. d.	n. d.	n. d.	n. d.	n. d.	n. d.
toluene	93	7.9	18.4	3.1	12	31	4	16	38	6	12	22	6
<i>o</i> -xylene	107	14	28	6	14	43	4	n. d.	n. d.	n. d.	n. d.	n. d.	n. d.
α -pinene	137	80	220	-20	220	410	-60	80	670	-10	160	300	-50
dichloro-benzene	148	Inf	Inf	Inf	39	56	-20	n. d.	n. d.	n. d.	n. d.	n. d.	n. d.

Table S12: SNR at 1 ppb \pm 95% confidence interval, based on product ion counts normalized to 10^6 reagent ion counts, $df = 7$) of the SIFT-MS of the different compounds and relative humidities at 25°C. NA: LOD was over 2 ppb so that not enough calibration points remained for a calibration.

compound	$m/z_{\text{reag}} / m/z_{\text{prod}}$	dry			30% humidity			60% humidity			90% humidity		
		SNR	CI ^u	CI ^l	SNR	CI ^u	CI ^l	SNR	CI ^u	CI ^l	SNR	CI ^u	CI ^l
methanol	19 / 33	1.1	1.6	0.8	1.3	1.8	0.9	1.3	2.3	0.5	1.4	2.3	0.7
acetonitrile	19 / 42	18	182	-1	21	1013	-1	15	46	4	10	30	2
acetaldehyde	19 / 45	1.2	1.5	0.9	1.2	1.5	0.9	1.2	1.6	0.9	1.3	1.7	0.9
acrolein	19 / 57	1.7	2.6	1.1	2.1	3.6	1	2.3	3.5	1.4	2.4	3.6	1.5
acetone	19 / 59	1.8	2.8	1.1	2.3	3.6	1.4	1.6	2.5	0.9	2.2	3.3	1.3
isoprene	19 / 69	3.6	8.4	1.2	4.6	12	1.3	2.8	5.5	1.1	3.5	9.2	0.7
2-butenal	19 / 71	2.1	4.5	0.5	4.6	7	2.8	2.5	4.7	0.9	2.8	4.1	1.8
butanone	19 / 73	3.3	4.8	2.1	4.3	7.4	2.2	3.2	5.4	1.6	4.1	6.8	2.2
benzene	19 / 79	13	34	4	15	56	2	9.4	31.8	1.9	11	38	2
toluene	19 / 93	30	145	5	22	162	1	9.8	28.2	1.9	9.7	25.9	2.3
<i>o</i> -xylene	19 / 107	24	177	1.9	26	86	6	18	75	3	12	30.2	3.7
α -pinene	19 / 137	14	37	3	19	65	4	12	46	2	13	27.1	5.3
dichlorobenzene	19 / 147	33	188	2	34	225	0	21	1129	-3	11	53	0
isoprene	30 / 68	9.4	35.8	1.4	8.6	96.1	-0.7	11	116	-1	12	61	0
2-butenal	30 / 69	3.3	8.1	0.8	7.5	17.1	2.4	4.7	11.6	0.9	5.3	10.1	2.5
benzene	30 / 78	17	52	4	23	97	3	20	61	3	22	71	5
toluene	30 / 92	59	234	11	55	167	14	54	144	17	62	200	15
butanone	30 / 102	8.5	119.8	-1.3	6.4	63.1	-0.7	4.1	18.7	-0.2	6.8	62.1	-0.3
<i>o</i> -xylene	30 / 106	27	278	2	42	156	6	29	173	3	25	93.7	5.6
chlorobenzene	30 / 112	6.1	10.2	3.1	6.4	12.9	2.8	6.7	13.4	2.7	6.5	11.7	3.1
α -pinene	30 / 136	10	48	-4	7.3	64.8	-1.4	5.5	35.8	-0.5	4.7	19.3	0.1
dichlorobenzene	30 / 146	37	952	-1	32	202	2	26	136	2	38	174	6
2-butenal	32 / 69	2.3	5.3	0.7	5.2	12.9	1.6	2.4	4.9	0.9	2.7	5.6	0.9
butanone	32 / 72	2.8	10.3	-0.2	3.3	8.8	0.6	2.1	6.6	0.3	2.7	5.6	0.9
benzene	32 / 78	12	43	3	12	34	3	9	22.7	3	12	35	3
toluene	32 / 92	28	165	4	40	350	2	31	472	-1	27	105	5
α -pinene	32 / 93	24	170	1	22	103	3	21	157	1	17	147	0
chlorobenzene	32 / 112	11	32	3	11	27	4	9.9	18.1	5	11	30	3
dichlorobenzene	32 / 146	43	259	-12	70	1233	-1	25	268	0	24	113	3

Supplementary Material

Table S1: product ions tracked in the SIM scan

reagent ion (m/z (u))	product ion m/z (u)	ion formula (substance)
H_3O^+ (19)	19	H_3O^+
	37	H_5O_2^+
	55	H_7O_3^+
	69	C_5H_9^+ (isoprene / MBO)
	73	H_9O_4^+
NO^+ (30)	30	NO^+
	48	$\text{NO}^+\cdot\text{H}_2\text{O}$
	68	C_5H_8^+ (isoprene)
	69	C_5H_9^+ (MBO)
O_2^+ (32)	32	O_2^+
	43	C_3H_7^+ (MBO)
	53	C_4H_5^+ (isoprene)
	58	$\text{C}_3\text{H}_6\text{O}^+$ (MBO)
	59	$\text{C}_3\text{H}_7\text{O}^+$ (MBO)
	67	C_5H_7^+ (isoprene)
	68	C_5H_8^+ (isoprene)
	69	C_5H_9^+ (MBO)
	71	$\text{C}_4\text{H}_7\text{O}^+$ (MBO)
	86	$\text{C}_5\text{H}_{10}\text{O}^+$ (MBO)

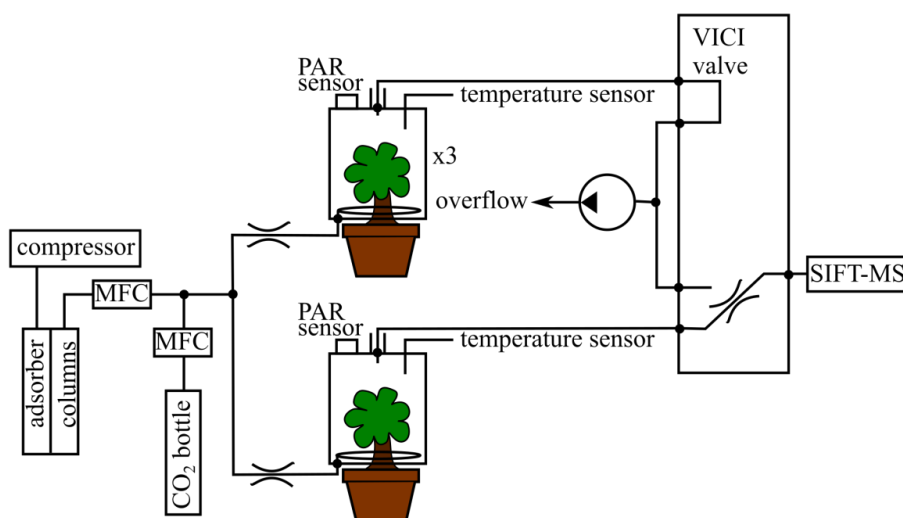


Figure S1: Scheme of the tree chamber setup

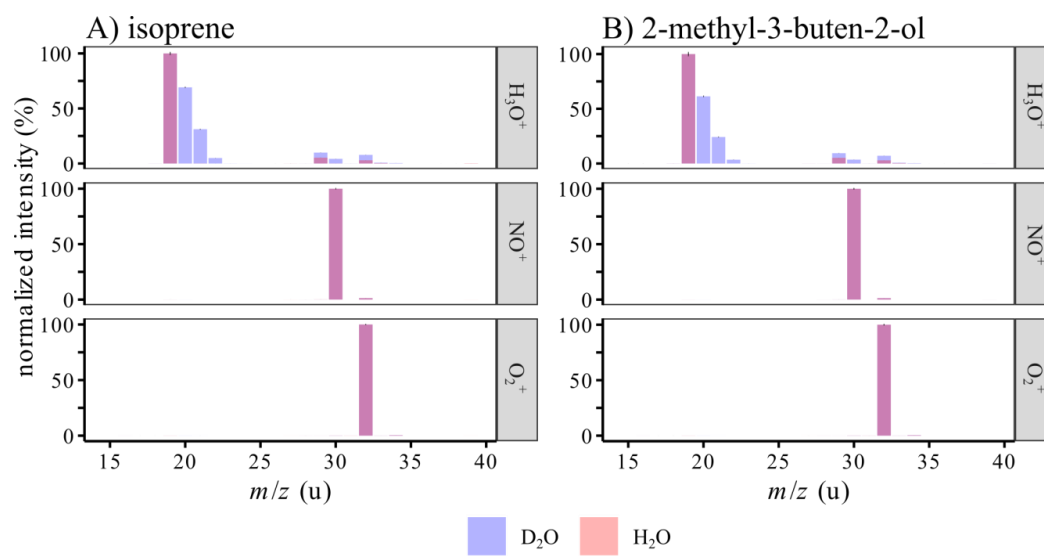


Figure S2: Relative intensity of the reagent ions (normalized to the biggest intensity in the peak area) when measuring isoprene and MBO that is humidified by normal and deuterated water.

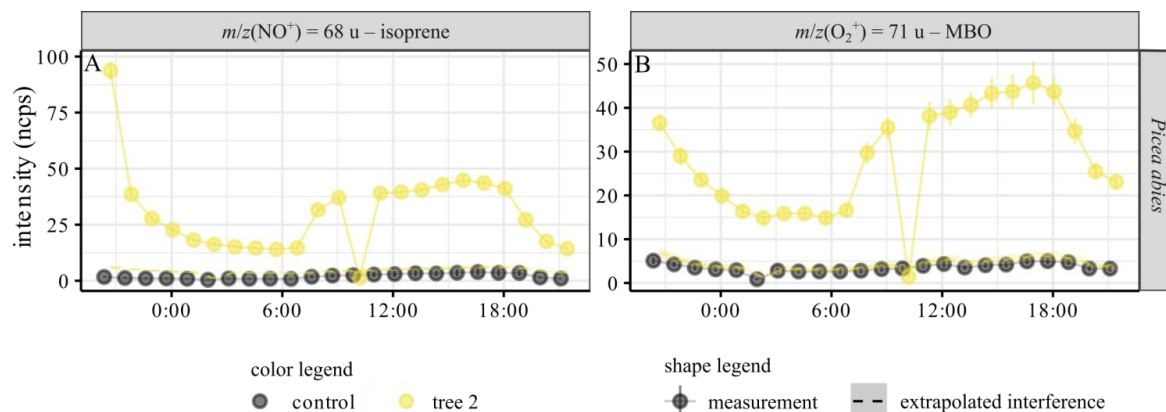


Figure S3: Diurnal cycle of isoprene and MBO emissions of the second *Picea abies* tree (for all trees, cf. Figure 5). The measured intensities were normalized to 10^6 reagent ion counts. Black: control, empty chamber. Yellow: the tree, individual 2. Dots: mean \pm 95% CI of the SIFT-MS measurement. A sudden Zero value indicates instrument malfunctioning (before a firmware update, software did not always switch on the VICI valve for long measurements). Dashed lines: interference extrapolated from $m/z(\text{NO}^+) = 69$ u (MBO interference on the isoprene signal,) and $m/z(\text{O}_2^+) = 67$ u (isoprene interference on the MBO signal) – mean \pm 95% CI. Basically, if the signal at $m/z(\text{O}_2^+) = 67$ u is isoprene, then a maximum of 1.4% (for lower carrier gas flows) and 2.9% (for higher carrier gas flows) of this signal will be seen at $m/z(\text{O}_2^+) = 71$ u where we measure MBO. These values are represented by the dashed lines in the graphs. If the intensity of $m/z(\text{O}_2^+) = 71$ u is higher than this signal, we also measure MBO. This also works the other way round, for MBO interference on isoprene.

Table S2: Needle/leaf dry weights of the three replicates of the different tree species.

Tree species / replicate	1 ●	2 ●	3 ●
Pinus ponderosa	7.27 g	4.40 g	2.11 g
Picea abies	22.60 g	37.00 g	14.26 g
Picea glauca sp. 1	20.34 g	28.04 g	16.05 g
Picea glauca sp. 2	9.50 g	6.04 g	5.89 g
Poplar	4.05 g	6.17 g	7.39 g

Table S3: Air flow through the chambers.

Chamber	1 ●	2 ●	3 ●	Control
Flow	3.2 L/min	3.5 L/min	3.5 L/min	3.4 L/min

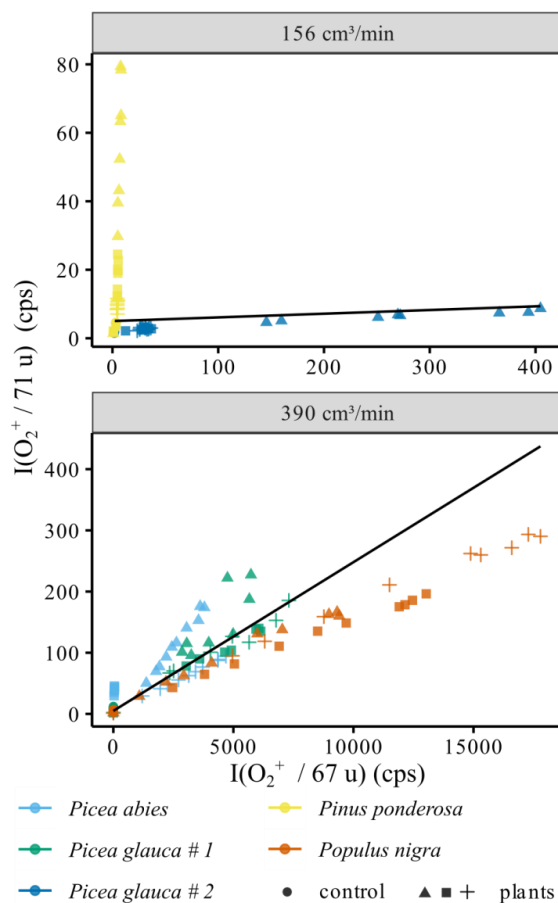


Figure S4: Ratio of the MBO signal at $m/z(\text{O}_2^+) = 71$ u versus the isoprene signal at $m/z(\text{O}_2^+) = 67$ u. The black lines mark an extrapolation of the ratio calculated based on the standard measurements under humid conditions, cf. Error! Reference source not found.. Points below this range are considered to be the result of isoprene interference on the MBO signal, points above the range are considered to represent genuine MBO signals.

Figure S5: Isoprene and MBO emission rate in μg per g leaf/needle dry weight per hour (mean \pm 95% CI) for the five different tree species evaluated. The extrapolated interference background was subtracted before calculating the emission rates.

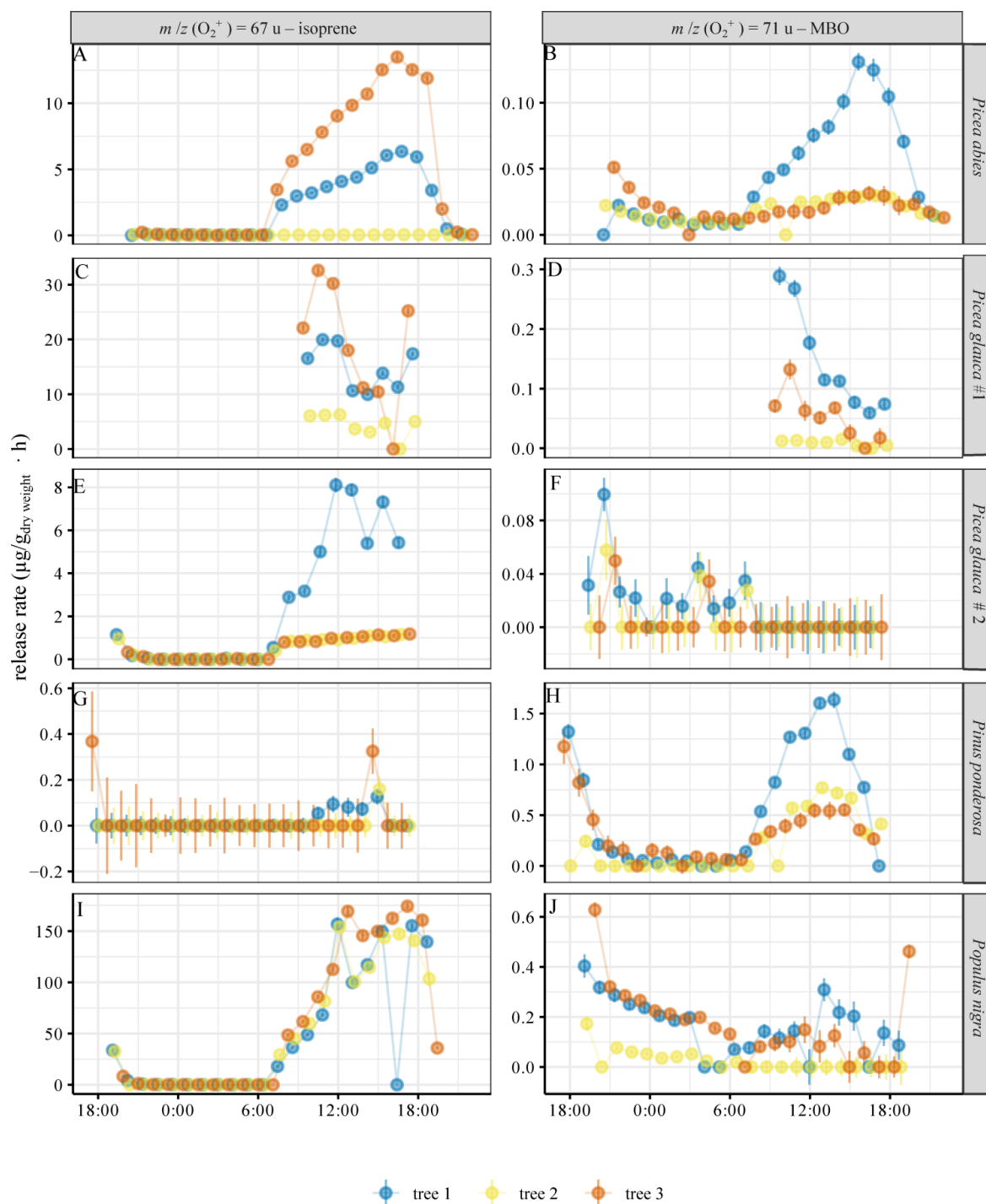


Figure S6: Isoprene and MBO emission rate in μg per g leaf/needle dry weight per hour (mean \pm 95% CI) for the five different tree species evaluated. Both are based on their signals upon reaction with O_2^+ . The extrapolated interference background was subtracted before calculating the emission rates.

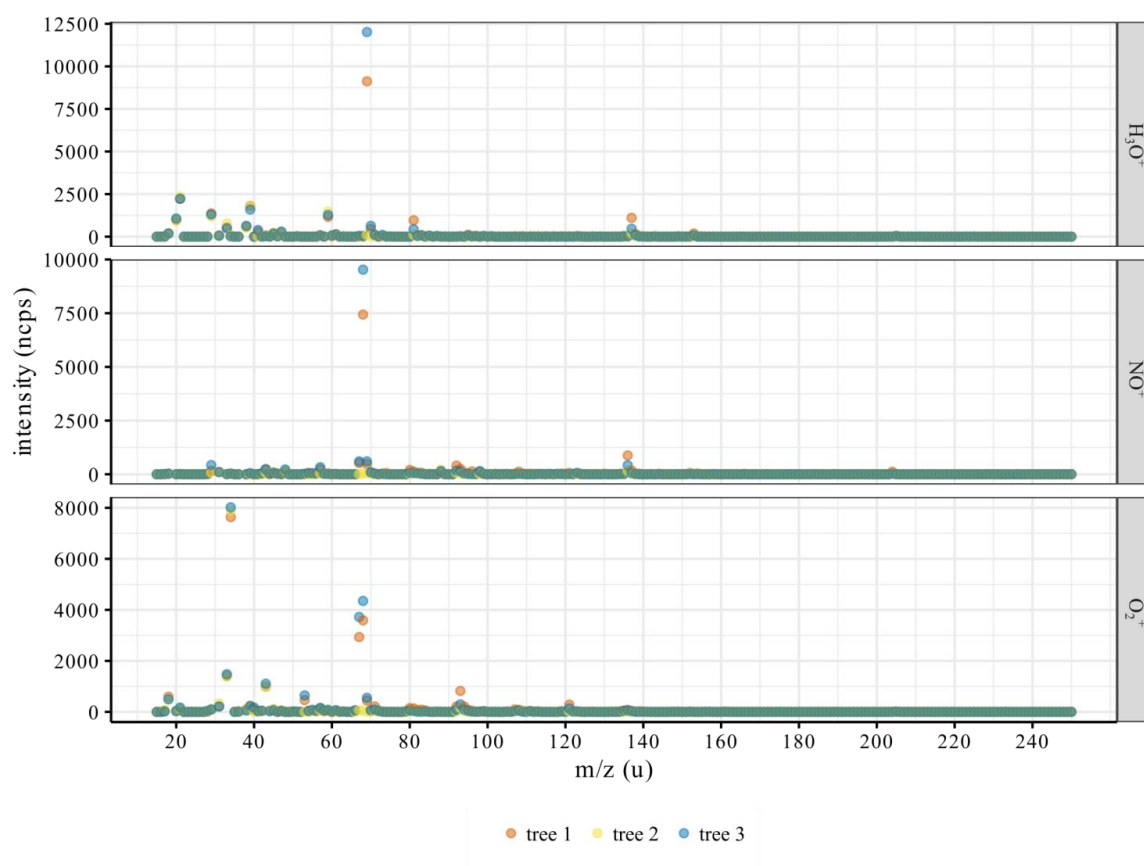


Figure S7: SIFT-MS mass spectra of the three *P. abies* trees at 3 pm (where the emissions are highest in this tree). The intensities are normalized to 10^6 reagent ion counts. Since only one spectrum was measured, no error bars could be calculated. $m/z = 19, 30, 32, 37$ u (the reagent ions) are not shown due to their high intensity. Monoterpenes as sum parameter can be measured on $m/z(\text{H}_3\text{O}^+) = 137$ u, $m/z(\text{NO}^+) = 136$ u, and $m/z(\text{O}_2^+) = 136$ u, sesquiterpenes on $m/z(\text{H}_3\text{O}^+) = 205$ u, $m/z(\text{NO}^+) = 204$ u, and $m/z(\text{O}_2^+) = 204$ u.

Supplementary Information for

Dimethyl sulfide emissions from freshwater
wetlands result more from organic matter
degradation than sulfate reduction

Ann-Sophie Lehnert^{1,2}, Rebecca E. Cooper³, Rebecca Ignatz^{1,2}, Alexander Ruecker¹, Eliane
Gomes-Alves¹, Kirsten Küsel³, Georg Pohnert², Susan E. Trumbore¹*

¹ Department of Biogeochemical Processes, Max Planck Institute for Biogeochemistry, Jena,
Germany

² Institute for Inorganic and Analytical Chemistry, Friedrich Schiller University, Jena, Germany

³ Institute for Biodiversity, Friedrich Schiller University, Jena, Germany

*Corresponding author

THIS PDF FILE INCLUDES:

Supplementary text

Figures S1 to S45

Tables S1 to S11

SI References

SUPPLEMENTARY INFORMATION TEXT

INTRODUCTION: HYPOTHESES.

(1) There are two main processes leading to VSC emissions: sulfate reduction with subsequent methylation and cleavage of organic matter. Sulfate reduction needs a redox potential of 0 mV at pH = 4.1 (see Table S6), whereas methylation and cleavage reactions are independent of the redox potential. We can thus separate sulfate-reduction-originated VSC emissions from organic-matter originated emissions both by tracking redox potential changes and by labelling with $^{34}\text{SO}_4^{2-}$.

(2) VSC emissions can not only be generated by (methylated) methionine and cysteine, but from all compounds in the organic matter that contain methylthio and dimethyl sulfonio groups. We can find these other precursors for VSCs by identifying the structures of sulfur-containing dissolved and acetonitrile-extractable organic metabolites whose abundance correlates with VSC emissions.

(3) The initially formed VSCs may be transformed by rapid reactions altering the profile of what is emitted in the environment. In a dynamic chamber, the air gets exchanged quickly (every

2-3 min in our case), so that VSCs cannot build up in the headspace. In a static chamber, we do not flush out the headspace, so an equilibrium can be formed. With this, we can look at the quick, immediate formation reactions in dynamic chambers (like in hypothesis (2)), and then see how they are transformed into each other in static chambers.

(4) Methanogens, sulfate reducers and methylotrophs are the main contributors to VSC formation in the fen. Bromoethanesulfonate (BES) inhibiting methanogens, tungstate inhibiting sulfate reducers, and chloroform inhibiting methylotrophs indicate whether those microbial groups are involved in VSC cycling. Other microbes potentially involved in VSC cycling can be identified by correlating their abundance with VSC emissions.

RESULTS: COS AND DMSO.

In dynamic chamber incubations, N-acetyl methionine, and thiophene-3-carboxylic acid enhance COS emissions substantially from our soils (Figure S23). This might be interference signals from acetate, but we did not see a similar behavior on other acetate signals. No significant DMSO or CS₂ emissions were observed (Figure S24-25).

In static chamber incubations, we observed substantial carbonyl sulfide (COS) and dimethyl sulfoxide (DMSO) emissions when adding organic sulfur compounds to soil in static chamber incubations (Figure S30, S31). Due to the small headspace volume, we had to restrict our methods to VSCs and could not verify COS and DMSO against interfering compounds. Assuming the signals we measured were actually COS and DMSO, we did see an interesting pattern: DMSO appeared to spike after 1-2 d, whereas COS mixing ratios steadily increased over

the duration of the incubation. Therefore, COS could be a terminal metabolite for organic S or VSC degradation.

When adding inhibitors, COS was increased with glutaraldehyde and stayed constant for the others (Figure S30), whereas DMSO emissions increased in the presence of all inhibitors except BES (Figure S31). This suggests that COS and DMSO can be produced abiotically, and only their degradation is performed by microbes.

In the long-term incubation, COS increased in the first week, and then steadily decreased (Figure S34), indicating it might be consumed by the soils, as reported previously (1). This coincided with similar observations for other volatile aldehydes and acids we relate to general metabolism (Figure S33), although COS mixing ratios in the headspace persisted longer.

RESULTS: ³⁴S-LABELLING IN STATIC CHAMBERS.

An attempt to repeat the labelling experiment by incubating the same Na₂³⁴SO₄-labeled soils in static chambers after storing them for four weeks (4°C, aerobic in plastic bags) was unsuccessful. We found some labelled Me₂S emissions in the beginning, but even after a week of incubation, no sulfate reduction was observed (Figure S17). Either the sulfate reducing populations became inactive during storage or the septa of the chambers were not gas-tight anymore, preventing a decline in the redox potential and hence the occurrence of sulfate-reducing conditions. A depletion of organic food sources seems unlikely since the organic content of the soil was ~30%.

RESULTS: 16S RRNA MICROBIAL COMMUNITY ANALYSIS.

Amplicon sequencing of the bacterial and archaeal 16S rRNA gene revealed the microbial communities observed in the microcosm incubations across all time points were dominated by Acidobacteria, Proteobacteria, Firmicutes, Verrucomicrobia, and Actinobacteria which accounted for up to 86.8% of the sequence reads in each sample, all of which have members associated with dissimilatory S cycling processes (sulfate/sulfite reduction and sulfur oxidation). In addition, members of the Chloroflexi, Nitrospirae, Planctomycetes, Spirochaetes, Rokubacteria, Omnitrphicaeota, Crenarchaeota, and Euryarchaeota phyla also contain lineages involved in dissimilatory S cycling and are present in the amplicon sequencing data at relative abundances ranging between 0.04% (Omnitrphicaeota) and 2.2% (Chloroflexi). Overall, the microbial community composition on the phylum level remained stable throughout the course of the incubation period, with exception of Firmicutes, which increased from 0.13% (n=1) at T0 to 11.5% (n=4) after 3 weeks (Figure S43, 44).

Upon further investigation into the representative amplicon sequences, we identified microorganisms on the Genus-level involved in dissimilatory S cycling and potentially linked to microbially-mediated Me₂S, H₂S and MeSH emissions in the Schlöppnerbrunnen fen. *Acidobacteria* subdivisions 1, 2, and 3 (SD1, SD2, SD3) were the most abundant subset of genera present in both the native soil and over time in the microcosm incubations, and are known active sulfur cycling microorganisms with a putative dissimilatory S metabolism (2). In total, 33 genera were identified with known representative members capable of either sulfate reduction, sulfite

reduction, or S oxidation. In addition to *Acidobacteria* SD1, SD2, and SD3, among the most abundant sequences linked to dissimilatory S cycling were *Thermodesulfovibrio* (up to 2.9% total abundance), *Acidobacteria* SD13 (up to 2.2% total abundance), *Syntrophobacter* (up to 1.1% total abundance), and *Desulfobacca* (up to 0.8% total abundance). *Hyphomicrobium* and *Thiobacillus*, both of which have been previously linked to Me₂S, H₂S and MeSH degradation (3-5), were also detected in abundances ranging from 0.018-0.043% and 0.004-0.21%, respectively. At T4, a noticeable shift in the number of sequences linked the less abundant genera (Fig 4D) linked to S cycling was observed. The average number of sequences (n=4 or n=5) linked to *Sulfurimonas* (0.22-1.18% total abundance), *Sulfuricella* (0.12-0.68% total abundance), *Pseudomonas* (0.06-0.25% total abundance), *Sulfuritalea* (0.03-0.13% total abundance), *Thiobacillus* (0.03-0.17% total abundance), *Sulfuricurvum* (0.02-0.05% total abundance), uncultured *Hydrogenophilaceae* (0.03-0.06%), *Paludibacterium* (0.02-.67%), and *Desulfosporosinus* (0.03-0.13% total abundance) all increased in abundance from T0 to week 3, suggesting the contribution of these microorganisms to dissimilatory S cycling and potentially Me₂S, H₂S and MeSH degradation/emissions, increases over time in the microcosm incubations (Figure S45).

DISCUSSION: SOIL DRYOUT.

The exact shape of the emission over time is not only dependent on the redox potential, but also on soil humidity and substrate availability. We observe the typical optimum curve of VSC emissions over the dryout which can also emerge from the soil humidity: At high humidity, the

soil is completely flooded such that gases diffuse slowly through the water-filled pores. Gas exchange improves when pores start to become air-filled instead of water-filled, but eventually, microbial activity will drop again when water becomes limiting. Also, in the three weeks of incubation, the more labile carbon might be degraded, as no new food source was added. There is also considerable variability between the three soil replicates. Since we did not homogenize the soil by sieving, but kept the complete fibrous material of the organic layer, this can reflect soil heterogeneity, different pore sizes and substrate availabilities in the soil. Large variations were also observed in the redox potentials in the small chambers as it dried out. Still, Me₂S and MeSH peak between 2 and 4 g H₂O/g_{dw}, whereas H₂S peaks at 4-5 g H₂O/g_{dw} and towards dry soil, so indicates that there are different processes and/or microbial groups involved in their formation.

SUPPLEMENTARY METHODS

GENERAL.

Nitrogen and Helium gases were 6.0 grade and purchased from Westfalen AG, Münster, Germany. VOC-free air was generated using a PAG 003 pure air generator (Ecophysics, Dürnten, Switzerland). Deionized water was produced using a TKA GenPure pure water system with X-CAD and UV-UF (JWT GmbH, Jena, Germany). Acetonitrile and water used for the organic matter metabolomics extractions were UHPLC grade (Thermo Fischer Scientific GmbH, Dreieich, Germany). KCl, agarose, and the organic sulfur substrates were analytical grade

(Sigma Aldrich/Merck, Darmstadt, Germany). Methylcysteine S-oxide was purchased from BIOZOL Diagnostika Vertrieb GmbH, Eching, Germany. Gonyol and Dimethylsulfonylacetate were synthesized as described in literature (6). A VSC-standard with 1 ppm hydrogen sulphide, methanethiol, dimethyl sulphide, carbonyl sulphide, and carbon disulfide in nitrogen (Air Liquide Deutschland GmbH, Krefeld, Germany) was used to calibrate the SIFT-MS. A gas calibration unit (GCU, Ionicon, Innsbruck, Austria) was used to humidify the air and dilute the standard gas in VOC-free air.

STATISTICAL ANALYSES.

Statistical analyses were done using R 4.0.3, in RStudio 1.3.1093, with the packages tidyverse 0.4.3, corrplot 0.84, chron 2.3-56, factoextra 1.0.7, GGally 2.1.0, ggplot2 3.3.3, Hmisc 4.4-2, lme4 1.1-26, lubridate 1.7.9.2, mgcv 1.8-33, nlme 3.1-149, plot3D 1.3, RColorBrewer 1.1-2, reshape2 1.4.4, sjPlot 2.8.7, stats 4.0.3, and xlsx 0.6.5. 95% confidence intervals were calculated as $CI(c) = sd(x) * t(0.95, n_x - 1) / sqrt(n_x)$.

SOIL PARAMETERS

Soil humidity. 20 g field-moist soil samples were dried at 40°C for 72 h in a drying oven (E28, BINDER GmbH, Germany). Their weight before and after drying was noted. These samples were used for the N_{min} and sulfate extractions. Then, the soil was dried at 105°C for 24 h, cooled down in an exsiccator with fresh desiccant and weighed.

Redox potential. For the incubation, the redox potential was measured directly in the soil slurry using a GMH 3511 handheld redox-meter with a GR105 redox electrode (Greisinger, Regenstauf, Germany). For the soil dryout curves, redox probes were built into the chamber like displayed in Figure S 2. 30 small platinum electrodes were distributed in the chamber in six clusters. For each cluster, there was a salt bridge connecting it to an Ag/AgCl reference electrode (3M KCl, Merck Millipore, Darmstadt, Germany). Additionally, the temperature was tracked at the chamber bottom by two temperature sensors. The salt bridge was manufactured by adding a hot 3 M KCl solution with 1% agarose and 1.5 g/L Akasolv AquaCare water bath conserver (Akadia-Chemie, Mannheim, Germany) into 1/8" PFA tubes. One end was inserted into the redox chamber and covered with a lit whenever unused, the other end was inserted into the container for the reference electrode filled with 3 M KCl.

pH. 5 g air-dried soil was extracted with 25 mL deionized water using an overhead shaker (1 h shaking, 1 h settling, Reax20, Heidolph Instruments GmbH & CO. KG, Schwabach, Germany), decanted and then the pH of the supernatant was measured using a pH Meter 538 MultiCal® (WTW, Weilheim, Germany). The same procedure was repeated with 1 M KCl solution.

Sulfate content. 5 g air-dried soil was extracted with 50 mL 0.0125 M CaCl₂ solution for 1 h using an overhead shaker (Reax20, Heidolph Instruments GmbH & CO. KG, Schwabach, Germany). The soil was filtered off over Whatman folded paper filters (GE Healthcare Europe GmbH, Frankfurt a.M., Germany) and the filtrate was measured with a DX 500 Ion chromatograph (Thermo Fisher Scientific GmbH, Idstein, Germany).

Nitrite/nitrate and ammonia content. 5 g air-dried soil was extracted with 50 mL 2 M KCl solution for 1 h using an overhead shaker (Reax20, Heidolph Instruments GmbH & CO. KG, Schwabach, Germany). The soil was filtered off over Whatman folded paper filters (GE Healthcare Europe GmbH, Frankfurt a.M., Germany) and the filtrate was measured via Flow Injection Analysis (Quikchem QC85S5, Lachat Instruments, Hach Company, Loveland CO, USA)

Nitrite was measured in situ by filtering off 10 mL of the water in the submerged soil using the Whatman folded paper filters and using the Spectroquant nitrite test kit measured by the Spectroquant Move100 Colorimeter (Merck KGaA, Darmstadt, Germany).

Element analysis. For measuring the C and N content, 250 mg of air-dried, sieved (4 mm), and ground soil samples were supplemented with 450 mg WO_3 and combusted and analyzed using a Vario MAX Elemental Analyzer (Elementar Analysensysteme GmbH, Hanau, Germany). To measure the inorganic carbon content, the samples were combusted at 450°C for 16 h prior to the WO_3 addition.

For measuring the S content, 30 mg air-dried, sieved, ground soil samples were added to 6x6 mm tin boats. These were folded and placed in 8x8 mm tin boats that were additionally filled with 60 mg WO_3 . The samples were analyzed using a Vario EL II Elemental Analyzer (Elementar Analysensysteme GmbH, Hanau, Germany).

Organic Matter Composition and Metabolomics. The frozen samples were stored until the water content was determined. With the dry weights, it was calculated how much fresh soil would be needed to resemble 5 g air-dry soil. As the soil was already submerged, the soil was centrifuged off directly using a Z 383K Universal High Speed Centrifuge (Hermle LaborTechnik GmbH, Wehingen, Germany) at 6000 rpm. 4 mL of the filtrate were dried down using a RVC 2-25 CDplus rotary vacuum concentrator (Martin Christ Gefriertrocknungsanlagen GmbH, Osterode, Germany) and resuspended in 400 μ L acetonitrile:water (1:1 v/v) mixture. 10 μ L 40 μ M ribitol in water was added as an internal standard. This was measured using UHPLC-MS. A quality control sample was created by pipetting aliquots of every sample together. The sample sequence was set up in a way that all samples were measured in a random order, and every 8 samples, an acetonitrile/water blank and the quality control was measured. The samples were measured on a Dionex UltiMate 3000 (Thermo Fisher Scientific, Dreieich, Germany) coupled to a Q-Exactive Plus mass spectrometer (Thermo Fisher Scientific, Dreieich, Germany). A Synergi™ 4 μ m Hydro-RP polar end-capped C18 analytical column (Phenomenex, Aschaffenburg, Germany) was flushed using a gradient (0-1 min: 100 % H₂O with 1% ACN and 0.1 % formic acid, 1-10 min: linear gradient to 100% ACN with 0.1% formic acid, 10-12 min: 100% ACN with 0.1% formic acid). Each sample was measured with three technical replicates. Positive and negative polarity were measured in separate runs. A window of $m/z = 100-1200$ u was used with a resolution of 280.000.

The residual soil was then extracted with 10 mL acetonitrile, centrifuged, and the supernatant was again dried down and resuspended in 400 μ L acetonitrile. Enough quality control sample for 8 individual QC samples was prepared from aliquots of these samples. 10 μ L 40 μ M ribitol in water was added as an internal standard. The samples and QC sample was dried down in an exsiccator overnight. 50 μ L methoxyamine in pyridine was added (20 μ g/mL), heated to 60°C for 1 h and then left to derivatize completely at room temperature overnight. The QC sample was split up into the individual QC samples. 2 μ L of alkane standard mix (C₇-C₄₀, 100 μ g/ml in hexane, Supelco, Munich, Germany) was added to one QC sample. The samples were measured using a Q Exactive GC Orbitrap GC-MS/MS with a Q Exactive orbitrap mass spectrometer, a Trace™ 1310 GC equipped with a TriPlus™ RSH™ Autosampler (Thermo Fisher Scientific, Dreieich, Germany) with automatic sample derivatization. The samples were additionally derivatized by adding 50 μ L BSTFA and heating to 60°C for 1 h directly before the analysis. The analysis was performed on a Zebtron ZB-SemiVolatiles column (30 m \times 0.25 mm \times 0.25 μ m, Phenomenex, Aschaffenburg, Germany) using a temperature gradient (2 min at 80°C, then heat to 120°C with a rate of 20°/min, hold for 1 min, then heat to 250°C with a rate of 5°C/min, then heat to 320°C at 10°C/min and hold for 2 min). 1 μ L sample was injected into the injector at 250°C at a split ratio of 1:10. Masses were recorded between $m/z = 60$ and 500 u with a resolution of 120.000.

The data analysis was done using Xcalibur and Compound Discoverer 4.0 (Thermo Fisher Scientific, Dreieich, Germany) as well as Metaboanalyst (7) and R 3.6.1 to 4.0.3 (8). Features

were detected and integrated with Compound Discoverer. Peaks were picked between 100 and 5000 Da, with a minimum signal to noise ratio threshold (SNR) of 1.5. The peaks were aligned with a maximum shift of 2 min and a mass tolerance of 5 ppm. Compounds were detected with a mass tolerance of 5 ppm, an intensity tolerance of 30%, a SNR-threshold of 3, a minimum peak intensity of 105, and a sum formula up to $C_{90}H_{190}Br_3F_6K_2N_{10}Na_2O_{18}P_3S_5$, with adducts of H^+ , Na^+ , K^+ , NH_4^+ , Cl^- , acetonitrile, formic acid, methanol, and H abstractions. Compounds were grouped and merged with a mass tolerance of 5 ppm and a maximum retention time shift of 0.1 min. Fragments of $[M+H]^+$ and $[M-H]^-$ were used in the feature list. ChemSpider, mzCloud, mzVault, and MassList search was done by sum formula and mass, with a maximum mass deviation of 5 ppm and an SFit Threshold and Range of 20. Gaps were filled with a 5 ppm mass tolerance and an ANR threshold of 1.5. Background compounds were eliminated if the sample/blank ratio was below 5. The S isotopic pattern was matched with a mass tolerance of 5 ppm, an intensity tolerance of 30%, and an SNR threshold of 3. Element compositions were predicted with 5 ppm mass tolerance, sumformulas between CH and $C_{90}H_{190}Br_3Cl_8F_{18}N_{10}O_{18}P_3S_5$, 0-40 double-bond equivalents, a H/C ratio between 0.1 and 3.5, and pattern matching.

Statistical Analyses were done with MetaboAnalyst. Therefore, the data was normalized using log transformation and Pareto scaling. Principal component analyses and partial-least squares discriminant analyses (PLS-DA) were done with the data. From the PLS-DA, the variable importance in projection (VIP score) was calculated for the first axis. For the selection of

individual features, we used the VIP score and not the correlation coefficient, as it would also capture substances first increasing and then decreasing during the analysis. The feature selection criteria were: $VIP > 1$, $\max(\text{intensity, autoclaved controls})/\min(\text{intensity, autoclaved controls}) < 5$, $\max(\text{intensity, samples})/\min(\text{intensity, samples}) > 5$, $\max/\min(\text{intensity, sample}) > 2 * (\max/\min(\text{intensity, autoclaved controls}))$. These features were then investigated manually. MS² spectra were acquired on the samples with the highest peak intensity using the same LC-method as above, at NCE = 50 eV. If possible, we coinjected organic sulfur compound standards for confirming the substances. These compounds were also used in a calibration between 10 ng/L and 10 µg/L. The calibration was used to quantify these substances in the incubation samples.

NUCLEIC ACID EXTRACTION AND ILLUMINA MISEQ AMPLICON SEQUENCING OF THE 16S RRNA GENE.

DNA was extracted from sediment sampled from microcosm incubations described in section ‘Prolonged Incubation in Closed Chambers under Argon’ using the DNeasy PowerSoil Extraction kit (Qiagen) following the manufacturer's protocol at 5 different time points. DNA was extracted in triplicate from samples taken at the following pre-selected time points: 0, 1, 7, 14, 21, 28 d. Amplicon sequencing of prokaryotes (bacteria and archaea) 16S rRNA genes was carried out targeting the V4 region using the Earth Microbiome Project primer pair, 515F-806R (9-12). Illumina libraries were generated using the NEBNext Ultra II FS DNA library preparation kit (New England Biolabs) according to the manufacturer's protocol. Size selection

was performed using the AMPure XP beads (Beckman Coulter). The sequencing was performed in-house on an Illumina MiSeq platform using v3 chemistry with 2×300 bp read lengths.

Amplicon sequence reads were first subjected to primer sequence removal by cutting the 5' to 3' end based on primer sequence length. Next, read pairs were paired-end assembly and checked for quality control using the `-fastq_mergepairs` (`-fastq_minmergelen = expected amplicon size`) and `-fastq_filter` (`-fastq_maxee = 0.5`) functions implemented in *usearch* (v 11)(13). The operational taxonomic units (OTU) were clustered using *vsearch* (v 1.10.2) (97% sequence identity, *de novo*)(14). Low abundant OTUs (<10 sequence reads) were removed. The representative sequences were taxonomically assigned against SILVA (release 128) (15) using the *uclust* algorithm (13) implemented in *vsearch* (minimum similarity of 90%). An OTU table including determined taxonomic affiliations and available metadata was assembled for downstream analysis with QIIME 2 (v 2020.2). Raw reads were deposited at the ENA under accession xxx.

The correlation and the heatmap was done in R 4.0.3 using the Hmisc 4.4-2, tidyverse 1.3.0, and corrplot 0.4.3 packages. Correlation with time was done for all individual samples; results were considered significant if the correlation was larger than 0.5 or smaller than -0.5. For the heatmap, the relative abundance data was averaged for each time point ($n = 4$ for $t = 4$ w, $n = 5$ for the others). These results were centered and scaled by their mean relative abundance, i.e. $rel.A.change(T_1) = (A(T_1) - \bar{A})/\bar{A}$.

CO₂, CH₄, AND N₂O EMISSIONS.

To make sure the samples are well equilibrated with room air, the chambers were opened for 10 min before the analysis. Then, Schott bottle caps with butyl rubber plugs were placed onto the Schott bottles containing the sample. After 5, 20, and 35 min, 50 mL headspace was taken out with a syringe and inserted into a previously evacuated 20 mL headspace vial. The headspace was measured using a Nexis GC-2030 with a BID discharge ionization detector and a HS-20 autosampler (Shimadzu, Jena, Germany). The sample was injected using a split ratio of 1:9, and a purge flow of 2 mL/min. Sample and transfer line were kept at 150°C, the auto sampler at 60°C. The SH-Rt-QBond column (30 m x 0.53 mm x 20 µm) was operated with a temperature gradient (40°C for 2.5 min, then heat to 120°C at 10°C/min, then hold for 1.5 min) and 3.34 mL/min He carrier gas flow.

SIFT-MS MEASUREMENTS – GENERAL.

Volatile gas emissions were measured using a Syft Voice200ultra SIFT-MS equipped with a positive ion source (Syft Technologies GmbH, Darmstadt, Germany). The instrument was optimized as published in (16). 100 mL/min sample gas flow, 312 mL/min Helium carrier gas flow, 140°C flow tube temperature and 50 V flow tube voltage were used. Unless stated otherwise, 1 s scan time and 100.000 cps count limit were used. A calibration at 0, 0.2, 0.5, 1, 2, 5, 10, 20 ppb of the VSC standard diluted with VOC-free air, in dry air and at 30%, 60% and 90% humidity at 25°C was done every six months.

Mixing ratios were calculated from the calibration as

$$\chi = a \cdot \frac{I_{prod}}{I_{reag}} + b \cdot \frac{I_{H_3O^+ \cdot H_2O}}{I_{H_3O^+}} + c \quad (1)$$

a, b, c are regression parameters from the calibration, I_{prod} and I_{reag} the intensity (cps) of the product ion of the analyte and its corresponding reagent ion, and $I_{H_3O^+ \cdot H_2O}$ and $I_{H_3O^+}$ the intensity (cps) of the $H_3O^+/37$ u water cluster and its corresponding reagent ion $H_3O^+/19$ u, as a measure of the air humidity.

In case there was no calibration available, the mixing ratios (in ppb) were calculated as

$$\chi = 1.0035 \cdot 10^{-10} \frac{\text{Torr} \cdot \text{cm}^3}{\text{K} \cdot \text{molecule} \cdot \text{s}} \cdot \frac{T_{FT}}{p_{FT}} \cdot \left(\frac{\varphi_{carr}}{\varphi_{samp}} + 1 \right) \cdot \frac{\sum_i I_{reag,i} \frac{ICF_i}{br_i}}{\sum_j k_j \cdot I_{prod,i} \cdot ICF_j} \quad (2)$$

Where T_{FT} and p_{FT} are the flow tube temperature and pressure, φ_{carr} and φ_{samp} the carrier gas and sample gas flow, $I_{reag,i}$ and $I_{prod,i}$ the reagent and their corresponding product ions, ICF_i and ICF_j the corresponding instrument calibration factors, as determined from the instrument validation, br_i the branching ratio of the product ion as listed in the library, and k_j the kinetic constant of the ionization reaction as listed in the library.

The first scan was always discarded and the remaining scans were averaged. The gas release rate was calculated as

$$\phi = \frac{\chi \cdot M \cdot \varphi_{air}}{V_{mol} \cdot m_{soil\ dw}} \quad (3)$$

ϕ being the release rate in $\mu\text{mol} / \text{g}_{\text{dw}} \text{ h}$, M the molar mass of the compound, φ_{air} the air flow through the incubation chamber (cf. Table S3), V_{mol} the molar volume, used 24 L/mol, and $m_{soil\ dw}$ the soil dry mass.

The error of the emission rate was calculated as

$$\Delta\phi = t(95\%, n_{meas} - 1) \cdot M \cdot \left(\frac{\phi_{air} \cdot \Delta\chi}{m_{soil\ dw}} + \frac{\chi \cdot \varphi_{air} \cdot \Delta V_{mol}}{V_{mol}^2 \cdot m_{soil\ dw}} + \frac{\chi \cdot \Delta\varphi_{air}}{V_{mol} \cdot m_{soil\ dw}} + \frac{\chi \cdot \varphi_{air} \cdot \Delta m_{soil\ dw}}{V_{mol} \cdot m_{soil\ dw}^2} \right) \quad (4)$$

$t(95\%, n_{meas} - 1)$ is the t-distribution at 95% and the degrees of freedom being the number of measurements per time point – 1. $\Delta\chi$ is the standard deviation of the mixing ratios that was calculated based on the individual measurements per time point. $\Delta V_{mol} = 0.72 \text{ L/mol}$ is the error of the molar volume for 5 K and 0.02 bar deviation of the temperature and pressure. $\Delta\varphi_{air}$ is the reading error of the gas flow measurements, and $\Delta m_{soil\ dw}$ the reading error of the weight measurement.

SIFT-MS MEASUREMENTS FOR PROLONGED INCUBATION.

11 scans were done per measurement. Scan time per ion was 500 ms for most ions, 1 s for the reagent ion $m/z = 19, 30, \text{ and } 32 \text{ u}$, and 5 s for dimethyl sulfide ($\text{H}_3\text{O}^+ / 63 \text{ u}$ and $\text{O}_2^+ / 62 \text{ u}$), methanethiol ($\text{H}_3\text{O}^+ / 49 \text{ u}$) and carbonyl sulfide ($\text{O}_2^+ / 60 \text{ u}$), Table S1.

Table S1: Details of the SIFT-MS settings of the method used in the prolonged incubation with 11 measurement repetitions each.

Reagent ion	Product ion m/z	Analyte and product ion
H_3O^+	18	ammonia, NH_4^+
H_3O^+	31	formaldehyde, CH_3O^+
H_3O^+	33	methanol, CH_5O^+
H_3O^+	35	hydrogen sulfide, H_3S^+
H_3O^+	36	ammonia, $\text{NH}_4^+ \cdot \text{H}_2\text{O}$
H_3O^+	43	pyruvic acid, $\text{C}_2\text{H}_3\text{O}^+$
H_3O^+	45	acetaldehyde, $\text{C}_2\text{H}_5\text{O}^+$
H_3O^+	49	methyl mercaptan, $\text{CH}_4\text{S} \cdot \text{H}^+$
H_3O^+	49	formaldehyde, $\text{H}_2\text{CO} \cdot \text{H}^+ \cdot \text{H}_2\text{O}$
H_3O^+	51	methanol, $\text{CH}_3\text{OH}_2^+ \cdot \text{H}_2\text{O}$
H_3O^+	53	hydrogen sulfide, $\text{H}_3\text{S}^+ \cdot \text{H}_2\text{O}$
H_3O^+	59	acetone, $\text{C}_3\text{H}_7\text{O}^+$
H_3O^+	59	propanal, $\text{C}_3\text{H}_7\text{O}^+$
H_3O^+	61	acetic acid, $\text{CH}_3\text{COOH}_2^+$
H_3O^+	63	dimethyl sulfide, $(\text{CH}_3)_2\text{S} \cdot \text{H}^+$
H_3O^+	63	acetaldehyde, $\text{C}_2\text{H}_5\text{O}^+ \cdot \text{H}_2\text{O}$
H_3O^+	67	methyl mercaptan, $\text{CH}_4\text{S} \cdot \text{H}^+ \cdot \text{H}_2\text{O}$
H_3O^+	69	methanol, $\text{CH}_3\text{OH} \cdot \text{H}^+ \cdot (\text{H}_2\text{O})_2$
H_3O^+	77	ethyl methyl sulfide, $\text{CH}_3\text{SHC}_2\text{H}_5^+$
H_3O^+	77	acetone, $(\text{CH}_3)_2\text{CO} \cdot \text{H}^+ \cdot \text{H}_2\text{O}$
H_3O^+	77	propanal, $\text{C}_3\text{H}_7\text{O}^+ \cdot \text{H}_2\text{O}$

Reagent ion	Product ion <i>m/z</i>	Analyte and product ion
H ₃ O ⁺	79	acetic acid, CH ₃ COOH ₂ ⁺ .H ₂ O
H ₃ O ⁺	81	acetaldehyde, C ₂ H ₅ O ⁺ .2H ₂ O
H ₃ O ⁺	89	butanoic acid, C ₃ H ₇ COOH ₂ ⁺
H ₃ O ⁺	91	lactic acid, CH ₃ CH(OH)COOH ₂ ⁺
H ₃ O ⁺	95	dimethyl disulfide, (CH ₃) ₂ S ₂ .H ⁺
H ₃ O ⁺	95	ethyl methyl sulfide, CH ₃ SHC ₂ H ₅ ⁺ .H ₂ O
H ₃ O ⁺	95	propanal, C ₃ H ₇ O ⁺ .2H ₂ O
H ₃ O ⁺	97	acetic acid, CH ₃ COOH ₂ ⁺ .2H ₂ O
H ₃ O ⁺	107	butanoic acid, C ₃ H ₇ COOH ₂ ⁺ .H ₂ O
H ₃ O ⁺	123	benzoic acid, C ₇ H ₆ O ₂ .H ⁺
H ₃ O ⁺	137	alpha-pinene, C ₁₀ H ₁₇ ⁺
H ₃ O ⁺	145	octanoic acid, C ₈ H ₁₆ O ₂ .H ⁺
H ₃ O ⁺	159	dimethyl tetrasulfide, C ₂ H ₆ S ₄ ⁺
H ₃ O ⁺	163	octanoic acid, C ₈ H ₁₆ O ₂ .H ⁺
H ₃ O ⁺	177	dimethyl tetrasulfide, C ₂ H ₆ S ₄ H ⁺ .H ₂ O
NO ⁺	43	acetaldehyde, CH ₃ CO ⁺
NO ⁺	57	propanal, C ₃ H ₅ O ⁺
NO ⁺	61	acetaldehyde, CH ₃ CO ⁺ .H ₂ O
NO ⁺	62	methanol, NO ⁺ .CH ₃ OH
NO ⁺	71	Butanoic acid, C ₃ H ₇ CO ⁺
NO ⁺	73	lactic acid, CH ₃ CH(OH)CO ⁺
NO ⁺	78	dimethyl sulfoxide, C ₂ H ₆ OS ⁺
NO ⁺	79	acetaldehyde, CH ₃ CO ⁺ .2H ₂ O
NO ⁺	88	acetone, NO ⁺ .C ₃ H ₆ O

Reagent ion	Product ion m/z	Analyte and product ion
NO^+	90	acetic acid, $\text{NO}^+ \cdot \text{CH}_3\text{COOH}$
NO^+	94	dimethyl disulfide, $(\text{CH}_3)_2\text{S}_2^+$
NO^+	104	propanoic acid, $\text{NO}^+ \cdot \text{C}_2\text{H}_5\text{COOH}$
NO^+	108	acetic acid, $\text{NO}^+ \cdot \text{CH}_3\text{COOH} \cdot \text{H}_2\text{O}$
NO^+	118	butanoic acid, $\text{NO}^+ \cdot \text{C}_3\text{H}_7\text{COOH}$
NO^+	118	pyruvic acid, $\text{C}_3\text{H}_4\text{O}_3 \cdot \text{NO}^+$
NO^+	120	lactic acid, $\text{NO}^+ \cdot \text{CH}_3\text{CH}(\text{OH})\text{COOH}$
NO^+	124	dimethylsulfone, $\text{C}_2\text{H}_6\text{O}_2\text{S} \cdot \text{NO}^+$
NO^+	126	dimethyl trisulfide, $\text{C}_2\text{H}_6\text{S}_3^+$
NO^+	136	alpha-pinene, $\text{C}_{10}\text{H}_{16}^+$
NO^+	146	hexanoic acid, $\text{C}_6\text{H}_{12}\text{O}_2 \cdot \text{NO}^+$
NO^+	156	dimethyl sulfate, $\text{C}_2\text{H}_6\text{O}_4\text{S} \cdot \text{NO}^+$
NO^+	158	dimethyl tetrasulfide, $\text{C}_2\text{H}_6\text{S}_4^+$
O_2^+	17	ammonia, NH_3^+
O_2^+	18	ammonia, NH_4^+
O_2^+	34	hydrogen sulfide, H_2S^+
O_2^+	35	ammonia, $\text{NH}_3^+ \cdot \text{H}_2\text{O}$
O_2^+	36	ammonia, $\text{NH}_4^+ \cdot \text{H}_2\text{O}$
O_2^+	43	acetone, $\text{C}_2\text{H}_3\text{O}^+$
O_2^+	45	formic acid, HCOO^+
O_2^+	48	methyl mercaptan, CH_4S^+
O_2^+	57	propanal, $\text{C}_3\text{H}_5\text{O}^+$
O_2^+	58	acetone, $\text{C}_3\text{H}_6\text{O}^+$
O_2^+	58	propanal, $\text{C}_3\text{H}_6\text{O}^+$
O_2^+	60	carbonyl sulfide, COS^+

Reagent ion	Product ion m/z	Analyte and product ion
O_2^+	60	butanoic acid, CH_3COOH^+
O_2^+	62	dimethyl sulfide, $(CH_3)_2S^+$
O_2^+	74	propanoic acid, $C_2H_5COOH^+$
O_2^+	88	butanoic acid, $C_3H_7COOH^+$
O_2^+	93	alpha-pinene, $C_7H_9^+$
O_2^+	94	dimethyl disulfide, $(CH_3)_2S_2^+$
O_2^+	94	dimethylsulfone, $C_2H_6O_2S^+$
O_2^+	95	dimethylsulfone, $C_2H_7O_2S^+$
O_2^+	96	dimethyl sulfate, $CH_4O_3S^+$
O_2^+	122	benzoic acid, $C_7H_6O_2^+$
O_2^+	126	dimethyl trisulfide, $C_2H_6S_3^+$

SIFT-MS MEASUREMENTS FOR DRYOUT.

All chambers were measured in an alternating fashion. Each time every chamber was measured, a one-point calibration was done with the VSC calibration standard that was diluted to 1 ppb in pure air.

Full scans of all three reagent ions were measured between $m/z = 15$ and 150 u, with 1 s scan time and a count limit of 100.000 counts. For the ions of hydrogen sulfide, methanethiol, carbonyl sulfide and dimethyl sulfide with $H_3O^+ / 35, 49, 63$ u, and $O_2^+ / 34, 48, 60, 62$ u, the scan time was extended to 5 s.

SIFT-MS MEASUREMENT FOR SUBSTANCE ADDITION, AND SULFATE LABELLING EXPERIMENTS.

Six scans of the analytes mentioned in table were done with a scan time of 1 s and 100.000 cps count limit, Table S2.

Table S2: Details of the SIM scan used for the substance addition in dynamic chambers and the labelling experiment.

Reagent ion	Product ion <i>m/z</i>	analyte and product ion
H ₃ O ⁺	35	hydrogen sulphide, H ₃ S ⁺
H ₃ O ⁺	49	methanethiol, CH ₄ S·H ⁺
H ₃ O ⁺	51	methanethiol- ³⁴ S, CH ₄ ³⁴ S·H ⁺
H ₃ O ⁺	53	hydrogen sulphide, H ₃ S ⁺ ·H ₂ O
H ₃ O ⁺	63	dimethyl sulphide, (CH ₃) ₂ S·H ⁺
H ₃ O ⁺	65	dimethyl sulphide- ³⁴ S, (CH ₃) ₂ ³⁴ S·H ⁺
H ₃ O ⁺	67	methanethiol, CH ₄ S·H ⁺ ·H ₂ O
H ₃ O ⁺	77	carbon disulfide, CS ₂ ·H ⁺
H ₃ O ⁺	77	methyl ethyl sulfide, C ₃ H ₈ S·H ⁺
H ₃ O ⁺	79	dimethyl sulphoxide, C ₂ H ₆ OS·H ⁺
H ₃ O ⁺	79	carbon disulphide- ³⁴ S, C ³² S ³⁴ S·H ⁺
H ₃ O ⁺	81	dimethyl sulphoxide- ³⁴ S, C ₂ H ₆ O ³⁴ S·H ⁺
H ₃ O ⁺	81	carbon disulphide-(³⁴ S) ₂ , C ³⁴ S ₂ ·H ⁺
H ₃ O ⁺	89	methyl propenyl sulfide, C ₄ H ₈ S·H ⁺
H ₃ O ⁺	91	diethyl sulfide, C ₄ H ₁₀ S ⁺

H ₃ O ⁺	95	dimethyl disulphide, (CH ₃) ₂ S ₂ ·H ⁺
H ₃ O ⁺	95	dimethylsulphone, C ₂ H ₆ O ₂ S·H ⁺
H ₃ O ⁺	95	methyl ethyl sulfide, C ₃ H ₈ S·H ⁺ ·H ₂ O
H ₃ O ⁺	97	dimethyl disulphide- ³⁴ S, (CH ₃) ₂ ³² S ³⁴ S·H ⁺
H ₃ O ⁺	97	dimethylsulphone- ³⁴ S, C ₂ H ₆ O ₂ ³⁴ S·H ⁺
H ₃ O ⁺	99	dimethyl disulphide-(³⁴ S) ₂ , (CH ₃) ₂ ³⁴ S ₂ ·H ⁺
H ₃ O ⁺	99	sulfuric acid, H ₃ SO ₄ ⁺
H ₃ O ⁺	113	dimethylsulphone, C ₂ H ₆ O ₂ S·H ₂ O·H ⁺
H ₃ O ⁺	115	di-2-propenyl sulfide, (C ₃ H ₅) ₂ S·H ⁺
H ₃ O ⁺	115	dimethylsulphone- ³⁴ S, C ₂ H ₆ O ₂ ³⁴ S·H ⁺ ·H ₂ O
H ₃ O ⁺	123	ethyl disulfide, C ₄ H ₁₀ S ₂ ·H ⁺
H ₃ O ⁺	127	methyl sulfate, C ₂ H ₆ O ₄ S·H ⁺
H ₃ O ⁺	127	methyl sulfate, C ₂ H ₆ O ₄ S·H ⁺
H ₃ O ⁺	127	dimethyl trisulphide, C ₂ H ₆ S ₃ H ⁺
H ₃ O ⁺	129	dimethyl trisulphide- ³⁴ S, C ₂ H ₆ (³² S) ₂ ³⁴ S·H ⁺
H ₃ O ⁺	145	methyl sulfate, C ₂ H ₆ O ₄ S·H ₂ O·H ⁺
H ₃ O ⁺	145	dimethyl trisulfide, C ₂ H ₆ S ₃ H ⁺ ·H ₂ O
H ₃ O ⁺	159	dimethyl tetrasulphide, C ₂ H ₆ S ₄ ·H ⁺
H ₃ O ⁺	161	dimethyl tetrasulphide- ³⁴ S, C ₂ H ₆ (³² S) ₃ ³⁴ S·H ⁺
H ₃ O ⁺	177	dimethyl tetrasulfide, C ₂ H ₆ S ₄ ·H ⁺ ·H ₂ O
NO ⁺	62	dimethyl sulphide, (CH ₃) ₂ S ⁺
NO ⁺	64	dimethyl sulphide- ³⁴ S, (CH ₃) ₂ ³⁴ S ⁺
NO ⁺	78	dimethyl sulphoxide, C ₂ H ₆ OS ⁺
NO ⁺	80	dimethyl sulphoxide- ³⁴ S, C ₂ H ₆ O ³⁴ S ⁺
NO ⁺	88	methyl propenyl sulfide, C ₄ H ₈ S ⁺
Reagent ion	Product ion <i>m/z</i>	Product ion

NO ⁺	90	diethyl sulfide, C ₄ H ₁₀ S ⁺
NO ⁺	94	dimethyl disulphide, (CH ₃) ₂ S ₂ ⁺
NO ⁺	96	dimethyl disulphide- ³⁴ S, (CH ₃) ₂ ³² S ³⁴ S ⁺
NO ⁺	98	dimethyl disulphide-(³⁴ S) ₂ , (CH ₃) ₂ (³⁴ S) ₂ ⁺
NO ⁺	99	glutaraldehyde, C ₅ H ₇ O ₂ ⁺
NO ⁺	108	dimethyl sulphoxide, C ₂ H ₆ OS·NO ⁺
NO ⁺	108	dimethyl sulphoxide- ³⁴ S, C ₂ H ₆ O ³⁴ S·NO ⁺
NO ⁺	114	di-2-propenyl sulfide, (C ₃ H ₅) ₂ S ⁺
NO ⁺	122	ethyl disulfide, C ₄ H ₁₀ S ₂ ⁺
NO ⁺	124	dimethylsulphone, C ₂ H ₆ O ₂ S·NO ⁺
NO ⁺	126	dimethyl trisulphide, C ₂ H ₆ S ₃ ⁺
NO ⁺	126	dimethylsulphone- ³⁴ S, C ₂ H ₆ O ₂ ³⁴ S·NO ⁺
NO ⁺	128	dimethyl trisulphide- ³⁴ S, C ₂ H ₆ (³² S) ₂ ³⁴ S ⁺
NO ⁺	156	methyl sulfate, C ₂ H ₆ O ₄ S·NO ⁺
NO ⁺	158	dimethyl tetrasulphide, C ₂ H ₆ S ₄ ⁺
NO ⁺	160	dimethyl tetrasulphide- ³⁴ S, C ₂ H ₆ (³² S) ₃ ³⁴ S ⁺
O ₂ ⁺	34	sulphur dioxide- ³⁴ S, ³⁴ SO ₂ ⁺
O ₂ ⁺	36	hydrogen sulphide, H ₂ S ⁺
O ₂ ⁺	46	hydrogen sulphide- ³⁴ S, H ₂ ³⁴ S ⁺
O ₂ ⁺	46	dimethyl sulphide, CH ₂ S ⁺
O ₂ ⁺	46	dimethyl disulphide, CH ₂ S ⁺
O ₂ ⁺	47	dimethyl disulphide- ³⁴ S, CH ₂ ³⁴ S ⁺
O ₂ ⁺	47	dimethyl sulphide, CH ₃ S ⁺
O ₂ ⁺	48	methanethiol, CH ₃ S ⁺
O ₂ ⁺	48	dimethyl sulphide- ³⁴ S, CH ₂ ³⁴ S ⁺
O ₂ ⁺	48	methanethiol, CH ₄ S ⁺
O ₂ ⁺	48	dimethyl disulphide-(³⁴ S) ₂ , CH ₂ ³⁴ S ⁺

O ₂ ⁺	49	dimethyl disulphide- ³⁴ S, CH ₂ ³⁴ S ⁺
O ₂ ⁺	49	dimethyl sulphide- ³⁴ S, CH ₃ ³⁴ S ⁺
O ₂ ⁺	50	methanethiol- ³⁴ S, CH ₃ ³⁴ S ⁺
O ₂ ⁺	60	methanethiol- ³⁴ S, CH ₄ ³⁴ S ⁺
O ₂ ⁺	61	carbonyl sulphide, COS ⁺
O ₂ ⁺	61	diethyl sulfide, C ₂ H ₅ S ⁺
O ₂ ⁺	61	dimethyl disulphide, CH ₃ CH ₂ S ⁺
O ₂ ⁺	61	dimethyl disulphide- ³⁴ S, CH ₃ CH ₂ ³² S ⁺
O ₂ ⁺	61	dimethyl trisulphide, C ₂ H ₅ S ⁺
O ₂ ⁺	62	dimethyl trisulphide- ³⁴ S, C ₂ H ₅ ³² S ⁺
O ₂ ⁺	62	dimethyl sulphide, (CH ₃) ₂ S ⁺
O ₂ ⁺	62	carbonyl sulphide- ³⁴ S, CO ³⁴ S ⁺
O ₂ ⁺	63	diethyl sulfide, C ₂ H ₆ S ⁺
Reagent ion	Product ion <i>m/z</i>	analyte and product ion
O ₂ ⁺	63	dimethyl disulphide-(³⁴ S) ₂ , CH ₃ CH ₂ ³⁴ S ⁺
O ₂ ⁺	63	dimethyl disulphide- ³⁴ S, CH ₃ CH ₂ ³⁴ S ⁺
O ₂ ⁺	64	dimethyl trisulphide- ³⁴ S, C ₂ H ₅ ³⁴ S ⁺
O ₂ ⁺	73	dimethyl sulphide- ³⁴ S, (CH ₃) ₂ ³⁴ S ⁺
O ₂ ⁺	75	methyl propenyl sulfide, C ₃ H ₅ S ⁺
O ₂ ⁺	76	diethyl sulfide, C ₃ H ₇ S ⁺
O ₂ ⁺	78	carbon disulfide, CS ₂ ⁺
O ₂ ⁺	78	dimethyl sulphoxide, C ₂ H ₆ OS ⁺
O ₂ ⁺	78	dimethyl sulphoxide- ³⁴ S, C ₂ H ₆ O ³⁴ S ⁺
O ₂ ⁺	78	carbon disulphide- ³⁴ S, C ³² S ³⁴ S ⁺
O ₂ ⁺	78	dimethyl trisulphide, CH ₂ S ₂ ⁺
O ₂ ⁺	79	dimethyl trisulphide- ³⁴ S, CH ₂ ³⁴ S ₂ ⁺

O_2^+	79	dimethyl disulphide, $CH_3S_2^+$
O_2^+	79	dimethyl trisulphide, $CH_3S_2^+$
O_2^+	80	dimethylsulphone, $CH_3O_2S^+$
O_2^+	80	carbon disulphide- ^{34}S , $C(^{34}S)_2^+$
O_2^+	80	dimethyl trisulphide, $CH_4S_2^+$
O_2^+	81	dimethyl trisulphide- ^{34}S , $CH_4(^{32}S)_2^+$ and $CH_2^{32}S^{34}S^+$
O_2^+	81	dimethyl disulphide- ^{34}S , $CH_3^{32}S^{34}S^+$
O_2^+	81	dimethyl trisulphide- ^{34}S , $CH_3^{32}S^{34}S^+$
O_2^+	82	dimethylsulphone- ^{34}S , $CH_3O_2^{34}S^+$
O_2^+	82	dimethyl trisulphide- ^{34}S , $CH_4^{32}S^{34}S^+$
O_2^+	83	glutaraldehyde, $C_5H_6O^+$
O_2^+	83	dimethyl disulphide- ^{34}S , $CH_3(^{34}S)_2^+$
O_2^+	85	trichloromethane, $CH(^{35}Cl)_2^+$
O_2^+	88	trichloromethane, $CH^{35}Cl^{37}Cl^+$
O_2^+	90	methyl propenyl sulfide, $C_4H_8S^+$
O_2^+	94	diethyl sulfide, $C_4H_{10}S^+$
O_2^+	94	ethyl disulfide, $C_2H_6S_2^+$
O_2^+	94	dimethyl disulphide, $(CH_3)_2S_2^+$
O_2^+	95	dimethylsulphone, $C_2H_6O_2S^+$
O_2^+	96	dimethylsulphone, $C_2H_7O_2S^+$
O_2^+	96	dimethyl disulphide- ^{34}S , $(CH_3)_2^{32}S^{34}S^+$
O_2^+	97	dimethylsulphone- ^{34}S , $C_2H_6O_2^{34}S^+$
O_2^+	98	dimethylsulphone- ^{34}S , $C_2H_6O_2^{34}SH^+$
O_2^+	111	dimethyl disulphide- ^{34}S , $(CH_3)_2(^{34}S)_2^+$
O_2^+	113	dimethyl trisulphide, $CH_3S_3^+$
O_2^+	122	dimethyl trisulphide- ^{34}S , $CH_3(^{32}S)_2^{34}S^+$
O_2^+	126	ethyl disulfide, $C_4H_{10}S_2^+$

O_2^+	128	dimethyl trisulphide, $C_2H_6S_3^+$
---------	-----	-------------------------------------

SIFT-MS MEASUREMENTS FOR STATIC CHAMBER MEASUREMENTS.

A 60 s SIM scan with 1 s scan time per ion and a count limit of 100,000 counts was done for measuring dimethyl sulfide, methanethiol, hydrogen sulfide, carbonyl sulfide, and dimethyl sulfoxide, Table S3.

Table S3: Details of the SIFT-MS settings of the short (60 s) VSC method with 5 measurement repetitions each, as used for the substance manipulation in closed chambers.

Reagent ion	Product ion m/z	Analyte and product ion
H_3O^+	35	hydrogen sulphide, H_3S^+
H_3O^+	49	methanethiol, $CH_4S \cdot H^+$
H_3O^+	63	dimethyl sulfide, $(CH_3)_2S \cdot H^+$
NO^+	62	dimethyl sulfide, $(CH_3)_2S^+$
NO^+	78	dimethyl sulfoxide, $C_2H_6OS^+$
O_2^+	48	methanethiol, CH_4S^+
O_2^+	60	carbon sulfoxide, COS^+
O_2^+	62	dimethyl sulfide, $(CH_3)_2S^+$
O_2^+	78	dimethyl sulfoxide, $C_2H_6OS^+$

SETUPS

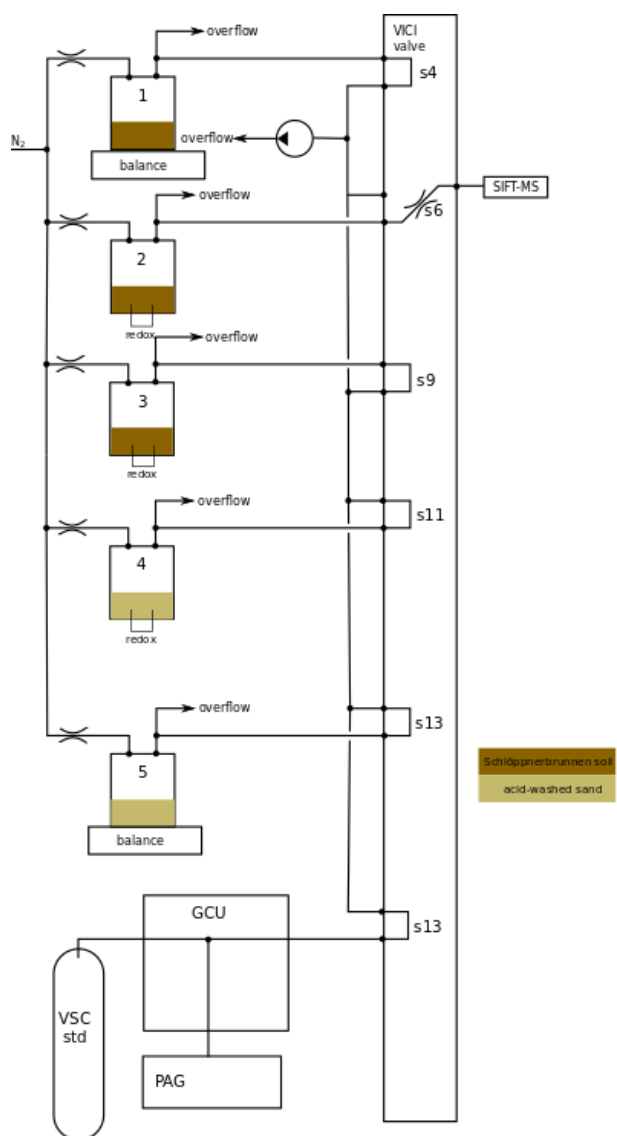


Figure S 1. Scheme of dryout chamber setup. Three replicates of Schlöppnerbrunnen soil and two replicates of an acid-washed sand control were incubated under nitrogen. One replicate each was placed on a balance to track the water loss directly; the other ones were placed in redox chambers as indicated in Figure S 2. All tubes were continuously flushed, both by the nitrogen stream flowing through the chambers and by the pump downstream the instrument. The VSC standard was diluted to 1 ppb and measured daily (though flowing constantly, to ensure the VSC mixing ratios are in equilibrium with the tube walls). The balance weight was also noted down daily. The VSC emissions of the chambers were measured continuously one after the other.

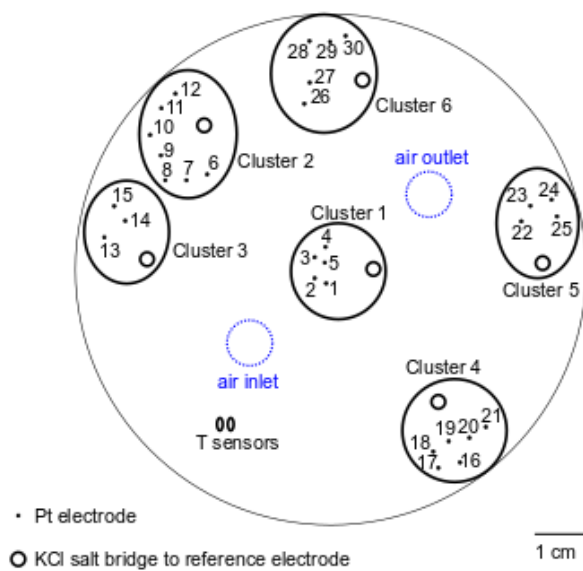


Figure S 2. Scheme of the redox chambers as viewed from above. Six clusters of platinum redox electrodes (small black dots) are distributed in the floor of the chamber, sticking out ca. 2 mm. Each cluster is connected to the Ag/AgCl reference electrode via a salt bridge (small circles). The temperature is measured by two sensors (small ellipses). Air inlet and outlet are on the top of the chamber, with the positions approximately shown by the blue dashed circles.

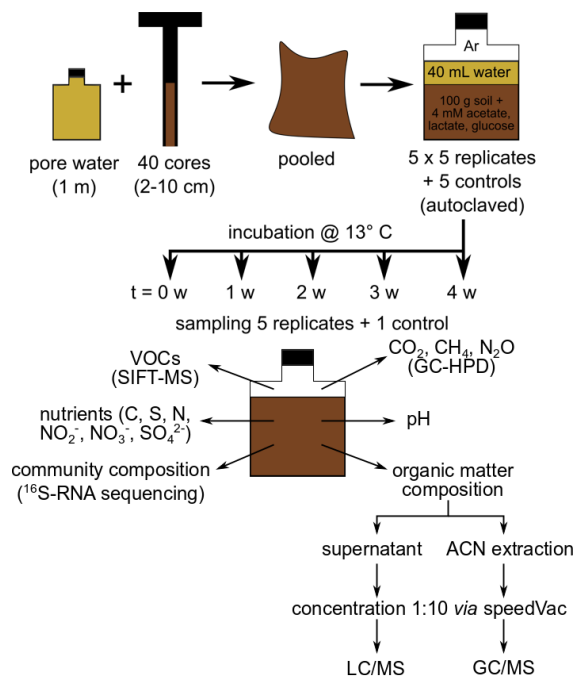


Figure S 3. Sampling scheme of long-term anoxic incubation experiment. Pore water and cores were sampled, pooled and distributed on 30 flasks which were flushed with Argon for 1 h. 5 flasks were autoclaved. Every week, 5 samples + 1 autoclaved control sample were used for the different measurements indicated.

SOIL SPECIFICATIONS

Table S4: Overview over the soils used in the soil screening experiment. The soils were air-dried, rewetted to 0%, 30%, 60%, 100%; and 150% of their field capacity, and then, their VSC emissions were measured. Mean $\pm 95\%$ CI for nitrate/nitrite, ammonia, and sulfate contents. Fertilizers were applied at Julius-Kühn-Feld after harvest in autumn. We sampled before the new crops were planted. Initials of the people who sampled: ML: Mariela Leidermann, Ben-Gurion University of the Negev, Israel, ASL: Ann-Sophie Lehnert, Max-Planck-Institute for Biogeochemistry, Jena, JW: John Wang, University of North Carolina, USA, TB: Thomas Behrendt, Max-Planck-Institute for Biogeochemistry, Jena. EC: Elisa Catão, Max-Planck-Institute for Biogeochemistry, Jena

Country	Sampling site	Soil horizon	Vegetation	Specifications	Soil type	pH	C (%)	Org. C (%)	N (%)	S (%)	NO ₂ / NO ₃ (µg/g _a)	NH ₄ ⁺ (µg/g _a)	SO ₄ ²⁻ (µg/g _w)	Sampled by	Sampling date	Ref
Israel	Kibbutz Sede Boker	0-5 cm	Olive orchard, irrigated by dripping irrigation	Taken from irrigated zone	Cambisol	6.6	5.13±0.02	2.27±0.01	0.21±0.02	0.08	20010	16.7±0.6	1000±100	ML	03/2019	(17, 18)
Germany	Hainich	Or	Beech forest	Managed beech forest, samples taken between trees, trying not to take the root zone	Cambisol	5.4	12.07±0.04	12.01±0.04	0.72±0.01	0.08	27±5	43±2	42±2	ASL	02/2019	(19)
		A 0-5 cm				4.4	3.35±0.08	3.31±0.08	0.25±0.01	<0.06	4.5±0.2	5.3±0.5	15±2	ASL		
	Würzbachgrund	Or	Beech forest	Managed beech forest, samples taken between trees, trying not to take the root zone	Cambisol	3.6	34.92±0.02	34.78±0.05	1.28±0.02	0.23	<1.04	10.7±0.6	40±1	ASL	02/2019	(20)
		A 0-5				3.8	1.36±0	1.36±0	0.05±0	<0.06	<1.04	3.2±0.8	8±1	ASL		

Julius-Kühn-Feld	A, 0-10 cm	Cropland, rotation: corn, spring wheat, spring barley, potato	40/80 kg/ha KCl C	Haplic Phaeozem	5.9	.13	.02	<0.06	12±1	2±1	10±3	ASL	03/201 ₉	(21)
	A, 0-10 cm				6.1	1.03±0	0.09±0	1±0.02	<0.06	4.5±0.5	1.57±0.07	8±3	ASL	
Schlößpnebrunnen	A, 0-10 cm	peat	80/160 kg/ha KCl ^D	Fibric Histosol	4.1	.13	.02	<0.06	<1.04	14.6±0.9	120±1	ASL	05/201 ₉	(22)
	O, 10-20 cm				4.2	1.13±0.01	0.08±0.01	0.09±0.01	0.09	8±1	<0.5	35±2	ASL	
USA	South Carolina	Forested freshwater fen	M site, downhill, more saturated, more redox potential changes, higher Fe content	Sediment	4.1	.13	.02	<0.06	<1.04	12.9±0.7	55±2	ASL		
					O, 10-20 cm	4.1	1.12±0.01	0.08±0.01	1.03±0.02	<0.06	4±1	<0.5	10±3	ASL
Brazil	ATTO	Sediment	Flooded 6 m/a	Sediment	5.2	.13	.02	<0.06	30±40	80±20	19±16	EC	06/201 ₆	(23)
					3-6 cm	5.2	30.99±0.01	30.93±0.01	1.41±0.01	0.31	<1.04	12.9±0.7	55±2	ASL
USA	South Carolina	Degraded organohaline fen	Salt marsh	Sediment	5.8	.13	.02	0.53	13±7	14.1±0.3	210±2	JW	03/201 ₉	
					3-6 cm	5.8	35.33±0.03	34.99±0.03	2.16±0.01	0.53	13±7	14.1±0.3	210±2	JW
Brazil	ATTO	Forest	Flooded 3 m/a	Ferralsol	4.4	.13	.02	0.89	<1.04	13.3±0.7	1000±70	JW		
					3-6 cm	4.4	34.62±0.03	34.5±0.07	1.87±0.02	0.89	<1.04	13.3±0.7	1000±70	JW
Brazil	ATTO	forest	Not flooded	Ferralsol	4.4	.13	.02	1.33	8±3	45±3	5600±160	JW		
					3-6 cm	4.4	15.84±2.92	15.78±2.93	17	1.33	8±3	45±3	5600±160	JW
Brazil	ATTO	forest	Not flooded	Ferralsol	5.9	.13	.02	0.08	30±70	80±30	5±1	EC	06/201 ₆	
					3-6 cm	5.9	2.6±0.02	2.57±0.02	1.14±0.01	0.08	30±70	80±30	5±1	EC
Brazil	ATTO	forest	Not flooded	Ferralsol	4.4	.13	.02	<0.06	45±49	29±8	15±1	TB	04/201 ₈	
					3-6 cm	4.4	4.37±0.02	4.34±0.02	0.29±0.01	<0.06	45±49	29±8	15±1	TB
Brazil	ATTO	forest	Not flooded	Ferralsol	4.4	.13	.02	<0.06	12±5	60±20	28±1	TB	04/201 ₈	
					3-6 cm	4.4	2.54±0.04	2.53±0.05	0.2±0.01	<0.06	12±5	60±20	28±1	TB

DRYOUT AND REWETTING

Table S5: pH of soil slurries from fresh fen soil before the anoxic dryout incubation and air-dry soil after being dried under a constant nitrogen flow (anoxic incubation) or a constant flow of VOC-free air (oxic incubation) over three weeks. Slurries were prepared by adding distilled water such that the amount of water was equal to 10 x the air-dry soil mass.

Soil replicate	pH of soil slurry		
	Before incubation	After anoxic incubation	After oxic incubation
1	4.47	4.13	3.79
2	4.57	3.90	3.75
3	4.54	4.90	4.44

Table S6: Redox potential of possible half reactions happening in soil-water systems at 25°C (24). Referenced to Standard Hydrogen Electrode. pH = 3.9, 4.1, and 4.5 are the pH reached in the anoxic dryout experiments. For the calculation of the Fe^{2+}/Fe^{3+} -potential, the correct phase was selected from the phase diagrams in Evangelou (24), and the used Fe^{2+} and Fe^{3+} contents were 140 and 30 $\mu\text{mol}/g_{\text{dw}}$ as reported by Reiche, Torburg and Küsel (25).

	E_H (V)			
	pH = 7	pH = 4.5	pH = 3.9	pH = 4.1
$O_2 + 4 H^+ + 4 e^- \rightleftharpoons 2 H_2O$	1.23	0.96	1.00	0.99
$NO_3^- + 6 H^+ + 5 e^- \rightleftharpoons NO_2^- + H_2O$	0.85	0.58	0.62	0.61
$Fe(OH)_3(\text{amorphous}, s) + 3H^+ + e^- \rightleftharpoons Fe^{2+} + 3 H_2O$	-0.33	0.11	0.21	0.18
$SO_4^{2-} + 10 H^+ + 8 e^- \rightleftharpoons H_2S + 4 H_2O$	0.31	-0.02	0.02	0.01
Acetic Acid: $2CO_2 + 8 H^+ + 8 e^- \rightleftharpoons C_2H_4O_2 + 2 H_2O$	0.10	-0.13	-0.14	-0.17
Glucose: $6 CO_2 + 24 H^+ + 24 e^- \rightleftharpoons C_6H_{12}O_6 + 6 H_2O$	-0.01	-0.28	-0.24	-0.26

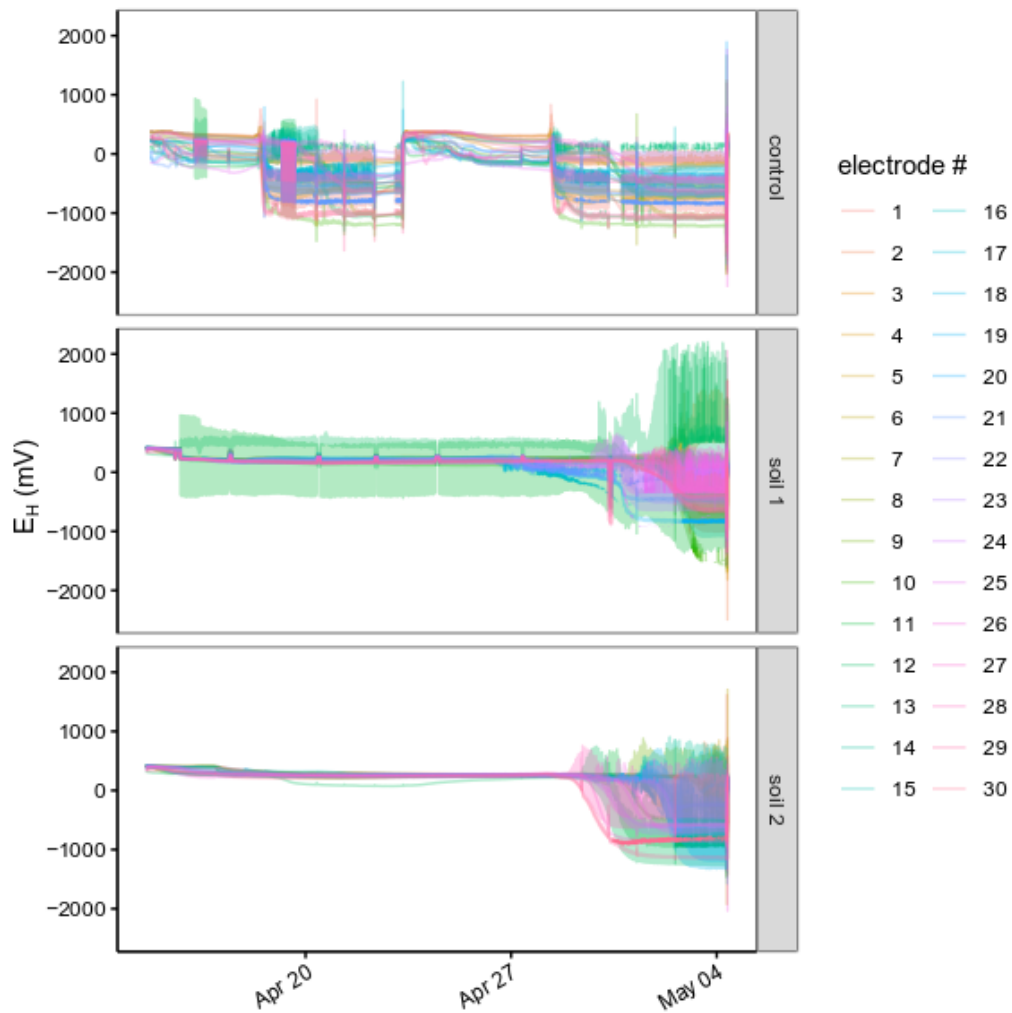


Figure S 4. change of redox potential signal for all electrodes in the three chambers during anoxic dryout of the Schlöppnerbrunnen soils and the acid-washed sand control over the course of 21 d. Secondly raw data shown. The sand had to be re-wetted after 10 d, since it dried out rather quickly.

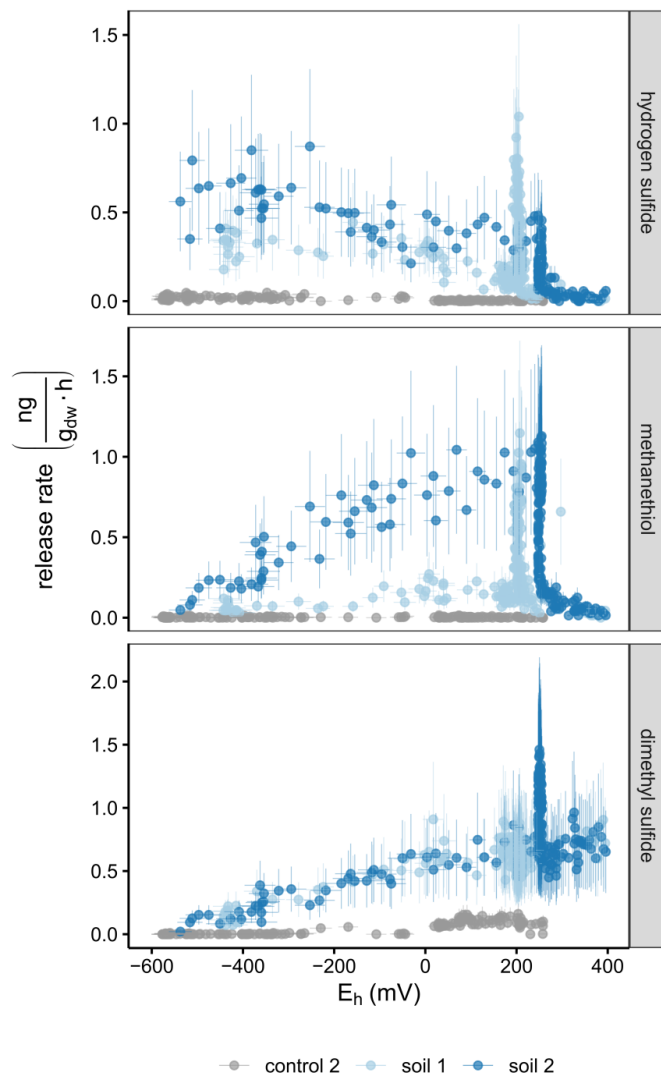


Figure S 5. Change of VSC emissions with redox potential change for the three chambers where the redox potential was measured during the anoxic dryout of the Schlöppnerbrunnen soils and acid-washed sand controls over the course of 21 d. Mean \pm 95% CI $n_{\text{tech, intensity}} = 4$. Redox potential distribution was summarized from all 3 electrodes over 1000 s for each data point ($n = 30000$).

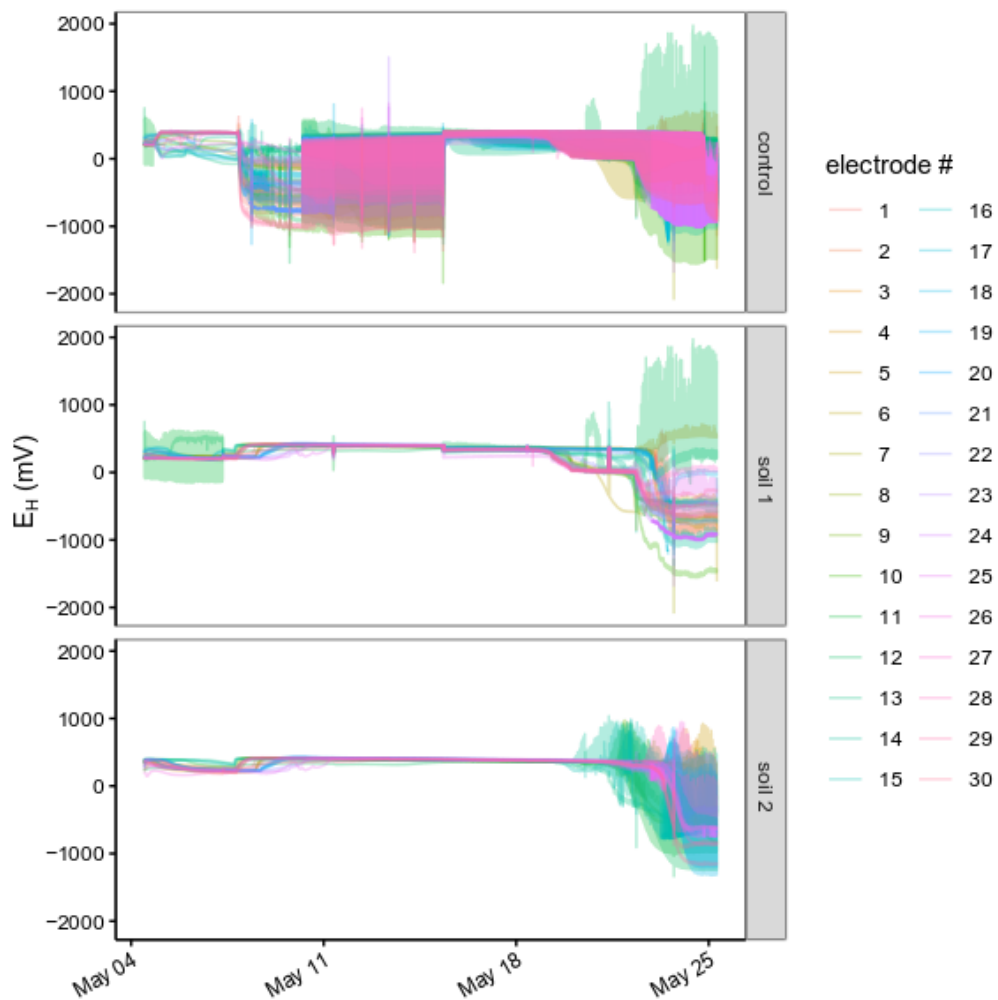


Figure S 6. change of redox potential signal for all electrodes in the three chambers during oxic dryout of the Schlöppnerbrunnen soils and the acid-washed sand control over the course of 21 d. Secondly raw data shown. The sand had to be re-wetted after 10 d, since it dried out rather quickly.

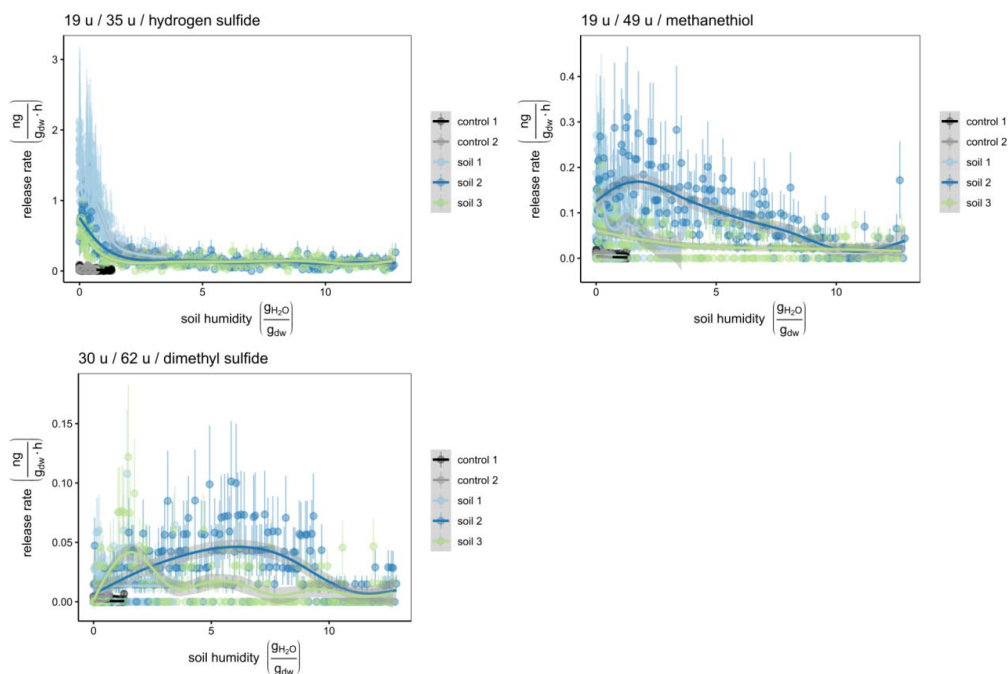


Figure S 7. VSC emission rates during dryout of Schlöppnerbrunnen soil under VOC-free air (acid-washed sand control $n = 2$, Schlöppnerbrunnen soil $n = 3$). Every data point is 10 scans, mean \pm 95% CI. A GAM smoother was applied over all times. The controls only had a very low soil humidity, as their density was much higher and even though the water added was the same as for the other soils, it never reached that high humidities.

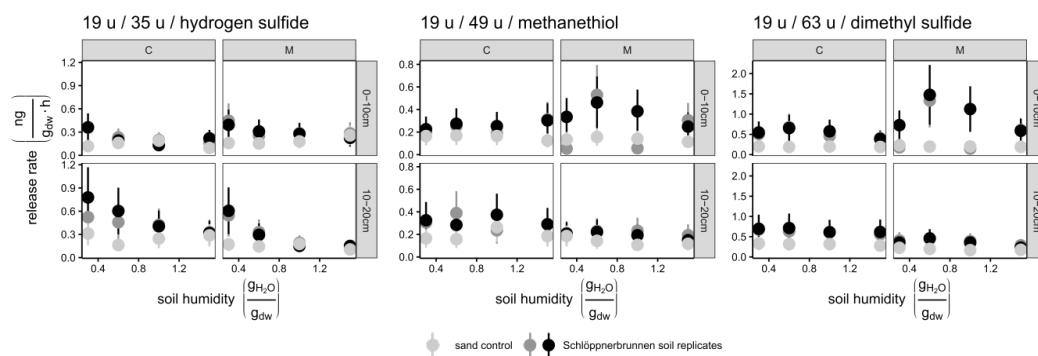


Figure S 8: VSC emissions from the two sites at the Schläppnerbrunnen fen, the M and the C site differing in their waterlogging and the amount of iron. Samples were taken from two depths as well, to see the influence of a changing water table. They were dried and rewetted to 30%, 60%, 100%, and 150% of their water holding capacity.

VSC emissions from other soils

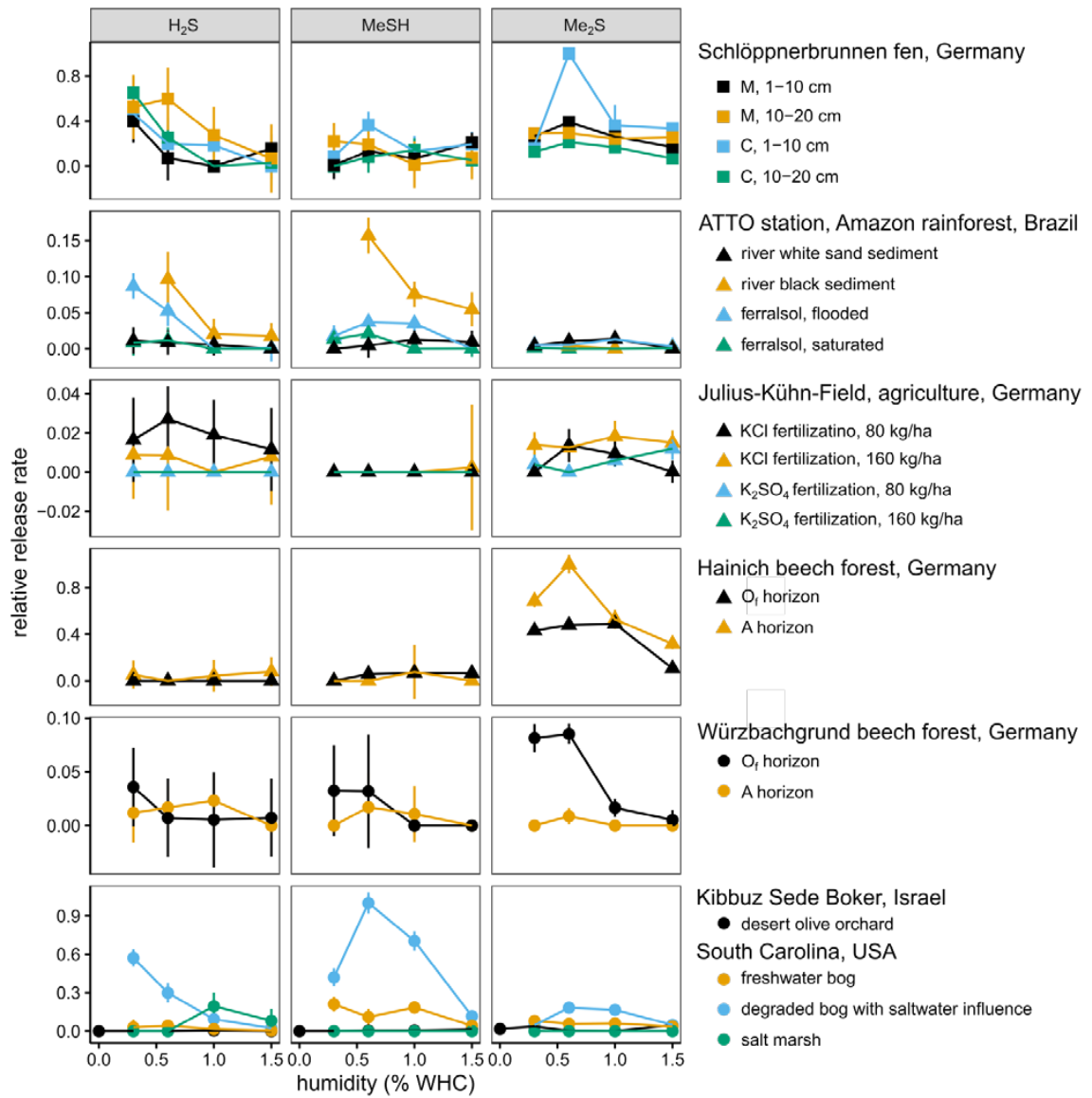


Figure S 9: Humidity-dependence of VSC emissions from soils from sites from different locations. Due to technical difficulties and limited sample size, the data could not be quantified properly. Release rates with the same point shapes (squares vs. triangles vs. points) were comparable and are normalized to the highest VSC emission from this group. Mean \pm 95% CI ($n_{\text{soil}} = 3$, $n_{\text{tech}} = 10$, $n_{\text{soil}} = 2$ for ATTO and Schlöppnerbrunnen sites). Soil from Disko Island, Greenland, was dried out for a similar result, but did not yield significant VSC emissions. Since the method was different, it was not included in this graph.

LABELLING

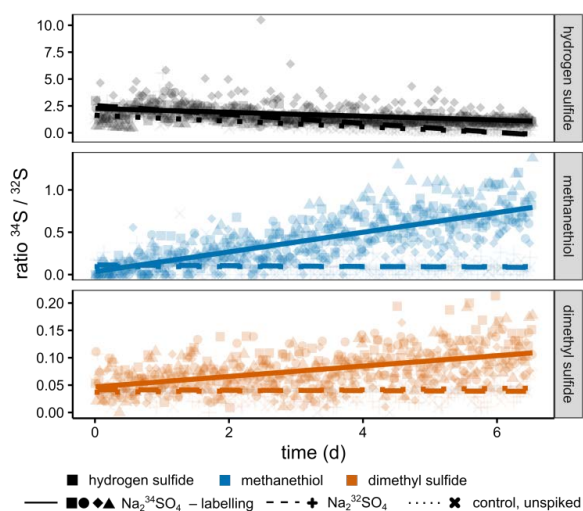


Figure S 10. Ratio of ^{34}S to ^{32}S emissions for hydrogen sulfide (black), methanethiol (blue) and dimethyl sulfide (red) when labelling with $\text{Na}_2^{34}\text{SO}_4$ ($n = 4$, solid line, replicates have different shapes), and the two controls $\text{Na}_2^{32}\text{SO}_4$ (dashed line) and unspiked soil control (dotted line). Whereas hydrogen sulfide and methanethiol reach labelling ratios of approx. 1, dimethyl sulfide shows much less labelling, only about 10% of the unlabeled signal.

Table S 7. Amount of $^{34}\text{SO}_4^{2-}$ converted to the emitted volatile sulfur compounds. Other labelled sulfur compounds were not detected.

VSC	Incorporated amount of ^{34}S (ppm)
Hydrogen sulfide	18±3
Methanethiol	5±3
Dimethyl sulfide	1.4±0.7

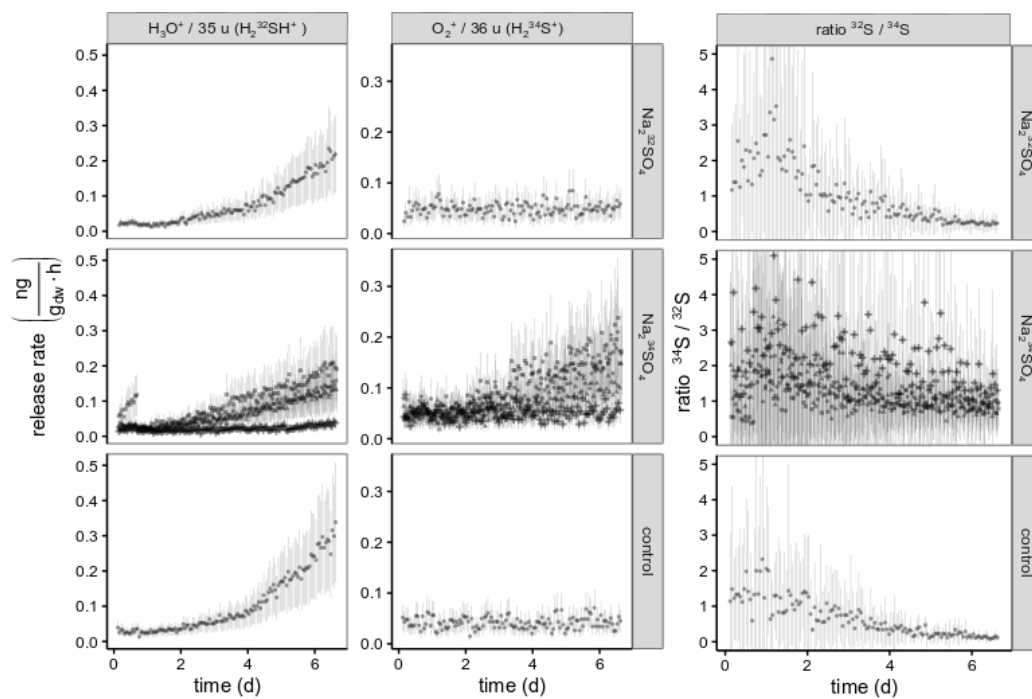


Figure S 11. Emissions of H_2^{32}S and H_2^{34}S as well as the ratio of labelled to unlabelled H_2S in dynamic chamber incubation when adding $\text{Na}_2^{32}\text{SO}_4$, $\text{Na}_2^{34}\text{SO}_4$, and a control. $N = 3$ for $^{34}\text{SO}_4$ -amended soil replicates (different shapes), and $N=1$ for $^{32}\text{SO}_4$ addition and control. Each data point is the mean \pm 95% CI of 5 scans.

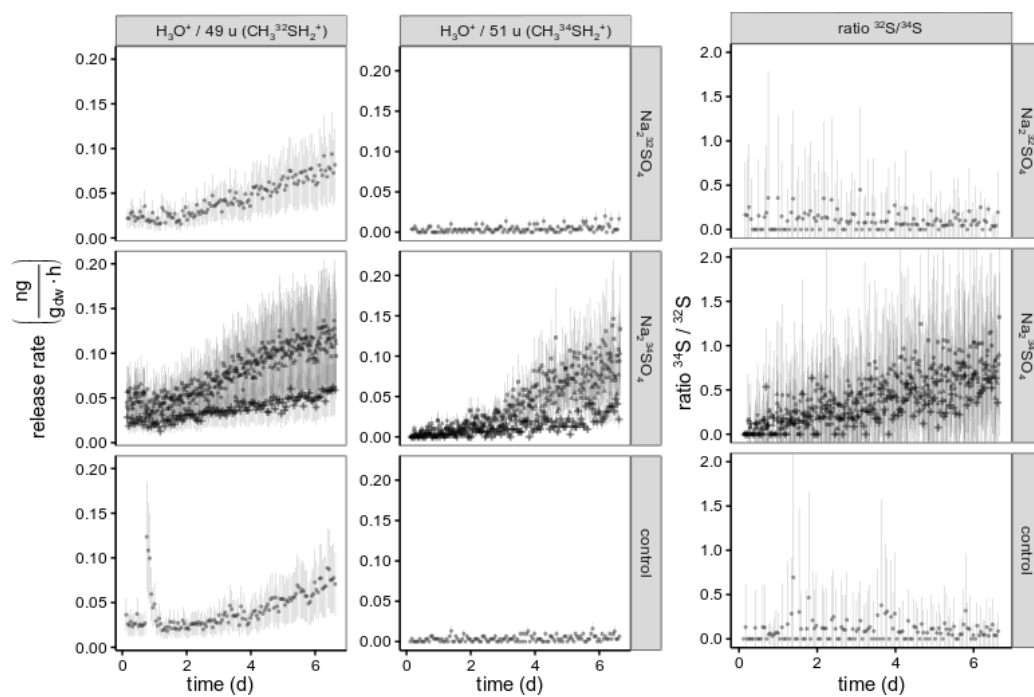


Figure S 12. Emissions of Me^{32}SH and Me^{34}SH as well as the ratio of labelled to unlabeled MeSH in dynamic chamber incubation when adding $\text{Na}_2^{32}\text{SO}_4$, $\text{Na}_2^{34}\text{SO}_4$, and a control. $n = 3$ for $^{34}\text{SO}_4$ -amended soil replicates (different shapes), and $n=1$ for $^{32}\text{SO}_4$ addition and control. Each data point is the mean \pm 95% CI of 5 scans.

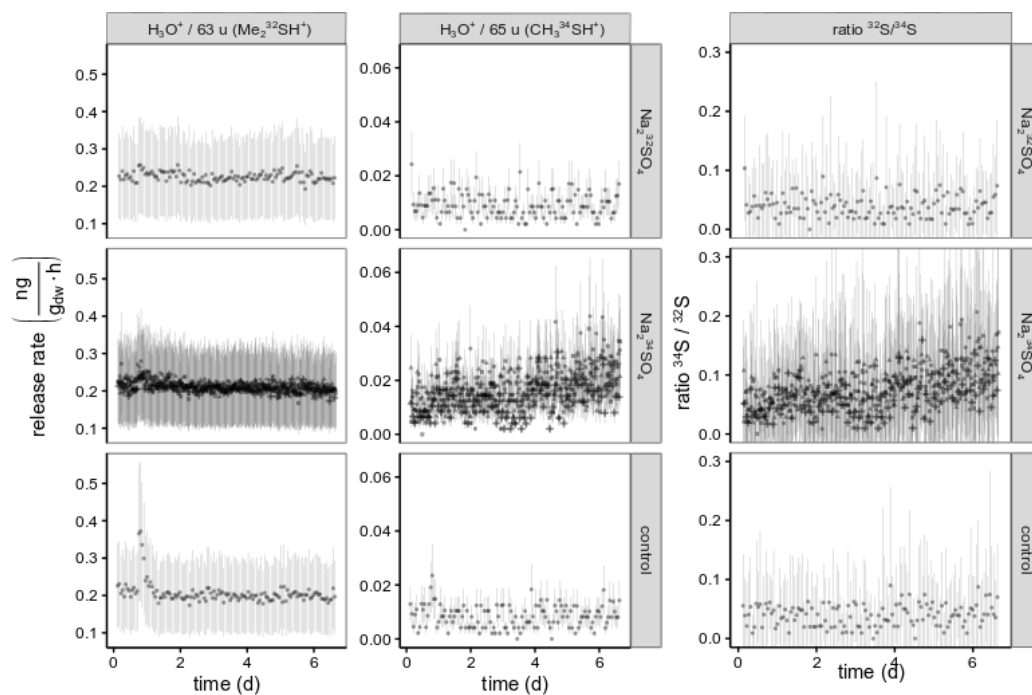


Figure S 13. Emissions of Me_2^{32}S and Me_2^{34}S as well as the ratio of labelled to unlabeled Me_2S in dynamic chamber incubation when adding $\text{Na}_2^{32}\text{SO}_4$, $\text{Na}_2^{34}\text{SO}_4$, and a control. $n = 3$ for $^{34}\text{SO}_4$ -amended soil replicates (different shapes), and $n=1$ for $^{32}\text{SO}_4$ addition and control. Each data point is the mean \pm 95% CI of 5 scans.

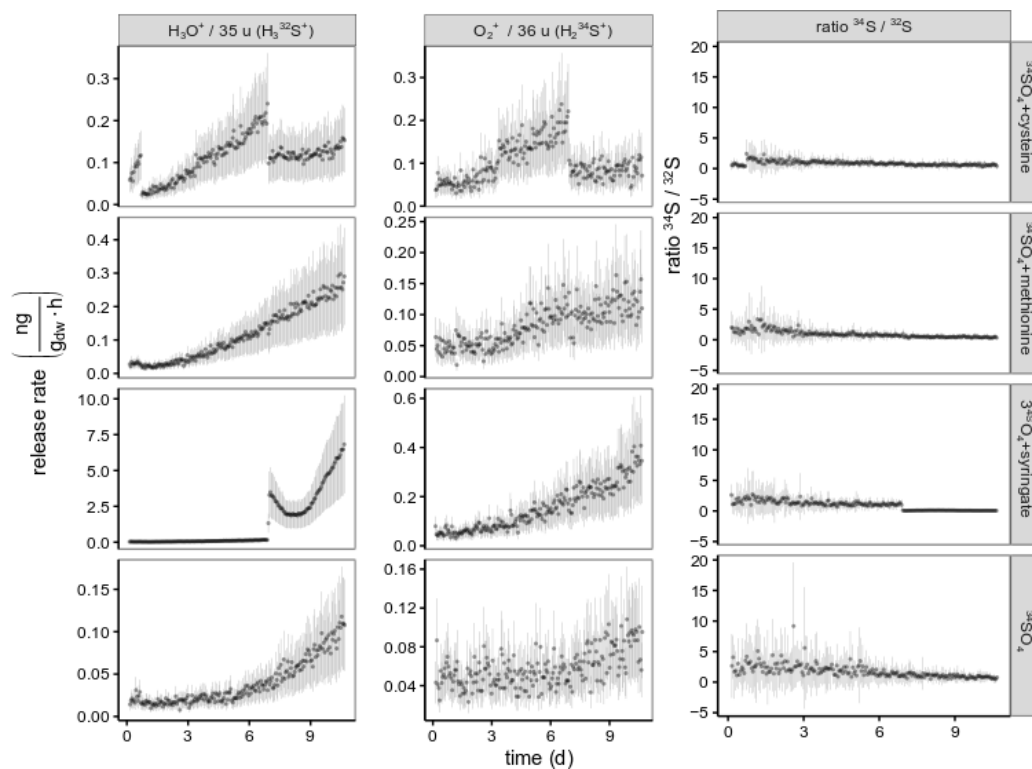


Figure S 14. Emissions of $^{32}\text{S}\text{-H}_2\text{S}$ and $^{34}\text{S}\text{-H}_2\text{S}$ as well as the ratio of labelled to unlabeled H_2S in dynamic chamber incubation when adding cysteine, a 1:1 mixture of S-methyl methionine and methionine, and a 1:1 mixture of syringic acid and trimethoxybenzoic acid to $\text{Na}_2^{34}\text{SO}_4$ -labelled soil. Each manipulation was done on one soil. Each data point is the mean \pm 95% CI of 5 scans.

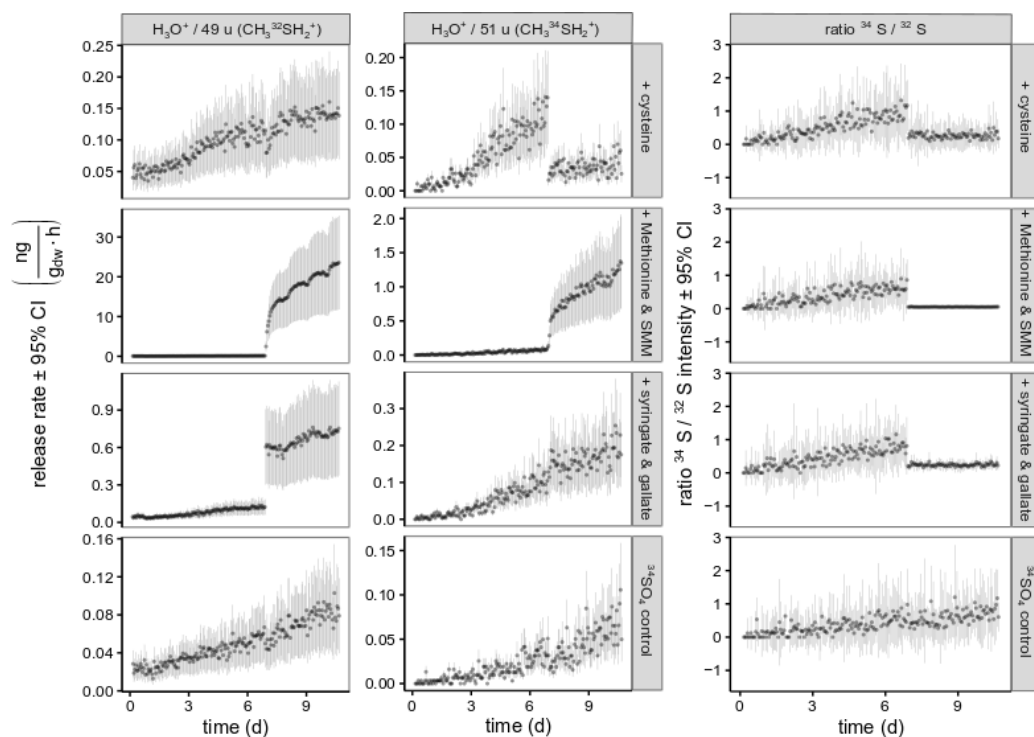


Figure S 15. Emissions of ^{32}S -MeSH and ^{34}S -MeSH as well as the ratio of labelled to unlabeled MeSH in dynamic chamber incubation when adding cysteine, a 1:1 mixture of S-methyl methionine and methionine, and a 1:1 mixture of syringic acid and trimethoxybenzoic acid to $\text{Na}_2^{34}\text{SO}_4$ -labelled soil. Each manipulation was done on one soil. Each data point is the mean \pm 95% CI of 5 scans.

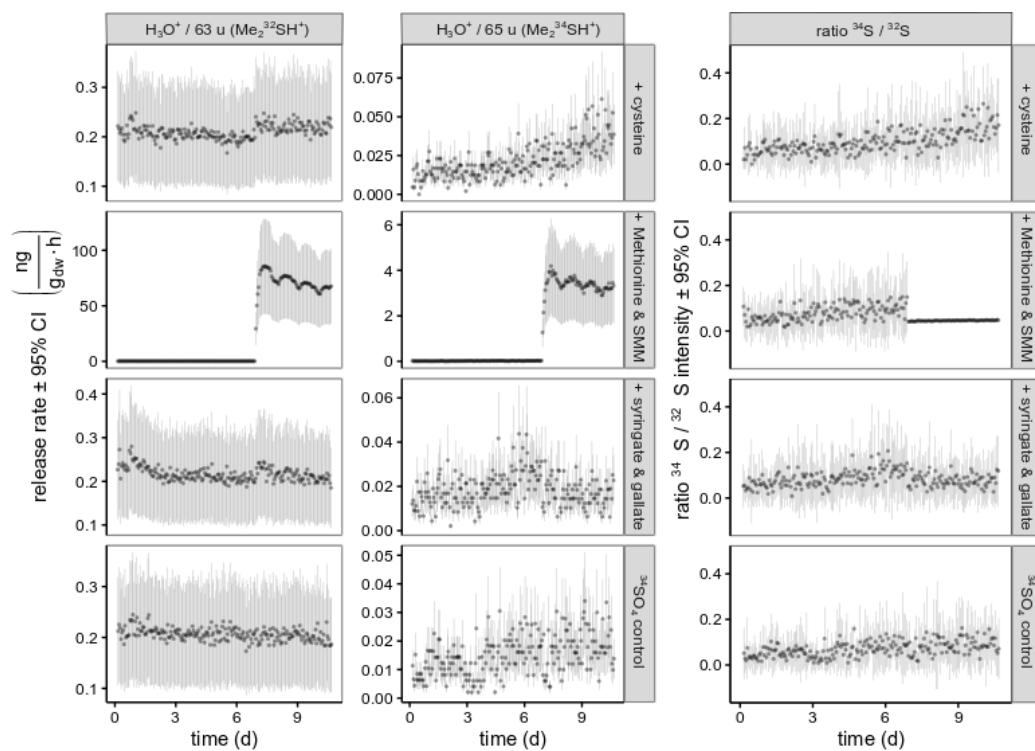


Figure S 16. Emissions of Me_2^{32}S and Me_2^{34}S as well as the ratio of labelled to unlabelled Me_2S in dynamic chamber incubation when adding cysteine, a 1:1 mixture of S-methyl methionine and methionine, and a 1:1 mixture of syringic acid and trimethoxybenzoic acid to $\text{Na}_2^{34}\text{SO}_4$ -labelled soil. Each manipulation was done on one soil. Each data point is the mean \pm 95% CI of 5 scans.

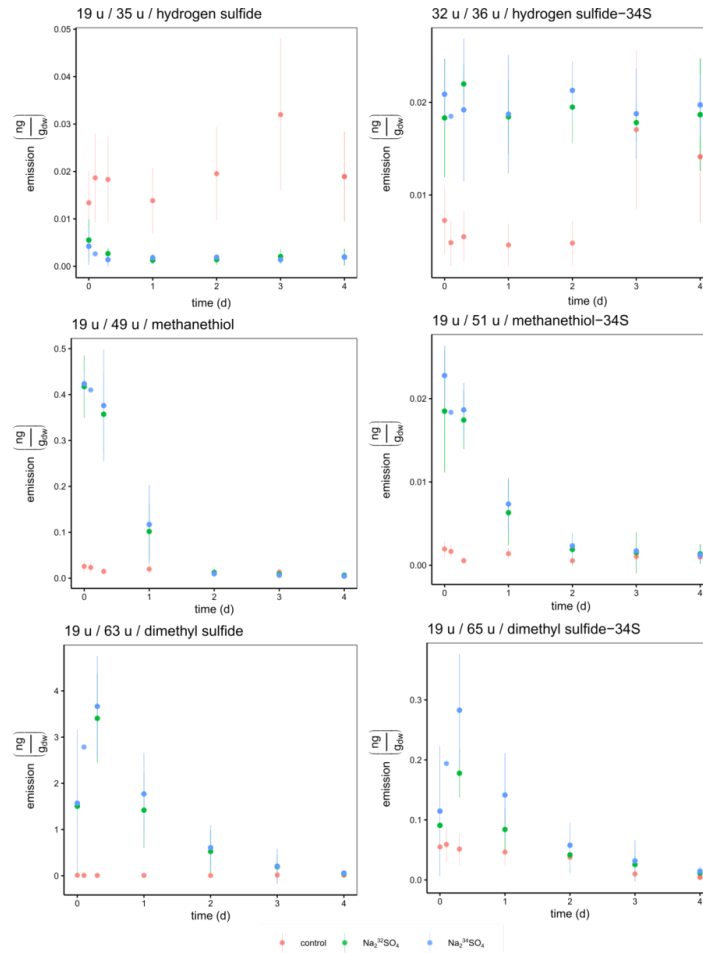


Figure S 17. VSC emission upon incubation of the $\text{Na}_2^{34}\text{SO}_4$ -labelled soils (from the dynamic labelling experiment) in closed chambers vs. an empty bottle as control. $N_{\text{soil}} = 3$ for the labelled soils, mean \pm 95% CI. The control was just one chamber, here the error bars are the 95% CI of the 5 technical replicates of each measurement.

SUBSTANCE MANIPULATION

Table S 8. Maximum VSC emissions upon addition of sulfur-substances and inhibitors. A) headspace concentrations relative to the utilized soil dry weight when incubating in closed chambers. $n_{\text{soil}} = 3$, $n_{\text{tech}} = 4$ B) release rates of the VSCs as determined in continuously-flushed dynamic chambers, normalized to the dry weight of the incubated soil. $n_{\text{soil}} = 1$, $n_{\text{tech}} = 5$. Values in *italic* are unreliable since they are higher than the calibration (MeSH , Me_2S , COS , CS_2) or higher than 5% of the reagent ion signal (H_2S , DMSO , DMSO_2 , DMDS , H_2SO_4). *Inf* marks values higher than 20% of the reagent ion signal, where quantification is just not possible anymore. Stars mark significant difference to control: * $p < 0.05$, ** $p < 0.01$, *** $p < 0.001$.

	A) incubation in static chambers					B) incubation in dynamic chambers								
	Maximum hydrogen sulfide (H ₂ S) / (H ₂ O+ / 35u)	methanethiol (H ₃ C-S- / 49u)	dimethyl sulfide (H ₃ C-S-CH ₃ / 65u)	dimethyl sulfoxide (H ₃ C-S-CH ₃ -O / 78u)	carbonyl sulfide (O=C=S / 60u)	Maximum hydrogen sulfide (19 / 35u)	methanethiol (19 / 49u)	dimethyl sulfide (19 / 65u)	dimethyl sulfoxide (19 / 79u)	dimethyl sulfone (30 / 124u)	dimethyl disulfide (19 / 95u)	carbon disulfide (19 / 77u)	carbonyl sulfide (32 / 60u)	sulfuric acid (19 / 99u)
literature-known aminoacid precursors	0.3±0.2	90±40**	2500±200***	4±2*	3.6±8***	2±1*	80±40**	15±7***	7±3	0.3±0.1	30±20*	9±4	6±3	2±1
methionine	0.15±0.07	25±7***	200±100**	1.3±0.3**	3.0±1.0***	0.3±0.2*	1.9±0.9*	600±300***	600±300***	0.3±0.2	50±20	12±6	13±6*	3±1
cysteine	0.11±0.09	20±10*	200±200	1.18±0.06**	1.2±4**	0.3±0.1*	1.2±6*	1.6±0.8	1.8±0.9*	0.12±0.06*	3±2*	8±4*	2±1*	1.8±0.9
S-methyl methionine	0.9±0.4*	30±20*	<i>Inf</i>	1.6±0.6**	5.0±5.0*	0.2±0.1*	3.0±2.0**	9±5**	1.1±0.6**	0.08±0.04**	1.7±0.8**	2±1**	3±2	1.3±0.7*
cysteic acid	0.09±0.08	1.1±0.3**	1.3±6	1±0.1**	0.4±0.1*	0.6±0.3	0.19±0.09**	0.3±0.1*	0.11±0.05**	0.06±0.03**	0.3±0.2**	0.9±0.4**	0.7±0.4**	1.1±0.5*
taurine	1±3	0.5±0.2**	3±2**	0.8±0.2**	0.5±0.2*									
potential precursors from metabolomics experiment	0.04±0.04	0.9±0.3**	4±1**	0.8±0.1**	10±5**	1.4±0.7*	3±2	1.5±0.7	0.09±0.05**	0.08±0.04**	0.7±0.4**	7±4*	6±3	1.5±0.7*
sulfosuccinate	0±1	0.9±0.3**	7±6	0.6±0.1**	0.4±0.2	20±10**	10±5	200±100**	20±10*	0.13±0.07*	30±20	600±300**	30±10**	1.7±0.9
3-(methylthio)-	0.26±0.06	3±3*	140±20***	0.89±0.09**	7±2***									

precursors with methylthio and dimethylsulfonio groups	propionic acid	15±4***	1.9±0.3***	2000±400***	0.8±0.1**	30±10**	20±10**	0.5±0.2**	40±20**	0.2±0.1**	0.03±0.02**	0.5±0.2**	3±1**	0.13±0.06**	0.7±0.4*
	gonyol dimethylsulfonio acetate														
literature-known sulfate reduction	sodium sulfate	0.014±0.002	0.7±0.1***	4±1**	0.74±0.06**	0.52±0.02**	1.5±0.7*	1.1±0.6**	1.8±0.9	0.1±0.05**	0.06±0.03**	0.4±0.2**	2±1**	7±4	1.2±0.6*
	sodium sulfide	0.8±0.6	3±2**	16±6	0.74±0.06**	3±2*	6±3	6±3	1.5±0.7	20±10**	0.8±0.4*	50±20	15±7	3±1	3±1
	sodium metholate	0.11±0.02	200±200*	130±50**	4±3*	3.5±0.4***									
	Me ₂ S	130±90*	<i>Inf</i>	<i>Inf</i>	<i>Inf</i>	<i>Inf</i>									
	DMSO	1±2	26±7***	<i>Inf</i>	10±40	2.7±0.5***									
	coenzyme M	1±0.1*	3±3*	7±2*	0.81±0.04**	0.8±0.5*									
precursors and intermediates	syringic acid	0.05±0.06	0.52±0.1***	30±20*	0.8±0.07**	0.8±0.3**	2±1*	5±2	0.2±0.1**	0.09±0.04***	0.02±0.01**	0.2±0.1**	1.8±0.9**	0.4±0.2**	1.1±0.6*
	1,3,5-trimethoxybenzoic acid	0.04±0.07	0.5±0.4*	13±5	0.72±0.07**	3±2*	0.4±0.2*	1.3±0.7**	0.4±0.2*	0.07±0.03**	0.14±0.07*	0.6±0.3**	2±1**	1.6±0.8*	1.1±0.6*
antibiotics and inhibitors control	bromoethanesulfonate	1±1	0.2±0.1	21±4**	12±3*	0.4±0.2	0.7±0.4	6±3	1.1±0.6	5±2	0.4±0.2	60±50	15±7	4±2	3±1
	chloroamphenicol	0.02±0.02	0.5±0.7	60±20**	50±30**	0.43±0.04*									
	chloroform	0.1±0.1	0.4±0.2*	24±4***	17±6*	0.9±1									
	gluturaldehyde	0.05±0.008	0.5±0.4*	200±200*	110±10***	1.1±0.5**									
	tungstate control	0.017±0.007	0.22±0.08	30±8**	26±9**	0.31±0.05									
control	0.3±0.6	0.17±0.06	11±4	8±3	0.29±0.09										

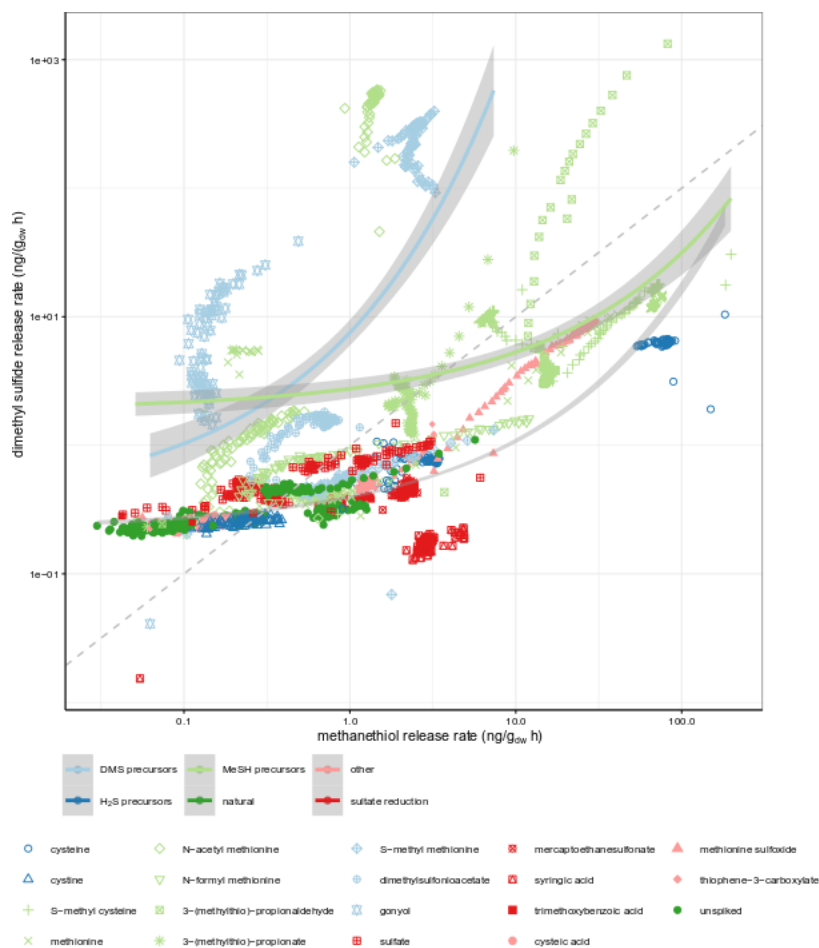


Figure S 18. Relation of Me₂S and MeSH release rates when spiking with precursor substances (colored by substance class) in a dynamic chamber incubation. Every point is a measurement in time. Grey dashed line: 1:1 line. Regression curves done for Me₂S precursors (light blue), MeSH precursors (light green) and all other incubations (gray):

$$DMS\ release = A \cdot exp(MeSH\ release) + B, \text{ mean } \pm 95\% \text{ CI.}$$

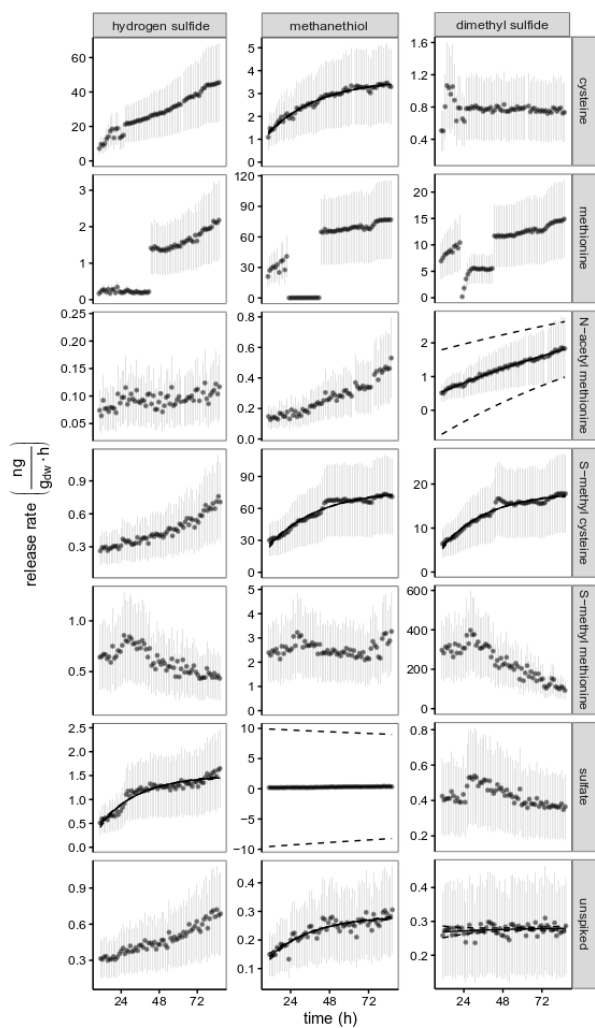


Figure S 19. VSC release rates during dynamic chamber incubation with different VSC precursors (amino acids and derivatives). $n_{\text{tech}} = 10$ per data point, mean \pm 95% CI.

Wherever possible, applied exponential fit $\Phi = a \cdot \exp\left(-\frac{t}{b}\right) + c$, solid lines: fit, dashed

lines:

95%

CI.

2

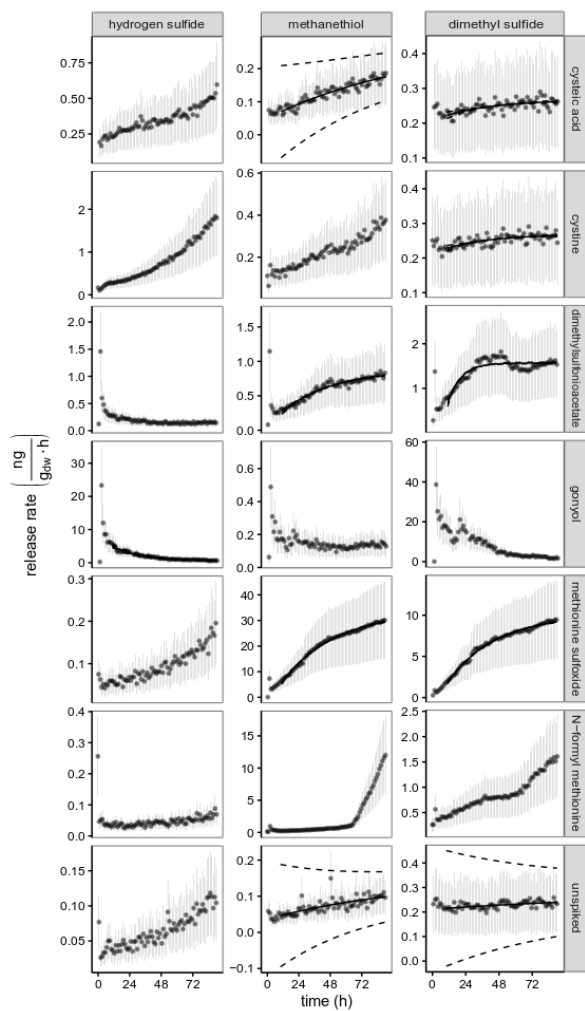


Figure S 20. VSC release rates during dynamic chamber incubation with different VSC precursors (amino acids and derivatives). $n_{\text{tech}} = 10$ per data point, mean \pm 95% CI. Wherever possible, applied exponential fit $\Phi = a \cdot \exp\left(-\frac{t}{b}\right) + c$, solid lines: fit, dashed lines: 95% CI.

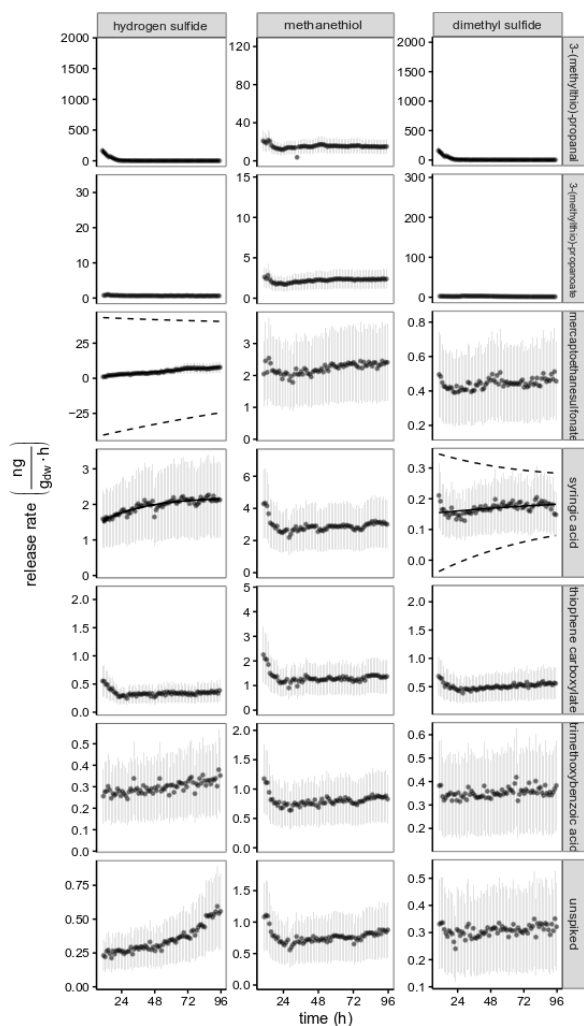


Figure S 21. VSC release rates during dynamic chamber incubation with different VSC precursors. $n_{\text{tech}} = 10$ per data point, mean \pm 95% CI. Wherever possible, applied exponential fit $\Phi = a \cdot \exp\left(-\frac{t}{b}\right) + c$, solid lines: fit, dashed lines: 95% CI.

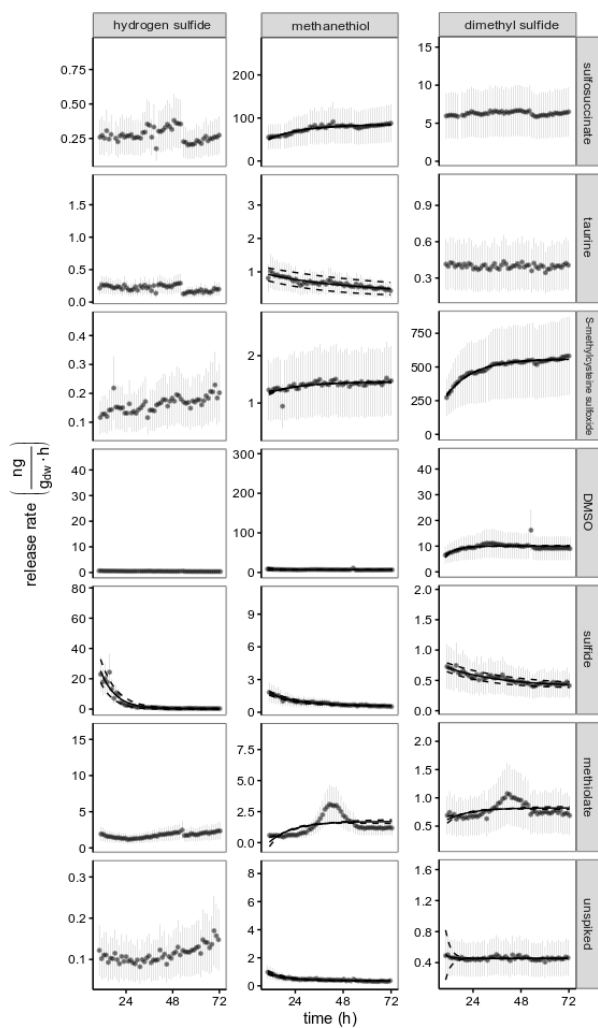


Figure S 22. VSC release rates during dynamic chamber incubation with different VSC precursors. $n_{\text{tech}} = 10$ per data point, mean \pm 95% CI. Wherever possible, applied exponential fit $\Phi = a \cdot \exp\left(-\frac{t}{b}\right) + c$, solid lines: fit, dashed lines: 95% CI.

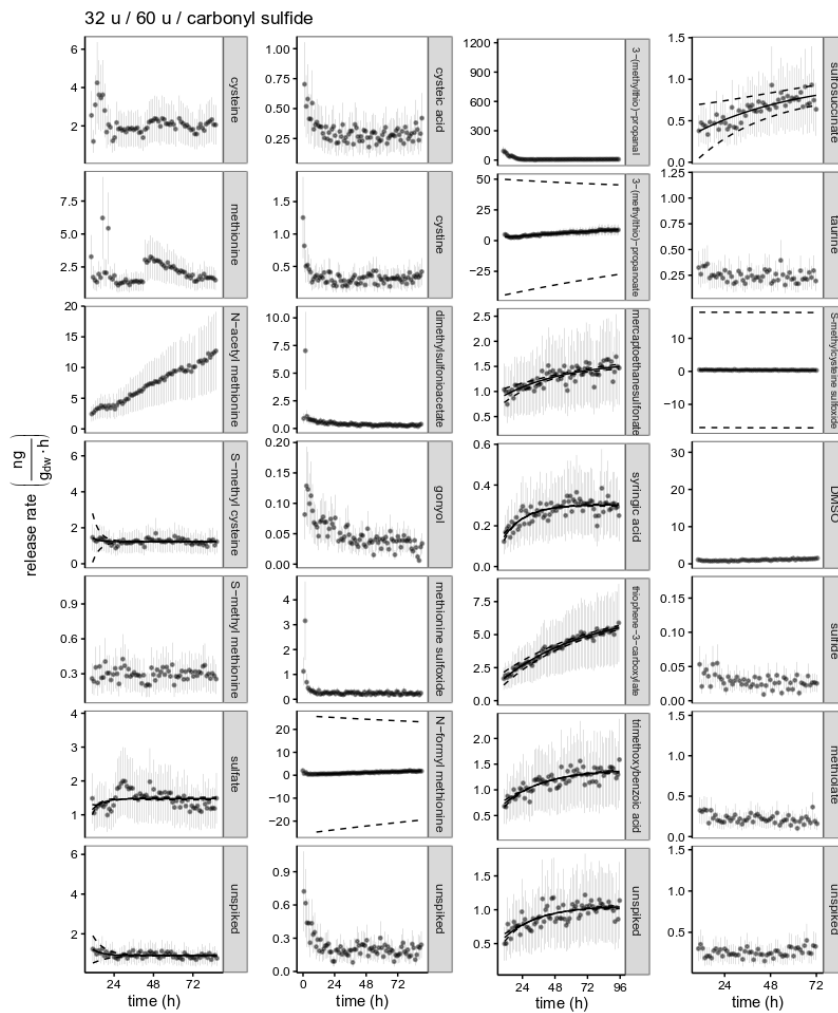


Figure S 23. VSC release rates during dynamic chamber incubation with different VSC precursors. $n_{\text{tech}} = 10$ per data point, mean \pm 95% CI. Wherever possible, applied exponential fit $\Phi = a \cdot \exp\left(-\frac{t}{b}\right) + c$, solid lines: fit, dashed lines: 95% CI.

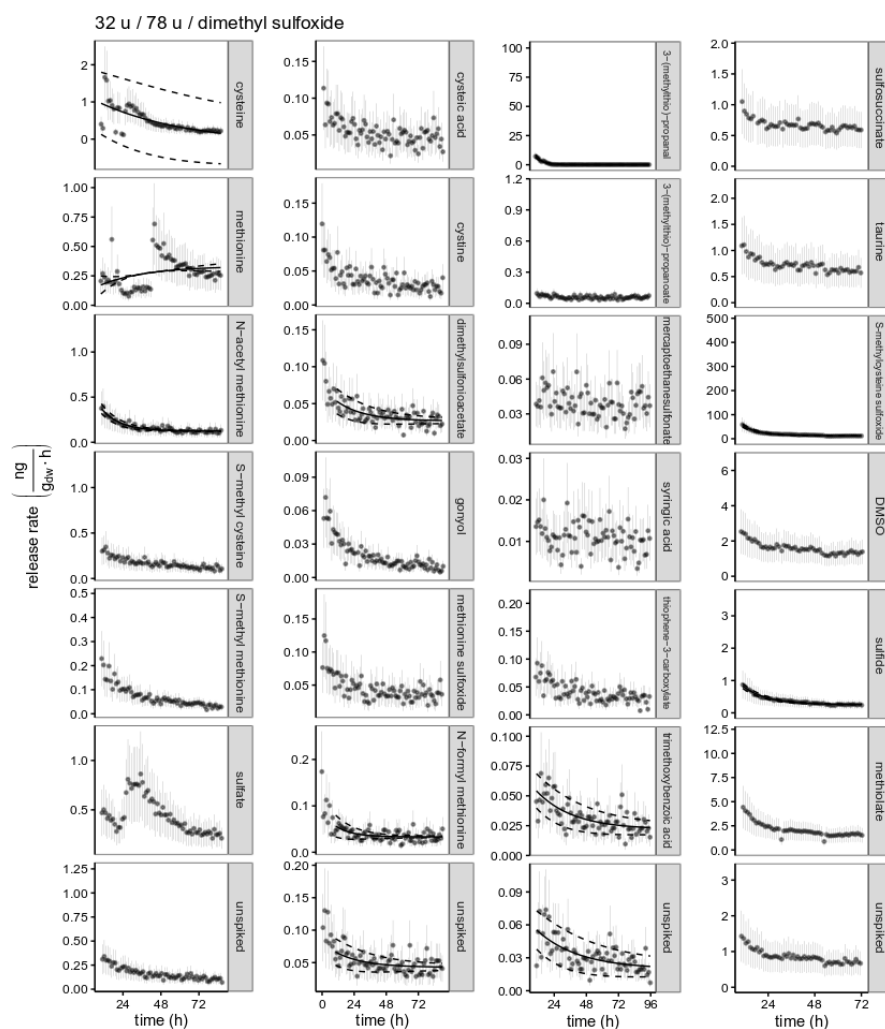


Figure S 24. DMSO release rates during dynamic chamber incubation with different VSC precursors. $n_{\text{tech}} = 10$ per data point, mean \pm 95% CI. Wherever possible, applied exponential fit $\Phi = a \cdot \exp\left(-\frac{t}{b}\right) + c$, solid lines: fit, dashed lines: 95% CI.

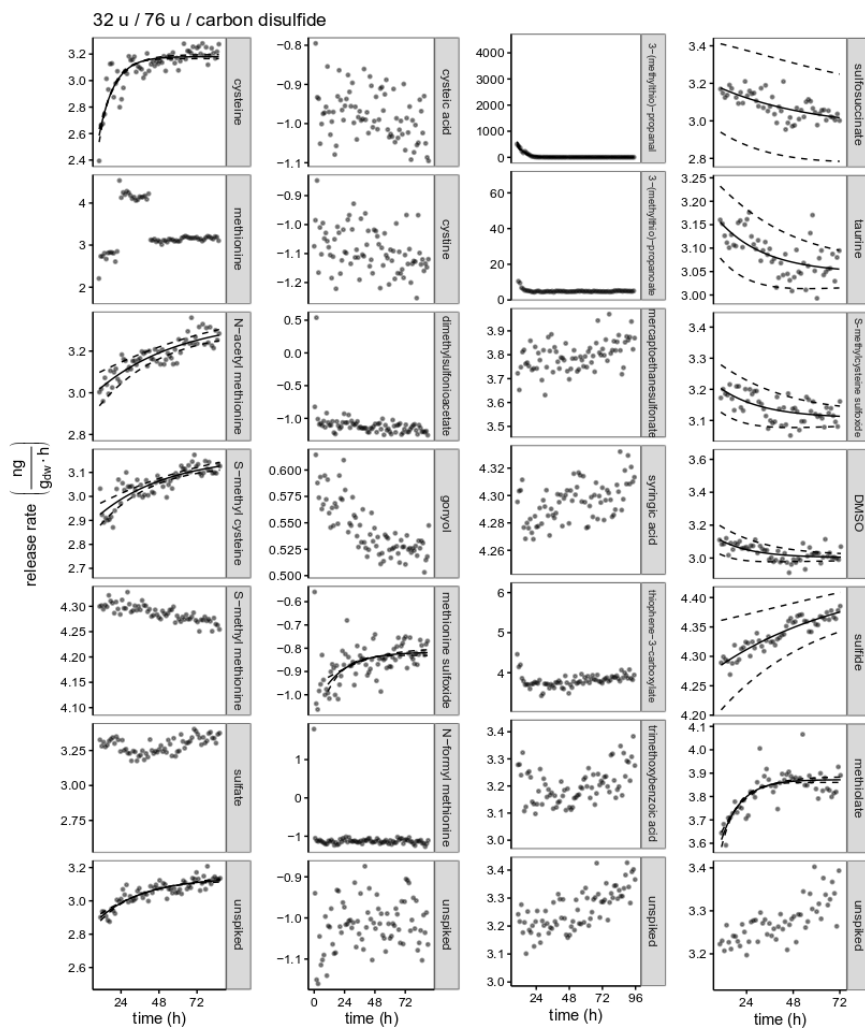


Figure S 25. CS₂ release rates during dynamic chamber incubation with different VSC precursors. ntech = 10 per data point, mean ± 95% CI. Wherever possible, applied exponential fit $\Phi = a \cdot \exp\left(-\frac{t}{b}\right) + c$, solid lines: fit, dashed lines: 95% CI.

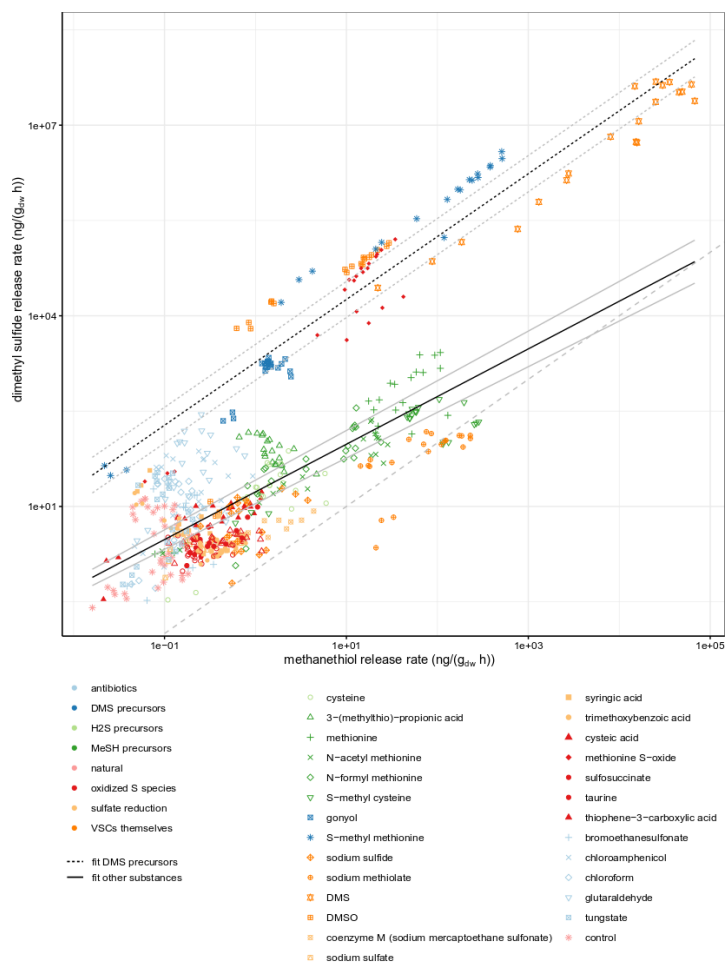


Figure S 26. Relation of Me₂S and MeSH release rates when spiking with precursor substances (colored by substance class) in a dynamic chamber incubation. Every point is a measurement in time. Separate regression curves for Me₂S precursors (dotted lines, mean ±95% CI) and other substances that do not contain dimethyl sulfonio groups (solid lines, mean ±95% CI). Grey dashed line: 1:1 line.

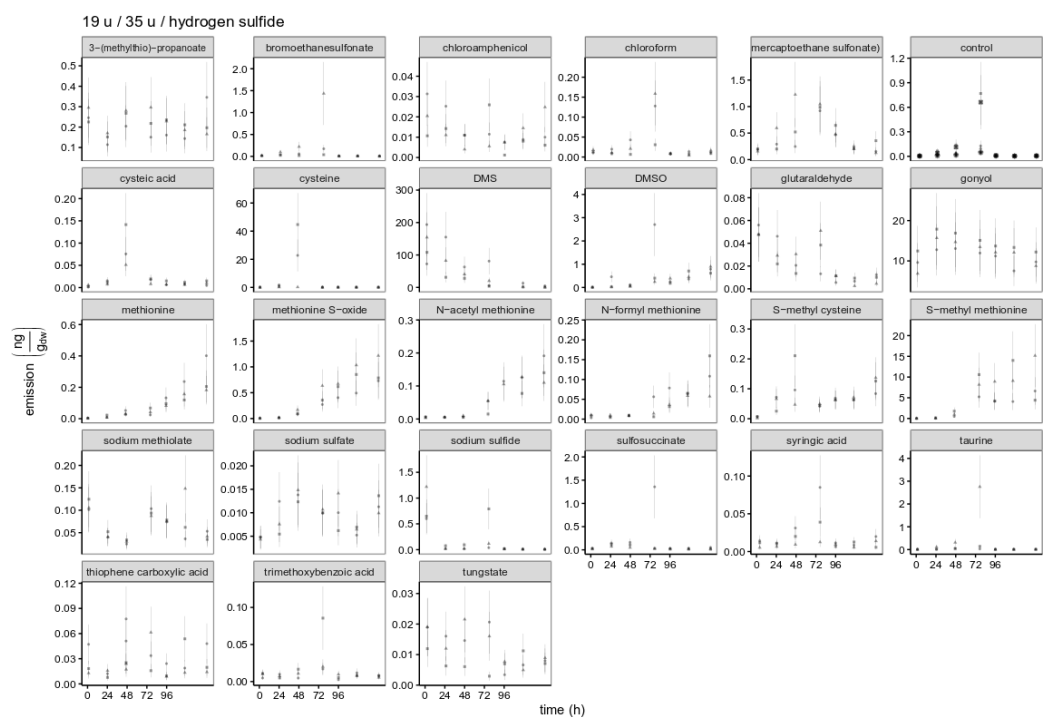


Figure S 27. H₂S emissions when spiking with different VSC precursor compounds in static chambers. $n_{\text{soil}} = 3$ (6 for control), $n_{\text{tech}} = 5$. Mean \pm 95% CI. The different shapes mark the 3 (6) different soil replicates.

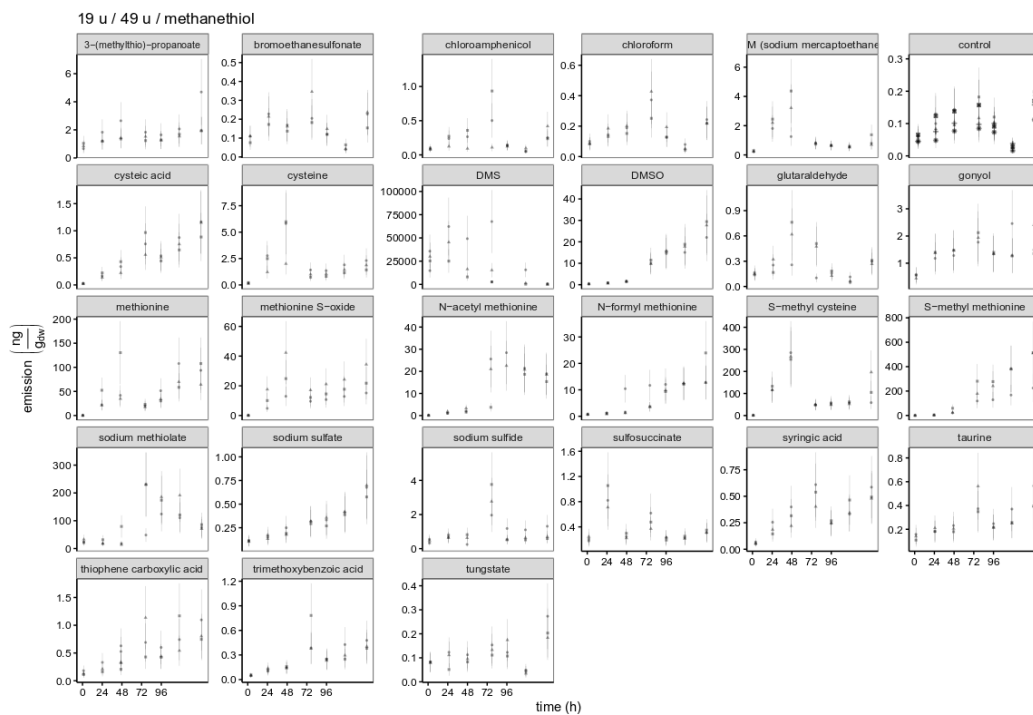


Figure S 28. MeSH emissions when spiking with different VSC precursor compounds in static chambers. $n_{\text{soil}} = 3$ (6 for control), $n_{\text{tech}} = 5$. Mean \pm 95% CI. The different shapes mark the 3 (6) different soil replicates.

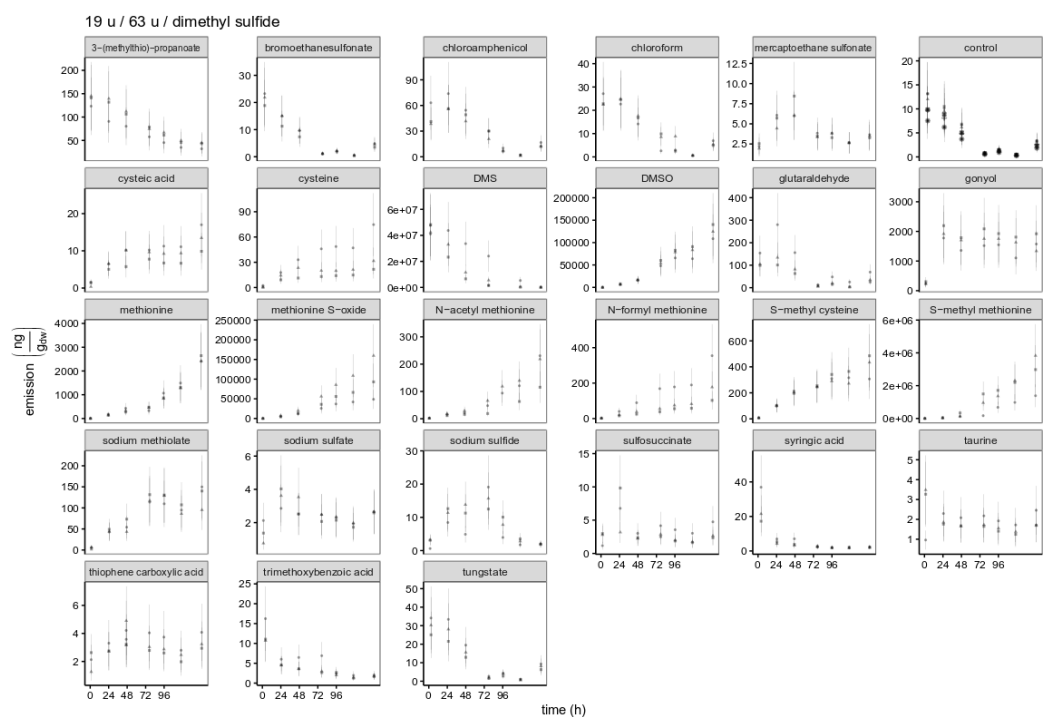


Figure S 29. Me₂S emissions when spiking with different VSC precursor compounds in static chambers. $n_{\text{soil}} = 3$ (6 for control), $n_{\text{tech}} = 5$. Mean \pm 95% CI. The different shapes mark the 3 (6) different soil replicates.

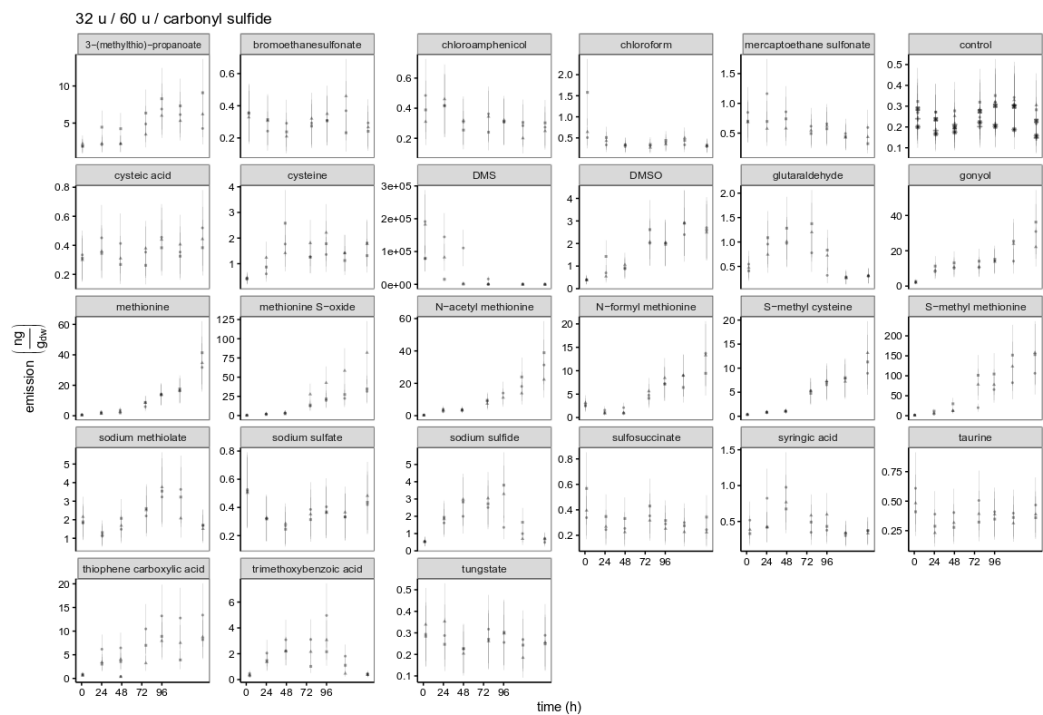


Figure S 30. COS emissions when spiking with different VSC precursor compounds in static chambers. $n_{\text{soil}} = 3$ (6 for control), $n_{\text{tech}} = 5$. Mean \pm 95% CI. The different shapes mark the 3 (6) different soil replicates.

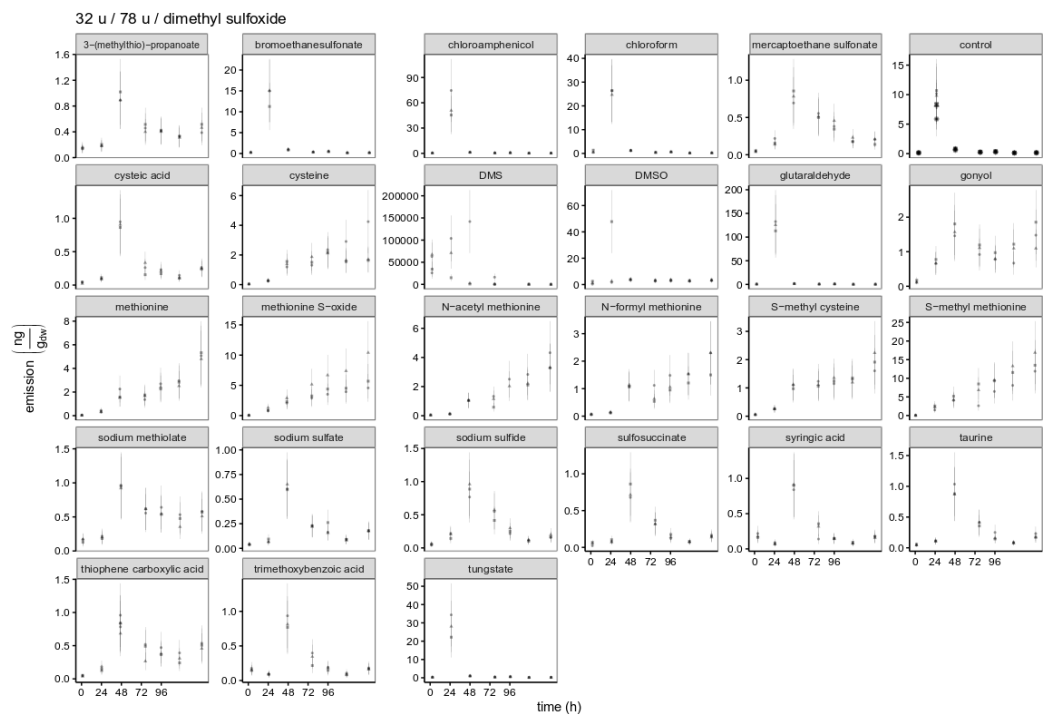


Figure S 31. DMSO emissions when spiking with different VSC precursor compounds in static chambers. $n_{\text{soil}} = 3$ (6 for control), $n_{\text{tech}} = 5$. Mean \pm 95% CI. The different shapes mark the 3 (6) different soil replicates.

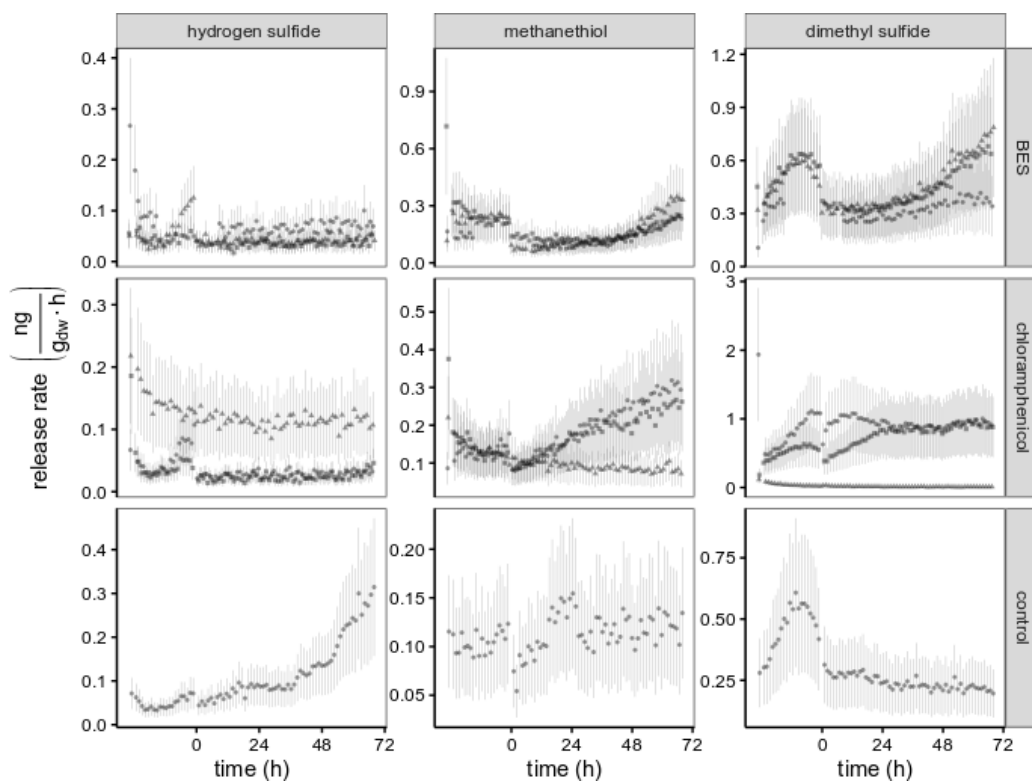


Figure S 32. VSC emissions upon incubation with antibiotics in dynamic chambers. Mean \pm 95% CI, $n_{\text{tech}} = 10$, $n_{\text{soil}} = 3$ for the treatments (different shapes), 1 for the untreated control.

LONG-TERM INCUBATION AND METABOLOMICS

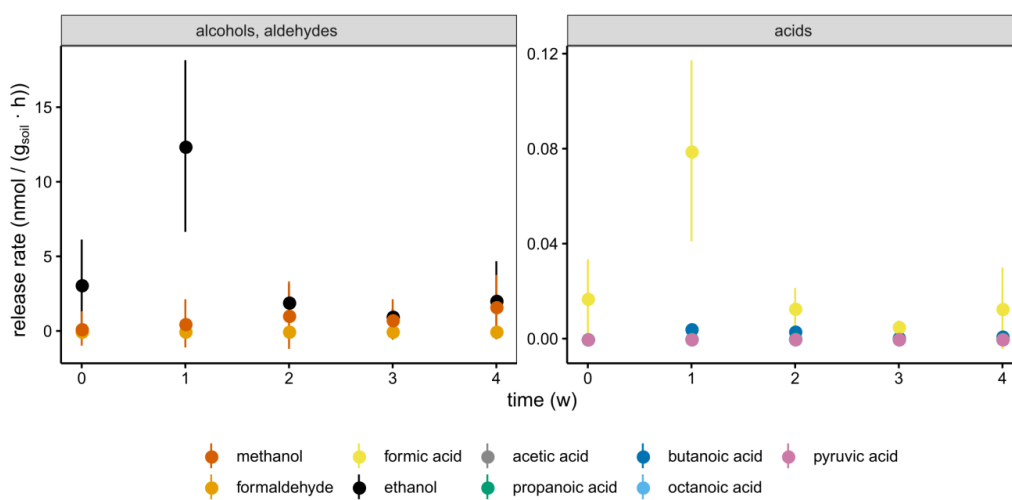


Figure S 33. Release rates of VOCs related to general metabolism in long-term incubation over 4 weeks. $n_{\text{soil}} = 5$ per time point. Mean $\pm 95\%$ CI.

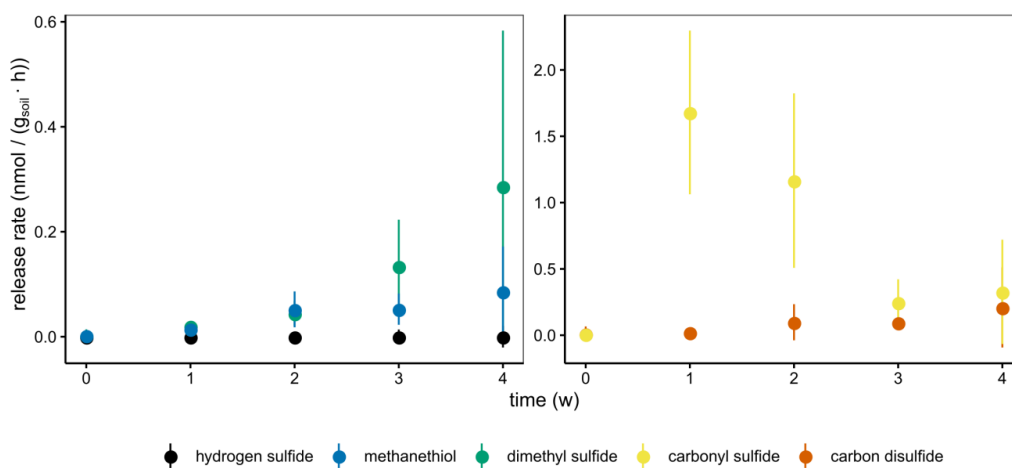


Figure S 34. Release rates of the different volatile sulfur compounds in long-term incubation over 4 weeks. $N_{\text{soil}} = 5$ per time point. Mean \pm 95% CI.

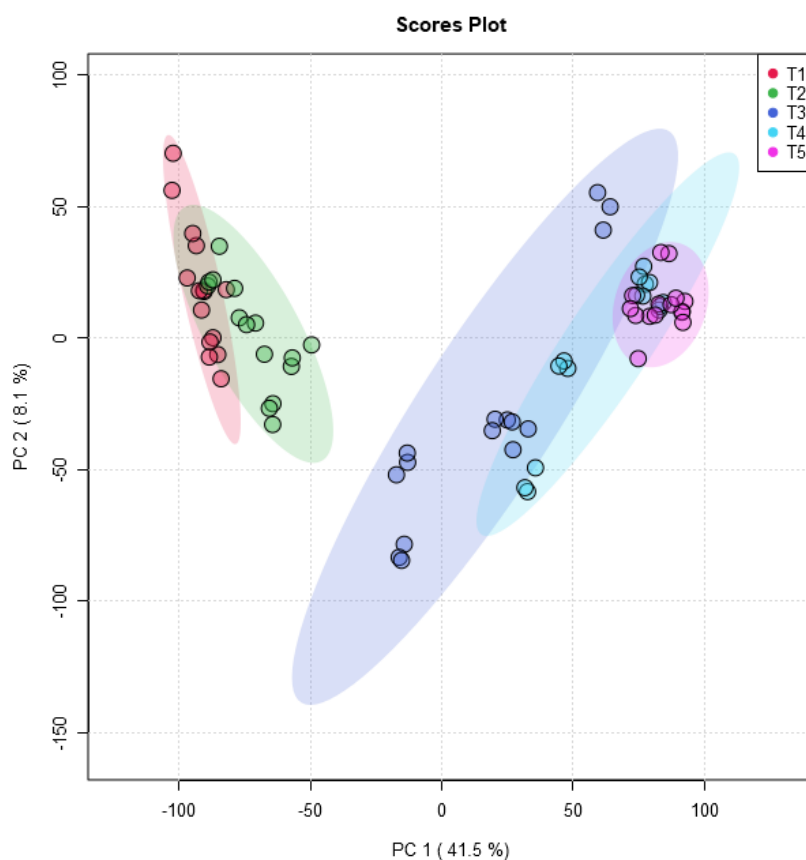


Figure S 35. Principle Component Analysis Scores plot of the organic matter extracts measured with UHPLS-Orbitrap-MS in negative polarity. Obtained from MetaboanalystR after log-transformation and Pareto-Scaling of the data. The five replicates analyzed each week were measured three times each ($n = 15$). The ellipses represent the 95% confidence interval of each time point.

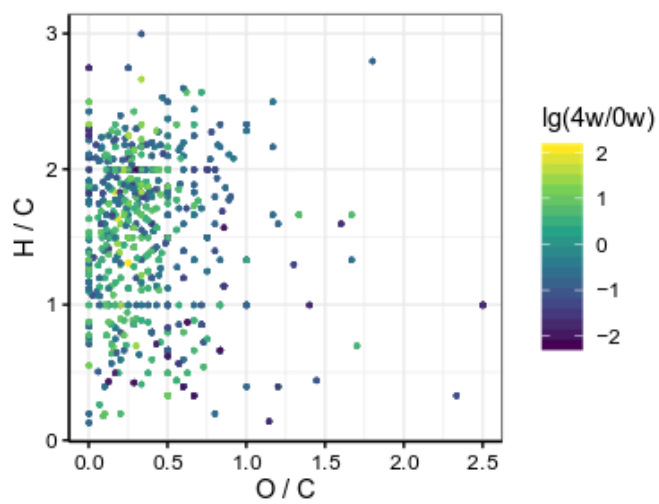


Figure S 36. Van Krevelen Diagram of significantly changing substances, as detected via UHPLC-MS in positive polarity. Substances are filtered to be at least 3x up-/downregulated.

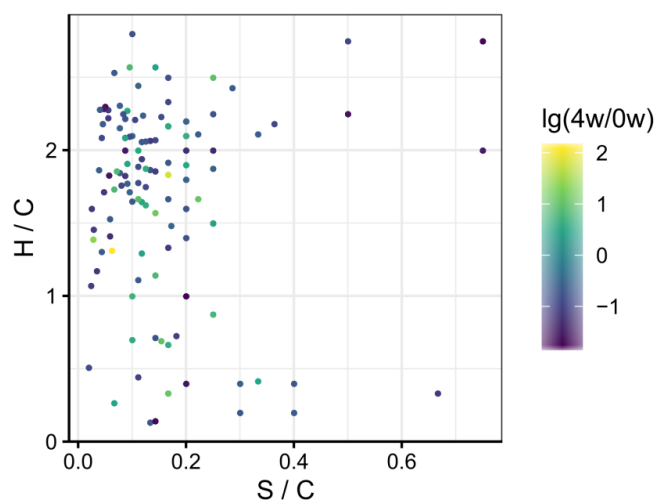


Figure S 37. Modified Van Krevelen Diagram (with S/C ratio) of significantly changing substances, as detected via UHPLC-MS in positive polarity. Substances are filtered to be at least 3x up-/downregulated.

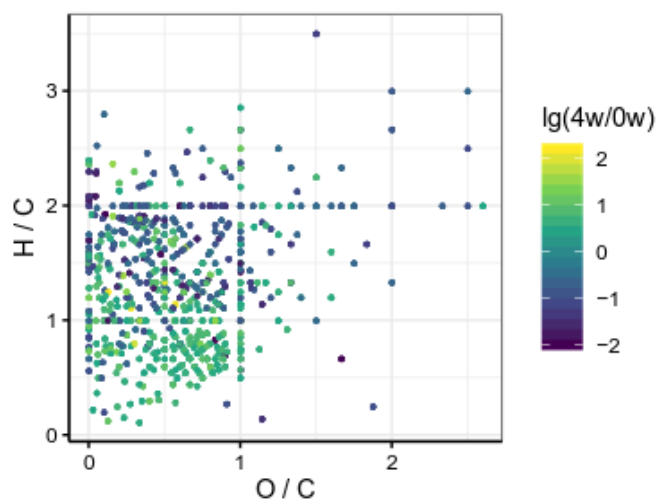


Figure S 38. Van Krevelen Diagram of significantly changing substances, as detected via UHPLC-MS in negative polarity. Substances are filtered to be at least 3x up/downregulated.

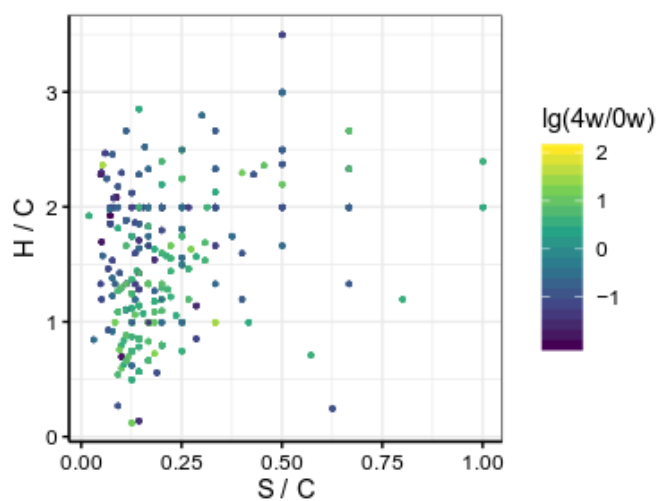


Figure S 39. Modified Van Krevelen Diagram (with S/C ratio) of significantly changing substances, as detected via UHPLC-MS in negative polarity. Substances are filtered to be at least 3x up-/downregulated.

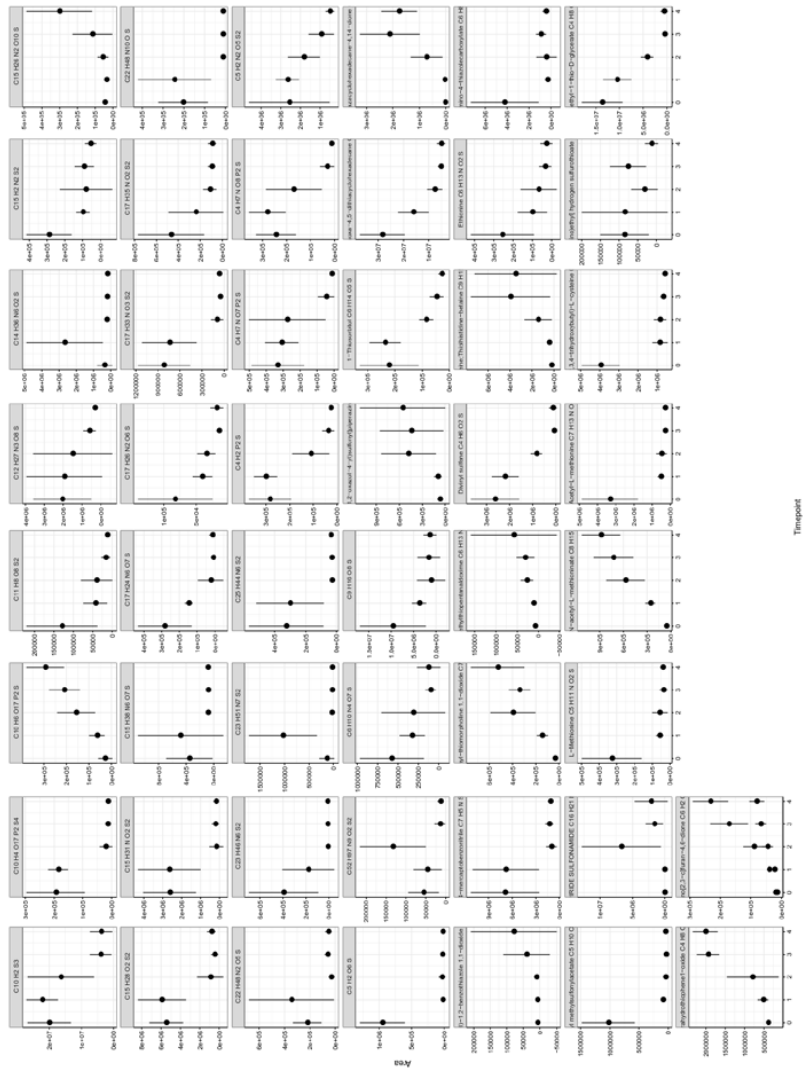


Figure S 40. Time course of significantly dysregulated Sulfur compounds, as detected with UPLC-MS in positive polarity.

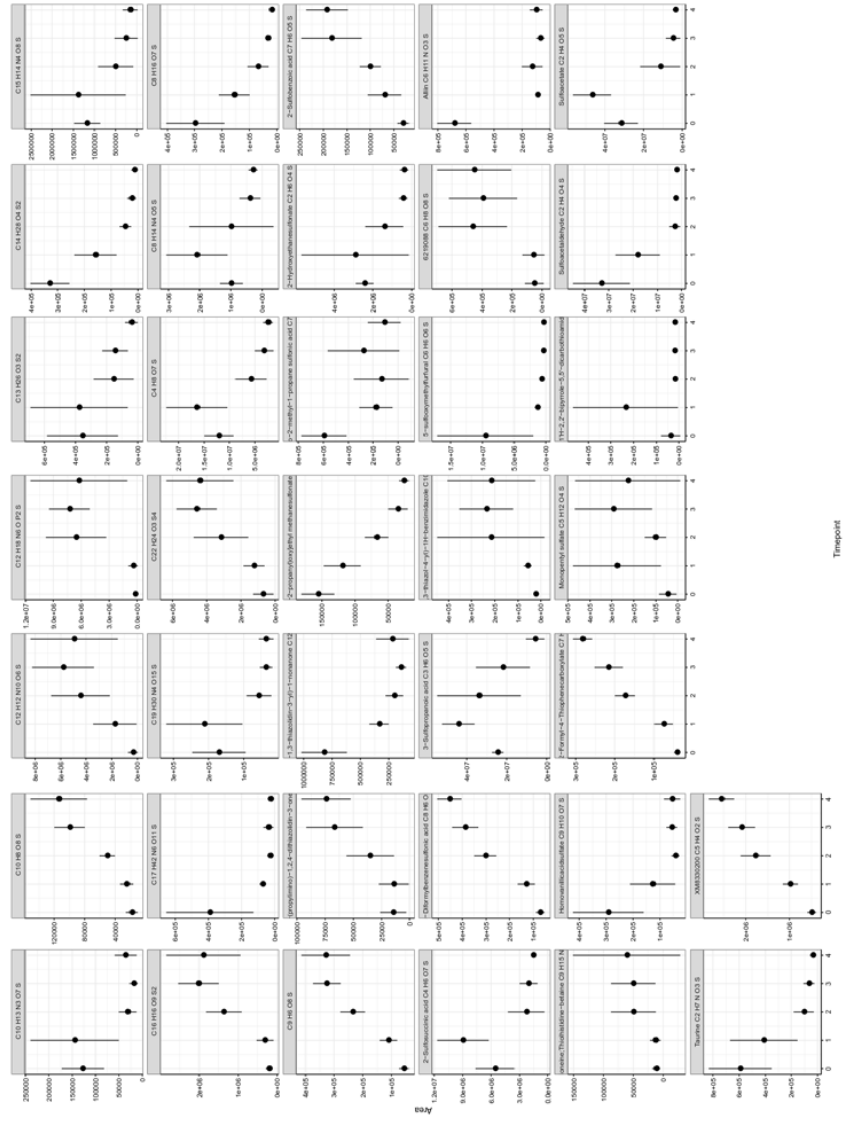


Figure S 41. Time course of significantly dysregulated Sulfur compounds, as detected with UPLC-MS in positive polarity.

Table S 9. Significantly dysregulated putative sulfur compound features as determined with UHPLC-MS in positive polarity. Features were considered significant if VIP > 1 (VIPscore of the PLS regression over time, as calculated by Metaboanalyst, after log-transformation and Pareto-scaling of the data), the change in control sample intensity was maximum 5 x, and the mean sample intensity change was at least 5-fold, and the sample intensity was at least two times the control intensity. Names and sum formulas are putative as suggested from Compound Discoverer unless an MS² spectrum could be obtained. Many features had a very small intensity or other peaks close-by, so that no MS² spectrum could be measured.

Formula	m/z (u)	rt (min)	log₂(4w/0w)	Putative	MS²	Coinjection	Name
C ₄ H ₈ OS	105.0371	1.4	2.37	x			tetrahydrothiophene 1-oxide
C ₄ H ₆ O ₂ S	119.0163	1.4	-4.43	x			Divinyl sulfone
C ₇ H ₅ NS	136.0217	9.3	-2.59	x			4-mercaptobenzonitrile
C ₄ H ₈ O ₃ S	137.0269	1.4	-4.55	x			S-Methyl-1-thio-D-glycerate
C ₄ H ₂ P ₂ S	144.9429	0.9	-3.42	x			5-
C ₆ H ₁₃ NOS	148.0792	8.2	2.84	x			methylthiopentanaloxime
C ₅ H ₁₁ NO ₂ S	150.0587	7.8	-3.05	x			L-Methionine
C ₆ H ₂ O ₃ S	154.98	7.7	3.64	x			Thieno[2,3-c]furan-4,6-dione
C ₆ H ₂ O ₃ S	154.98	7.5	2.53	x			Thieno[2,3-c]furan-4,6-

$C_6H_{13}NO_2S$	164.0742	0.9	-3.26	x				dione
								Ethionine
								Ethyl
$C_5H_{10}O_4S$	167.0376	1.4	-4.41	x				methylsulfonylacetate
								Ethyl 2-amino-4-
$C_6H_8N_2O_2S$	173.0448	1.4	-3.24	x				thiazolecarboxylate
								4-Prop-2-ynyl-
$C_7H_{11}NO_2S$	174.0587	6.6	3.88	x				thiomorpholine 1,1-dioxide
$C_5H_2O_6S$	190.9643	1.5	-5.28	x				
$C_7H_{13}NO_3S$	192.0694	7.8	-3.58	x	x	x		N-Acetyl-L-methionine
$C_6H_{14}O_5S$	199.0605	1.1	-2.98	x				1-Thiosorbitol
$C_9H_{15}NO_3P_2S_5$	204.4635	0.8	3.98	x				
								Methyl N-acetyl-L-
$C_8H_{15}NO_3S$	206.0851	8.1	3.47	x				methioninate
$C_{10}H_2S_3$	218.9396	0.8	-2.38	x				
$C_9H_{15}N_3O_2S$	230.0962	1.1	4	x	x			Ergothioneine
$C_5H_2N_2O_5S_2$	234.9475	1.1	-2.35	x				
								1-[(3,5-Dimethyl-1,2-
								oxazol-4-
$C_9H_{15}N_3O_3S$	246.0907	1.2	2.96	x				yl)sulfonyl]piperazine
								N-Acetyl-S-(2,3,4-
								trihydroxybutyl)-L-
$C_9H_{17}NO_6S$	268.0852	1.1	-2.69	x				cysteine
								1,8,11,14-Tetraoxa-4,5-
$C_{10}H_{20}O_4S_2$	269.0869	1.1	-2.46	x				dithiacyclohexadecane
$C_{15}H_2N_2S_2$	274.9728	1.5	-2.37	x				
$C_4H_7NO_7P_2S$	275.9504	0.9	-4.69	x				
								3-(Phenylsulfanyl)-1,2-
$C_{13}H_9NO_2S_2$	276.0152	9.3	3.39	x				benzothiazole 1,1-dioxide

C ₉ H ₁₆ O ₈ S	285.0586	1.2	-2.81	x		
C ₄ H ₇ NO ₈ P ₂ S	291.9626	0.9	-4.22	x		
Formula	m/z (u)	rt (min)	log₂(4w/0w)	Putative	MS²	Coinjection Name
C ₁₃ H ₂₉ NO ₃ S ₂	312.166	8.0	-2.68	x		S-[2-(Undecylamino)ethyl] hydrogen sulfurothioate
C ₁₅ H ₂₈ O ₂ S ₂	322.1864	8.9	-3.81	x	(x)	
C ₁₁ H ₈ O ₈ S ₂	332.9572	0.9	-3.4	x		
C ₁₇ H ₃₅ NO ₂ S ₂	350.2176	8.4	-2.33	x		?, from MS ² maybe β-lactam. CD suggests
C ₁₆ H ₂₁ N ₃ O ₄ S	352.1329	7.0	6.92	x	x	glimepiridine sulfoneamide
C ₁₄ H ₃₆ N ₆ O ₂ S	353.2694	10.0	-0.87	x		
C ₁₇ H ₃₃ NO ₃ S ₂	364.1971	9.1	-3.61	x		
C ₁₂ H ₂₇ N ₃ O ₈ S	374.1592	1.0	-2.62	x		
C ₁₇ H ₂₆ N ₂ O ₆ S	387.1566	8.1	-2.16	x		
C ₁₅ H ₂₆ N ₂ O ₁₀ S	427.1364	1.0	2.76	x		
C ₁₅ H ₃₈ N ₆ O ₇ S	447.2593	9.5	-2.08	x		
C ₂₂ H ₄₈ N ₂ O ₅ S	453.3368	9.5	-2.04	x		
C ₁₇ H ₂₄ N ₆ O ₇ S	457.1506	6.7	-4.33	x		
C ₂₃ H ₄₆ N ₆ S ₂	471.3322	9.1	-5.12	x		
C ₂₅ H ₄₄ N ₆ S ₂	493.3139	9.9	-3.15	x	x	
C ₂₂ H ₄₈ N ₁₀ OS	501.379	10.0	-4.08	x		
C ₁₀ H ₆ O ₁₇ P ₂ S	984.7681	0.9	-2.02	x		

Table S 10. Significantly dysregulated putative sulfur compound features as determined with UHPLC-MS in negative polarity. Features were considered significant if $VIP > 1$ (VIPscore of the PLS regression over time, as calculated by Metaboanalyst, after log-transformation and Pareto-scaling of the data), the change in control sample intensity was maximum 5 x, and the mean sample intensity change was at least 5-fold, and the sample intensity was at least two times the control intensity. Names and sum formulas are putative as suggested from Compound Discoverer unless an MS2 spectrum could be obtained. Many features had a very small intensity or other peaks close-by, so that no MS2 spectrum could be measured.

Formula	<i>m/z</i> (u)	rt (min)	$\log_2(4w/0w)$	Putative	MS ²	Coinjection	Name
C ₂ H ₄ O ₄ S	122.9758	1.0	-4.02	x	x		Sulfoacetaldehyde
C ₂ H ₇ NO ₃ S	124.0074	1.1	-4.05	x	x	x	Taurine
C ₂ H ₆ O ₄ S	124.9914	1.0	-2.7	x			2-Hydroxyethanesulfonate
C ₅ H ₄ O ₂ S	126.986	7.8	2.36	x	x	x	thiophene-3-carboxylate
C ₂ H ₄ O ₅ S	138.9707	1.0	-3.15	x	x		acetylsulfonic acid
C ₃ H ₆ O ₅ S	152.9865	1.1	-2.07	x	x		3-Sulfopropanoic acid
C ₅ H ₁₂ O ₄ S	167.0385	8.3	2.32	x			Monopentyl sulfate
C ₇ H ₆ O ₃ S	168.9967	7.6	2.81	x	x	x	Methyl 2-Formyl-4-Thiophenecarboxylate
C ₆ H ₁₁ NO ₃ S	176.0389	7.6	-2.8	x	x	x	N-formyl methionine
C ₇ H ₁₆ O ₄ S	195.0698	8.9	-2.6	x			2-[(2-Methyl-2-propanyl)oxy]ethyl methanesulfonate
C ₄ H ₆ O ₇ S	196.9762	1.0	-1.86	x	x	x	2-Sulfosuccinic acid
C ₄ H ₈ O ₇ S	198.9919	1.0	-2.3	x	x		3,4-dihydroxy-2-

							oxobutylsulfate
C ₇ H ₆ O ₅ S	200.9865	7.3	2.68	x			2-Sulfobenzoic acid
C ₆ H ₆ O ₆ S	204.9814	1.4	-4.71	x			5-sulfooxymethylfurfural
C ₇ H ₁₃ NO ₄ S	206.0494	1.5	-2.42	x	x		N-acetyl methionine sulfoxide
C ₈ H ₆ O ₅ S	212.9865	7.6	2.69	x			2,3-Diformylbenzenesulfonic acid
C ₈ H ₁₄ N ₂ OS ₂	217.0467	1.2	2.35	x			(5Z)-4-Propyl-5-(propylimino)-1,2,4-dithiazolidin-3-one
C ₉ H ₁₅ N ₃ O ₂ S	228.0807	1.2	2.4	x			Ergothioneine;Thiolhistidine-betaine
C ₆ H ₈ O ₈ S	238.9868	1.2	3.1	x			
C ₉ O ₆ S	245.0127	8.3	3.25	x	x		3-(3-sulfooxyphenyl)propanoate
C ₈ H ₁₆ O ₇ S	255.0547	1.3	-3.96	x			
C ₉ H ₁₀ O ₇ S	261.0074	7.5	-2.43	x	(x)		Homovanillicacidsulfate
C ₉ H ₆ O ₈ S	272.9712	7.8	2.56	x	x		2-[3-(Carboxymethyl)-5-sulfophenyl]acetic acid
C ₁₀ H ₈ O ₈ S	286.987	7.7	2.64	x			
C ₁₃ H ₂₆ O ₃ S ₂	293.1246	8.0	-3.15	x			
C ₁₀ H ₁₃ N ₃ O ₇ S	318.041	1.4	-1.84	x			
C ₁₄ H ₂₈ O ₄ S ₂	323.1354	7.9	-4.63	x			
C ₁₂ H ₁₈ N ₆ OP ₂ S	355.0678	7.7	4.92	x	(x)		acid

Formula	m/z (u)	rt (min)	log ₂ (4w/0w)	Putative	MS ²	Coinjection	Name
C ₁₅ H ₁₄ N ₄ O ₈ S	409.0455	7.2	-2.92	x	(x)		
C ₁₆ H ₁₆ O ₉ S ₂	415.0165	1.5	3.24	x	(x)		
C ₁₂ H ₁₂ N ₁₀ O ₆ S	423.0579	7.9	3.85	x			
C ₂₂ H ₂₄ O ₃ S ₄	463.0525	8.1	2.68	x			
C ₂₈ H ₄₆ N ₄ S ₂	501.3071	10.0	-1.02	x			N,N'-Dinonyl-1H,1'H-2,2'-bipyrrrole-5,5'-dicarbothioamide
C ₁₇ H ₄₂ N ₆ O ₁₁ S	537.2555	8.5	-4.03	x	(x)		

$C_{19}H_{30}N_4O_{15}S$	585.1355	1.1	-2.24	x	(x)
--------------------------	----------	-----	-------	---	-----

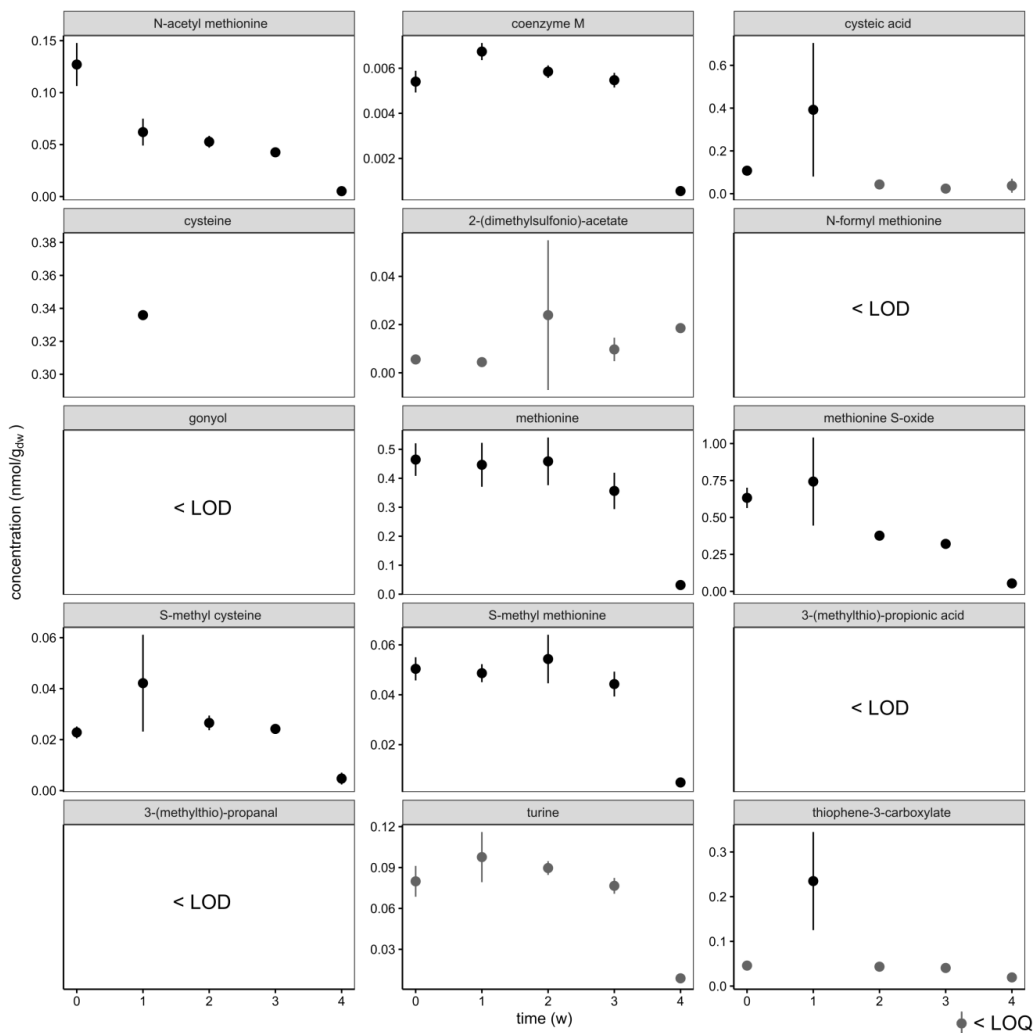


Figure S 42: Concentration of organic sulfur substances during the long-term anoxic incubation, mean \pm 95% CI ($n_{\text{soil}} = 5$, $n_{\text{tech}} = 3$, $n_{\text{ges}} = 15$). Quantified by UPLC-MS via calibration. Gray points were below the limit of quantification ($10 * \text{sd}(\text{blank concentration})$). Sample concentrations below the limit of detection were not plotted.

Table S 11: Fraction of Sulfur present as the following compounds at the different time points of the long-term incubation. The molar abundance of those compounds was normalized to the sulfur content of the soil sample (mol/mol).

time (w)	sulfate	N-acetyl methionin	Coenzyme M	Cysteic acid	Cysteine	Methionine	Methionine S-oxide	S-methyl cysteine	S-methyl methionine	Taurine	thiophene 3- carboxylate
	%	$\times 10^{-7}$	$\times 10^{-8}$	$\times 10^{-7}$	$\times 10^{-7}$	$\times 10^{-6}$	$\times 10^{-7}$	$\times 10^{-8}$	$\times 10^{-7}$	$\times 10^{-7}$	$\times 10^{-7}$
0	2.6±1.1	1.4±5.2	5.9±1.8	1.2±4.2	< LOD	5.0±1.7	69±22	2.5±7.8	5.4±1.7	8.7±3.1	5.0±1.6
1	2.5±0.9	5.5±2.2	6.0±1.4	35±36	3.0±5.4	4.0±1.4	66±40	37±25	4.3±1.1	8.7±3.3	21 ±14
2	1.8±0.8	4.6±1.5	5.1±1.4	3.8±1.7	< LOD	4.0±1.6	33±10	2.3±7.8	4.7±1.9	7.8±2.2	3.8±1.3
3	1.4±0.6	4.2 ±1.1	5.3±1.1	0.23±0.80	< LOD	3.5±1.2	3.1±7.2	2.3±5.4	4.3±1.2	7.4±1.7	0.39±0.88
4	2.3±0.9	0.52±0.23	0.55±0.16	3.8±4.0	< LOD	0.32±0.12	5.4±3.5	4.8±3.1	0.49±0.15	0.88±0.39	2.0±1.3

Microbial community shifts

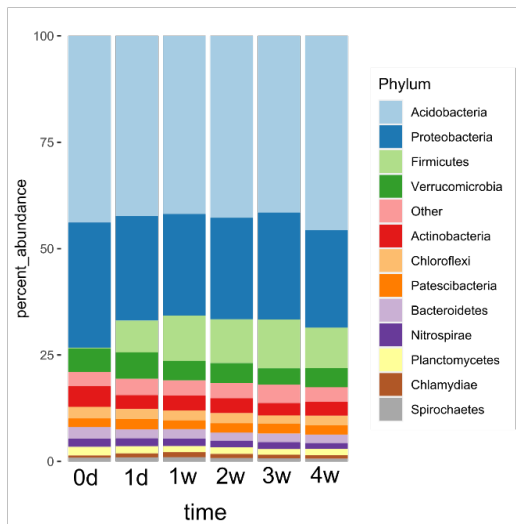


Figure S 43: Microbial community composition in microcosms containing soil collected in the Schlöppnerbrunnen II peatland. 16S rRNA amplicon abundance of phyla relative to all classified reads/sequences in the native soil (0d) and microcosm incubations over time (1d – 4w). Taxa representing less than 1% (Phylum-level) are grouped together as ‘Others’ (pink). Each bar represents the average 16S rRNA amplicon abundance (n=5) of phyla or genera for each time point (1d, 1w, 2w, 3w, 4w). 0d represents the microbial composition directly after sampling, before peat water addition, 1d the T = 0 for the other analyses, when the peatwater was added and the microcosm could adjust overnight. Note, at t = 4 w only 4 replicates are shown due to a failed library preparation for this sample prior to amplicon sequencing.

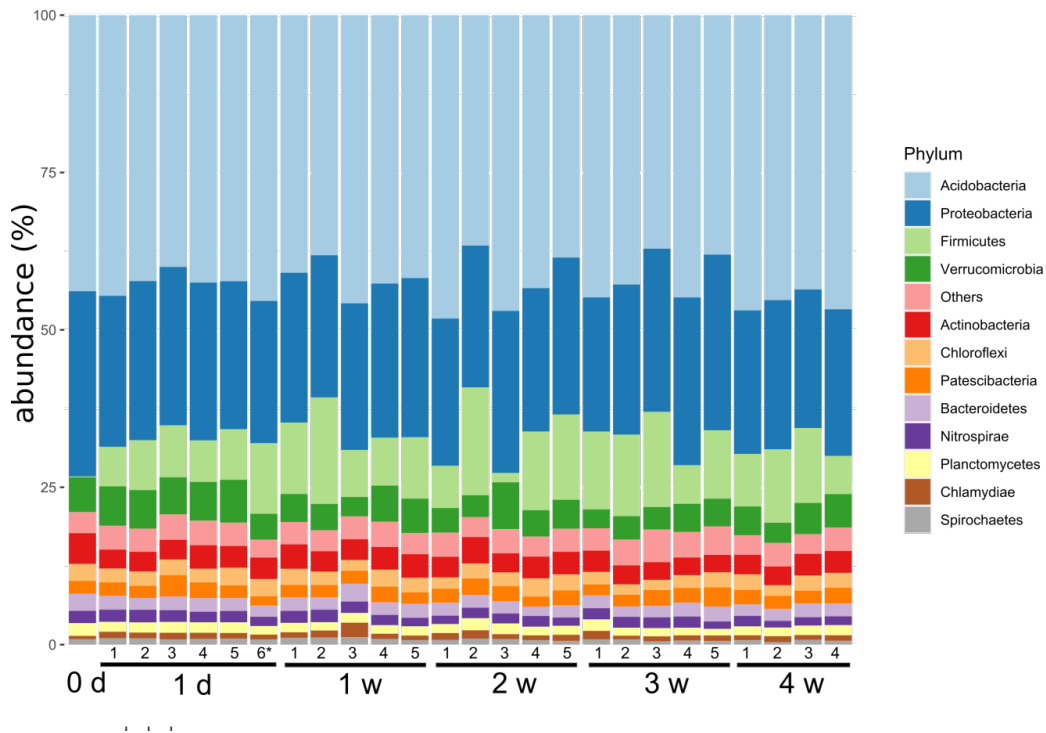


Figure S 44: Microbial community composition in microcosms containing soil collected in the Schlöppnerbrunnen II peatland. 16S rRNA amplicon abundance of phyla relative to all classified reads/sequences in the native soil (0d) and microcosm incubations over time (1d – 4w). Taxa representing less than 1% (Phylum-level) are grouped together as ‘Others’ (pink). Each bar represents the 16S rRNA amplicon abundance of phyla or genera for each sample at each time point (1d, 1w, 2w, 3w, 4w).

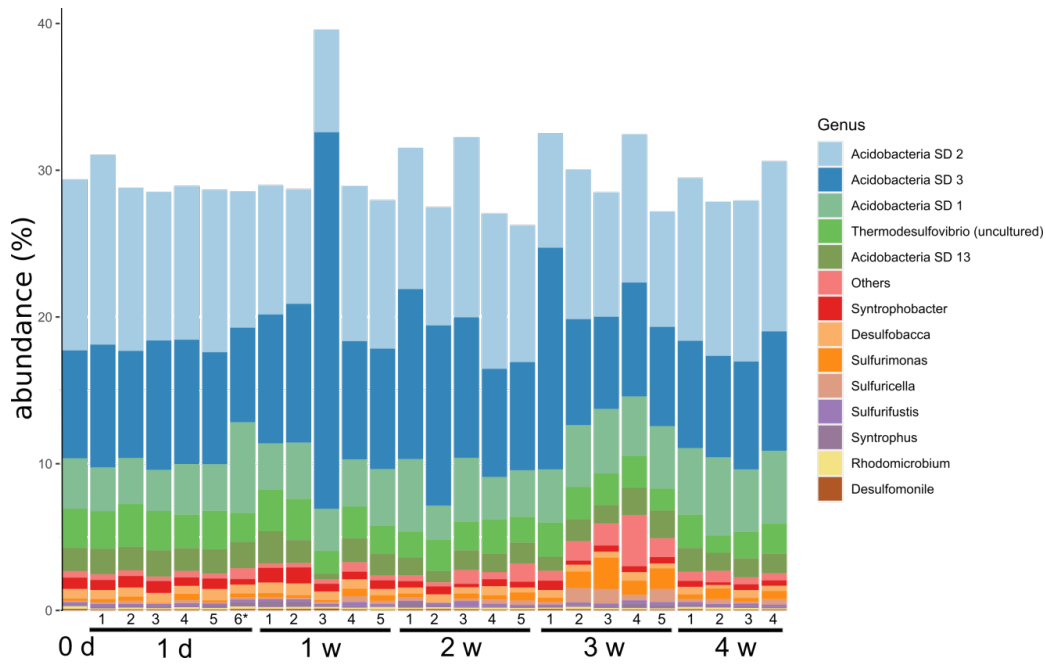


Figure S 45: Relative abundance of genera associated with dissimilatory S cycling were subset (33 total) from the total microbial community composition dataset. 16S rRNA amplicon abundance of genera associated with dissimilatory S cycling (sulfate/sulfite reduction and S oxidation). Each bar represents the relative 16S rRNA amplicon abundance of the selected genera for each sample and time point (1d, 1w, 2w, 3w, 4w).

SI REFERENCES

1. Kuhn U, et al. (1999) Carbonyl sulfide exchange on an ecosystem scale: soil represents a dominant sink for atmospheric COS. *Atmos. Environ.* 33(6):995-1008.
2. Hausmann B, et al. (2018) Peatland Acidobacteria with a dissimilatory sulfur metabolism. *ISME J* 12(7):1729-1742.
3. Gould WD & Kanagawa T (1992) Purification and properties of methyl mercaptan oxidase from *Thiobacillus thioparus* TK-m. *J. Gen. Microbiol.* 138(1):217-221.
4. Boden R, et al. (2011) Purification and characterization of dimethylsulfide monooxygenase from *Hyphomicrobium sulfonivorans*. *J. Bacteriol.* 193(5):1250-1258.
5. Hayes AC, Liss SN, & Allen DG (2010) Growth kinetics of *Hyphomicrobium* and *Thiobacillus* spp. in mixed cultures degrading dimethyl sulfide and methanol. *Appl. Environ. Microbiol.* 76(16):5423-5431.
6. Gebser B & Pohnert G (2013) Synchronized regulation of different zwitterionic metabolites in the osmoadaptation of phytoplankton. *Mar. Drugs* 11(6):2168-2182.
7. Chong J, Wishart DS, & Xia J (2019) Using MetaboAnalyst 4.0 for Comprehensive and Integrative Metabolomics Data Analysis. *Curr Protoc Bioinformatics* 68(1):e86.
8. Team RC (2020) R: A language and environment for statistical computing (R Foundation for Statistical Computing, Vienna, Austria), 4.0.3.

9. Apprill A, McNally S, Parsons R, & Weber L (2015) Minor revision to V4 region SSU rRNA 806R gene primer greatly increases detection of SAR11 bacterioplankton. *Aquat. Microb. Ecol.* 75(2):129-137.
10. Caporaso JG, et al. (2012) Ultra-high-throughput microbial community analysis on the Illumina HiSeq and MiSeq platforms. *ISME J* 6(8):1621-1624.
11. Caporaso JG, et al. (2011) Global patterns of 16S rRNA diversity at a depth of millions of sequences per sample. *Proc Natl Acad Sci U S A* 108 Suppl 1:4516-4522.
12. Parada AE, Needham DM, & Fuhrman JA (2016) Every base matters: assessing small subunit rRNA primers for marine microbiomes with mock communities, time series and global field samples. *Environ. Microbiol.* 18(5):1403-1414.
13. Edgar RC (2010) Search and clustering orders of magnitude faster than BLAST. *Bioinformatics* 26(19):2460-2461.
14. Rognes T, Flouri T, Nichols B, Quince C, & Mahe F (2016) VSEARCH: a versatile open source tool for metagenomics. *PeerJ* 4:e2584.
15. Klindworth A, et al. (2013) Evaluation of general 16S ribosomal RNA gene PCR primers for classical and next-generation sequencing-based diversity studies. *Nucleic Acids Res.* 41(1):e1.
16. Lehnert A-S, Behrendt T, Ruecker A, Pohnert G, & Trumbore SE (2020) SIFT-MS optimization for atmospheric trace gas measurements at varying humidity. *Atmos. Meas. Tech.* 13(7):3507-3520.

17. Steinmetz Z, Kurtz MP, Dag A, Zipori I, & Schaumann GE (2015) The seasonal influence of olive mill wastewater applications on an orchard soil under semi-arid conditions. *J. Plant Nutr. Soil Sci.* 178(4):641-648.
18. Ben-Gal A, et al. (2009) Evaluating water stress in irrigated olives: correlation of soil water status, tree water status, and thermal imagery. *Irrigation Science* 27(5):367-376.
19. Roth VN, Dittmar T, Gaupp R, & Gleixner G (2015) The molecular composition of dissolved organic matter in forest soils as a function of pH and temperature. *Plos One* 10(3):e0119188.
20. Michalzik B & Martin S (2013) Effects of experimental duff fires on C, N and P fluxes into the mineral soil at a coniferous and broadleaf forest site. *Geoderma* 197-198:169-176.
21. Merbach W, Garz J, Schliephake W, Stumpe H, & Schmidt L (2000) The long-term fertilization experiments in Halle (Saale), Germany - Introduction and survey. *J. Plant Nutr. Soil Sci.* 163:629-638.
22. Kugler S, et al. (2019) Iron-organic matter complexes accelerate microbial iron cycling in an iron-rich fen. *Sci. Total Environ.* 646:972-988.
23. Bourtsoukidis E, et al. (2018) Strong sesquiterpene emissions from Amazonian soils. *Nat Commun* 9(1):2226.
24. Evangelou V (1998) *Environmental soil and water chemistry* (John Wiley).
25. Reiche M, Torburg G, & Küsel K (2008) Competition of Fe(III) reduction and methanogenesis in an acidic fen. *FEMS Microbiol. Ecol.* 65(1):88-101.

A.5. Litter VOC Emissions over Time

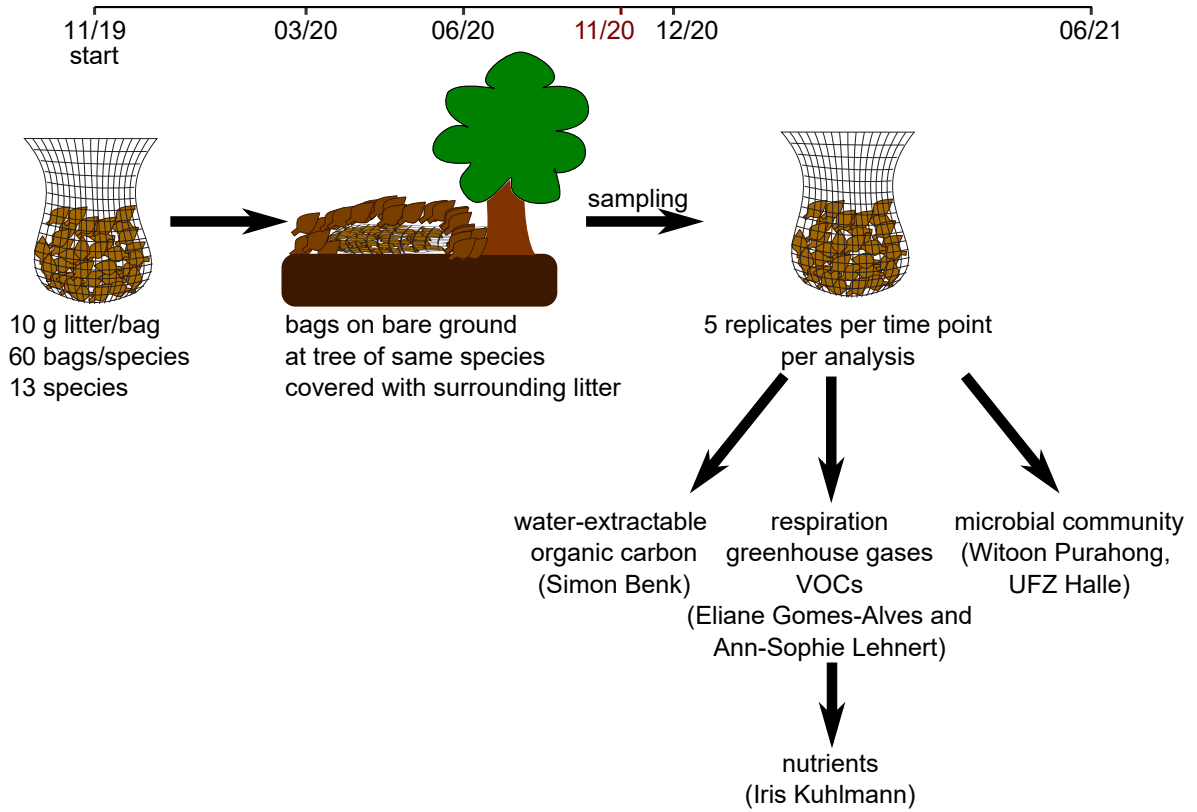


Figure A.1.: General scheme of the litter degradation in the field and the analyses done for understanding the degradation processes. Red date: date where we resampled fresh litter for the VOC analysis.

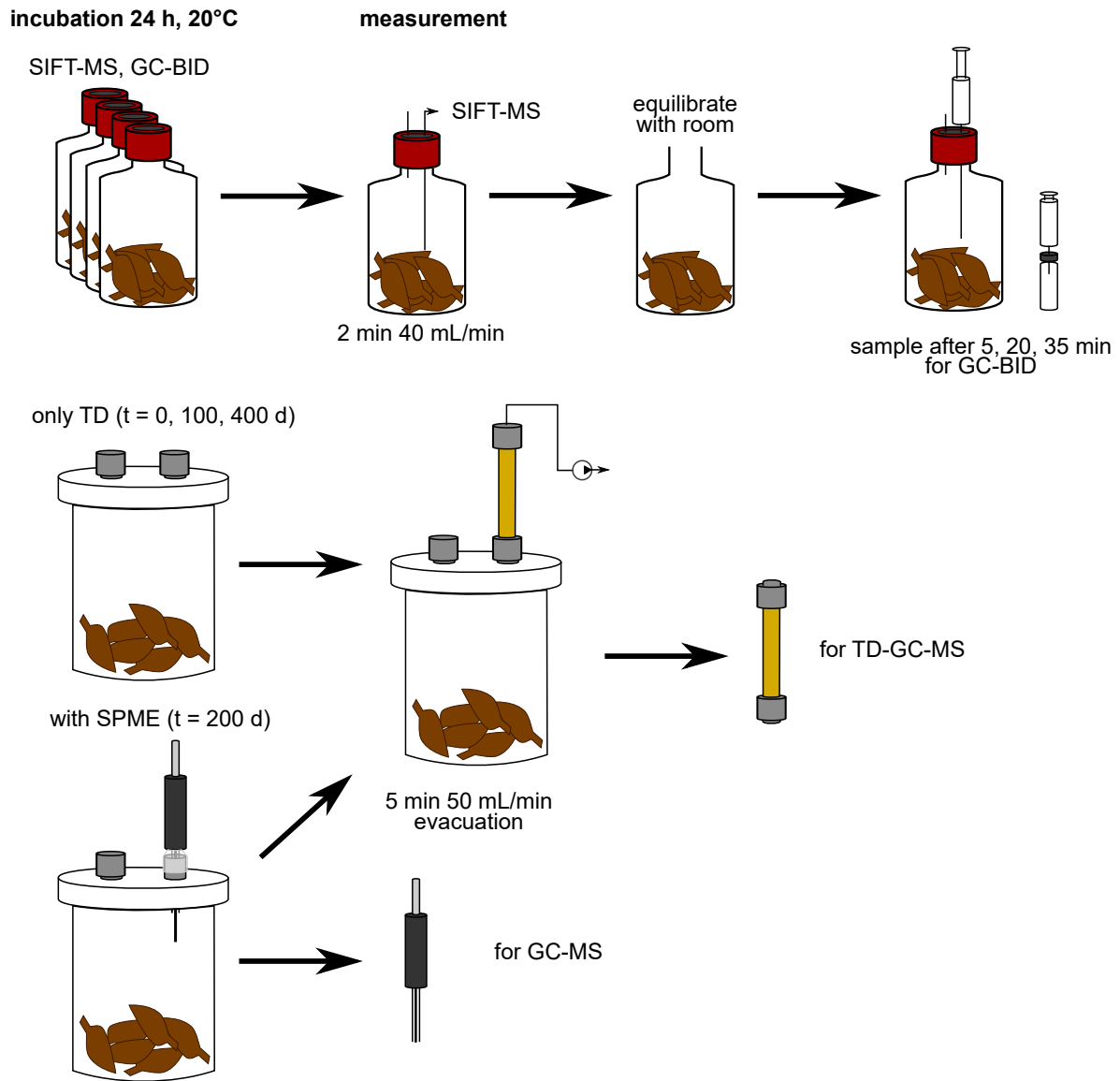


Figure A.2.: Scheme of the litter incubation and different types of gas samples analyzed for the litter degradation project.

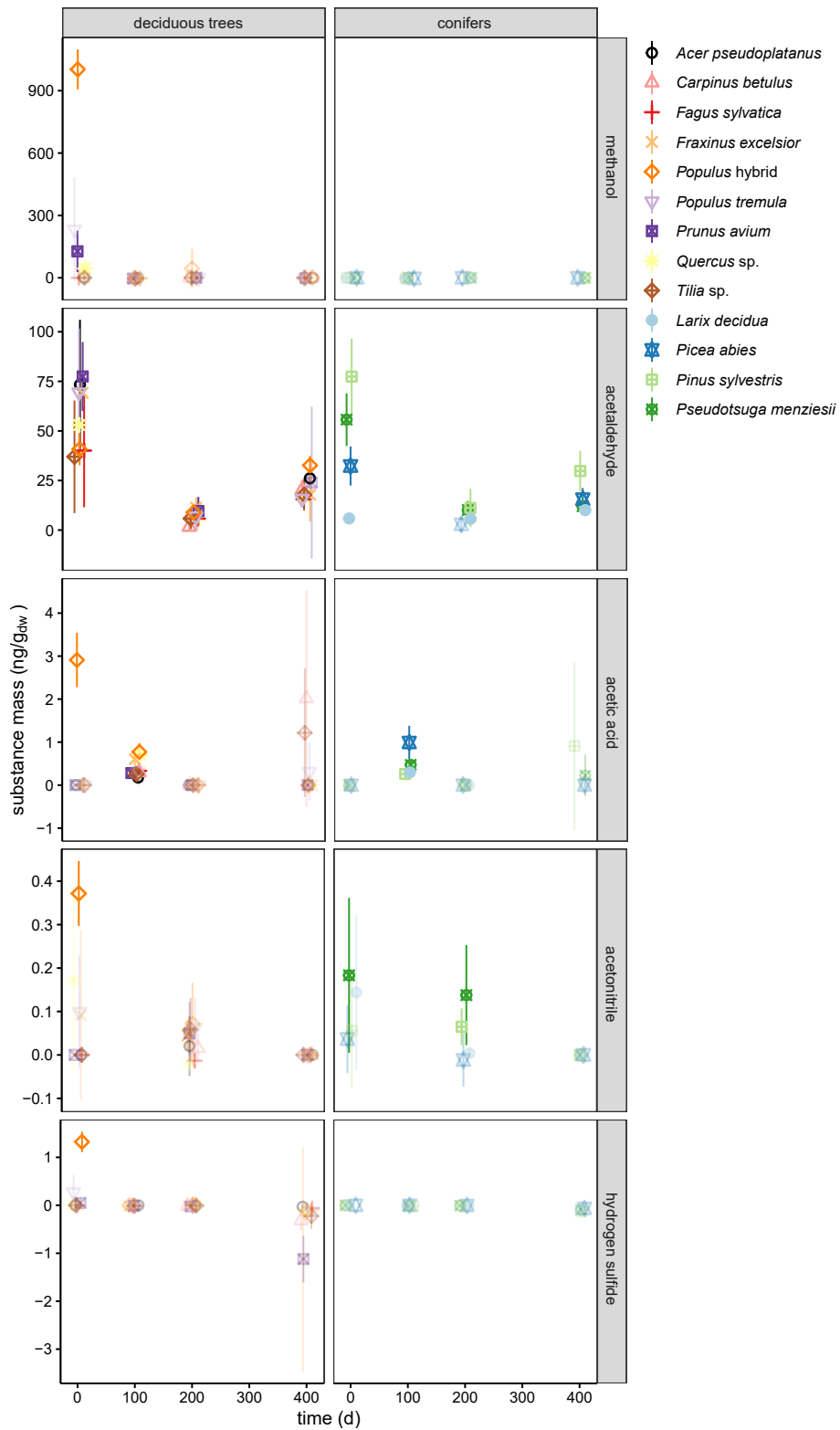


Figure A.3. Methanol, acetaldehyde, acetic acid, acetonitrile, and hydrogen sulfide emission of the different tree litter types over time. Mean \pm 95% CI, (n = 4 per litter type and time point).

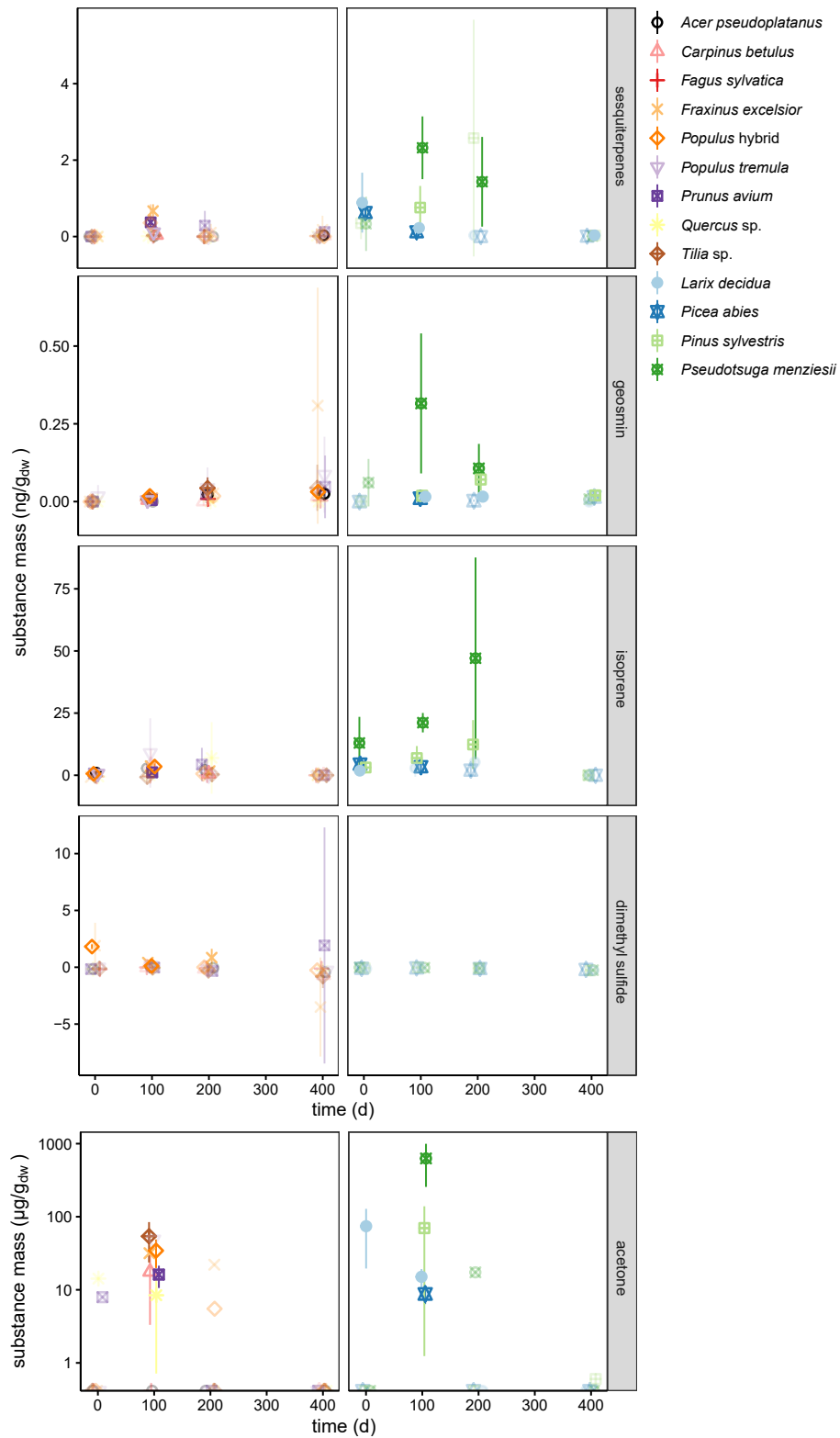


Figure A.4.: Sum sesquiterpene, geosmin, isoprene, dimethyl, and acetone emission of the different tree litter types over time. Mean \pm 95% CI, (n = 4 per litter type and time point). Note that the acetone emission is depicted on a logarithmic scale.

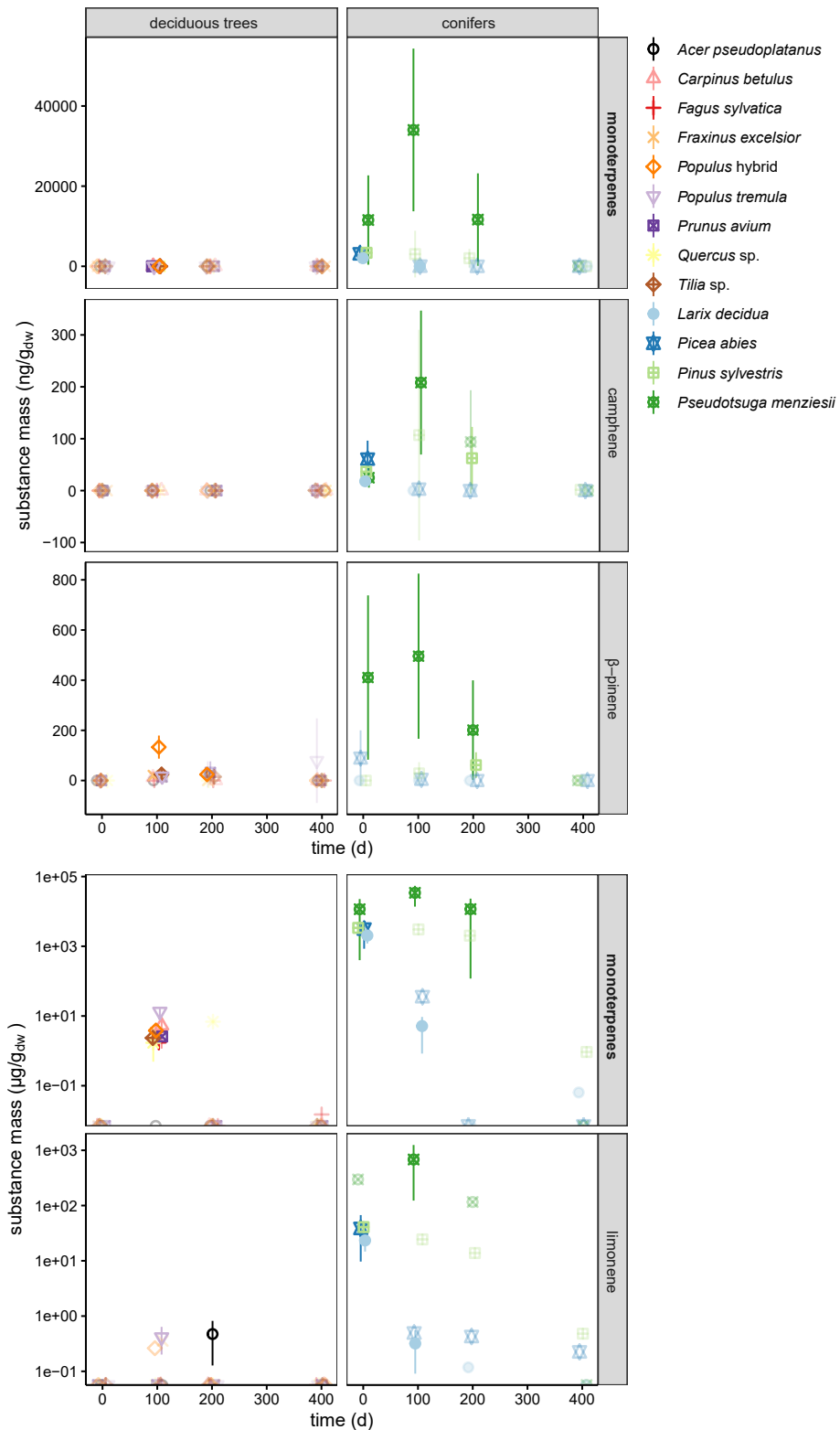


Figure A.5.: Sum monoterpene, β -pinene, camphene, and limonene emission of the different tree litter types over time. Mean \pm 95% CI, (n = 4 per litter type and time point). Note that the monoterpene and limonene emissions are depicted on a logarithmic scale; monoterpene emissions are depicted twice for comparability on both axis types.

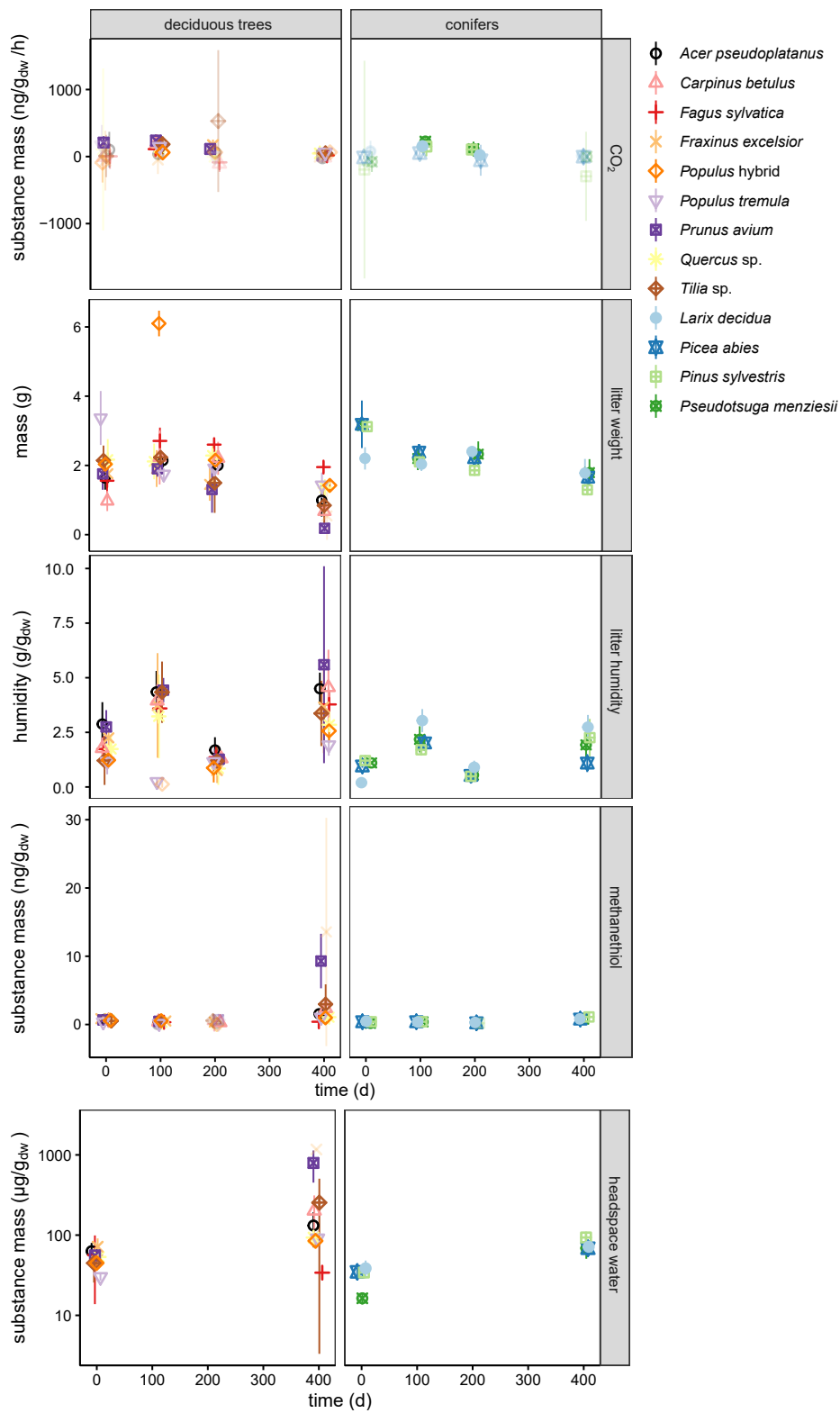


Figure A.6.: CO₂ release rate, headspace and sample humidity, litter weight, and methanethiol emission of the different tree litter types over time. Mean \pm 95% CI, (n = 4 per litter type and time point). Note that the headspace humidity is depicted on a logarithmic scale.

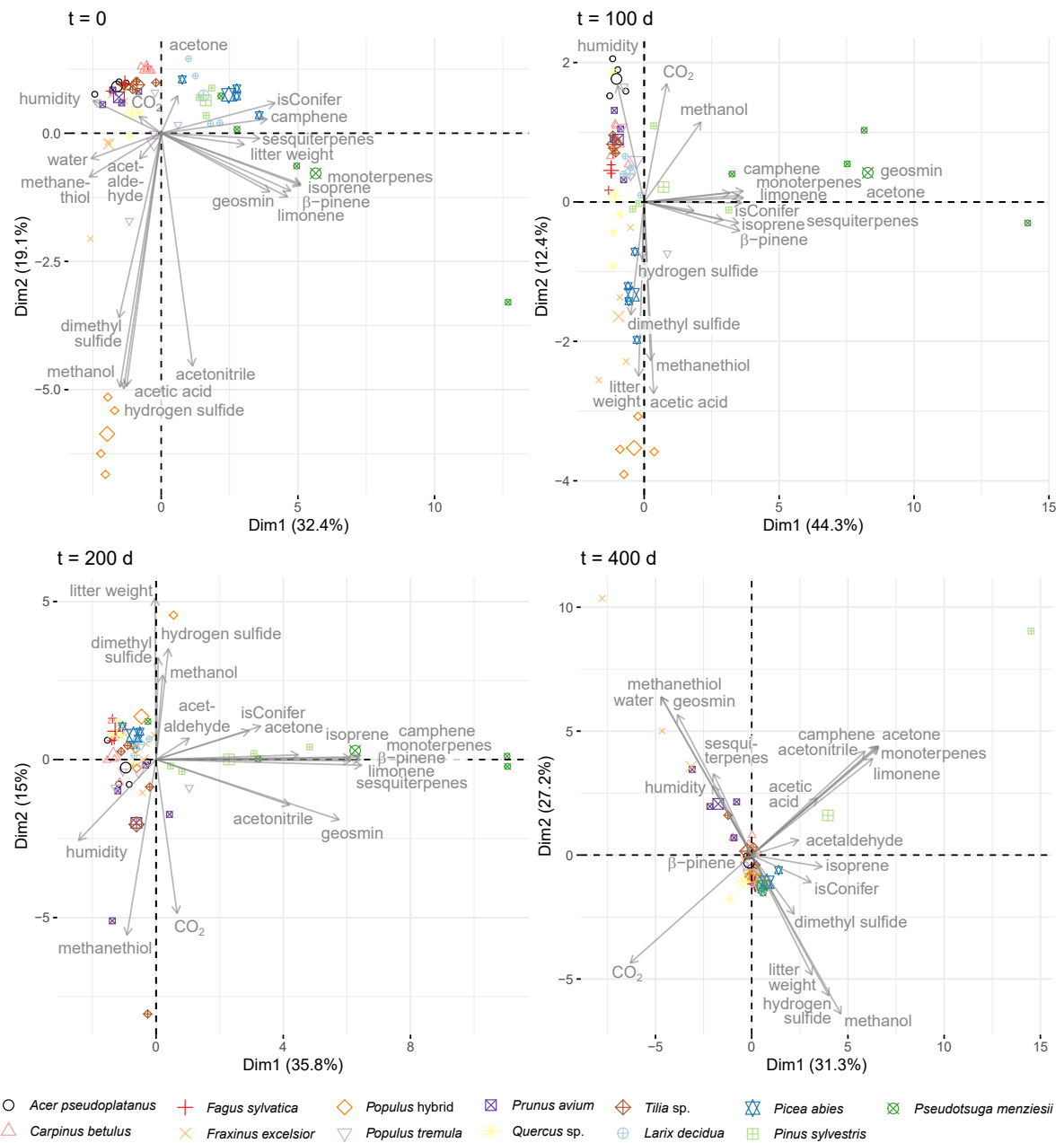


Figure A.7.: Principal component analyses of VOC emissions from litter of different tree species on the different sampling dates. Bigger symbols represent the mean of each species. The data for the PCA was centered and scaled. The individual contributions of the third and higher axes are smaller than 10% and very similar to each other and thus considered negligible..

Table A.12.: Mixed-effect model for acetaldehyde emissions. The model is $\text{ACETALDEHYDE} \sim \text{EXPTIME} + \text{HUMIDITY} + (\text{EXPTIME}|\text{PLANT})$. $\text{EXPTIME} = e^{-\text{time}}$. The confidence intervals are bootstrapped ($n_{sim} = 1000$), p -values were calculated *via* the Kenward-Roger approximation.

Predictors	Estimates	CI	p
Intercept	2.8	-1.2 – 6.9	0.167
expTime	41	30 – 53	<0.001
humidity	5.0	3.7 – 6.4	< 0.001
Random effects			
σ^2	123		
$\tau_{00plant}$	9.48		
$\tau_{00plant.isConiferTRUE}$	263		
$\rho_{01plant}$	0.48		
ICC	0.46		
N_{plant}	13		
Observations	150		
Marginal R^2 / Conditional R^2	0.623 / 0.796		

Table A.13.: Mixed-effect model for acetone emissions. The model is $\text{ACETONE} \sim \text{PLANT}$. The confidence intervals are bootstrapped ($n_{sim} = 1000$), p -values were calculated *via* the Kenward-Roger approximation.

Predictors	Estimates	CI	p
Intercept (<i>P. menzesii</i>)	162	112 – 211	p < 0.001
plant (<i>Quercus</i> sp.)	-156	-228 – -82	p < 0.001
plant (<i>F. excelsior</i>)	-148	-218 – -78	p < 0.001
plant (<i>P. abies</i>)	-159	-230 – -89	p < 0.001
plant (<i>C. betulus</i>)	-157	-233 – -81	p < 0.001
plant (<i>P. avium</i>)	-156	-226 – -86	p < 0.001
plant(<i>P. sylvestris</i>)	-142	-214 – -72	p < 0.001
plant (<i>L. decidua</i>)	-140	-210 – -870	p < 0.001
plant (<i>Tilia</i> sp.)	-148	-218 – -78	p < 0.001
plant (<i>P. tremula</i>)	-149	-220 – -79	p < 0.001
plant(<i>Populus</i> hybrid)	-152	-222 – -82	p < 0.001
Observations	170		

Table A.14.: Mixed-effect model for methanol emissions. The model is $\text{METHANOL} \sim \text{expTime} + (\text{expTime}|\text{PLANT})$. $\text{expTime} = e^{-\text{time}}$. The confidence intervals are bootstrapped ($n_{sim} = 1000$), p -values were calculated *via* the Kenward-Roger approximation.

Predictors	Estimates	CI	p
Intercept	0.1	-6.6 – 6.7	0.984
expTime	116	-60 – 293	0.179
Random effects			
σ^2	1.29E3		
$\tau_{00plant}$	13		
$\tau_{11plant.expTime}$	73E3		
$\rho_{01plant}$	1.00		
ICC	0.93		
N_{plant}	13		
Observations	202		
Marginal R^2 / Conditional R^2	0.115 / 0.938		

Table A.15.: Mixed-effect model for monoterpene emissions. The model is $\text{MONOTERPENES} \sim \text{TIME} * \text{isCONIFER} + (\text{isCONIFER}|\text{PLANT})$. The confidence intervals are bootstrapped ($n_{sim} = 1000$), p -values were calculated *via* the Kenward-Roger approximation.

Predictors	Estimates	CI	p
Intercept	1.82	-1200 – 1200	0.998
time	-0.0	- 5.2 – 5.2	0.999
isConiferTRUE	7500	-780 – 16000	0.069
time:isConiferTRUE	-17	-26 – -8	<0.001
Random effects			
σ^2	2.0E7		
$\tau_{00plant}$	0		
$\tau_{00plant.isConiferTRUE}$	3.2E7		
$\rho_{01plant}$			
N_{plant}	13		
Observations	202		
Marginal R^2 / Conditional R^2	0.236 / NA		

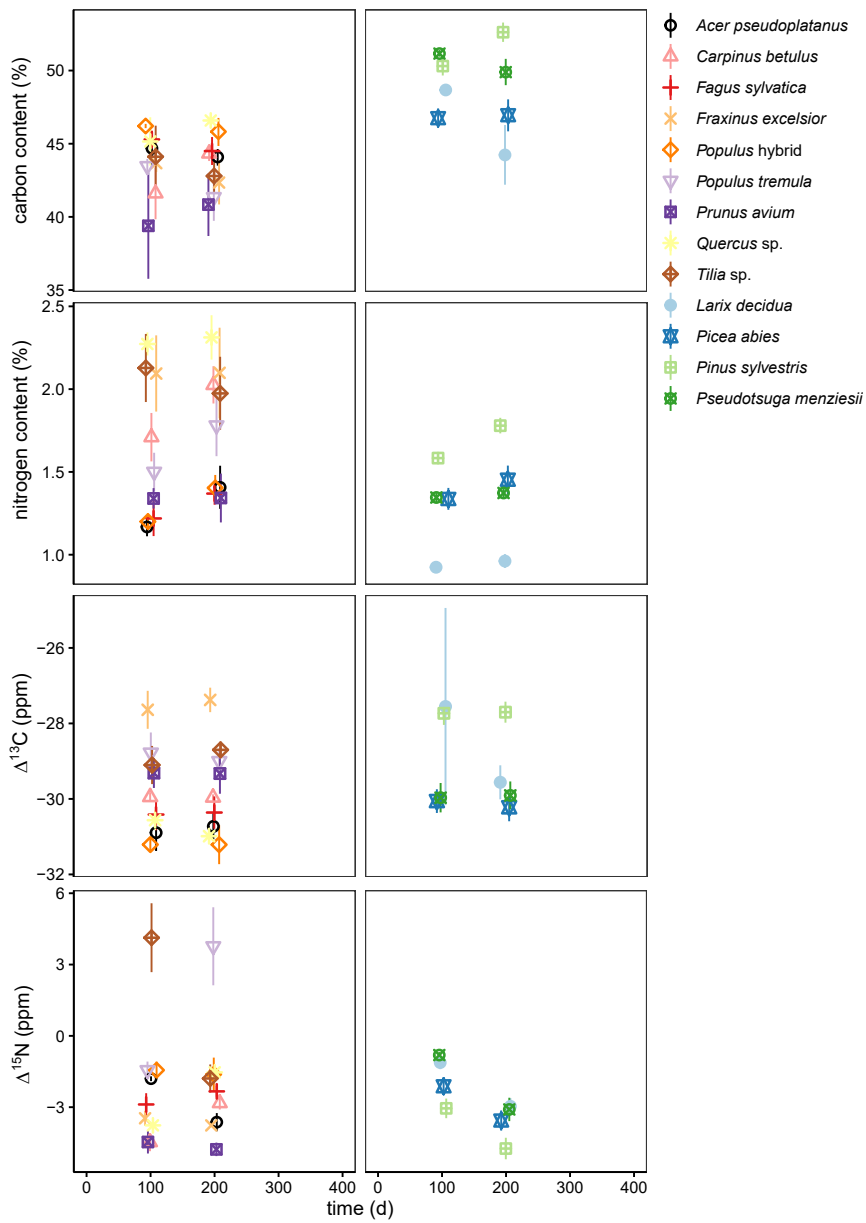


Figure A.8.: Carbon and nitrogen contents (mass percent relative to dry mass) as well as $\Delta^{13}\text{C}$ and $\Delta^{15}\text{N}$ signals of the different tree litter types over time. Mean \pm 95% CI, (n = 5 per litter type an time point).

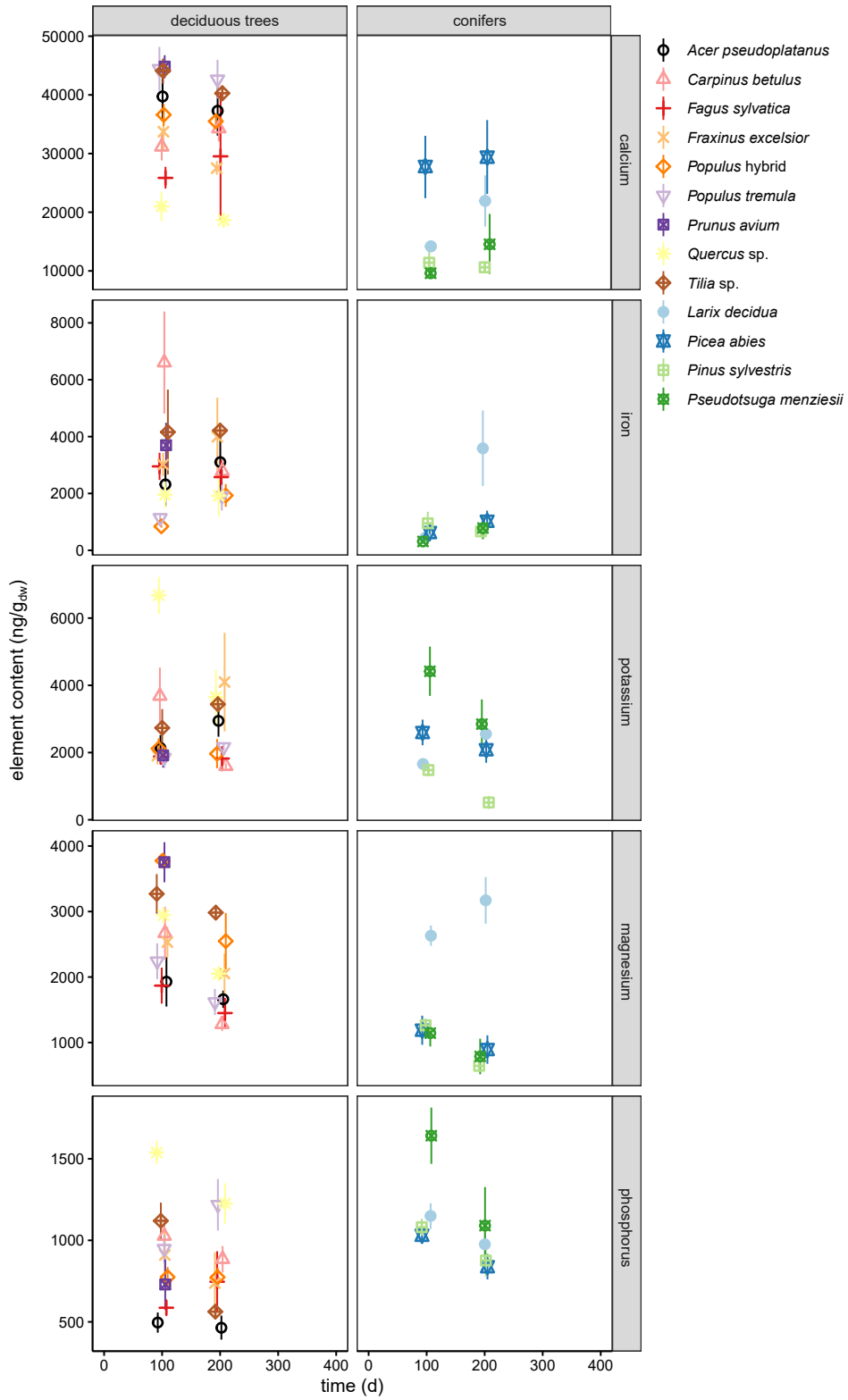


Figure A.9: Ca, Fe, K, Mg, and P contents of the different tree litter types over time. Mean \pm 95% CI, (n = 5 per litter type at a time point).

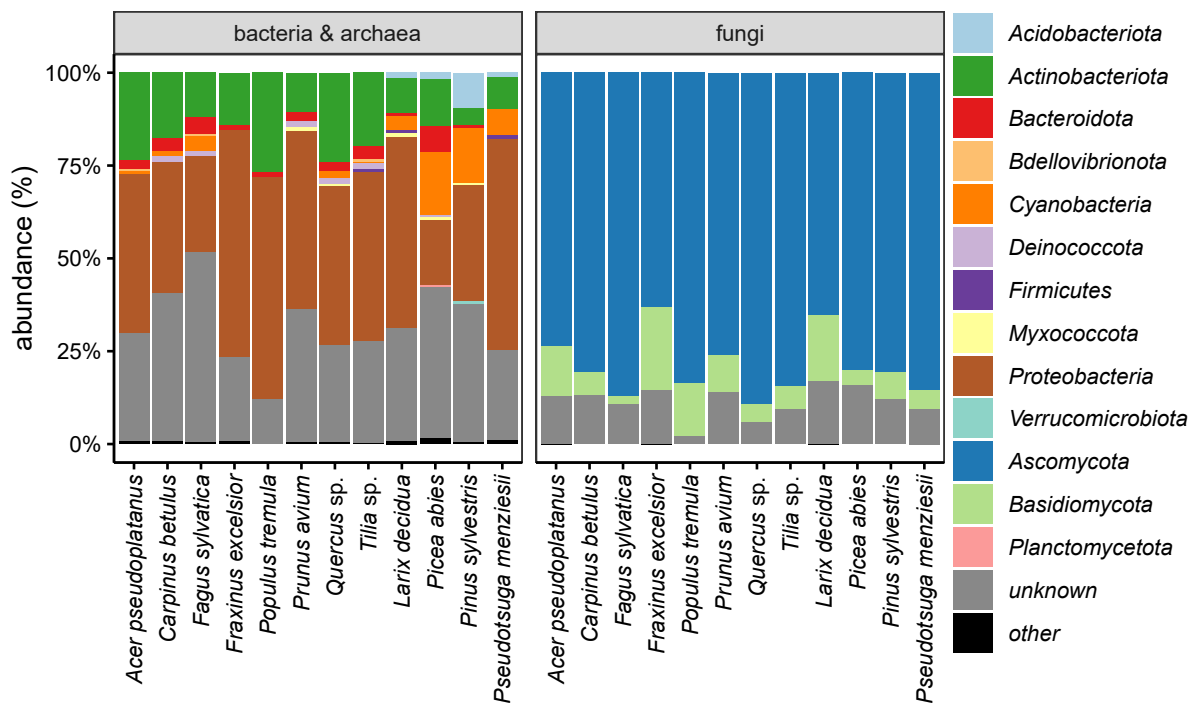


Figure A.10.: Relative abundance of the different bacterial/archaeal and fungal phyla at $t = 0$ for the different tree species, based on their 16S-RNA-sequences. Phyla with an abundance $< 0.5\%$ were merged to "other".

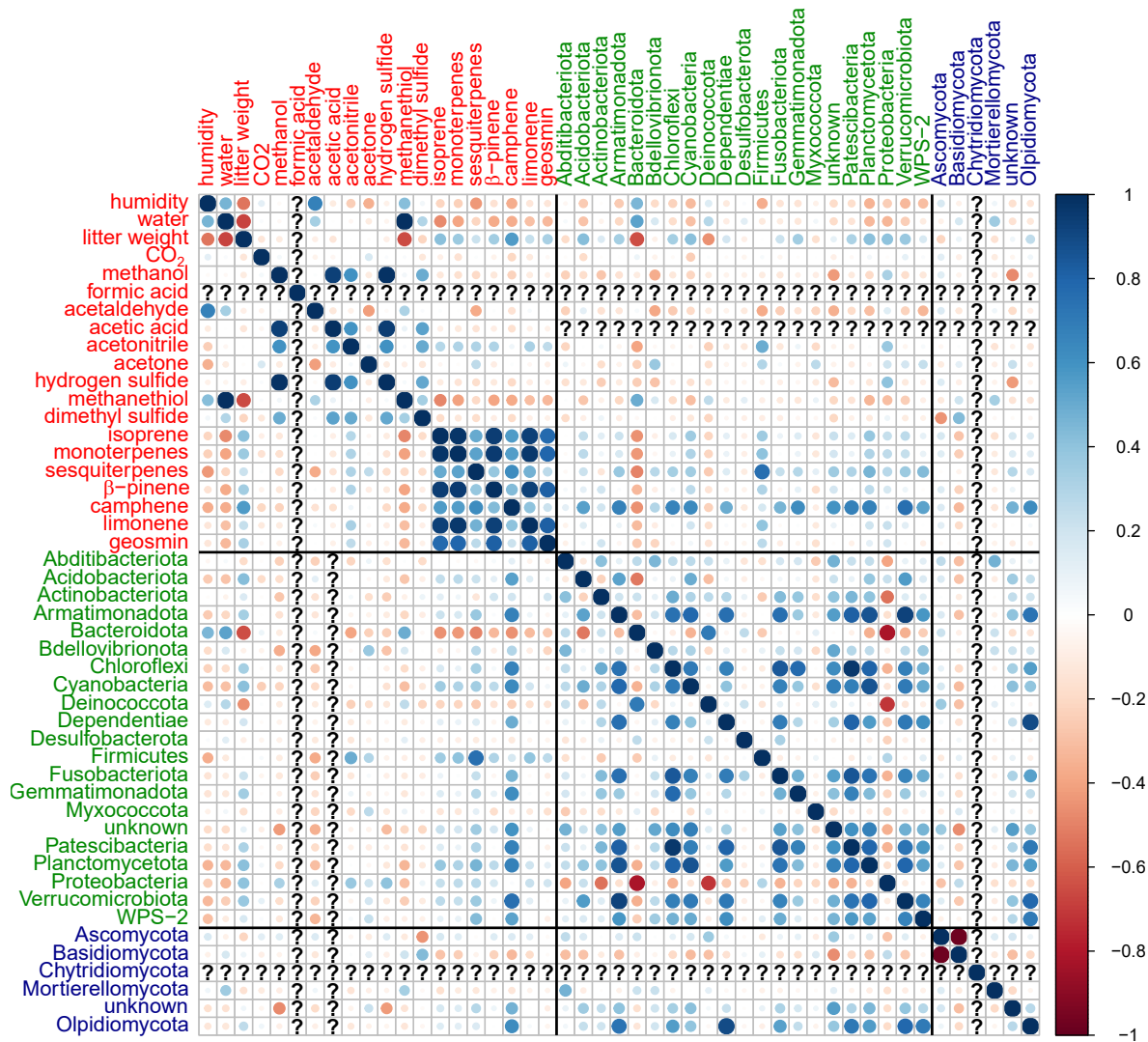


Figure A.11.: Correlation coefficients of the different VOCs correlating with the bacterial/archaeal and fungal phylum abundances at t = 0.